



UCTEA Turkish Chamber of Civil Engineers

# Teknik Dergi

*Technical Journal*

Volume 33    Issue 5    Semtember 2022

## **TEKNİK DERGİ PUBLICATION PRINCIPLES**

Teknik Dergi is a scientific and technical journal indexed by the Science Citation Index Expanded. Annually six issues are published, three in Turkish in the months of January, May and September, three in English in March, July and November. Its main principles of publication are summarized below:

1. Articles reporting original scientific research and those reflecting interesting engineering applications are accepted for publication. To be classified as original, the work should either produce new scientific knowledge or add a genuinely new dimension to the existing knowledge or develop a totally new method or substantially improve an existing method.
2. Articles reporting preliminary results of scientific studies and those which do not qualify as full articles but provide useful information for the reader can be considered for publication as technical notes.
3. Discussions received from the readers of the published articles within three months from publication are reviewed by the Editorial Board and then published together with the closing remarks of the author.
4. Manuscripts submitted for publication are evaluated by two or three reviewers unknown to the authors. In the light of their reports, final decision to accept or decline is taken by the Editorial Board. General policy of the Board is to get the insufficient manuscripts improved in line with the reviewers' proposals. Articles that fail to reach the desired level are declined. Reasons behind decisions are not declared.
5. A signed statement is taken from the authors, declaring that the article has not been published as a "journal article or book chapter". In case the Editorial Board is in the opinion that the article has already been published elsewhere with minor changes or suspects plagiarism or a similar violation of ethics, then not only that article, but none of the articles of the same authors are published.
6. Papers reporting works presented as conference papers and developed further may be considered for publication. The conference it was presented to is given as a footnote in the first page.
7. Additionally, a document signed by all authors, transferring the copyright to UCTEA Chamber of Civil Engineers is submitted together with the manuscript.



UCTEA Turkish Chamber of Civil Engineers

# Teknik Dergi

*Technical Journal*

Volume 33    Issue 5    Semtember 2022



**UCTEA (TMMOB)**

**Turkish Chamber of Civil Engineers (*İnşaat Mühendisleri Odası*)**

Necatibey St. No: 57, Kızılay 06440 Ankara, Turkey

Tel: +90.312.294 30 00 - Faks: +90.312.294 30 88

E-mail: imo@imo.org.tr - www.imo.org.tr

**Publisher (*Sahibi*):**

Taner YÜZGEÇ

On behalf of UCTEA Turkish Chamber of Civil Engineers

**Administrative Officer (*Yazı İşleri Müdürü*):**

Özer AKKUŞ

Volume 33 - Issue 5 - September 2022 (*Cilt 33 - Sayı 5 - Eylül 2022*)

Published bi-monthly. Local periodical. (*İki ayda bir yayınlanır, yerel süreli yayın*)

Date of Print: September 1, 2022 (*Baskı Tarihi: 1 Eylül 2022*)

Number of copies: 1.000 (*1.000 adet basılmıştır*)

Quotations require written approval of the Editorial Board.

(*Yayın Kurulunun yazılı onayı olmaksızın alıntı yapılamaz.*)

**ISSN: 1300-3453**

Teknik Dergi is indexed by

- Science Citation Index Expanded
- Scopus
- Journal Citation Reports / Science Edition
- Engineering Index
- Concrete Abstracts (American Concrete Institute)
- National Technical Information Service (US NTIS)
- CITIS
- Ulrich's International Periodical's Directory
- Google Scholar
- TR Index

Teknik Dergi is a peer reviewed open access periodical publishing papers of original research and interesting practice cases. It addresses both the research community and the practicing engineers.

Teknik Dergi ekidir.

---



UCTEA Turkish Chamber of Civil Engineers

# Teknik Dergi

## Editor in Chief:

Alper İLKİ

## Co-Editors:

İsmail AYDIN

Özer ÇİNİCİOĞLU

Metin GER

Gürkan Emre GÜRCANLI

Kutay ORAKÇAL

İsmail ŞAHİN

Özkan ŞENGÜL

Tuğrul TANKUT

Emine Beyhan YEĞEN

## Secretary:

Cemal ÇİMEN

## Advisory Board:

Prof. M. Aral, USA

Prof. D. Arditi, USA

Prof. A. Aydilek, USA

Prof. K. Beyer, Switzerland

Prof. N. Çatbaş, USA

Prof. M. Çetin, USA

Prof. M. Dewoolkar, USA

Prof. T. Edil, USA

Prof. K. Elwood, New Zealand

Prof. M. Fardis, Greece

Prof. G. Gazetas, Greece

Prof. P. Gülkan, Türkiye

Prof. J. Han, USA

Prof. I. Hansen, Netherlands

Prof. T. Hartmann, Germany

Prof. F. Imamura, Japan

Prof. T. Kang, Korea

Prof. K. Kusunoki, Japan

Prof. S. Lacasse, Norway

Prof. R. Al-Mahaidi, Australia

Prof. K. Özbay, USA

Prof. H. Özer, USA

Prof. G. Özmen, Türkiye

Prof. S. Pampanin, Italy

Prof. A. J. Puppala, USA

Prof. M. Saatçioğlu, Canada

Prof. C. Santamarina, Saudi Arabia

Prof. S. Sheikh, Canada

Prof. E. C. Shin, South Korea

Prof. J. Smallwood, South Africa

Prof. M. Sümer, Türkiye

Dr. H. A. Şentürk, Türkiye

Dr. S. S. Torisu, Japan

Prof. E. Tutumluer, USA

Prof. M. Tümay, USA

## Reviewers:

This list is renewed each year and includes reviewers who served in the last two years of publication.

Şükran AÇIKEL	Halil İbrahim BURGAN	Fazlı Erol GÜLER	Umut OKKAN	Serhan TANYEL
Merve AÇIKGENÇ	Erdem CANBAY	İlgin GÜLER	Derviş Volkan OKUR	Yüksel TAŞDEMİR
ULAŞ	Zekai CELEP	Hamza GÜLLÜ	Mehmet Hakkı OMURTAG	Kerem TAŞTAN
Stüleyman ADANUR	Cihan CENGİZ	Gürkan GÜNAY	Engin ORAKDÖĞEN	Gökmen TAYFUR
Ali Mardani	Halim CEYLAN	Taylan GÜNAY	Şeref ORUÇ	Beytullah TEMEL
AGHABAGLOU	Hüseyin CEYLAN	Murat GÜNAYDIN	Akin ÖNALP	Rasim TEMÜR
Perviz AHMEDZADE	Ömer CİVALEK	Samet GÜNER	Halil ÖNDER	Egemen TEOMETE
Bülent AKBAŞ	Ayşe COŞKUN BEYAN	Ülker GÜNER BACANLI	Jülide ÖNER	Serdal TERZİ
Ragıp AKBAŞ	Melih ÇALAMAK	Oğuz GÜNEŞ	Bihra ÖNÖZ	Berrak TEYMUR
Samir Oğuzhan AKBAŞ	Gülben ÇALIŞ	Mehmet Şükri GÜNEY	Ali Hakan ÖREN	Hüseyin Onur TEZCAN
Şeref Doğuşcan AKBAŞ	Süheyla Pelin ÇALIŞKANELLİ	Tuba GÜRBÜZ	Mustafa ÖZAKÇA	Mesut TİĞDEMİR
Rıfat AKBIYIKLI	Dilay ÇELEBİ	Melike GÜREL	Ceyhan ÖZÇELİK	Şahnaz TİĞREK
Özge AKBOĞA KALE	Tevfik Kutay ÇELEBİOĞLU	İbrahim GÜRER	Yiğit ÖZÇELİK	Salih TİLEYLİOĞLU
Hüseyin AKBULUT	Ahmet Ozan ÇELİK	Aslı Pelin GÜRGÜN	Gökhan ÖZDEMİR	Vedat TOĞAN
Sarven AKCELYAN	Oğuz Cem ÇELİK	İman HAJİRASOULİHA	Osman Nuri ÖZDEMİR	Onur Behzat TOKDEMİR
Burcu AKÇAY	Semret ÇELİK	Soner HALDENBİLEN	Halit ÖZEN	İrem Dikmen TOKER
ALDANMAZ	Hilmi Berk ÇELİKOĞLU	Mustafa HATİPOĞLU	Murat ÖZEN	Cengiz TOKLU
Cihan Taylan AKDAĞ	Mahmut ÇETİN	Bo-Tao HUANG	Pelin ÖZENER	Ali TOPAL
Cem AKGÜNER	Mecit ÇETİN	Zeynep İŞİK	Cem ÖZER	İlker Bekir TOPÇU
Muhammet Vefa AKPINAR	Gökhan ÇEVİKBİLEN	Hande İŞİK ÖZTÜRK	Hasan ÖZER	Cem TOPKAYA
Atakan AKSOY	Erdal ÇOKÇA	Sabriye Banu İKİZLER	Serkan ÖZGEN	Kamile TOSUN
Hafızullah AKSOY	İsa ÇÖMEZ	Ragıp İNCE	Eren Arman ÖZGÜVEN	ÇELEKOĞLU
Hakan AKSU	İsmail DABANLI	Recep İYİSAN	Hakkı Oral ÖZHAN	Gökçe TÖNÜK
Tülay AKSU ÖZKUL	Ömer DABANLI	Nihat KABAY	M. Hulusi ÖZKUL	Ülgen Mert TUĞSAL
Büşra AKTÜRK	Atilla DAMCI	Mehmet Sedat KABDAŞLI	Zeynep Huri ÖZKUL	Gürşen TURAN
Zuhal AKYÜREK	Yakup DARAMA	Mehmet Rifat KAHYAOĞLU	BİRGÖREN	Ö. Tuğrul TURAN
Uğurhan AKYÜZ	Osama M.F. DAWOUD	Özkan KALE	Ahmet ÖZTÜRAL	Cüneyt TÜZÜN
Sadık ALASHAN	Tayfun DEDE	Volkan KALPAKÇI	Sadık ÖZTOPRAK	Eren UÇKAN
Centk ALHAN	Özgür DEĞERTEKİN	Murat KARACASU	Turan ÖZTURAN	Ergin ULUTAŞ
Ayşe Burcu ALTAN	Abdullah DEMİR	Halil KARAHAN	Hasan Tahsin ÖZTÜRK	Berna UNUTMAZ
SAKARYA	Cem DEMİR	Centk KARAKURT	Mustafa ÖZUYSAI	Tayfun UYGUNOĞLU
Sinan ALTIN	Emre DEMİR	Mustafa KARASAİN	Ahmet Onur PEHLİVAN	Volkan Emre UZ
Adlen ALTUNBAŞ	Munise Didem DEMİRBAŞ	Zülküf KAYA	Onur PEKCAN	Nihal UZCAN ERATLI
Ahmet Can ALTUNBAŞ	Ender DEMİREL	Hasan Ahmed KAZMEE	Seval PINARBAŞI	İbrahim Mert UZUN
Ahmet Can ALTUNİŞİK	Mehmet Cüneyd DEMİREL	Mustafa Kubilay KELEŞOĞLU	ÇUHADAROĞLU	Deniz ÜLGEN
Yalçın ALVER	Fatih DİKBAŞ	Elçin KENTEL	Elişan Filiz PİROĞLU	Mehmet ÜLKER
Bahadır ALYAVUZ	Seyyit Ümit DİKMEN	Havvanur KILIÇ	Selim PUL	Mehmet Barış Can ÜLKER
Özgür ANIL	Ali Ersin DİNÇER	Young Hoon KIM	Selçuk SAATÇI	Yurdanur ÜNAL
Necati ARAS	İsmail DURANYILDIZ	Ufuk KIRBAŞ	Selman SAĞLAM	Cüneyt VATANSEVER
Yalın ARICI	Selim DÜNDAR	Veysel Şadan Özgür KIRCA	Mehmet SALTAN	Syed Tanvir WASTI
Yalçın ARISOY	Nurhan ECEMİŞ ZEREN	Cem KIRLANGIÇOĞLU	İlyas SARIBAŞ	Ahmet YAKUT
Musa Hakan ARSLAN	Volkan Ş. EDİGER	Güven KIYMAZ	Metin SARIGÖL	Mehmet Cem YALÇIN
Deniz ARTAN İLTER	Muhammet Emin EMİROĞLU	Kasım KOÇAK	Afşin SARITAŞ	Aslı YALÇIN
Şenay ATABAY	Murat Altuğ ERBERİK	Salih KOÇAK	Altuğ SAYGILI	DAYIOĞLU
Ali Osman ATAHAN	Ali ERCAN	Niyazi Uğur KOÇKAL	Serdar SELAMET	Ahmet Cevdet YALÇINER
Hakan Nuri ATAHAN	Hakan ERDEM	Mehmet Melih KOŞUCU	Senem SEYİS	İsmail Özgür YAMAN
Bekir Özer AY	Sinan Turhan ERDOĞAN	Baha Vural KÖK	Alper SEZER	Arcan YANIK
Ersin AYDIN	Ramazan Cüneyt ERENOĞLU	Mete KÖKEN	Osman SİVRİKAYA	Mert Yücel YARDIMCI
Gökçe AYDIN	Esin ERGEN PEHLEVAN	Şerife Yurdağül KUMCU	Behzad SOLTANBEİGI	Ufuk YAZGAN
Hakan AYGÖREN	Gökmen ERGÜN	Murat KURUOĞLU	Celal SOYARSLAN	Anıl YAZICI
Mustafa Tamer AYVAZ	Bülent ERKMEN	Akif KUTLU	Serdar SOYÖZ	Halit YAZICI
İhsan Engin BAL	Barış ERKUŞ	Abdullah KÜRKCÜ	Rifat SÖNMEZ	Seda YEŞİL MEN
Selim BARADAN	Tuğba ESKİŞAR TEFCİ	Hilmi LUŞ	Tayfun Altuğ SÖYLEV	Tahsin Alper YIKICI
Eray BARAN	Burak FELEKOĞLU	Kasım MERMERTAŞ	Erol ŞADOĞLU	İrem Zeynep YILDIRIM
Türkay BARAN	Okan FİSTİKOĞLU	Mehmet Murat MONKUL	Güvenç ŞAHİN	Mehmet YILDIRIMOĞLU
Bekir Oğuz BARTIN	Abdullah GEDİKLİ	Hamid MORTEZAEİ	Olca ŞAHİN	Abdülazim YILDIZ
Eyüp Ensar BAŞAKIN	Ömer GİRAN	Yetiş Şazi MURAT	Ömer Lütfi ŞEN	Koray Kamil YILMAZ
Özgür BAŞKAN	Zehra Canan GİRGIN	Sepanta NAİMİ	Burak ŞENGÖZ	Mehmet YILMAZ
Niyazi Özgür BEZGİN	İlgın GÖKAŞAR	Öcal NECMİOĞLU	Özkan ŞENGÜL	Mustafa Tolga YILMAZ
Senem BİLİR	Serdar GÖKTEPE	Sinan Melih NİĞDELİ	Aynur ŞENSOY ŞORMAN	Mustafa Tuğrul YILMAZ
MAHÇİÇEK		Elif OĞUZ	Karin ŞEŞETİYAN	İsmail YÜCEL
Gökçen BOMBAR		Fuad OKAY	Okan ŞİRİN	Ömer YÜKSEK
Burak BOYACI			Ali Ünal ŞORMAN	Shaban Isamel Albrka Ali ZANGENA
İlknur BOZBEY			Gülüm TANIRCAN	Abdullah Can ZÜLFİKAR
Zafer BOZKUŞ				
Atıl BULU				
Burcu BURAK BAKIR				

## CONTENTS

Utilising Building Information Models in Facility Maintenance and Operations ....	12351
<b>Esa HALMETOJA, Natalija LEPKOVA</b>	
Experimental Investigation on Hydraulic Efficiency of Vertical Drop Equipped with Vertical Screens .....	12379
<b>Rasoul DANESHFARAZ, Sina SADEGHFAM, Vadoud HASANNIYA, John ABRAHAM4, Reza NOROUZI</b>	
Seismic Performance of a Hybrid Coupled Wall System Using different Coupling Beam Arrangements .....	12401
<b>Molham SALAMEH, Mohsenali SHAYANFAR, Mohammad Ali BARKHORDARI</b>	
Investigating the Service Quality of Kocaeli Tram Service Using Artificial Neural Networks .....	12429
<b>Selim DÜNDAR</b>	
Improvement of Shear Strength of Zeolite-Bentonite Liner Material under High Temperatures with Tincal and Pumice .....	12457
<b>Sukran Gizem ALPAYDIN, Esra GUNERI, Yeliz YUKSELEN-AKSOY</b>	
Challenges and Benefits of the Use of AASHTOWare for 3 Climatic Regions in Turkey .....	12473
<b>Bevhyan IPEKYUZ, Hediye TUYDES YAMAN, Hande Isik OZTURK</b>	
Investigating the Influence of Dam-Breach Parameters on Dam-Break Connected Flood Hydrograph .....	12501
<b>Mohamed NAJAR, Ali GÜL</b>	
Buckling of Laminated Elliptical and Super-Elliptical Thin Plates .....	12525
<b>Erkin ALTUNSARAY, İsmail BAYER</b>	
Modification in Response of a Bridge Seismically Isolated with Lead Rubber Bearings Exposed to Low Temperature .....	12553
<b>Esengul CAVDAR, Volkan KARUK, Gokhan OZDEMIR</b>	
Comparing Performances of Machine Learning Techniques to Forecast Dispute Resolutions .....	12577
<b>Murat AYHAN, Irem DIKMEN, M. Talat BIRGONUL</b>	
Transit Frequency Optimization in Bi-modal Networks Using Differential Evolution Algorithm .....	12601
<b>Mehmet Metin MUTLU, İlyas Cihan AKSOY, Yalçın ALVER</b>	

Numerical Study on the Deformation Behavior of Geosynthetic-Encased Stone Columns Supporting Embankments .....	12617
<b>Tuncay DOĞAN, Mehmet Rifat KAHYAOĞLU</b>	
Identification and Prioritization of Key Performance Indicators for the Construction Small and Medium Enterprises .....	12635
<b>Ozan OKUDAN, Cenk BUDAYAN, Yusuf ARAYICI</b>	
Hydrological Considerations in Designing Roadways: Avoiding Hydroplaning.....	12663
<b>Sevgi CAVDAR, Ali UYUMAZ</b>	
A Numerical Investigation on the Limitations of Design Equations for Steel Plate Shear Walls.....	12677
<b>Muhammed GÜRBÜZ, İlker KAZAZ</b>	
Evaluation of Occupational Safety in the Operation and Maintenance Activities of Dams .....	12709
<b>Özge AKBOĞA KALE, Ömer Levend AŞIKOĞLU, Selim BARADAN</b>	
<b>TECHNICAL NOTE</b>	
Effect of Blasting During Tunnel Excavation on an Existing Adjacent Tunnel.....	12725
<b>Van Kien DANG, Trong Hung VO</b>	

# Utilising Building Information Models in Facility Maintenance and Operations

Esa HALMETOJA<sup>1</sup>  
Natalija LEPKOVA<sup>2</sup>

## ABSTRACT

Utilising the digital capital of buildings, including building information modelling (BIM), is crucial for building owners from the perspective of high-level maintenance. This case study concerns a company in which building information models are received as files complying with the Industry Foundation Classes (IFC) standard. An analysis of the information content of the IFC files was performed to investigate whether the files, which were generated in a construction project using traditional procedures, contained relevant information for maintenance. The critical needs were evaluated based on the aspects highlighted in an online survey. As a result, essential content requirements for BIM are presented for facility maintenance and operations (FMO). It has been shown that existing building information models cannot close the information gap from a facility maintenance perspective. Still, they have significant potential due to their ability to contain technical information and provide a graphical representation. With information exchange requirements (IEXs), a great deal of progress could be made by utilising BIM for FMO. A property service company's capabilities must also be evolved before the benefits of digital capital can be reaped. This paper provides insights for developing the information content of computerised maintenance management systems (CMMS) and demonstrates the crucial need to harmonise them using BIM. Finally, as a new use case for BIM, this paper presents an operations and maintenance model (OMM).

**Keywords:** Operations and maintenance model, property maintenance, building information models in facility maintenance and operations.

## 1. INTRODUCTION

Facility maintenance and operations (FMO) contains two main task areas: (1) the care and maintenance of building and technical systems (including the repair and replacement of technical systems), and (2) care and maintenance of outdoor areas [1]. In this case study,

---

Note:

- This paper was received on June 5, 2020 and accepted for publication by the Editorial Board on August 13, 2021.
  - Discussions on this paper will be accepted by November 30, 2022.
- <https://doi.org/10.18400/tekderg.748397>

1 Senate Properties, Maintenance Unit, Helsinki, Finland  
[esa.halmetoja@senaatti.fi](mailto:esa.halmetoja@senaatti.fi) - <https://orcid.org/0000-0002-0631-273X>

2 Department of Construction Management and Real Estate, Vilnius Gediminas Technical University, Vilnius, Lithuania - [Natalija.Lepkova@vilniustech.lt](mailto:Natalija.Lepkova@vilniustech.lt) - <https://orcid.org/0000-0002-9760-1747>

FMO is considered to be an activity that continually keeps a building in good shape, uses the building's technology appropriately, optimises energy use, and ensures that occurrences and deviations do not cause damage or become a danger to people, equipment or structures.

In the last twenty years, digitalisation has appeared and big data has emerged, but the operation models of FMO are still old-fashioned and integrations between systems are inadequate. Digitalisation also plays a crucial role in the design of buildings and the management of construction projects. Building information models have been commonplace in significant construction projects [2, 3, 4].

The specific objective of this case study is to investigate whether it is possible to digitalise facility management (FM) by introducing BIM in post-construction and to discover what the crucial requirements are. This study focuses on the practical FMO processes of the principal company, and other use cases are excluded. The primary research questions are:

- Could BIM operate as an information source for FMO?
- What are the crucial requirements for BIM in FMO?

Because the case company's aim is to introduce BIM to post-construction use, as has been presented in the related standards, it is crucial to investigate existing BIM files to validate their usability in FM. It is also essential to define what information must be added to BIM to enable its post-construction use.

## **2. THEORETICAL BACKGROUND**

The term BIM is used to describe a building information model, building modelling, and technology related to building modelling. For the sake of clarity, the explanatory terms modelling, technology or process are used in this paper. BIM is an evolving approach concerning digital information in facilities [5]. Besides the geometry and structures, BIM includes definitions about the building's other elements, such as heat, ventilation and air conditioning (HVAC) equipment, spaces, zones, furniture and specific properties [6]. The National BIM Standard of the United States (2015) describes BIM as a digital presentation of the physical and functional characteristics of a facility that explains how a building is conceived, designed, constructed and operated [7].

Krygiel et al. (2008) noted that BIM allows lifetime information management, promotes sustainable development, and enables optimal service life and environmentally friendly construction [8]. BIM applications have also been used increasingly to support sustainability in the construction industry [9]. At present, BIM technology is widely used in construction projects for building site management, quality, time management and financial control [10,11]. BIM modelling is essentially a software-facilitated process used by architects, engineers and contractors (AEC designers) in the construction industry [12].

According to Azhar et al. (2015), BIM modelling supports the real estate business and the high-level management of the investment process [13]. Typically, as-built BIM is transferred to a client after a construction project for post-construction use. BIM can also generate and maintain the information produced during the whole life cycle of a building project – from design to maintenance – and can be applied to various fields [14, 15].

The strength of BIM modelling is the ability to store, synthesise and visualise both semantic and relational information along with geometric information. The geometric information identifies the location, while relational information contextualises the work order within the building (at the room, system or equipment level), and semantic information contains the key content [16]. A few examples in the related literature are presented in which data transferred from BIM for maintenance are used [11, 17, 18]. For example, Chen et al. (2018) proposed a facility maintenance management framework based on BIM and facility management systems that can provide the automatic scheduling of maintenance work orders in order to enhance good decision-making in facility maintenance management [17]. Because BIM software is not intended for FM functions, priority should be given to finding solutions for transferring semantic data from BIM for use by FM software.

Ustinovičius et al. (2018) presented the conceptual model of BIM-based design and refurbishment [19]. The proposed new approach presented in this model creates a knowledge-based decision-making environment for refurbishment strategies and quality control, thus creating the preconditions to bridge the gap between expected and actual energy performance. Heaton et al. (2019) presented a methodology that enables the extraction of BIM-related data directly from a model into a relational database, for integration with existing asset management systems [20]. The article presented a case study which demonstrates that if BIM is designed from the start with consideration for operations and maintenance requirements, it can be exploited for development into an asset information model.

The Industry Foundation Classes (IFC) standard is an XML-based international ISO/PAS 16739 (2018) construction industry standard for the transfer of object-oriented data from one computer system to another in BIM [21]. It is used to transfer design data between CAD systems and from design software to various analysis and production software. The IFC process only transfers 3D geometry and parameters. An IFC file is thus a kind of tabular description of the contents of BIM.

It is standard practice for AEC designers to adhere to the coverage of plans defined by the subscriber. Therefore, in order to include the information required in the FM, it is essential to define information exchange requirements (ER or IER), as well as principles of data management, shared product libraries, etc. at the contract stage.

The Construction Operations Building Information Exchange (COBie) standard is an international standard relating to managed asset information, including space and equipment. It is closely associated with BIM modelling approaches to the design, construction and management of built assets [22]. COBie is still a relevant standard for delivering standardised data in aid of asset management cost reductions. However, additional rules are required, because COBie does not provide details on what information is to be provided when, and by whom [23].

FM is a form of asset management that is concerned with the successful and profitable maintenance, operation and monitoring of buildings or properties [24]. FM presents an integrated approach to maintaining, improving and adapting an organisation's buildings in order to promote a fertile environment that supports an organisation's primary objectives [25, 26]. FM encompasses the workplace, facility, support services, property, corporate real estate and infrastructure [27].

The ISO 41011:2017 standard defines FM as an organisational function that integrates people, places and processes within the built environment in order to improve the quality of life for people and the productivity of the core business [28]. FM covers two primary areas: space and infrastructure (including planning, programming, design, construction, leasing, occupancy, maintenance, renovating, energy, the environment, waste, workplace design, furniture, moving and cleaning), and people and the organisation (including reception, catering, hospitality, ICT, information technology (IT), office supplies, travel, car parking, accounting and marketing). On a general level, FM thus aims to provide safe, healthy and efficient work environments for clients [29].

ISO 19650:2018 series 1 describes and defines information management across the whole life cycle of an asset [30]. To support this, there needs to be close links with the approaches used for asset and project management, and for organisational management. ISO 19650-1 allows for an inexperienced appointing party to seek assistance with completing its information management activities [31].

BIM-based application initiatives in FM can be found in newly published research papers. By linking the BIM-based structural elements with FM work information, BIM and FM databases can be integrated for easy information accessibility and utilisation. Kim et al. (2018) proposed an approach to effectively manage BIM-based FM information by linking the BIM-based building elements and FM work information in an FM system database [32]. The authors presented a web-based FM information system that semantically links BIM data to relevant historical work records. Chen et al. (2020) developed a specification-compliant FM system based on BIM using the Lingxia tunnel in Wenzhou, China, as a testbed [33]. The application of the system in the mountainous tunnels demonstrates the feasibility and benefits of BIM-based FM related to productivity improvement.

Ustinovičius et al. (2017) noted that BIM modelling allows them to analyse the current situation, solving problems with information management using team-based collaborations and integrated project delivery [19, 54]. Motawa and Almarshad (2013) developed an integrated system to capture information about and knowledge of building maintenance operations when maintenance is carried out and afterwards in order to understand how a building deteriorates, and to support preventive/corrective maintenance decisions [34]. Halmetoja (2019) presented a way to combine the information content of BIM and field data on the same platform to provide real-time information for improving FM operations [35].

Kang and Choi (2015) showed that BIM modelling could enhance the FM process by expediting tasks and reducing time loss [36]. Aziz et al. (2016) underlined that using BIM for FM could lead to a reduction of operational costs; less time spent on decision-making; a better documentation procedure; greater collaboration and more work flexibility [37]. The research by Pishdad-Bozorgi et al. (2018) analysed BIM for FM case studies presented in the literature by different authors from 2010 to 2016 [38]. By using a project example, the authors showed the importance of the implementation of FM-enabled BIM. Gao and Pishdad-Bozorgi (2019) studied academic articles, industry reports and guidelines pertaining to the use of BIM to improve selected facility O&M activities, including maintenance and repair, emergency management, energy management, change/relocation management and security [39]. Content analysis results showed that research on using BIM for O&M is still in the early stages and most of the current research has focused on energy management. Wong et al. (2018) analysed the digitalisation process in facility management. The authors analysed 120



academic journal papers, conference proceedings and other technical notes published on the subject (BIM concept, combined geographic information systems (GIS) and BIM technology, IoT, reality capture technology with photogrammetry and laser scanning tools application for FM) mainly between 2004 and 2017 [40]. Araszkievicz (2017) presented the results of the latest research related to the application of digitisation in facility management based on a literature review from 2010 to 2016. The article investigated the potential application of BIM for data integration for the building life cycle, providing information for facility management and maintenance, as well as FM for smart buildings [41].

Applying BIM for FM requires changes within organisations. Cavka et al. (2017) developed a methodology for understanding owner requirements and identifying BIM-related information [42]. Their method covers a lot of the requirements for BIM-enabled asset management and leads to significant changes in workflows.

According to the literature, many FM applications have adopted BIM technology and provide functions for building maintenance, but knowledge management is not usually offered. For example, lessons learnt from investigations into the causes of failure, or the consequences of selecting a specific method of maintenance, and the ripple effects on other building elements have not been thoroughly researched. The current article describes how to enrich the content of the models so that they can be utilised in FMO. This was not reported in the analysed literature.

### **3. CASE STUDY DESCRIPTION**

The principal company is a sizeable property-owning company that is known as a pioneer and leader in the use of digital tools for FMO. For example, their CMMS has been used for as long as they have existed. The company owns about 9,200 buildings, covering approximately six million square metres and serving nearly 55,000 occupants daily. The company is also a pioneer in utilising BIM in design and construction. Similar material is rarely found in other companies when researching the FMO field. The company uses smart building technologies and aims to introduce a digital twin of each building in everyday use in four years. This study reveals the current state of the digital material and shows how it should be developed to achieve this goal.

As BIM for FM is an entirely new use case, it is not relevant to assume that previous BIM files will comprehensively contain FM information, especially insofar as they differ from the information needed for a construction project. However, it is crucial to investigate whether existing BIM can be utilised in FM or whether they need to be regenerated entirely for this purpose.

In this study, we exploited the task lists and device lists of the CMMS. We were permitted to use the online repository system of the case company. The total number of BIM files amounted to over 10,000, from which 15 buildings with 238 BIM files produced using a computer-aided design (CAD) modelling program were chosen for analysis. These buildings were similar regarding the CMMS and scope of BIM. The target was to explore the compatibility of the CMMS and BIM using traditional analysis tools.

Three types of buildings were involved: *office buildings*, which included standard offices (nine buildings), *education buildings* for schools (three buildings), and *special premises*, including research and laboratory buildings (three buildings).

Besides exploiting the available files, we used an online survey to investigate the availability and quality of crucial information. Further, if a gap in the information needed for property maintenance occurred, we examined whether BIM could close the gap. The accordance of the FMO service provider's and the property owner's values was also assessed, and the ability of the CMMS to support this target was investigated. A web link to the online survey was emailed to 479 janitors, supervisors and property service bidders working in the five largest property service companies in Finland. About 23,000 employees work for these companies in the Finnish property service market. All the respondents had working experience of the principal company's properties.

#### **4. METHODOLOGY**

The current BIM Modelling guidelines were studied, and the FMO needs were observed using relevant literature. Gaps in the current research were detected. The information content of current IFC files were analysed to find out whether they contained useful data for FM. The CMMS device lists and task lists were also explored. The FMO information requirements, quality and availability were examined using an online survey. Finally, the essentials of the research were conceptualised, and conclusions were drawn using qualitative analysis.

##### *The online survey*

The purpose of the online survey was a) to determine the information requirements, qualifications and availability for day-to-day work of the personnel, and b) to map the personnel's BIM know-how. Those issues are crucial to evaluating the current availability of information and considering how to utilise BIM in property maintenance work.

An online survey was selected as a method because it enables remote access to individuals. It can also reach challenging-to-contact participants and can enable automated data collection [43, 44, 45]. Further, the author cannot influence the responder during the survey through their attitudes or behaviour [46].

The questions were compiled with the principal company's maintenance team and tested in advance. The questions are based on CMMS task lists. The questions were designed to be unambiguous so that they were easy to answer regardless of the educational background of the respondents, and did not contain demanding terminology. The questions reflected the general values of the real estate and construction industries and were designed to reveal correlations with the service providers, who provide property services for the case company. The questions about BIM were hypothetical because BIM was not yet in use in the case company. The questionnaire was designed to enable the researchers to develop proposals to introduce BIM for a property owner who already owns a significant number of building information models and who is continually ordering them.

Scores were calculated using the weighted average method, according to ISO Standard ISO 41011:2017 Facility Management – Part 7: Guidelines for Performance Benchmarking [48]. A five-step Likert scale was used, wherein the minimum score was 0 and the maximum rating

was 5 [49]. The same score was used multiple times. Every question had the option for a textual comment.

### *The empirical analysis of BIM and CMMS*

Empirical research methods are usually associated with inductive approaches, which are based on empirical evidence [47,50]. According to Ghauri et al. (2002), “The research design is the overall plan for connecting the conceptual research problems to pertinent (and achievable) empirical research.” [51] The purpose of empirical research is to obtain research results by making actual observations of the subject and analysing and measuring them. In empirical research, concrete and aggregated research material serves as the starting point for research [52].

In the empirical analysis, the information content of the BIM files was explored, and an analysis of the device lists and task lists of the CMMS was made. The online survey answers were utilised in order to specify the content analysis of the building information models. The tool used was Microsoft Excel®, and the data was collected manually by using the Solibri model checker (SMC).

We decided to examine the current IFC files instead of the original CAD files for better readability. IFC files are compatible with all standard analytics applications, and a licence for the initial modelling application is not needed. Thus, differences in the models caused by the design software can be excluded. The same applies to the architectural models, structural models, and mechanical, electrical and plumbing (MEP) models [53]. The IFC format is the most practical when utilising the information content of BIM for external use. The central idea was to investigate the usability of the content of existing IFC files. The conclusions take into account that when creating these files, the subscriber had not submitted any content requirements for the information required in the FM.

Fifteen buildings were chosen for the comparison process. The criteria for selecting buildings for the study were:

- the model should cover the entire property
- MEP models should exist
- the models should cover the same area as the device list of the CMMS

The content of the architectural model was based on the authors’ view of the required information, which was evaluated according to the results of the online survey and reviewed by FM-related professionals. The following issues were examined in order to determine whether or not there was data on them:

- a. The total area and volume of a building
- b. The borders (spatial separations) of users in the multi-user buildings
- c. Architectural space objects
- d. Emergency exits and hauling routes
- e. Care and maintenance instructions
- f. The technical details of structures and surfaces

The verification of the content of the MEP model was based on CMMS task lists and made in the online survey. The following issues were examined in order to determine whether they exist or not:

- a. Pipes, ducts and cable ladders
- b. Equipment to maintain and/or indicate alarms (compared to the CMMS device list)
- c. The technical details of the HVAC equipment (including capacities and set-points)
- d. Fire and automatic air volume control dampers, and shut-off and automatic valves (compared to the CMMS device list)
- e. The operation areas of the HVAC systems

The buildings were categorised by their use/purpose (office/education/special premises), and their gross floor area (GFA) and gross volume (GV) were described. The date of the IFC file was also recorded.

## **5. RESULTS**

### *Online survey*

In the online survey, a total of 479 people were contacted, and 161 replies were received (33.6% reply rate). The majority of the respondents were men (96%), and the majority were aged 31–40 (58%). Eighteen per cent were under 30 years of age, and 12% were over 60 years of age. A total of 44% had more than 20 years of work experience. The next largest group had 11–15 years of work experience (23%), followed by 6–10 years (20%) and 16–20 years (18%). About 12% had less than five years of work experience. The distribution of occupations among the respondents was as follows: 55% were janitors or mechanics; 13% were foremen or managers; 15% were technical managers or supervisors; 4% were directors or chief officers; 3% were bidders or controllers; and 2% were the space user's representatives. The remaining 9% were mostly service managers and system specialists. The statistical review is presented in Table 1.

In the first question, we asked about the significance of the features of a building in general. The principal company is aiming to improve the efficiency of the space users' work and hopes to manage life cycle costs by implementing technically advanced (smart) buildings. Other essential features are safety and security, energy efficiency, healthiness, value retainability and a good user experience. Additionally, the ease of care and maintenance and the economic viability for the service company are important when pursuing good maintainability.

Figure 1 presents the results of the first question. According to the responses, healthiness was the most highly valued feature (4.86/5), followed by safety and security (4.86/5), and then by the building's ability to retain its value (4.63/5). The fourth most valued feature was the provision of a good user experience (4.54/5); and energy efficiency was only fifth (4.46/5). The ease of maintenance (4.30/5) and economic viability for the service company (4.04/5) were the sixth and seventh most valued features. The technical intelligence of the building was the least valued feature (3.67/5).

Table 1 - Distribution of respondents according to different features.

Distribution of respondents	Description
Distribution of respondents to professions	Janitors or mechanics (58%); various supervisors and managers (28.8 %). The smallest respondent group is managers working for space user organisations (2.6 %).
Distribution of respondents to education	Most of the responders have completed vocational education (51.3%). The next most relevant group has engineering-level education (34.0%). The smallest groups of respondents are university graduates (3.5%) and those without any professional education (1.7%).
Distribution of age of respondents	The largest group is 31–40 years old (58%). The next largest groups are 41–50 (23.5%) and 51–60 years old (22.6%).
Distribution of work experience of respondents	Most of the respondents had over 21 years of work experience (30.4%). The next largest group had 11–15 years of work experience (23.5%). The smallest group had 0–5 years of work experience (9.6%).

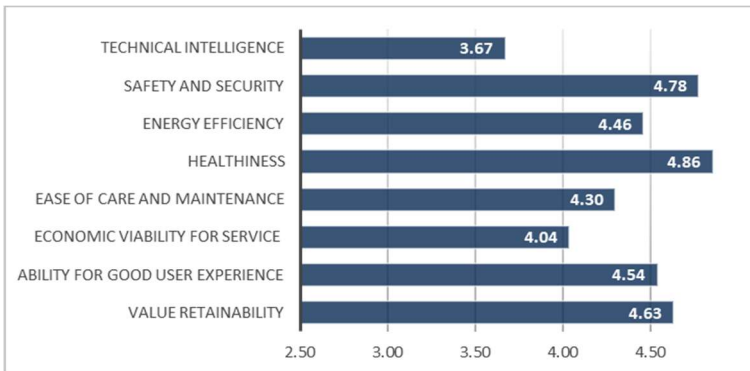


Figure 1 - Valuations of the features of a building in general.

In the second question, the respondents were asked to rank the ten most frequent property maintenance and service tasks (see Figure 2). Fault repairs emerged as the most important function (4.74/5) but receiving and managing alarms was almost equal (4.73/5). The third most important function was receiving and managing customer SRs (4.57/5), general care was fourth (4.50/5) and indoor conditions management was fifth (4.46/5). The sixth most important function was user satisfaction management (4.41/5). Respondents also found that calendar-based maintenance tasks (4.24/5), outdoor work (4.23/5) and controlling service and maintenance (4.23/5) had some importance. Energy use management and reporting (4.15/5) were considered the least important items.

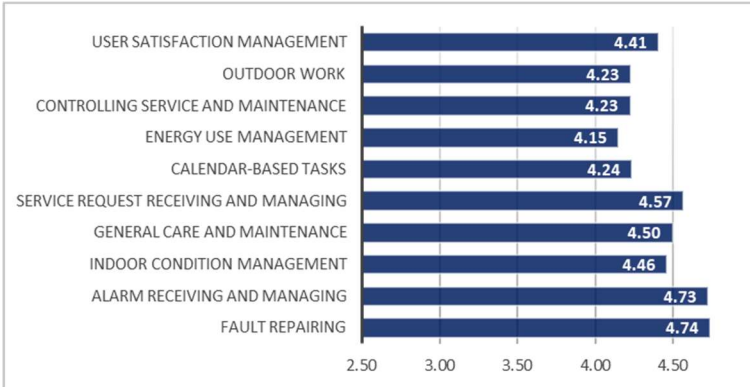


Figure 2 - Importance of property service tasks

Next we asked about the availability of the information required for the same maintenance and service tasks as used previously. Figure 3 presents the results of the third question. The best availability was for receiving and managing customer SRs (4.19/5), followed by calendar-based maintenance tasks (4.11/5) and receiving and managing alarms (4.10/5). The fourth best availability was for energy use and management (4.00/5) and the fifth was for controlling service and maintenance (3.89/5). Almost equal were outdoor work (3.87/5) and general care and maintenance (3.86/5). The availability of information on fault repairing was the third poorest (3.81/5). The weakest availability was for indoor conditions management (3.78/5) and user satisfaction management (3.75/5).

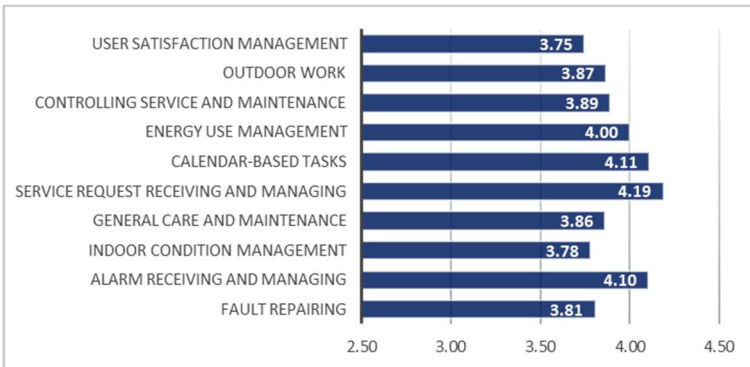


Figure 3 - Availability of information for certain service tasks.

About half of the respondents (45.7%) considered the availability of information to generally be good. Nearly one fifth (21.7%) found that information availability was very good, and about one fifth (19.1%) considered it acceptable. Only 3.1% thought that it was poor, and 1.0% considered it very poor.

The fourth question was related to sources of information concerning day-to-day tasks and running the building given by various people or from a variety of sources. The respondents were asked to rank the importance of the information sources related to their own task areas (see Figure 4). The CMMS was reported to be the most important source of information (4.29/5). The second most important information source was the owner’s customer SR management system (4.27/5), and the next two highest were colleagues or the support centre and the internet (both 4.14/5). The property manager ranked fifth (4.07/5), paper documents sixth (3.91/5) and the energy management system (EMS) seventh (3.89/5). The importance of the property service company’s IT system was estimated to be small (3.25/5). The owner’s online repository was considered to be the least relevant source of information (3.05/5).

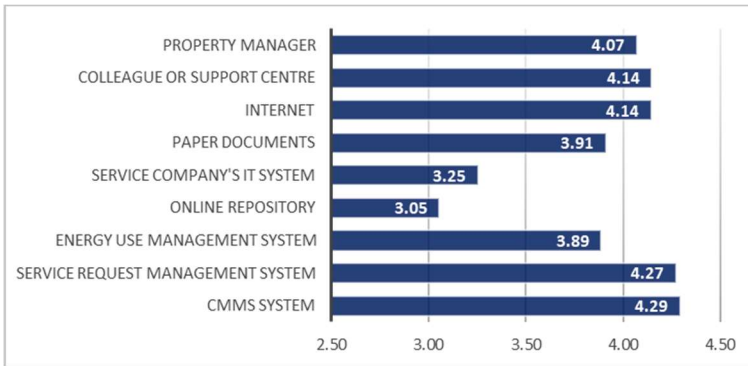


Figure 4 - Meaning on information sources

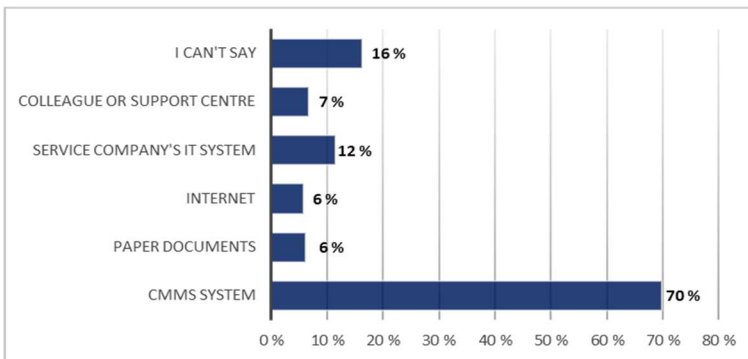


Figure 5 - First-used information sources.

Next, the first-used source of information was mapped when the respondents searched for information on the most essential tasks (see Figure 5). The CMMS was the most commonly used source of information, as 70% of respondents chose it as their first source. The property service company’s IT system was the second most commonly used source (12%) and a colleague or the service company’s support centre came in third (7%). Using the internet and

paper documents as sources were seen as a last resort (both sources being chosen by 6%). Unlike the other questions, the share of the 'I can't say' answers was significant (16%).

Then the respondents were asked about their experience of using BIM over the last two years. The results reveal that 74% of respondents had not used BIM over the last two years. Only 2.49% had used BIM regularly (see Figure 6).

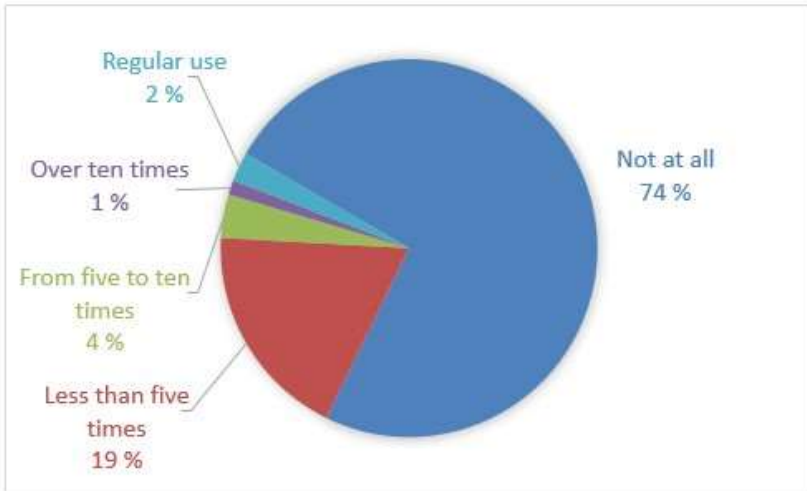


Figure 6 - BIM use over the last two years.

Figure 7 presents the most usual current reason for BIM use. BIM was mostly used for the planning of service and maintenance actions because 37.2% of the respondents used them for that purpose. The next most common use was identifying HVAC system operating areas (32.6%) and controlling service and maintenance operations (30.2%). The two lowest-ranked uses were using BIM to check care categories and design staff resources (both accounting for 2.3%). Only those who had experience of using BIM (10% of all respondents) answered this question.

The next question concerned the importance of BIM features (see Figure 8). Showing the operation areas of HVAC systems was the most important feature (4.30/5). Showing pipes, ducts and cable ladders (4.20/5) and showing dampers and shut-off valves (4.19/5) were next. Showing equipment to maintain was fourth (4.11/5), while showing technical details of equipment and showing the service and maintenance instructions (4.06/5) were fifth and sixth, respectively. The monitoring of emergency and hauling routes was ranked seventh (3.93/5), and identifying users' spaces came eighth (3.77/5). Showing the areas and volumes of the building was seen as the least important feature (3.49/5). Lastly, we asked about the importance of BIM for specific maintenance tasks. Figure 9 presents the results of this question. BIM was seen to be the most important for fault repairs (4.06/5). The next highest importance was given to indoor conditions management (4.04/5). The next two most important items were receiving and managing customer SRs and receiving and managing alarms (both scoring 4.03/5). The fifth was general care and maintenance (3.91/5), and the



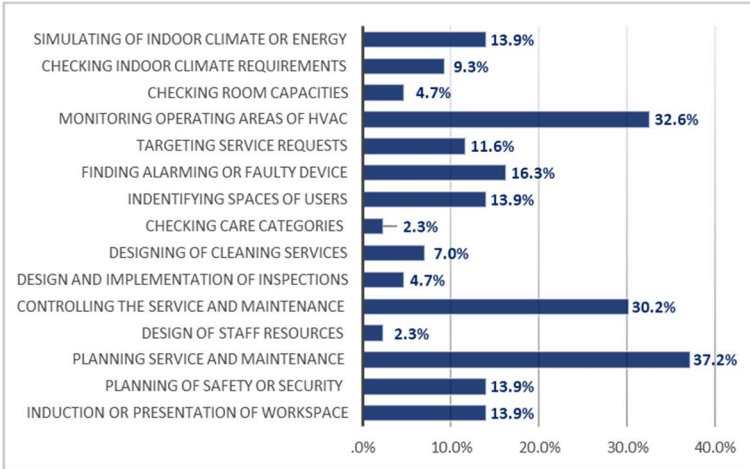


Figure 7 - Current BIM use purposes.

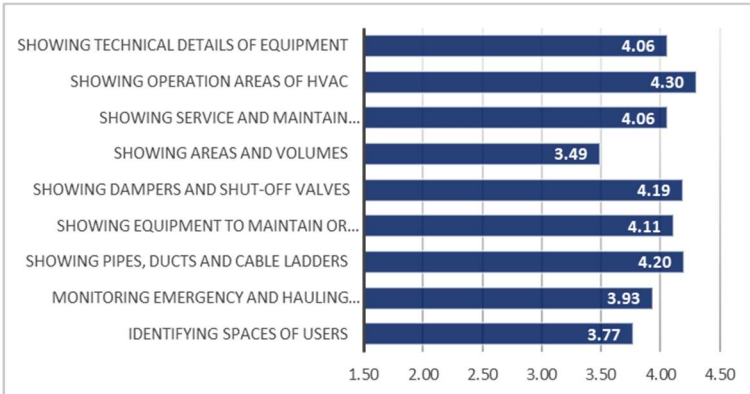


Figure 8 - Importance of BIM features.

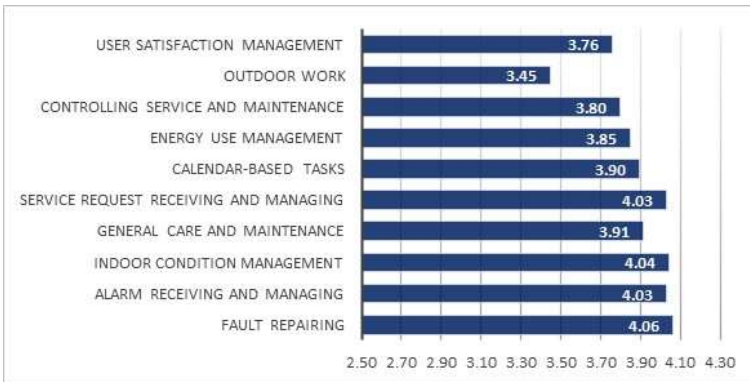


Figure 9 - The importance of BIM features for certain tasks.

sixth was for calendar-based tasks (3.90/5). The seventh most important use was for energy use management (3.85/5). Controlling service and maintenance activities was the eighth most important use (3.80/5), and user satisfaction management was ninth (3.76/5). The least significant was seen to be outdoor work (3.45/5).

*The textual comments*

The textual comments revealed that the current availability and level of information were insufficient for everyday FMO work. For example, the respondents said that more information was needed about materials, such as information about their surfaces. They also reported that tacit information is often lost, and the history of previous repairs is not available. It is known that the current systems enable history recording but, according to the comments, the feature is not widely used. The respondents also wanted more detailed customer feedback. They considered the building automation system as an important source of information, especially in exploring the history of indoor conditions.

Most of the respondents were not familiar with BIM. Therefore, many of the comments were irrelevant. For example, the most desired feature for BIM was the real-time monitoring of indoor conditions.

The respondents reminded us that the most important FMO task is to ensure the continuity of the user's actions in good conditions, without hampering the service work. They also emphasised that property maintenance was all too often criticised based on external factors, such as lawns or plants on the property, when the main emphasis of the work is on matters that remain unseen, such as indoor conditions.

In the comments, the role of a remote control room was considered significant. For example, the respondents said that the responsibility for the control of energy consumption had been transferred to remote control room specialists from the local service staff.

*The analysis of IFC files and the CMMS*

The purpose of comparing the content of the IFC files and the CMMS was to explore whether they included the same components and if the components were recognisable. According to the device lists of the CMMS, the most commonly maintained devices were control and automatic valves, fire dampers, automatic airflow control dampers, fans, pumps, replaceable filters, expansion vessels and different controllable tanks. A comparison was made on a per-building basis.

Table 2 indicates that the CMMS contains only one of the two automatic and control valves from the IFC files. Similarly, the CMMS only includes one third of the fire dampers and automatic airflow dampers. In turn, only 16% of the listed fans and 28% of the pumps of the CMMS were found in the IFC files. Only 12% of the replaceable filters and 52% of the expansion vessels and controllable tanks were presented in the IFC files.

The areas and volumes of the building were defined in 53% of the studied buildings. This issue is not very important for service staff in their daily work, but it is crucial when using BIM as base data for other systems. For example, calculations on energy consumption, effective space use and rentals, as well as many simulations, require this sort of data.

Data on the spatial separation of the users was missing from all BIM files. In this context, this refers to the interfaces between different tenant-managed spaces in multi-user buildings

and spaces rented to outsiders, in addition to owner-managed areas. The information about user organisations may not necessarily be available at the planning stage. However, the borderlines are essential to the service provider. The maintenance tasks can be different with different occupants, and emergency escapes may not be possible through other organisations' spaces.

*Table 2 - Comparison of contents of CMMS and IFC file*

<b>Control and automatic valves</b>	824	1,538
<b>Fire and automatic dampers</b>	665	2,273
<b>Fans (incl. integrated)</b>	1,205	197
<b>Pumps</b>	497	141
<b>Replaceable filters</b>	476	55
<b>Expansion vessels and tanks</b>	109	57
<b>Total</b>	3,776	4,261

Architectural space objects, which usually represents a cubicle accompanying the walls of a room, were defined in 53% of the studied buildings. Space objects are needed when a device (e.g. a ventilation machine) is to be connected to a particular room. Additionally, space objects are required when visualising the conditions in the external UI. Lacking space objects in an IFC file is mainly due to defective definition in an IFC exporter. Many IFC exporters and importers are defective and limited, and require special care in their use.

The exits and hauling routes were also presented adequately in 53% of the studied buildings. In the other buildings, the information must be collected manually. This matters when planning an emergency exit as premises change and when heavy or large equipment needs to be moved.

None of the care and maintenance instructions were included or linked to any IFC files. This leads to the need to manually search for the information in other systems. In the studied portfolio, the task was complicated because the devices were described differently in BIM and the CMMS. Often, even the names were not the same.

The technical details of structures were presented in 67% of the studied buildings. This information is relevant to property maintenance when there is a need to replace or repair a damaged construction product. The information facilitates the selection of a replacement product and helps to evaluate repair methods.

Pipes, ducts and cable ladders were presented comprehensively. Service staff can use location and size information to plan repairs and to locate faulty components.

The equipment requiring maintenance according to the CMMS task list was only presented adequately in one building. The question is not always one of missing information; often it was that things were presented differently. For example, the MEP designer may use a packed object in an IFC file, while the CMMS author may unpack it as components that are to be

maintained. Respectively, a CMMS author may state that only the main item of equipment is to be maintained while the designer creates all the components in an IFC file. In some buildings, only the mandatory information for creating an object was given, and all other fields were left blank. Also, building service technology equipment was often only defined as space reservation, and the design discipline was assigned as *architectural*.

The technical details of the building’s technology devices were created in 93% of the studied buildings. Although comparability with the CMMS assignments was poor, the designers had provided a lot of technical information. That information is relevant to property service staff when replacing a damaged device with a new one.

Dampers and shut-off valves were presented in 87% of the studied buildings. This information is needed by property service staff when seeking a reason for a problem with indoor conditions or when a broken pipe or another reason for a water leak threatens to damage the building. The information is also useful when replacing or repairing a damaged component.

No HVAC operation areas were presented for any buildings. This information is needed by property service staff when seeking a reason for a problem with indoor conditions. It also facilitates planning changes to spaces when the capacity and operation area of a ventilation or air-cooling machine is seen from BIM.

Table 3 - Usable BIM features in most crucial FMO tasks.

<b>BIM features</b>	<b>FMO tasks (see the list below)</b>	<b>A</b>	<b>B</b>	<b>C</b>	<b>D</b>	<b>E</b>	<b>F</b>	<b>G</b>	<b>H</b>
<b>Pipes, ducts, and cable ladders</b>		x	x						
<b>Care and maintenance instructions</b>		x	x		x		x	x	
<b>Equipment to maintain or alarm</b>		x	x		x		x	x	x
<b>Technical details of equipment and structures</b>		x	x		x	x		x	x
<b>Fire and automatic dampers, shut-off valves</b>		x	x		x	x		x	x
<b>Operation areas for building services</b>		x	x	x		x			x
<b>User spaces and common areas</b>		x		x		x			
<b>Emergency exits and hauling routes</b>		x		x					
<b>Areas and volumes</b>		x							

The numbers of FMO tasks:

- A. General care and maintenance
- B. Fault repair
- C. User satisfaction
- D. Calendar-based tasks
- E. Service request managing
- F. Outdoor care
- G. Alarm receiving and managing
- H. Energy management

Table 3 shows which features of BIM are needed for specific FMO tasks. Table 3 only presents the priority needs and does not cover all the particular cases. It can be seen that general care and maintenance can take advantage of all the features. Fault repair operations may benefit from the top six features, which are comprised of technical data and information on the operation areas. The calendar-based tasks and receiving and managing alarms mostly require technical details and instructions, and user satisfaction management and maintenance control require information about the spaces in the building. Outdoor care would benefit from care and maintenance instructions and information on the devices that need to be maintained. The receiving and managing of service requests can take advantage of technical details and information about different areas of the building. Energy management could reap benefits from technical details and information about the operating areas of building service systems.

In summary, the visual appearance of BIM can be utilised in almost all use cases. For example, equipment that needs to be maintained or for which alarms need to be installed or monitored, the technical details of equipment and structures, fire and automatic air volume control dampers, and shut-off valves should always be presented. Only rare-use cases utilise areas and volumes, as well as information on pipes, ducts and cable ladders.

## 6. DISCUSSION

### *Previous research*

Previous research has focused on using BIM-based visualisations on construction sites, for purposes such as construction safety planning and training [55] and production planning [56], as well as design review sessions [57, 58, 59]. Additionally, BIM has previously been studied from the perspective of FM, and pilot projects have successfully integrated BIM with a CMMS. However, previous investigations have primarily concentrated on investigating IT using certain software and IT solutions. Instead, we studied use cases and preparedness for using BIM's visual features in FMO.

Previous efforts have not provided information on how the content of BIM, created in a practical construction project, meets the requirements of real-life service and maintenance. In this case study, we present the elaborated content for the introduction of BIM for FMO.

This investigation confirms previous findings that there is a need to expand BIM beyond the design and construction phases and to consider using it for facility maintenance activities. To benefit, the design for maintenance should be considered in the early design phase [60,61]. Previously, it has also been found that specific information requirements for building information models to support FM systems are needed [62]. The study also confirms an earlier finding that facility managers can benefit from the advantages of BIM to enhance managing the significant amount of information [63].

### *Key findings on FMO tasks*

The results reveal that the service personnel found reactive tasks, such as fault repairing and receiving alarms, as the most important tasks. Proactive tasks are often seen to be useless routines. The values of the service personnel do not necessarily coincide with the values of the building owner. For example, the technical intelligence of a building was the least-valued feature, yet it is highly rated by the principal company. It can be concluded that the weak

appreciation of proactive tasks correlates with the weak appreciation of the technical intelligence of a building.

Also, it was indicated that outdoor tasks are not adequately described in the CMMS. Because up to 52% of on-site time is used in outdoor activities [64], half of the maintenance work is carried out using incomplete instructions or general knowledge. According to the comments, the most experienced service staff primarily do their jobs without any IT systems. IT systems were only used when it was not possible to resolve the problem otherwise.

In contrast to preconceptions, energy management was a poorly appreciated task. The result seems to contradict the principal company's environmental objectives, which are highlighted in its *Corporate Social Responsibility Report*. The result is a consequence of the fact that the importance of energy management has declined in public debate. Respectively, the importance of indoor conditions and health of the building has increased. The significance of on-site energy management has also decreased because large service providers have shifted the primary responsibility for that to remote control rooms.

*The availability of information in daily tasks*

The results reveal that the availability of information is deficient in several FMO tasks. This is primarily due to the insufficient content of the CMMS. Figure 10 shows that the gap is the most extensive concerning fault repairs. The next most substantial gap is for the items receiving and managing alarms, indoor condition management, user satisfaction management and general care. The gap is only at an acceptable level for calendar tasks and energy management.

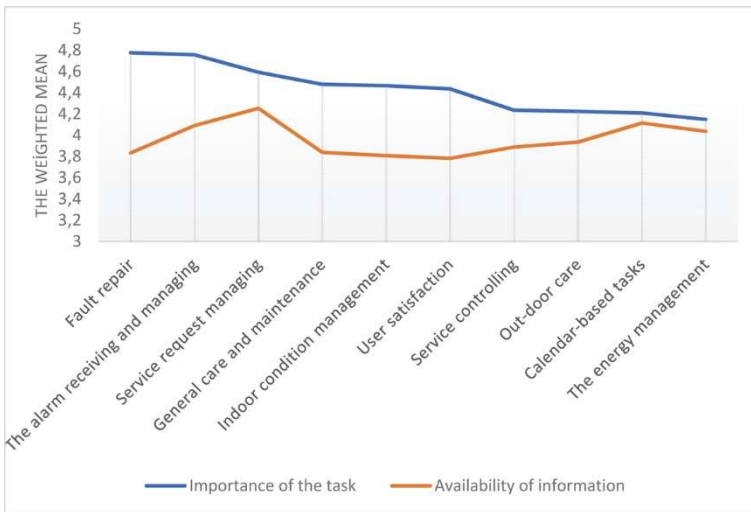


Figure 10 - The availability of information in relation to the importance of the task.

The traditional FM management systems, such as CMMSs, were seen by the respondents in this study as primary sources of information. Also, communication with other professionals was considered essential. A contradiction to this was found when asking respondents to

evaluate the use of the internet as a source of information. The internet was seen to be the third most meaningful source of obtaining semantic information, but it was a last resort when we asked about the order of importance of information sources. This indicates that the information content of official sources that support the task were not considered adequate. It also shows that the information was deemed to eventually be found on the internet if it cannot be found elsewhere.

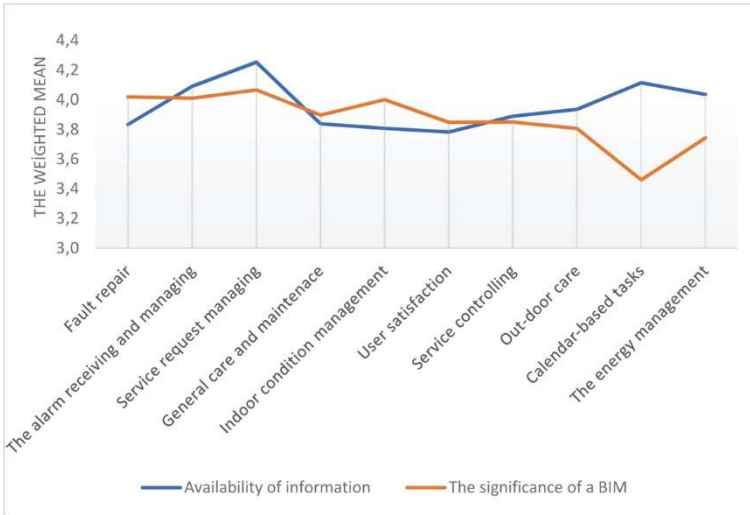


Figure 11 - The availability of information in relation to the significance of BIM.

The chart in Figure 11 shows the significance of BIM (orange polyline) and the availability of information (blue polyline) in the same diagram. The significance of BIM is evaluated to be higher than the availability of information for four tasks: (a) fault repairs, (b) general care, (c) indoor management and (d) user satisfaction management. That means that respondents expect the BIM to improve the availability of information specifically for these tasks.

Most of the service personnel are interested in BIM and are eager to use it in their daily work. However, at this time, BIM is little known. Three crucial reasons for this are: current BIM files do not contain the required information; BIM files are not available to the service personnel; and the property service company does not have the required visualisation tools. Additionally, BIM is often considered to be complicated among service staff.

The primary research question was successfully answered by presenting a new use case for BIM: an operations and maintenance model (OMM). The OMM is based on an as-built BIM, created and updated by the construction project planning team and enriched by maintenance professionals.

Figure 12 presents a flow chart for creating an OMM. The left side of the chart shows the construction stakeholders, and the right side shows the post-construction stakeholders. In the middle of the chart, BIM's lifespan is shown, starting with the design stage. The OMM is based on the as-built model, enriching it with additional information needed for maintenance.

The recommended content of the OMM is presented in Annexe 1. The use cases of the owner, the workplace’s service provider and the space users are given in Annexe 2.

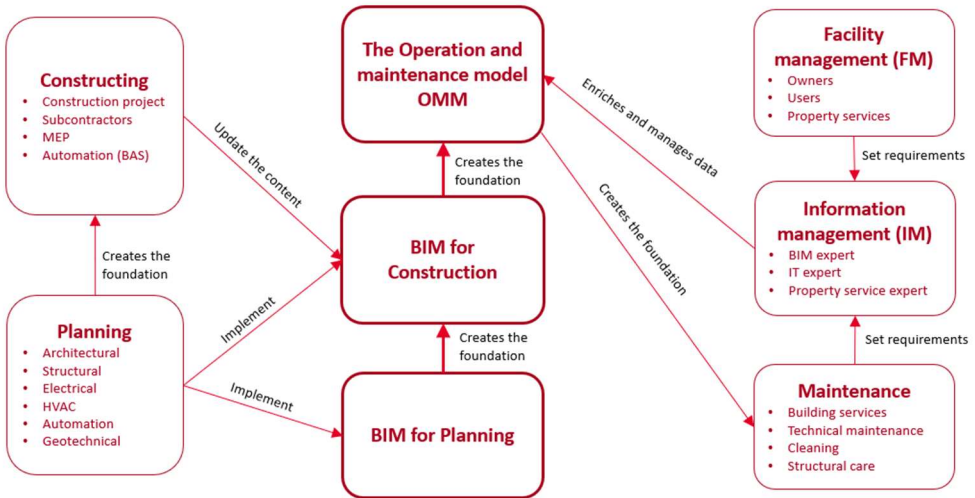


*Figure 12 - The evolution of BIM*

## 7. CONCLUSIONS

Existing building information models cannot close the information gap for property maintenance as such, but they have significant potential. Most devices and components are named in an informal way, which hampers their recognition and discovery. CMMS maintenance tasks are difficult to connect to devices. Ducts, pipes and cable trays are mainly well displayed, but the operation areas of HVAC systems are not usually shown. The technical detail coverage for devices also varies greatly.

The results show that graphical presentation is the greatest strength of BIM. The service personnel require detailed information on the operational areas of the building service systems and the devices they need to maintain. Additionally, devices that can affect indoor conditions must be shown, as well as the components that must be detected in fault correction cases; and general information on different routes and detailed information about spaces are required.

The results of the empirical research show that the required content is incomplete or missing, despite long-used design methods, advanced tools and detailed instructions. One of the most serious deficiencies is the lack of a connection between BIM and CMMS. Changing the situation requires a complete renewal of the design process.

Based on results, it is possible to create IER guidelines for the principal company, as well as for the entire real estate industry. In creating IER, ISO 19650 and COBie standards must also be followed. After introducing the IER and using the right design tools, a significant leap could be taken in the exploitation of digital data in FM. Additionally, maintenance experts must be assigned to the project at an early stage in order to determine how the building will



be maintained. This will ensure sufficient information content in the OMM and the easy maintenance of technical systems and structures.

The principal company's drive to adopt smart buildings and promote the introduction of a digital twin of buildings requires the BIM process to be reformed. The current as-built material as such is not sufficient – it needs to be significantly developed. The property service company's capabilities must also be evolved before the benefits of digital capital can be reaped.

### References

- [1] COBIM2012, *Common BIM Requirements of Finland Series 12 Use of models in facility management*, Rakennustieto Oy, Finland, p. 5.
- [2] Xin, Q. (2011), "Building information modelling (BIM) adoption of construction project management based on Hubei Jinzhou bus terminal case", in 2011 International Conference on Business Computing and Global Informatization, pp. 282-284.
- [3] Han, N., Yue, Z.F. and Lu, Y.F. (2012), "Collision detection of building facility pipes and ducts based on BIM technology", *Advanced Material Research*, Vol. 346, pp. 312-317.
- [4] Wang, Y., Wang, X., Wang, J., Yung, P. and Jun, G. (2013), "Engagement of facilities management in design stage through BIM: Framework and a case study", *Advances in Civil Engineering*, Vol. 8.
- [5] Hardin, B. and McCool, D. (2015), *BIM and Construction Management, Proven Tools, Methods, and Workflows*, Wiley Publishing, IN, US, p. 12.
- [6] Kensek, K. (2015), "BIM guidelines inform facilities management databases: A case study over time", *School of Architecture, University of Southern California, LA, US*, p. 904.
- [7] National BIM Standard-United States NBIMS-US™ (2015), *National Institute of Building Sciences, 1090 Vermont Avenue, NW, Suite 700 Washington, DC US*, p. 1.
- [8] Krygiel, E. and Nies, B. (2008), *Green BIM: Successful Sustainable Design with Building Information Modelling*, John Wiley & Sons, US, p. 26.
- [9] Gurgun, A., Koc, K., Atabay, S. (2021). Impacts of Using Building Information Modeling (BIM) in Sustainable Green Building Projects (in Turkish). *Teknik Dergi*. 33. <https://doi.org/10.18400/tekderg.715574>
- [10] Li Juan, C. and Hanbin, L. (2014), "A BIM-based construction quality management model and its applications", *School of Civil Engineering & Mechanics, Huazhong University of Science & Technology, Wuhan 430074, China*, p. 1.
- [11] Eastman, C., Teicholz, P., Sacks, R. and Liston, K. (2011), *BIM Handbook: A Guide to Building Information Modelling for Owners, Managers, Designers, Engineers and Contractors*, second ed., Wiley US, p. 1.

- [12] Fountain, J, and Langar, S, (2018), “Building information modelling (BIM) outsourcing among general contractors”, *Automation in Construction*, Vol. 95, pp. 107-117.
- [13] Azhar, S., Khalfan, M. and Maqsood, T. (2015), “Building information modelling (BIM): Now and beyond”, *Australasian Journal of Construction Economics and Building*, Vol. 12 No. 4, pp. 15-28.
- [14] Yoon, S., Park, N. and Choi J. (2009), “A BIM-based design method for energy-efficient building”, in *Proceedings of the 2009 Fifth International Joint Conference*, pp. 376-381.
- [15] Pittard, S. and Sell, P. (2016), *BIM and Quantity Surveying*, Routledge, ISBN: 978-0-415-87042-9
- [16] McArthur, J.J., Shahbazi, N., Fok, R., Raghubar, C., Bortoluzzi, B. and An, A. (2018), “Machine learning and BIM visualization for maintenance issue classification and enhanced data collection”, *Advanced Engineering Informatics*, Vol. 38., pp. 101-112.
- [17] Chen, W., Chen, K., Cheng, J.C.P., Wang, Q. and Gan, V.J.L. (2018), “BIM-based framework for automatic scheduling of facility maintenance work orders”, *Automation in Construction*, Vol. 91, pp. 15-30.
- [18] Pärn E.A., Edwards D.J. and Sing, M.C.P. (2017), “The building information modelling trajectory in facilities management: A review”, *Automation in Construction*, Vol. 75, pp. 45-55.
- [19] Ustinovičius, L., Popov, V., Čepurnaitė, J., Vilutienė, T., Samofalov, M. and Miedziąłowski, C. (2018), “BIM-based process management model for building design and refurbishment”, *Archives of Civil and Mechanical Engineering*, Vol. 18 No. 4, pp. 1136-1149. <https://doi.org/10.1016/j.acme.2018.02.004>
- [20] Heaton, J., Parlikad, A.K. and Schooling, J. (2019), “Design and development of BIM models to support operations and maintenance”, *Computers in Industry*, Vol. 111, pp. 172-186. <https://doi.org/10.1016/j.compind.2019.08.001>
- [21] ISO 16739:2013 Industry Foundation Classes (IFC) for data sharing in the construction and facility management industries. ISO International Organization for Standardization, 2013.
- [22] East, W. (2009) BIM Enables Success on WTC Mega Project. *Journal of Building Information Modeling*, Fall 2009, pp. 18-20.
- [23] East, W., Carrasquillo-Mangual, M. (2013) The COBie Guide: A commentary to the NBIMS-US COBie standard. [https://www.bimpedia.eu/static/nodes/1010/COBie\\_Guide\\_-\\_Public\\_Release\\_3.pdf](https://www.bimpedia.eu/static/nodes/1010/COBie_Guide_-_Public_Release_3.pdf)
- [24] Alexander, K. (2013), *Facilities Management: Theory and Practice*, Routledge, New York.
- [25] Atkin, B. and Brooks, A. (2009), *Total Facilities Management*, third ed., Wiley and Blackwell, Hong Kong.
- [26] Barrett, P. and Baldry, D. (2009), *Facilities Management: Towards Best Practice*, Blackwell Science, Oxford, USA.

- [27] Lepkova, N. and Uselis, R. (2013), “Development of a quality criteria system for facilities management services in Lithuania”, in 11th International Conference on Modern Building Materials, Structures and Techniques, MBMST, p. 2.
- [28] ISO Standard ISO 41011:2017 Facility Management – Part 1: Terms and definitions
- [29] GSA (2011) BIM Guide for Facility Management, U.S. General Services Administration, the National 3D-4D-BIM Program, [Cited 2018, 30.1.2018] Available at: <https://www.gsa.gov/real-estate/design-construction/3d4d-building-information-modeling>
- [30] ISO 19650-1:2018 Organization and digitization of information about buildings and civil engineering works, including building information modelling (BIM) — Information management using building information modelling — Part 1: Concepts and principles.
- [31] UK BIM Alliance (2019). Information management according to BS EN ISO 19650. Guidance Part 1: Concepts.
- [32] Kim, K., Kim, H., Kim, W., Kim, C., Kim, J., Yu, Y. (2018). “Integration of IFC objects and facility management work information using Semantic Web”, *Automation in Construction*, Vol. 87, pp. 173-187.
- [33] Chen, L., Shi, P., Tang, Q., Liu, W., Wu, Q. (2020). “Development and application of a specification-compliant highway tunnel facility management system based on BIM”, *Tunnelling and Underground Space Technology*, Vol. 97, pp. 103262.
- [34] Motawa, I. and Almarshad, A. (2013), “A knowledge-based BIM system for building maintenance”, *Automation in Construction*, Vol. 29, pp. 173-182.
- [35] Halmetoja, E. (2019), “The conditions data model supporting building information models in facility management”, *Facilities*, <https://doi.org/10.1108/F-11-2017-0112>
- [36] Kang, T.-W. and Choi, H.-S. (2015), “BIM perspective definition metadata for interworking facility management data”, *Advanced Engineering Informatics*, Vol. 29, pp. 958-970.
- [37] Aziz, N.D., Nawawi, A.H. and Ariff, N.R.M. (2016), “Building information modelling (BIM) in facilities management: Opportunities to be considered by facility managers”, *Procedia – Social and Behavioural Sciences*, Vol. 234, pp. 353362.
- [38] Pishdad-Bozorgi, P., Gao, X., Eastman, C. and Self, A.P. (2018), “Planning and developing facility management-enabled building information model (FM-enabled BIM)”, *Automation in Construction*, Vol. 87, pp. 22-38.
- [39] Gao, X. and Pishdad-Bozorgi, P. (2019), “BIM-enabled facilities operation and maintenance: A review”, *Advanced Engineering Informatics*, Vol. 39, pp. 227-247. <https://doi.org/10.1016/j.aei.2019.01.005>
- [40] Wong, J. K. W., Ge, J., & He, S. X. (2018). Digitisation in facilities management: A literature review and future research directions. *Automation in Construction*, Vol. 92, pp. 312-326.

- [41] Araszkiwicz, K. (2017). Digital technologies in Facility Management—the state of practice and research challenges. *Procedia Engineering*, 196, 1034-1042.
- [42] Cavka, H.B., Staub-French, S. and Poirier, E.A. (2017), “Developing owner information requirements for BIM-enabled project delivery and asset management”, *Automation in Construction*, Vol. 83, pp. 169-183.
- [43] Wright, K.B. (2005), “Researching internet-based populations: Advantages and disadvantages of online survey research, online questionnaire authoring software packages, and web survey services”, *Journal of Computer-Mediated Communication*, Vol. 10 No. 3, available at: <https://academic.oup.com/jcmc/article/10/3/JCMC1034/4614509> (accessed 18 Jan 2020).
- [44] Garton, L., Haythornthwaite, C. and Wellman, B. (1999), “Studying on-line social networks”, in Jones, S. (Ed.), *Doing Internet Research: Critical Issues and Methods for Examining the Net*, Sage, Thousand Oaks, CA., pp. 75-105.
- [45] Wellman, B. (1997), “An electronic group is virtually a social network”, in Kiesler, S. (Ed.), *Culture of the Internet*, Lawrence Erlbaum, Mahwah, NJ. pp. 179-205.
- [46] Hirsijärvi, S., Remes, P. and Sajavaara, P. (2010), *Tutki ja kirjoita*, Tammi. Helsinki, p. 195.
- [47] Bharadwaj A.S. (2000), “A resource-based perspective on information technology capability and firm performance: An empirical investigation”, *MIS Quart.*, Vol. 24 No. 1, pp. 169-196.
- [48] ISO Standard ISO 41011:2017 Facility Management – Part 7: Guidelines for Performance Benchmarking.
- [49] Joshi, A., Kale, S., Chandel, S. and Pal, D.K. (2015), “Likert scale: Explored and explained”, *British Journal of Applied Science & Technology*, Vol. 7 No. 4, pp. 396-403.
- [50] Keil, M., Mann, J. and Arun, R. (2000), “Why software projects escalate: An empirical analysis and test of four theoretical models”, *MIS Quart.*, Vol. 24 No. 4, pp. 631-664.
- [51] Ghauri, P.N. and Gronhaug K. (2002), *Research Methods in Business Studies*, Financial Times Ltd, New York, USA.
- [52] Burns, R. (2000), *Introduction to Research Methods*, Sage, London.
- [53] COBIM2012 Common BIM Requirements of Finland Series 4 MEP Design, Rakennustieto Oy, Finland, p. 9.
- [54] Ustinovičius, L., Peckienė, A. and Popov, V. (2017), “A model for spatial planning of site and building using BIM methodology”, *Journal of Civil Engineering and Management*, Vol. 23 No. 2, pp. 173-182. <https://doi.org/10.3846/13923730.2016.1247748>
- [55] Hafsia, M., Monacelli, E., Martin, H. (2018). Virtual Reality Simulator for Construction workers. In *Proceedings of the Virtual Reality International Conference (VRIC 18)*, Laval, France.

- [56] Muhammad, A. A., Yitmen, I., Alizadehsalehi, S., Celik, T. (2019). Adoption of Virtual Reality (VR) for Site Layout Optimization of Construction Projects. *Teknik Dergi*, 31(2).
- [57] Roupé, M., Johansson, M., Viklund Tallgren, M., Jörnebrant, F., Tomsa, P. (2016). Immersive visualization of Building Information Models. In: *Living Systems and Micro-Utopias: Towards Continuous Designing (Proceedings of CAADRIA 2016)*, 21, pp. 673-682.
- [58] Zaker, R., Coloma, E. (2018). Virtual reality-integrated workflow in BIM-enabled projects collaboration and design review: a case study. *Visualization in Engineering*, 6(1), 4.
- [59] Wolfartsberger, J. (2019). Analyzing the potential of Virtual Reality for engineering design review. *Automation in Construction*, 104, pp. 27-37.
- [60] Liu, R. and Issa, R.R.A. (2013) "BIM for Facility Management: Design for Maintainability with BIM Tools." The 30th International Symposium on Automation and Robotics in Construction and Mining, Montreal, Canada. <https://doi.org/10.22260/ISARC2013/0035>
- [61] Ghosh, A., Chasey, A.D., Mergenschroer, M. (2015) in *Building information modeling: applications and practices*, R. R. A. Issa and S. Olbina, Eds., ed: American Society of Civil Engineers, 2015.
- [62] Matarneh S.T., Danso-Amoako, M.O., Al-Bizri, S., Gaterell, M., Matarneh, R.T. (2020), "BIM for FM: Developing information requirements to support facilities management systems", *Facilities*, Vol. 38 No. 5/6, pp. 378-394. <https://doi.org/10.1108/F-07-2018-0084>
- [63] Naghshbandi, S. (2016) "BIM for Facility Management: Challenges and Research Gaps." *Civil Engineering Journal*, Vol. 2, No. 12, December 2016.
- [64] Kangasluoma, M., Jaatinen, A., Kaivanto, K., Kortelampi, A., Kämpymäki, T., Fränti, H., Peltonen, K., Suomäki, J., Hännikäinen, J., Vepsäläinen, S., Tuomivaara, O., Väyrynen, L. (2018), *Handbook of Property Maintenance*, Kiinteistöalan Kustannus Oy, Helsinki, Finland, pp. 336-351.

## **ANNEXE 1.**

Lists 1a and 1b include the visual information content of the OMM. These lists are based on responses to the online survey's Question 8. Lists 2a and 2b are based on the content of the studied IFC MEP files, CMMS device lists and maintenance task lists.

List 1a. The indispensable information content of the OMM:

1. The operation areas of building service systems (HVAC)
2. Pipes, ducts and cable ladders
3. Dampers and shut-off and automatic valves
4. Equipment to maintain or alarm
5. Technical details of equipment to maintain
6. Service and maintenance instructions

List 1b. Optional information content of the OMM:

7. Escape and hauling routes
8. User-specific spaces, shared spaces and boundaries between spaces
9. Areas and volumes

List 2a. Devices to present in the OMM:

1. Electric distribution boards and transformers
2. Safety and emergency lighting distribution boards and luminaires
3. Fire alarm panels and fire detection devices
4. Fixed luminaires
5. Elevators, hoists and escalators
6. Uninterruptible power suppliers (UPS), generators and other power suppliers
7. Heat distribution units, heat transmitters, pumps, tanks and piping
8. Heating radiators and other heating terminals
9. Water system pipelines, pumps, tanks, transmitters, reservoirs, separators and filters
10. Water fittings and basins
11. Air conditioning machines, closing dampers, filters, radiators, heat recovery (HR) equipment and ducts
12. Air conditioning terminals, grease filters and fume hoods and cubicles
13. Cooling machines and compressors, radiators, convectors, steamers and condensers
14. Firefighting pumps, valves, installations and piping
15. Compressed air compressors, tanks, coolers, dryers, filters and piping
16. Building automation sensors

List 2b. Obligatory device details in the OMM:

1. Device type and use purpose
2. Manufacturer and/or vendor
3. Year of manufacture and installation
4. Key operating values
5. Service periods and instructions (text, attachment or URI)
6. Maintenance periods and measures (text, attachment or URI)

## **ANNEXE 2.**

Besides the property maintenance operator, the building owner and building users can also utilise the OMM. The vendors of workplace services, such as cleaning and catering vendors, can also benefit from the OMM.

1. The owner's use cases for OMM

The shapes, spaces and other details can be visualised by the OMM. The following opportunities for a building owner are detected, based on visual information:

1. Illustrating the building's special features
2. Identifying structural opportunities for space and purpose changes
3. Identifying the building service system's opportunities from the rebuilding perspective
4. Identifying the building service system's opportunities from the property servicing tendering perspective
5. Evacuation safety review and planning
7. Access control planning
8. Presenting space arrangements to users
9. Illustrating the interfaces and dimensions of the different users' spaces

2. The workplace service's use cases for the OMM

Some of workplace services can utilise the technical information and some the visual information. The following opportunities are detected:

1. Visualising and identifying office equipment
2. Verifying the areas to be cleaned and maintained
3. Identifying the boundaries between different users
4. Ensuring transportation routes
5. Viewing maintenance classes and surface materials
6. Defining the operating areas of security services
7. Orientating service personnel

3. The user's use cases for the OMM

The following are some of the building operation uses of the OMM, based on visual information:

1. Verifying the use purpose of rooms
2. Workstation and furniture planning
3. Identifying the locations and equipment under one's own care
4. Verifying the boundaries between different spaces
5. Service request positioning
6. Evacuation safety and access control planning
7. Employee induction to facility safety and security





# **Experimental Investigation on Hydraulic Efficiency of Vertical Drop Equipped with Vertical Screens**

**Rasoul DANESHFARAZ<sup>1</sup>**

**Sina SADEGHFAM<sup>2</sup>**

**Vadoud HASANNIYA<sup>3</sup>**

**John ABRAHAM<sup>4</sup>**

**Reza NOROUZI<sup>5</sup>**

## **ABSTRACT**

In the present study, vertical screens were utilized at downstream of vertical drops to increase the energy dissipation of subcritical flow. The experiments were carried out using screens with two different porosity ratios (40% and 50%) and three different distances from the drop brink (30, 60 and 90 cm). The results reveal that drops equipped with screens increase the relative downstream depth, the relative pool depth, and the relative energy dissipation compared with a plain vertical drop. By increasing porosity ratios and the screen distance from the drop brink, the relative downstream depth and relative energy dissipation increase, whereas the relative pool depth decreases. Also, by increasing the relative critical depth, the relative energy dissipation of the vertical drop decreases, whereas the energy dissipation related to the screens increases. However, increasing the relative critical depth initially increases and then decreases the performance of the hydraulic jump in terms of total energy dissipation.

**Keywords:** Energy dissipation, hydraulic jump, screen, vertical drop.

---

## Note:

- This paper was received on June 22, 2020 and accepted for publication by the Editorial Board on March 10, 2021.
- Discussions on this paper will be accepted by November 30, 2022.
- <https://doi.org/10.18400/tekderg.755938>

1 Department of Civil Engineering, University of Maragheh, East Azerbaijan, Iran  
daneshfaraz@maragheh.ac.ir - <https://orcid.org/0000-0003-1012-8342>

2 Department of Civil Engineering, University of Maragheh, East Azerbaijan, Iran  
s.sadeghfam@maragheh.ac.ir - <https://orcid.org/0000-0002-9018-547X>

3 Department of Civil Engineering, University of Maragheh, East Azerbaijan, Iran  
vadoodh733@gmail.com - <https://orcid.org/0000-0002-8200-582X>

4 School of Engineering, University of St. Thomas, St Paul, MN, USA  
jpabraham@stthomas.edu - <https://orcid.org/0000-0002-3818-8681>

5 Department of Water Engineering, University of Tabriz, East Azerbaijan, Iran  
rezanorouzi1992@tabrizu.ac.ir - <https://orcid.org/0000-0002-3756-8746>

## **1. INTRODUCTION**

Screens have been introduced by Rajaratnam and Hurtig [1] as a new method to enhance effectiveness of energy dissipation in rivers and downstream of hydraulic structures. These structures are located perpendicular to the flow direction to impose regime transformation by a hydraulic jump and consequently dissipate energy. Screens are commonly used downstream of drops to reduce energy. Also, vertical drops are commonly used as the structure to dissipate the energy of flow in rivers and open channels. This study combines drops with screens to achieve a higher performance in terms of energy dissipation.

When the natural slope in a river is high, drops compensate for differences between the existing slope and the desired slope for controlling the energy of the flow. Rouse' [2] was one of the first research studies on this; he derived an equation to estimate the discharge by measuring the brink depth. The results by Rouse [2] were later modified by Blasidell [3] and Rajaratnam and Chamani [4]. Rajaratnam and Chamani [4] used the data developed in prior studies of Moore [5] and Rand [6] to derive an equation relating to energy dissipation and pool depth. Chamani and Beirami [7] investigated the effect of supercritical flow upstream of a vertical drop on the hydraulic parameters. They revealed that increasing the Froude number for a constant discharge decreases the relative pool depth, the relative downstream depth, and the relative energy dissipation. Chamani et al. [8] presented an equation for the relative energy dissipation using shear layer theory and a fully developed surface jet.

A literature review also highlights studies that investigated the geometry of drops and adjunct structures. Esen et al. [9] evaluated the performance of a step with different dimensions downstream of a vertical drop and revealed that increasing the height of step increases the energy dissipation. Hong et al. [10] investigated the effect of downstream slope on hydraulic performance. Their results showed that increasing the downstream slope of a drop increases the drop length and the collision forces. Liu et al. [11] studied the effect of the upstream slope of a drop on hydraulic performance. Their results revealed that increasing the Froude number and the upstream slope will decrease the values of brink depth, the depth of water in the pool, and the angle of jet collision.

In recent years, many theoretical and empirical studies have been conducted to understand the energy dissipation process through screens (e.g., Rajaratnam and Hurtig [1]; Daneshfaraz et al. [12]; Bozkus et al. [13]; Şimsek et al. [14] and Sadeghfam et al. [15]). Rajaratnam and Hurtig [1] investigated the energy dissipation through screens and revealed that screens with 40% porosity can efficiently dissipate energy. Sadeghfam et al. [16] evaluated the performance of screens when a submerged hydraulic jump occurs and revealed that screens successfully perform in both free and submerged hydraulic jumps. On the other hand, they observed that the gap between screens had an insignificant effect on energy dissipation. Daneshfaraz et al. [17] investigated the energy dissipation through screens equipped with baffles. They observed that screens with 40% porosity reduce more energy compared to screens with 50% porosity. Also, their results revealed that screens equipped with baffles exhibit a greater energy dissipation compared to plain screens. investigated the behaviour of screens in movable-bed channels. They derived a set of equations to describe the dimensions of a scouring pit induced by screens.

Sharif and Kabiri-Samani [18] investigated a drop equipped with a horizontal screen in subcritical flow. They observed two types of bubble impinging jet flow regimes and a surface

flow regime occur downstream of drops equipped with screens. They also found that when the relative downstream depth is increased, air/water mixing decreases the relative length of the first jet collision point. However, it increases the relative pool depth. Norouzi et al. [19] studied energy dissipation through vertical screens downstream of inclined drops. Their results showed that screens cause a significant increase (between 400-900%) in the total relative energy dissipation compared to a plain inclined drop. Daneshfaraz et al. [20] investigated the performance of a drop equipped with dual horizontal screens. They observed that dual horizontal screens transformed supercritical flow to subcritical downstream of the drop. Daneshfaraz et al. [21] studied the efficiency of support vector machine for predicting vertical drop with dual horizontal screens. The results showed that capacity for this approach to predict the hydraulic performance of these systems with accuracy. Using vertical screens with two porosity ratios located downstream of inclined drops was investigated by Daneshfaraz et al. [22] investigated an inclined drop equipped with a screen in subcritical flow. Results revealed that compared to a plane inclined drop, the screen also caused an increase of at least 407% and up to 903% in total relative energy dissipation.

From this prior research, the use of screens can improve energy dissipation. However, there are limited studies have been performed for investigating energy dissipation on drops equipped with screens. Jet collisions with the pool floor have not been performed in the previous studies. So, the aim of this study is to investigate the performance of drop with vertical screen and pool downstream of the drop. Then, the hydraulic parameters of the drop with vertical screen such as the relative pool depth, the relative downstream depth and average percentage of the energy dissipation contribution for each of the components will be examined. The results of this study will also be compared with the results of the others.

## **2. MATERIALS AND METHODS**

### **2.1. Experimental Set-up**

Experiments were conducted on a flume with 5m length, 0.3m width and 0.55m depth in the hydraulic laboratory at the University of Maragheh. The flume is horizontal and has a rectangular cross-section. Figure 1 illustrates the flume. The flow was supplied via two pumps with a flow rate capacity of 900 liters per minute. The discharge was measured using two rotameters which were located at the outlet of the pumps and have a  $\pm 2\%$  accuracy. The flow depth was measured using a point gauge with  $\pm 1\%$  accuracy.

The body of the drop was made of plexiglass planes with 0.3m width and 0.15m height. Screens were made of polyethylene planes with a thickness of 1cm and porosity ratios of 40% and 50% through circular holes. All screens were located perpendicular to the flow direction at downstream of the drop with 30, 60 and 90 cm distance from the drop brink. The Range of variables used illustrated in Table 1.

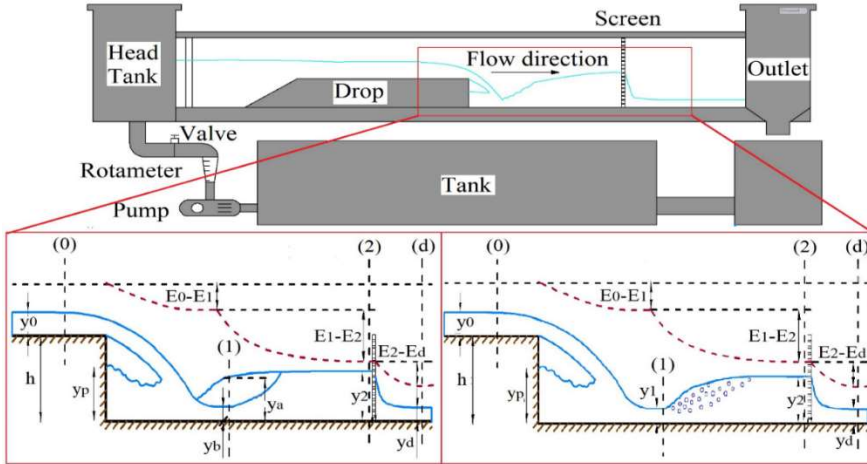


Figure 1 - Schematic of experimental setup and water circulation system

Table 1 - Range of variables used in the experimental study

Measured variables	Range of variables				
	Drop	Drop equipped with vertical screen in different distances			
		p (%)	d/h=2	d/h=4	d/h=6
Q (l/min)	150-850	40	150-850	150-850	150-850
		50	150-850	150-850	150-850
y <sub>0</sub> (cm)	2.45-6.86	40	2.34-7.6	2.38-6.98	2.33-7
		50	2.35-7.2	2.39-7.1	2.39-7.1
y <sub>b</sub> (cm)	1.38-4.12	40	1.3-4.22	1.27-4.27	1.28-4.25
		50	1.32-4.22	1.33-4.28	1.32-4.22
y <sub>p</sub> (cm)	3.78-8.97	40	4.15-14	4-13.02	3.88-12.4
		50	3.9-11.48	3.9-10.43	3.78-9.99
y <sub>a</sub> (cm)	0.62-2.55	40	1.35-4.08	1.39-4.33	1.45-4.37
		50	1.48-4.22	1.46-4.61	1.51-4.62

## 2.2. Specific Energy Dissipation

The specific energy at upstream of the drop is calculated using  $E_0=h+1.5y_c$  and specific energy at downstream (after the screen) of the drop is calculated as follows:

$$E_d=y_d+\frac{q^2}{2gy_d^2} \tag{1}$$

where  $E_0$  is the energy at upstream;  $h$  is the drop height;  $y_c$  is the critical depth;  $E_d$  is the energy downstream of the drop;  $q$  is the discharge per unit width;  $g$  is the gravitational acceleration; and  $y_d$  is the flow depth downstream of the drop measured approximately 20 to 30 cm after screen.

The relative energy dissipation of the total system is calculated as follows:

$$\frac{\Delta E}{E_0} = 1 - \frac{E_d}{E_0} \quad (2)$$

where  $\Delta E$  is the energy that has been dissipated. The energy dissipation efficiency of the drop equipped with screens compared to a plain vertical drop ( $\eta$ ) can be calculated as follows:

$$\eta = \frac{\Delta E_{\text{with screen}} - \Delta E_{\text{without screen}}}{\Delta E_{\text{without screen}}} \quad (3)$$

By measuring the flow depth at the location where the jet collides with the pool floor and the depths before and after screen, and also by calculating the energy at each section, the relative energy dissipation in each component of energy dissipation can be calculated as follows:

$$\frac{\Delta E_{\text{(Energy dissipator systems)}}}{E_0} = \frac{E_n - E_{n-1}}{E_0} \quad (4)$$

where  $E_n$  is energy at  $n^{\text{th}}$  component and  $E_{n-1}$  is energy at  $(n-1)^{\text{th}}$  component. The energy of the jet at the collision point with the floor for a submerged hydraulic jump is calculated as follows (see Fig. 1).

$$E = y_a + \frac{q^2}{2gy_b^2} \quad (5)$$

### 2.3. Dimensional Analysis

The equation describing energy dissipation as a function of independent parameters can be written as follows:

$$\Delta E = f_1(\rho, \mu, g, Q, B, h, p, t, d, y_c, y_0, y_b, y_1, y_2, y_d) \quad (6)$$

where  $\rho$  is the density of water [ $\text{ML}^{-3}$ ];  $\mu$  is the dynamic viscosity of water [ $\text{ML}^{-1}\text{T}^{-1}$ ];  $g$  is gravitational acceleration [ $\text{LT}^{-2}$ ];  $Q$  is the flow discharge [ $\text{L}^3\text{T}^{-1}$ ];  $B$  is the channel width [ $\text{L}$ ];  $h$  is the drop height [ $\text{L}$ ];  $p$  is the porosity of screen [-];  $t$  represents thickness of the screen [ $\text{L}$ ];  $d$  is the distance of the screen from the drop brink [ $\text{L}$ ];  $y_c$  is the critical depth [ $\text{L}$ ];  $y_0$  is the depth of flow at upstream depth of drop [ $\text{L}$ ];  $y_b$  is the drop brink depth [ $\text{L}$ ];  $y_1$  is the depth of water after the jet collides with the floor [ $\text{L}$ ];  $y_2$  is the depth of water at upstream of screen

[L];  $y_d$  is the depth of water at downstream screen [L]; and  $y_p$  is the pool depth under the falling jet [L].

Upstream energy and downstream Froude number can be expressed by Eqs. (7) and (8):

$$E_0 = f_2(g, Q, B, h, y_0) \quad (7)$$

$$Fr_d = f_3(g, Q, B, y_d) \quad (8)$$

Since the channel width is fixed, 30 cm, in all experiments it can be ignored. So, Eq. (6) can be rewritten as follows:

$$\Delta E = f_4(\rho, \mu, g, Q, h, p, t, d, y_c, y_0, y_b, y_1, y_2, Fr_d) \quad (9)$$

Considering  $y_0$ ,  $\rho$  and  $g$  as the repeating variables, the dimensionless Eq. (10) is obtained through Buckingham  $\pi$  theorem as follows:

$$\frac{\Delta E}{E_0} = f_5(Re_0, Fr_0, \frac{h}{y_0}, p, \frac{t}{y_0}, \frac{d}{y_0}, \frac{y_c}{y_0}, \frac{y_b}{y_0}, \frac{y_1}{y_0}, \frac{y_2}{y_0}, Fr_d) \quad (10)$$

where  $Re_0$  is upstream Reynolds number,  $Fr_0$  is upstream Froude number and  $Fr_d$  is downstream Froude number of the drop. After simplifications, Eq. (11) is obtained as follows:

$$\frac{\Delta E}{E_0} = f_6(Re_0, Fr_0, p, \frac{t}{h}, \frac{d}{h}, \frac{y_c}{h}, \frac{y_b}{y_c}, \frac{y_2}{y_1}, Fr_d) \quad (11)$$

Since the Reynolds number varied in the range of 7000 to 34000 in the present study, the flow was turbulent and viscosity effects can be neglected [23]. It was also observed that the Froude number ( $Fr_0$ ) varied in the range of 0.68 to 0.84. Considering the small range of Froude numbers, the effect of this parameter on the hydraulic characteristics was neglected. The thickness of the screens was also identified as an insignificant parameter Cakir [24] and Balkis [25].

Although the parameters  $y_b/y_c$  and  $y_2/y_1$  can be included in the experiments, quantifying their impact is beyond the scope of the present study. Therefore, relative energy dissipation can be described as a function of the reduced set of non-dimensional parameters as follows:

$$\frac{\Delta E}{E_0} = f_7(p, \frac{d}{h}, \frac{y_c}{h}) \quad (12)$$

The relative pool depth and relative downstream depth are expressed in terms of the dimensionless parameters are found as follows:

$$\frac{y_p}{h} = f_8(p, \frac{d}{h}, \frac{y_c}{h}) \tag{13}$$

$$\frac{y_d}{h} = f_9(p, \frac{d}{h}, \frac{y_c}{h}) \tag{14}$$

In this study, 48 experiments were conducted based on the non-dimensional parameters  $p$ ,  $d/h$ , and  $y_c/h$ . Also, eight experiments were conducted for the case of drops without screens. The non-dimensional parameters of the porosity ratios of the screens are 40% or 50%; the distance to height ( $d/h$ ) equals 2, 4 and 6; and relative critical depth ( $y_c/h$ ) are in the range (0.13-0.406). All the experiments required 15 minutes to warrant a steady-state condition.

### 2.4. Performance Metrics

Three performance metrics were used to evaluate the results. RMSE is the Root Mean Square Error,  $R^2$  is the determination coefficient, and  $RE$  is the relative error (see Table 2).

Table 2 - Performance Metrics for Evaluation Results

Performance Metrics	Equation
Root Mean Square Error	$RMSE = \sqrt{\frac{1}{n} \sum_1^n (X_{exp} - X_{cal})^2}$
Determination coefficient	$R^2 = \left( \frac{n \sum X_{exp} X_{cal} - (\sum X_{exp})(\sum X_{cal})}{\sqrt{n(\sum X_{exp}^2) - (\sum X_{exp})^2} \sqrt{n(\sum X_{cal}^2) - (\sum X_{cal})^2}} \right)^2$
Relative Error	$RE = \frac{ X_{exp} - X_{cal} }{X_{exp}}$

$X_{exp}$  is an experimental value and  $X_{cal}$  is calculated values.

### 3. RESULTS AND DISCUSSIONS

While the flow regime is subcritical upstream of the drop, the flow regime changes initially to critical and then supercritical near the drop brink. After the brink, due to gravity, the flow falls and impacts the pool. The flow then is divided into two parts, part of which flows towards the pool and the other part flows downstream [26]. The presence of a returned rotating flow leads to greater pool depth. Fluctuations, air/water mixing and the presence of a returned flow inside the pool result in a non-hydrostatic pressure distribution [27]. Also,

turbulence inside the pool reduces the energy of flow [26, 28]. The flow regime becomes supercritical by moving downstream (Fig. 2).

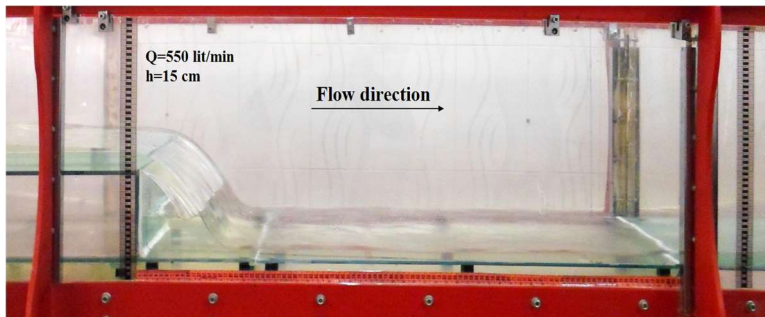


Figure 2 - Flow overview in plain vertical drop

### 3.1. The Drop Relative Depth

Previous studies on subcritical flow upstream of vertical drops indicated that the fluid depth is initially greater than the critical depth and as the flow approaches the drop brink, the flow depth decreases and reaches the critical flow depth. Then, at a slight distance upstream of the drop brink it reaches a supercritical depth [26]. Laboratory observations in the present study confirm these findings. Also, experiments conducted on the vertical drop equipped with screens show that screens had an insignificant effect on the general behavior of flow at upstream of the drop. The equation  $y_c = \sqrt[3]{\frac{q^2}{g}}$  can be useful to relate the critical depth and discharge values. Table 3 presents a comparison between the present drop brink and critical depths with prior studies. It is observed that the drop relative depth in the present study agrees with previous studies. Therefore, it can be concluded that the results of the present study and the experimental findings are accurate.

Table 3 - Comparison of the drop brink depth and the critical depth of the present study with previous studies

Studies	Diskin [29]	Andersen [30]	Strelkoff and Moayeri [31]	Present study
$y_b/y_c$	0.667	0.694	0.672	0.674

After the flow passes through the drop brink, it collides with the downstream bed. When the jet moves further downstream towards the screen, the screen acts as a barrier against the flow and increases the flow depth just upstream of the screen and consequently causes a hydraulic jump between the screen and the collision location. Laboratory observations revealed that hydraulic jump increases turbulence and roller flows and air/water mixing between the screen and the collision location. Figure 3 shows the behavior of the flow along with the screen and hydraulic jump formation.





Figure 3 - Vertical drop equipped with a screen and hydraulic jump formation

It was observed that for low discharges, the free hydraulic jump occurred, and the toe of jump formed a slight distance upstream of the screens. By increasing the discharge, the toe of hydraulic jump moves towards the drop and ultimately reaches the collision location of a jet, which forms a submerged hydraulic jump. For all the cases where the hydraulic jump was submerged, it was observed that pool depth increased. It was also observed that flow passing through the screens produce severe air/water mixing.

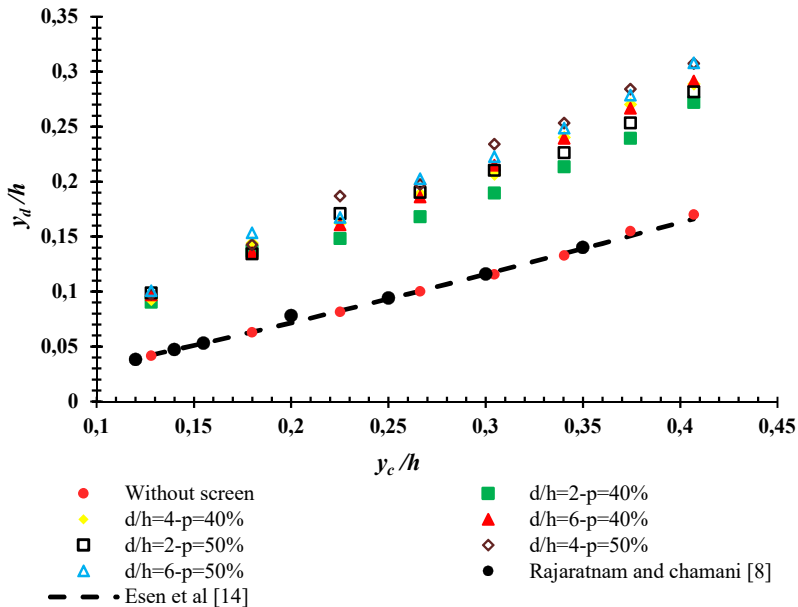


Figure 4 - Effect of screens on the relative downstream depth

### 3.2. Relative Downstream Depth

Figure 4 shows the effect of screens on the relative downstream depth versus the relative critical depth. According to the figure,  $y_d/h$  increases by increasing  $y_c/h$ . The figure also shows that screens downstream of the vertical drop increase the relative downstream depth compared to a plain vertical drop. Also, increasing screen porosity and the downstream location of screens from the drop brink increase the relative downstream depth.

During the experiments, it was observed that the downstream Froude number decreases from a range of 3.5-5.5 to a range of 1.25-2.1. Notably, the downstream Froude number has a direct relationship with the destructive energy of flow. In some experiments, it was also observed that at low relative critical depth, an undular jump is formed.

Table 4 presents the reduction of downstream Froude number for vertical drops equipped with screens compared to plain vertical drops. The table shows that the increase in screen porosity decreases the Froude number. Also, with the increase in distance of screens from 2h to 4h, the Froude number increases. However, there is no significant difference in the results for screens which are located at 4h to 6h.  $h$  is the height of drop.

*Table 4 - Reduction of downstream Froude number for vertical drops equipped with screens compared to plain vertical drops*

Location	Decrease in Froude number for the screen with 40% porosity (%)	Decrease in Froude number for the screen with 50% porosity (%)
2h	56.6	61.1
4h	62	65.5
6h	62	65.1

### 3.4. Relative Pool Depth

The depth of the pool behind the falling jet was measured as an important parameter in the design of vertical drops. By estimating this parameter, it is possible to control submergence of the drop. Figure 5 shows a comparison of the relative pool depth in the present and previous studies for vertical drops equipped with screens. The figure also shows that screens in vertical drops increase the relative pool depth compared to plain vertical drops.

A submerged hydraulic jump occurred for all relative critical depths and all locations of screens with a porosity of 40%, while a free hydraulic jump occurred for the screen with a porosity of 50%. Therefore, experimental results provide evidence that a vertical drop equipped with a screen with a porosity of 50% located at a distance of 6h from the drop brink is appropriate for preventing drop submergence. However, by increasing the relative critical depth of submergence, the backflow moves to the pool and thus the pool depth increases in both cases. Furthermore, by increasing the screen distance from the drop brink, the submergence depth and the relative pool depth decreases. Table 5 shows the increase in relative pool depth for vertical drops equipped with screens compared to the plain vertical drop.

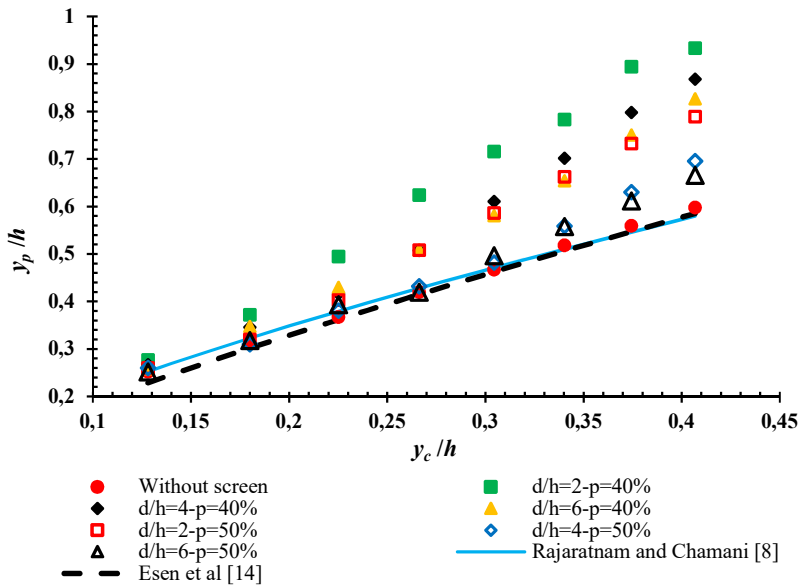


Figure 5 - Effect of screens on the relative pool depth for a drop equipped with a screen

Table 5- Increase in relative pool depth for the vertical drop equipped with screens relative to the plain vertical drop

Location	Increase in relative pool depth for the screen with 40% porosity (%)	Increase in relative pool depth for the screen with 50% porosity (%)
2h	41.5	19
4h	25.5	6
6h	21.8	5.4

In order to derive an empirical equation for describing relative pool depth, experimental data were divided randomly into calibration and validation sets with ratios of 80% and 20%, respectively. Then, Eq. (15) were derived by using a Generalized Reduced Gradient (GRG) algorithm as one of the most robust nonlinear programming methods (see [32]). Figure 6 compares the experimental and estimated values of the relative pool depth. According to the figure, the average relative error is 3.9% and the maximum error between experimental and the estimated values is 10.5%.

$$\frac{y_p}{h} = 1.31 \left( \frac{y_c}{h} \right)^{1.4} \left( \frac{d}{h} \right)^{-0.193} (p)^{-1.058} + 0.1164 \quad R^2 = 0.9952 \quad \text{and} \quad \text{RMSE} = 0.019 \quad (15)$$

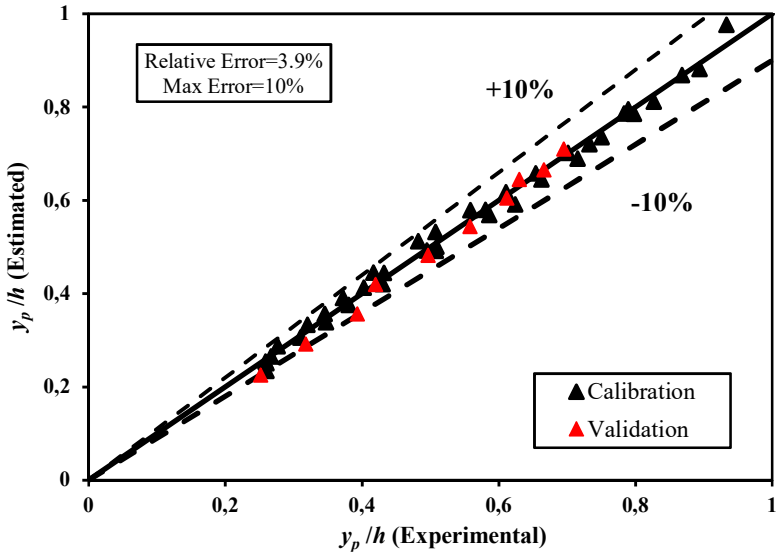


Figure 6 - Comparison between experimental values of  $y_p/h$  and estimated values

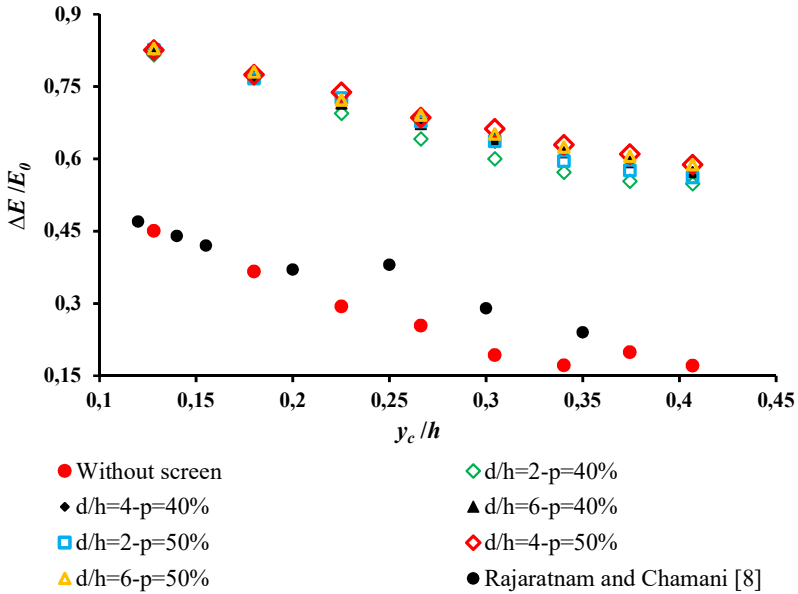


Figure 7 - Effect of screens on relative energy dissipation

### 3.5. Relative Energy Loss

Energy dissipation in vertical drops with the subcritical flow in upstream of the drop, usually occurs due to the collision effect of the jet to floor of pool and flow turbulence in the pool below the jet [26]. Figure 7 compares the relative energy dissipation versus changes in the relative critical depth in the present and prior studies. According to the figure, the relative energy dissipation decreases with increasing relative critical depth for plain vertical drops and vertical drops equipped with screens by varying porosities and locations. The figure provided evidence that using screen increases the relative energy dissipation compared with the plain vertical drop. Also, it is observed that increasing porosity and downstream position both increase the relative energy dissipation.

Similar to Section 3.3, the GRG algorithm was used to derive Eq. (16) for describing the relative energy dissipation in vertical drops equipped with screens. Figure 8 compares the estimated and experimental values for the relative energy dissipation. It is seen that the average relative error is 1.61% and the maximum error between experimental and estimated values is 3.29%.

The energy dissipation efficiency (the ratio of the energy dissipation difference of the plain vertical drop with screens to the energy dissipation of the plain vertical drop) is presented in Table 6 for different models versus changes in the relative critical depth.

$$\frac{\Delta E}{E_0} = 1.023 \left( \frac{y_c}{h} \right)^{0.4853} \left( \frac{d}{h} \right)^{-0.05} p^{-0.088} + 0.252 \quad R^2 = 0.9934 \quad \text{and} \quad \text{RMSE} = 0.012 \quad (16)$$

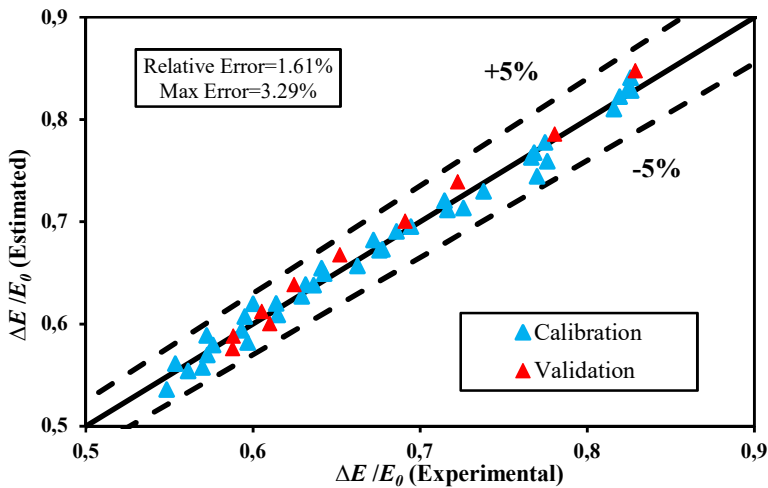


Figure 8 - Comparison of experimental values of  $\Delta E / E_0$  and estimated values

Table 6 - Summary of the loss efficiency for the vertical drop equipped with energy dissipate

$y_c/h$	The efficiency of the energy dissipation increases in the screen with a porosity of 40% at various downstream locations			The efficiency of the energy dissipation increases in the screen with a porosity of 50% at various downstream locations		
	2h	4h	6h	2h	4h	6h
0.13	0.81	0.82	0.83	0.83	0.83	0.84
0.18	1.1	1.12	1.1	1.09	1.11	1.13
0.225	1.36	1.44	1.43	1.47	1.5	1.46
0.266	1.52	1.66	1.64	1.66	1.7	1.72
0.3	2.1	2.27	2.33	2.29	2.4	2.38
0.34	2.34	2.59	2.58	2.47	2.67	2.65
0.37	1.78	2	1.98	1.89	2.06	2.04
0.406	2.36	2.33	2.35	2.28	2.44	2.45

According to Table 6, it can be concluded that by increasing the relative critical depth, the efficiency of energy dissipation increases for all distances and different porosities. It is also observed that energy dissipation efficiency increases with increasing screen distance from the drop brink and by increasing the porosity of the screen for a constant relative critical depth. Figure 9 shows the average energy dissipation efficiency versus the relative critical depth and ratio of distance to drop height.

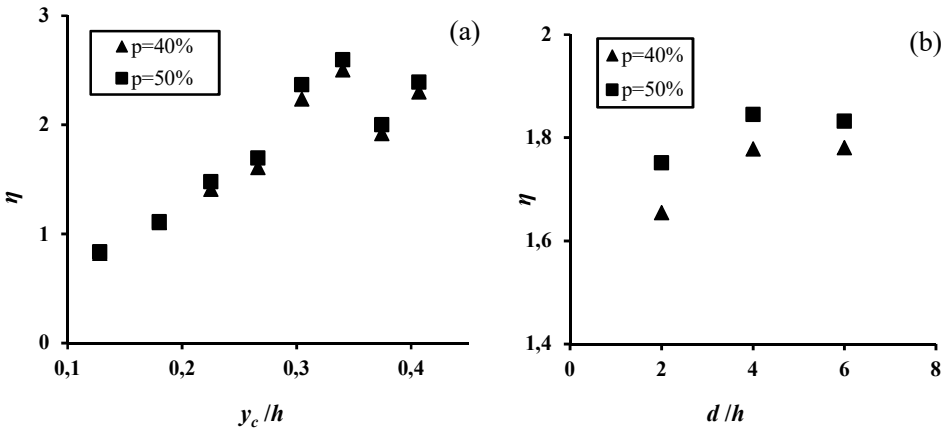


Figure 9 - Variation of energy dissipation efficiency versus (a) Relative critical depth; and (b) ratio of distance to screen height

Figure 9(a) shows that the average energy-loss efficiency increases by increasing relative critical depth, in general. However, there are fluctuations due to the high turbulence of flow for the relative critical depth greater than 0.3. As shown in Fig. 9(b), the energy-loss efficiency generally increases with the increase in the ratio of the distance from drop height. Also, both figures show that the energy dissipation efficiency for vertical drops equipped with screens with a porosity of 50% is higher than screens with the porosity of 40%.

### 3.6. Contribution of Different Components in Energy Dissipation

Three components play major roles in dissipating flow energy in a vertical drop: (1) the drop structure; (2) the hydraulic jump imposed by the screen; and (3) turbulence as fluid passes through a screen. Figure 10 depicts the contributions of these components in energy dissipation. The relative energy dissipation of the drop equipped with the screen is significantly greater than that for the plain vertical drop, while the total relative energy dissipation of a vertical drop equipped with the screen is smaller than that of the plain vertical drop. It can be concluded that for a drop equipped with a screen, an increase in critical depth can cause the hydraulic jump to become submerged and the pool depth to increase. This factor reduces the impact of the jet on the pool floor and thereby reduces the energy dissipation. On the other hand, by investigating the hydraulic jump mechanism for a vertical drop equipped with a screen, it can be concluded that a free hydraulic jump is formed at low discharge. By increasing the discharge, the toe of jump moves upstream and reaches the collision location of the jet with the floor and the relative energy dissipation of hydraulic jump reaches a maximum value. With further increase in the discharge, the hydraulic jump becomes submerged and its relative energy dissipation is reduced.

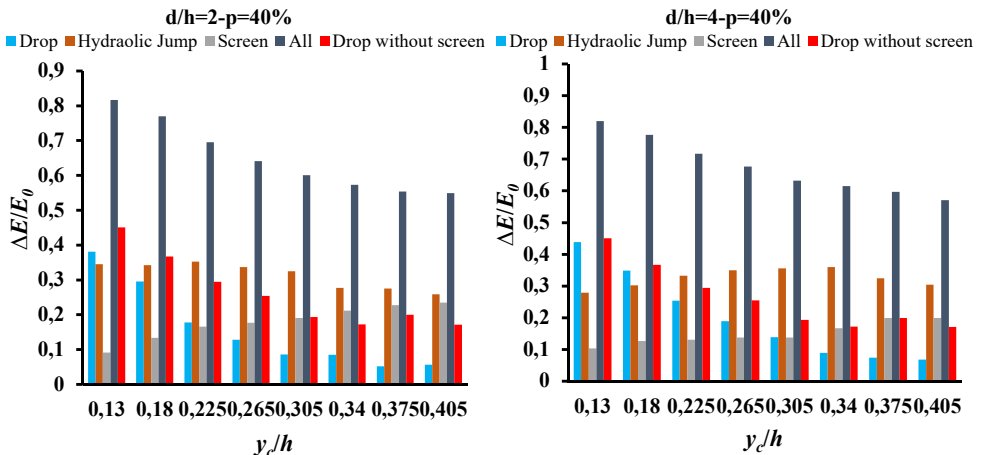


Figure 10- Contribution of different components in energy dissipation

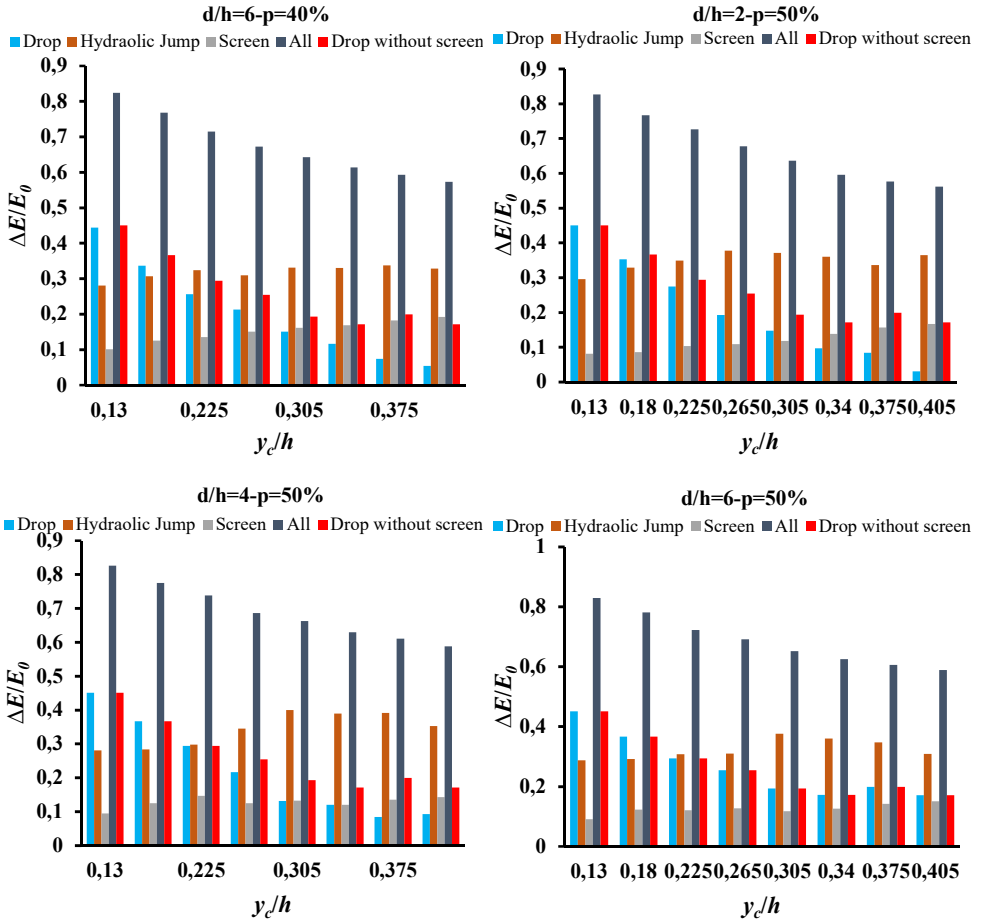


Figure 10- Contribution of different components in energy dissipation (continue)

Figure 11 shows the average percentage contribution for each of the components of the energy dissipation. It can be observed that by increasing the distance of the screens from the drop brink, the average contribution of the energy dissipation for a vertical drop increases. Furthermore, increase in the screen distance reduces the contribution in total energy dissipation of hydraulic jump and screen components.

It is seen that by increasing screen porosity, both the contribution in total energy dissipation of the vertical drop and hydraulic jump increase while contribution of the screen decreases. Generally, the results show that the hydraulic jump provides the greatest contribution to total energy dissipation.



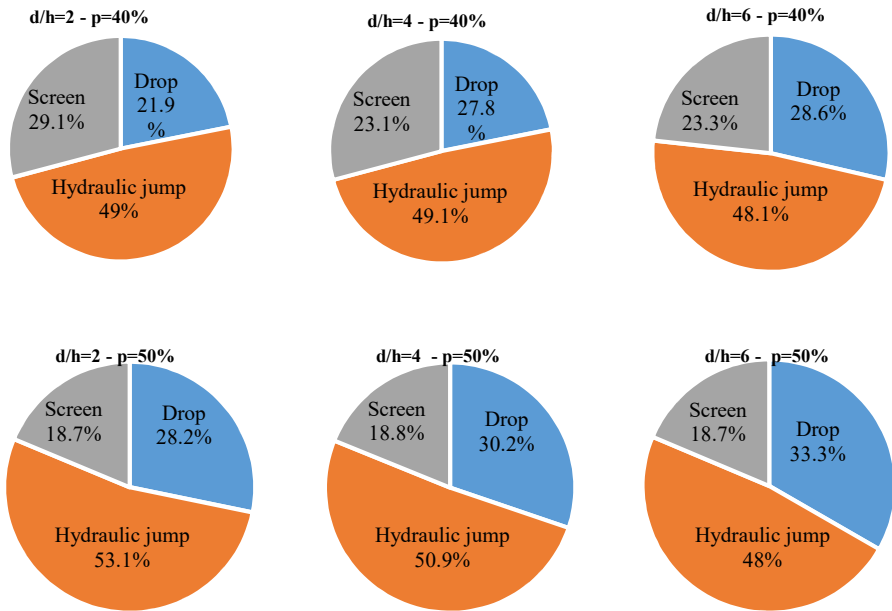


Figure 11 - Variation of energy dissipation percentage for different components

#### 4. DISCUSSION

Recent studies confirm that using screens downstream of small hydraulic structures can increase energy dissipation by imposing a hydraulic jump and turbulence and thereby control erosion and scouring on rivers beds and open channels. The present study suggests that screens can be utilized along with drops as one of the common structures to achieve higher energy dissipation and control the hydraulic jump location. This system is a step towards less polluted water and provide an important environmental benefit by aeration mechanism.

However, screen-type dissipaters have been used less in practice and research is ongoing in this field. One of the major obstacles to the use of these systems is the potential of clogging or blocking of pores with natural material and sediment. Therefore, the determination of pore diameters and pore shapes are critical and require further attention. Maintenance systems are needed to control the possible blocking if the system is to be used in practices. On the other hand, this feature can be useful to remove unfavorable floating or submerged objects in the flow.

The present study is a step towards providing a guideline to design such systems. For example, the pool depth under the falling jet is an important parameter for determining the amount of the submergence in the vertical drop design. The results of this study show that the use of screens downstream of a vertical drop increases the pool depth and decreases the performance of the drop structures. However, according to the design regulations, the drop structure should not be totally submerged. Equations are developed to calculate the relative pool depth in vertical drops equipped with screens. These equations can be used in the design of this system.

A comparison of the screen porosity on energy dissipation has shown that a screen with a porosity of 40% dissipates more energy than screens with a porosity of 50% in the hydraulic jump, in agreement with [1] and [16]. However, since submergence of the jump reduces the performance of energy dissipating in the drop and screen with porosity of 40% leads to submergence, a vertical drop equipped with a screen of porosity of 50% leads to more energy dissipation than a screen of porosity of 40%.

Screens are another type of energy dissipation structure whose performance is based on a relative critical depth, as shown in Fig. 10. By increasing water height behind the screen the amount of air/water mixing and energy dissipation increase. Therefore, by increasing the discharge and thus increasing the depth at upstream of the screen, the screen performance increases.

## **5. CONCLUSION**

The present study investigates the effect of using screens in vertical drops to increase energy dissipation. The experiments were run for a vertical drop equipped with screens with two porosity ratios, 40% and 50% and three different screen locations, 30 cm, 60 cm, and 90cm downstream the drop brink. It was observed that a screen installed at downstream of a vertical drop imposes a hydraulic jump between the jet collision position and the screen and provides the depth necessary to create a hydraulic jump. This phenomenon increases energy dissipation. The screen also increases energy dissipation by enhanced air/water mixing. The results show that the use of screens increases the relative downstream depth, the relative pool depth, and the relative energy dissipation. It was also found that by increasing porosity and the distance of screens from the drop brink, the relative downstream depth and the energy dissipation are increased, and the relative pool depth is decreased. It was also found that by increasing relative critical depth, the relative energy dissipation of the drop component decreases, the contribution of hydraulic jump initially increases upto a certain point and then decreases, and the contribution of energy dissipation of the screen increases. Also, by increasing the distance of the screen from the drop brink, the energy dissipation in the vertical drop increases and the contributions to energy dissipation by the hydraulic jump and the screen decreases. It was also found that hydraulic jump provides the greatest contributions (~50%) in total energy dissipation followed by almost equal contributions from vertical drop and screen.

### **Notation**

The following symbols are used in this paper:

$B$ = channel width (m)

$d$ = the distance of the screen from the drop brink (m)

$E_0$ = Energy at the upstream(m)

$E_1$ = energy at cross-section (1) (m)

$E_2$ = energy at cross-section (2) (m)

$E_d$  = energy at the downstream (m)

$Fr_u$  = upstream Froude number (-)

$g$  = gravitational acceleration ( $m/s^2$ )

$h$  = drop height (m)

$p$  = porosity of the screen (%)

$Q$  = flow discharge ( $m^3/s$ )

$q$  = discharge inflow per unit width ( $m^2/s$ )

$Re_u$  = Reynolds number at upstream of screen (-)

$t$  = represents the thickness of the screen (m)

$y_u$  = upstream depth (m)

$y_l$  = depth after the jet collides with the floor (m)

$y_2$  = depth before the screen (m)

$y_b$  = drop brink depth (m)

$y_c$  = critical depth (m)

$y_d$  = downstream depth (m)

$y_p$  = pool depth under the falling jet (m)

$\Delta E$  = energy dissipation (m)

$\eta$  = energy dissipation efficiency; (-)

$\rho$  = density of water; ( $kg/m^3$ )

$\mu$  = the dynamic viscosity; ( $kg/m.s$ )

## References

- [1] Rajaratnam, N., Hurtig, K., Screen-type energy dissipator for hydraulic structures. *Journal of Hydraulic Engineering*, Vol 126, No (4), 310-312. 2000.
- [2] Rouse, H., Discharge characteristics of the free overfall: Use of crest section as a control provides easy means of measuring discharge. *Civil Engineering*, Vol 6, No (4), 257-260. 1936.
- [3] Blaisdell, F., Hydraulics of rectangular vertical drop structures. *Journal of Hydraulic Research*, Vol 17, No (4), 289-302. 1980.
- [4] Rajaratnam, N., Chamani, M.R., Energy loss at drops. *Journal of Hydraulic Research*, Vol 33, No (3), 373-384. 1995.
- [5] Moore, W.L. Energy loss at the base of a free overfall. in *Proceedings of the American Society of Civil Engineers*. ASCE, 1943.

- [6] Rand, W. Flow geometry at straight drop spillways. in Proceedings of the American Society of Civil Engineers. ASCE, 1955.
- [7] Chamani, M.R., Beirami, M., Flow characteristics at drops. journal of Hydraulic Engineering, Vol 128, No (8), 788-791. 2002.
- [8] Chamani, M.R., Rajaratnam, N., Beirami, M., Turbulent jet energy dissipation at vertical drops. Journal of Hydraulic Engineering, Vol 134, No (10), 1532-1535. 2008.
- [9] Esen, I.I., Alhumoud, J.M., Hannan, K.A., Energy Loss at a Drop Structure with a Step at the Base. Water international, Vol 29, No (4), 523-529. 2004.
- [10] Hong, Y.M., Huang, H.S., Wan, S., Drop characteristics of free-falling nappe for aerated straight-drop spillway. Journal of Hydraulic Research, Vol 48, No (1), 125-129. 2010.
- [11] Liu, S.-I., Chen, J.-Y., Hong, Y.-M., Huang, H.-S., Raikar, R.V., Impact characteristics of free over-fall in pool zone with upstream bed slope. Journal of Marine Science and Technology, Vol 22, No (4), 476-486. 2014.
- [12] Daneshfaraz, R., Hasannia, V., Norouzi, R., Sihag, P., Sadeghfam, S., Abraham, J., Investigating the Effect of Horizontal Screen on Hydraulic Parameters of Vertical Drop. Iranian Journal of Science and Technology, Transactions of Civil Engineering. 2021.
- [13] Bozkus, Z., Çakir, P., Ger, A.M., Energy dissipation by vertically placed screens. Canadian Journal of Civil Engineering, Vol 34, No (4), 557-564. 2007.
- [14] Şimsek, O., Göksu Soydan, N., Gumus, V., Sami Akoz, M., Salih Kirkgoz, M., Numerical modeling of B-type hydraulic jump at an abrupt drop. Teknik Dergi, Vol 26, No (4), 7215-7240. 2015.
- [15] Sadeghfam, S., Daneshfaraz, R., Khatibi, R., Minaei, O., Experimental studies on scour of supercritical flow jets in upstream of screens and modelling scouring dimensions using artificial intelligence to combine multiple models (AIMM). Journal of Hydroinformatics, Vol 21, No (5), 893-907. 2019.
- [16] Sadeghfam, S., Akhtari, A.A., Daneshfaraz, R., Tayfur, G., Experimental investigation of screens as energy dissipaters in submerged hydraulic jump. Turkish Journal of Engineering and Environmental Sciences, Vol 38, No (2), 126-138. 2015.
- [17] Daneshfaraz, R., Sadeghfam, S., Ghahramanzadeh, A., Three-dimensional numerical investigation of flow through screens as energy dissipaters. Canadian Journal of Civil Engineering, Vol 44, No (10), 850-859. 2017.
- [18] Sharif, M., Kabiri-Samani, A., Flow regimes at grid drop-type dissipaters caused by changes in tail-water depth. Journal of Hydraulic Research, 1-12. 2018.
- [19] Norouzi, R., Daneshfaraz, R., Bazayr, A., The Study of Energy Depreciation due to the use of Vertical Screen in the Downstream of Inclined Drops by Adaptive Neuro-Fuzzy Inference System (ANFIS). AUT Journal of Civil Engineering. 2019.

- [20] Daneshfaraz, R., Majedi Asl, M., Razmi, S., Norouzi, R., Abraham, J., Experimental investigation of the effect of dual horizontal screens on the hydraulic performance of a vertical drop. *International Journal of Environmental Science and Technology*. 2020.
- [21] Daneshfaraz, R., Bagherzadeh, M., Esmaeeli, R., Norouzi, R., Abraham, J., Study of the performance of support vector machine for predicting vertical drop hydraulic parameters in the presence of dual horizontal screens. *Water Supply*. 2020.
- [22] Daneshfaraz, R., Majedi Asl, M., Baziyar, A., Abraham, J., Norouzi, R., The laboratory study of energy dissipation in inclined drops equipped with a screen. *Journal of Applied Water Engineering and Research*. 2020.
- [23] Ghaderi, A., Daneshfaraz, R., Abraham, J., Torabi, A., Effect of Different Channels on Discharge Coefficient of Labyrinth Weirs. *Teknik Dergi*, Vol 32. 2021.
- [24] Cakir, P., Experimental investigation of energy dissipation through screens in Department of Civil Engineering. Middle East Technical University: Ankara, Turkey, 2003.
- [25] Balkis, G., Experimental investigation of energy dissipation through inclined screens in Department of Civil Engineering Middle East Technical University: Ankara, Turkey, 2004.
- [26] Rajaratnam, N., Chamani, M., Energy loss at drops. *Journal of Hydraulic Research*, Vol 33, No (3), 373-384. 1995.
- [27] Robinson, K., Predicting stress and pressure at an overfall. *Transactions of the ASAE*, Vol 35, No (2), 561-569. 1992.
- [28] White, M., Discussion of moore. *Tran. ASCE*, Vol 108, 1361-1364. 1943.
- [29] Diskin, M., End depth at a drop in trapezoidal channels. *Journal of the Hydraulics Division*, Vol 87, No (4), 11-32. 1961.
- [30] Andersen, V.M., Non-uniform flow in front of a free overfall. *Acta polytechnica scandinavica-civil engineering and building construction series*, Vol 42, No (3). 1967.
- [31] Strelkoff, T., Moayeri, M.S., Pattern of potential flow in a free overfall. *Journal of the Hydraulics Division*, Vol 96, No (4), 879-901. 1970.
- [32] Lasdon, L.S., Fox, R.L., Ratner, M.W., Nonlinear optimization using the generalized reduced gradient method. *Revue française d'automatique, informatique, recherche opérationnelle. Recherche opérationnelle*, Vol 8, No (V3), 73-103. 1974.



# **Seismic Performance of a Hybrid Coupled Wall System Using different Coupling Beam Arrangements**

**Molham SALAMEH<sup>1</sup>**

**Mohsenali SHAYANFAR<sup>2</sup>**

**Mohammad Ali BARKHORDARI<sup>3</sup>**

## **ABSTRACT:**

This study implemented multi-record nonlinear dynamic and fragility analysis in order to gain better insight into the hybrid coupled wall (HCW) system. Two potentials are used to construct coupling beams, which are the typical steel coupling beam and the replaceable steel coupling beam. Furthermore, an innovative idea for replaceable beams is discussed using reinforced concrete infill instead of steel stiffeners. A new simplified FE model for such beams is carried out in order to explore how this new beam influences the seismic performance of HCW system. An additional equivalent bare RC wall case study is also taken into account for a comprehensive comparison. A precise 2D modelling method using OpenSees platform is adopted after validation against experimental and complex 3D numerical simulations. The results indicate a good effect of the replaceable coupling beams concept upon reducing the vulnerability of wall piers under low and moderate events. In terms of coupling beams fragility, the replaceable steel coupling beams also demonstrate better damage resistance when compared with typical steel beams under low and moderate seismic events. Using reinforced concrete infill instead of steel stiffeners can significantly protect beam maintenance without deteriorating wall piers vulnerability.

**Keywords:** Hybrid coupled wall (HCW), replaceable steel coupling beam (RSCB), replaceable composite coupling beam, nonlinear dynamic analysis, fragility assessment.

## **1. INTRODUCTION**

Recent investigations have demonstrated that the modern buildings have good performance in terms of life safety. However, post-earthquake repair of buildings is costly and time

---

Note:

- This paper was received on August 19, 2020 and accepted for publication by the Editorial Board on April 9, 2021.
- Discussions on this paper will be accepted by November 30, 2022.
- <https://doi.org/10.18400/tekderg.782642>

1 Iran University of Science and Technology, School of Civil Engineering, Tehran, Iran - molham\_sl88@yahoo.com - <https://orcid.org/0000-0003-2871-0074>

2 Iran University of Science and Technology, School of Civil Engineering, Tehran, Iran - shayanfar@iust.ac.ir - <https://orcid.org/0000-0001-6358-2771>

3 Iran University of Science and Technology, School of Civil Engineering, Tehran, Iran - barkhordar@iust.ac.ir - <https://orcid.org/0000-0001-7760-0475>

consuming. Therefore, recent advances in structural engineering are more than ever oriented towards construction of economical and easily repairable earthquake-proof buildings. Use of hybrid coupled shear walls is one of these interesting systems which has gained attention over the past decade. It consists of two or more RC walls connected by means of steel or composite concrete-steel coupling beams. Much effort has been devoted to study the seismic behaviour of HCW systems [1-19]. Generally, since basic damage extent is substantially concentrated in the coupling beams, the latest research is oriented to make them replaceable after being damaged (e.g. Fortney et al. [20], Christopoulos and Montgomery [21] and Ji et al. [22]). Among them, the replaceable steel coupling beam (RSCB) (Fig. 1-a) seems to be the most practical. The RSCB constitutes of a “fuse” shear link connected at its two ends to steel beam segments which are supposed to remain elastic even under high lateral displacement demand. Appropriate link-to-beam connection produced by Ji. et al. [22] can permit easy replacement of the damaged shear link even when residual drifts exist. However, typical steel moment critical coupling beams (Fig. 1-b) can still be used in current projects because of easy construction. Ji. et al. [23] assessed the seismic performance of a HCW system with RSCBs against the traditional RCW with RC coupling beams. They concluded that the expected damage to the walls, even under extreme events, is limited to cracks and slight spalling of concrete. Moreover, the HCW system with RSCBs illustrates enhanced performance over the conventional RCW with RC coupling beams in terms of beams vulnerability. Herein a similar assessment is carried out to assess HCW system with RSCBs against HCW system with typical steel coupling beams. Furthermore, an innovative replaceable composite coupling beam method will be estimated. Coupling beams in such systems have a similar principle as the links of eccentrically braced frames (EBFs). Accordingly, they can be classified as long, intermediate and short links. According to Euro Code 8 [24] the steel link is classified as short link when the link length  $e < e_s = 1,6 M_{p,link}/V_{p,link}$  and as long link when  $e > e_L = 3,0 M_{p,link}/V_{p,link}$  where  $M_{p,link}$  and  $V_{p,link}$  are link design yielding bending and shear. When link length is between  $e_s$  and  $e_L$ , it is classified as intermediate link. Recently, Ji et al. [25] produced the very short link type when web plate is made from lower yield strength than flanges, and  $e/(M_{p,link}/V_{p,link})$  ratio is less than 1. These links can provide very high inelastic ductility on the order of 0.14 rad rather than 0.08 rad which is stated by Euro Code 8 [24]. Furthermore, the over-strength factor of such links can reach 1.9 due to substantial participation of shear strength in flanges and high inelastic rotation capacity. This type of links has been adopted by Ji et al. [23] for RSCB method in HCW system. Whereas typical steel coupling beams are usually moment-critical elements and are classified as long links with an inelastic ductility which equals only 0.02 rad as stated by Euro Code 8 [24].

Using reinforced concrete infill instead of steel stiffeners has not yet been proposed in such fuse shear links. The details of this method are portrayed in Fig. 2, noting that the stirrups and the web of steel link are welded together in order to ensure safe transformation of shear forces between the web and concrete infill. There is a significant lack in the literature about this component performance when used as shear force resisting element. Composite link idea has originated in Technical University of Darmstadt in 1989 using an experimental program to assess the concrete infill efficiency to prevent web buckling rather than typical web stiffeners. Kanz et al. [26] produced an experimental study to estimate the behaviour of two-storey eccentrically braced composite frame. The results show that concrete infill with closely spaced stirrups is an effective replacement of steel stiffeners typically used in



eccentrically braced frame system (EBFs). Shayanfar et al. [27] also studied composite shear link to be utilized in EBFs with vertical links (V-EBFs). The results reveal an increase in shear strength and dissipated energy up to 100 and 38 per cent, respectively over using steel link only.

This study aims to make quantitative fragility assessment of HCW system when using different schematic potentials to construct coupling beams as portrayed in Fig. 3. Case 1 is conventional RC wall which represents the most frequent system, and the easiest to be construct. Case 2 represents using HCW system with typical steel coupling beams (TSCBs). Case 3 represents using HCW system with replaceable steel coupling beams (RSCBs). Case 4 represents using HCW system with a newly proposed type of links; this type includes using reinforced concrete infill instead of steel stiffeners in RSCB case. The new type can be called RCCBs (Replaceable Composite Coupling Beams). Using reinforced concrete infill instead of steel stiffeners may present some challenges in construction. Nevertheless, it may be chosen as a retrofitting or strengthening solution in order to dissipate seismic energy through concrete crushing. This will contribute to protecting the steel portion of the link from extra damage. It not only prevents buckling in web but also attains up to 2 times the shear capacity of bare steel link without affecting its initial stiffness. Since increasing initial stiffness of links will increase the seismic demand for the HCW system.

In this study a new simplified FE model for such link will also be carried out in order to explore how this new beam influences the seismic performance of HCW system. With a view to ease the ability to follow the text and figures, the following abbreviations will be used: RC wall, HCW-TSCB, HCW-RSCB and HCW-RCCB for Case 1, Case 2, Case 3 and Case 4, respectively.

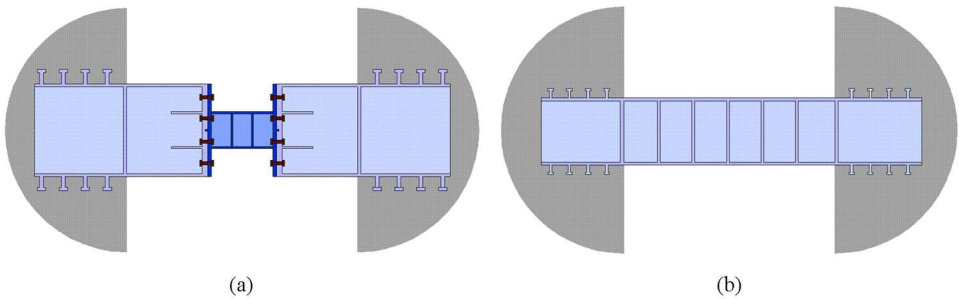


Fig. 1 - (a) Replaceable steel coupling beam (b) Typical steel coupling beam

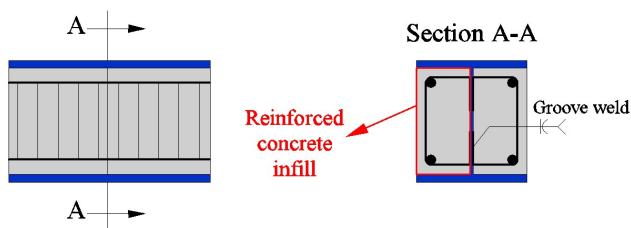


Fig. 2 - The details of using reinforced concrete infill in steel link

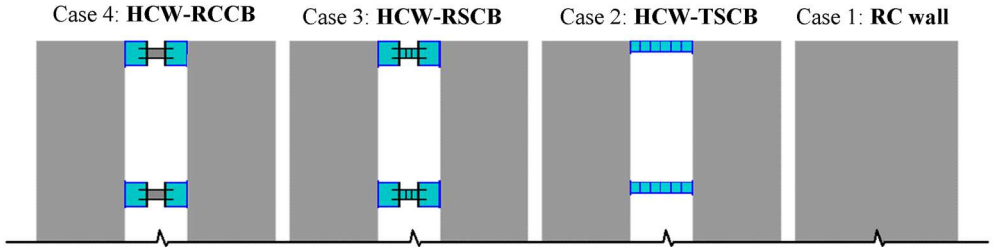


Fig. 3 - The case studies proposed for lateral force resisting system

## 2. PROTOTYPE STRUCTURE:

The prototype structure constitutes of a six-storey building; the plan is depicted in Fig. 4. The lateral resisting system is composed of four steel moment frames in the long direction and two HCW systems in the short direction. The short direction case is only considered in this study using a 2D model. Three case studies are selected to represent HCW system in addition to one case representing conventional RC wall system (RC wall) as shown in Fig. 3. First, the building is designed using HCW-RSCB case according to Euro Code8 [24]. Ground type A and peak design acceleration 0.3 g in accordance with Euro Code 8 are considered with behaviour factor  $q = 3,3$ . Dead load for all floors is assumed to be 4.4 kN/m<sup>2</sup> and 3 kN/m<sup>2</sup> for the roof. Live load for all floors is assumed to be 2 kN/m<sup>2</sup> and 1.5 kN/m<sup>2</sup> for the roof. The self-weight loads of structural elements are taken into account. The allowable drift checks are also verified according to Euro Code8 [24]. The wall pier details for all HCW cases are shown in Fig. 5-a. The original assumption is to implement similar coupling ratio for HCW-TSCB and HCW-RSCB cases. Coupling ratio (CR) is defined as the proportion of overturning moment resisted by coupling action over the overall system resistant moment stated as follows:

$$CR = \frac{L \sum V_{beam}}{L \sum V_{beam} + \sum M_w} \quad (1)$$

Where  $\sum V_{beam}$  is the accumulation of the coupling beam shears acting at the edge of one wall pier;  $L$  is the lever arm between the centroids of the wall piers, and  $\sum M_w$  is the total overturning moment resisted by the wall piers. Accordingly, given the same strength of wall piers and same distance between walls, both coupling beams of HCW-TSCB and HCW-RSCB cases should give similar shear force resistance value at the ends in order to achieve the same CR ratio. El-Tawil and Kuenzli [7] recommend that the CR ranges from 30 percent to 45 percent for an efficient design. In this research, the HCW systems are conceived to have a CR equals 40 percent. The conventional shear wall system (RC-wall) is designed to have similar lateral strength and initial stiffness as HCW-RSCB, thus it has similar fundamental period as HCW-RSCB. RC-wall details are shown in Fig 5-b. The steel stiffeners of steel link are designed in accordance with Euro Code8 [24] guidelines with 10 mm thickness. In HCW-RCCB, a high confined concrete fills the inner space of HCW-RSCB link instead of steel stiffeners. The inner reinforced concrete of this case is composed of (characteristic compressive strength  $f_{ck}=25$  MPa) concrete and (characteristic yield stress  $f_{yk}=400$  MPa)

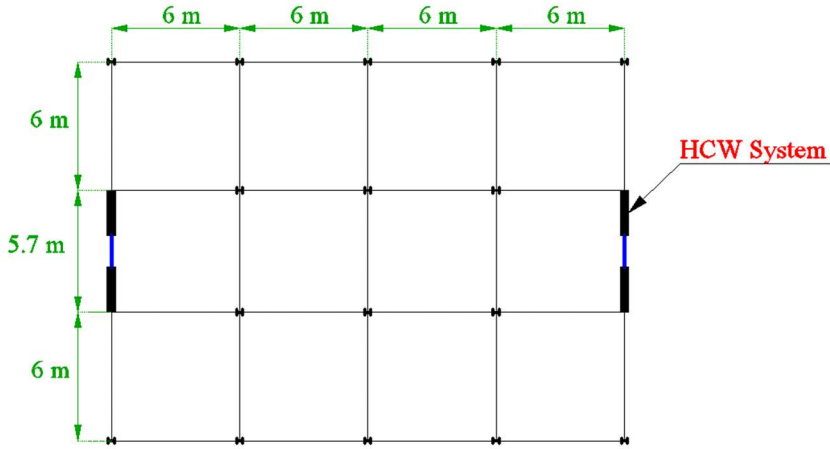


Fig. 4 - Plan configuration of the prototype structure

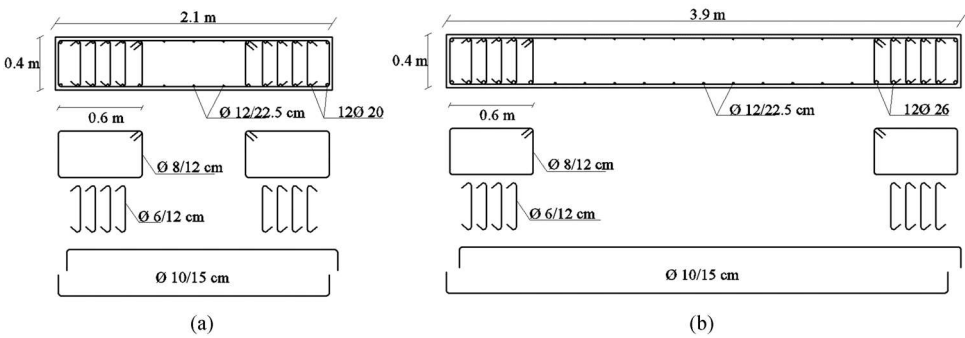


Fig. 5 - Arrangement of wall reinforcement: (a) Wall piers of HCW system (b) RC wall

for both longitudinal and transverse reinforcements. The coupling beam configurations used in this study are depicted in Fig. 6; and additional details of steel and composite links are portrayed in Fig. 7. The links of HCW-RSCB and HCW-RCCB have been previously tested by Shayanfar et al. [27] to be used in eccentrically braced frames. Based on Ji et al. [25], the links with a length ratio  $e/(M_p/V_p)$  less than 1 are assumed to be classified as very short links with a maximum link angle rotation which equals 0.11 rad. Therefore, this value will be adopted for the links in HCW-RSCB. As consequence of the Shayanfar et al. [27] study, using steel profiles partially embedded in concrete does not affect rotation capacity of the original steel beam section. Thus, the same 0.11 rad value is adopted as maximum rotation capacity for the composite link. The properties of utilized links and fundamental periods T1 for all cases are reported in Table1. The embedded profiles are designed to transfer maximum probable shear and moment forces resulting in the coupling links without exceeding the yielding limit. The embedded profiles are equipped with sufficient shear studs and can fulfil rigid connection with the wall. They are made of S355 steel ( $f_y = 355$  MPa). C30 concrete ( $f_{ck}=30$  MPa) and B450C reinforcements ( $f_{yk}=450$  MPa) are used for concrete and rebars in

all RC walls. Reinforcement bars are designed according to the DCM (medium ductility class) rules stated in Euro Code 8 [24], Clause 5.4.3.4 for ductile walls. The link is connected to beam segments using the end-plate connection with high-strength bolts and shear keys. This connection is designed such that the shear force is resisted by shear keys and the bending moment is resisted by the bolts.

Table 1 - Fundamental periods and Coupling beams links properties

	T1 (sec)	Link Length (m)	Link cross section (mm)	Fy (Flange, Web) (Mpa)	$e/(M_p/V_p)$	Link classification	Max angle rotation (rad)
RC wall	0.687	-	-	-	-	-	-
HCW-TSCB	0.91	1.5	IPE 270 O	(275,275)	3.91	Long	0.02
HCW-RSCB	0.688	0.4	Built up (240,6,220,15)	(300,249)	0.35	Very Short	0.11
HCW-RCCB	0.67	0.4	Built up (240,6,220,15) + RC infill	(300,249)	0.68	Very Short	0.11

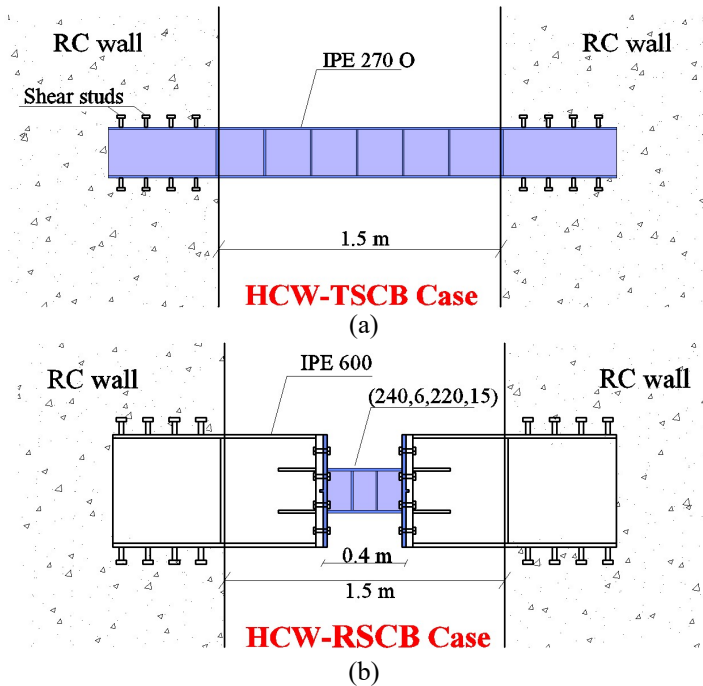
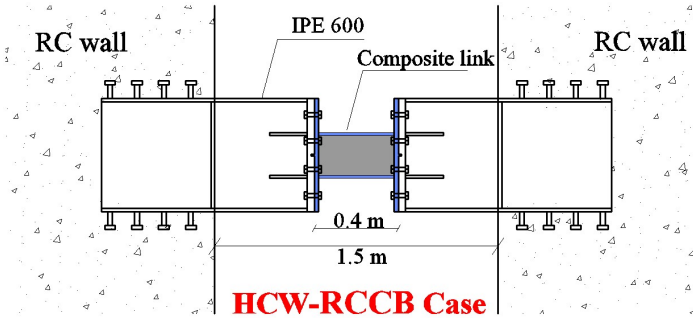


Fig. 6 - Adopted coupling beams configurations: (a) Typical steel coupling beam (HCW-TSCB), (b) Replaceable steel coupling beam RSCB (HCW-RSCB), (c) Replaceable composite coupling beam RCCB (HCW-RCCB)



(c)

Fig. 6 (Cont.) - Adopted coupling beams configurations: (a) Typical steel coupling beam (HCW-TSCB), (b) Replaceable steel coupling beam RSCB (HCW-RSCB), (c) Replaceable composite coupling beam RCCB (HCW-RCCB)

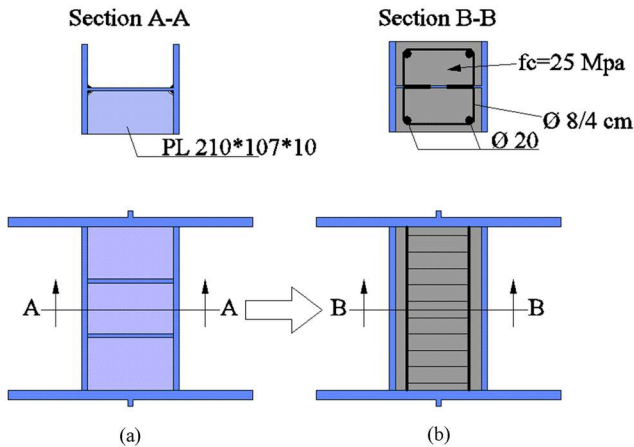


Fig. 7 - Arrangement of: (a) Steel link of HCW-RSCB, (b) Composite link of HCW-RCCB

### 3. NUMERICAL MODEL SPECIFICATIONS

#### 3.1. Steel Coupling Beams Modelling:

The frame model with lumped plasticity model proposed by Bosco et al. [28] will be adopted to represent the steel coupling link. This model is derived from the elasto-plastic model introduced by Zona and Dall'Asta [29] and implemented in OpenSees software [30]. The schematic shape of this model is illustrated in Fig. 8-a. The elasto-plastic model presented by Zona and Dall'Asta [29] needs the following parameters: initial stiffness, yielding force, maximum force for asymptotically fully developed hardening, post-elastic stiffness, elastic-to-plastic transition shape parameter  $\alpha$ , hardening rate parameter  $\delta r$ . The initial stiffness  $k_0$ , yield and maximum flexural and shear forces are obtained from the cross section properties of the link. The other parameters are calibrated based on experimental responses and three-

dimensional finite-element simulations. The steel link used in HCW-RSCB is experimentally studied by Shayanfar et al. [27] to be used in EBF system. It will be used for the elastic-plastic OpenSees model validation due to displacement history shown in Fig. 8-b. The results indicate a very acceptable performance with OpenSees model as shown in Fig. 9. Guiding lines are used in order to indicate the initial stiffness for each case. The initial stiffness of this model will be rearranged in order to accommodate the real behaviour of the link which is investigated in this study. However, by applying a simple sub-study using nonlinear pushover analysis and eigenvalue analysis, it could be easily concluded that even the high variation in link initial stiffness value (up to 30 percent) cannot make a substantial effect in structure response. For the long link type representing the HCW-TSCB case, there are no experimental investigations. Therefore, a complex 3D numerical simulations will be carried out using Abaqus software[31] in order to validate OpenSees modelling of this case due to displacement history shown in Fig. 8-b. The results indicate very acceptable performance as shown in Fig. 10.

The link resistance is terminated in the model when its rotation exceeds the allowed values reported in Table 1. This procedure represents the actual response of the system under extreme seismic events. Hence, once a link fails, the shear force will be redistributed among the rest of the links.

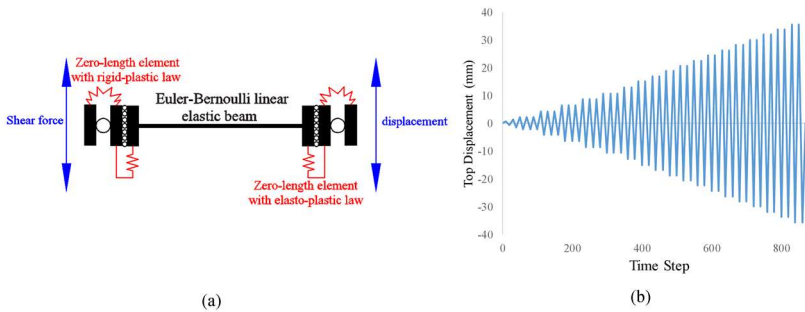


Fig. 8 - (a) Frame element model of the steel link (b) Displacement history

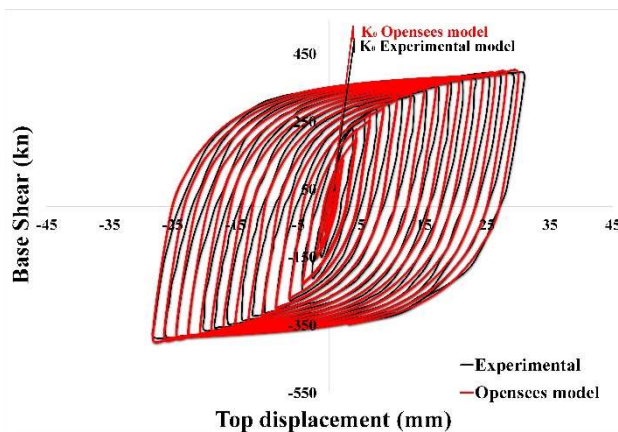


Fig. 9 - Comparison between the responses of experimental test and simplified FE model for the steel link of HCW-RSCB case

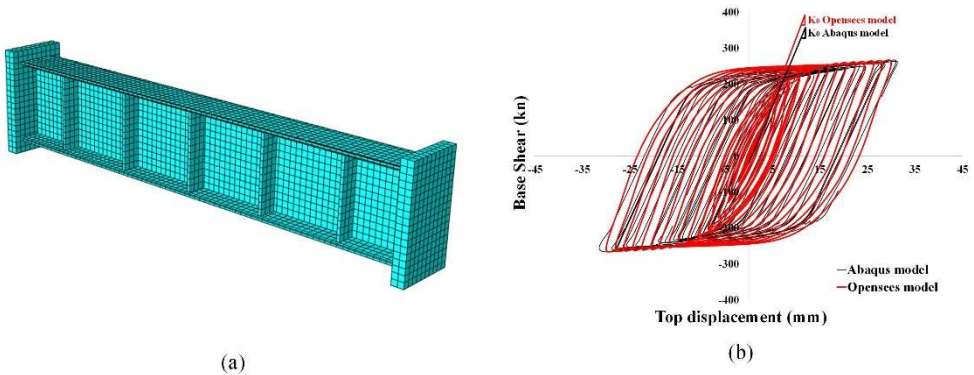


Fig. 10 - Link of HCW-TSCB case (a) ABAQUS simulation (b) Comparison between the responses of ABAQUS model and simplified FE model

### 3.2. Composite Coupling Beams Modelling

Steel profiles partially embedded in concrete are usually used in columns and rarely in beams. There is a lack of investigations concerned with using such components to serve as shear critical elements. Therefore, there is no finite element model in the literature to represent such elements so far. However, in order to estimate the effect of such element in HCW system, a correct model is extremely needed. Here, the attempt is done to create rational simplified model, taking advantage of similar structures concept such as (concrete-filled steel moment frame)[32] and (composite panel zone in composite moment frames)[33]. By observing the experimental results of the Shayanfar et al.[27] test program, it can be concluded that the final behaviour of the composite link is simply a contribution of the bare steel link and the confined concrete segment. The steel link can be presented by the Bosco et al. [28] model without considering moment behaviour to enhance the stability of the model analysis. This assumption could be accepted since the model behaviour will be governed by shear force as the  $\epsilon/(M_p/V_p)$  ratio is much lower than 1.6, and the steel link will not experience plastic yielding under moment. Based on the experimental test of this link [27], the results show diagonal cracks in concrete with inclination at approximately 30 degrees, which indicates the main direction of concrete strut efficiency. Therefore, firstly two pinned stiff elastic elements should be modelled to represent the flanges restriction of concrete strut without impacting the shear capacity. The second step is to determine concrete strut dimensions. For this purpose, the inner concrete is divided into three regions: unconfined, partially confined and highly confined concrete as presented in Fig. 11-a. Concrete02 material is used to represent strut concrete. The stress-strain relation of concrete is described using Mander et al. [34], Denavit et al. [35] and Paulay et al. [36] studies. Afterwards, an equivalent highly confined concrete cross section is adopted to express a unified behaviour of internal concrete Fig. 11-b. The two sides of concrete parts are assembled to express first the concrete strut dimension. To conclude the second strut dimension, the inner concrete compression strut relations of composite panel zone reported by ASCE Task Committee [33] are used in this case boundary conditions. It is concluded



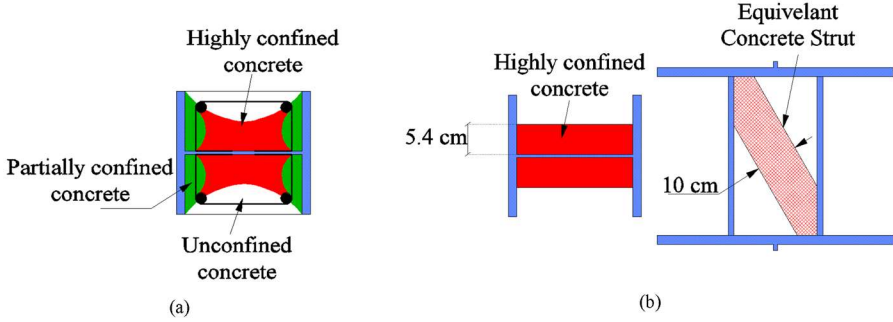


Fig. 11 - (a) The confinement zones, (b) Concrete Strut dimensions

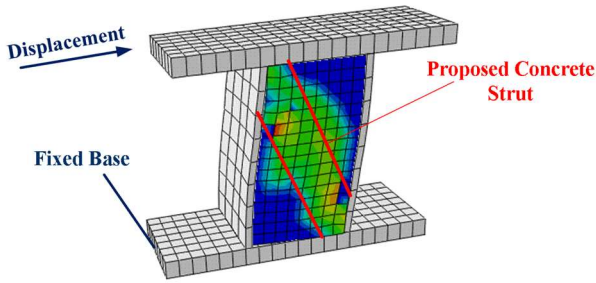


Fig. 12 - ABAQUS simulation of the composite link case and compression damage contours of the inner concrete

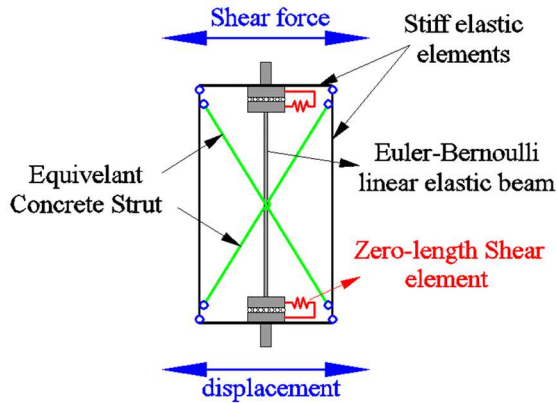


Fig. 13 - Proposed simplified finite element model of composite link



that the strut width equals approximately one quarter of strut length value. In order to assure this conclusion, a refined Abaqus model of the composite link is carried out; Fig. 12 shows the contours of compression damage in concrete. It indicates good agreement with the calculated value of strut width as well as the inclination angle shown in the empirical observations. The displacement-based distributed-plasticity fibre frame element available in OpenSees is used to describe the axial behaviour of concrete struts. Finally, the proposed resulted model (Fig. 13) is validated against experimental hysteresis diagram presented by Shayanfar et al [27] investigation as shown in Fig. 14. It illustrates sufficient reliance to be utilized in final HCW system model. The initial stiffness value of this model is rearranged in order to accommodate the real behaviour of a coupling beam which is investigated in this study.

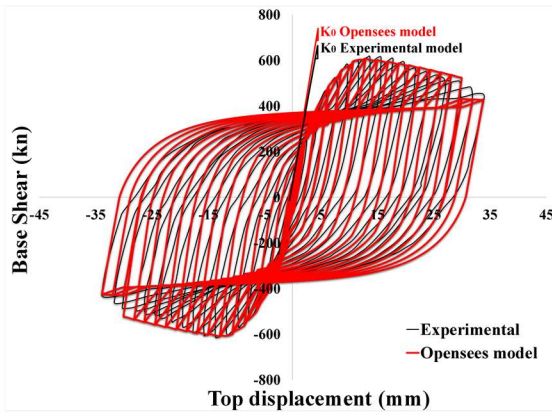


Fig. 14 - Comparison between the responses of experimental test and simplified FE model for the composite link of HCW-RCCB case

### 3.3. Modelling of RC Wall and HCW Systems:

Multi-layered shell element is selected to express the RC shear walls. This method has been previously verified by Lu. et al. [37] and Ji. et al. [38]. The results indicate highly acceptable agreement with the experimental response. Lu et al. [37] applied it in OpenSees program. Concrete is represented by multi-layered elements, Fig. 15a[37]. The damage mechanics concept and fixed smeared crack model are the basis of the nonlinearity of the concrete in a plane stress state of the multi-layered model. The confined concrete at boundary elements is represented by the Saatcioglu–Razvi model [39]. Kent–Park model [40] defines the uniaxial stress-strain of unconfined concrete relation. The Giuffre–Menegotto–Pinto steel model [41] represents the uniaxial stress-strain relation for structural steel and rebars. The truss elements represent the longitudinal rebars in boundary elements. Equivalent smeared rebar layers in vertical and horizontal directions define the internal longitudinal and horizontal reinforcement, Fig. 15b[37]. The embedded beam elements are designed to remain elastic under earthquake, thus they are modelled by elastic column-beam element produced by OpenSees. A zero-length shear element should be set between the link and the embedded beam elements as shown in Fig. 16 to represent elastic shear stiffness which equals  $GA_w/l_b$ ; where  $G$  represents shear modulus and  $A_w$ ,  $l_b$  denote web area and length of the expanded

beam, respectively [23]. Rayleigh damping model for the first and second vibration modes is used in analysis with a damping ratio of 5 percent. A gravity column is modelled in order to assign superimposed permanent live and dead loads of each floor. It is joined to the original system using pinned rigid beams. Self-weight mass is lumped at both ends of each element.

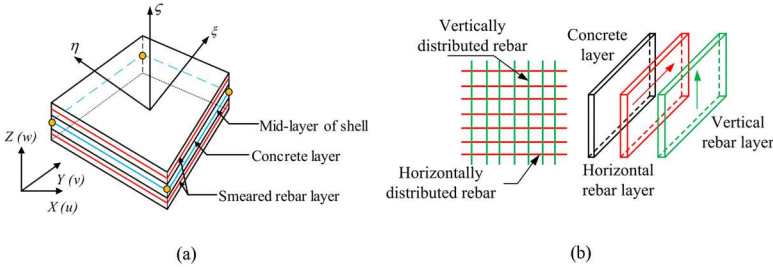


Fig. 15 - Sketch of multi-layer shell element for RC wall (Lu et al. [37])

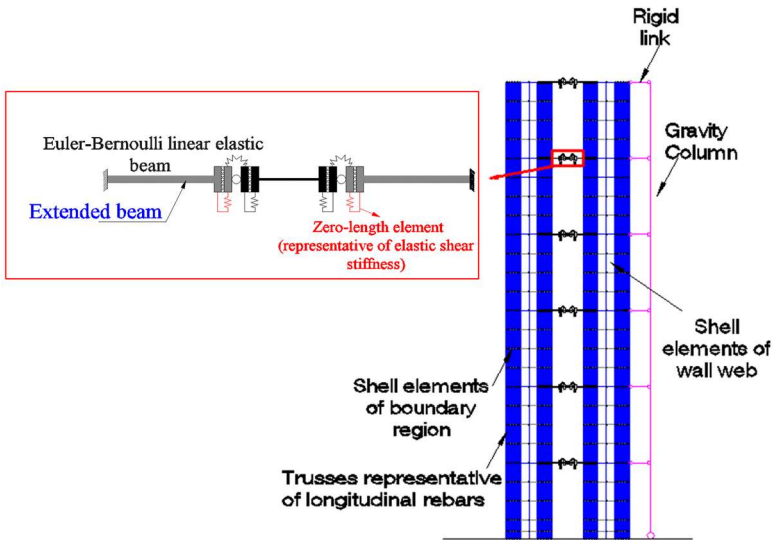


Fig. 16 - Finite element modelling for HCW system with replaceable steel coupling beam (HCW-RSCB case)

#### 4. NONLINEAR DYNAMIC ANALYSIS AT VARIOUS TARGET SPECTRA

A set of 30 natural ground motion records are chosen using Pacific Earthquake Engineering Research (PEER) NGA database [42] with far-field type in accordance with soil type A. These records are scaled to fit in average the Euro Code 8 elastic spectrum with ground acceleration 0.3 g and soil type A. These ground motions are provided in Table 2.

Three levels of ground motion intensities are adopted to study the dynamic response of prototype structures. The first is representing DBE design basis earthquake level with 10 percent probability of exceedance in 50 years and a return period equal to 475 years. The

second is computed for ground motion earthquake with 2 percent probability of exceedance in 50 years and a return period equal to 2475 years. The third is computed for ground motion earthquake with a 0.5 percent probability of exceedance in 50 years and a return period equal to 9975 years. The last two levels are estimated based on Euro Code 8 recommendation paragraph 3.2.1 (3)P [24] to represent maximum credible earthquake MCE and very rare earthquake VRE. Fig. 17 shows acceleration response spectra of the adopted 30 records with geometric mean and the target spectra of the three levels of ground motion intensities.

Table 2 - The ground motions utilized in nonlinear dynamic analysis

No.	Event	Year	Station	Mw	PGA(g)
1	San Fernando	1971	Cedar Springs_ Allen Ranch	6.61	0.32
2	Loma Prieta	1989	Piedmont Jr High School Grounds	6.93	0.34
3	Loma Prieta	1989	SF - Rincon Hill	6.93	0.32
4	Loma Prieta	1989	So. San Francisco_ Sierra Pt.	6.93	0.24
5	Chi-Chi_ Taiwan	1999	TTN042	7.62	0.26
6	Chi-Chi_ Taiwan-03	1999	TCU085	6.2	0.25
7	Chi-Chi_ Taiwan-03	1999	TTN042	6.2	0.32
8	Chi-Chi_ Taiwan-04	1999	HWA002	6.2	0.24
9	Chi-Chi_ Taiwan-04	1999	TTN042	6.2	0.32
10	Chi-Chi_ Taiwan-05	1999	HWA002	6.2	0.34
11	Chi-Chi_ Taiwan-05	1999	ILA015	6.2	0.36
12	Chi-Chi_ Taiwan-05	1999	TAP075	6.2	0.28
13	Chi-Chi_ Taiwan-05	1999	TAP086	6.2	0.34
14	Chi-Chi_ Taiwan-05	1999	TTN042	6.2	0.44
15	Chi-Chi_ Taiwan-06	1999	CHY102	6.3	0.34
16	Chi-Chi_ Taiwan-06	1999	ILA015	6.3	0.26
17	Chi-Chi_ Taiwan-06	1999	ILA063	6.3	0.39
18	Chi-Chi_ Taiwan-06	1999	TAP086	6.3	0.26
19	Chi-Chi_ Taiwan-06	1999	TCU085	6.3	0.31
20	Chi-Chi_ Taiwan-06	1999	TTN042	6.3	0.26
21	Tottori_ Japan	2000	HYG004	6.61	0.33
22	Chuetsu-oki_ Japan	2007	FKSH15	6.8	0.43
23	Chuetsu-oki_ Japan	2007	NGN013	6.8	0.41
24	El Mayor-Cucapah_ Mexico	2010	El Monte County Park	7.2	0.54
25	El Mayor-Cucapah_ Mexico	2010	San Diego Road Dept	7.2	0.36
26	Tottori_ Japan	2000	KOC008	6.61	0.59
27	Tottori_ Japan	2000	KYT005	6.61	0.25
28	Tottori_ Japan	2000	SMN013	6.61	0.34
29	Niigata_ Japan	2004	FKSH15	6.63	0.45
30	Niigata_ Japan	2004	YMTH03	6.63	0.40

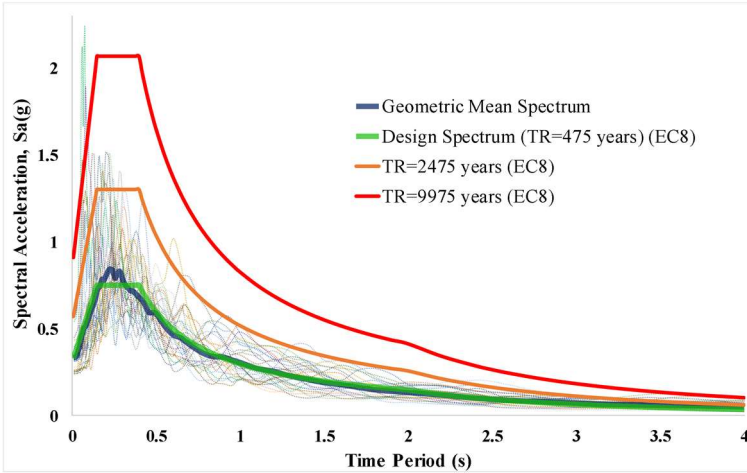


Fig. 17 - Target spectra and response spectra of the 30 scaled ground motion records

The maximum responses for each accelerogram are defined, then the mean values of the responses are presented. The lateral displacements, inter-storey drifts and links rotations normalized with respect to rotation capacity values are provided in Fig. 18 for the three earthquake intensity levels. Taking into consideration the analysis results, the conclusions below can be derived:

- Under TR=475 years (intensity level DBE), using replaceable steel and composite beams shows relatively similar lateral displacement demand. In the case of composite coupling beams, the inter-storey drifts tend to be uniform. In terms of links rotations, composite links demonstrate considerably lower rotation demand than the steel links with minimal values in the last storey. In comparison with typical steel coupling beam case, the inter-storey drift in the last storey of composite links case attains a reduction of 28 percent, and steel links case attains 25 percent reduction. Despite the high stiffness of the conventional wall system, all cases can achieve lower inter-storey drifts because of the high energy dissipation of HCW systems compared with bare RC wall system.

- Under TR=2475 years (intensity level MCE), both steel and composite links cases show similar behaviour. In comparison with typical steel coupling beam case, the inter-storey drift in the last storey of composite links case attains 15.4 percent reduction, and steel links case attains 13.8 percent reduction. In terms of links rotations, composite links still demonstrate lower rotation demand than the bare steel links with minimal values in the last storey.

- Under TR= 9975 years (intensity level VRE), all cases indicate similar displacement demand. It is worth mentioning that rotation demand values of the three cases are still lower than their rotation capacities.

For the purpose of estimating the seismic demand of the case studies, an incremental dynamic analysis (IDA) using (Base shear-  $S_a(T1)$ ) relation is performed for each record then the mean values are depicted in Fig. 19. The range of  $S_a(T1)$  scaling factors used in IDA analysis is from 0.02 to 1.3 with 0.03 interval value. Such analysis can illustrate the seismic force

demand of each case. This will provide indications of required shear and flexural reinforcements as well as substructures design complications such as designing of foundations against uplift which is considered a quite perilous issue in such kind of systems.

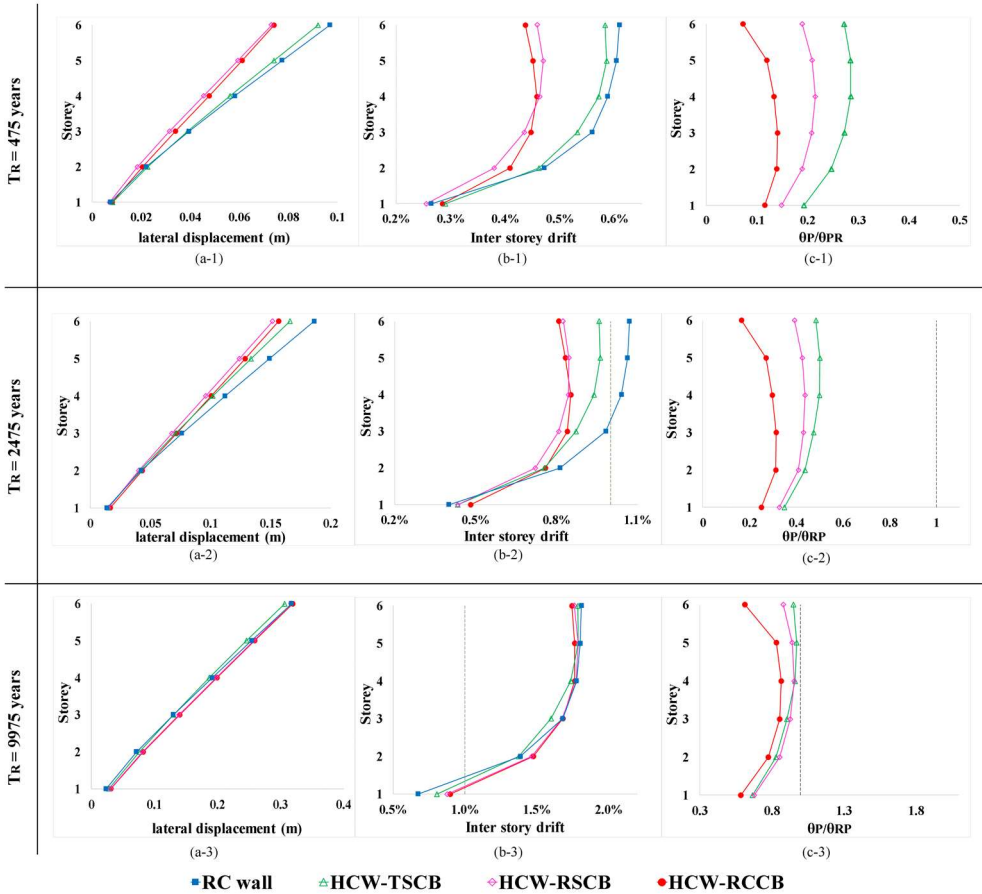


Fig. 18 - Mean over 30 accelerograms for all case studies (a) Lateral displacement (b) Inter-storey drifts (c) Links rotation demand normalized with respect to links rotation capacity

The vertical lines shown in Fig. 19 demonstrate the values of spectral accelerations at fundamental periods of each case. These lines are presented for the three seismic intensity levels illustrated previously. HCW-TSCB always has the lowest spectral acceleration value because it has the highest fundamental period among the case studies.

The results show that seismic demand values under DBE level for all cases are approximately comparable. Under extreme events (MCE and VRE levels), it should be noted that RC wall

system demonstrates the highest seismic demand values while the typical coupling beam case shows the lowest ones. It is worth noting that despite the large shear force capacity shown by composite links, the seismic demand of HCW-RCCB has values close to the bare steel link case (HCW-RSCB) values under DBE and MCE levels; and smaller values than HCW-RSCB case under VRE level. This indicates that using composite links method will not require extra design detailing for wall piers and foundations.

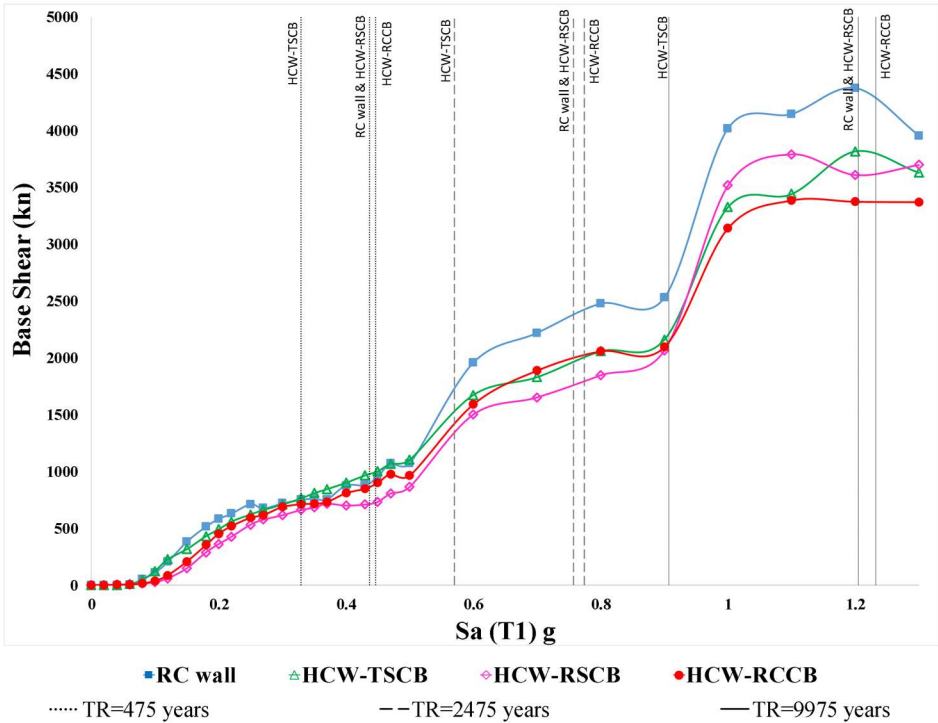


Fig. 19 - Mean over 30 accelerograms for nonlinear incremental dynamic analysis (IDA)

With a view to further explore the seismic performance of case studies, the mean residual storey drifts are reported in Table 3. Based on FEMA P-58 [43] recommendation, 0.2 percent expresses the limit value of residual storey drift below which no structural realignment is necessary for structural stability (however, the building may require adjustment and repairs to non-structural and mechanical components that are sensitive to building alignment (e.g., elevator rails, curtain walls, and doors)). It is noted that all results are far below 0.2 percent limit value for all cases and seismic intensity levels.

Nevertheless, the residual storey drift value can be a good indicator for self-centering capacity of the adopted systems. In this regard, using composite links may provide better centering capacity than the bare steel link under MCE level. Furthermore, using HCW system produces significant self-centering capacity compared with the conventional shear wall system under DBE and MCE levels.

Table 3 - Mean values of residual storey drifts percent

	TR=475 years	TR=2475 years	TR=9975 years
RC wall	0.014	0.067	0.142
HCW-TSCB	0.010	0.035	0.156
HCW-RSCB	0.008	0.039	0.144
HCW-RCCB	0.008	0.035	0.144

## 5. FRAGILITY ANALYSIS

Fragility assessment has usually been used for performance-based earthquake purposes in order to predict the probability of exceedance of structural damage as a function of earthquake motion intensity. Generally, the damage level in certain structural element or whole structure is expressed by a damage index like element rotation value or IDR (inter storey drift). The approach to describe motion intensity is usually accomplished by using ground motion indices, such as PGA (peak ground acceleration), peak ground velocity or spectral acceleration at the fundamental period of the building,  $S_a(T1)$ . In accordance with the fact that fragility curve formation using  $S_a(T1)$  measure is more efficient than PGA; and allows lower limit of uncertainty when assessing the drift response (Iervolino and Manfredi) [44], it will be employed in this study.

To build fragility curves, there is a necessity to clearly determine damage states, which are defined as threshold levels of damage sustained by structural components. To this end, the damage states that are defined by the FEMA P-58 for slender RC shear walls [45] and links in the EBFs [46] will be used to express corresponding damage state of RC wall piers and typical steel coupling beams. The demand parameter of typical links is taken as plastic link rotation, whereas for slender RC wall, the demand parameter will be expressed by effective wall drift as defined by FEMA P-58[45]. In case of very short replaceable steel links, the damage parameter is total link rotation and the damage states that are concluded from the tests performed by Ji et al. 2017[47]. In the case of composite links, the basic segment is imposed to be the steel link and the concrete part damage will not be taken into account. Based on Shayanfar et al. [27] results, where concrete portion does not affect damage sequence of the steel link; the same fact is supposed to be true in the situation of this research. Subsequently, the similar damage parameter and damage states of the very short steel link will be adopted for the case of the composite link.

In order to provide fragility data of RC slab above the RSCB element, the parameters suggested by Ji. et al. 2017 [47] will be used for HCW-RSCB and HCW-RCCB cases. Since there is no data in the literature about the slab fragility in case of using long links (HCW-TSCB), it will not be considered in this study. However, the RC slab in such case seems to suffer minimal damage when be compared with other cases because of low rotation demand values obtained in coupling beams. Table 4 provides a summary of the median values, dispersions related to the RC wall and links fragility, damages description and associated repair methods.

Fragility curves produced in this investigation rely on lognormal cumulative distribution, the mathematical relation of fragility function is reported in Eq.2

$$F(D) = \Phi \left( \frac{\ln(D/\theta)}{\beta} \right) \tag{2}$$

Where D is demand parameter.  $\Phi$  is cumulative lognormal function.  $\theta$  is median of damage limit states.  $\beta$  is the logarithmic standard deviation. It involves the participation of record-to-record demand variability and the uncertainty related to component capacity.

The resulting fragility curves are plotted in Figures 20-23 for all aforementioned limit states. The links are numbered based on storey number.

Table 4 - Structural elements fragility data

Structural component	Damage state	Damage parameter	Fragility data		Damage discription	Repair method
			Median	Dispersion		
Wall	DS1	Effective wall drift	0.118 <i>percent</i>	0.762	Formation of initial cracking.	Cosmetic repair
	DS2		0.927 <i>percent</i>	0.476	Spalling of concrete cover	Inject cracks with epoxy and replace finishes
	DS3		1.28 <i>percent</i>	0.341	Exposure of longitudinal wall reinforcement	Patch spalled concrete, epoxy inject cracks and replace finishes
	DS4		1.86 <i>percent</i>	0.441	Crushing of concrete	Replacement of the wall or concrete jacketing
Long link	DS2	Plastic rotation (rad)	0.010	0.58	Flange local buckling	Heat straightening
	DS3		0.018	0.48	Flange fracture or Lateral torsional buckling	Link replacement
Very Short Link	DS1	Total rotation (rad)	0.05	0.3	Substantial slab damage	Cosmetic repair or Injection of epoxy or Replacement of the local slab above the RSCB
	DS2		0.09	0.19	Buckling of the web or flanges in the shear link	Heat straightening buckled elements or replacement of shear link.
	DS3		0.11	0.15	Fracture of the web in the shear link or fracture of the link flange-to-end plate welds.	Link replacement



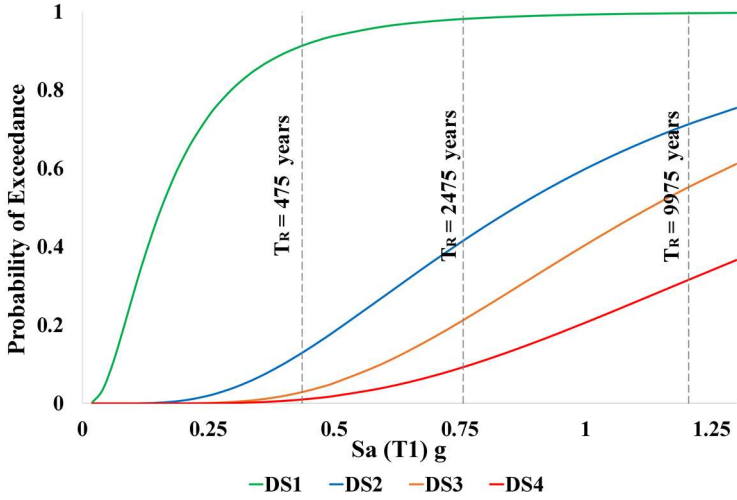


Fig. 20 - Fragility curves of the wall of RC wall case

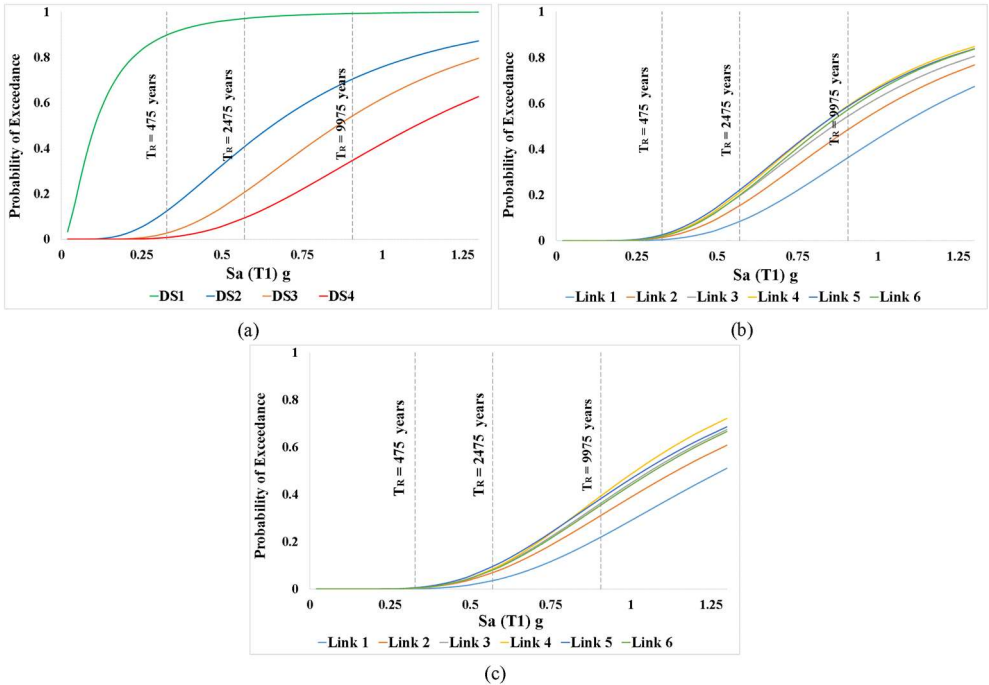


Fig. 21 - Fragility curves for HCW-TSCB case: (a) Wall piers (b) DS2 performance level for all links (c) DS3 performance level for all links

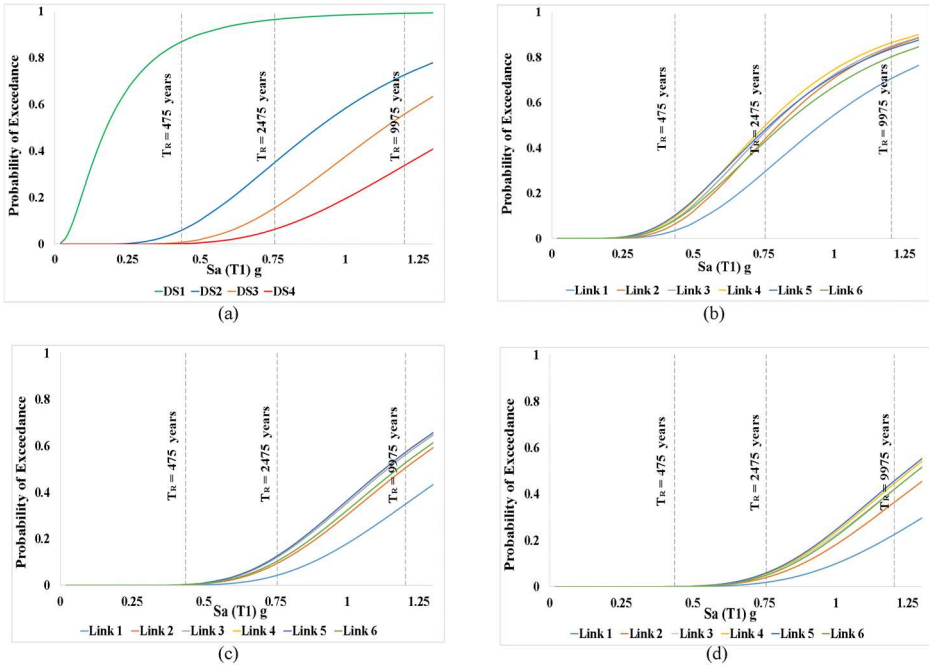


Fig. 22 - Fragility curves for HCW-RSCB case: (a) Wall piers (b) DS1 performance level for all links (c) DS2 performance level for all links (d) DS3 performance level for all links

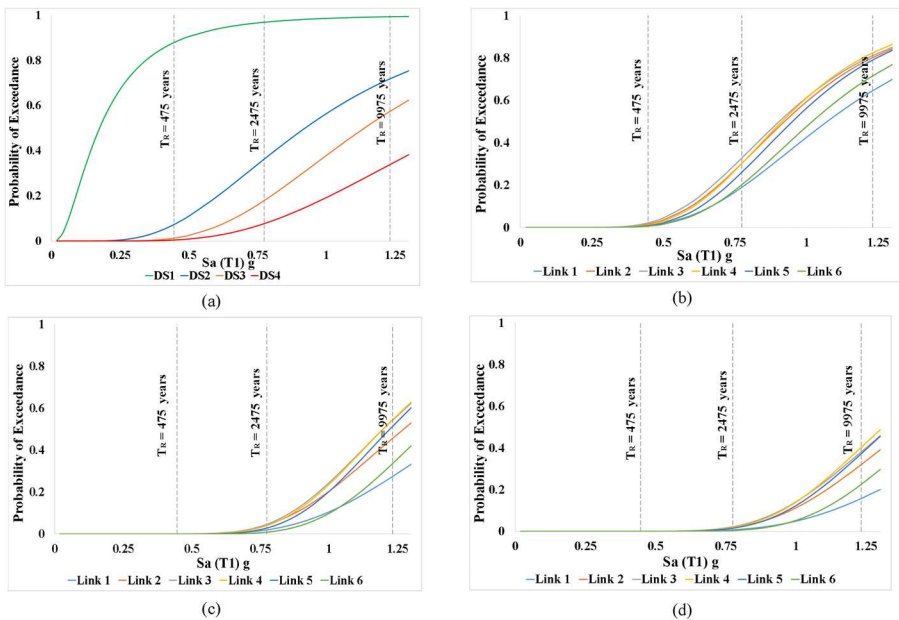


Fig. 23 - Fragility curves for HCW-RCCB case: (a) Wall piers (b) DS1 performance level for all links (c) DS2 performance level for all links (d) DS3 performance level for all links

In order to explain thoroughly fragility results and produce clear comparison between the case studies, the probability of exceedance will be determined at fixed values of the three earthquake intensity levels for all structural components and damage states. The results are plotted in Fig. 24,25 .

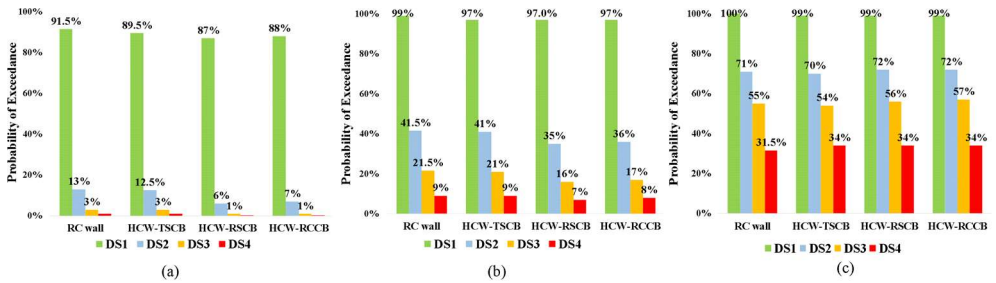


Fig. 24 - Probability of exceedance for wall damage states: (a) 475 years level, (b) 2475 years level, (c) 9975 years level

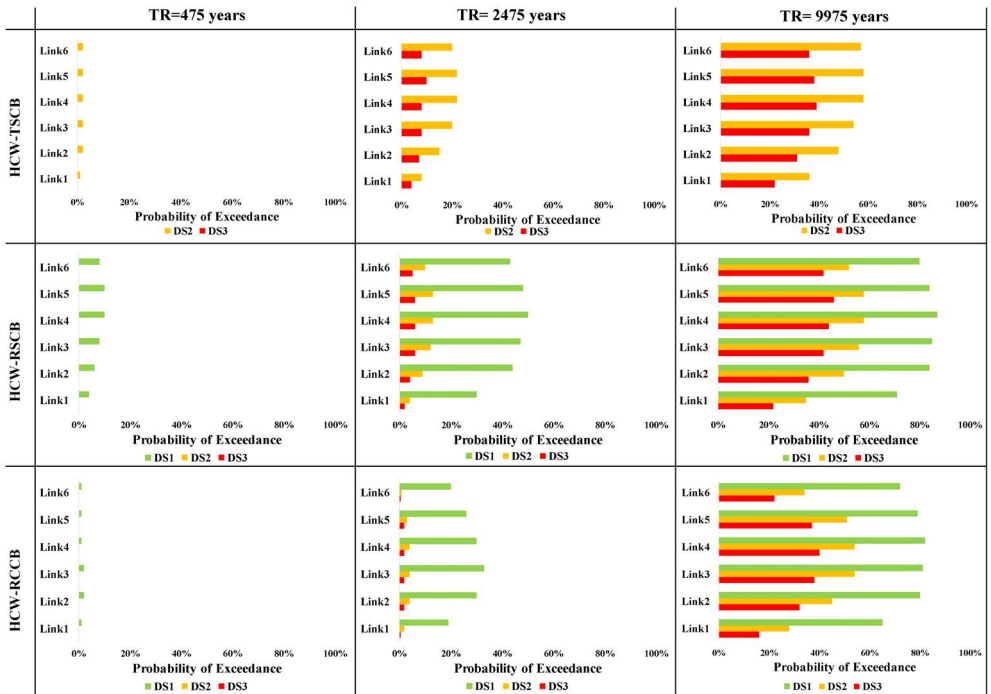


Fig. 25 Probability of exceedance for the damage states of all links

Fig. 24 indicates higher damage levels for RC wall piers in moderate-rise buildings than had been shown for high-rise buildings by Ji. et al. [23]. Using typical steel coupling beam does not show high improvement in damage resistance of RC wall piers when compared to the stiff conventional RC wall system. However, expected damage to all walls under DBE and MCE levels is limited to cracks or slight spalling of concrete. Under VRE level, exposure of longitudinal wall reinforcement and crushing of concrete may be confidently expected for both the HCW and the conventional RC wall. Using replaceable steel coupling beams shows lower values of vulnerability in RC wall piers under DBE and MCE levels. Despite the higher energy dissipation of composite links, their impact is not noted in RC wall piers. Under VRE level, all cases show a relatively similar behaviour.

In contrast to RC wall fragility data, the level of damage in links between the cases is not convergent. In accordance with Fig. 25, it is observed that all the cases indicate a limited probability of damage in links under DBE level.

- In regard to RC slab fragility, using reinforced concrete infill can achieve 83 percent, 40 percent and 7 percent lower damage probability than using steel stiffeners under DBE, MCE and VRE levels, respectively.

- Under MCE level, replaceable steel links case can achieve 43 percent and 35 percent lower damage probability than typical coupling beams case for DS2 and DS3, respectively. Using reinforced concrete infill (HCW-RCCB) presents acceptable improvement against using steel stiffeners (HCW-RSCB) with 40 percent reduction for buckling of the web damage state and 44 percent reduction for web failure damage state. The upper links in composite links case demonstrate an evident reduction in damage amount compared with middle links.

- In the case of VRE level, the variation between the performances of links is minimized. Replaceable steel links case shows very limited reduction in damage probability at DS2 level and 15 percent increase in damage probability in DS3 level compared with typical coupling beams case. Using reinforced concrete infill presents 14 percent damage reduction in buckling of the web damage state and 23 percent reduction in web failure damage state compared with using the steel stiffeners.

## **6. CONCLUSIONS:**

This study attempts to gain more insight into the (HCW) hybrid coupled wall system when different potentials of coupling beams are utilized. These possibilities include using typical steel coupling beam and the replaceable steel coupling beam (RSCB) proposed by Ji. et al.[22]. Furthermore, a novel composite shear link is proposed and modelled using the OpenSees platform by employing reinforced concrete infill rather than steel stiffeners in the inner space of steel link. A comparison with stiff bare RC wall system shows similar initial stiffness and flexural strength capacity as the HCW system with RSCB case is also carried out. An attempt has been made to accurately assess the dynamic response and to present a quantitative estimation of vulnerability of the wall and links for each case. It is assumed that all of which have identical wall pier configurations and CR coupling ratio equals 0.4. The main conclusions are listed below:

-Using reinforced concrete infill instead of steel stiffeners proves similar lateral displacement demand values and vulnerability in wall piers. However, this method does not require extra

design detailing for walls and foundations. The essential advantage of this method is the high efficiency to preserve upper RC slab and steel links maintenance than using steel stiffeners. It can achieve 40 percent lower damage probability for RC slab and steel links under the maximum credible earthquake level (MCE) compared with using the steel stiffeners.

- The RSCB case presents the least lateral displacement demand under DBE level. For extreme seismic levels, the RSCB case start behaving similar to typical steel coupling beams case. However, the RSCB method can attain 35 percent reduction in links fracture probability compared with typical steel coupling beams case under MCE seismic level. But it causes higher damage in links than typical steel coupling beams case under VRE seismic level.

- The typical steel coupling beams illustrate poor performance in terms of lateral displacement restriction at DBE level, but behaves well under extreme seismic events.

-The stiff bare RC wall reveals high lateral displacements demand for both DBE and MCE levels, whereas in terms of VRE level it has similar behaviour as other cases.

These outcomes give designers the required database to make the decision in regard of the method of construction due to their particular architectural and constructional considerations.

## **Symbols**

$A_w$	: Web area of the expanded beam
CR	: Coupling ratio
D	: Demand parameter
e	: Link length
$e_s$	: Critical length of short links
$e_L$	: Critical length of long links
$f_c$	: Concrete compressive strength
$f_y$	: Yield stress of steel
G	: Shear modulus
$K_0$	: Initial stiffness
L	: Lever arm between the centroids of the wall piers
$l_b$	: Length of the expanded beam
$\Sigma M_w$	: Total overturning moment resisted by the wall piers
$M_p$	: Plastic resistant moment of link
q	: Behaviour factor
$S_a$	: Spectral acceleration
TR	: Return period of the earthquake
$V_{beam}$	: Shear force of the beam

$V_p$	: Plastic resistant shear of link
$\beta$	: Logarithmic standard deviation
$\theta$	: Median of damage limit states
$\Phi$	: Cumulative lognormal function
EBF	: Eccentrically braced frame system
DBE	: Design basis earthquake
DCM	: Medium ductility class
DS	: Damage state
HCW	: Hybrid coupled wall
IDA	: Incremental dynamic analysis
MCE	: Maximum credible earthquake
PEER	: Pacific Earthquake Engineering Research
PGA	: Peak ground acceleration
RCCB	: Replaceable composite coupling beam
RCW	: Reinforced concrete wall
RSCB	: Replaceable steel coupling beam
TSCB	: Typical steel coupling beam
V-EBF	: Eccentrically braced frames with vertical link
VRE	: Very rare earthquake

### References

- [1] Harries, K.A., Gong, B., Shahrooz, B.M., Behavior and design of reinforced concrete, steel, and steel-concrete coupling beams, *Earthquake Spectra*, 16, 4, 775-800, 2000.
- [2] El-Tawil, S., Harries, K.A., Fortney, P.J., Shahrooz, B.M., Kurama, Y., Seismic design of hybrid coupled wall systems: state of the art, *Journal of structural engineering*, 136, 7, 755-69, 2010.
- [3] Hajjar, J.F., Composite steel and concrete structural systems for seismic engineering, *Journal of Constructional Steel Research*, 58, 5-8, 703-23, 2002.
- [4] Harries, K.A., Mitchell, D., Cook, W.D., Redwood, R.G., Seismic response of steel beams coupling concrete walls, *Journal of Structural Engineering*, 119, 12, 3611-29, 1993.
- [5] Park, W.-S., Yun, H.-D., Seismic behaviour of coupling beams in a hybrid coupled shear walls, *Journal of Constructional Steel Research*, 61, 11, 1492-524, 2005.
- [6] Shahrooz, B.M., Remmetter, M.E., Qin, F., Seismic design and performance of composite coupled walls, *Journal of Structural Engineering*, 119, 11, 3291-309, 1993.

- [7] El-Tawil, S., Kuenzli, C.M., Pushover of hybrid coupled walls. II: Analysis and behavior, *Journal of Structural Engineering*, 128, 10, 1282-9, 2002.
- [8] El-Tawil, S., Kuenzli, C.M., Hassan, M., Pushover of hybrid coupled walls. I: Design and modeling, *Journal of Structural Engineering*, 128, 10, 1272-81, 2002.
- [9] Fortney, P.J., Shahrooz, B.M., Rassati, G.A., Seismic performance evaluation of coupled core walls with concrete and steel coupling beams, *Steel and Composite Structures*, 7, 4, 279-301, 2007.
- [10] Gong, B., Shahrooz, B.M., Steel-concrete composite coupling beams—behavior and design, *Engineering Structures*, 23, 11, 1480-90, 2001.
- [11] Gong, B., Shahrooz, B.M., Concrete-steel composite coupling beams. I: Component testing, *Journal of Structural Engineering*, 127, 6, 625-31, 2001.
- [12] Gong, B., Shahrooz, B.M., Concrete-steel composite coupling beams. II: Subassembly testing and design verification, *Journal of Structural Engineering*, 127, 6, 632-8, 2001.
- [13] Gong, B., Shahrooz, B.M., Gillum, A.J., Cyclic response of composite coupling beams, *Special Publication*, 174, 89-112, 1998.
- [14] Harries, K.A., McNeice, D.S., Performance-based design of high-rise coupled wall systems, *The Structural Design of Tall and Special Buildings*, 15, 3, 289-306, 2006.
- [15] Harries, K.A., Mitchell, D., Redwood, R.G., Cook, W.D., Nonlinear seismic response predictions of walls coupled with steel and concrete beams, *Canadian Journal of Civil Engineering*, 25, 5, 803-18, 1998.
- [16] Shahrooz, B.M., Deason, J.T., Tunc, G., Outrigger beam–wall connections. I: component testing and development of design model, *Journal of Structural Engineering*, 130, 2, 253-61, 2004.
- [17] Shahrooz, B.M., Gong, B., Tunc, G., Deason, J.T., An overview of reinforced concrete core wall–steel frame hybrid structures, *Progress in Structural Engineering and Materials*, 3, 2, 149-58, 2001.
- [18] Shahrooz, B.M., Tunc, G., Deason, J.T., Outrigger beam–wall connections. II: subassembly testing and further modeling enhancements, *Journal of Structural Engineering*, 130, 2, 262-70, 2004.
- [19] Doran, B., Polat, Z., A proposal for estimation of coupling beam stiffness of shear walls, *IMO, Teknik Dergi*, 10, 3, 1973-82, 1999.
- [20] Fortney, P.J., Shahrooz, B.M., Rassati, G.A., Large-scale testing of a replaceable “fuse” steel coupling beam, *Journal of structural engineering*, 133, 12, 1801-7, 2007.
- [21] Christopoulos, C., Montgomery, M., Viscoelastic coupling dampers (VCDs) for enhanced wind and seismic performance of high-rise buildings, *Earthquake Engineering & Structural Dynamics*, 42, 15, 2217-33, 2013.
- [22] Ji, X., Wang, Y., Ma, Q., Okazaki, T., Cyclic behavior of replaceable steel coupling beams, *Journal of Structural Engineering*, 143, 2, 04016169, 2017.

- [23] Ji, X., Liu, D., Sun, Y., Molina Hutt, C., Seismic performance assessment of a hybrid coupled wall system with replaceable steel coupling beams versus traditional RC coupling beams, *Earthquake Engineering & Structural Dynamics*, 46, 4, 517-35, 2017.
- [24] Standardization, E.C.f., Euro Code 8: Design of structures for earthquake resistance-part 1: general rules, seismic actions and rules for buildings, Brussels: European Committee for Standardization, 2005.
- [25] Ji, X., Wang, Y., Ma, Q., Okazaki, T., Cyclic behavior of very short steel shear links, *Journal of Structural Engineering*, 142, 2, 04015114, 2016.
- [26] Kanz, R., Schneider, B., Bouwkamp, J., Results and correlative analysis of a composite two storey eccentric braced frame, *Earthquake Engineer 10th World*, 3441, 1992.
- [27] Shayanfar, M., Barkhordari, M., Rezaeian, A., Experimental study of cyclic behavior of composite vertical shear link in eccentrically braced frames, *Steel & Composite Structures*, 12, 1, 13-29, 2012.
- [28] Bosco, M., Marino, E.M., Rossi, P.P., Modelling of steel link beams of short, intermediate or long length, *Engineering structures*, 84, 406-18, 2015.
- [29] Zona, A., Dall'Asta, A., Elastic-plastic model for steel buckling-restrained braces, *Journal of Constructional Steel Research*, 68, 1, 118-25, 2012.
- [30] Mazzoni, S., McKenna, F., Scott, M.H., Fenves, G.L., OpenSees command language manual, Pacific Earthquake Engineering Research (PEER) Center, 264, 2006.
- [31] ABAQUS, A.u.s.M.V., ABAQUS, Inc., Dassault Systèmes, USA, 2018.,
- [32] Sun, G., Chuang-Sheng, W.Y., Gu, Q., DesRoches, R., An effective simplified model of composite compression struts for partially-restrained steel frame with reinforced concrete infill walls, *Earthquake Engineering and Engineering Vibration*, 17, 2, 403-15, 2018.
- [33] ASCE Task Committee on Design Criteria for Composite Structures in Steel and Concrete, Guidelines for design of joints between steel beams and reinforced concrete columns, *Journal of Structural Engineering*, 120, 8, 2330-57, 1994.
- [34] Mander, J.B., Priestley, M.J., Park, R., Theoretical stress-strain model for confined concrete, *Journal of structural engineering*, 114, 8, 1804-26, 1988.
- [35] Denavit, M.D., Hajjar, J.F., Leon, R.T. Seismic behavior of steel reinforced concrete beam-columns and frames. In: *Structures Congress 2011*, pp. 2852-61, 2011.
- [36] Paulay, T., Priestley, M.N., *Seismic design of reinforced concrete and masonry buildings*, 1992.
- [37] Lu, X., Xie, L., Guan, H., Huang, Y., Lu, X., A shear wall element for nonlinear seismic analysis of super-tall buildings using OpenSees, *Finite Elements in Analysis and Design*, 98, 14-25, 2015.
- [38] Ji, X., Sun, Y., Qian, J., Lu, X., Seismic behavior and modeling of steel reinforced concrete (SRC) walls, *Earthquake Engineering & Structural Dynamics*, 44, 6, 955-72, 2015.



- [39] Saatcioglu, M., Razvi, S.R., Strength and ductility of confined concrete, *Journal of Structural engineering*, 118, 6, 1590-607, 1992.
- [40] Kent, D.C., Park, R., Flexural members with confined concrete, *Journal of the Structural Division*, 1971.
- [41] OpenSees Wiki. Steel02 Material-Giuffr -Menegotto-Pinto Model with Isotropic Strain Hardening. [http://OpenSees.berkeley.edu/wiki/index.php/Steel02\\_Material\\_GiuffrpercentC3percentA9-MenegottoPinto\\_Model\\_with\\_Isotropic\\_Strain\\_Hardening](http://OpenSees.berkeley.edu/wiki/index.php/Steel02_Material_GiuffrpercentC3percentA9-MenegottoPinto_Model_with_Isotropic_Strain_Hardening) [Accessed on 2019].
- [42] PEER, N. Pacific Earthquake Engineering Research Center NGA Database. 2011.
- [43] ATC. Seismic Performance Assessment of Buildings Volume 1-Methodology (FEMA P-58-1). Applied Technology Council: Redwood City, CA, 2012.
- [44] Iervolino, I., Manfredi, G. A review of ground motion record selection strategies for dynamic structural analysis. In: *Modern Testing Techniques for Structural Systems*, Springer, 2008, pp. 131-63.
- [45] Birely, A.C., Lowes, L.N., Lehman, D.E., Fragility Functions for Slender Reinforced Concrete Walls (FEMA P-58/BD-3.8.9), Federal Emergency Management Agency, Washington, DC, 2011.
- [46] Gulec, C.K., Gibbons, B., Chen, A., Damage States and Fragility Functions for W-Shape Steel Link Beams in Eccentrically Braced Frames (FEMA P-58/BD-3.8.5), Federal Emergency Management Agency, Washington, DC, 2010.
- [47] Ji, X., Wang, Y., Zhang, J., Okazaki, T., Seismic behavior and fragility curves of replaceable steel coupling beams with slabs, *Engineering Structures*, 150, 622-35, 2017.



# **Investigating the Service Quality of Kocaeli Tram Service Using Artificial Neural Networks**

**Selim DÜNDAR<sup>1</sup>**

## **ABSTRACT**

Service quality is one of the main issues of today's world. Firms operating in the passenger transportation sector are also trying to improve the quality of the services they provide to their passengers. It is crucial to determine the passenger service quality perceptions and priorities to evaluate and improve the service in this context. In this study, Kocaeli tram user service quality perceptions have been evaluated by applying a survey consisting of 20 questions and user satisfaction levels from different service dimensions. Then, an artificial neural network model was developed using the demographic data of the users and their responses to the survey questions to mimic their service quality satisfaction. The artificial neural network model developed has been examined to understand the importance that tram users give to service quality. Using the developed "change of score" method, how the changes to be made in the tram system will affect the quality of service and, hence, how the opinions of different user groups will be affected can be examined in detail. The artificial neural network model prediction capability was compared with that of the multiple linear regression model, and found its superiority. Based on the developed Change of Score Method, the most frequent user attaches the highest importance to the service dimensions of the convenience to pay for the tram, getting his/her destination on time, and reducing environmental pollution.

**Keywords:** Service quality, public transportation, artificial neural networks, tram services, transportation planning, transportation modelling.

## **1. INTRODUCTION**

The rapid growth of the population and the intense migration from the village to the city are some of the main reasons for the increasing traffic, especially in the big cities of developing countries. The public enterprises and municipalities are working together and creating plans to minimize the adverse effects of traffic problems. Transportation planning is needed to decrease the existing problems such as accidents, stress, environmental pollution, and energy use brought by increasing traffic.

---

Note:

- This paper was received on August 20, 2020 and accepted for publication by the Editorial Board on April 9, 2021.
- Discussions on this paper will be accepted by November 20, 2022.

• <https://doi.org/10.18400/tekderg.783110>

<sup>1</sup> Istanbul Okan University, Civil Engineering Department, Istanbul, Turkey - [selim.dundar@okan.edu.tr](mailto:selim.dundar@okan.edu.tr)  
<https://orcid.org/0000-0003-4433-1998>

Developed communities are formed in environments where people can easily travel without chaos and turmoil. Since economic prosperity creates mobility for various social activities, it has become imperative to establish transportation systems as a requirement created by the desire to travel. Public enterprises have the task of examining and evaluating travel demands and finding solutions for the prospective problems.

Consumer-oriented *Service Quality* (SQ) perception has become one of the most critical urban transportation dynamics [1]. Due to the public transport sector structure, competition occurs with private car use and within the sector itself. This competition requires the sector's components to continually improve the quality of the service and achieve the comfort level provided by personal automobiles.

When the SQ of public transportation is improved, some citizens could prefer public transportation instead of private automobiles. This situation leads to increased mobility with less marginal costs such as gas emissions or noise pollution. Determining the criteria that affect the SQ perceptions of public transportation system users is of great importance for increasing the general SQ.

This study investigates the SQ of Kocaeli tram service from the most frequent user type perspective, using *the Artificial Neural Networks* (ANN) method. Although some studies in the literature focus on SQ from the users' perspective, the presented study differs from them by developing a new method to investigate each SQ dimension's effect from various perspectives. The study is the first to investigate the SQ perception of various tram users' perspectives using ANN to the author's knowledge. The developed *Change Of a Score* (COS) *Method* is a simple but powerful method that uses a trained ANN to evaluate the possible effects of the changes planned or already applied to the tram system. The decision-makers and/or operators can also analyze various user groups' needs thoroughly and develop solutions focusing on their needs easily using this method. For this reason, it will not only fill a gap in the literature, state agencies or companies can also use it to prepare their investment plans more effectively.

This paper's organization is as follows; in the next section, a brief literature review is presented. In the third section, the methodology of the study is described. In the fourth and fifth sections, the study results and discussions about them are presented, respectively. The paper concludes in the sixth and the final section.

## **2. LITERATURE REVIEW**

There are various studies in the literature regarding the SQ of public transport and users' perception of the system.

Dell'Olio et al. [2] investigated the differences between perceived quality and systematic expectations of users from the public transportation agencies in terms of SQ. The users valued public transportation service variables, such as waiting time, cleanliness, and comfort the most, but the magnitude of the values varied according to the user type. Users gave less weight to the variables such as driver courtesy, bus occupancy, and journey. For potential users, the essential variables when determining the quality expected from public transport were waiting time, travel time, and above all, the occupancy level of the vehicles.

Friman and Felleson [3] compared the agencies providing public transportation service by examining public transportation service performance in Europe over 6000 participants. They collected data from six different European cities. They considered three objective service performance measures for each city from the UITP Millennium Database. A total of 6021 participants evaluated three subjective satisfaction criteria obtained from the Benchmarking in European Service of Public Transport [4]. They also used general satisfaction as a subjective measure, in addition to the subjective criteria of quality. Correlational analyses show that the relationship between satisfaction and service performance in public transport is far from perfect.

Eboli and Mazzulla [5] proposed a tool to measure customer satisfaction in public transportation. The study created a structural equation model to investigate the relationship between global customer satisfaction and SQ features. The public transportation service investigated is a bus service used by Calabria University students in Cosenza's (Southern Italy) urban area to reach the campus. To calibrate the model, they used the data collected from a survey conducted on the students. They defined the proposed model as useful for transport agencies and planners to examine the relationship between qualities of service qualifications and identify more appropriate qualifications to improve the service provided.

Noor et al. [6] presented criteria that affect the bus SQ. They defined 24 criteria under three main headings: comfort, accessibility, and safety. After that, they applied the specified criteria to the city of Kinabalu in Malaysia. The study revealed a small difference in satisfaction with the minibus and bus services in the city. The essential features that affected user satisfaction emerge as feeling overcrowded and insecure during the night. Islam et al. [7] conducted a customer satisfaction survey with 300 passengers in Kadeh. According to the results, safety, driver performance, and bus condition were the criteria that affect SQ the most. According to Directorate General Mobility and Transport [8], bus SQ's most important criteria were frequency, cleanliness, and safety. The results show that 70% of the passengers are satisfied with the bus frequency and punctuality. Verbich and Geneidy [9] identified different passenger groups such as the disabled, luggage-carrying. They determined that different types of passenger groups have different needs and priorities. While information is a critical priority for disabled passengers, available spaces for those carrying luggage are essential.

Ardıç and Sadaklıoğlu [10] conducted a local study on customer-based satisfaction levels and demands regarding the measurement and development of SQ levels of institutions that show intercity passenger transportation activities. In the study, they aimed to reveal the SQ levels for the target groups. The research determined seven different attitudes and behaviors of employees that affect customer satisfaction as bus features, timeliness, accommodation and break, reservation procedures, office operations, shuttle service, and luggage operations. Imre and Çelebi [11] have linked user satisfaction to several factors for public transportation systems. They expressed that transportation public services and customer satisfaction should be designed in a connected way to increase public transportation use. The study examined the effect of comfort and convenience on public transportation using qualitative and quantitative data. The research provides a new method to evaluate comfort in public transport systems. It has developed a new index based on a series of qualitative and quantitative indicators. It also provides a better understanding of passenger attitudes towards public transport and the perception of comfort in public transport services.

Özuysal et al. [12] have investigated the effects of utility-based accessibility, one of the SQ criteria on transportation mode choice. They have found that linear approaches like correlation and elasticity analysis, the accessibility indices like residential and social infrastructure, are effective but not enough to predict aggregate mode choice ratios. On the other hand, ANN, as a nonlinear approach, has high prediction capability, especially for private car choices. Doğan and Özuysal [13] have investigated the factors affecting waiting time in public transportation in terms of reliability, passenger information system, and physical condition. As a result of the constituted linear multiple regression models, they have found that passenger information system and reliability have reduced the effect on waiting time by 2 and 1.3 minutes, respectively. Besides, it is concluded that the passenger information systems are more efficient if implemented properly for the stops respecting their geometry and the ones used by the lines coming from the city center.

The bus system is the type of public transportation service preferred by many city administrations due to its low investment cost. For this reason, in many cities, public transportation services are provided by a network of bus lines. Therefore, studies on the SQ of public transport have focused primarily on the SQ of buses. Kahraman and Yıldız [14] aimed to measure the quality of service offered by bus companies that provide public transportation services by associating customers' expectations in addition to their perceptions and demographic characteristics. As a result of the research, they observed that a significant relationship exists between customer satisfaction and demographic characteristics, such as gender, age, education, and income level. In the research conducted by Koçoğlu and Aksoy [15] on 274 customers, they investigated the relationship between the demographic characteristics and their satisfaction with an agency that provides public bus transportation. As a result of the research, there was a relationship between the customer age and satisfaction, while there was no relationship between gender, educational status, income status, and customer satisfaction. In their research, Gökaşar et al. [16] aimed to evaluate Istanbul's bus services. As a result of the online surveys conducted on 2177 people, they determined that the users were least satisfied with the frequency of the buses, comfort of the seats, the availability of sufficient space, and ease of moving within the bus, while they were most satisfied with the convenience of the payment method, the clean clothing of the employees and the benefit of the buses to reduce environmental pollution. Gökaşar et al. [17] created a multiple linear regression model using factor analysis to evaluate the service quality of the buses using 2177 satisfaction surveys. When the two factors that emerged were analyzed, they revealed that users attach more importance to service access than comfort. They compared the user survey results with the service providers' opinions and observed only a 1.733% difference between the two stakeholder groups' opinions.

As a result of the increasing population and travel demand in recent years, the investments in urban rail systems have also increased. Therefore, in recent years studies investigating the SQ of rail systems have also been started to increase. In their study, Girginer and Cankuş [18] examined the customer satisfaction of public trams. The study carried out in Eskişehir examined the quality of service expectations of students from the public transport companies using data obtained from approximately 300 students. They used a latent variable at the binomial level related to student satisfaction in their model. As a result of the applied Binomial Logistic Regression Analysis, all the independent variables included in the model had adverse effects on students' satisfaction from the Eskişehir tram system (Estram). Hemedoğlu [19] aimed to determine the SQ of the agencies that provide urban public

transportation services and determine the user satisfaction levels regarding a metro line. In the research, they interviewed 761 consumers using the face-to-face survey technique. As a result of the research, customer expectations for all SQ variables were significantly higher than their perceptions. The variable with the lowest difference between the level of SQ consumers expect and the level of SQ they perceive is the presence of direction signs in the stations. According to the research, the most significant difference between the level of SQ that consumers expect and the level of SQ they perceive was the crowdedness of vehicles. Seçilmiş et al. [20] tried to evaluate the SQ of public transportation vehicles that provide rail service by investigating customer expectations regarding comfort, accuracy, timed, and service facilities. In the results of the study, they stated that there is a significant and positive relationship between the "comfort", "service", "information and accuracy", and "time" sub-dimensions of the problems regarding SQ in railways. Akyıldız et al., [21] aimed to measure the quality of service of *the high-speed rail system* (HSRS) serving between the two cities in Turkey. They prepared the questionnaire to ask users to rate satisfaction ratings from 61 features created for seven SQ dimensions for public transport systems: passenger information, fare level and type, accessibility, station environment, vehicle environment, service delivery and security. By analyzing the results, they identified the most problematic areas of the service provided by HSRS. According to the model results, the system operator should provide improvements, especially in the vehicle seat design and the time and frequency of the service. Šojat et al. [22] analyzed the tram network of Zagreb using two hypothetical tram priority scenarios. Study results show that by implementing yellow line enforcement, 7% better operating speed, 7% saving in passenger spaces, and 22 million € investment cost savings can be obtained. However, if absolute tram priority is applied, the operating speed is 41% better, with 29% saving in passenger spaces and 94 million € of investment cost savings, resulting in a significant increase in the tram's SQ. Vujicic and Prester [23] applied the P-Transqual model to public tram transport in Zagreb to assess its service quality. Their study investigated trams service quality using four quality dimensions: comfort, tangible, personnel, and reliability. They have observed 50, 8, 4, and 23 defects in terms of comfort, tangible, personnel, and reliability, respectively, in 10 days. However, they stated that the results were still positive because, in 9 of 10 cases (90%), public tram transport quality was satisfactory. Khelf et al. [24] investigated the tram service quality and its impact on the passenger modal choice in Constantine City (Algeria). The study results show that despite the tram's different advantages, the population is not satisfied with its exploitation and service quality. Almost 40% of passengers declared that they preferred to use their cars or taxis to using tram. They also provided some suggestions to increase the performance and the SQ of the tram in the study.

ANN is a useful method to predict people's decisions [25]. In SQ studies, ANN is used to estimate which criteria are more important than others. For example, De Oña and De Oña [25] proposed a model that uses ANN to analyze the SQ perceived by passengers of a public transport system. In 2007, they carried out a customer satisfaction survey on the Granada metropolitan bus transport system. They developed an ANN model to investigate customer satisfaction. They used to determine each feature's relative contribution and applied a statistical analysis to each method's outputs to identify groups of features that differ significantly in their relative importance. Statistical results have shown that frequency is the most useful feature in SQ. Islam et al. [26] proposed various ANN approaches to define which feature of the SQ criteria is more important than others. They presented a comparative

study using *Generalized Regression Neural Network* (GRNN), *Probabilistic Neural Network* (PNN), and *Pattern Recognition Neural Network* (PRNN). According to the results, punctuality and reliability, frequency of service, free seats, and travel experience were essential.

### 3. METHODOLOGY

Within the scope of this study, a 20-question survey created by the *International Bus Benchmarking Group* (IBBG) [27] was adapted for the *light rail transit* (LRT) system. User preferences were derived from the answers given to the first 19 questions using the ANN model. The ANN model developed can predict passenger SQ perception using the survey results and how a change in the public transport system's feature affects SQ accurately. Therefore, the *Perturb Method* suggested by De Oña and De Oña [25] has been adapted to develop a new and more straightforward estimation method, namely the *Change Of a Score* (COS) *Method*. The ANN model created using this method can also predict the SQ perception of different user groups, so decision-makers can focus on meeting various customer groups' needs.

Kocaeli, located in the Marmara Region of north-western Turkey, is the tenth most populous city of Turkey with a population of 1,953,035. The city is one of the largest industrial and commercial cities in the country. Kocaeli is the most developed city after Istanbul, Ankara, and Izmir according to the Socio-Economic Development Ranking of Regions – SEGE 2017 [28] ranking. It is a neighbor of important cities, such as Istanbul and Yalova in the west, Sakarya in the east, and Bursa in the south. Due to these features, it is a critical travel generation and attraction center.

Kocaeli Metropolitan Municipality presented the tram service to the public in 2017. They determined the most suitable route by evaluating passenger demand, integration with other transportation systems, and construction costs. The tramline named *Akçaray*, consists of 15 stations along 14.8-kilometer line between Otogar and Sekapark. The route of Akçaray is presented in Figure 1.



Figure 1 - Route of Akçaray [29]



The research was carried out in the survey model to examine user satisfaction with Kocaeli tram system. The research subjects are defined in the conditions they exist and are not attempted to be changed in any way. The study sample consists of individuals over the age of 15 who live in Kocaeli in May 2019 and benefit from the tram system in public transport. According to the *Turkish Statistical Institute* (TSI) address-based information system [30], the number of persons with the age of 15 or over living in Kocaeli Centre in 2019 are 289577. Meyer [31] and Fox et al. [32] suggest the values shown in Table 1 for the population range and the corresponding sample size. For the universe of non-homogeneous subjects, the required sample size was calculated as  $n = 384$ . To reach more general results, the sample size was selected as 500 people.

*Table 1 - Population range and approximate sample size [31, 32]*

<b>Population Range</b>	<b>Approximate Sampling Size (n)</b>
Infinity	384
500000	384
100000	383
50000	381
10000	370
5000	357
3000	341
2000	322
1000	278

In the research, the data were collected using the surveys that were conducted online in May 2019. The survey was published on a web site and was advertised using various channels such as social media and text messages to members of non-governmental organizations located in Kocaeli. The questionnaire form consists of two parts. The first part consists of 7 questions that aim to obtain the participants' demographic information, such as age and gender. Descriptive statistics are shown in Table 2. The most of the respondents were males, with a percentage of 65.6. The respondents were from various education levels, but mostly with a bachelor's degree. The percentage of married and single (or divorced) respondents are close to each other with percentages of 54.2 and 45.8, respectively. 47.2% of the respondents were in the age range of 18-30, and 47.6% had a monthly income between 2000-5000 TL. Most of the respondents (53%) used the tram service less than once a month, and 46.4% used it for hobby/socializing journeys. In the second part, a questionnaire consisting of 20 questions to measure the SQ of buses developed by the International Bus Benchmarking Group was adapted to the tram and used. The answers to the survey questions were evaluated using the 5-point Likert scale ranging from 1 to 5. One indicates the worst case (strongly disagree), and five indicates the best case (strongly agree). 44 of 500 participants left some questions empty and contained missing information. Therefore, these surveys were not taken

into consideration in developing the ANN model. Table 3 shows the average of the scores given to each survey question.

*Table 2 - Descriptive statistics*

<b>Groups</b>	<b>Frequency (n)</b>	<b>Percentage (%)</b>
<b>Sex</b>		
Male	328	65.6
Female	172	34.4
<b>Education</b>		
Elementary School	27	5.4
High School	69	13.8
Associate	51	10.2
Bachelor's	279	55.8
Graduate	70	14.0
Post Graduate	4	0.8
<b>Marital status</b>		
Married	271	54.2
Single (or divorced)	229	45.8
<b>Age Range</b>		
<18	2	0.4
18-30	236	47.2
31-40	153	30.6
41-50	55	11.0
51-60	37	7.4
61-70	15	3.0
>70	2	0.4
<b>Monthly Income Range</b>		
< 2000 TL	98	19.6
2000-5000 TL	238	47.6
5001-7000	94	18.8
>7000 TL	70	14.0

Table 2 - Descriptive statistics (Continued)

<b>Frequency of Tram Use</b>	
Less than once a month	265 53.0
Between once a month and once a week	83 16.6
Between once a week and thrice a week	82 16.4
Between thrice a week and six times a week	57 11.4
Everyday	13 2.6
<b>Purpose of Tram Use</b>	
Hobby/socializing journeys	232 46.4
Work/school journeys	160 32.0
Shopping journeys	127 25.4
Doctor/hospital journeys	32 6.4
Other	20 4.0

### 3.1. ANN Model

ANN is an artificial intelligence method developed based on the human brain's fundamental functions such as learning, remembering, generalizing, and memorizing. The ANN consists of interconnected processing units called neurons, developed in the form of layers. Learning in ANN is done by adjusting the values of the connections (weights) between neurons. There are different network structures developed in the literature. In this study, the feed-forward neural network type, a *multilayer perceptron (MLP)* procedure, and error backpropagation algorithm were used to develop the ANN model. In backpropagation algorithm, which is a type of supervised learning, the difference (error) between the actual (observed) result and the result produced by ANN is propagated backward by updating the weight values in the network towards the previous layers to reduce the obtained error [33].

In ANN, a black box modeling technique, instead of deriving a mathematical relationship between input values and output values, aims to produce appropriate output values from the given input values. Therefore, what mathematical operations are performed between input and output or how they are performed is not essential. For this reason, the number of hidden layers between the input and output layers and the number of neurons in the hidden layer(s) are found in a way that optimizes the performance of the model using the *trial-and-error method*. It is also crucial for the model to be as simple as possible, reducing the amount of necessary calculations. For this reason, model development is carried out by taking into account the trade-off between model simplicity and performance [34].

An ANN model has been developed to mimic the satisfaction of Akçaray users. In the developed model, the demographic variables and the first 19 questions asked to obtain the users' SQ satisfaction level were used as the input values. The only output value of the ANN was the answer to the 20<sup>th</sup> question of the survey, "How satisfied are you overall with the

tram services in the city?”. In other words, the ANN model tries to estimate the level of satisfaction of the users from the system by using the demographic data of the users and the satisfaction levels of different aspects of service offered by the tram.

*Table 3 - Average score given to survey questions*

<b>Nr.</b>	<b>Question</b>	<b>Average Score</b>
1	The tram service is usually reliable	3.798246
2	The trams are frequent	3.464912
3	The tram route is convenient for me	3.405702
4	It is easy for me to get on and off the tram	3.688596
5	It is easy to move inside the tram	3.541667
6	It is convenient to pay for the tram	3.800439
7	It is easy to get information about the tram services	3.392544
8	It is easy to find out how well the trams are running	3.559211
9	If there are problems, I can easily find an alternative route	3.015351
10	The tram gets me to my destination on time	3.642544
11	Staff are well dressed	3.710526
12	Staff are helpful	3.480263
13	It is easy to resolve problems or complaints	3.368421
14	The seats are comfortable, and there is enough space	2.980263
15	The tram is well driven and gives a comfortable ride	3.541667
16	The tram is clean	3.587719
17	The tram is quiet, well lit, ventilated, and at an adequate temperature	3.592105
18	The tram is a secure place for me	3.640351
19	The tram does not cause too much pollution	3.760965
20	How satisfied are you overall with the tram services in the city?	3.578947

Since only gender and marital status belong to 2 different classes among the input values of ANN, they were represented by a single neuron. For example, the input value is 0 when the user was male and 1 when the user was female. For other demographic data, input neurons as many as the number of classes were used. Education level was represented by 6, the age range was represented by 7, the monthly income range was represented by 4, frequency and purpose of tram use were represented by 5 neurons each. For each demographic data, the

neuron representing this class takes the value 1, and the others take the value 0. For example, for a 45-year-old user, the 4<sup>th</sup> of the neurons showing the age range takes the value 1, while the remaining ones take the value of 0. A single neuron was used for each of the 19 questions of the survey. Since the answers to the questions ranged from 1 to 5, this range was normalized between 0 and 1 using Eq. 1. In other words, 0 indicates the lowest level of satisfaction, and 1 indicates the highest level of satisfaction. The answers to the survey's 20<sup>th</sup> question, which constitute the single output of the ANN model, were also normalized between 0 and 1, just like the other 19 questions representing the survey's other questions.

$$\text{Normalized Value} = \frac{\text{Answer given to the question} - 1}{4} \tag{1}$$

In the ANN model, which was developed using the Matlab® Neural Networks Toolbox, 48 neurons were forming the input and a single neuron forming the output, while the number of hidden layers and the number of neurons in the hidden layer were determined by trial-and-error approach suggested by Murat and Başkan [35] due to its simplicity. The sigmoid function in Eq. 2 was selected as the activation function in the hidden layer and a linear function on the output layer. Levenberg Marquardt (LM) algorithm was preferred in the training of ANN because of its fast convergence and its need for fewer iterations. The parameters of the LM algorithm were selected as initial  $\mu = 0.001$ ,  $\mu$  decrease factor = 0.1,  $\mu$  increase factor = 10, maximum  $\mu = 10000000000$ , which are also the default values of MATLAB®. The ANN model developed can be seen in Figure 2.

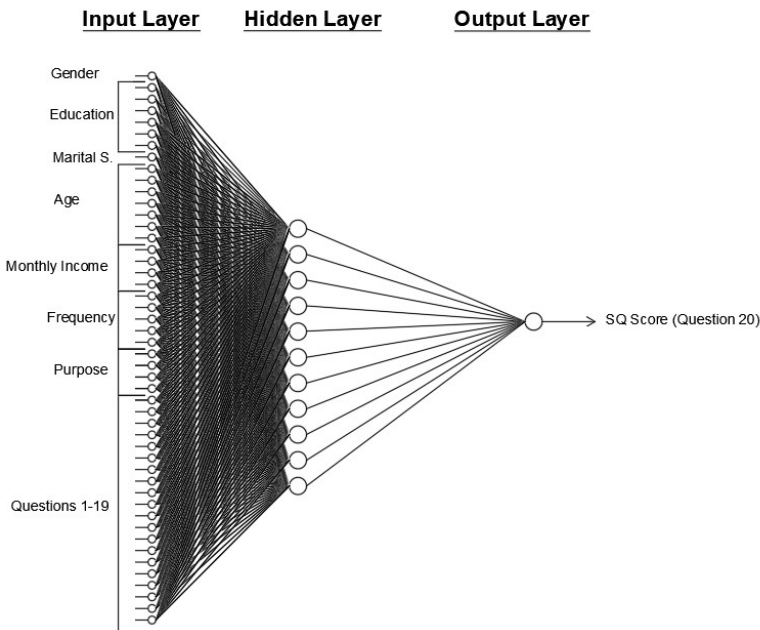


Figure 2 - The ANN model developed

$$\sigma(x) = \frac{1}{1+e^{-x}} \tag{2}$$

The outputs obtained from the ANN model were denormalized between 1 and 5 using Eq. 3 for the evaluation of its performance.

$$\text{Denormalized Value} = \text{Normalized Value} \times 4 + 1 \tag{3}$$

The three-way data split method by Osuna [36] was used to prevent the over-fitting problem and determine the best network architecture. The flow chart of the three-way data split methodology is given in Figure 3. First, the data were divided into three parts as training (80%), test (10%), and validation (10%) sets. Then the best network architecture was investigated considering the combinations of the data sets given in Table 4. For each partition, the network architecture was trained and tested with the test dataset that was not used in training. The best network architectures obtained from different trials and partitions and corresponding error values are given in Table 5. For each run, the best network architecture was selected with the best network performance. One and two hidden layers with a maximum of 15 neurons were tried at each layer.

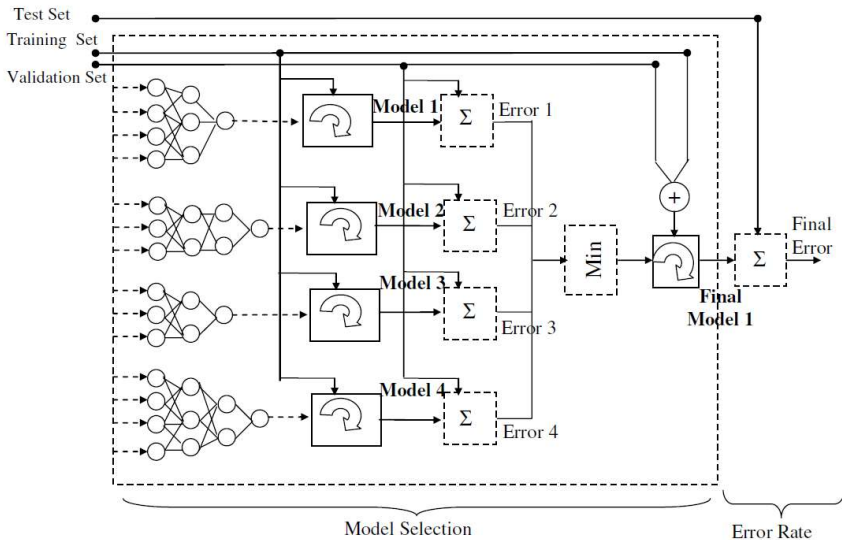


Figure 3 - Flow chart of the three-way data split validation method [37]

Table 4 - Partitions of the data used

<b>Partition I</b>	Training				Validation	Test
<b>Partition II</b>	Training			Validation	Test	Training
<b>Partition III</b>	Training		Validation	Test	Training	
<b>Partition IV</b>	Training	Validation	Test	Training		
<b>Partition V</b>	Validation	Test	Training			

Table 5 - Samples from network architectures searching and corresponding errors

Partition no	Best network architecture	Train errors	Validation Errors	Test Errors
I	$48 \times 10 \times 1$	0.348	0.324	0.434
II	$48 \times 15 \times 1$	0.391	0.427	0.425
III	$48 \times 9 \times 1$	0.361	0.410	0.434
IV	$48 \times 11 \times 1$	0.302	0.358	0.391
V	$48 \times 12 \times 1$	0.371	0.272	0.322

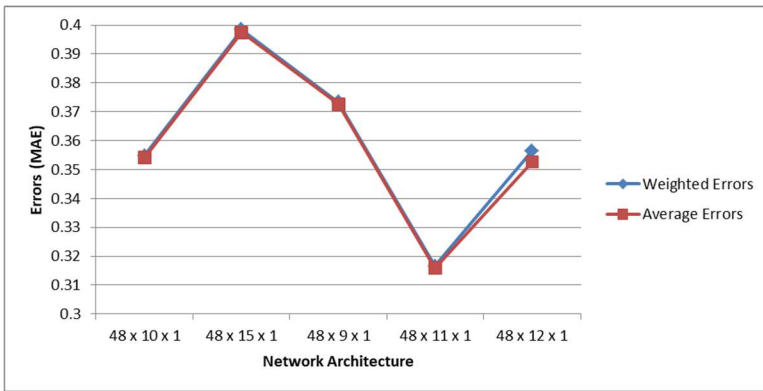


Figure 4 - Weighted and average error values for different network architectures.

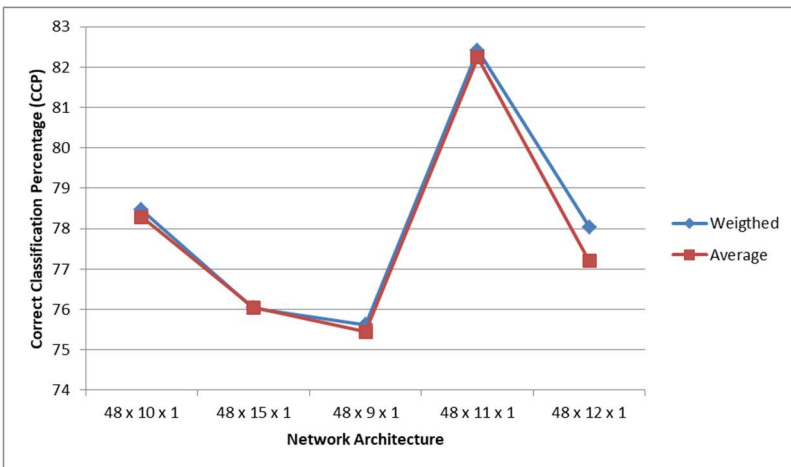


Figure 5 - Weighted and average correct classification percentages for different network architectures.

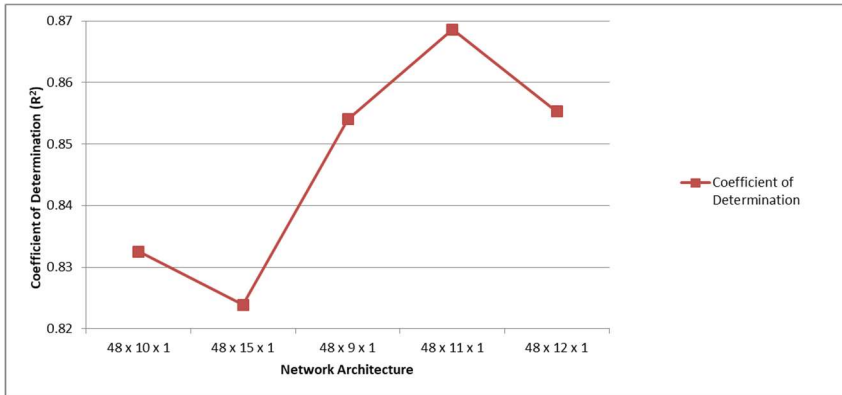


Figure 6 - Coefficient of determination values for different network architectures.

Three criteria, the correct classification percentage (CCP), the Mean Absolute Error (MAE) values, and coefficient of determination ( $R^2$ ) values, were taken into consideration for searching the best network architecture using the train, test, and validation data. The ultimate network architecture was determined as  $[48 \times 11 \times 1]$  based on the evaluations. The MAE, CCP, and  $R^2$  values of different network architectures are indicated in Figures 4, 5, and 6, respectively.

Since most of the respondents (53%) were not regular users and used the tram service for less than once a month, another ANN has been developed and trained using the data of the 223 users who use the system at least once a week. For this reason, the input neuron that corresponds to non-regular users has been removed from the ANN. The same method has been applied to the development of the ANN for regular users. The best network architecture for every partition was obtained as  $[47 \times 12 \times 1]$  based on the evaluations. The error values obtained for each partition and MAE CCP, and  $R^2$  values of the network architecture are indicated in Table 6.

Table 6 - Errors of ANN developed using regular users

Partition no	I	II	III	IV	V
<b>Train errors</b>	0.087	0.076	0.088	0.095	0.091
<b>Validation errors</b>	0.154	0.194	0.039	0.066	0.108
<b>Test errors</b>	0.027	0.076	0.126	0.050	0.037
<b>Weighted error</b>	0.087	0.087	0.087	0.087	0.088
<b>Weighted CCP</b>	0.960	0.959	0.960	0.964	0.959
<b>Overall</b>					
<b>Average error</b>			0.087		
<b>Average CCP</b>			0.960		
<b><math>R^2</math></b>			0.943		



Although the ANN developed using regular user data only seems to provide better results; it cannot predict non-regular users' evaluations. The predicted values for both ANN models have been compared with each other and are shown as a scatter diagram in Figure 7.  $R^2$  value between the two ANNs predicted values was found as 0.825, and both models predicted the same scores for 77% of the regular users. These values show that although most of the respondents were non-regular users due to the sampling method used, ANN can still learn and mimic every user type's opinions.

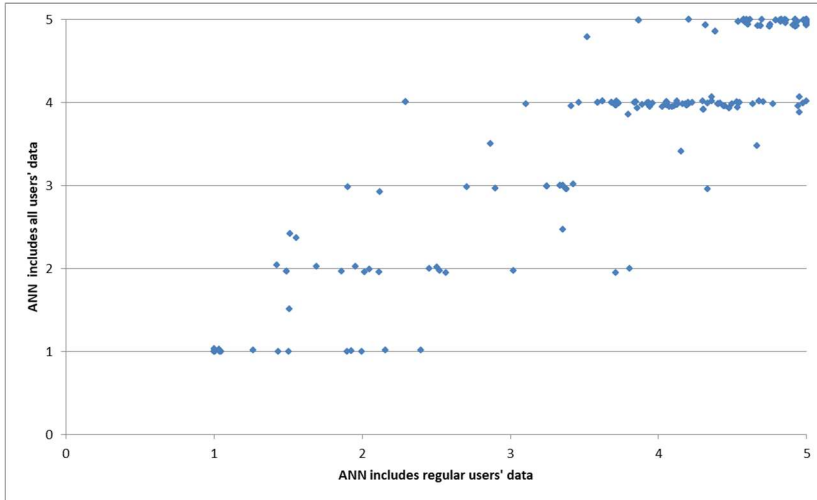


Figure 7 - Scatter diagram between the two ANN models' predicted values

### 3.2. Multiple Linear Regression Model

A *Multiple Linear Regression (MLR)* model has been developed to compare the ANN model performance. Although some machine learning methods such as *Support Vector Machines (SVM)*, *k-nearest neighbor*, and *random forest* may provide better classification performance, MLR was used in performance evaluation because it provides continuous output results just like the ANN model. For this reason, the COS method described in the next subsection can also be applied to the MLR model. The data split method was also used in the MLR model to evaluate the model prediction performance. However, this time the data was split into two-ways as training and test set. Hence, the validation set of each partition was included in the test set. The performance obtained for each partition using the ANN and MLR models are given in Table 7. Results show that the ANN model performs better in estimating the SQ perception of tram system users than the MLR model.

MLR developed for partition III provides the best performance as seen in Table 5. For this reason, this model was taken into consideration. The formulation of the MLR model is given in Eq. 4 where  $SQ$  is dependent variable,  $\beta$ 's are the coefficients and  $x_i$ 's are the independent variables.

$$SQ = \beta_0 + \beta_1 \times x_1 + \beta_2 \times x_2 + \dots + \beta_n \times x_n \quad (4)$$

The goodness of fit statistics, analysis of the variance, and MLR model parameters are given in Tables 8, 9, and 10, respectively.

*Table 7 - Comparison of ANN and MLR methods*

Partition no	Weighted MAE		Average MAE		Weighted CCP		Average CCP		R <sup>2</sup>	
	ANN	MLR	ANN	MLR	ANN	MLR	ANN	MLR	ANN	MLR
I	0.355	0.418	0.354	0.414	78.466	72.382	78.289	73.210	0.833	0.808
II	0.398	0.424	0.398	0.424	76.031	66.006	76.046	65.755	0.824	0.804
III	0.373	0.411	0.373	0.410	75.616	73.900	75.439	73.632	0.854	0.797
IV	0.317	0.428	0.316	0.427	82.419	69.738	82.237	69.475	0.869	0.806
V	0.357	0.410	0.353	0.409	78.038	70.395	77.193	70.131	0.855	0.809

*Table 8 - Goodness of fit statistics of MLR model*

Observations	365
Sum of weights	365
DF	320
R <sup>2</sup>	0.825
Adjusted R <sup>2</sup>	0.801
MSE	0.328
RMSE	0.573
MAPE	14.038
DW	2.102
Cp	45.000
AIC	-364.768
SBC	-189.273
PC	0.224

*Table 9 - Analysis of variance of MLR model*

Source	DF	Sum of squares	Mean squares	F	Pr > F
Model	44	495.532	11.262	34.323	0.000
Error	320	105.000	0.328		
Corrected Total	364	600.532			

Table 10 - MLR model parameters

Source	$\beta$ Value	Standard error	t	Pr >  t	Lower bound (95%)	Upper bound (95%)
Intercept	0.187	0.673	0.277	0.782	-1.138	1.512
Sex	-0.077	0.081	-0.951	0.342	-0.237	0.083
Elementary School	0.166	0.456	0.363	0.717	-0.732	1.064
High School	0.389	0.435	0.893	0.372	-0.467	1.245
Associate	0.102	0.435	0.234	0.815	-0.754	0.959
Bachelor's	0.261	0.426	0.613	0.541	-0.577	1.100
Graduate	0.357	0.431	0.827	0.409	-0.492	1.206
Post Graduate	0.000	0.000				
Marital	-0.001	0.086	-0.009	0.993	-0.171	0.169
<18	-0.239	0.642	-0.372	0.710	-1.501	1.024
18-30	0.273	0.451	0.605	0.546	-0.614	1.159
31-40	0.207	0.445	0.465	0.642	-0.668	1.081
41-50	0.247	0.452	0.546	0.586	-0.643	1.137
51-60	0.245	0.455	0.540	0.590	-0.649	1.140
61-70	-0.175	0.476	-0.368	0.713	-1.112	0.762
>70	0.000	0.000				
<2000	0.132	0.137	0.968	0.334	-0.136	0.401
2000-5000	0.088	0.116	0.756	0.450	-0.141	0.317
5001-7000	0.028	0.117	0.237	0.813	-0.202	0.258
>7000	0.000	0.000				
<once a month	-0.592	0.195	-3.036	<b>0.003</b>	-0.975	-0.208
oncem.-oncew.	-0.459	0.209	-2.193	<b>0.029</b>	-0.871	-0.047
oncew.-thricew.	-0.319	0.196	-1.623	0.105	-0.705	0.068
thricew.-everyday	-0.303	0.198	-1.528	0.127	-0.692	0.087
everyday	0.000	0.000				
hobby	-0.043	0.093	-0.460	0.646	-0.226	0.140
workschool	0.100	0.088	1.146	0.253	-0.072	0.272
shopping	-0.015	0.086	-0.175	0.861	-0.185	0.154
medical	0.039	0.140	0.277	0.782	-0.236	0.313
other	-0.063	0.172	-0.368	0.713	-0.401	0.274

Table 10 - MLR model parameters (continue)

Source	$\beta$ Value	Standard error	t	Pr >  t	Lower bound (95%)	Upper bound (95%)
Q1	-0.107	0.066	-1.620	0.106	-0.237	0.023
Q2	0.041	0.047	0.872	0.384	-0.051	0.133
Q3	0.215	0.051	4.202	<b>0,000</b>	0.114	0.316
Q4	-0.134	0.058	-2.326	<b>0.021</b>	-0.247	-0.021
Q5	0.029	0.054	0.528	0.598	-0.078	0.135
Q6	-0.052	0.069	-0.756	0.450	-0.189	0.084
Q7	0.038	0.058	0.648	0.517	-0.077	0.152
Q8	0.047	0.063	0.746	0.456	-0.077	0.170
Q9	-0.068	0.041	-1.667	0.097	-0.148	0.012
Q10	0.167	0.063	2.633	<b>0.009</b>	0.042	0.292
Q11	0.074	0.079	0.938	0.349	-0.082	0.231
Q12	0.174	0.086	2.031	<b>0.043</b>	0.005	0.342
Q13	-0.157	0.077	-2.033	<b>0.043</b>	-0.308	-0.005
Q14	-0.030	0.042	-0.713	0.476	-0.111	0.052
Q15	-0.078	0.069	-1.124	0.262	-0.214	0.059
Q16	0.172	0.081	2.137	<b>0.033</b>	0.014	0.331
Q17	0.078	0.077	1.010	0.313	-0.074	0.229
Q18	0.250	0.078	3.217	<b>0.001</b>	0.097	0.403
Q19	0.260	0.067	3.866	<b>0.000</b>	0.128	0.392

The results of the MLR indicated the predictors explained 82.5% of the variance ( $R^2 = 0.825$ ,  $F(2,320) = 34.323$ ,  $p < 0.05$ ). The analysis shows that using the tram less than once a month ( $\beta = -0.592$ ,  $t(364) = 0.003$ ,  $p < 0.05$ ), using the tram between once a month and once a week ( $\beta = -0.459$ ,  $t(364) = 0.029$ ,  $p < 0.05$ ), Question3 ( $\beta = -0.215$ ,  $t(364) = 0.000$ ,  $p < 0.05$ ), Question4 ( $\beta = -0.134$ ,  $t(364) = 0.021$ ,  $p < 0.05$ ), Question10 ( $\beta = 0.167$ ,  $t(364) = 0.009$ ,  $p < 0.05$ ), Question12 ( $\beta = 0.174$ ,  $t(364) = 0.043$ ,  $p < 0.05$ ), Question13 ( $\beta = -0.157$ ,  $t(364) = 0.043$ ,  $p < 0.05$ ), Question16 ( $\beta = 0.172$ ,  $t(364) = 0.033$ ,  $p < 0.05$ ), Question18 ( $\beta = 0.250$ ,  $t(364) = 0.001$ ,  $p < 0.05$ ) and Question19 ( $\beta = 0.260$ ,  $t(364) = 0.000$ ,  $p < 0.05$ ) did significantly predict the SQ value. The value of  $\beta$  indicates the order of importance of the independent variables. The variable with the highest  $\beta$  value is relatively most important independent variable [38]. Positive  $\beta$  values indicate that increasing the independent variable also increases the SQ value, whereas negative  $\beta$  values indicate that increasing the independent variable decreases the SQ value.

### 3.2. Change of Score Method

The developed ANN model was then used to examine to what extent each of the dimensions related to the tram system's SQ affected the general level of satisfaction from itself. For this purpose, first of all, the most frequent user profile has been defined. The highest frequency features were selected from the demographic variables (shown in Table 2) while creating the profile. However, the most frequent user was defined as a person who uses the tram every day. Therefore, the profile determined as a standard user is a male, with an undergraduate degree, married, between the ages of 18-30, with a monthly income of 2000-5000 TL, using the tram every day, and mostly for hobby/socialization journeys. The score that such an individual would give to each SQ dimension was determined by taking the mean of the total scores given to them. This individual's characteristics and preferences were presented in the ANN model. An overall satisfaction score of 4.42 was obtained as the overall SQ score of the most frequent user. Since none of the 456 respondents fitted precisely into the defined profile, such a user's actual opinion could not be obtained.

To measure the effect of dimensions on the overall SQ, *the Change Of a Score (COS)* method, similar to the Perturb Method suggested by De Oña and De Oña [25], has been developed. In the Perturb Method, small amounts of noise are applied to each input neuron until 50% of the original value is perturbed, while the remaining input neurons keep unaltered. The change in the Mean Square Error (MSE) assesses each attribute's relative importance; therefore, the larger the MSE for each input perturbation, the more the corresponding attribute's relative importance. In the developed COS method, instead of perturbing the original values by a small amount of noise, the values given by the most frequent user to each dimension were increased and decreased by 1 point, respectively. The most frequent user's modified preferences are presented to the ANN model, and their output is considered as the overall SQ score. By dividing the difference between these two values into two, how the 1-point change in SQ dimensions will change the overall satisfaction level has been calculated. This method can be considered as a modified and simplified version of the perturb method. An example of the COS method is as follows:

The most frequent user's overall score for the SQ, in other words, the ANN model's output is 4.42283. Similarly, his score for the first dimension, the tram service is usually reliable, is 3.79824. First of all, the first-dimension score is increased by 1 point, keeping every other input value constant, obtaining a new score of 4.79824. The most frequent user's new opinion is supplied to the ANN model, obtaining an overall score of 4.52438. It means that 1 point of an increase in dimension 1 increases the SQ perception of the most frequent user by 0.10155. Then, the first-dimension score is decreased by 1 point, obtaining a new score of 4.28902. Furthermore, this shows that 1 point of a decrease in dimension 1 decreases the SQ perception of the most frequent user by 0.13380. The average of both values, 0.11768, shows the impact of dimension 1 on the overall SQ.

## 4. RESULTS

Figure 8 shows the scatter diagram between user satisfaction with SQ and trained ANN's predicted values. When the figure is examined, it is seen that the outputs of the ANN model is not only composed of integers between 1 and 5 but also includes intermediate

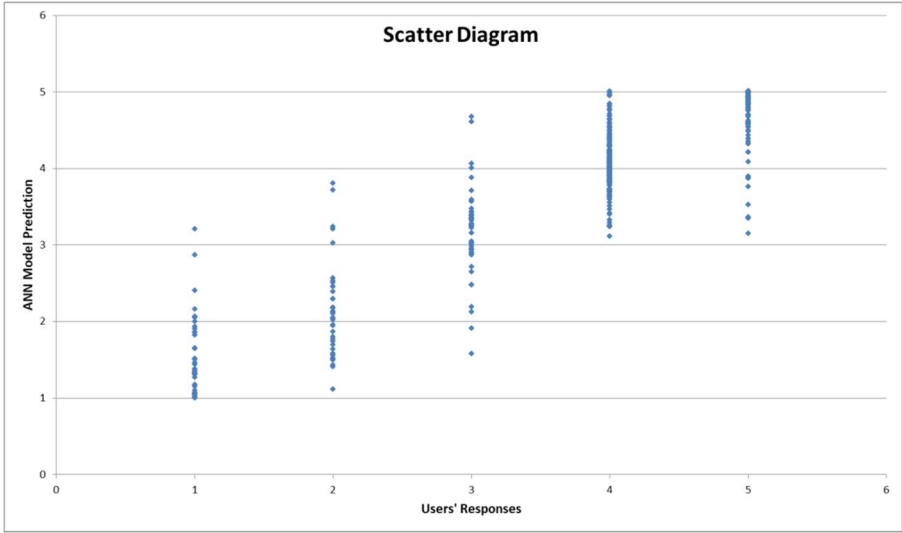


Figure 8 - Scatter diagram between user satisfaction with SQ and ANN's predicted values

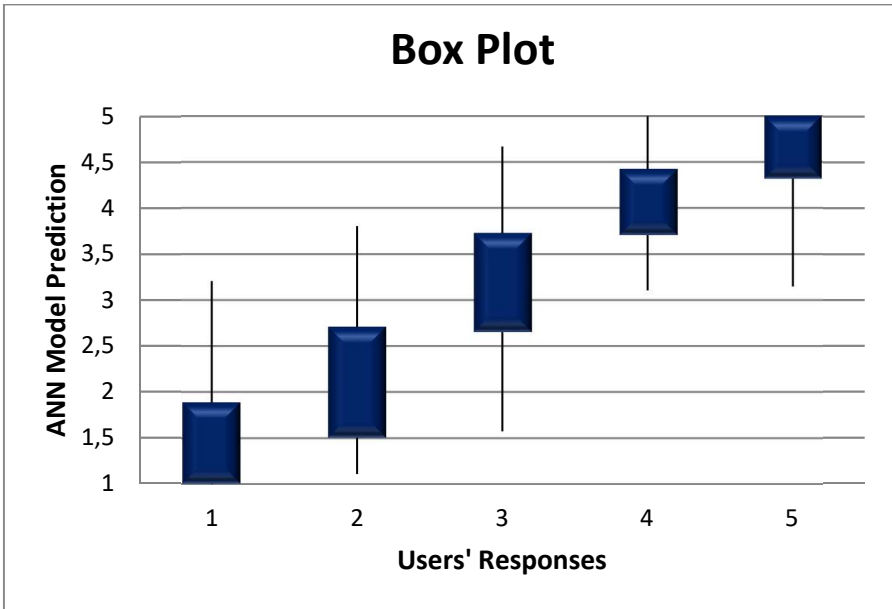


Figure 9 - Box plot showing the mean and the standard deviations estimated by ANN for each respondent with respect to their overall SQ satisfaction

values. This feature also investigates how the changes of SQ dimensions related to the tram system affect their overall satisfaction with the tram service.  $R^2$  value between the users SQ scores and ANN's predicted values was found as 0.8604 and Pearson correlation statistic ( $r$ ) as 0.928. The box plot that shows the mean and the standard deviations estimated by ANN for each respondent regarding overall SQ satisfaction can be seen in Figure 9. The developed ANN model correctly estimated the satisfaction score of 82% of the respondents with an error margin of  $\pm 0.5$  and 97% of the respondents with an error margin of  $\pm 1$ . This performance stands out as an appropriate value, especially considering the stochastic nature of human thoughts and behaviors and also that different people with similar characteristics may have different evaluations.

Table 11 shows the most frequent user scores on SQ dimensions and each dimension's effect on the overall SQ. The values shown in the table show that the user is most satisfied with the convenience of paying for the tram, the tram's reliability, and the trams being useful in reducing environmental pollution. On the other hand, he/she is least satisfied with the comfort of the seats and the space inside the trams, finding an alternative route in case of problems and ease to resolve problems or complaints. Furthermore, the dimensions that most affect the overall satisfaction level of the most frequent user from tram service are the convenience to pay for the tram, the tram getting him/her to his destination in time, and the benefits of trams in reducing the environmental pollution. The cleanliness of the trams, their frequency, and dress of the staff affect the level of general satisfaction the least. Figure 10 shows the most frequent user score of each dimension and its impact on overall SQ.

*Table 11 - The most frequent user scores on SQ dimensions and each dimension's effect on the overall SQ*

<b>Dim.</b>	<b>Question</b>	<b>Most Freq. User Score</b>	<b>Impact on Overall SQ</b>
6	It is convenient to pay for the tram	3.800439	0.42324
10	The tram gets me to my destination on time	3.642544	0.32150
19	The tram does not cause too much pollution	3.760965	0.30908
18	The tram is a secure place for me	3.640351	0.29437
4	It is easy for me to get on and off the tram	3.688596	0.20247
3	The tram route is convenient for me	3.405702	0.17710
9	If there are problems, I can easily find an alternative route	3.015351	0.15540
7	It is easy to get information about the tram services	3.392544	0.13452
12	Staff are helpful	3.480263	0.12301
1	The tram service is usually reliable	3.798246	0.11768
17	The tram is quiet, well lit, ventilated, and have adequate temperature	3.592105	0.11643

Table 11 - The most frequent user scores on SQ dimensions and each dimension's effect on the overall SQ (continue)

Dim.	Question	Most Freq. User Score	Impact on Overall SQ
5	It is easy to move inside the tram	3.541667	0.11368
8	It is easy to find out how well the trams are running	3.559211	0.10693
15	The tram is well driven and gives a comfortable ride	3.541667	0.10401
13	It is easy to resolve problems or complaints	3.368421	0.07868
14	The seats are comfortable, and there is enough space	2.980263	0.06630
11	Staff are well dressed	3.710526	0.04185
2	The trams are frequent	3.464912	0.04025
16	The tram is clean	3.587719	0.03815

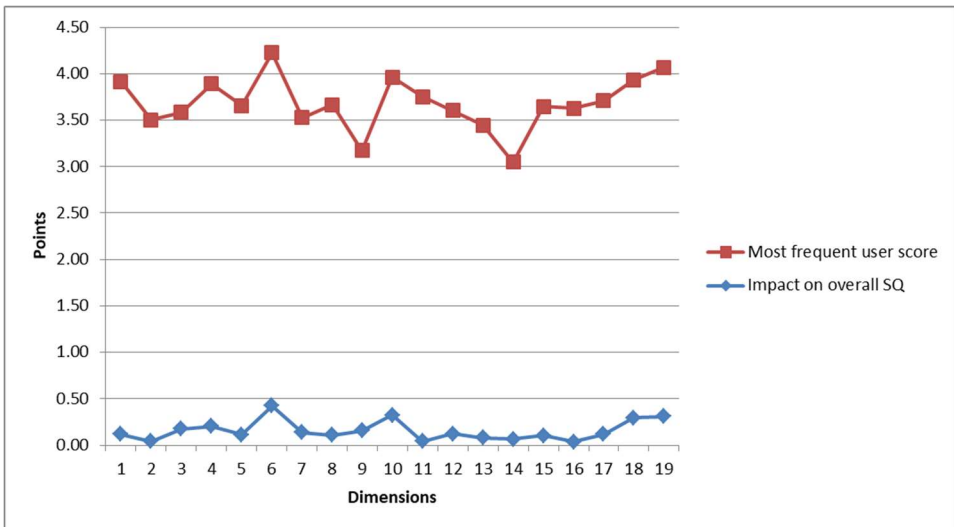


Figure 10 - The most frequent user score of each dimension and its impact on overall SQ.

## 5. DISCUSSIONS

Within the scope of this study, general satisfaction level of tram services were tried to be estimated using the demographic characteristics of tram users in Kocaeli and their evaluation for tram SQ dimensions. The ANN model developed for this purpose has an accurate classification level of 82%. The values obtained indicate that the developed ANN model has a good performance level when the stochastic and complex human thoughts and behaviors



are considered. Thanks to the ANNs generalization feature, by which the developed model can predict how different users would evaluate the SQ.

After developing the ANN model, a most frequent user profile was created using the surveyed users' dominant demographic features. The most frequent user opinions about the dimensions that make up the quality of the service were also formed by taking the average of the participants' scores to the survey questions. The most frequent user seems to be entirely satisfied with the city's tram service, with a score of 4.42/5 obtained from ANN.

In the survey applied to the tram system users, only the satisfaction levels of 19 dimensions related to the tram system were considered, and how vital these levels were for them if ignored. The most frequent user's score for each dimension has been altered by 1 point width, and these preferences have been provided as an input to the ANN to determine each dimension's importance. The average of the changes in SQ perception when the dimension is improved and disturbed by 1 point shows the impact of the subject dimension into the overall SQ level, or in other words, it shows how much the tram users attach importance to this feature.

According to the survey results applied, the most frequent user is most satisfied with the convenience to pay for the tram, reliability of the tram service, and the positive environmental effects of the tram. In recent years, the implementation of smart cards instead of paying with money, ticket, or coin in all transportation systems throughout the city and the integrated payment system seems to be the primary reason behind the satisfaction. A high satisfaction level from the tram service reliability shows that the tram operations do not deviate much from the announced time table. It also shows that the waiting time, which is the service variable that the users valued most, according to Dell'Olio et al. [2], is also low or predictable. This finding is also interesting from another point of view. According to Akyıldız et al. [21], the HSRS operator should improve the servicetime and frequency. Both studies reveal that the reliability of the rail system services is an essential aspect for their users. Since Kocaeli is an industrial city and its Dilovası district is the most polluted district of Turkey, it is not surprising that users are satisfied with trams' help in reducing the environmental pollution. The finding is similar to the study conducted by Dell'Olio et al. [2] since cleanliness is one of the service variables that users valued most.

Dimensions that most frequent user is least satisfied with are the seats being comfortable and providing enough space in vehicles, the possibility to find an alternate route in case of service disruption, and easiness to resolve problems or complaints. Comfort level in the vehicles is also found significant by Noor et al. [6] and Seçilmiş et al. [20]. However, this dimension was ranked as the fourth lowest in affecting the most frequent user's general SQ level, which is an interesting finding. Since the tram does not have an alternate route as parallel lines, the low satisfaction from finding an alternate route in case of problems is not surprising. Still, the passengers can use other public transportation systems, such as the city's bus transit services, in case of service disruption. Unlike the bus system, users do not communicate with the driver, or other staff of the tram system. Therefore, it is not surprising that their satisfaction with easiness to resolve problems or complaints is low.

The most frequent user's most important dimension in tram service is the convenience of paying for the tram. It is an interesting finding that this dimension ranked first in terms of both satisfaction and importance. It reveals that the operator knows their customers'

expectation, or in other words, their passengers' will and is successful in satisfying them, in some way. The most frequent user assigns the second highest importance to get his destination on time. This finding is not surprising considering that Kocaeli is the tenth most populated and fourth most developed city in Turkey, hence, people pay high importance to the time spent on the transportation system. It can be thought that the dimension to which the most frequent user attaches the third highest importance in terms of tram service is the beneficial in reducing the environmental pollution of trams. Because Kocaeli is an industrial city, and especially the high level of air pollution in the city affects this evaluation.

The trams' cleanliness, frequency, and dress of the staff stand out as the most frequent user's least important dimensions. However, the low importance of cleanliness assigned is contrary to Dell'Olivo et al. [2] and Directorate General Mobility and Transport [8]. This finding reveals that while cleanliness is an important aspect for European cultures, it loses its importance in Turkey and some Asian countries like Malaysia [6] and Afghanistan [7]. The second lowest important dimension for the most frequent user, the tram frequency, is somewhat a controversial issue. One may consider that this finding is contrary to Directorate General Mobility and Transport [8] and Gökaşar et al. [16]. Akçarar provides services with an interval of 6 minutes at peak hours and 10-15 minutes at off-peak hours. Since the most frequent user is using the tram service every day and for hobby/socializing journeys, it reveals that waiting a few minutes less or more does not significantly affect his SQ perception. It is not surprising that the most frequent user attaches low importance to the staff's dress since the driver and other staff of the tram system have no or minimum level of communication with the passengers. It should be noted that this is the contrary to the bus system, from which the questionnaire has been adapted .

## **6. CONCLUSIONS**

Using the COS method developed within this study, it can be examined to what extent a change of 1 point in each dimension that constitutes SQ will change the perception of general service quality. This 1-point change may be in the direction of improving or reducing the dimension of SQ. Due to this feature, the study differs from other studies evaluating the SQ in the literature. Furthermore, the developed method enables the decision-makers to determine which dimensions need betterment to improve the tram system users' general SQ perception. They can also evaluate to what extent improvements in dimensions will change the SQ perception of society. In this way, they can plan the investments to be made in the tram system and perform a benefit/cost analysis that will reveal the benefits to be provided in return for these investments. Also, it can be ensured that limited resources are optimally used. Besides, decision-makers can use this method to create different user profiles instead of most frequent user and measure the SQ perception of different users and develop improvement solutions specific to user types. In this way, it can be ensured that the vulnerable part of the society, especially the children, the elderly, and the disabled, benefit from this service more efficiently. Thus, it can be stated that the improvements to be put forward through the developed method will also support social justice.

There are some weak points of the method applied in this study. For example, the survey applied to tram users may have some questions developed by IBBG for the bus system that is not suitable for the tram. Developing a global benchmarking survey on tram would be

beneficial for more appropriate and objective assessments. Another issue that can be considered the weakness is that some user groups may be more dominant in this survey data, obtained from the internet users by using a random sampling method. Developing a method that will ensure uniform distribution of each group may provide a more appropriate evaluation method. However, thanks to ANN's ability to mimic user through its abilities to learn and generalize, it also reduces the applied method's weakness. Similarly, 53% of respondents using the tram less than once a month may create the impression that a group of non-regular users has the dominant assessment. In contrast, the developed ANN has been trained to include the opinions of users of each group. In the subsequent evaluation, a person who uses the system every day has been identified as the most frequent user. This way, the opinion of the users who know the system better has been evaluated. However, it is natural that users who use the system less than once a month also have opinions about the service, as they may have experienced and dissatisfied with the system and/or may have relatives who regularly use the tram. Thanks to the method applied, the opinions of these people were able to be added to the model. In this way, the kind of improvements applied to increase their tram usage can also be evaluated. This way, the decision-makers can develop user-oriented investment plans and strategies.

In future studies for tram user satisfaction, the development and implementation of a global survey structure specific to the tram system will enable more appropriate evaluations. Periodic application of such a survey will help assess the change of user opinions or the effects of different service implementations on the system. Besides, thanks to the developed method, evaluations specific to certain user groups such as women, children, and older adults can also be made. In this way, special applications can be made to increase each group's satisfaction and thus usage of tram system.

### **Acknowledgement**

The author would like to thank the graduate thesis students Damla Yaşar and Cihan Bahadır Yaşar for their help in collecting and evaluating the survey data.

### **References**

- [1] Yaşar, D., Kocaeli tramvay sistemi kullanıcı memnuniyetinin incelenmesi, M.Sc. Thesis, İstanbul Okan Üniversitesi, 2020 (In Turkish).
- [2] Dell'Olio, L., Ibeas, A., Cecin, P., The quality of service desired by public transport users. *Transport Policy*, 18(1), 217-227, 2011.
- [3] Friman, M., Fellesson, M., Service supply and customer satisfaction in public transportation: The quality paradox. *Journal of Public Transportation*, 12(4), 57-69, 2009.
- [4] Benchmarking in European Service of public Transport (BEST), Results of the 2004 survey, <http://benchmarkingpublictransport.org/content/download/292/1328/file/Report%20BEST%20Survey%20-%202004.pdf>, 2004. Accessed 08 August 2020.

- [5] Eboli, L., Mazzulla, G., Service quality attributes affecting customer satisfaction for bus transit. *Journal of public transportation.*, 10 (3), 21-34, 2007.
- [6] Noor, H.M., Nasrudin, N., Foo, J., Determinants of Customer Satisfaction of SQ: City Bus Service in Kota Kinabalu, Malaysia. *Procedia - Social and Behavioural Sciences.*, 153, 595-605, 2014.
- [7] Islam, R., Chowdhury, M.S., Sarker, M.S., Ahmed, S., Measuring Customer's Satisfaction on Bus Transportation. *American Journal of Economics and Business Administration.*, 6(1), 34-41, 2014.
- [8] Directorate General Mobility and Transport and Co-ordinated by the Directorate General for Communication. Europeans' Satisfaction with Urban Transport, England, Transport for NSW., [https://ec.europa.eu/commfrontoffice/publicopinion/flash/fl\\_382b\\_en.pdf](https://ec.europa.eu/commfrontoffice/publicopinion/flash/fl_382b_en.pdf), 2014, Accessed 08 August 2020.
- [9] Verbich, D., Geneidy, A., The pursuit of satisfaction: Variation in satisfaction with bus transit service among riders with encumbrances and riders with disabilities using a large-scale survey from London, UK. *Transport Policy.*, 47(1), 64-71, 2015.
- [10] Ardiç, K., Sadaklıođlu, H., Şehirlerarası yolcu taşımacılığında hizmet kalitesinin ölçümü: Tokat örneđi. *Atatürk Üniversitesi İktisadi ve İdari Bilimler Dergisi.*, 23(3), 167-190, 2009 (In Turkish).
- [11] İmre, Ş., Çelebi, D., Measuring comfort in public transport: a case study for İstanbul. *Transportation Research Procedia.*, 25, 2441-2449, 2017.
- [12] Özuysal, M., Tanyel, S., Oral, M.Y., Fayda esaslı erişilebilirliđin ulaşım türü seçimi üzerindeki etkisi. *İMO Teknik Dergi.*, 23(113), 5987-6016, 2012 (In Turkish).
- [13] Dođan, G., Özuysal, M., Toplu ulaşımında bekleme süresini etkileyen faktörlerin incelenmesi: Güvenilirlik, yolcu bilgilendirme sistemi ve fiziksel koşullar. *İMO Teknik Dergi.*, 28(3), 7927-7975, 2017 (In Turkish).
- [14] Kahraman, Ç., Yıldız, M.S., Şehirlerarası otobüs işletmelerinde hizmet kalitesinin ölçülmesi ve bir uygulama. *Hacettepe Üniversitesi İktisadi ve İdari Bilimler Fakültesi Dergisi.*, 23(2), 121-144, 2005 (In Turkish).
- [15] Koçođlu, C.M., Aksoy, R., Hizmet kalitesinin servperf yöntemi ile ölçülmesi: otobüs işletmeleri üzerinde bir uygulama. *Akademik Bakış Dergisi.*, 29(1), 1-25, 2012 (In Turkish).
- [16] Gökaşar, I., Dündar, S., Buran, B., Yolcu ihtiyaçlarının incelenmesi. *İETT Örneđi. İBB Transist 2017 Bildiri Kitabı.*, 2-4 Kasım, İstanbul, 386-395, 2017 (In Turkish).
- [17] Gökaşar, I., Buran, B., Dündar, S., Kent içi otobüs memnuniyet anketi verileri ve faktör analizinden yararlanılarak otobüslerin hizmet kalitesinin modellenmesi: İETT örneđi. *Pamukkale Üniv Müh Bilim Derg.*, 24(6), 1079-1086, 2018 (In Turkish).
- [18] Girginer, N., Cankuş, B., Tramvay yolcu memnuniyetinin lojistik regresyon analiziyle ölçülmesi: Estram örneđi. *Yönetim ve Ekonomi: Celal Bayar Üniversitesi İktisadi ve İdari Bilimler Fakültesi Dergisi.*, 15(1), 181-193, 2008 (In Turkish).

- [19] Hemedođlu, E., Toplu taşımacılık sektöründe hizmet kalitesini ölçme: Algılanan hizmet kalitesi ve müşterinin arzuladığı hizmet kalitesi üzerindeki etkileri (Master Thesis). Yıldız Technical University, Graduate School of Natural and Applied Sciences, Istanbul, Turkey, 2010 (In Turkish).
- [20] Seçilmiş, C., Kaşlı, M., Kılıçlar, A., Sarı, Y., The effect of quality at railway services on customer satisfaction in terms of fee paid. *Ege Academic Review.*, 11(4), 573-586, 2011 (In Turkish).
- [21] Akyıldız Alçura, G., Kuşakçı, S.Ş., Gölbaşı Şimşek, G., Gürsoy, M., Tanrıverdi, S.C., Impact score technique for analyzing the service quality of a high-speed rail system. *Transportation Research Record: Journal of the Transportation Research Board.*, 2541(1): 64-72, 2016.
- [22] Šojat, D., Brcic, D., Slavulj, M., Analysis of public transport service improvements on tram network in the City of Zagreb. *Tehnički vjesnik.*, 24, 217-223, 2017.
- [23] Vujičić, M., Prester, J., Assessing service quality of public tram transport in Zagreb city using P-TRANSQUAL mode. *Zbornik Ekonomskog fakulteta u Zagrebu.*, 17, 19-31, 2019.
- [24] Khelf, M., Boukebbab, S., Bhouri, N., Boulahlib, M.S. Tram Service Quality and Its Impact on the Passengers' Modal Choice in Constantine City (Algeria), Selected Papers from the 18th International Conference on Reliability and Statistics in Transportation and Communication, RelStat'18, 17-20 October 2018, Riga, Latvia, 2018.
- [25] De Oña, R., De Oña, J., Neural Networks for Analyzing Service Quality in Public Transportation. *Expert Systems with Applications.*, 41(15), 6830–6838, 2014.
- [26] Islam, M.R., Hadiuzzaman, M., Banik, R., Hasnat, M.M., Musabbir, S.R, Hossain, S., Bus Service Quality Prediction and Attribute Ranking: a Neural Network Approach. *Public Transport.*, 8(1), 295–313, 2016.
- [27] International Bus Benchmarking Group (IBBG), <https://busbenchmarking.org>. Accessed 08 August 2020.
- [28] Acar, S., Bilen Kazancık, L., Meydan, M.C., Işık, M., İllerin ve bölgelerin sosyo-ekonomik gelişmişlik sıralaması araştırması SEGE-2017., *Kalkınma Ajansları Genel Müdürlüğü Yayını Sayı: 3* 2018 (In Turkish).
- [29] KBB Ulaşım Dairesi Başkanlığı., Akçaray güzergay haritası, 2017 <https://twitter.com/kocaeliulasim/status/876024582746066944/photo/1> Accessed 08 August 2020.
- [30] Turkish Statistical Institute TSI, Outcomes of Address Based Population Registration System 2018. TUIK, Ankara, Turkey, 2019 <https://biruni.tuik.gov.tr/medas/?kn=95&locale=tr>. Accessed 08 August 2020.
- [31] Meyer, J.T., *Fundamental Research Statistics for the Behavioural Sciences.*, New York: Holt Rinehart & Winston, 1979.
- [32] Fox, N., Hunn, A., Mathers, N., *Sampling and Sample Size Calculation. The NIHR RDS for the East Midlands / Yorkshire & the Humber*, 2007.

- [33] Dündar, S., Şahin, İ., Train re-scheduling with genetic algorithms and artificial neural networks for single-track railways. *Transportation Research Part C: Emerging Technologies* Volume 27(1), 1-15, 2013.
- [34] Yardım, M.S., Değer Şitilbay, B., Dündar, S., Modelling the effects of hydrated lime additives on asphalt mixtures by fuzzy logic and ANN. *Teknik Dergi*, Vol. 30(6), 9533-9559, 2019.
- [35] Murat, Y.Ş., Başkan, Ö., Modelling vehicle delays at signalized junctions: Artificial neural networks approach. *Journal of Scientific & Industrial Research*, Vol. 65(1), 558-564,2006.
- [36] Osuna, R.G., CS790: Selected Topics in Computer Science, Lecture Notes, Texas A&M University, 2002.
- [37] Murat, Y.Ş., Comparison of fuzzy logic and artificial neural networks approaches in vehicle delay modeling. *Transportation Research Part C* Vol. 14(1), 316–334, 2006.
- [38] Kaya Uyanık, G., Güler, N., A study on multiple linear regression. *Procedia - Social and Behavioral Sciences*, Vol. 106, 234-240, 2013.

# Improvement of Shear Strength of Zeolite-Bentonite Liner Material under High Temperatures with Tincal and Pumice\*

Sukran Gizem ALPAYDIN<sup>1</sup>  
Esra GUNERİ<sup>2</sup>  
Yeliz YUKSELEN-AKSOY<sup>3</sup>

## ABSTRACT

Thermal changes (high temperature and thermal cycles) occur around energy structures, such as energy piles, nuclear waste repositories, etc. Sometimes these temperature changes affect the engineering properties of surrounding soils undesirably. Hence, there is a need for durable soils that can keep their engineering properties unchanged under high temperature and thermal cycles for a long time. Tincal and pumice are used in the production of temperature-resistant and heat-insulated materials. Therefore, in the present study, 10% and 20% tincal and pumice additives were added to zeolite-bentonite mixtures and the shear strength behavior of the mixtures was investigated under room and high temperature (80°C). According to the results, the maximum shear stress values of zeolite-bentonite mixtures generally increased in the presence of tincal and pumice additives under high temperature. Both additives are effective for improvement the effect of pumice can be more pronounced.

**Keywords:** Energy geo-structures, pumice, tincal, zeolite, bentonite, shear strength.

## 1. INTRODUCTION

There has been an enormous increase in the number of energy structures in last decades. Since energy structures are in a direct contact with soil, there has been an increase in the number of studies on the behavior of soils under high temperatures in recent years. The

---

Note:

- This paper was received on August 31, 2020 and accepted for publication by the Editorial Board on April 13, 2021.
- Discussions on this paper will be accepted by November 30, 2022.
- <https://doi.org/10.18400/tekderg.788422>

1 Dokuz Eylul University, The Graduate School of Natural and Applied Sciences, Izmir, Turkey  
sukrangizem.alpaydin@ogr.deu.edu.tr - <https://orcid.org/0000-0002-0784-2361>

2 Dokuz Eylul University, The Graduate School of Natural and Applied Sciences, Izmir, Turkey  
esra\_cetinorgu@hotmail.com - <https://orcid.org/0000-0002-1840-2118>

3 Dokuz Eylul University, Department of Civil Engineering, Izmir, Turkey  
yeliz.yukselen@deu.edu.tr - <https://orcid.org/0000-0002-9145-765X>

\* A part of this study was presented at the 8<sup>th</sup> International Geotechnical Symposium. This article is an expanded version.

former studies have shown that the engineering properties of soils change depending on temperature. This change in engineering properties under high temperatures can often lead to cases that can damage energy structures, decrease their efficiency and affects human health and environment. Therefore, there is a need for the soils and/or soil mixtures that can maintain their properties unchanged at high temperatures or thermal cycles. A soil material that is durable to the thermal changes can be developed by help of thermally resistant materials such as boron, pumice, perlite, or fiber glass.

High temperatures affect the engineering properties of soils. The magnitude of this effect depends on density, water content, soil type, mineralogical and chemical composition [1]. The thermo-mechanical behavior of disturbed and natural clay soils was investigated using triaxial cell tests with controlled temperature (20°C to 60°C) [2]. In this study, it was found that the temperature increment caused change in the sample volume and the particles were rearranged. However, this volumetric deformation may be contraction or expansion. The change in deviator stresses due to high temperature and temperature cycling was investigated by Abuel-Naga et al. (2006) [3]. The water temperature in the triaxial cell was increased to 90°C, then tests were performed under this temperature. In terms of shear strength, higher peak shear strength values were obtained under high temperatures. Similar to this, previous studies show that the shear strength of clays increases with an increase in temperature. The change in the shear strength of clays with an increase in temperature is largely dependent on the volume change caused by high temperature [4]. The volume change that occurs with increase in temperature can be explained by the effects of high temperature on the interparticle forces and the viscous shear resistance of the adsorbed water, which affects the resistance of the clay particles to the fabric change [5]. Wang et al. (2017) reported that as the temperature increases, the viscosity of the adsorbed water decreases under the same consolidation stress and consequently decreases the porosity [6]. Accordingly, it can be concluded that the clays shrink in volume at high temperature. Hong et al. (2013) observed that thermal shrinkage increased the shear strength as a result of their study [4]. Although it is concluded that the shear strength of clays increases with high temperature, there is not much study on the behavior of soil mixtures at high temperature.

Bentonite, a montmorillonitic clay, often used as a liner, has low permeability and high plasticity. However, in cases where the water content decreases, bentonite shrinks and cracks occur. These cracks cause an increase in hydraulic conductivity and this situation will negatively affect the long-term performance of the liner. Therefore, the use of compacted clay is suitable in areas where temperature and humidity changes are insignificant [7]. Due to these adverse conditions when clay is used alone, sand-bentonite mixtures are widely used as barrier materials. The sand component increases the strength and the bentonite component fills the pore gap between the sand grains to reduce hydraulic conductivity [8]. Natural zeolites consist of acidic and volcanic tuffs that form rock-forming minerals [9]. Zeolites have ability to absorb smaller molecules and are therefore called "molecular sieves". It was observed that zeolite-bentonite mixtures were not affected by changes in water content, and also had very low hydraulic conductivity and low volumetric shrinkage potential, and these mixtures are proposed as an alternative to sand-bentonite mixtures [10]. Yukselen-Aksoy (2010) investigated the swelling potential, compressibility, hydraulic conductivity and shear strength behaviors of two different natural zeolites. In this study, it was found that zeolites did not have high compressibility and swelling potential and hydraulic conductivity was suitable for limitation of landfill liners [11]. Galvão et al. (2008) compared sand-bentonite



and zeolite-bentonite compression characteristics, volumetric shrinkage strain and hydraulic conductivity. In this study, it was reported that zeolite-bentonite was a good material for regular liner material [12]. The use of zeolite bentonite mixtures in waste storage is more advantageous than sand-bentonite mixtures thanks to the high adsorption property of zeolite [13].

Boron minerals and pumice are two of the materials commonly used in industry for various areas like temperature resistance and heat insulation. Pumice which is used as an additive, is a volcanic rock formed during volcanic eruptions [14]. It is found in two different forms as acidic and basic in nature. Pumice that consists of Si, Al, K, Na and Fe oxides, is also contains a small amount of Ca, Mg, Mn and Ti oxides [15-17] (Table 1). Pumice is used in different fields such as construction, textile, agriculture, chemistry, filtration and brick-ceramic production. Boron is found very commonly in the earth's crust. The boron is present in the minerals form in nature by bonding with oxygen. One of the most widely used boron minerals in the industry is tincal. Tincal is very rich in terms of sodium minerals ( $\text{Na}_2\text{B}_4\text{O}_7 \cdot 10\text{H}_2\text{O}$ ). Boron minerals are used in the various areas such as; energy, metallurgy, cement, glass and ceramics in order to reduce the thermal expansion of glasses and protect the glass from acid and scratches. In addition, Alpaydin (2019) reported an increase in the shear strength of tincal added sand-bentonite mixtures under high temperature (80°C) [16].

Due to such superior thermal properties of tincal and pumice, the motivation behind of the present study is improvement of engineering properties of zeolite-bentonite mixtures with these additives under high temperatures. The aim of this study is to investigate the change of the shear strength parameters of 10B-90Z and 20B-80Z mixtures under high temperature (80°C) with 10% and 20% pumice and tincal additives. In this way, durable soil material may be developed with the addition of tincal and pumice against high temperature.

Table 1 - Chemical composition of pumice [17]

	SiO <sub>2</sub>	Al <sub>2</sub> O <sub>3</sub>	Fe <sub>2</sub> O <sub>3</sub>	TiO <sub>2</sub>	CaO	MgO	Na <sub>2</sub> O
%	48.37	12.49	8.07	1.78	8.43	9.58	4.63

## 2. MATERIAL CHARACTERIZATION AND TEST METHODS

### 2.1. Material Characterization

In this study, zeolite-bentonite mixtures, pumice and as a boron mineral tincal were used. Bentonite was gathered from Esan Eczacıbaşı Industrial Raw Materials Industry and Trade Inc. and zeolite was obtained from Rota Mining Inc.. The X-Ray analyses of bentonite and zeolite were performed with Rigaku D/Max-2200/PC X-Ray diffractometer (XRD) and Thermo Scientific ARL X'TRA devices, respectively. XRD data of powders were recorded with a 2°/min scanning speed in the range of 20<2θ<80°. The analyses were performed with Win XRD software. After the analyses data were received, the relevant quantitative crystallographic information via Material Analysis Using Diffraction (MAUD) software, based on Rietveld refinement was used. The analyses results are shown in Figure 1. According to the results of the analyses, the bentonite consists of mostly quartz (SiO<sub>2</sub>), montmorillonite  $\text{Na}_{0.3}(\text{Al},\text{Mg})_2\text{Si}_4\text{O}_4(\text{OH})_24\text{H}_2\text{O}$  and illite (Figure 1a). Clinoptilolite, silica

(SiO<sub>2</sub>), silicon oxide hydrate, sodium tecto-alumosilicate hydroxide, and silicon aluminum oxide were obtained in the zeolite sample (Figure 1b).

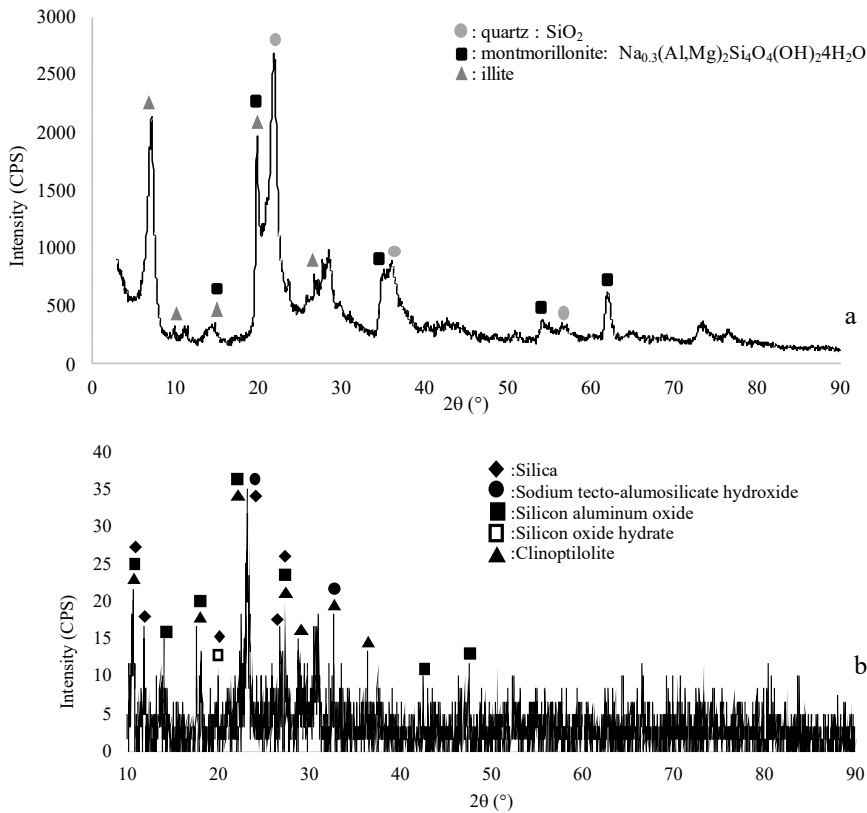


Figure 1 - XRD analysis results a) bentonite, b) zeolite

Pumice sample used as additive was gathered Pumice Export Mining Industry Inc. and tincal was obtained from Eti Mining Operations General Directorate. The grain size distribution of pumice is given in Figure 2. Because of the crystal structure of tincal, this experiment could not be performed for tincal.

According to XRD analyses, silicate and sodium-aluminum silicate compounds were determined in the pumice. Tincalconite, borax, jadeite and silica contents were observed in the tincal mineral.

The structure of the additives used in this study was observed using scanning electron microscopy (SEM). SEM analyses were performed using the COXEM EM-30 Plus device. Physico-chemical properties of all materials used in this study are given in Table 2. For the tests, zeolite and bentonite samples were prepared by drying in an oven (105°C) for 24 h. Pumice and tincal samples were used by sieving through No.40 sieve. Natural water contents of pumice and tincal were determined before the tests and calculations were made by taking these data into consideration. While giving the name to the mixtures, bentonite was

abbreviated as "B", zeolite "Z", pumice "P" and tincal "T". For example, the mixture of 18B-72Z-10P contains 10% pumice, 18% bentonite, 72% zeolite. While preparing the mixtures, 10% or 20% of the total weight of the dry mixture was taken as tincal or pumice, 10% or 20% of the remaining amount was bentonite and the rest of was zeolite. The material ratios in the sample were chosen such that bentonite / bentonite + zeolite ratios (B / B + Z) were 10% and 20%. For example, the B / B + Z ratio for an 9B-81Z-10T mixture was 0.10, while it was 0.20 for a 18B-72Z-10T mixture.

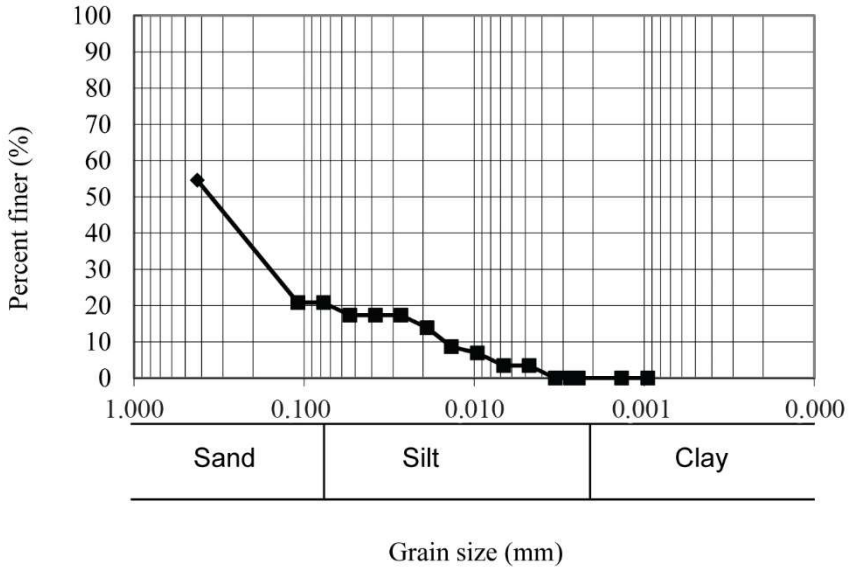


Figure 2 - Grain size distribution of pumice

Table 2 - Physico-chemical characteristics of all materials

	Bentonite	Zeolite	Pumice	Tincal
Specific gravity	2.70	2.30	2.50	1.67
Liquid limit (%)	476.0	42.0	37.1	60.5
Plastic limit (%)	70.1	NP	NP	42.9
pH	9.50	8.50	8.86	9.12

## 2.2. Test Methods

### 2.2.1. Compaction Tests

In this study, compaction tests were performed to obtain compaction parameters to be used in sample preparation for the direct shear tests of 10B-90Z and 20B-80Z mixtures in the presence of 10% and 20% pumice and tincal additives. In addition, the changes in the

compaction parameters of zeolite-bentonite mixtures with additives were determined. The compaction tests were performed according to ASTM D-698 (2012) standard [18]. While preparing the samples, the natural water content of pumice and tincal was taken into consideration for the calculations. The dry materials were mixed in a bowl with scoop. After mixing the dry materials homogeneously, these samples were prepared at four different water contents. The water was added by spraying method. The prepared samples were kept closed for 24 h in a plastic bag. After the tests were carried out, the samples were kept in an oven to determine the final water content. The Standard Proctor tests were and maximum dry unit weight ( $\gamma_{dmax}$ ) and optimum water content ( $w_{opt}$ ) values were determined.

### 2.2.2. Direct Shear Tests

In this study, the direct shear tests were performed according to ASTM D3080 (2018) standard [19]. These tests were carried out for 10B-90Z and 20B-80Z mixtures in the presence of 10% and 20% pumice and tincal at room temperature and 80°C. The samples were prepared at the  $w_{opt}+2\%$  and  $\gamma_d$  values corresponding obtained from Standard Proctor tests. The samples were placed in 6x6 cm<sup>2</sup> mold by compacting in three layers. The samples were placed as submerged condition in a tray filled with water for 24 h and 25 kPa vertical pressure was applied on the mold to prevent swelling. At the end of this period, the tests were performed under three different normal stresses (49, 98, 196 kPa). In the tests at 80°C, the temperature increment was provided with a specially designed heat rod for the shear box. The temperature of the water in the cell was kept around 80°C by using a thermostat. When the water temperature increased, the thermostat deactivated the heat rod, and when it decreased, it activated the heat rod to ensure that the water temperature

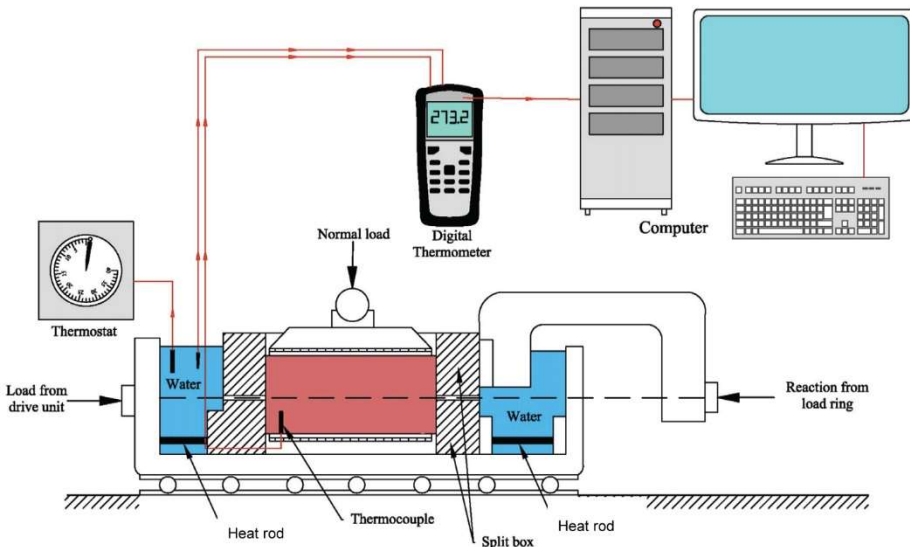


Figure 3 - Schematic presentation of the test set-up

remained at adjusted level. During the tests, the temperature of the sample and water were measured with K-type thermocouples. Measured values were recorded by digital thermometer. The schematic presentation of the test set-up is given in Figure 3.

At the end of the tests, the sample was left in the oven (105°C) to determine the water content. The shear strength parameters (internal friction angle,  $\phi'$ ; cohesion,  $c'$ ), maximum shear stress ( $\tau_{max}$ ) of the sample were determined with the data obtained during the tests.

### 3. RESULTS AND DISCUSSION

#### 3.1. Compaction Test Results

The changes in the compaction parameters of 10B-90Z and 20B-80Z mixtures in the presence of 10% and 20% pumice and tincal were determined and the results are given in Figure 4.

As shown in Figure 4, when 10% pumice was added to 10B-90Z mixture, max. dry unit weight did not change significantly, while 20% pumice additive increased the max. dry unit weight. It should be noted that the specific gravity value of pumice is 2.5 which is higher than zeolite (2.3) and lower than bentonite (2.7). Whereas the optimum water content of this mixture decreased with 20% pumice, it increased slightly with 10% pumice additive. When additive was added to the mixture the bentonite content decreased. The liquid limit values of the bentonite, pumice and tincal are 476%, 37.1% and 60.5%, respectively. For that reason, when bentonite content decreased, the optimum water content values decreased. For 20B-80Z mixture, 10% and 20% pumice additive increased the max. dry unit weight values, while the optimum water content showed a tendency as in the 10B-90Z mixture.

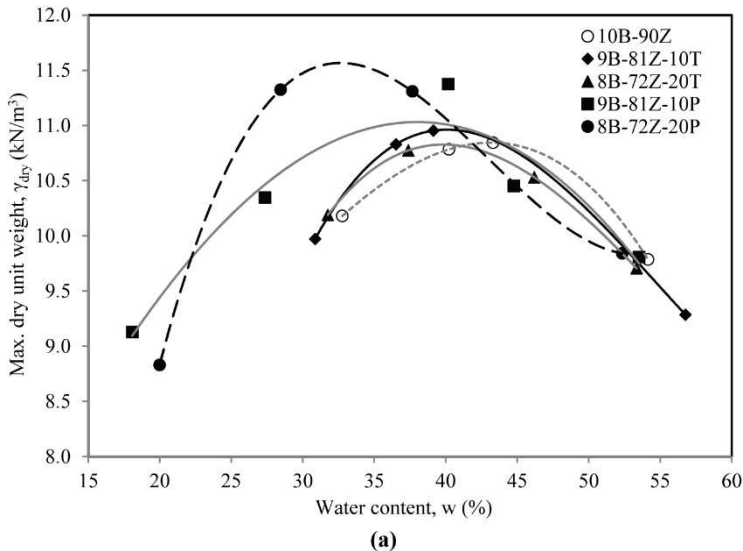


Figure 4 - Compaction curves of pumice and tincal added zeolite-bentonite mixtures  
 a)10B-90Z mixtures, b)20B-80Z mixtures



Figure 4 - Compaction curves of pumice and tincal added zeolite-bentonite mixtures a)10B-90Z mixtures, b)20B-80Z mixtures (continue)

As shown in Figure 4a, when tincal added to the 10B-90Z mixture, there was no significant change in the  $\gamma_{d,max}$  value, while the  $w_{opt}$  value decreased slightly. This decrease was around 3.5% and did not change with increasing tincal additive from 10% to 20%. According to the results given in Figure 4b, when 10% tincal was added to the 20B-80Z mixture, while the  $\gamma_{d,max}$  value increased by 0.4 kN/m<sup>3</sup>, there was no significant change in the  $w_{opt}$  value. When the tincal percentage was increased to 20%, the  $\gamma_{d,max}$  value increased slightly (0.3 kN/m<sup>3</sup>) while the  $w_{opt}$  value decreased.

### 3.2. Direct Shear Test Results

The change in the shear strength parameters of 10B-90Z and 20B-80Z mixtures in the presence of 10% and 20% pumice and tincal additives was determined at room temperature and 80°C. The shear strength parameters are given in Table 3 and failure envelopes are shown in Figure 5.

The angle of internal friction value of 10B-90Z was determined as 30.9°. The angle of internal friction value of pure zeolite is around 34-44° [11, 20]. According to the direct shear test results, when the temperature increased, the internal friction angle of the 10B-90Z mixture increased from 30.9° to 32.0°, and the cohesion value increased from 5.2 to 9.8 kPa. With increasing temperature, the internal friction angle of the 20B-80Z mixture increased by 5.2° and reached to 27.9°.

When additives (tincal and pumice) were added to the 10B-90Z mixture at room temperature, the internal friction angle and cohesion values generally increased. So much as 20% pumice additive, the internal friction angle value of 10B-90Z mixture increased from 31° to 36°. For

20B-80Z mixtures, while the internal friction angle generally decreased at room temperature, cohesion values increased. As an exception, an inverse trend was observed for the 18B-72Z-10P mixture (i.e. the internal friction angle increased while the cohesion value decreased). The internal friction angle value ( $32^\circ$ ) of the 10B-90Z mixture at  $80^\circ\text{C}$  temperature increased in the presence of 10% additives (tincal-pumice), while it decreased in the presence of 20% additives. The cohesion value of the 10B-90Z mixture at  $80^\circ\text{C}$  increased in the presence of pumice and tincal just like at room temperature. The internal friction angle of the 20B-80Z mixture increased in the presence of pumice, but decreased in the presence of tincal at  $80^\circ\text{C}$ . The cohesion values of 20B-80Z mixture also increased with additives at  $80^\circ\text{C}$  as in general. In addition, the effect of temperature increment on the internal friction angle of 10B-90Z mixtures was not as much as that of 20B-80Z mixtures.

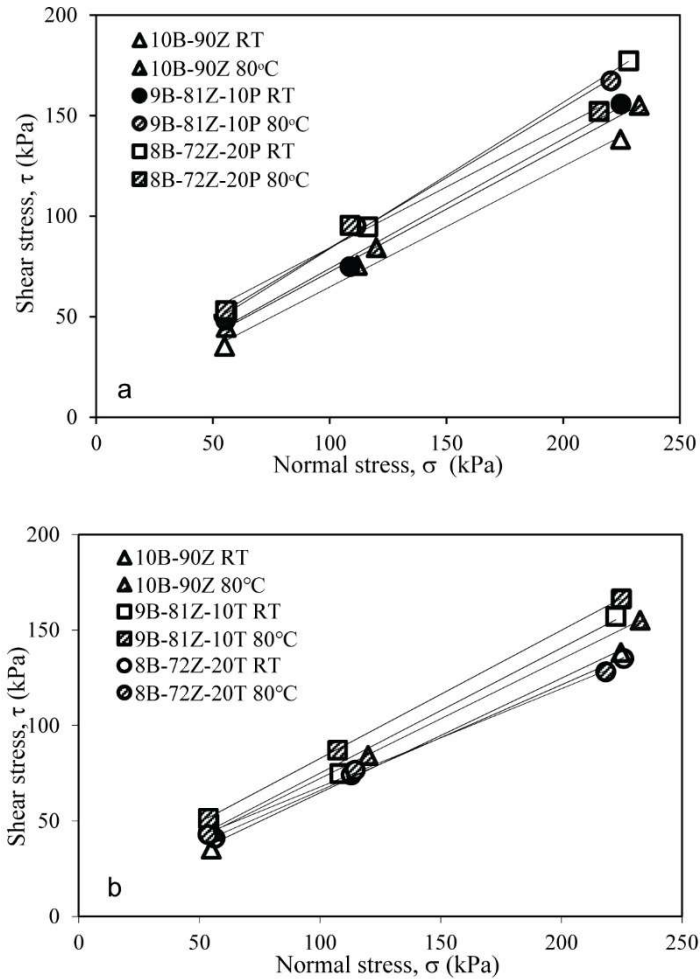


Figure 5 - Shear failure envelopes of 10B-90Z mixtures at room temperature and  $80^\circ\text{C}$  in the presence of a) pumice, b) tincal

Table 3 - Shear strength parameters of samples

Samples	Room Temperature		80°C	
	$\phi'$ (°)	$c'$ (kPa)	$\phi'$ (°)	$c'$ (kPa)
100 P	36.8	29.6	37.3	13.1
100 T	15.6	40.6	*	*
10B-90Z	30.9	5.2	32.0	9.8
9B-81Z-10P	32.9	9.5	35.0	14.4
8B-72Z-20P	36.1	11.0	31.5	23.6
9B-81Z-10T	33.3	9.5	33.9	15.6
8B-72Z-20T	29.0	10.6	27.2	16.3
20B-80Z	22.7	18.3	27.9	15.4
18B-72Z-10P	25.5	15.1	28.7	12.4
16B-64Z-20P	21.4	36.0	31.5	16.8
18B-72Z-10T	20.5	25.3	22.7	23.4
16B-64Z-20T	18.7	30.8	25.0	20.3

\*: Tincal collapsed when it was heated to 80°C

The maximum shear stress values of bentonite-zeolite mixtures in the presence of pumice and tincal at room temperature and 80°C are given in Table 4. According to Table 4, when the temperature of additive-free zeolite-bentonite mixtures was increased, an increase up to about 10 kPa in maximum shear strength values was observed.

The results show that the shear strength of 10B-90Z and 20B-80Z mixtures were not affected negatively much by the additives at both temperatures. However, there was an increase up to 20 kPa in the maximum shear strength in the presence of 20% pumice. However, when the temperature of 20% pumice mixtures (8B-72Z-20P and 16B-64Z-20P) was increased to 80°C, the change in maximum shear strength was almost negligible. The effect of additives other than this on the shear strength was either insignificant or negative at room temperature. In addition to this, another remarkable point was that the maximum shear strength of all mixtures increased only with the effect of temperature increment, while only 20% pumice added mixtures decreased slightly. It can be concluded that the improvement in the shear strength of the mixture obtained by pumice additive occurred independently of the temperature increment.

The maximum shear stress values of bentonite-zeolite mixtures in the presence of additives at both temperatures are presented in Figure 6. As can be seen from this figure, there was generally an improvement in maximum shear stress for 20B-80Z mixtures at 80°C, and this improvement also valid for 10B-90Z mixtures.



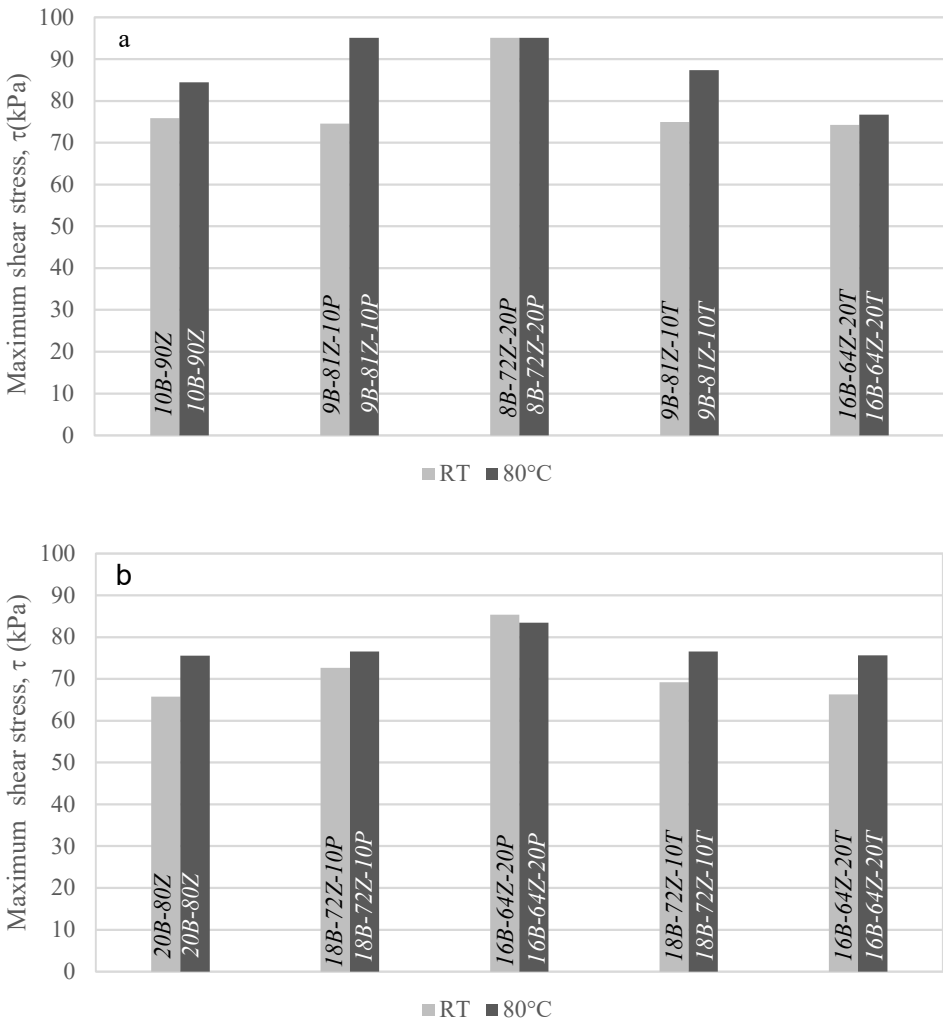


Figure 6 - Maximum shear stress a) 10B-90Z mixtures at room temperature and 80°C, b) 20B-80Z mixtures at room temperature and 80°C

The results have shown that, when temperature increased the maximum shear stress of additive-free zeolite-bentonite mixtures increased slightly. Moreover, generally the addition of tincal and pumice increased the  $\tau_{max}$  more. In the presence of 20% pumice the maximum shear strength value of 20B-80Z mixture increased from 75.5 to 83.4 kPa under 80°C. However, the effect of tincal on the  $\tau_{max}$  was insignificant. Previous studies have shown that the increase in temperature transforms the smectite mineral into more constant silicate phases. Smectite transforms to illite depending on temperature, time and  $K^+$  pore-water doping [21]. As a result of this water retention capability of bentonite decreases. If the ability

of water adsorption of clay decreases, the strength of the clay should increase. In terms of zeolite, most zeolites undergo dehydration-induced reductions in volume. Clinoptilolite can undergo a large, very anisotropic decrease in unit-cell dimensions [22]. The water retention capability decreased in bentonite and volume reduction in zeolite caused an increase in shear strength of the zeolite-bentonite mixture by temperature increase. The results of this study confirm this behavior as well. The maximum shear strength value of 10B-90Z and 20B-80Z increased from 75.8 to 84.4 kPa, from 65.7 to 75.5 kPa, respectively. Previous studies showed that at a given water content the suction decreased with increasing temperature [23]. Moreover, as suction decreases, the shear strength increases. Hence, temperature increment causes an increase in the shear strength.

*Table 4 - Maximum shear stress of all mixtures at both temperatures*

Samples	Maximum Shear Stress (kPa)	
	Room Temperature (~25°C)	80°C
100P	127.5	87.3
100T	70.2	*
10B-90Z	75.8	84.4
9B-81Z-10P	74.5	95.1
8B-72Z-20P	95.1	95.1
9B-81Z-10T	74.9	87.3
8B-72Z-20T	74.2	76.7
20B-80Z	65.7	75.5
18B-72Z-10P	72.6	76.5
16B-64Z-20P	85.3	83.4
18B-72Z-10T	69.2	76.5
16B-64Z-20T	66.3	75.6

\*: Tincal collapsed when it was heated to 80°C

The results of this study have shown that the shear strength of both zeolite-bentonite mixtures increased in the presence of tincal. The tincal is held strongly by the aluminum or silicon tetrahedron portion in the clay structure [24]. For that reason, the tincal was held by bentonite particles. Eventually the shear strength of zeolite-bentonite increased as a result of both tincal adsorption and material replacement. Because when the tincal added to the sample both bentonite and zeolite content was decreased. The bentonite material was replaced with tincal mineral which has very high thermal resistivity and very low thermal expansion. For that reason, the material replacement may be another reason for the increase in the shear strength of zeolite-bentonite mixtures under high temperature.

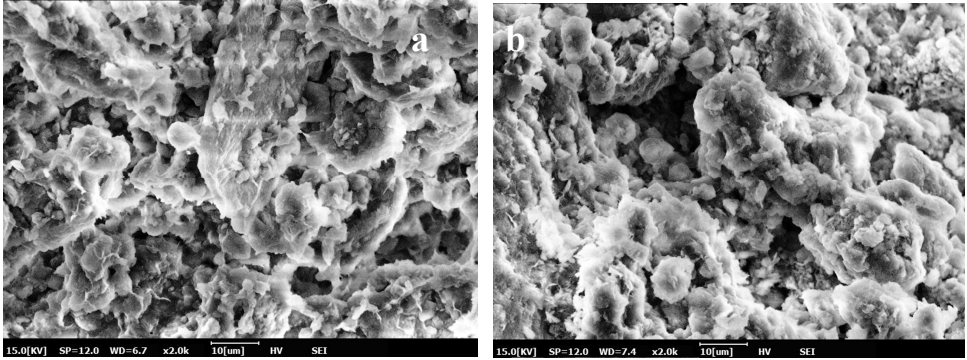


Figure 7 - Scanning electron microscope photographs of 20B-80Z mixture (x2000) at a) room temperature, b) 80°C

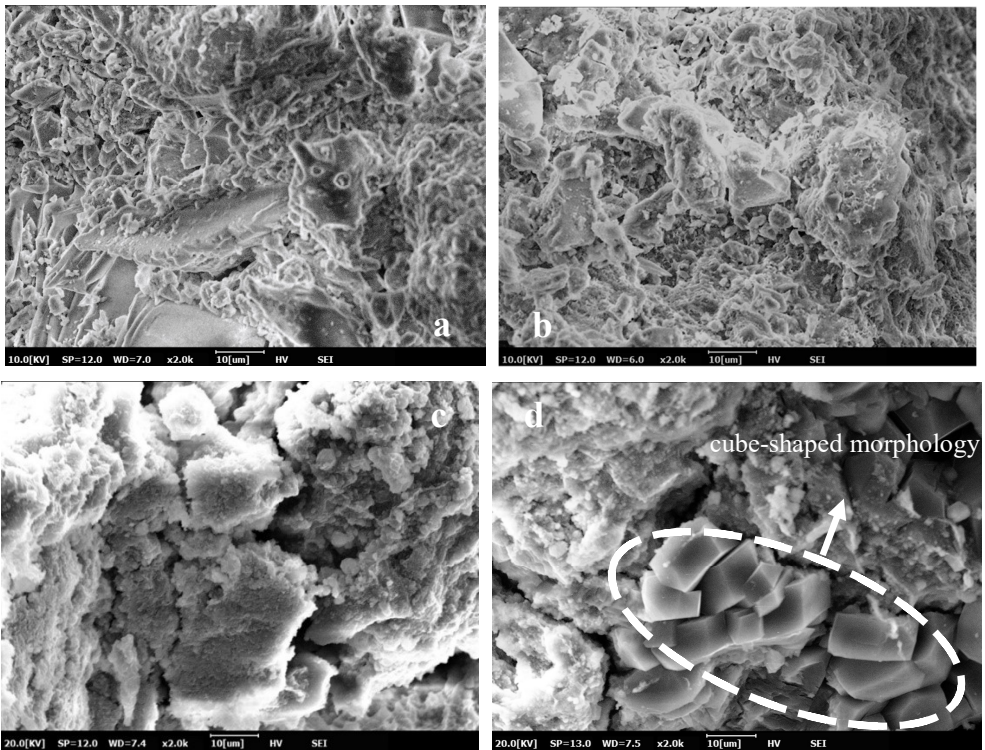


Figure 8 - Scanning electron microscope photographs of additives (x2000) a) pumice (RT), b) pumice (80°C), c) tincal (RT), d) tincal (80°C)

The SEM photos of the additive-free 20B-80Z mixtures at room temperature and 80°C are given in Figure 7. It was observed that the structure of the mixture almost same between the two SEM photos. This observation supports evaluated slight changes in the shear strength

parameters. The SEM photos of the additive materials (i.e. pumice and tincal) at room temperature and 80°C are given in Figure 8. The SEM photos of the pumice were taken at low voltage for best view. When structural view was compared between room temperature and 80°C, there was no change between these photos. However; the maximum shear stress value decreased when temperature increased. The direct shear test on the tincal collapsed under 80°C. However; at the SEM photo different structure like cubical particles clearly was observed under high temperature. According to the X-Ray analysis jadeite was found in the tincal sample and this cubical form belongs to jadeite mineral.

#### **4. CONCLUSIONS**

In this study, boron mineral (tincal) and pumice additives were used in order to improve engineering properties of zeolite-bentonite mixtures under high temperatures. The compaction and shear strength behavior of 10B-90Z and 20B-80Z mixtures were determined in the presence of 10% and 20% pumice and tincal. In addition, the direct shear tests were performed at 80°C and compared with the results at room temperature. According to the compaction test results, when pumice and tincal were added to the 10B-90Z mixture, the optimum water content generally decreased, while the maximum dry unit weight did not change much in the presence of tincal but increased in the presence of pumice. The maximum dry unit weight values of 20B-80Z mixtures generally increased with both additives. According to the direct shear test results, when pumice was added to zeolite-bentonite mixtures, the internal friction angles generally increased at 80°C. On the other hand, tincal additive generally decreased the angle of internal friction and increased cohesion. The highest internal friction angle values of zeolite-bentonite mixtures were obtained in the presence of pumice additive at both temperatures. Also, the shear strength of additive-free 10B-90Z and 20B-80Z mixtures increased under high temperature, when compared with the room temperature. However, this increment was more in the presence of pumice (10% and 20%) and tincal (10%). According to the results obtained from the present study, pumice and tincal additives may be used to increase the thermal durability of zeolite-bentonite mixtures at high temperatures. Considering the results of the present study, pumice and tincal additives increased the shear strength of zeolite-bentonite mixtures under high temperatures. The effect of pumice was slightly higher than that of tincal, however; both additives have positive effects. These mixtures have a good potential to be used as thermally durable materials, with additional research required in this regard. In future studies the hydraulic conductivity and volume deformation behavior in the presence of pumice and tincal should be investigated. In terms of shear strength with tincal and pumice additives promising results were observed. Moreover; in landfills and nuclear waste repository liners these additives are candidate additives in order to improve engineering properties of natural soil mixtures under high temperatures.

#### **Symbols**

- $\gamma_{d,max}$  is the maximum dry unit weight  
 $w_{opt.}$  is the optimum water content  
 $\phi'$  is the internal friction angle

$c'$  is the cohesion

$\tau_{\max}$  is the maximum shear stress

### **Acknowledgements**

The authors greatly acknowledged the support of TÜBİTAK (Grant no:217M553).

### **References**

- [1] Mitchell, J.K., Temperature Effects on the Engineering Properties and Behavior of Soils. Proceeding of International Conference on the Effects of Temperature and Heat on Engineering Behaviour of Soils, 9(6), 9–28, 1969.
- [2] Burghignoli, A., Desideri, A., Miliziano, S., A Laboratory Study on the Thermomechanical Behaviour of Clayey Soils. Canadian Geotechnical Journal, 37(4), 764–780, 2000.
- [3] Abuel-Naga, H.M., Bergado, D.T., Ramana, G.V., Grino, L., Rujivipat, P., Thet, Y., Experimental Evaluation of Engineering Behavior of Soft Bangkok Clay under Elevated Temperature. Journal of Geotechnical and Geoenvironmental Engineering, 132(7), 902–910, 2006.
- [4] Hong, Z.S., Bian, X., Cui, Y.J., Gao, Y.F., and Zeng, L.L., Effect of Initial Water Content on Undrained Shear Behaviour of Reconstituted Clays. Géotechnique, 63(6), 442–450, 2013.
- [5] Abuel-Naga, H.M., Effect of Temperature on Shear Strength and Yielding Behavior of Soft Bangkok Clay. Soils and Foundations, 47(3), 423–436, 2007.
- [6] Wang, S., Zhu, W., Qian, X., Xu, H., Fan, X., Temperature Effects on Non-Darcy Flow of Compacted Clay. Applied Clay Science, 135, 521–525, 2017.
- [7] Öncü, Ş., Bilsel, H., Effect of Zeolite Utilization on Volume Change and Strength Properties of Expansive Soil as Landfill Barrier. Canadian Geotechnical Journal, 54(9), 1320–1330, 2017.
- [8] Akgün, H., Koçkar, M.K., Aktürk, Ö., Evaluation of a Compacted Bentonite/sand Seal for Underground Waste Repository Isolation. Environmental Geology, 50, 331–337, 2006.
- [9] Bish, F., Guthrie, G.D., Mineralogy of Clay and Zeolite Dusts (exclusive of 1:1 layer silicates). In Health effects of mineral dusts. Edited by G.D. Guthrie and B.T. Mossman. Reviews in Mineralogy, 28, 139–184, 1993.
- [10] Kaya, A., Durukan, S., Ören, A.H., Yükselen, Y., Determining the Engineering Properties of Bentonite-zeolite Mixtures. Teknik Dergi, 17(3), 3879–3892, 2006.

- [11] Yükselen-Aksoy, Y., Characterization of Two Natural Zeolites for Geotechnical and Geoenvironmental Applications. *Applied Clay Science*, 50, 130-136, 2010.
- [12] Galvão, T.C.B., Kaya, A., Ören, A.H., Yükselen, Y., Geomechanics of Landfills-Innovative Technology for Liners. *Soil & Sediment Contamination*, 17(4): 411-424, 2008.
- [13] Kaya, A., Durukan, S., Utilization of Bentonite-Embedded Zeolite as Clay Liner. *Applied Clay Science*, 25, 83-91, 2004.
- [14] Witham, A.G., Sparks, R.S.J., Pumice. *Bulletin of Volcanology*, 48, 209-223, 1986.
- [15] Liguori, V., Sciorta, R., Ruisi, V., The Pumice Aggregates of Lipari Island (Aeolian Isles-Italy). *Bulletin of the International Association of Engineering Geology*, 30, 431-434, 1984.
- [16] Alpaydın, Ş.G., An Investigation of Effects of Boron Additives on the Permeability and Shear Strength Behavior of Sand-Bentonite Mixtures Under High Temperatures. MSc. Thesis, Dokuz Eylül University, 2019.
- [17] Abedi Koupai, J. Application of natural and synthetic water absorbers materials on soil hydraulic properties. Research Report, Isfahan University of Technology, 2012.
- [18] ASTM D 698., Standard Test Methods for Laboratory Compaction Characteristics of Soil Using Standard Effort, ASTM International, USA, 2012.
- [19] ASTM D 3080., Standard Test Method for Direct Shear Test of Soils Under Consolidated Drained Conditions, ASTM International, USA, 2018.
- [20] Georgiannou, V.N., Lefas, D., Konstadinou M., Perraki, M., Geotechnical properties of a natural zeolite. *Proceedings of the Institution of Civil Engineers - Geotechnical Engineering*, 170:5, 395-406, 2017.
- [21] Wersin, P., Johnson, L. H., Snellman, M., Impact of iron released from steel components on the performance of the bentonite buffer: A preliminary assessment within the framework of the KBS-3H disposal concept. *MRS Proceedings*, 932, 117, 2006.
- [22] Bish, D.L., Carey, B. Thermal Behavior of Natural Zeolites. *Reviews in Mineralogy and Geochemistry*, In book: *Natural Zeolites: Occurrence, Properties, Applications*, Editors: D. L. Bish and D. W. Ming, Mineralogical Society of America, Washington, DC, 45(1), 403-452, 2001.
- [23] Tang, A.M., Cui Y.J. Controlling Suction by the Vapour Equilibrium Technique at Different Temperatures and Its Application in Determining the Water Retention Properties of MX80 Clay. *Canadian Geotechnical Journal*, 42 (1), 287-296, 2005.
- [24] Privett, K. J.E. *Gillott Clay in Engineering Geology*, 2nd Edition. (Developments in Geotech Eng 41.) Elsevier Science Publishers, Amsterdam, 1987.

# Challenges and Benefits of the Use of AASHTOWare for 3 Climatic Regions in Turkey

Beyhan IPEKYUZ<sup>1</sup>

Hediye TUYDES YAMAN<sup>2</sup>

Hande Isik OZTURK<sup>3</sup>

## ABSTRACT

The economic growth in developing countries triggers investments in highway networks. Thus, this requires a re-evaluation of existing design practices, which are mostly empirical. An alternative is the relatively recently developed Mechanistic-Empirical (M-E) design method. It has major data challenges and must be identified before a major switch. In this study, three different climatic regions for Turkey were analyzed optimizing 162 design combinations. Results showed that climate, traffic, and reliability parameters extremely affect the performance of the pavement. As in the current practice of Turkey, climate and material effects are not currently considered; these should be further studied considering the local calibration steps.

**Keywords:** Mechanistic-Empirical design method, AASHTOWare, AASHTO, flexible pavement, pavement design, climate.

## 1. INTRODUCTION

In both developed and developing countries, a considerable amount of gross national product is spent on the expansion and maintenance of the road networks [1]. It is important to evaluate these investments based on service life perspective and follow a pavement design guide considering the climate, traffic, environmental, subgrade, and material properties all at once, using a method capable of predicting distress mechanisms.

In Turkey, the General Directorate of Highway (GDH-KGM) was established in 1950 to construct, maintain, rehabilitate, and manage the intercity roadway network. Today, within

---

Note:

- This paper was received on September 15, 2020 and accepted for publication by the Editorial Board on July 7, 2021.
- Discussions on this paper will be accepted by November 30, 2022.

• <https://doi.org/10.18400/tekderg.793889>

1 Middle East Technical University, Department of Civil Engineering, Ankara, Turkey  
ipekyuzb@metu.edu.tr - <https://orcid.org/0000-0001-8088-1896>

2 Middle East Technical University, Department of Civil Engineering, Ankara, Turkey  
htuydes@metu.edu.tr - <https://orcid.org/0000-0001-8088-1896>

3 Middle East Technical University, Department of Civil Engineering, Ankara, Turkey  
ozturkha@metu.edu.tr - <https://orcid.org/0000-0003-2053-992X>

their 30 000 km network, it has about 17 500 km flexible pavements, 13 000 km chip seals and the rest is majorly stabilized and earth. It is targeted to upgrade the poor roadway segments with flexible pavements, and to add new corridors.

In pavement design, starting with the American Association of State Highways Officials (AASHO) Interim Guide of 1962, the GDH adopted the AASHTO methods. The latest version, based on AASHTO'93 design guideline [2], has been in use in Turkey as in many countries for the design of both flexible and rigid pavements even though it is stated to overestimate/underestimate layer thicknesses in most design cases, leading to either high initial construction cost or inadequate pavement performance under traffic loading during its service life [3]. Alternatively, the AASHTO has introduced the new Mechanistic-Empirical Pavement Design Guide (MEPDG) based on the Mechanistic-Empirical (M-E) design method. The M-E method is embedded in the AASHTOWare software [4], which considers the material properties, climate, subgrade type, reliability, etc. and, predicts performance for the entire service life of the pavement. This software computes the stresses, strains, and deflections through the life of the pavement and estimates the distresses with the help of distress transfer functions [5]; and it gained popularity in European countries such as Italy [6], Poland [7, 8], and Romania [9].

Applying MEPDG may provide long term economic and performance evaluations for highway investments in developing countries. Some studies focused on the application of the M-E method as a design technique were conducted in emerging economies, e.g., Qatar [10, 11], Egypt [12, 13], and the Kingdom of Saudi Arabia, lately [14].

Despite the interest in adopting the M-E design method for future road investments in developing countries, such as Turkey, there are still limited experience and study in switching to the M-E design because the data needs create a major challenge, which must be carefully assessed a priori, and is the main motivation behind this study. In the case of Turkey, Shakhan et al. [15] focused on the data collection needs for pavement design in the city of Izmir, Turkey but it fell short in creating any specific design. Ozturk et al. [16] is the only study to use the M-E method for rigid pavement design for 8 different cities in Turkey. This follow-up study aimed to support the discussion of the challenges and benefits of switching to the M-E method for flexible pavement design.

To evaluate the potential use of the M-E method for different design cases and compare the results with those of AASHTO'93, various design cases were created based on traffic conditions (low, medium, high), subgrade types, reliability levels, and surface course mixtures, and all of which were assumed to have a fixed service life of 20 years. As climatic conditions affect many of these aforementioned parameters directly, the pavement design cases were repeated for three different climatic (CL) regions (cold, rainy, and warm/Mediterranean) in Turkey.

AASHTOWare Pavement software Version 2.2 (AASHTOWare in short) was used to determine the optimum design thicknesses by iteratively varying these thicknesses to meet the target levels of distresses at the end of the life of the pavement. Following the research methodology for the rigid pavement design using the M-E design in [16], this study first charted the effect of selected design factors on flexible pavement thickness (thus, ultimately the cost of it indirectly). Secondly, the evaluation of selected designs by AASHTO'93 in the AASHTOWare enabled the quantification of benefits of the latter using some pavement



performance criteria, as well. The numerical results and challenges of the need to adopt the M-E approach are expected to lead the researchers and government officials to better evaluate the use of the M-E for Turkey and other developing countries.

## **2. BACKGROUND**

### **2.1. Flexible Pavement Design Guide by AASHTO'93**

Based on empirical findings of the AASHO Road Test at Ottawa, Illinois, USA, the first pavement design guide of 1962 was further improved in 1972 and 1986. In its latest version, AASHTO'93, it is primarily aimed to predict the layer thicknesses with limited traffic, material, and climatic data; whereas other data are taken into consideration in a limited way, for example, the climatic conditions are only taken into account for drainage and seasonal variation of the subgrade strength [17, 18]. The major limitations of AASHTO'93 could be listed as follows [2, 3]:

- The design equations are based on the limited material properties, such as one subgrade type and one climatic condition. It indirectly considered the influence of the climate with resilient modulus and drainage coefficients.
- Traffic loads applications and repetitions in the equation are developed from identical axle loads and configurations and are calculated according to the Equivalent Single Axle Load (ESAL). However, increasing transportation demand and freight loads (even 10-20 times more), as well as different axle load configurations, are not met by ESAL.
- The design equations were developed in the accelerated two-year testing period, which did not address the long-term effects of climate and aging of materials. The results are extrapolated out to a longer period.

However, the AASHTO'93 guideline is still in use in 80% of states in the US [19], as well as many other countries including Turkey.

### **2.2. Flexible Pavement Design by Mechanistic-Empirical (M-E) Method**

Based on the limitations discussed above, the M-E design method is developed using mechanical relations in addition to the empirical data. The distress transfer functions, mechanical part of the M-E method, are nationally calibrated using design inputs and distress data gathered in the Long-Term Pavement Program (LTPP) database [20, 21]. The M-E design method requires extensive input to better simulate the design conditions to accurately predict the distresses. Due to the availability of the inputs, hierarchical design levels are defined as Level 1, 2, and 3: Level 1 inputs are most accurate and determined through field data collection or laboratory studies. Level 2 inputs are derived from correlations and regional values. Finally, Level 3 inputs are typical local estimates, and these are the default values suggested in the M-E design guide [3].

The M-E method utilizes an elastic model as well as it works by processing various inputs (traffic, climatic and environmental conditions, material properties, reliability, subgrade types, and design layer thicknesses) to compute the pavement performance indicators [22].

Thus, the procedure does not directly address the thicknesses. Specifically, this method is used to evaluate a trial design for a given set of site conditions and failure criteria at a specified level of reliability [23].

The M-E design allows for better modeling of pavements and yields closer results to real conditions in life, while the AASHTO'93 guide overestimates performance for pavements especially in warm regions and at high traffic levels [24]. In the M-E design, the performance is evaluated by the cumulative incremental damage at any point in a pavement structure; and it allows for the prediction of distresses over time including International Roughness Index (IRI), rutting, fatigue, and thermal cracking in asphalt pavements, considering stress, strain and deformations based on the interactions between traffic, climate and pavement structure. The major inputs in the M-E method are discussed as follows:

#### *Climate effect in the M-E method*

The major improvement is the consideration of climatic effects on pavement materials, responses, and distresses in an integrated manner [25, 26]. Climatic inputs are essential to predict the temperature and moisture profiles in the pavement over the design life. Pavement layer temperature and moisture predictions are calculated on an hourly basis and used to estimate the material properties for the foundation and pavement layers throughout the design life [15, 27]. It was shown that seasonal temperature variations carry out a considerable drop in pavement durability and significantly affect the overall performance of the pavement system, which is greatly affected by temperature and moisture [8, 28]. An increase in moisture content reduces the load-carrying ability of subgrade soils. Therefore, asphalt distresses such as total rutting, fatigue and the thermal cracking of asphalt pavement highly depend on the temperature [18]. Strong relationships between peak strain values and temperature were observed in the study of Shafiee et al. [29].

AASHTOWare has an extensive number of embedded weather station data. However, these stations are only limited to airfields around the US. On the other hand, many researchers studied ways to implement the M-E design outside the US by using different methods to generate local climate inputs and to convert the data to the required format. In Jannat's study [30], climatic inputs for the M-E design method for different climate zones in Canada were determined. In another study, the monthly minimum, maximum, and average temperature values were matched with the climatic data considering annual air temperature, annual precipitation, freezing index, and the average annual number of freeze-thaw days. The similarities in average and range of seasonal temperature, percent sunshine, and wind speed were considered and compared between Italy and Alabama [6]. A weather station in Alabama was used for climatic input examined the validity of this approach by comparing locally used surface temperature equation results and climate model output. In a more recent study, virtual station matching based on climatic similarity was performed to obtain climatic data for Qatar [11]. Researchers observed the climatic conditions in Needles Airport in California, US, to be reasonably resembling the climatic conditions in Qatar. Climatic data were generated with the AASHTOWare by the interpolation of data from six nearby weather stations in Oklahoma, US [31]. In one of the latest studies to implement the M-E design in Egypt, weather-related input data were divided into subgroups based on annual temperature, annual precipitation, wind speed, relative humidity, and sunshine [28].

### *Traffic conditions in the M-E method*

The M-E design method requires actual traffic data rather than a total ESAL number, which allows us to better simulate the traffic during the life of the pavement. The data briefly includes the traffic growth, axle configurations (axle spacing and wheelbase), axle load distribution factors, vehicle classification distribution, truck volume, hourly and monthly traffic volume adjustment factors, number of axles per truck and lateral traffic wander to perform analyses, in addition to standard single, tandem, tridem, and quad-axle loadings and specific percentages of each truck class [4].

### *Subgrade effect in the M-E method*

Subgrade plays a major role in the pavement bearing capacity, which directly affects pavement performance. The variations in the properties of the soils concerning seasonal climatic conditions are taken into consideration [6, 32]. As noted by Zofka et al. [7], the resilient modulus of the soil depends on the stress, moisture, and freeze-thaw cycle effects. Thus, subgrade type (soil properties) is directly affected by weather conditions and locations. On the other hand, the study of Aguib [12] showed that the change in subgrade type in AASHTO'93 do not influence the Asphalt Concrete (AC) layer thickness, since the influence of climate in this method is neglected, which is the major weakness of AASHTO'93.

### *Reliability in the M-E method*

In the M-E design method, the reliability level is another critical criterion, which can be defined as the probability of satisfactory performance over the traffic and climate conditions for the analysis period [2]. Therefore, the M-E method yields more realistic results in the observation of reliability for rutting performance. Note: High-level reliability ultimately leads to the conservative design and tends to over-thick pavements [27].

### *Material properties in the M-E method*

The M-E design method requires detailed material properties (e.g., aggregate gradation, air void, binder performance grade (PG), etc.). Material properties of surface course mixture are used for the climatic model, the pavement response models, and the distress models in the design process. The pavement response models need material properties considering the effects of traffic loading and temperature changes. Similarly, distress models are used to predict pavement performance [33, 34].

### *Performance criteria used in the flexible design*

The performance of flexible pavements is predicted based on selected threshold values of indicators of the embedded distress models, e.g., the terminal IRI ( $m/km$ ), rutting in total pavement ( $mm$ ), AC bottom-up (%), and AC top-down ( $m/km$ ) fatigue cracking, AC thermal cracking ( $m/km$ ) and rutting in AC only ( $mm$ ) through the design life. To optimize, the values of these indicators for various pavement thickness designs are monitored concerning the selected threshold limits. Although these threshold values may vary across agencies, the limits proposed by the AASHTO used in this study are shown in Table 1. At the beginning of the design procedure, the initial thicknesses of each layer in the software were selected according to layer thicknesses determined by the GDH based on AASHTO'93, as given in Table 2.

Table 1 - Flexible pavement performance criteria

Performance Criteria	Limit values
Terminal IRI (m/km)	2.7
Rutting - total pavement (mm)	19.0
AC bottom-up fatigue cracking (%)	25.0
AC thermal cracking (m/km)	189.4
AC top-down fatigue cracking (m/km)	378.8
Rutting - AC only (mm)	12.0

Table 2 - Layer design thicknesses by the GDH based on AASHTO '93

Reliability (%)	AADTT*								
	1000			7500			15000		
	85	90	95	85	90	95	85	90	95
Pavement Layer Thickness (cm)									
Surface course	5	5	5	5	5	5	5	5	5
Binder course	6	6	6	7	8	8	8	10	10
Bituminous base	8	8	8	10	11	11	11	12	12
Base course	15	20	20	20	20	20	20	20	20
Subbase course**	20	20	20	20	20	20	20	20	20

\* AADTT stands for average annual daily truck traffic.

\*\* The subbase course thickness is assumed constant throughout the analysis since 20 cm-thickness is the typical application in Turkey.

### 3. METHODOLOGY

#### 3.1. Determination of Climatic Regions for the M-E Pavement Design in Turkey

There are limited number of studies in Turkey on the M-E design. In the Izmir (city in Turkey) study [15], the focus was the data collection to implement the M-E design, but no runs were performed. In the only study performing the M-E based rigid pavement designs [16], 8 cities were studied individually by simply matching them with the selected US city/weather stations.

In this study, a more general evaluation was made by dividing the country into the climatic regions (CLs) based on Bitumen Class Selection Maps [35] respecting climatic characteristics. Accordingly, 81 provinces of Turkey were divided into 8 CLs as shown in Table 3. This suggested that many cities could be grouped in a single CL from the point of flexible pavement design based on the PG binder selection. It should be also noted that these CLs almost overlapped with climate regions from the Köppen-Geiger Climate Classification Map of Turkey (see Figure 1). For example, regions having hot-summer-Mediterranean climatic conditions based on Köppen-Geiger climate type exhibited similar conditions to climate characteristics of Izmir (Mediterranean/warm).

Table 3 - CLs classification table for Turkey

CL*	Share (%)	Provinces (81)
1	13.11	Antalya; Aydin; Balikesir; Denizli; Elazig; <b>Izmir</b> ; Manisa; Mugla;
2	13.48	Agri; Bolu; <b>Erzurum</b> ; Kars; Sivas; Yozgat; Bayburt; Ardahan;
3	7.36	Giresun; <b>Istanbul</b> ; Ordu; <b>Rize</b> ; Sakarya; Samsun; Sinop; Tekirdag; Trabzon; Zonguldak; Yalova;
4	16.14	<b>Afyonkarahisar</b> ; Artvin; Bilecik; Bitlis; Cankiri; Gumushane; Kastamonu; <b>Kayseri</b> ; Kutahya; Nevsehir; Nigde; Van; Duzce;
5	19.87	Adana; Ankara; Erzincan; Isparta; Kirklareli; Kirsehir; <b>Konya</b> ; Tokat; Usak; Aksaray; Karaman; Kirikkale; Karabuk;
6	15.25	Amasya; Bingol; Burdur; Bursa; Canakkale; Corum; Edirne; <b>Eskisehir</b> ; Hakkari; Kocaeli; Malatya; Mus; Tunceli; Bartin; Igdir;
7	7.78	Adiyaman; Diyarbakir; Mardin; Siirt; <b>Sanliurfa</b> ; Batman;
8	7.01	Gaziantep; Hatay; Mersin; Kahramanmaras; Sirkak; Kilis; Osmaniye;

\* CL stands for the climatic region

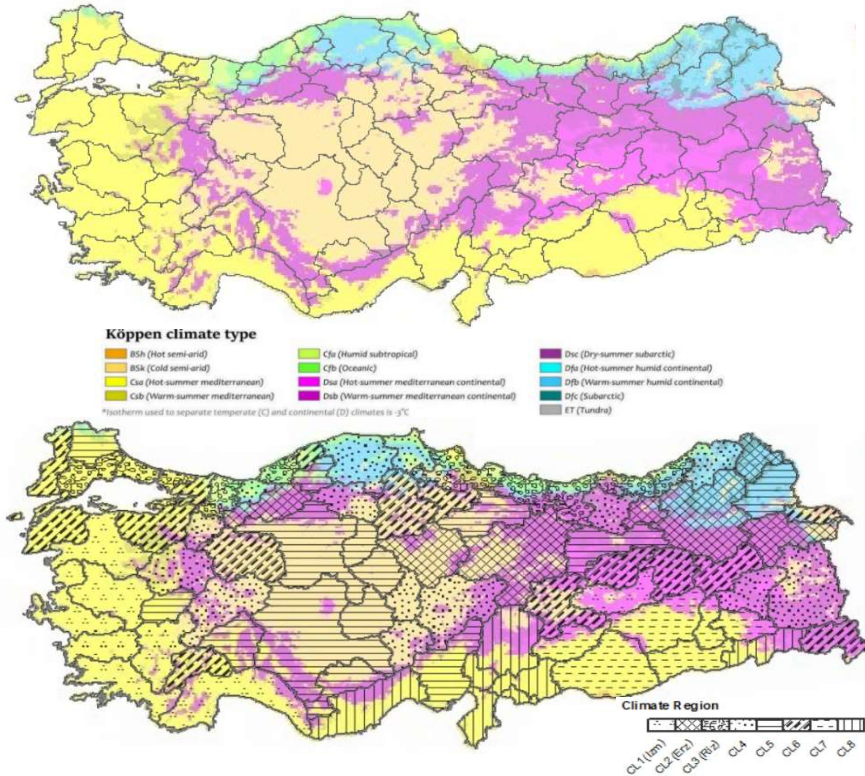


Figure 1 - Recommended climate regions for Turkey (adopted from Köppen-Geiger Climate Classification Map for Turkey) [40]

Due to data and time limitations, in this study, the M-E pavement design is performed for CL1 (Izmir-Izm), CL2 (Erzurum-Erz), and CL3 (Rize-Riz) climatic conditions, respectively, and the results of which can be generalized for 33.95% of Turkey by coverage area.

### 3.2. Factor Analysis Approach Using M-E Pavement Design Process

The M-E design process requires the design input parameters as well as performance criteria, as presented in Figure 2. The performance outputs include information on stresses, strains, and deformations that are directly converted to the performance criteria. If the outputs are within the acceptable threshold limits (see Table 1), the M-E design is finalized; if not, the evaluated trial design is modified to re-run, in other words, more iterations are done. Among the acceptable designs obtained by trial designs, the design that matches the performance criteria limits with the closest values was defined as the “optimized M-E design”.

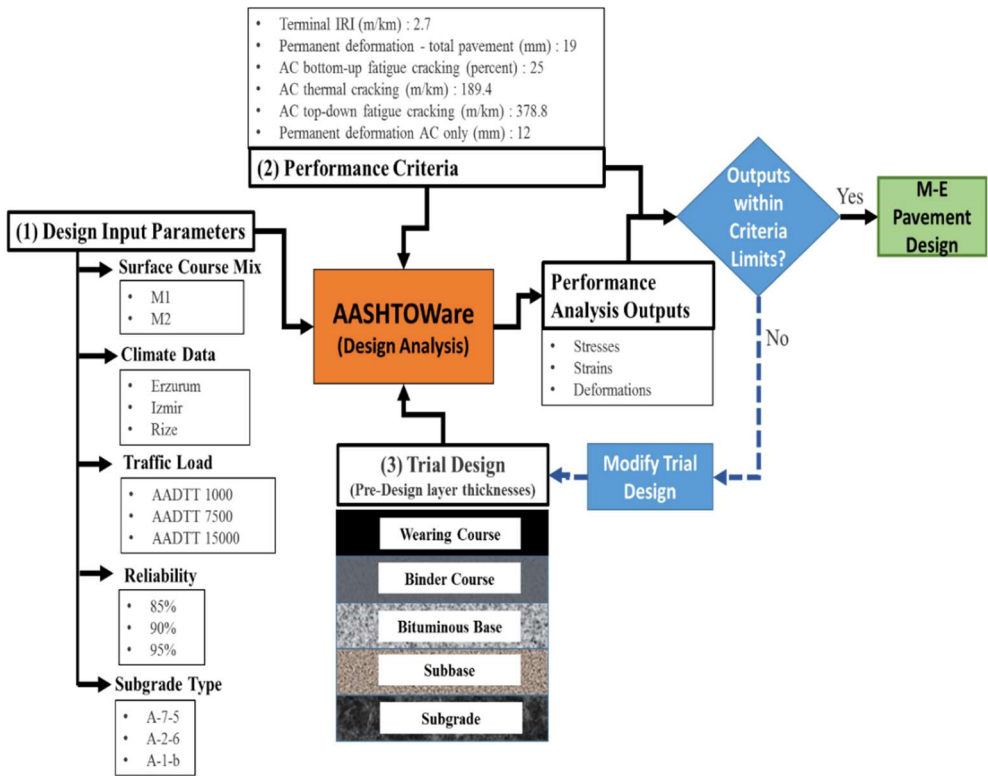


Figure 2 - M-E design process with selected input and performance criteria sets in this study

### 3.3. Selection of Design Input Parameters

The study investigated the effect of 5 design input parameters as follows:

- Climatic data: Izmir (warm/Mediterranean), Erzurum (cold) and Rize (rainy).
- Traffic load: Truck traffic volumes of AADTT-1000 (low), AADTT-7500 (medium), and AADTT-15000 (high).
- Surface course mixture gradation and asphalt cement: Mix designs of Mix 1 (M1-coarser) and Mix 2 (M2-finer). Note: The asphalt cement selection depends on the climate and traffic load.
- Subgrade type: clayey-silty soil (A-7-5), sandy pebble granular soil (A-2-6), rocky soil (A-1-b) and one subbase type (A-1-a).
- Reliability levels: 85%, 90%, and 95% selected to show the performance of the road quality (service level).

In this approach, evaluation is based on a total of 162 input design parameter sets composed of “3 climate regions x 3 traffic loads x 3 subgrade types x 3 reliability levels x 2 mix designs”. For each set, several M-E designs were generated based on the assumed trial designs. The resulting acceptable M-E designs were later reviewed to analyze the impact of the selected design parameters and discussed below in further detail.

#### 3.3.1. Determination of Climatic Regions in Turkey

The effect of the climate on the pavement design depends on the climatic inputs, which can affect the amount of heat transfer at the surface of the asphalt pavement, pavement layer

Table 4 - Climate data for the study regions [16]

Climate Data		Izmir	Erzurum	Rize
Annual Average Temperatures				
Winter- minimum	( <sup>o</sup> C)	6.60	-12	4.20
Summer- maximum	( <sup>o</sup> C)	32.30	29.00	25.43
Spring	( <sup>o</sup> C)	16.30	11.10	11.90
Autumn	( <sup>o</sup> C)	18.80	12.90	15.90
Annual average	( <sup>o</sup> C)	17.90	12.01	14.30
Annual precipitation	(mm)	690.30	402.20	2245.30
Elevation	(m)	30.0	1853.0	6.0
Wind speed	(m/s)	6.00	5.00	4.00
Moisture	(%)	70	65	75
Daily avg. solar radiation	(kWh/m <sup>2</sup> )	4.30	4.00	4.00
<b>Matched US Weather Stations</b>		Marysville Int. Airport, CA	Soda Springs Int. Airport, Idaho Falls-ID	Crescent City, CA

temperatures, and moisture conditions. The M-E method requires detailed inputs including annual air temperature ( $^{\circ}\text{C}$ ), annual precipitation ( $\text{mm}$ ), wind speed ( $\text{km/h}$ ), sunshine ( $\%$ ), cloud cover, relative humidity ( $\%$ ), and hourly air temperature distribution by month as well as the depth of groundwater table to properly calculate the temperature and moisture profile of a pavement section to predict the distresses. This detailed level of climatic data is significantly costly to provide in Turkey. Therefore, the climates of the study regions were matched with weather stations in the US. This approach has been used by many researchers implementing AASHTOWare outside the US [8, 14, 18, 28, 36]. For this purpose, annual average data for minimum winter and maximum summer temperatures, spring and autumn temperatures, average temperature, average precipitation, elevation, wind, and solar radiation were collected for three study regions and matched with the US weather stations as shown in Table 4 and Figure 3.

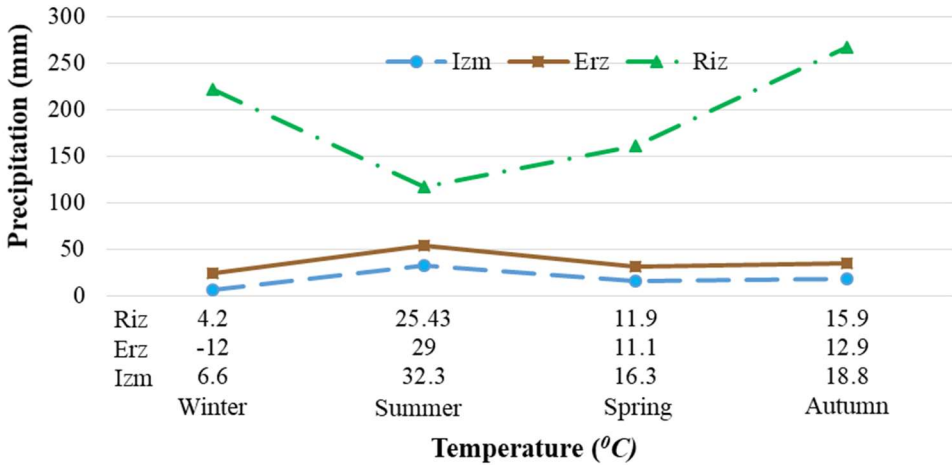


Figure 3 - Seasonal precipitation versus temperature data for the study locations [37]

### 3.3.2. Selection of Traffic Conditions

Three different AADTT values were selected considering different truck traffic in Turkey for each study region. These values were within the observed AADTT values, which range from 2800 to 37000 heavy vehicles on the Turkish Motorway network [38]. For traffic load calculations, the growth rate was fixed at 2% due to a drastic increase in the traffic volume in Turkey [39]. AASHTOWare requires detailed information on axle loads, configurations, and daily, monthly and seasonal changes in traffic volume. However, this information was not available at the time of this study, therefore default values of the software were used. Besides, vehicle class distributions were also assumed to be constant over the years.



### 3.3.3. Selection of Surface Course Mix Design

According to the specifications of the GDH, the following asphalt PG classes were selected based on the location and AADTT as shown in Figure 4. For the surface course, the GDH recommends majorly two different types of mixtures (M1 and M2) based on the aggregate gradation. M1 is a finer mix than M2. Job mix formulas used in this study were selected among various field applications. Eventually, two types of mixtures were determined according to their gradation limits; designated as M1 and M2 as shown in Table 5 and Figure 5.

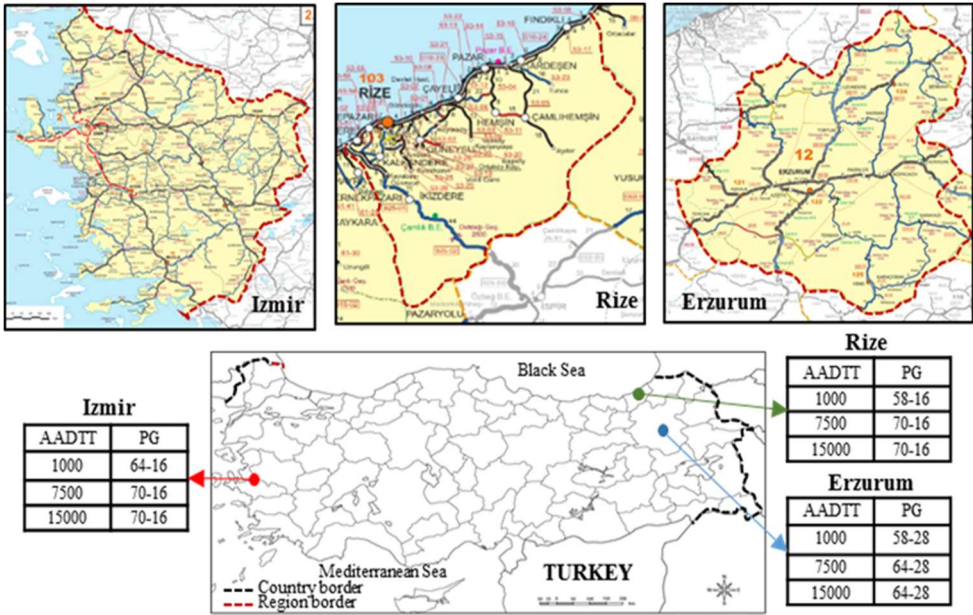


Figure 4 - PG class by AADTT for each study region (adopted from [35])

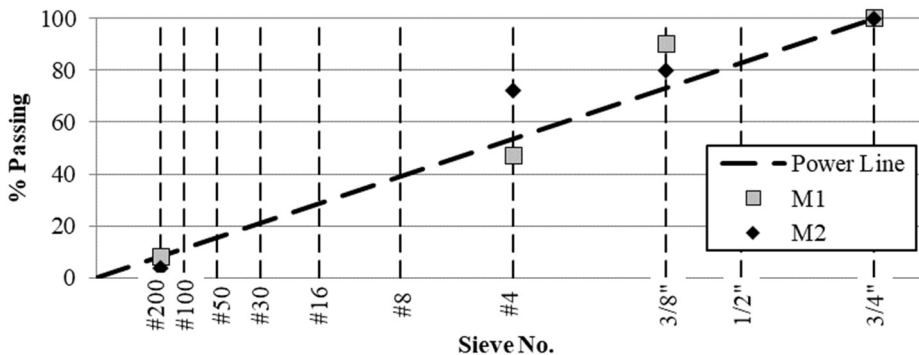


Figure 5 - Surface course mixture gradation limits

Table 5 - Mix properties for the surface course

Mixture Properties	M1	M2
3/4 in %	100.0	100.0
3/8 in %	90.0	80.0
#4 %	47.0	72.0
#200 %	8.0	4.0
V <sub>h</sub> (Void ratio %)	3.0	5.0
V <sub>b</sub> (Bitumen amount %)	11.5	14.0

### 3.3.4. Determination of Subgrade and Base Types

To define soil properties, the soil classification system developed by the AASHTO for pavement applications was used to determine the effect of subgrade type and granular base thickness on the M-E flexible pavement design. To observe the effect of the subgrade type on design, three types were specified for each region as follows:

- A-7-5 representing high plasticity clayey-silty soils,
- A-2-6 representing normal-strength sandy pebble granular soils,
- A-1-b representing rocky soils with high carrying capacity values.

Besides, A-1-a (non-stabilized) was selected as the base layer type, since it is the common practice in Turkey. It includes Level 3 inputs such as Poisson's ratio (0.35), coefficient of lateral earth pressure (0.5), maximum dry unit weight (2038.2 kgf/m<sup>3</sup>), saturated hydraulic conductivity (1.54e-02 m/hr), the specific gravity of solids (2.7), optimum gravimetric water content (7.4%) and resilient modulus (275.8 psi).

### 3.3.5. Determination of reliability

Reliability shows the probability of whether the predicted performance indicator of the trial design satisfies the design criteria [2]. In this study, to observe the reliability effect on the pavement, three reliability levels (i.e., secondary, interstate, and intercity roads) were chosen as 85%, 90%, and 95%, respectively.

## 3.4. Performance evaluations

To show the performance of the M-E method and the difference between the M-E and AASHTO'93, both the performance indicators and the effects of the parameters are presented in Table 6, which includes each comparison. The "Given" column refers to parameters that are fixed in the software and the last two columns include parameters and performance indicators that are analyzed to determine their effects on pavement performance. Each comparison is discussed in Section 4 in detail.

Table 6 - Comparison scenarios of the study

Comparisons	Given	Parameters	Indicators
Comp 1 (see Table 7)	T, S	C, R, M, LT	TR IRI FC
Comp 2 (see Table 8)	S, M, R	T, C, LT	
Comp 3 (see Table 9)	T, M, R	S, C, LT	
Comp 4 (see Table 7)	T, S, M	C, R, LT	
Comp 5 (see Table 10)	T, S	C, R, M, LT	

1) T, C, S, M, and R stand for traffic volume, climate, subgrade, surface course mix design, and reliability, respectively.

2) LT, TR, IRI, and FC stand for layer thicknesses, total rutting, International Roughness Index, and fatigue cracking, respectively.

#### 4. NUMERICAL RESULTS

To evaluate and compare the optimized designs, total pavement rutting was considered as the first indicator throughout the study, since TR was found to be the most dominant distress acting on pavements [6, 12, 18]. Secondly, the IRI and FC were investigated as the critical parameters [12, 31, 41]. It should be noted that IRI was also a function of other distresses in pavements [42, 43]. The designs were being carried out based on economy and safety by approaching the nearest level of threshold values of the three performance criteria through an iterative process. Overall, 162 designs were optimized based on limiting performance indicators. In the following subsections, various factors were discussed separately.

##### 4.1. Climate Effect

To observe the climate effect on flexible pavement design, results obtained from the three regions having different climatic conditions were analyzed by keeping the other aforementioned inputs the same. The results revealed that the climate effect is the main parameter influencing the pavement performance. As shown in Table 7, CL3(Riz) had equal or smaller pavement layer thicknesses compared with other regions under the same conditions, since CL3 has the least seasonal temperature change. On the other hand, drainage conditions in CL3(Riz) was assumed to be well-drained; however, in future studies, drainage should be considered more precisely. It should be noted that the PG classes for each region were different from each other. On the other hand, the FC results of CL3(Riz) were higher than both CL1(Izm) and CL2(Erz), because of the thinner sections. As the reliability level increases, cracking increases in general. In this case, FC was affected by colder climates with low temperatures and high precipitation rather than warmer temperatures or the reliability level. Thus, to maintain similar levels of FC, layer thicknesses should be varied highly between climatic regions. Moreover, it should be noted that IRI and rutting are also affected by climatic differences.

Table 7 - Climate effect on layer thicknesses (for 20-year service life) (Given: AADTT-7500; Subgrade = A-1-b)

CL	CL1(Izm)			CL2(Erz)			CL3(Riz)		
Reliability	85%	90%	95%	85%	90%	95%	85%	90%	95%
<b>M1</b>									
<b>Binder</b>	14	14	14	10	10	11	5	5	6
<b>Bituminous Base</b>	15	15	16	15	15	15	7	8	8
<b>Subbase</b>	20	20	20	20	20	20	10	10	10
<b>TR</b>	16.65	17.37	17.11	17.22	17.95	18.65	13.85	14.22	15.13
<b>IRI</b>	2.14	2.25	2.38	2.26	2.38	2.55	2.12	2.22	2.37
<b>FC</b>	1.28	1.56	1.95	1.36	1.64	2.01	16.41	12.28	6.44
<b>M2</b>									
<b>Binder</b>	12	12	12	10	10	12	5	5	6
<b>Bituminous Base</b>	16	18	18	15	15	15	7	8	8
<b>Subbase</b>	20	20	20	20	20	20	10	10	10
<b>TR</b>	17.99	16.25	17.25	17.48	18.21	17.11	14.09	14.47	15.4
<b>IRI</b>	2.17	2.22	2.39	2.27	2.39	2.52	2.13	2.22	2.36
<b>FC</b>	1.31	1.54	1.95	1.36	1.64	1.99	16.76	13.24	7.04

Note: i) Layer thickness values in cm. TR in mm. IRI in (m/km). FC in %. ii) Surface course thickness was kept constant at 5 cm for all analyses since, in typical construction practice, 5 cm thickness is constant according to the GDH practice. iii) These notes are acceptable for all the following tables.

#### 4.2. Traffic Effect

According to Table 8, the results indicated that under low traffic (AADTT-1000), layer thicknesses (Binder-Bituminous Base-Subbase) were found to be (6-7-10) for CL1(Izm), (5-6-15) for CL2(Erz) and (4-5-10) CL3(Riz). These estimated values were thinner than those of the standard application (6-8-20) in Turkey for 90% reliability level (Table 2). Comparisons of designs in terms of layer thickness based on traffic volume were also given in scaled cross-sections (see Figure 6). In this case, the M-E method indicated an economic design over the AASHTO'93 (typical application) under low traffic.

To compare the regions for climatic conditions only might be misleading, since the PG selection is based on both the climate and traffic load. PG of AC is the same for traffic load levels of 7500 and 15000 in each region (Figure 4). Therefore, results are evaluated for each region, separately. The layer thicknesses increase with the increase in traffic load. Current AASHTO'93 practice for AADTT-7500 (8-11-20) and AADTT-15000 (10-12-20) requires thinner thickness than M-E results for CL2(Erz) and CL1(Izm), but results for

Table 8 - Traffic effect on layer thicknesses (for 20-year service life) (Given: Subgrade = A-1-b; Mix design = M1; R= 90%)

CL	CL1(Izm)			CL2(Erz)			CL3(Riz)		
	AADTT 1000	7500	15000	1000	7500	15000	1000	7500	15000
<b>Binder</b>	6	14	15	5	10	11	4	5	6
<b>Bituminous Base</b>	7	15	18	6	15	18	5	8	8
<b>Subbase</b>	10	20	20	15	20	20	10	10	10
<b>TR</b>	16.53	17.37	18.93	14.97	17.95	18.62	10.62	14.22	17.27
<b>IRI</b>	2.24	2.25	2.29	2.32	2.38	2.4	2.11	2.22	2.31
<b>FC</b>	2.17	1.56	1.57	2.46	1.64	1.64	3.44	12.28	20.64

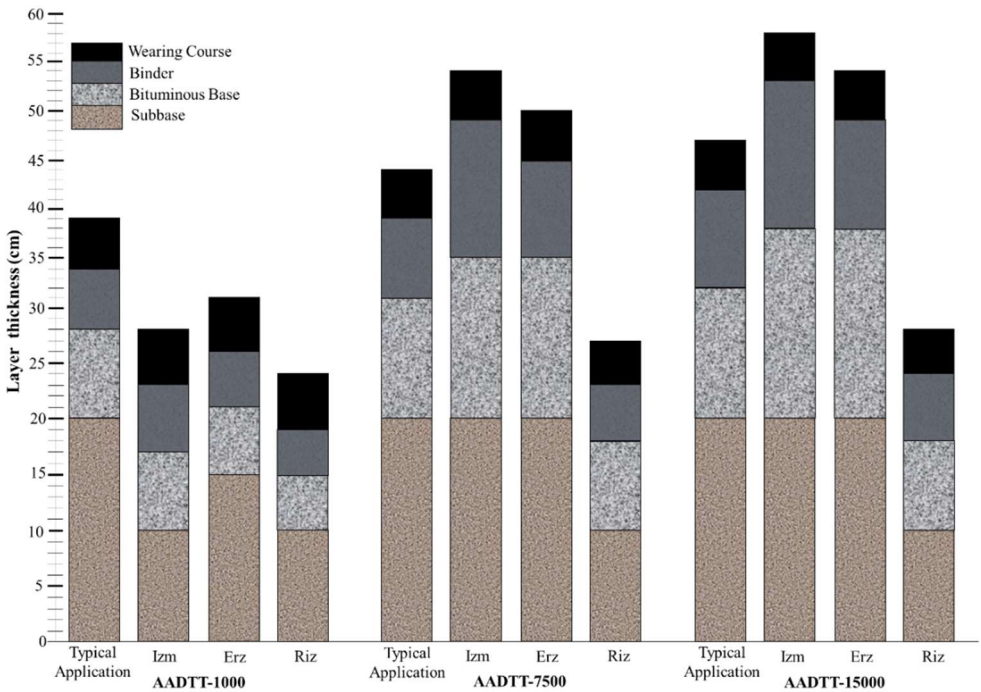


Figure 6 - Visual depiction of the typical and M-E designs for selected traffic volumes (R=90%)

CL3(Riz) were significantly thinner than current practice in Turkey. Therefore, the current practice may under-design the layer thicknesses as required regarding warmer and cold climatic conditions. The IRI is not significantly varied between the optimized designs under different traffic loads, whereas the TR considerably increases under different traffic loads (see Table 8). It can be concluded that both IRI and FC are affected by the traffic loading. It should be noted that traffic loading dominates rutting more. In CL1(Izm) and CL2(Erz), to keep the distresses around the same level under different traffic loads, the layer thicknesses should be increased. Only a slight increase is observed for the CL3(Riz) case. Since there is little variation in seasonal temperatures, the significant precipitation influence is eliminated by choosing good drainage conditions. Therefore, after local calibrations, the precipitation should be separately taken into consideration.

### 4.3. Subgrade Effect

To study the effect of subgrade, M-E designs with low traffic (AADTT-1000), coarser surface course (M1) and 85% reliability level were analyzed for three subgrade types (low strength A-7-5, medium-strength A-2-6, and high strength A-1-b) as shown in Table 9. The optimized designs indicated that subgrade type and its strength have significant impact on the flexible pavement performance, as expected. In the CL2(Erz) case, layer thicknesses were selected as (3-5-15) for all subgrade types, respectively. However, the A-7-5 subgrade yielded higher rutting and the A-1-b created a lower deformation due to its high strength with a high modulus. Similar results were obtained for CL1(Izm) and CL3(Riz), although the thicknesses of bituminous bases were decreased by 1 cm and 2 cm, respectively.

Table 9 - Subgrade type effect on layer thicknesses (for 20-year service life) (Given: AADTT-1000; Mix design = M1; R=85%)

CL	CL1(Izm)			CL2(Erz)			CL3(Riz)		
	A-7-5	A-2-6	A-1-b	A-7-5	A-2-6	A-1-b	A-7-5	A-2-6	A-1-b
<b>Binder</b>	4	4	4	3	3	3	3	3	3
<b>Bituminous Base</b>	7	7	6	5	5	5	5	5	3
<b>Subbase</b>	10	10	10	15	15	15	10	10	10
<b>TR</b>	17.61	17.80	16.24	16.94	17.15	15.13	13.63	13.46	11.33
<b>IRI</b>	2.32	2.27	2.15	2.42	2.37	2.24	2.24	2.18	2.07
<b>FC</b>	16.52	10.26	6.34	18.57	17.06	12.87	18.65	16.81	18.46

Designs conceived for CL1(Izm) had (4-7-10) layer thicknesses for A-7-5 and A-2-6, but A-1-b required thickness values of (4-6-10). Similarly, designs for CL3(Riz) involved (3-5-10) layer thicknesses for A-7-5 and A-2-6 subgrades, but A-1-b required thickness values of (3-3-10). In other words, subgrades with high strength required thinner layers. Also, the M-E

trial designs required thinner layers than typical application thicknesses in Turkey (Table 2). This also reveals the importance of calibration.

The IRI and FC exhibited a descending trend depending on the increased loading capacity of subgrades. A-1-b results generated the least cracking except for CL3 (Riz), which might be due to the drainage factor assumed to be well-drained. Although the results of the A-7-5 subgrade for CL2(Erz) indicated similar findings with CL1(Izm) concerning deformations, the IRI and FC in CL1(Izm) were smaller due to the differences in climatic conditions.

#### **4.4. Reliability Effect**

To analyze the reliability, a subset of the designs for medium traffic (AADTT-7500), coarser surface course (M1), and high strength subgrade (A-1-b) were examined as given in Table 7. Accordingly, the CL2(Erz) case had almost the same layer thicknesses of (10-15-20) for all reliability levels (for 95% level, the binder layer thickness is increased by 1 cm). Similarly, for CL1(Izm), layer thicknesses were estimated around (14-15-20) for values of the all reliability levels (at a 95% level, the bituminous base thickness was needed to be increased by 1 cm due to greater deformations). In CL3(Riz), layer thicknesses were estimated as (5-7-10) for 85% reliability level, the bituminous base needed an additional 1 cm thickness for 90% level, while at 95% level, the layer thicknesses of both binder and bituminous base were increased by 1 cm. However, in three climatic regions, greater deformations were observed at increased reliability levels.

On the other hand, the selected PG classes in Turkey in the standard application were different for all regions (See Figure 4). In terms of predicted IRI and FC, an ascending trend was found in all regions depending on the reliability level. Consequently, increases in reliability levels, i.e. road quality, resulted in increases in layer thickness values. However, findings for CL3(Riz) showed reverse results than other cities considering FC distresses, probably due to a significant increase in thickness.

#### **4.5. Surface Course Mix Design Effect**

To analyze mix design effect, low traffic (AADTT-1000), subgrade type A-2-6 for granular soil with medium strength, and three reliability levels (85%, 90%, and 95%) during 20-year service life were re-tabulated for each region in Table 10. Results of the selected two mix designs (M1-coarser and M2-finer) showed that for CL2(Erz) and CL1(Izm), layer thicknesses under the same conditions were almost the same (or slightly thicker with 1 cm difference for bituminous base). For example, in CL2(Erz), while the mix M1 required (3-5-15) thickness values, M2 required (3-6-15) for 85% reliability. Moreover, in 95% reliability, the M2 combination sometimes needs a greater thickness of about an increase of 3 cm. As the reliability level increases, the deformations arising from M1 and M2 increase, and the lower strength material led to lower performance. Typically, the mixture with finer gradation corresponds to higher rutting and requires thicker layers. Moreover, the surface course design significantly affects FC. For the cases with the same reliability level and layer thicknesses, the surface mix design change from coarser to finer leads to an increase in cracking. On the other hand, IRI increases based on the reliability level independent of the layer thickness increase. However, for the cases with the same reliability level and layer thicknesses, no considerable change is observed.

Table 10 - Surface mix design and reliability effect on layer thicknesses (for 20-year service life) (Given: AADTT-1000; Subgrade = A-2-6)

Reliability	85%		90%		95%	
	M1	M2	M1	M2	M1	M2
<b>CL1(Izm)</b>						
<b>Binder</b>	4	4	5	5	5	5
<b>Bituminous Base</b>	6	6	6	6	7	8
<b>Sub-Base</b>	15	15	15	15	15	15
<b>TR</b>	18.38	18.48	18.87	18.67	18.99	19.07
<b>IRI</b>	2.28	2.29	2.38	2.38	2.54	2.53
<b>FC</b>	10.81	11.34	5.4	5.81	3.47	2.85
<b>CL2(Erz)</b>						
<b>Binder</b>	3	3	3	3	5	5
<b>Bituminous Base</b>	5	6	5	6	6	7
<b>Sub-Base</b>	15	15	15	15	15	15
<b>TR</b>	17.15	17.3	17.76	17.92	17.68	17.24
<b>IRI</b>	2.37	2.37	2.37	2.49	2.63	2.61
<b>FC</b>	17.06	14.41	20.38	17.24	4.28	3.00
<b>CL3(Riz)</b>						
<b>Binder</b>	3	3	3	3	3	4
<b>Bituminous Base</b>	5	5	5	6	5	7
<b>Sub-Base</b>	10	10	10	10	10	10
<b>TR</b>	13.46	13.57	13.96	13.86	14.71	13.64
<b>IRI</b>	2.18	2.19	2.30	2.29	2.47	2.41
<b>FC</b>	16.81	17.05	20.09	15.90	24.96	3.34

#### 4.6. Supplementary Economic Analysis for Different Traffic Volumes

In order to discuss the economic impacts of the use of M-E method, a comparative cost table for selected cities is prepared based on the thicknesses predicted for different traffic volumes at 90% reliability. However, it should be re-noted that the economic analysis presented herein is based on the thicknesses predicted without regional calibration of the AASHTOWare. Therefore, the findings may contain some uncertainty. The cost calculation is implemented based on 1 km of 2 lane highway segment having a lane width of 3.5 m and a shoulder width of 0.5 m. The item numbers representing the unit price (TL) of the layers belong to the GDH and were published in 2020 [44]. Upon these unit prices, the cost per 1 cm thickness per layer was calculated to estimate the price of the overall 1 km section as given in Table 11. While M-E designs cost less at low traffic volume, the cost increases slightly as the traffic load increases, requiring thicker layers in CL1(Izm) and CL2(Erz). On the other hand, CL3(Riz) costs less with thinner layers under all traffic volumes. However, it should be reminded that the effect of the drainage is neglected from the analysis.



Table 11 - Economic analysis of selected provinces based on traffic volume (for 20-year service life, R = 90%)

Item Number	Unit Price (TL)	Cost of m <sup>2</sup> /cm or m <sup>3</sup> /cm (TL)	AADTT-1000		AADTT-7500		AADTT-15000	
			LT (cm)	Price (TL)	LT (cm)	Price (TL)	LT (m)	Price (TL)
<b>Typical Application (AASHTO 93)</b>								
W. Course	11.81 m <sup>2</sup>	2.36	5	94480	5	94480	5	94480
Binder	18.29 m <sup>2</sup>	2.29	6	109740	8	146320	10	182900
Bit. Base	23.28 m <sup>2</sup>	2.12	8	135447.3	11	186240	12	203170.9
Subbase	47.88 m <sup>3</sup>	0.48	20	76608	20	76608	20	76608
<b>Total Price (TL)</b>			<b>416275.3</b>		<b>503648</b>		<b>557158.9</b>	
<b>Izmir</b>								
W. Course	11.81 m <sup>2</sup>	2.36	5	94480	5	94480	5	94480
Binder	18.29 m <sup>2</sup>	2.29	6	109740	14	256060	15	274350
Bit. Base	23.28 m <sup>2</sup>	2.12	7	118516.4	15	253963.6	18	304756.4
Subbase	47.88 m <sup>3</sup>	0.48	10	38304	20	76608	20	76608
<b>Total Price (TL)</b>			<b>361040.4</b>		<b>681111.6</b>		<b>750194.4</b>	
<b>Erzurum</b>								
W. Course	11.81 m <sup>2</sup>	2.36	5	94480	5	94480	5	94480
Binder	18.29 m <sup>2</sup>	2.29	5	91450	10	182900	11	201190
Bit. Base	23.28 m <sup>2</sup>	2.12	6	101585.5	15	253963.6	18	304756.4
Subbase	47.88 m <sup>3</sup>	0.48	15	57456	20	76608	20	76608
<b>Total Price (TL)</b>			<b>344971.5</b>		<b>607951.6</b>		<b>677034.4</b>	
<b>Rize</b>								
W. Course	11.81 m <sup>2</sup>	2.36	5	94480	5	94480	5	94480
Binder	18.29 m <sup>2</sup>	2.29	4	73160	5	91450	6	109740
Bit. Base	23.28 m <sup>2</sup>	2.12	5	84654.6	8	135447.3	8	135447.3
Subbase	47.88 m <sup>3</sup>	0.48	10	38304	10	38304	10	38304
<b>Total Price (TL)</b>			<b>290598.6</b>		<b>359681.3</b>		<b>377971.3</b>	

**Definition Notes of Item Number:**

**GDH/6405:** Making 1 m<sup>2</sup> asphalt concrete wearing course in 5 cm compacted thickness (with crushed and sieved quarry stone) (Type-I).

**GDH/6308:** Making 1 m<sup>2</sup> asphalt concrete binder layer in 8 cm compacted thickness (with crushed and sieved quarry stone).

**GDH/6211-A:** Making 1 m<sup>2</sup> asphalt concrete bituminous base course in 11 cm compacted thickness on the unlined base (with crushed and sieved quarry stone).

**GDH/6000:** Making the subbase with crushed and sieved quarry stone (m<sup>3</sup>)

Notes: W, Bit, and LT stand for wearing, bituminous, and layer thickness in cm, respectively.

For example, for AADTT-7500 in Erzurum (10-15-20), standard application of AASHTO'93 costs 503 648 TL, but M-E costs 607 951.6 TL, thus, M-E requires approximately 20.71% more cost than the standard design. Considering the excessive budget that has been invested in the maintenance and rehabilitation of highways in Turkey, it could be anticipated that AASHTO'93 underestimates the layer thicknesses in some cases as revealed in this study.

#### **4.7. Monitoring the Benefits of Switching to the M-E design Method**

To better understand the benefits of switching to the M-E method, it is necessary to compare the optimized M-E designs using the AASTHOWare with those traditional ones determined by the AASHTO'93 method. As discussed above, IRI, TR, and FC values would be the performance indicators to be discussed against the total pavement thickness, which is a strong indicator of the cost of the pavement, and upcoming maintenance and rehabilitation. Since the traditional AASHTO'93 approach utilizes basic parameters and outputs, it does not provide the selected three performance indicators, directly. But it is possible to estimate those values, by simply running the traditional pavement design layer thickness in the AASTHOWare. Ultimately, this would allow us the comparisons of the best designs from the M-E and AASHTO'93 over the same performance indicators.

For the case of three CLs in Turkey the M-E based optimized designs (ME\_Izm, ME\_Erz, and ME\_Riz) were run to get the IRI, TR, and FC values, which are compared with the estimated ones for the AASHTO'93 based designs (93\_Erz, 93\_Izm and 93\_Riz). The performance of both approaches is illustrated in Figure 7. Since the surface and the subbase course layers were kept the same with 5 cm and 20 cm, respectively, the x-axis was selected as the total thickness of the binder, bituminous base, and base layers, only in all designs. In the AASHTO'93 method, only 5 different total thickness cases were created based on the input variables (denoted by the blue triangles in Figure 7). The overestimation/underestimation of performance indicators can be easily detected by comparing the desired levels shown by thick lines in the graphs. For example, some of the 93\_Izm and 93\_Erz designs are expected to have worse IRI than the 2.7 mm/km limit. The designs exceeding the limits were mostly the high traffic load (AADT-15000) or medium traffic load (AADT-7500) and high-reliability requirements (95%). A similar pattern was also detected in the case of the rutting performance of the traditional designs, going above the limit of 19 mm. For the FC, the traditional approach produced the highest value 18 mm/km FC which was still much lower than the allowed 25 mm/km, suggesting an extremely high overdesign from the fatigue performance perspective. When the optimized M-E designs were analyzed, the performance indicators were satisfied with the majority of the cases that also indicated much more total thickness due to the sensitivity of the model to various variables. For all three CLs, rutting performance was seemed to be the limiting value for most of the design cases, which were more critical for the CL1(Izm) and CL2(Erz). For the case of CL3(Riz), the M-E optimized results were obtained by much smaller pavement thickness without violating the desired performance limits. Besides the TR, FC performance values could be critical but lower than the allowed limit of 25 mm/km for most of the cases in the CL3(Riz). For the other two regions, IRI performance was observed as the second critical factor causing mostly higher pavement thicknesses, whereas optimized designs would have much safer FC values than the allowed limit.

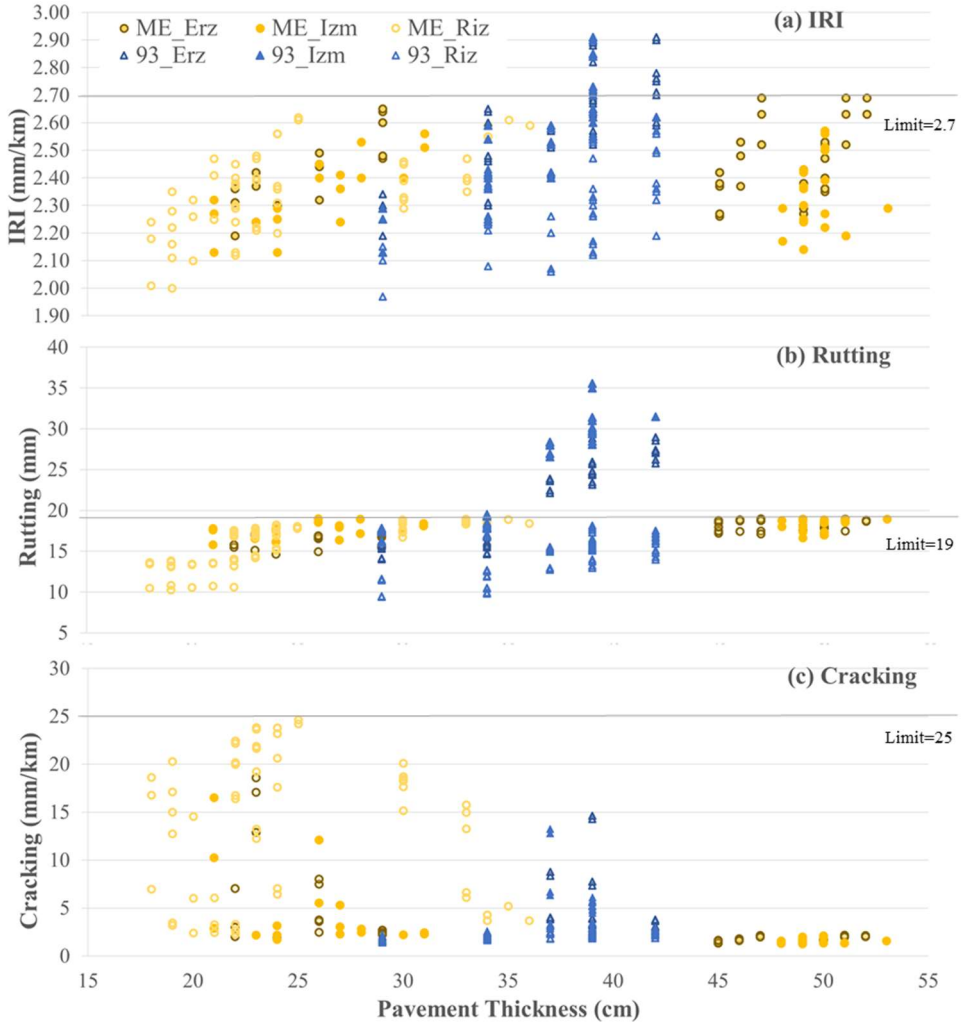


Figure 7 - Total thickness versus performance indicator effects

The pavement thickness change (DT) created using the M-E design is shown in Figure 8, where major reductions can be seen for the CL3(Riz), and drainage should be handled carefully. Higher pavement thicknesses for some of the cases in the M-E design compared to those in the AASTHO'93 method stemmed from the need to satisfy all three performance indicator limits, one or two of which were not met in the latter methodology (see Figure 8). Though the initial cost of these designs with the M-E method would be higher, they are expected to have a higher advantage when the total costs during the service life and quality of the service were considered.

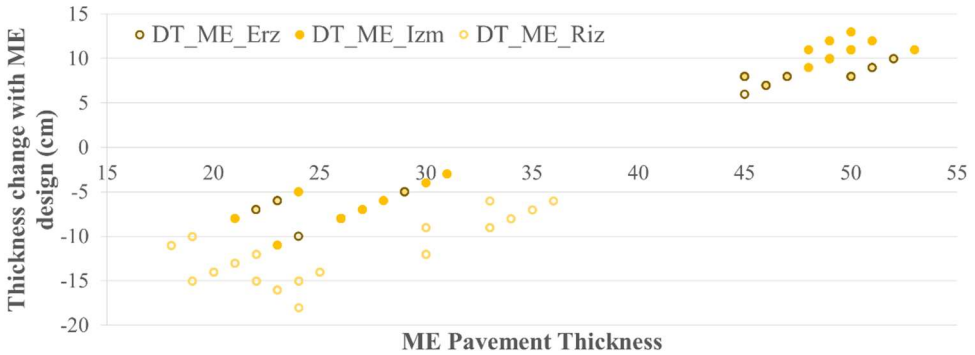


Figure 8 -Total thickness change due to use of the M-E design method

## 5. CONCLUSIONS AND FUTURE RECOMMENDATIONS

Developing countries need expanding their road network, as well as improving their existing road network. Budget limitations result in bigger challenges not only for the construction but also for the maintenance of the roadway networks. Due to its practicality, AASHTO'93 is currently in use in many countries, like Turkey. However, the AASHTO'93 method leads to overestimate or underestimate the layer design thicknesses, which may even result in poor pavement performance and/or high initial construction costs. As this method is empirical, it does not deeply take into account the project-specific properties like the climate, axle load distributions, etc. Thus, the main focus of this study is to implement the M-E analysis method in flexible pavements and state the differences from the current design method for Turkey. Although it has been suggested to calibrate the inputs of AASHTOWare based on region-specific properties, in this study, the global averages provided by AASHTO'93 were used due to the unavailability of the data. Therefore, comparative analysis based on different climatic regions, traffic patterns, subgrade types, reliability levels, and material choices are done for 20-year service life by utilizing new M-E and traditional AASHTO'93 design methods. Accordingly, the following findings are obtained:

- In all climatic conditions studied, thicker layer designs were predicted in the M-E pavement designs with high traffic volumes and poor soil conditions as compared to designs with AASHTO'93. This is parallel to the findings of the previous studies which reported that climate, subgrade, and traffic volume are the major parameters that influence the design thicknesses. Since realistic climatic properties are used in the M-E analysis, the findings indicated the influence of climate, as well as the poor side of AASHTO'93.
- In flexible pavement design, the mix gradation and the asphalt cement grade selection are critical in performance, as well as the design thickness selection. Because the asphalt grade selection depends majorly on the climatic conditions, the climate effect on the performance grade selection should be considered simultaneously.
- The results indicated that denser gradation with fewer air voids performed better compared to finer gradation with higher void content as expected. Therefore, better

mixture performance led to a thinner section. However, the influence of material characteristics cannot be taken into account in AASHTO'93 design.

- For low traffic volumes, the M-E design approach may produce more economical designs than those by the AASHTO'93 for Turkey; and, the current practice may be resulting in under-design situations of higher traffic conditions, whereas the M-E design method predicted higher layer thickness than AASHTO'93.
- Thus, it is revealed the importance that shifting from empirical design (AASHTO'93) to new M-E (AASHTOWare) may improve the overall design process and infrastructure budget allocation in developing countries, such as Turkey.

It should be noted that, in this study, some default values (e.g., subgrade properties) are used in the analysis, due to the unavailability of project-specific or regional data, though the analysis indicated the differences when the climatic properties varied from the region to region. As the M-E method is not currently in use in Turkey, climatic data for selected regions was not available, but it was assumed by matching weather station data from three cities in Turkey (Izmir-warm, Erzurum-cold, and Rize-rainy) with three similar weather stations in the US, as adapted by other studies considering the use of the M-E method for regions outside the US. However, since climatic conditions showed the strongest effect on the pavement design and performance, it is a critical step to use local data sets and produce calibration values for the M-E procedure and AASHTOWare to nationally adapt to the new design method. Thus, the challenges for changing the current design practice in Turkey are to develop climatic, material, subgrade, structural data library, as well as to analyze the current road network characteristics including distresses and propagation of distresses through the life of the pavement. Hence, the nationwide calibration of the M-E can be done for Turkey and the M-E can be used as a design method. Due to the presented limitations of the study, it is shown that thicker or thinner pavement layers can be designed when climatic, material, subgrade properties are considered. Thus, it will provide long-life pavements as well as economical savings.

### **Acknowledgment**

Authors thanks to "Turkish Cement Manufacturers' Association (TCMA)" for their support in the recruitment process of AASHTOWare Pavement M-E Design software (Version 2.2) license.

### **References**

- [1] OECD, *Fostering Investment in Infrastructure Lessons learned from OECD Investment Policy Reviews*, 2015.
- [2] AASHTO, *AASHTO Guide for Design of Pavement Structures*", American Association of State Highway and Transportation Officials, Washington, D.C. U.S.A., ISBN-10: 1-56051-055-2, 640 pp, 1993.

- [3] NCHRP, Mechanistic-Empirical Design of New and Rehabilitated Pavement Structures, National Cooperative Highway Research Program, NCHRP Project 1-37A Report, National Research Council. Washington, D.C., 2004.
- [4] Rahman, M. M., Gassman, S. L., Data collection experience for preliminary calibration of the AASHTO pavement design guide for flexible pavements in South Carolina, *International Journal of Pavement Research and Technology*, 11(5), 445-457, 2018. <https://doi.org/10.1016/j.ijprt.2017.11.009>
- [5] NCHRP, Recommended Practice for Local Calibration of the M-E Pavement Design Guide, National Cooperative Highway Research Program, ARA Inc. Texas, 2007.
- [6] Caliendo, C., Local calibration and implementation of the mechanistic-empirical pavement design guide for flexible pavement design, *Journal of Transportation Engineering*, 138(3), 348-360, 2011. [https://doi.org/10.1061/\(ASCE\)TE.1943-5436.0000328](https://doi.org/10.1061/(ASCE)TE.1943-5436.0000328)
- [7] Zofka, A., Urbanik, A., Maliszewski, M., Bankowski, W., Sybilski, D., Site specific traffic inputs for mechanistic-empirical pavement design guide in Poland, (No. 14-4534), 2014.
- [8] Haponiuk, B., Zbiciak, A., Mechanistic-empirical asphalt pavement design considering the effect of seasonal temperature variations, *Archives of Civil Engineering*, 62(4), 35-50, 2016. <https://doi.org/10.1515/ace-2015-0096>
- [9] Plescan, E., Plescan, C., Implementation of mechanistic empirical pavement design guide ME-PDG in Romania, *Bull. Transilvania Univ. Braşov*, 7(56), 323-329, 2014.
- [10] Masad, E., Kassem, E., Little, D., Characterization of asphalt pavement materials in the State of Qatar: A case study, *Road Materials and Pavement Design*, 12(4), 739-765, 2011. <https://doi.org/10.1080/14680629.2011.9713893>
- [11] Sadek, H. A., Masad, E. A., Sirin, O., Al-Khalid, H., Sadeq, M. A., Little, D., Implementation of mechanistic-empirical pavement analysis in the State of Qatar, *International Journal of Pavement Engineering*, 15(6), 495-511, 2014. <https://doi.org/10.1080/10298436.2013.837164>
- [12] Aguib, A., Flexible pavement design AASHTO 1993 versus mechanistic-empirical pavement design. MSc thesis, The American University in Cairo School of Sciences and Engineering Construction and Architectural Engineering, 2014. Available at: <http://dar.aucegypt.edu/handle/10526/3806>
- [13] Aguib, A. A., Khedr, S., The mechanistic-empirical pavement design: An Egyptian perspective, In: *Functional Pavement Design*, CRC Press, 2016, pp. 933-942. <https://doi.org/10.1201/9781315643274-102>
- [14] Khattab, A. M., El-Badawy, S. M., Elmwafi, M., Evaluation of Witczak E\* predictive models for the implementation of AASHTOWare-Pavement ME Design in the Kingdom of Saudi Arabia, *Construction and Building Materials*, 64, 360-369, 2014. <https://doi.org/10.1016/j.conbuildmat.2014.04.066>

- [15] Shakhan, M. R., Topal, A., Sengoz, B., Data Collection for Implementation of the Mechanistic Empirical Pavement Design Guide (MEPDG) in Izmir, Turkey, *Teknik Dergi*, 2021. <https://dx.doi.org/10.18400/tekderg.651399>
- [16] Ozturk, H. I., Tan, E. B., Sengün, E., Yaman, I. O., Comparison of jointed unreinforced rigid pavement systems designed with mechanistic-empirical (ME) method for different traffic, soil, material and climatic conditions, *Gazi Üniversitesi Mühendislik-Mimarlık Fakültesi Dergisi*, 2018. <https://doi.org/10.17341/gazimmfd.416536>
- [17] Kim, D., Nantung, T., Siddiki, N. Z., Kim, J. R., Implementation of new mechanistic-empirical design for subgrade materials: Indiana's experience, No. 07-0463, 2007.
- [18] Hasan, M. A., Tarefder, R. A., Development of temperature zone map for mechanistic-empirical (M-E) pavement design, *International Journal of Pavement Research and Technology*, 11(1), 99-111, 2018. <https://doi.org/10.1016/j.ijprt.2017.09.012>
- [19] FHWA, Geotechnical Aspects of Pavements Reference Manual, Federal Highway Administration, 2019. <https://www.fhwa.dot.gov/engineering/geotech/pubs/05037/ac.cfm> Accessed on 4 November 2019
- [20] Azadi, M., Nasimifar, S. M., Pouranian, M. R., Determination of local fatigue model calibration used in MEPDG for Iran's dry-no freeze region, *Arabian Journal for Science and Engineering*, 38(5), 1031-1039, 2013. <https://doi.org/10.1007/s13369-012-0340-0>
- [21] Li, Q. J., Wang, K. C., Yang, G., Zhan, J. Y., Qiu, Y., Data needs and implementation of the Pavement ME Design, *Transportmetrica A: Transport Science*, 1-30, 2018. <https://doi.org/10.1080/23249935.2018.1504254>
- [22] Rao, K. V., Mathew, T., Flexible Pavement Design, *Introduction to Transportation Engineering Lecture Notes*, 2007.
- [23] AASHTO, Mechanistic-empirical pavement design guide: A manual of practice, American Association of State Highway and Transportation Officials, 2008a.
- [24] Carvalho, R., Schwartz, C., Comparisons of flexible pavement designs: AASHTO empirical versus NCHRP Project 1-37A mechanistic-empirical, *Journal of the Transportation Research Board*, (1947), 167-174, 2006. <https://doi.org/10.1177/0361198106194700116>
- [25] Li, Q., Mills, L., McNeil, S., Attoh-Okine, N., Exploring the impact of climate change on pavement performance and design, Presented at the Transportation Research Board 91st Annual Meeting, 2012.
- [26] Elshaeb, M. A., El-Badawy, S. M., Shawaly, E. S. A., Development and impact of the Egyptian climatic conditions on flexible pavement performance, *American Journal of Civil Engineering and Architecture*, 2(3), 115-121, 2014. <https://doi.org/10.12691/ajcea-2-3-4>
- [27] AASHTO, Mechanistic-Empirical Pavement Design Guide, AASHTO Designation: MEPDG-1, American Association of State Highway and Transportation Officials, Washington, D.C, 2008b.

- [28] Elshaeb, M. A., El-Badawy, S. M., Shawaly, E. S. A., Development and impact of the Egyptian climatic conditions on flexible pavement performance, *American Journal of Civil Engineering and Architecture*, 2(3), 115-121, 2014. <https://doi.org/10.12691/ajcea-2-3-4>
- [29] Shafiee, M. H., Hashemian, L., Rostami, A., Bayat, A., Tabatabaee, N., Field measurement and modeling of vertical and longitudinal strains from falling weight deflectometer testing, *Journal of Transportation Engineering, Part B: Pavements*, 144(1), 2017. <https://doi.org/10.1061/JPEODX.0000022>
- [30] Jannat, G. E., Database Development for Ontario's Local Calibration of Mechanistic–Empirical Pavement Design Guide (MEPDG) Distress Models, MSc thesis, Ryerson University, 2012. Available at: <https://digital.library.ryerson.ca/islandora/object/RULA%3A1461>
- [31] Hossain, N., Singh, D., Zaman, M., Rassel, S. S., Local calibration of MEPDG rut models: Oklahoma's experience from an instrumented pavement section. *Analytical Methods in Petroleum Upstream Applications*, 135, 2015. <https://doi.org/10.1201/b17435-20>
- [32] Pereira, P., Pais, J., Main flexible pavement and mix design methods in Europe and challenges for the development of a European method, *Journal of Traffic and Transportation Engineering (English Edition)*, 4(4), 316-346, 2017. <https://doi.org/10.1016/j.jtte.2017.06.001>
- [33] Montuschi, A., Dondi, G., Pettinari, A. R. M., Flexible pavement design using Mechanistic-Empirical methods: the Californian approach, MSc thesis, Department of Civil, Chemical, Environmental and Material Engineering, Alma Mater Studiorum University of Bologna, 2012. Available at: [https://amslaurea.unibo.it/4914/1/tesi\\_file\\_unico.pdf](https://amslaurea.unibo.it/4914/1/tesi_file_unico.pdf)
- [34] Aflaki, S., Tabatabaee, N., Proposals for modification of Iranian bitumen to meet the climatic requirements of Iran, *Construction and Building Materials*, 23(6), 2141-2150, 2009. <https://doi.org/10.1016/j.conbuildmat.2008.12.014>
- [35] Saglik, A., Orhan, F., Gungor, A. G., BSK Kaplamalı Yollar İçin Bitüm Sınıfı Seçim Haritaları (Bitumen Class Selection Maps for BSK Coated Roads), General Directorate of Highways, 2012. Available at: <http://www.kgm.gov.tr/>
- [36] Dezotepe, G., Ksaibati, K., The Effect of Environmental factors on the implementation of the Mechanistic-Empirical Pavement Design Guide, Wyoming Technology Transfer Center, 2011.
- [37] Turkish State Meteorological Service (TSMS), Weather Statistic for 1950-2015 Period in City: Normal and Extreme Recordings, 2017. Retrieved on August 15, 2017, Available at: the <https://www.mgm.gov.tr/>
- [38] GDH, Trafik ve Ulaşım Bilgileri (Traffic and Transportation Information), General Directorate of Highways, 2019. Available at: <http://www.kgm.gov.tr/>
- [39] GDH, Karayolları Esnek Üstyapılar Projelendirme Rehberi (Flexible Pavement Design Guide for Highways), General Directorate of Highways, Ankara, 93, 7, 2008.



- [40] Kottek M., Grieser J., Beck C., Rudolf B., Rubel F., World Map of the Köppen-Geiger Climate Classification Updated, Meteorol Zeitschrift, 15:259–63, 2006.
- [41] Mehta, Y. A., Sauber, R. W., Owad, J., Krause, J., Lessons learned during implementation of mechanistic-empirical pavement design guide, No. 08-1670, 2008.
- [42] Mubaraki, M., Study the relationship between pavement surface distress and roughness data, In MATEC Web of Conferences (Vol. 81, p. 02012), EDP Sciences, 2016.
- [43] Lin, J. D., Yau, J. T., Hsiao, L. H., Correlation analysis between international roughness index (IRI) and pavement distress by neural network, In 82nd Annual Meeting of the Transportation Research Board (pp. 12-16), 2003.
- [44] KGM 2020 Birim Fiyatları (Item Numbers of GDH for 2020), 2021, Retrieved on April 01, 2021. Available at: <https://www.birimfiyat.net/>



# **Investigating the Influence of Dam-Breach Parameters on Dam-Break Connected Flood Hydrograph**

**Mohamed NAJAR<sup>1</sup>**

**Ali GÜL<sup>2</sup>**

## **ABSTRACT**

The dam-break connected flood hydrograph properties primarily depend on the breach geometry and the time for the breach to fully develop. Therefore, the prediction of dam's breach geometry is essential in dam-break studies. To understand the impact of breach parameters on flood peak hydrograph, five of the most common breach prediction methods are implemented in the presented study to estimate the flood hydrographs using 2-dimensional HEC-RAS model. The Ürkmez Dam is chosen as the case study due to the presence of a residential settlement located right at the dam downstream where undesirably any breach of the dam body can have inevitable and dramatical risks on downstream populations and properties. Various levels for reservoir storage are investigated in each method. To assess the impact of each breach parameter on the resulting flood hydrographs, sensitivity analysis is carried out. The peak discharge rates and the times to peak for each analyzed scenario are investigated and discussed. Results reveal that Froehlich approach is the most reasonable method for estimating dam-breach parameters as far as exemplified in the Ürkmez Dam case. Furthermore, sensitivity analysis points out that the parameter of the breach side slope has no major influence on the time to peak while having an insignificant impact on the peak discharge. Besides, the study exhibits that both the peak discharge and the time to peak characteristics are highly sensitive to breach time formation parameter. In the light of these targeted findings, the study is aimed to contribute to other relevant research in designating the set of key parameters in experimental or modeling efforts in a way to limit the uncertainty that substantially originates from personal judgment.

**Keywords:** Dam-break, dam breach flows, sensitivity analysis, uncertainty, flood hydrograph, Ürkmez Dam.

---

### Note:

- This paper was received on September 17, 2020 and accepted for publication by the Editorial Board on March 10, 2021.
- Discussions on this paper will be accepted by November 30, 2022.

• <https://doi.org/10.18400/tekderg.796334>

1 Dokuz Eylül University, Graduate School of Natural and Applied Sciences, GIS Dept., Izmir, Turkey  
eng.mhmd.najar@gmail.com - <https://orcid.org/0000-0002-9107-961X>

2 Dokuz Eylül University, Department of Civil Engineering, Izmir, Turkey  
ali.gul@deu.edu.tr - <https://orcid.org/0000-0001-8137-8950>

## **1. INTRODUCTION**

Dams are hydraulic structures that regulate the flow of rivers. They primarily serve to collect and control the water stored in their reservoirs for several purposes (e.g., hydropower generation, water supply, irrigation, etc.). Even though dams afford great benefits to societies, they could cause catastrophic damages for lives, properties, and environment in cases of accidental events or other emergency conditions. Dam-break (widely also called dam-breach) is a term used when the water behind the dam is released accidentally. Dam-break takes place due to various reasons (e.g., structural defects, insufficient spillway capacity, seepage & piping, overtopping, earthquakes, etc.).

When designing the dams, the failure probability is assigned to be very low during their operational life span. Dam critical design principles demand the dams to resist different kinds of loads, specifically dam body weight and storage water load in the upstream reservoir, with or without seismic load. The failure of a water retaining structure can be categorized with respect to the level of failure (e.g., partial or complete) or its duration (e.g., sudden or gradual). Sudden failure is associated with all types of dams: concrete dams, embankment or arch dams. When breaching is initiated; its development is faster for earth-fill dams than other types under the same conditions. Rock-fill and earth-fill dams - referred to as embankment dams, constitute the most significant portion of dams around the world. Thus, most events of dam-break are recorded for this category. Their failure, depending on the triggering factors, is mostly a gradual process rather than a sudden one.

Different factors can initiate the failure of the earth-fill dam, e.g., piping, overtopping, seepage, or foundation defect. One of the most basic failure modes for embankment dams is the overtopping. Overtopping failure occurs when the inflows become higher than the design inflow [1], malfunctioning reasons, lack of spillway operation systems, inadequate capacity of spillways, or as a consequence of landslides into the reservoir. Any earth-fill dam would collapse if the spillway capacity were inadequate and flood wave elevates high enough to stream over the crest of the dam for a fair amount of time; the initial breach would then start. Once the initial breach mechanism begins, and the upstream storage water levels continue to be high, the breaching would persist in developing and any effort made to stop it would be ineffective [2]. Overtopping failure mode may not lead to structural collapse, but still presents a significant flood hazard. Similarly, the rapid release of upstream stored water to drop the water level to safe limits could conclude to not commendable consequences for downstream areas [3]. The penetration of the water through the interior body of the dam or its foundation may progressively weaken soil from the embankment or its foundation, leading to the failure of the dam. Here, piping failure mode can be defined as a failure caused by water seeping through the dam's body, bearing with its small particles of dam material, continuously enlarging the gap [1].

In the recent decade, several researchers extensively studied both the dam breaks and the flood-wave propagation in both one-dimensional and two-dimensional models. Li et al. [4] examined six reservoirs - located north of Italy, to evaluate the flood damages to the downstream regions. The HCH/DIGHE model was used to measure the hydrograph generated from a dam-break flood event in a way combined with MIKE11 (1D) model to simulate the flood-wave in the downstream riverbed. The study covered also, some issue connected to dam-breach, the impact of the dam-breach parameters, and calculation of the

hydraulic resistance factors. Two early studies by Bozkuş and Kasap [5] and by Bozkuş and Güner [6] employed numerical models for simulating dam break flood events. Based on the comparison of the findings of these studies and an experimental physical dam break model revealed that there is a substantial difference between the physical and numerical results implying that the time to peak discharge ( $T_p$ ) is sensitive to the channel's bottom surface friction. Brufau et al. [7] modelled the flood wave propagation in both one and two dimensions using the shallow water flow equations for unsteady flow. Their model attempted to override the issue that arises when flow develops over dry beds of different slopes. Their model showed a satisfying performance in handling complex flow domains. Yanmaz and Beşer [8] investigated the safety of gravity dams by employing a probabilistic evaluation approach. A probabilistic strategy through random loading and resistance aspects were used for the safety analysis. One of the earliest two-dimensional models in the field of dam-breaks performed by Vásquez and Leal [9]. A finite element method was employed to discretize the computational domain by using a triangular mesh. Both dry (zero) and wet (non-zero) initial water depths were adopted as downstream boundary conditions to run the model. The model successfully simulated both the hydraulic jump that was produced from a wet downstream condition and the surge that was moving over an initially dry bed. Alcrudo and Mulet [10] studied the Tous Dam, which was experienced with a major dam-break event in 1982, to develop and validate a flood wave model. Due to the absence of a validated topography model of the area prior to dam-break occurring time, they run the flood propagation model on two different topography estimates to understand the uncertainties associated with the terrain variety. Palumbo et al. [11] simulated the dam-break flow by taking into consideration the turbulent stresses that may appear from the re-circulating flows in a limited extent. Macchione [12] developed a model to present the main aspects influencing both the formation of the hydrograph peak discharge and the breach development. He described the breach occurrence as a function of the shear stress generated by the flow. The geometry of the embankment, the shape of the breach and the planimetric shape of the reservoir had been taken into consideration. The result after the model calibration indicated a high accuracy of the physical layout for both overtopping and piping failure modes. In the following study by Macchione and Rino [13], sensitivity analysis was carried out to quantify the influence of the side slope parameter on the outputs. The sensitivity analysis showed that dam height, reservoir volume, and water mass in the reservoir are significant factors that influence the flood hydrograph. In a different effort that expands assessments through statistical analyses toward the estimation of expected breach parameters relationships, Froehlich [14] used the data compiled from 74 embankment dam failure cases and developed a set of empirical models for breach cases that form in the shape of a trapezoid. Based on the findings of the study, which also employed Monte Carlo simulation techniques to estimate the uncertainty degree of the predicted peak flows and water depths in the downstream, it was concluded that breach geometry has a non-vertical trapezoidal shape. Yochum et al. [15], on the other hand, modelled an actual dam break event using the HEC-RAS model. Because the study adapted the actual breach geometry parameters, the obtained results have a good agreement with the depths collected as post-flood dataset. Ying et al. [16] developed a dam-break model based on the finite volume method using an unstructured triangular mesh. To simplify the computation and reduce the numerical imbalance between source and flux terms, the model considered the effects of pressure and gravity in the shallow water equations. The developed model displayed capacity to simulate dam-break connected flows which may take place over complicated terrains with different flow types (e.g., subcritical flows, supercritical flows, or

trans-critical flows). Singh et al. [17] developed a two-dimensional numerical model for simulation of dam-break flow propagation. Experiment with a frictionless horizontal bottom was established to validate the 2D model. The agreement observed between the simulation and the experimental results indicated that the model was suitable for simulating dam-break flows. Marco et al. [18] studied the failure of Gleno Dam - located in the Central Italian Alps, caused by structural deficiencies. The study attempts to set-up a dam-break model valid for a mountainous terrains. One-dimensional modelling of dam wave propagation with a first-order finite volume numerical scheme was used to present the main results of the study. Bozkuş and Bağ [19] simulated a fictitious dam break that takes place under a set of pre-defined conditions. Their analysis focused on the post-failure consequences and attempted to estimate the inundation depth with respect to time in the downstream valley. FLDWAV software was used to forecast the flood characteristic. Based on the outputs, a set of recommendations were suggested to the local administrators in charge of public safety. Honghai and Altınakar [20] integrated the GIS and remote sensing technologies to develop a decision support system for dam-break flood management formed on two-dimensional flood simulations. They used HEC-RAS & HEC-FDA to validate their system. The results indicate that the decision support system provides a reliable setting for estimating different flood damage. Mahdizadeh et al. [21] followed up on their previously introduced one-dimensional (1D) shallow-water model for simulating free-surface interaction with the flows issuing vertically through finite gaps. They enhanced the model by using a modified wave propagation algorithm (e.g., extends the shallow-water scheme to two dimensions) to understand the interaction between the free-surface flow and large underground pipe networks used for sewage and storm drainage. Navier-Stokes equations were employed to validate the algorithm. Bosa and Petti [22] applied a two-dimensional numerical model (e.g., 2DH model) to understand the impacts of the overtopping flood wave in the Piave Valley - a region in Italy witnessed a catastrophic dam-break in 1900; about 1700 individual passed away in the valley region alone. They verified if the simplifications assumed by the two-dimensional model properly simulated the growth of the wave. Tsakiris and Spiliotis [23] employed a semi-analytical approach to simulate the breach formation as well as to estimate the outflow hydrograph resulting from a hypothetical overtopping type dam break event. Assumptions of constant vertical erosion rate for the breach formation and a parabolic shape of the breach were accepted through the analysis. The study presented two sets of solution based on the capacity of the reservoir (e.g., prismatic or a power function of the water depth in the reservoir). Moramarco et al. [24] aimed to exemplify the collected reservoir levels data of the studied dam break event (i.e., partial sudden collapse of the spillway of the Montedoglio dam in December 2010) by using discharge hydrographs at several downstream river sites. The work employed a one-dimensional model to simulate the breach development and the flood wave propagation in the downstream valley. In this study, the breach development time was obtained by using an optimization method. Several modeling studies were conducted to scrutinize the effect of densely populated areas subject to the propagation of dam break generated flood waves. For the models using coarse grid sizes, Chen et al., [25] employed two parameters, building coverage ratio (BCR) and conveyance reduction factor (CRF), to simulate flooding in an urban region by two-dimensional model. They found out that this enhanced the accuracy of the modeling and slightly increased the computational efficiency. In addition, Chen et al., [26] utilized a multi-layer approach to model dam break flood plain by taking into considerations two additional factors, elevation and roughness, over those of their previous study. The multilayer approach further increased the accuracy of

the model at grid cells around the buildings and marginally facilitated the computation. Bellos and Tsakiris [27] simulated a flood event in a built-up area using a fully dynamic numerical model (FLOW-R2D). They solved the two-dimensional Shallow Water Equations using the Finite Difference Method and the McCormack numerical system. The resistance caused by buildings (e.g., the reflection boundary, the local elevation rise, and the local increase of the Manning roughness coefficient) were employed to examine the performance of the model. The study concluded that the reflection boundary method proved to be the foremost successful building representation when applying FLOW-R2D model. Elçi et al., [28] investigated the impact of buildings and other obstacles defined through using two parameters, Area Reduction Factor (ARF) and Width Reduction Factor (WRF), on the propagation of the flood waves from dam break events in the examples of two separate dams by combining one-dimensional HEC-RAS and two-dimensional FLO-2D models. They assessed the associated impacts on flood velocity and depth by comparing three scenarios ranked with varying breach characteristics [29].

The literature mainly focused on the determination of flow characteristics at the break time, the collapse mechanism and flood-wave propagation, using both numerical idealized and experimental models. The presented research employs the case-study of Ürkmez Dam to examine failure consequences of any break event that may occur in the site under certain triggering conditions, counting on the significance of the populated downstream region which is greatly used for vacation houses and touristic purposes. In case of a flood resulting from a dam-break event, the loss of lives and properties would be disastrous. In this context, a number of previous studies were carried out to simulate the flood-wave in the downstream area of the dam. Güney et al. [30] carried out an experimental model to simulate the flood-wave propagation by construction a distorted physical model of Ürkmez Dam with vertical and horizontal scales of 1/30 and 1/150, respectively. The model consists of an upstream reservoir, dam body, and topographical representation of downstream region. As the model represents the topography and the building in the downstream area, the effect of the agriculture existence on the flood wave was not covered. Haltas et al. [31] utilized the one-dimensional hydraulic routing HEC-RAS model to estimate the flood hydrograph generated from a partial failure of the dam. Then, a two-dimensional routing model FLOW-2D was employed to simulate the spreading of the dam-break flood after the flood wave exits the valley. A very recent study - following the work of Güney et al. [30]- was carried out by Oguzhan and Aksoy [32]. The study aimed to understand the vegetation effects on the flood wave propagation resulting from a dam-break. It was shown that the presence of vegetation makes a significant decrease in water depths as the flood wave propagates and considerably reduces flooding impact on the downstream settlements.

The previous research show that dam-break studies have two central tasks: estimating the breach flood hydrograph and routing the generated hydrograph along the narrow valley downstream of the dam site. However, the flood hydrograph is determined by the breach geometry and breach formation time. In the dam break simulation models the user is required to estimate the breach geometry and dimensions independently and provide this information as input to the simulation model. Therefore, breach geometry prediction depends on personal judgments, thus it involves high uncertainty in estimating dam-break flood. To this end, the objectives of this study are: (1) to examine the impact of dam-break parameters on maximum breaching outflows, (2) to evaluate the effect of each breaching parameter on the resulting

flood hydrographs by carrying out a sensitivity analysis, and (3) to generate spatio-temporal series of hazard maps to be observed during the propagation of the flood waves to occur from varying approaches of dam break prediction, eventually to help decision makers, and vulnerable communities in the final end, against the flooding threat and for the sake of emergency preparedness. Concerning the targeted objectives in a way this study differs from the previous studies, in terms of (1) the consideration of five modelling approaches against comparatively different selections of some previous studies toward assessing dam break parameters, (2) the use of method-specific breach parameter estimations instead of user defined parameter assignments, (3) the consideration of Probable Maximum Flood (PMF) based on the computation of Probable Maximum Precipitation (PMP) to represent the worst-case scenario in hydrologic aspect, (4) the topography mapping based on precise and updated Digital Terrain Model (DTM) that represents the dam site downstream accurately by adapting the building volumes and other cadastral features onto the Digital Elevation Model (DEM) as well as the accurate reservoir geometry definition to allow level pool routing, (5) final disposition of hazard map series to aid in decision-making.

## **2. DAM BREAK PHENOMENON**

### **2.1. Dam Breach Characteristics**

Dam breaching is a very complex, time-dependent and non-linear mechanism. With the aim of avoiding non-linearity of the model, a simplification might be made regarding breach shape. Breach shape is usually predefined in the models. A uniform erosion behavior during the breaching development time and a constant breach shape are assumed. The breach cross-section is usually considered to be rectangular, trapezoidal, or triangular. One of the earliest research projects conducted by Jonson and Illes [33] by analyzing data from more than 100 dam breach events concluded that the breach initially develops in a "V" shape with a ratio of 4:1 or 3:1 wide to deep. While according to De Almeida & Franco [34] the final breach shape is trapezoidal, this conclusion is based on collected historical dam failure records. They also conclude that, for the earth-fill dams, triangular shape for the breach might be assumed up to the time that the breach reaches the base of the embankments. Once the apex of the triangle reaches the basement of embankments, the breach propagates forming a trapezoidal shape expanding because of the lateral erosion. Another conclusion, from numerous field and laboratory experiments conducted within a European Union funded project implemented in 10 different countries, is that the breach side keeps vertical during the breach growth [35]. Unfortunately, records that describe the progress of the breach cross-section with time are still unavailable for actual dam break events. The main parameters that define the shape of a breach are shown in Figure 1, where,  $B_b$  is the breach bottom width (meter),  $B_{avg}$  is the average breach width (meter),  $h_b$  is the breach height (meter),  $h_w$  is maximum depth of water stored behind the breach (meter),  $W_{avg}$  is the average width of dam in direction of flow (meter),  $C$  is the width of the dam crest (meter),  $Z_d$  and  $Z_u$  are the slopes of the downstream and upstream faces of the embankment, respectively, and  $Z_b$  is the side slope of breach.



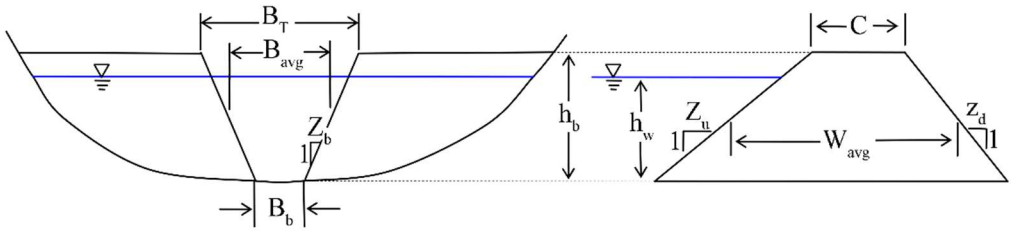


Figure 1 - Dam breach variable definition sketch. [36]

## 2.2. Breach Development

To understand the breach development, the progress of the breach in time and space should be investigated [37]. Breach initiation time is defined as the time starting from the first observable leak (e.g., overtopping, piping, and so forth) that launches warning, evacuation, or awareness, and ending when the breach formation phase started [38-39]. Within this stage phase (breach initiation), the flow amount is relatively small; and if the leak can be kept under control, the dam might not collapse. The phase of breach formation initiates at the moment when the dam failure is about to start and continues until when the breach reaches its maximum shape. The size of the dam reservoir plays a significant role. For a small capacity reservoir, the peak outflow from a dam breach may take place before the breach cross-section reaches its maximum shape, simply because of a rapid decline in reservoir water level during the breach progress. On the contrary, the peak outflow in the case of dams with a relatively large storage pool may occur when the breach fully develops. An initial assumption here is that a channel formed on the embankment body is often taken into consideration in all breach models. The initial channel determines the starting condition for the breaching progress. If no initial channel exists, then the succeeding phases of the breaching process will not happen. The fundamental characteristics of the breach channel define further breaching development. As the initial channel formation depends on many factors (e.g., flow characteristics, structure coverage, and improper/insufficient compaction), it is a difficult task to predict the exact initial location of the formed breach channel.

### 2.2.1. Hydraulics of Flow over the Dam

The breach flow hydrograph plays a significant role in the evaluation of the flood wave characteristics in the downstream regions. The flow through the breach channel can be simulated using either orifice equation (at the initial formation phase of piping failure), and the weir equation or the one-dimensional Navier-Stokes equation referred to as Saint-Venant equations.

The weir equation that estimates the discharge for the free flow (low tailwater) condition is expressed as:

$$Q = CLH^{3/2} \quad (1)$$

where,  $Q$  is the discharge,  $C$  ( $m^{1/2}.s^{-1}$ ) is weir coefficient,  $L$  (m) is the weir crest length, and  $H$  (m) is energy head over the weir crest. In extreme cases, if tailwater arises up to the embankment crest, Eq. 1 becomes,

$$Q = C_s L H^{3/2} \quad (2)$$

where  $C_s$  is a coefficient for the submergence effect.

Attention should be given to the difference between the weir coefficient and the discharge coefficient. The weir coefficient is an aggregate parameter that includes the discharge coefficient, the gravitational constant, and constants based on geometric properties.

$$C = \frac{2}{3} C_d \sqrt{2g} \quad (3)$$

where  $C_d$  again is the dimensionless discharge coefficient [40-41].

#### Empirical Approaches to Dam-Break Analysis

A group of the most common experimental approaches for forecasting dam breach size and breach formation time were applied to evaluate breach parameters for a dam-break event. The employed approaches are MacDonald and Langridge-Monopolis [42], Bureau of Reclamation [36], Von Thun and Gillette [43], Froehlich [14]; and Xu and Zhang [44]. Furthermore, the type of failure, either overtopping or piping, was also examined in the study based on the parameters defined in Fig. 1. The empirical methods were formulated based on a statistical analysis of the data extracted from documented dam failures.

To estimate the width of the dam breach recommendations of Singh and Snorrason [45] was integrated. Their empirical formula was calculated in the approach based on twenty documented dam failure cases. The breach width is a function of only one variable, dam height, ranging between twice and five times of the height. Also, according to this study, they expressed that the dam failure time varied from a quarter-hour to one hour.

The study by MacDonald and Langridge-Monopolis [42], on the other hand, provides two sets of equations to accommodate the differences between the types of dams (e.g., earth-fill dam or other type dams). In their study, data set of forty-two dam failure events were assessed to develop the regression equation that predicts the breach factors. Eqs. 4 and 5 that estimate the volume of eroded material ( $V_{er}$ ,  $m^3$ ) are functions of the volume of water that passes through the breach ( $V_{out}$ ,  $m^3$ ) and water depth ( $h_w$ , m) in the reservoir at the time of failure, for earth-fill dam type and other types, respectively. This study covered a range of dams with the height ranging between 4.27 m and 92.96 m and the available water volume between 0.0037 and 660.0 ( $10^6 m^3$ ). For the time of failure, based on the calculated volume of material eroded, ( $t_f$ , hr) Eq. 6 was recommended.

$$V_{er} = 0.0261(V_{out} * h_w)^{0.769} \quad (\text{for earthfill dams}) \quad (4)$$

$$V_{er} = 0.00348(V_{out} * h_w)^{0.852} \quad (\text{for earth-fill dams with a clay core or rockfill dams}) \quad (5)$$

$$t_f = 0.0179(V_{er})^{0.364} \quad (6)$$

U.S. Department of the Interior, Bureau of Reclamation [36] provided a third approach to obtain the width of rectangular breach with respect to depth of the water in the upstream reservoir (Eq. 7). This formula can be used as a rule of thumb for choosing the ultimate breach width that can be used mostly in the hazard classification studies. This approach suggests that the time for breach to develop is around 1% of the breach width (Eq. 8).

$$B = 3 h_w \quad (7)$$

$$t_f = 0.011 B \quad (8)$$

The fourth method put forward by Von Thun and Gillette [43] used the data obtained from fifty-seven historically recorded dam failure cases that were previously studied by both Froehlich [46] and MacDonald & Langridge-Monopolid [42] to recommend a relationship for predicting average breach width,  $B_{avg}$ . In the relationship, Eq. 9,  $B_{avg}$  is a function of reservoir water depth ( $h_w$ , m) and the coefficient ( $C_b$ , m). the data covered a range of where  $V_{out}$  ( $10^6$  m<sup>3</sup>) between 0.027 and 660 and height of dams ( $h_d$ , m) between 3.66 and 92.96. Besides, Von Thun and Gillette [43] stated that the majority of dams (89 %) have  $h_d$  less than 30 m and  $V_{out}$  less than 25 ( $10^6$  m<sup>3</sup>). The  $C_b$  values were directly related to the reservoir size and varied from 6.1 m for relatively small reservoirs to 54.9 m for large sized reservoirs.

$$B_{avg} = 2.5 h_w + C_b \quad (9)$$

In addition to the developed relationship, it was also recommended to use 1H:1V breach slope side except for the dams with cohesive cores for which a ratio of 1H:2V or even 1H:3V may be more suitable. Regarding to the breach formation time, the approach provides two set of equations based on the dam fill material Eqs. 10 through 13.

$$t_f = 0.02 h_w + 0.25 \quad (\text{erosion resistive material}) \quad (10)$$

$$t_f = 0.015 h_w \quad (\text{easily erodible}) \quad (11)$$

Breach development time as a function of ( $h_w$  and  $B_{avg}$ ):

$$t_f = \frac{B_{avg}}{4h_w} \quad (\text{erosion resistive material}) \quad (12)$$

$$t_f = \frac{B_{avg}}{4h_w + 61.0} \quad (\text{highly erodible}) \quad (13)$$

The next approach investigated in the present study was originally developed by Froehlich [14] and exemplifies one of the most recent studies on dam breach. The study is seemingly an enhancement of one of his previous studies (Froehlich, 1987) covering a larger number of documented dam breach cases. The study states that in the case of overtopping type failure, the side slope ratio is 1H:1V, while for the piping or seepage failure the side slope ratio is 0.7H:1V.

Froehlich's suggested the following relationship (Eq. 14) for the average width of the breach ( $B_{avg}$ , m),

$$B_{avg} = 0.27 K_o V_w^{0.32} h_b^{0.04} \quad (14)$$

where,  $K_o = 1.3$  for overtopping, and  $K_o = 1.0$  for other failure modes. The equation below considers that the breach formation time is directly proportional to reservoir volume ( $V_w$ ,  $m^3$ ) and inversely proportional to the breach height ( $h_b$ , m) (Eq. 15).

$$t_f = 63.2 \sqrt{\frac{V_w}{g h_b^2}} \quad (15)$$

In the last approach, considered in the present work, by Xu and Zhang [44], analyses were performed using a wide range of historically documented dam failure cases – 182 earth and rockfill dams from both U.S and China. However, due to data limitations their final formulas were developed using a relatively smaller subset (75 dams) of those dam break cases. The ranges of  $h_d$  and  $V_{out}$  used in the study are very similar to the ranges that were used by Von Thun and Gillette [43] (i.e.,  $3.2 \text{ m} \leq h_d \leq 92 \text{ m}$ ; and  $0.105 \times 10^6 \text{ m}^3 \leq V_{out} \leq 660 \times 10^6 \text{ m}^3$ ). However, in this study most dams (around 80 %) have heights less than 30 m and  $V_{out}$  less than  $25 \times 10^6 \text{ m}^3$ . They also, developed an equation (Eq. 16) to calculate the average breach width ( $B_{avg}$ , m).

$$\frac{B_{avg}}{h_b} = 0.787 \left(\frac{h_d}{h_r}\right)^{0.133} \left(\frac{V_w^{1/3}}{h_w}\right)^{0.652} e^{B_3} \quad (16)$$

where,  $h_r$  is 15 meters, which is the reference height used to distinguish between small and large dams,  $B_3$  is the coefficient that depends on dam properties and equal to the summation of  $b_3$ ,  $b_4$ , and  $b_5$ ;  $b_3$  is -0.226 for homogenous/zoned-fill,  $b_4$  is equal to -0.389 and 0.149 for piping and overtopping, respectively, and  $b_5$  represents the effect of erodibility of the dam (e.g., Ürkmez dam was considered to be medium erodible with  $b_5 = -0.14$ )

Unlike the previous methods, Xu & Zhang [44] method does not estimate the side slopes of the breach. Alternatively, the method calculates the top width of the breach ( $B_T$ , m) through Eq. 17 that governs the relationship between the breach top width and the height of the final breach.

$$\frac{B_T}{h_b} = 1.062 \left(\frac{h_d}{h_r}\right)^{0.092} \left(\frac{V_w^{1/3}}{h_w}\right)^{0.508} e^{(b_3+b_4+b_5)} \quad (17)$$

where  $b_3$  is -0.089 for homogenous/zoned-fill,  $b_4$  is equal to -0.239 and 0.299 for piping and overtopping, respectively; and  $b_5$  is -0.062 for medium erodible dam.

All of the equations above help to estimate the breach geometry parameters suggested by the different approaches of earlier studies which then serve as input for hydraulic modelling.

### 3. METHODS

In the presented study, five of the most popular experimental approaches for predicting dam breach characteristics (e.g., dam breach size and breach formation time) were employed to estimate breach parameters for the Ürkmez Dam. The study site of Ürkmez Dam was selected as it is in a touristic region with the residential area right on the dam downstream (Fig. 2). It is located 3 km north of Ürkmez township in the province of İzmir in Turkey. The dam was built to supply drinking water and provide irrigation. The General Directorate for State Hydraulic Works (DSI) completed the construction in 1990 and the dam started with the irrigation function. In 2004, a municipal water treatment plant was built and started functioning.

The breach modelling techniques were formulated from the statistical analysis of data derived from the recorded dam failures of a wide range of dam sizes. These approaches were used to estimate Ürkmez Dam breach characteristics subjected to numerous scenarios of failure mode type (e.g., overtopping and piping) with varying ranges of initial upstream reservoir water levels. A decreasing interval of 2 m - from the maximum upstream reservoir storage level (48 m a.s.l.), were studied for these methods. The centerline of the dam was assumed to be the dam breach location for both piping and overtopping failure types. As the weir and piping coefficients for the earthen sand and gravel type of dams (similar to the Ürkmez Dam case) are recommended to be between 2.6 and 3.0 in case of overtopping mode, and 0.5 to 0.6 in piping failure mode [1], these coefficients were set to be as 2.8 and 0.55, for overtopping and piping failure modes, respectively. In the case of piping failure mode, the breach start level though piping was considered to be at the level equal to the half of the water height in the reservoir ( $h_w/2$ ).



Figure 2 - Ürkmez Dam Location Map

The Probable Maximum Precipitation (PMP) was calculated using [47] statistical method based on the annual maximum precipitation observations for 67 years in the period 1938-2015. The Probable Maximum Flood (PMF) hydrograph generated from the PMP was used as input hydrograph feeding the HEC-RAS 5.0.7 hydraulic model. Since the topography of upstream reservoir was modeled accurately, the level pool routing method was used conveniently. The study area was modelled using inline structure to present the dam body, a storage area to model the upstream reservoir and a continuous 2-dimensional mesh with 20-meter resolution to model the downstream area, while a 1-meter mesh resolution was used in representing the river and spillway centerlines. The main riverbed was assumed to be the breach final bottom elevation. The Saint-Venant full-momentum set of equations were used to determine the flood hydrograph produced by a dam breach for each scenario setting.

#### 4. RESULTS AND DISCUSSION

##### 4.1. Maximum Discharge and Time of its Occurrence

The resulting flood hydrograph associated with dam-break in the case of Ürkmez Dam was calculated by using the Saint-Venant full momentum set of equations in HEC-RAS 5.0.7 with a different initial reservoir level for five different empirical approaches for both overtopping and piping failure modes as shown in Table 1. The flood hydrographs were

Table 1 - Maximum discharge & Time to peak discharge for all scenarios

Approach	Variable	Unit	Failure Type	Initial Reservoir Level (m)				
				48.0	46.0	44.0	42.0	40.0
USBR	Q <sub>p</sub>	(10 <sup>3</sup> m <sup>3</sup> /s)	Over top.	5.85	5.89	5.91	5.92	5.93
	T <sub>p</sub>	min.		23.05	22.92	22.88	22.90	22.95
	Q <sub>p</sub>	(10 <sup>3</sup> m <sup>3</sup> /s)	Piping	4.87	4.92	4.95	4.97	4.98
	T <sub>p</sub>	min.		25.05	24.82	24.93	27.88	25.02
Von Thun & Gillette	Eq. (10) Q <sub>p</sub>	(10 <sup>3</sup> m <sup>3</sup> /s)	Overtopping	7.64	7.69	7.71	7.72	7.72
	T <sub>p</sub>	(min.)		16.05	15.83	15.88	15.92	16.02
	Eq. (12) Q <sub>p</sub>	(10 <sup>3</sup> m <sup>3</sup> /s)	Overtopping	7.37	7.41	7.44	7.44	7.45
	T <sub>p</sub>	(min.)		18.00	17.87	17.88	17.93	17.59
MacDonald & Monopolis	Q <sub>p</sub>	(10 <sup>3</sup> m <sup>3</sup> /s)	Over top.	2.90	2.98	3.00	3.02	3.03
	T <sub>p</sub>	min.		64.00	64.82	64.88	63.90	63.95
	Q <sub>p</sub>	(10 <sup>3</sup> m <sup>3</sup> /s)	Piping	2.73	2.78	2.81	2.85	2.85
	T <sub>p</sub>	min.		64.02	61.82	61.88	61.90	61.98
Xu & Zhang	Q <sub>p</sub>	(10 <sup>3</sup> m <sup>3</sup> /s)	Over top.	3.75	3.82	3.87	3.89	3.91
	T <sub>p</sub>	min.		56.12	55.83	54.88	55.90	54.97
	Q <sub>p</sub>	(10 <sup>3</sup> m <sup>3</sup> /s)	Piping	2.88	2.94	2.98	3.00	3.02
	T <sub>p</sub>	min.		65.08	64.83	64.88	64.93	64.95

obtained at a point immediately after the downstream face of the dam. Here, slight increases are observed in the outflow hydrograph peak quantities in a pattern inversely proportional with the initial reservoir levels. The rationale behind this is that the dam becomes subject to different rates of inflow (observed from the PMF hydrograph) as the time passes from the initial reservoir water elevation. Indeed, higher rates of flow will have been accessed at the breach formation time in the case of lower initial reservoir elevations so that longer time will be required to allow the breach process to initiate (also considering the additional time for the full development of breach geometry on top of the breach start through the gradual development of breach geometry). As shown in Figs. 3a and 3b, the overtopping failure type has also a tendency to provide higher peak discharge value than the piping failure type. It was observed also that, Von Thun & Gillette approach (Eq. 12), which estimates the breach development time as a function of  $h_w$  and  $B_{avg}$ , provides time to peak longer than the one obtained by Eq. 10 (i.e., time to peak as function of  $h_w$ ). Besides, the peak discharge obtained using  $(t_r)$  from Eq. 12 is always less than the peak quantity obtained through using  $(t_r)$  from Eq. 10.

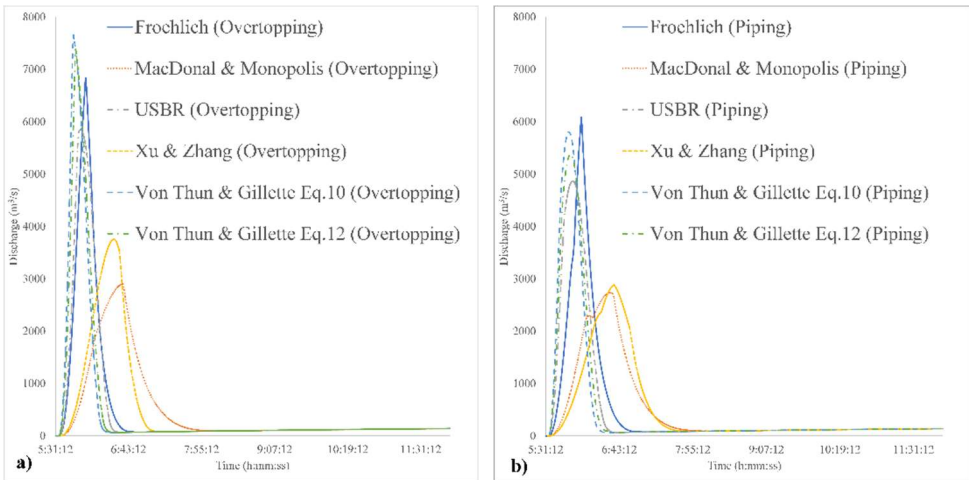


Figure 3 - a) Flood hydrographs when reservoir elevation is at 48 m a.s.l. for all approaches for Overtopping failure mode, b) Flood hydrographs when reservoir elevation is at 48 m a.s.l. for all approaches for piping failure mode

#### 4.2. Failure Mode Impact on Flood Hydrographs

With the aim of examining the effect of failure type on the resulting hydrograph. Firstly, the geometry of the breach for all the approaches were predicted for the maximum reservoir level for both overtopping and piping failure mode (Figs. 3a, 3b). Figs. 3a, and 3b clearly reveal that, for the same reservoir level (i.e.,48 m), there are two differentiated sets of hydrograph patterns that are associated with the different methods applied. The first set of hydrographs has the highest amplitudes with higher discharge peaks that resulted in less times to peaks as well as the lower base times. The hydrographs of this first pattern were calculated by using

Von Thun & Gillette, USBR, and Froehlich approaches. Xu & Zhang and MacDonald & Monopolis prediction approaches established the second set of hydrographs which are characterized by relatively longer times to peak discharges (and longer base times) and approximately halved peak values with respect to the former group values. This pattern remains the same for both overtopping and piping failure types. Besides, while Xu & Zhang approach provides a higher peak value (e.g., +22.5 %) in the overtopping failure mode than MacDonald & Monopolis method, its peak attenuates to become nearly at the same level with MacDonald & Monopolis method for the piping mode. Secondly, the effect of failure mode was also investigated by varying the initial water level for the upstream reservoir (e.g., 40 m, 42 m, 44 m, 46 m, and 48 m).

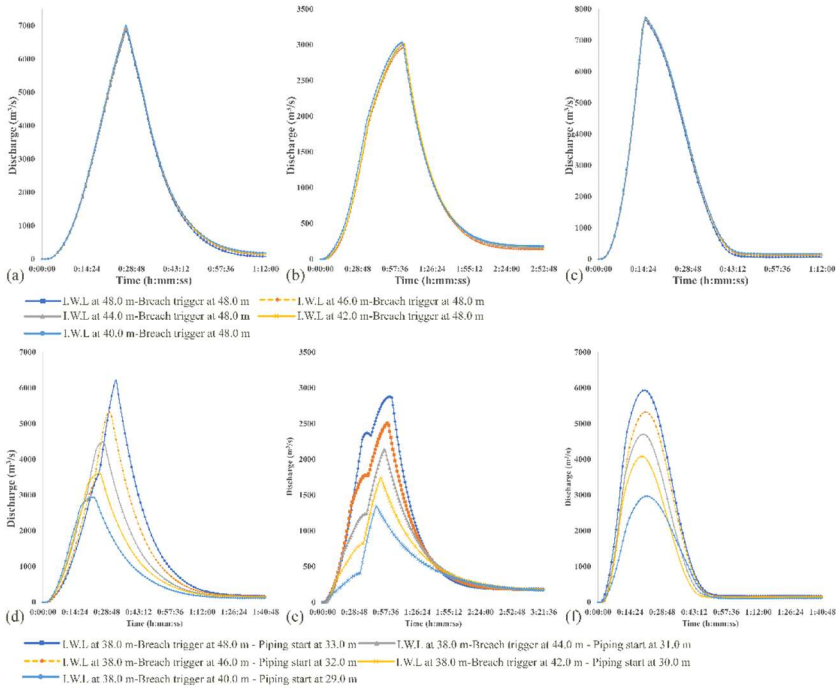


Figure 4 - Flood hydrographs for different initial water levels (I.W.L.) using (a) Froehlich approach, (b) MacDonald & Monopolis approach, (c) Von Thun & Gillette (Eq. 10) approach for overtopping failure modes, and (d) Froehlich approach, (e) MacDonald & Monopolis approach, and (f) Von Thun & Gillette (Eq. 10) approach for piping failure modes.

Figs. 4a to 4c show that a very minimal change was observed when varying the initial water level for the overtopping failure mode, where, the breach trigger at elevation 48.0 m. Figs. 4d to 4f illustrate the flood hydrographs that were generated using piping failure modes (for piping to start at the half of the water height in the reservoir above the reservoir bottom elevation ( $Z_b$ ) of 18 m; i.e.,  $Z_b + h_w/2$ ) against the initial water level (I.W.L.) assumption of 38 m. (e.g., the piping breach elevation of 33.0 m is computed for the breach trigger



consideration at the reservoir water level of 48.0 m that corresponds to 30.0 m reservoir water depth ( $h_w$ ) above  $Z_b$ ). It is also apparent from the graphs of the piping mode that the time to peak evolved gradually for the Froehlich hydrographs for varying initial water levels associated with corresponding piping start levels, while in the latter two, the changing input variables for inducing the piping did not make significant effect on the peak arrival time.

### 4.3. Sensitivity Analysis

With the aim to investigate which parameter of dam breach has more influence on the result, a sensitivity analysis was applied by using the Froehlich (2008) [14] approach with the overtopping failure type and dam maximum operating water elevation at 48 m a.s.l. To determine the controlling parameter, the breach formation time ( $t_f$ ), the average breach width ( $B_{avg}$ ), and side slope ( $Z_b$ ) were increased by 25 %, 50 %, 75 % and 100 % and then reduced by 25 %, 50 % and 75 %, respectively. The resulting flood hydrographs directly at the downstream side of the dam were estimated for each individual case. The sensitivity analysis for  $B_{avg}$  clearly shows that an increase of breach width by a constant percentage tends to increase the maximum discharge value and at the same time decrease  $T_p$  and vice versa. As Figs. 5a and 5b reveal, doubling the value of  $B_{avg}$  leads to an increase in the maximum discharge value by 34 % while dropping the time to peak up to 50 %.

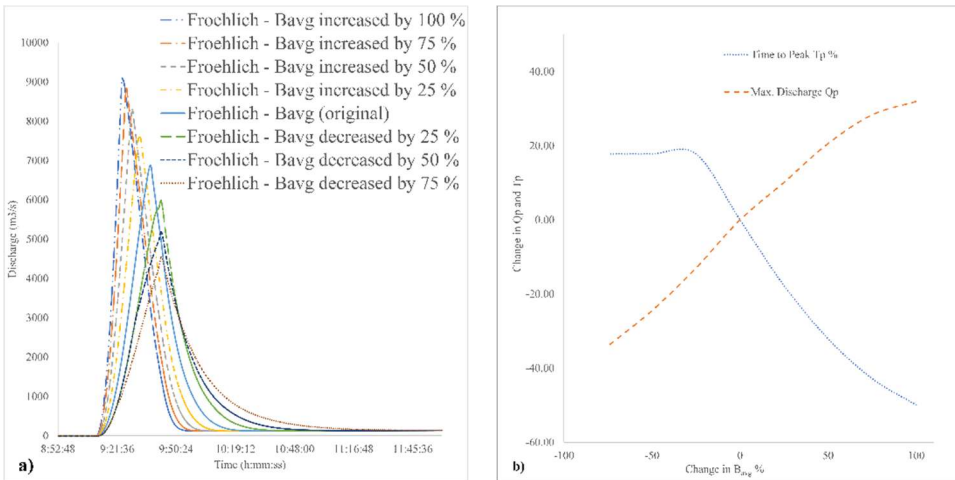


Figure 5 - a) Flood hydrographs for different  $B_{avg}$  values at dam site, and b) percent change in  $Q_p$  and  $T_p$  with  $B_{avg}$

Apparently, no remarkable variation was distinguished in time to peak and a minor difference in peak discharge value with respect to the corresponding changes in breach side slopes. Although, adjusting the breach side slope leads to a change in breach cross-section area, decreasing the breach side slope by 75 % led to change by 0.0 % and -15 % in time to peak and peak discharge, respectively. Therefore, the breach side slope effect in the case of Ürkmez dam can be considered negligible, as Figs. 6a and 6b indicate.

The results obtained by varying the time of breach formation - with standardization of all other parameters (e.g., average breach width ( $B_{avg}$ ) and side slope ( $Z_b$ ) of the breach cross-section) - suggest that maximum discharge value,  $Q_p$  and the time of peak discharge,  $T_p$  are significantly sensitive to the change in time for the breach to fully develop. As Table 2, Figs. 7a and 7b suggest, increasing the breach formation time by 50 %, from 0.55 hr to 0.83 hr, led to a decrease in  $Q_p$  by 23.18 % and an increase in  $T_p$  by 46.44 %. Nevertheless, declining breach formation time by 50 %, from 0.55 hr to 0.14 hr, led to an increase in  $Q_p$  by 32 % while  $T_p$  was halved.

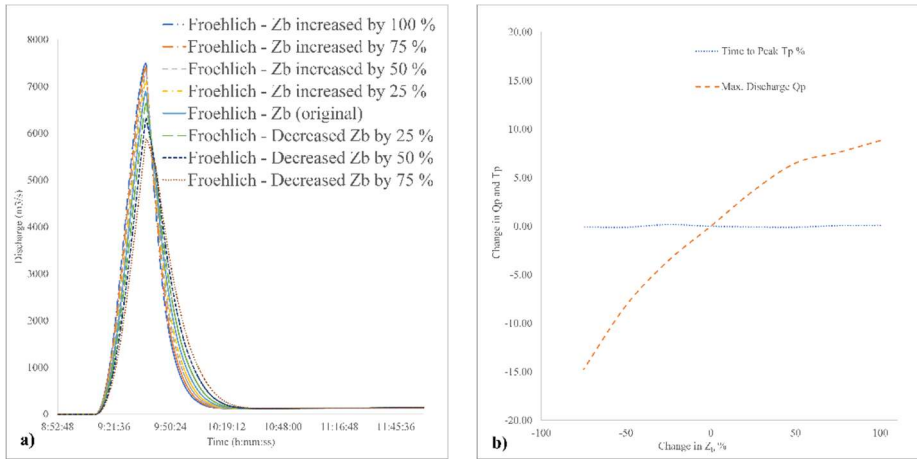


Figure 6 - a) Flood hydrographs for different  $Z_b$  values at the dam site, and b) percent change in  $Q_p$  and  $T_p$  against varying  $Z_b$ .

Table 2 - The maximum discharge and time to the maximum values against varying breach formation times

$t_f$ (hr)	$t_f$ dif. (%)	$Q_p$ ( $10^3$ m <sup>3</sup> /s)	$Q_p$ dif. (%)	$T_p$ (min)	$T_p$ dif. (%)	Note
<b>1.10</b>	$t_f + 100\%$	4.17	-39.33	53.07	88.86	<b>Increased <math>t_f</math></b>
<b>0.96</b>	$t_f + 75\%$	4.66	-32.24	47.15	67.79	
<b>0.83</b>	$t_f + 50\%$	5.29	-23.18	41.15	46.44	
<b>0.69</b>	$t_f + 25\%$	6.04	-12.25	35.08	24.84	
<b>0.55</b>	$t_f + 0\%$	6.88	0.00	28.10	0.00	<b>Original <math>t_f</math></b>
<b>0.41</b>	$t_f - 25\%$	7.87	14.32	21.13	-24.80	<b>Decreased <math>t_f</math></b>
<b>0.28</b>	$t_f - 50\%$	9.08	31.97	14.08	-49.89	
<b>0.14</b>	$t_f - 75\%$	10.77	56.57	8.07	-71.28	

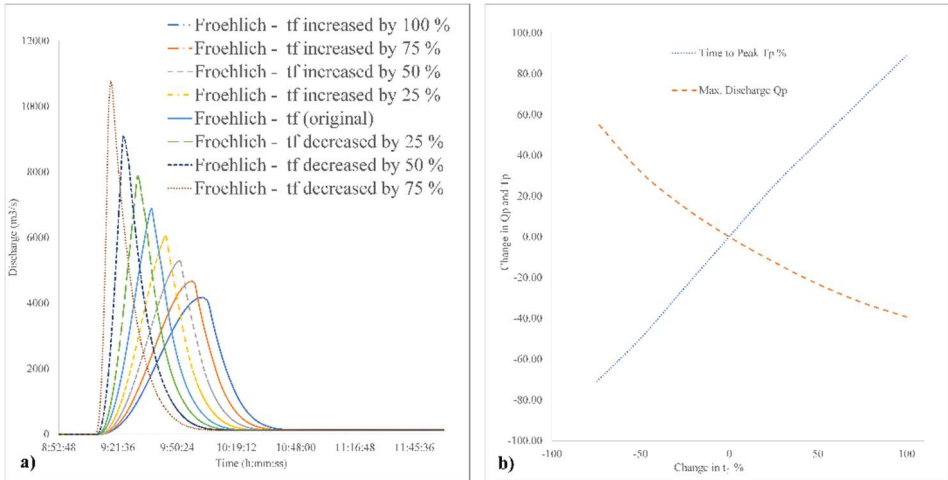


Figure 7 - a) Flood hydrographs for different  $t_f$  at the dam site, and b) percent change in  $Q_p$  and  $T_p$  with respect to  $t_f$ .

The results from the sensitivity analysis in the current study help reveal that the breach side slope has no significant impact on neither the peak discharge arrival time nor the peak discharge value itself. Nevertheless, the outflow hydrograph is remarkably sensitive to the breach width and is extremely sensitive to the breach formation time. These findings that resulted from the disconnected study on a site with varied dam characteristics and topography features as such proved to be in a reconfirmed agreement with the previous studies on the same subject in support of the sensitivity aspects of the breach parameters (e.g., [6], [38], [48-50]).

#### 4.4. Flood Inundation and Hazard Mapping

The main objective of flood hazard mapping is to identify areas under the risk of flooding, and thus to contribute to both flood risk management and the post-disaster recovery planning. Dam break connected flood hazard maps typically unveil the expected flood extent, depth, and velocity characteristics in the downstream. In the case of dam break flood mapping, flood hazard can vary significantly across both the temporal and spatial scales, particularly with a combined impact of flood velocity and depth.

U.S. Bureau of Reclamation (1988) provides guidance (Downstream Hazard Classification Guideline [36]) to evaluate the fluctuating degrees of flood hazard that occurs across a floodplain. For the scope of this study, a classification for possible hazard for adults, considered to be over 150 cm tall and weighing over 54 kg [36], is mainly carried out based on the flood danger relationship with depth and velocity. The classification scheme produces three hazard levels (through high-danger zone, judgment/transition zone, and low-danger zone definitions). In the context of the presented study, a comparison between the hazard inundation mapping produced by using the Froehlich [14] (Fig. 8) and MacDonald & Monopolis [42] methods (Fig. 9) both for overtopping breach types were provided since these

literature sources yielded notably dissimilar results for both the time to peak and the peak discharge quantities as clearly shown in Fig. 3a. Figs. 8 and 9 show the temporal series of flood hazard mapping that covered an area of 5 km<sup>2</sup> downstream of the dam. It is worth to note here that the resulting hazard zones associate with the probable maximum event that may be experienced in the case study, though there may be other studies that deal with the flood issue in different aspects. Differing from the main objective of sensitivity analysis, some relate to the modeling and validation of an actual flood event experience (e.g., [10], [15], [24]) while some others more consider scenario analyses (e.g., [19]).

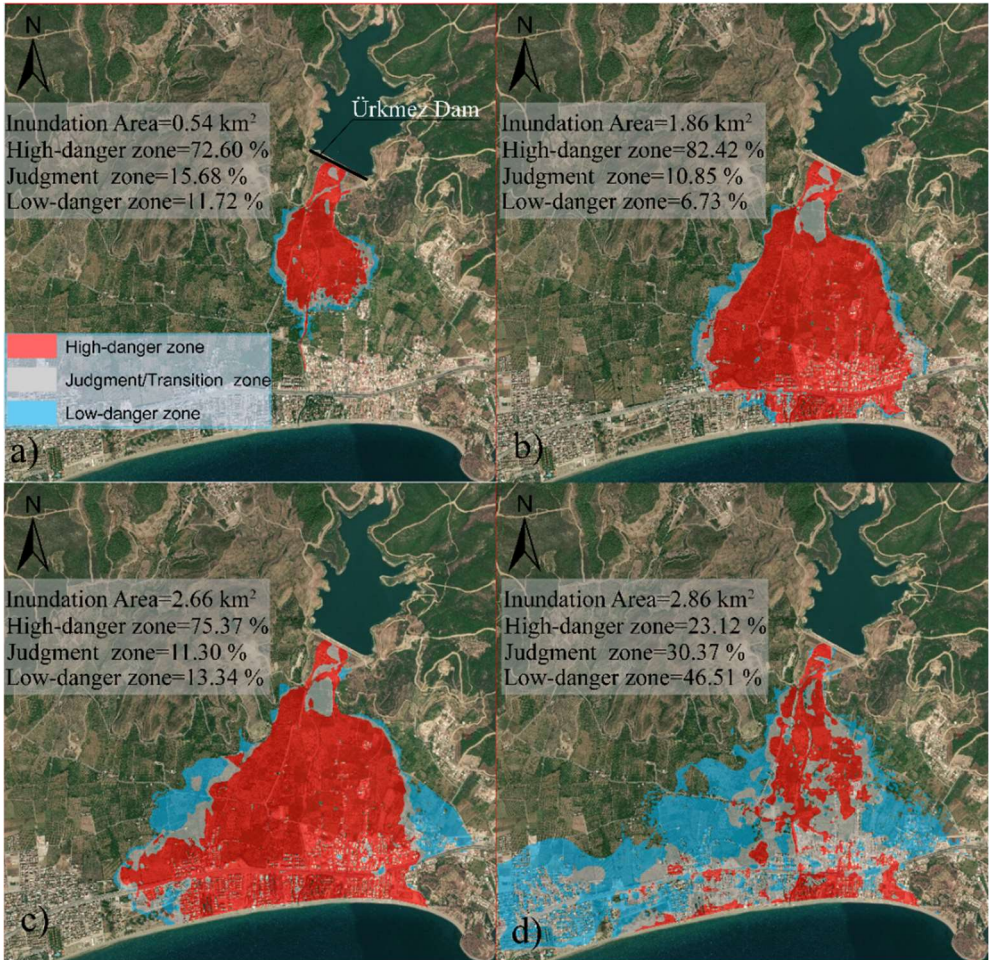


Figure 8 - The Spatio-temporal change in water extent and hazard classification using Froehlich [14] method after a) 15 min, b) 25 min, c) 35 min, d) 60 min.



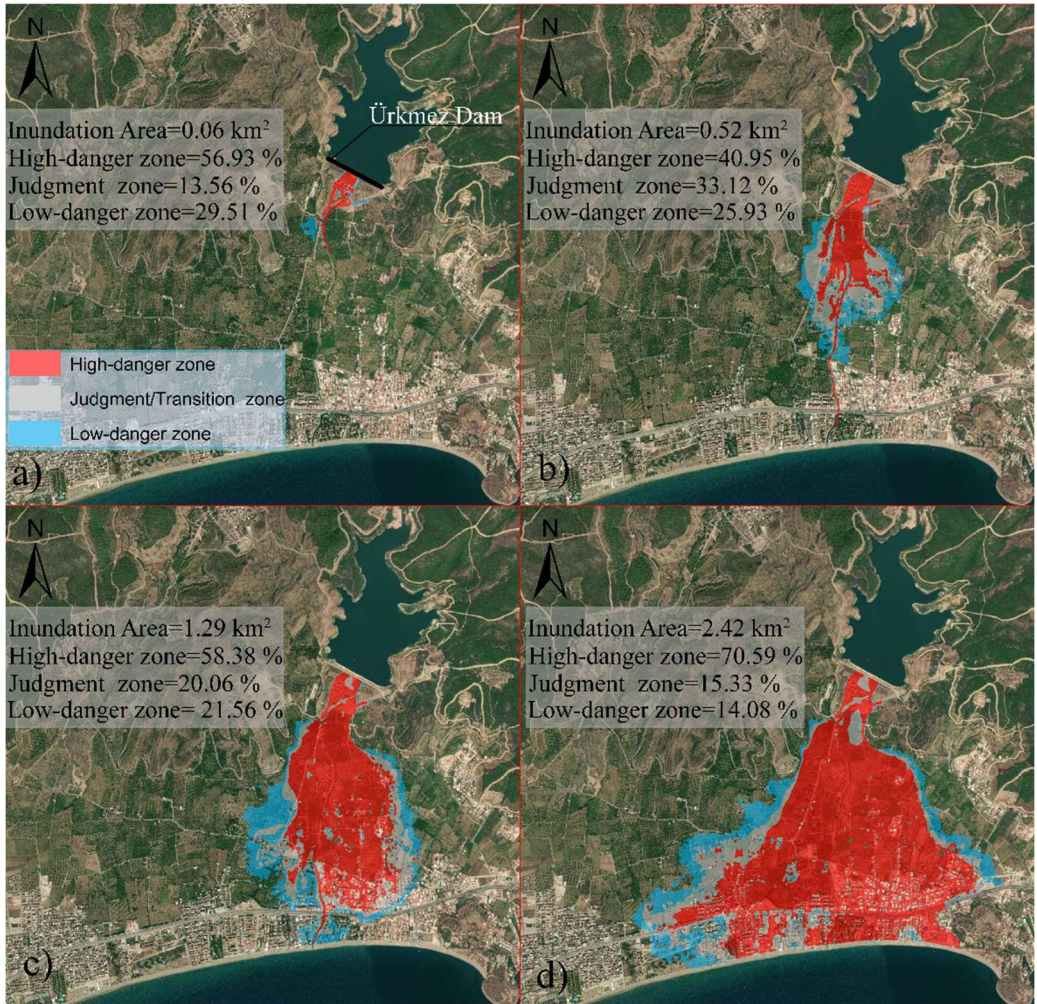


Figure 9 - The Spatio-temporal change in water extent and hazard classification using MacDonald & Monopolis [51] method after a) 15 min, b) 25 min, c) 35 min, d) 60 min.

## 5. CONCLUSIONS

This study explored the consequences of a hypothetical dam failure in the case of an embankment dam with a built-up downstream area of 5 km<sup>2</sup>. The HEC-RAS two-dimensional hydrodynamic model was used to simulate dam failure and propagation of the flood wave for extensive set of scenarios (96 in total varying with respect to initial conditions and breach formation characteristics). Scenarios were practiced testing the varying impacts of overtopping and piping failure modes. Besides, 5 initial reservoir levels (e.g., 48 m, 46 m, 44 m, 42 m and 40 m a.s.l) were studied in each approach. A very sensitive DTM was developed as well as the worst-case scenario was studied by considering the PMF hydrograph as input

for the hydraulic model. The differences in the hydraulic model predictions caused by alternating the initial conditions were analyzed. A sensitivity analysis on the breaching parameters was mainly performed. The study investigated flooding impacts based on the flood hydrographs resulting from dam break phenomenon. A series of breach prediction methods that commonly appeared in relevant scientific literature were employed in the case study.

Based on comparisons with an observational judgment among all the methods employed in the study, the USBR and Von Thun & Gillette approaches estimated the highest peaks and the lowest times to corresponding peaks, Froehlich (2008) method provided moderate outputs for the both quantities (peak discharge and peak time) while the lowest peaks against delayed peak arrival times were estimated through the MacDonald & Langridge-Monopolis and Xu & Zhang equations. In general, the piping failure modes that were simulated in all empirical approaches tend to give lower peak flood discharges in comparison to the overtopping failure mode as expected.

The sensitivity analysis points out that both the peak discharge and the peak arrival time (i.e., time to peak) show great sensitivity to the breach full development time ( $t_f$ ) parameter (even following an almost identity line relationship with  $T_p$ ) and again a considerable sensitivity to the breach width ( $B_{avg}$ ) parameter. Besides, the results provided strong indication to infer that the breach side slope ( $Z_b$ ) does not affect the time to peak discharge at all, even though its negligible impact on the evolution of the peak discharge may still be observed.

Concerning the targeted study area, the obtained results show that the case study area, Ürkmez reservoir, represents a significant threat to downstream areas in a probable event of dam break; as indicated by the hazard maps; greater portion of the inundated area is subject to high-danger hazard level in around 30 mins after the break event.

The obtained results provide decision makers, urban & emergency planners, and vulnerable communities in the end, to help formulate evacuation procedures and to consider an adapted site planning in the areas especially associated with high and intermediate (transition) hazard levels. The presented work is targeted to provide a contribution to the field of dam break studies in its tailored context with the use of method-specific breach parameter estimations instead of user defined assignments (i.e., through the suggestions of the methods themselves) when investigating the sensitivity of the parameters governing the outflow discharge characteristics.

## References

- [1] G. Brunner, Using HEC-RAS for Dam Break Studies, TD-39, 2014.
- [2] M. Zagonjoli, Dam break modelling, risk assessment and uncertainty analysis for flood mitigation, Delft University of Technology & UNESCO-IHE Institute for Water Education, 2007.
- [3] C. A. Pugh and D. W. Harris, Prediction of landslide-generated water waves, 1982.
- [4] L. Li, M. Cargnelutti, and C. Mosca, Dam-break events, flood damage, Piemonte region, Italy, *Water Resour. Manag.*, vol. 5, pp. 261–270, 1991.

- [5] Z. Bozkuş and A. Kasap, Comparison of physical and numerical dam-break simulations, *Turkish J. Eng. Environ. Sci.*, vol. 22, no. 5, pp. 429–443, 1998.
- [6] Z. Bozkuş and A. I. Güner, Pre-event dam failure analyses for emergency management, *Turkish J. Eng. Environ. Sci.*, vol. 25, no. 6, pp. 627–641, 2001.
- [7] P. Brufau, M. E. Vázquez-Cendón, and P. García-Navarro, A numerical model for the flooding and drying of irregular domains, *Int. J. Numer. Methods Fluids*, vol. 39, no. 3, pp. 247–275, May 2002, doi: 10.1002/flid.285.
- [8] A. M. Yanmaz and M. R. Beşer, On the reliability-based safety analysis of the Porsuk Dam, *Turkish J. Eng. Environ. Sci.*, vol. 29, no. 5, pp. 309–320, 2005, doi: 10.3906/sag-1203-6.
- [9] J. A. Vásquez and J. G. A. B. Leal, Two-dimensional dam-break simulation over movable beds with an unstructured mesh, *Proc. Int. Conf. Fluv. Hydraul. - River Flow 2006*, vol. 2, pp. 1483–1491, 2006, doi: 10.1201/9781439833865.ch158.
- [10] F. Alcrudo and J. Mulet, Description of the Tous Dam break case study (Spain), *J. Hydraul. Res.*, vol. 45, no. sup1, pp. 45–57, Dec. 2007, doi: 10.1080/00221686.2007.9521832.
- [11] A. Palumbo, S. Frazão, L. Goutiere, D. Pianese, and Y. Zech, Dam-break flow on mobile bed in a channel with a sudden enlargement, in *Proceedings international conference on Fluvial Hydraulics*, 2008, pp. 645–654.
- [12] F. Macchione, Model for Predicting Floods due to Earthen Dam Breaching. I: Formulation and Evaluation, *J. Hydraul. Eng.*, vol. 134, no. 12, pp. 1688–1696, Dec. 2008, doi: 10.1061/(ASCE)0733-9429(2008)134:12(1688).
- [13] F. Macchione and A. Rino, Model for Predicting Floods due to Earthen Dam Breaching. II: Comparison with Other Methods and Predictive Use, *J. Hydraul. Eng.*, vol. 134, no. 12, pp. 1697–1707, Dec. 2008, doi: 10.1061/(ASCE)0733-9429(2008)134:12(1697).
- [14] D. C. Froehlich, Embankment Dam Breach Parameters and Their Uncertainties, *Environ. Prot.*, vol. 134, no. May 2011, pp. 1708–1721, Dec. 2008, doi: 10.1061/(ASCE)0733-9429(2008)134:12(1708).
- [15] S. E. Yochum, L. A. Goertz, and P. H. Jones, Case Study of the Big Bay Dam Failure: Accuracy and Comparison of Breach Predictions, *J. Hydraul. Eng.*, vol. 134, no. 9, pp. 1285–1293, 2008, doi: doi:10.1061/(ASCE)0733-9429(2008)134:9(1285).
- [16] X. Ying, J. Jorgeson, and S. S. Y. Wang, Modeling Dam-Break Flows Using Finite Volume Method on Unstructured Grid, *Eng. Appl. Comput. Fluid Mech.*, vol. 3, no. 2, pp. 184–194, 2009, doi: 10.1080/19942060.2009.11015264.
- [17] J. Singh, M. S. Altinakar, and Y. Ding, Two-dimensional numerical modeling of dam-break flows over natural terrain using a central explicit scheme, *Adv. Water Resour.*, vol. 34, no. 10, pp. 1366–1375, 2011, doi: https://doi.org/10.1016/j.advwatres.2011.07.007.

- [18] P. Marco, M. Andrea, T. Massimo, and V. Giulia, 1923 Gleno Dam Break: Case Study and Numerical Modeling, *J. Hydraul. Eng.*, vol. 137, no. 4, pp. 480–492, Apr. 2011, doi: 10.1061/(ASCE)HY.1943-7900.0000327.
- [19] Z. Bozkuş and F. Bağ, Virtual Failure Analysis of the Çınarcık Dam, *Tek. Dergi/Technical J. Turkish Chamb. Civ. Eng.*, vol. 22, no. 4, pp. 5675–5688, 2011.
- [20] Q. Honghai, S. M. Altinakar, H. Qi, and M. S. Altinakar, GIS-Based Decision Support System for Dam Break Flood Management under Uncertainty with Two-Dimensional Numerical Simulations, *J. Water Resour. Plan. Manag.*, vol. 138, no. 4, pp. 334–341, Jul. 2012, doi: doi:10.1061/(ASCE)WR.1943-5452.0000192.
- [21] H. Mahdizadeh, S. K. Peter, and R. D. Benedict, Flood Wave Modeling Based on a Two-Dimensional Modified Wave Propagation Algorithm Coupled to a Full-Pipe Network Solver, *J. Hydraul. Eng.*, vol. 138, no. 3, pp. 247–259, Mar. 2012, doi: 10.1061/(ASCE)HY.1943-7900.0000515.
- [22] S. Bosa and M. Petti, A Numerical Model of the Wave that Overtopped the Vajont Dam in 1963, *Water Resour. Manag.*, vol. 27, no. 6, pp. 1763–1779, 2013, doi: 10.1007/s11269-012-0162-6.
- [23] G. Tsakiris and M. Spiliotis, Dam- Breach Hydrograph Modelling: An Innovative Semi- Analytical Approach, *Water Resour. Manag.*, vol. 27, no. 6, pp. 1751–1762, 2013, doi: 10.1007/s11269-012-0046-9.
- [24] T. Moramarco, S. Barbetta, C. Pandolfo, A. Tarpanelli, N. Berni, and R. Morbidelli, Spillway Collapse of the Montedoglio Dam on the Tiber River, Central Italy: Data Collection and Event Analysis, *J. Hydrol. Eng.*, vol. 19, no. 6, pp. 1264–1270, Jun. 2014, doi: 10.1061/(ASCE)HE.1943-5584.0000890.
- [25] A. S. Chen, B. Evans, S. Djordjević, and D. A. Savić, A coarse-grid approach to representing building blockage effects in 2D urban flood modelling, *J. Hydrol.*, vol. 426–427, pp. 1–16, 2012, doi: 10.1016/j.jhydrol.2012.01.007.
- [26] A. S. Chen, B. Evans, S. Djordjević, and D. A. Savić, Multi-layered coarse grid modelling in 2D urban flood simulations, *J. Hydrol.*, vol. 470–471, pp. 1–11, 2012, doi: 10.1016/j.jhydrol.2012.06.022.
- [27] V. Bellos and G. Tsakiris, Comparing Various Methods of Building Representation for 2D Flood Modelling In Built-Up Areas, *Water Resour. Manag.*, vol. 29, no. 2, pp. 379–397, 2015, doi: 10.1007/s11269-014-0702-3.
- [28] Ş. Elçi, G. Tayfur, İ. Haltas, and B. Kocaman, Baraj Yıkılması Sonrası İki Boyutlu Taşkın Yayılımının Yerleşim Bölgeleri İçin Modellenmesi, *Tek. Dergi/Technical J. Turkish Chamb. Civ. Eng.*, vol. 28, no. 3, pp. 7955–7975, Jul. 2017, doi: 10.18400/tekderg.307456.
- [29] İ. Haltas, S. Elçi, and G. Tayfur, Numerical Simulation of Flood Wave Propagation in Two-Dimensions in Densely Populated Urban Areas due to Dam Break, *Water Resour. Manag.*, vol. 30, no. 15, pp. 5699–5721, Dec. 2016, doi: 10.1007/s11269-016-1344-4.



- [30] M. Ş. Güney, G. Tayfur, G. Bombar, and S. Elci, Distorted Physical Model to Study Sudden Partial Dam Break Flows in an Urban Area, *J. Hydraul. Eng.*, vol. 140, no. 11, p. 5014006, 2014, doi: doi:10.1061/(ASCE)HY.1943-7900.0000926.
- [31] I. Haltas, G. Tayfur, and S. Elci, Two-dimensional numerical modeling of flood wave propagation in an urban area due to Ürkmez dam-break, İzmir, Turkey, *Nat. Hazards*, vol. 81, no. 3, pp. 2103–2119, 2016, doi: 10.1007/s11069-016-2175-6.
- [32] S. Oguzhan and A. Ozgenc Aksoy, Experimental investigation of the effect of vegetation on dam break flood waves, *J. Hydrol. Hydromechanics*, no. 2016, pp. 231–241, 2020, doi: 10.2478/johh-2020-0026.
- [33] F. Jonson and P. Illes, A Classification of Dam Failures, *Water Power Dam Constr.*, vol. 28, no. 12, pp. 43–45, 1976.
- [34] A. B. De Almeida and A. B. Franco, Modeling of Dam-Break Flow BT - Computer Modeling of Free-Surface and Pressurized Flows, M. H. Chaudhry and L. W. Mays, Eds. Dordrecht: Springer Netherlands, 1994, pp. 343–373.
- [35] M. Morris, Final Technical Report – January 2005, 2005.
- [36] USBR, Downstream Hazard Classification Guidelines, Bureau of Reclamation, United States Department of the Interior, 1988, Denver, Colorado, 1988.
- [37] K. A. Vaskinn et al., Physical Modeling of Breach Formation - Large scale field tests, in *Proceedings of Dam Safety*, 2004, pp. 1–16.
- [38] T. L. Wahl, Prediction of Embankment Dam Breach Parameters - A Literature Review and Needs Assesment, 1998. doi: DSO-98-004.
- [39] S. Dhiman and K. C. Patra, Experimental study of embankment breach based on its soil properties, *ISH J. Hydraul. Eng.*, no. December, pp. 1–11, 2018, doi: 10.1080/09715010.2018.1474500.
- [40] R. P. George, C. R. David, P. Miller, H. G. Yung, E. C. Paul, and M. Temple, Mechanics of Overflow Erosion on Embankments. II: Hydraulic and Design Considerations, *J. Hydraul. Eng.*, vol. 115, no. 8, pp. 1056–1075, Aug. 1989, doi: 10.1061/(ASCE)0733-9429(1989)115:8(1056).
- [41] C. Goodell, Weir Equations in HEC-RAS, The RAS Solution - The Place for HEC-RAS Modellers, 2016. <https://www.kleinschmidtgroup.com/ras-post/weir-equations-in-hec-ras/> (accessed Jul. 16, 2020).
- [42] C. T. MacDonald and J. Langridge-Monopolis, Breaching Characteristics of Dam Failures, *J. Hydraul. Eng.*, vol. 110, no. 5, pp. 567–586, May 1984, doi: 10.1061/(ASCE)0733-9429(1984)110:5(567).
- [43] J. L. Von Thun and D. R. Gillette, Guidance on breach parameters. Denver, Colorado: U.S. Dept. of the Interior, Bureau of Reclamation, 1990.
- [44] Y. Xu and L. M. Zhang, Breaching Parameters for Earth and Rockfill Dams, *J. Geotech. Geoenvironmental Eng.*, vol. 135, no. 12, pp. 1957–1970, Dec. 2009, doi: 10.1061/(ASCE)GT.1943-5606.0000162.

- [45] K. P. Singh and A. Snorrason, Sensitivity of outflow peaks and flood stages to the selection of dam breach parameters and simulation models, *Journal of Hydrology*, vol. 68, no. 1–4, pp. 295–310, 1984, doi: 10.1016/0022-1694(84)90217-8.
- [46] D. C. Froehlich, Embankment-Dam Breach Parameters, in *Hydraulic Engineering, Proceedings of the 1987 National Conference.*, 1987, pp. 570–575, [Online]. Available: <http://pubs.er.usgs.gov/publication/70014497>.
- [47] D. M. Hershfield, Method for Estimating Probable Maximum Rainfall, *J. Am. Water Works Assoc.*, vol. 57, no. 8, pp. 965–972, 1965, doi: 10.1002/j.1551-8833.1965.tb01486.x.
- [48] A. W. Petrascheck and P. A. Sydler, Routing of dam break floods, *Int. Water Power Dam Constr.*, vol. 36, no. 7, 1984.
- [49] Z. Bozkuş, Dam Break Analyses for Disaster Management (in Turkish), *Tek. Dergi*, vol. 15, no. 74, pp. 3335–3350, 2004.
- [50] T. A. Basheer, A. Wayayok, B. Yusuf, M. D. R. Kamal, and M. Rowshon, Dam breach parameters and their influence on flood hydrographs for Mosul dam, *J. Eng. Sci. Technol.*, vol. 12, no. 11, pp. 2896–2908, 2017.
- [51] T. C. MacDonald and J. Langridge-Monopolis, Breaching Characteristics of Dam Failures, *J. Hydraul. Eng.*, vol. 110, no. 5, pp. 567–586, May 1984, doi: 10.1061/(ASCE)0733-9429(1984)110:5(567).

# **Buckling of Laminated Elliptical and Super-Elliptical Thin Plates**

**Erkin ALTUNSARAY<sup>1</sup>**

**İsmail BAYER<sup>2</sup>**

## **ABSTRACT**

In this computational study the buckling analysis of symmetrically laminated elliptical and super-elliptical thin plates was carried out. The plates were considered as clamped or simply supported at the boundary. The minimum buckling load was determined using the Rayleigh-Ritz method and the Galerkin Method based on the Classical Laminated Plate Theory (CLPT). The influence of the solution methods, shape functions, boundary conditions, super-elliptical power, lamination type, aspect ratio, and thickness on the critical buckling load were investigated using a parametric study. The verification of the isotropic case was performed comparing some results in the open literature, and good agreement was obtained. Convergence studies of the composite case with increasing terms (up to 10 terms) were achieved and sufficient accuracy was provided. During the preliminary design stage of composite structures, many design parameters such as panel sizes, panel thickness, stacking sequences, boundary conditions and loading conditions are taken into consideration. It is possible to evaluate these parameters quickly by using appropriate shape functions with the Rayleigh-Ritz method.

**Keywords:** Super-elliptical composite thin plates, buckling, Classic Laminated Plate Theory (CLPT), Rayleigh-Ritz method, The Galerkin Method, shape function.

## **1. INTRODUCTION**

Composite panels have high specific strength and high specific rigidity, which are the most important advantages especially when compared to steel structures. Hence, they are used in engineering applications such as civil, aerospace and marine engineering as building materials [1-3]. With developing technology, analysis of super-elliptical plates under wind loads has been studied recently [4]. For the accurate designing of structures, it is important to analyze their critical buckling loads. Numerous studies on the buckling of composite

---

Note:

- This paper was received on December 11, 2020 and accepted for publication by the Editorial Board on July 7, 2021.
- Discussions on this paper will be accepted by November 30, 2022.

• <https://doi.org/10.18400/tekderg.839435>

1 Dokuz Eylul University, Institute of Marine Sciences and Technology, Izmir, Turkey  
erkin.altunsaray@deu.edu.tr - <https://orcid.org/0000-0003-3099-6059>

2 Yildiz Technical University, Department of Naval Architecture and Marine Engineering, Istanbul, Turkey  
bayer@yildiz.edu.tr - <https://orcid.org/0000-0002-8589-671X>

rectangular, elliptical or circular plates analyzed by the Rayleigh–Ritz method have been demonstrated in the review paper [5].

The buckling of rectangular isotropic plates was studied by Timoshenko and Gere [6] and Szilard [7]. Dawe and Craig [8] analyzed the buckling and vibration of rectangular laminated plates subject to in-plane stress systems using the Rayleigh-Ritz Method and the finite strip method based on shear deformation plate theory. Leissa [9] presented a review of laminated composite plate buckling from the extensive available literature. Aiello and Ombres [10] examined the buckling and vibration of unsymmetrical rectangular laminates resting on elastic foundations under in-plane and shear forces.

The authors have used the Rayleigh-Ritz Method based on the first order shear deformation theory. Darvizeh et al. [11], studied the buckling analysis of generally laminated composite rectangular plates by generalized differential quadrature rules and the Rayleigh–Ritz Method. The authors compared the results with some available experimental and analytical results. Reddy [12] presented the buckling analysis of orthotropic and anisotropic rectangular plates by using analytical and numerical methods. Shufrin et al. [13] dealt with the buckling of laminated composite plates for general boundary conditions using the semi-analytical Kantorovich method. Seifi et al. [14] presented the critical buckling loads and related buckling modes of cross-ply laminated annular plates using the Rayleigh-Ritz Method and finite element analysis based on Classical Laminate Plate Theory (CLPT).

Altunsaray and Bayer [15] presented the buckling of symmetrically laminated quasi-isotropic rectangular plates by using the Finite Difference Method, the Galerkin Method and the Finite Element Method (ANSYS software). Afsharmanesh et al. [16] examined the buckling and vibration of laminated composite angle-ply and cross-ply circular plates on a Winkler-type foundation by the Ritz Method and the Finite Element Method (ABAQUS software). Ghaheri et al. [17] studied the buckling and vibration of symmetrically laminated angle-ply and cross-ply composite elliptical plates on an elastic foundation using the Ritz Method.

Rectangular plates having rounded corners are named as super-elliptical plates having the advantage of diffusing the stress at the corner of rectangular plates [18]. The buckling of isotropic, thin, super-elliptical plates was studied at first by Wang et al. [19]. Solutions were obtained by using the Rayleigh-Ritz Method based on the Kirchhoff–Love theory in this study [19]. Altekin [20] studied the free linear vibration and buckling of isotropic super-elliptical plates resting on symmetrically distributed point-supports on the diagonals by using the Rayleigh-Ritz Method and Lagrange multipliers. Hasheminejad et al. [21] investigated the dynamic stability of isotropic super-elliptical plates resting on elastic foundations under periodic in-plane loads. The Galerkin procedure is used based on the thin plate small deflection theory. Jazi and Farhatnia [22] examined the buckling analysis of a functionally graded super elliptical plate. They obtained their results by using the Rayleigh-Ritz Method based on classical plate theory for clamped and simply supported boundary conditions. Sayyad and Ghugal [23] investigated the buckling analysis of isotropic and laminated cross-ply composite rectangular plates, subjected to in-plane uniaxial and biaxial compressions, based on a new trigonometric shear and normal deformation theory.

Ghaheri et al. [24] demonstrated the analyses of composite plates (cross-ply and angle-ply) resting on Winkler-type foundations subject to in-plane harmonic loads, under different edge conditions (clamped, simply supported and free). The authors found that the static and

parametric characteristics were influenced by fiber orientation, stacking sequences, super-elliptical power, aspect ratio, foundation stiffness parameter and in-plane loads. Zhang [25] studied the nonlinear bending and thermal post-buckling analysis of functionally graded super elliptical thin plates by using the Rayleigh-Ritz method based on the Classical Laminated Plate Theory (CLPT). Bending and free transverse vibration of shear deformable super-elliptical plates were analyzed based on the Mindlin plate theory using the finite element method by Altekin [4, 26]. Mirzaei [27] investigated the thermal buckling response of functionally graded super elliptical plates reinforced with carbon nano tubes. The author performed the parametric analyses based on the first-order shear deformation plate theory with the aid of the Ritz method.

The reason for the preference of the symmetrically laminated plates in production was explained in the study of Altunsaray and Bayer [28]. The vibration analysis of symmetrically laminated quasi-isotropic super-elliptical thin plates has been presented by the author [29]. The buckling analysis of symmetrically laminated rectangular thin plates under biaxial compression was studied by Altunsaray and Bayer [30] recently.

This paper is a development of previous work [30] studied by the authors. In their previous studies, the authors examined the biaxial buckling analyzes of simply supported laminated quasi-isotropic, cross-ply and angle-ply rectangular plates according to the Classical Laminated Plate Theory (CLPT). In this study, unlike previous studies and other studies in the open literature; laminated quasi-isotropic, cross-ply and angle-ply elliptical and super-elliptical plates were investigated with Rayleigh-Ritz Method and Galerkin Method, which is known to be a powerful method among the weighted residual methods. Three different shape functions were considered at the beginning of this analysis, one of which was chosen for the parametric investigation, because it was more favorable than the other two in terms of accuracy and computing time. It has been shown that the Rayleigh-Ritz Method is more suitable than Galerkin Method for this particular problem, which is the buckling analysis of both elliptical and super-elliptical plates in simple support and clamped boundary conditions.

In this parametric study, the effects of the super-elliptical power ( $n$ ), lamination type, boundary conditions (simply supported and clamped) and the aspect ratio ( $a/b$  and  $b/a$ ) on the critical buckling load of symmetrically laminated quasi-isotropic, cross-ply and angle-ply super-elliptical thin plates were investigated.

The verification of the isotropic case was investigated by comparing the results of buckling of isotropic plates only available in the literature. The convergence study for the buckling of LT1 ( $[-45_2/0_2/45_2/90_2]_s$ ) plate was performed up to 10 terms, hence sufficient accuracy was obtained. The critical buckling loads of symmetrically laminated plates with different super-elliptical powers, lamination types, boundary conditions and aspect ratios have also been presented with tables and graphics.

## 2. EQUATIONS AND FORMULATION

The periphery of a super-elliptical plate between an ellipse and a rectangle is shown in (Fig. 1).

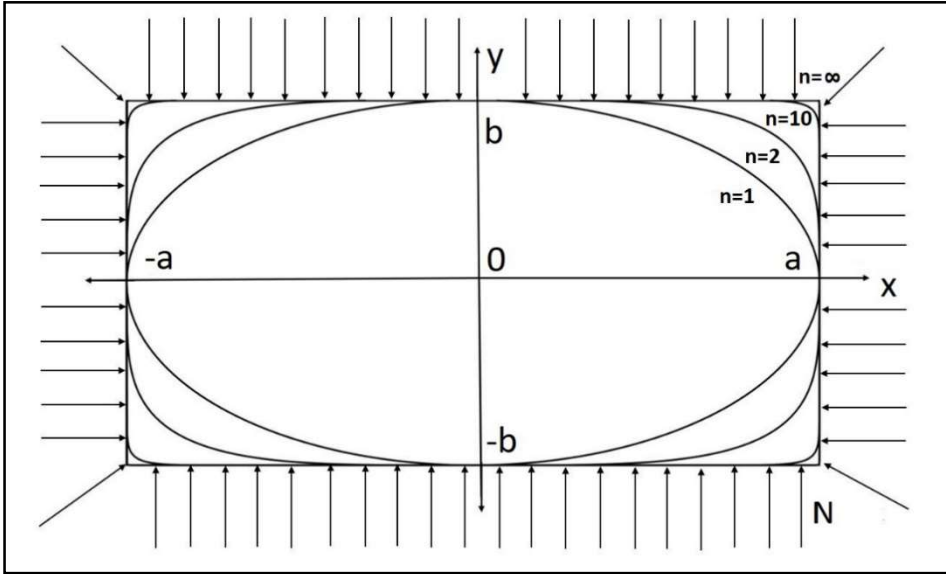


Figure 1 - Geometry of super-elliptical plate in the Cartesian co-ordinates

The equation of the super-ellipse is given in Eq. (1), where  $n$  is the power of the super ellipse ( $n=1$  is an ellipse and  $n=\infty$  is a rectangle);  $a$  and  $b$  are the half lengths of the plate.

$$\frac{x^{2n}}{a^{2n}} + \frac{y^{2n}}{b^{2n}} = 1, \quad n=1, 2 \dots \infty \quad (1)$$

The plates in this study are considered to be within the scope of the Classical Laminated Plate Theory (CLPT), because the ratio of thickness to the short side of plates is small enough. The Rayleigh-Ritz Method and The Galerkin Method were used for the analyses.

### 2.1. The Rayleigh-Ritz Method

The strain energy ( $U$ ) of the symmetrically laminated plate is given by the following expression [12]:

$$U = \frac{1}{2} \int_{-a}^a \int_{-b}^b \sqrt{1 - \frac{x^{2n}}{a^{2n}}} \sqrt{1 - \frac{y^{2n}}{b^{2n}}} \left[ D_{11} \left( \frac{\partial^2 w}{\partial x^2} \right)^2 + 2D_{12} \left( \frac{\partial^2 w}{\partial x^2} \right) \left( \frac{\partial^2 w}{\partial y^2} \right) + D_{22} \left( \frac{\partial^2 w}{\partial y^2} \right)^2 + 4D_{16} \left( \frac{\partial^2 w}{\partial x^2} \right) \left( \frac{\partial^2 w}{\partial x \partial y} \right) + 4D_{26} \left( \frac{\partial^2 w}{\partial y^2} \right) \left( \frac{\partial^2 w}{\partial x \partial y} \right) + 4D_{66} \left( \frac{\partial^2 w}{\partial x \partial y} \right)^2 \right] dx dy \quad (2)$$

where  $w$  indicates the transverse deflection, and  $D_{11}$ ,  $D_{12}$ ,  $D_{22}$ ,  $D_{16}$ ,  $D_{26}$ ,  $D_{66}$  denote the elements of the bending stiffness matrix  $D_{ij}$  which are found by the following [12]:

$$D_{ij} = \frac{1}{3} \sum_{k=1}^N \bar{Q}_{ij}^k (z_{k+1}^3 - z_k^3) \quad (3)$$

where  $(\bar{Q}_{ij})$  indicates the transformed reduced stiffness matrix, while  $n$  is the total number of plies.  $z_k$  and  $z_{k-1}$  are the distance from the reference plane [12]: Calculation of members of transformed reduced stiffness matrix  $(\bar{Q}_{ij})$  for each lamina is

$$\begin{aligned}
 \bar{Q}_{11} &= Q_{11}c^4 + 2(Q_{12} + 2Q_{66})s^2c^2 + Q_{22}s^4 \\
 \bar{Q}_{12} &= (Q_{11} + Q_{22} - 4Q_{66})s^2c^2 + Q_{12}(s^4 + c^4) \\
 \bar{Q}_{22} &= Q_{11}s^4 + 2(Q_{12} + 2Q_{66})s^2c^2 + Q_{22}c^4 \\
 \bar{Q}_{16} &= (Q_{11} - Q_{12} - 2Q_{66})sc^3 + (Q_{12} - Q_{22} + 2Q_{66})s^3c \\
 \bar{Q}_{26} &= (Q_{11} - Q_{12} - 2Q_{66})s^3c + (Q_{12} - Q_{22} + 2Q_{66})sc^3 \\
 \bar{Q}_{66} &= (Q_{11} + Q_{22} - 2Q_{12} - 2Q_{66})s^2c^2 + Q_{66}(s^4 + c^4)
 \end{aligned} \tag{4}$$

where  $c=\cos(\theta)$ ,  $s=\sin(\theta)$  and  $\theta$  is angle of the lamina, respectively. The reduced stiffness matrix elements  $Q_{ij}$  are given below

$$\begin{aligned}
 Q_{11} &= \frac{E_{11}}{1-\nu_{12}\nu_{21}}, \\
 Q_{12} &= \frac{\nu_{12}E_{11}}{1-\nu_{12}\nu_{21}}, \\
 Q_{22} &= \frac{E_{22}}{1-\nu_{12}\nu_{21}}, \\
 Q_{66} &= G_{12}
 \end{aligned} \tag{5}$$

The potential energy of the uniform in-plane load ( $N$ ) acting on the periphery of the symmetrically laminated plate, in other words the work done by this external load, is given below [12]:

$$V = -\frac{1}{2} \int_{-a}^a \int_{-b}^b \sqrt{1-\frac{x^{2n}}{a^{2n}}} \sqrt{1-\frac{y^{2n}}{b^{2n}}} N \left[ \left( \frac{\partial w}{\partial x} \right)^2 + \left( \frac{\partial w}{\partial y} \right)^2 \right] dx dy \tag{6}$$

Then the total potential energy functional may be given as follows:

$$F = U - V \tag{7}$$

Substituting Eq. (2) and Eq. (6) into Eq. (7), the total potential energy is

$$F = \frac{1}{2} \int_{-a}^a \int_{-b}^b \sqrt{1 - \frac{x^{2n}}{a^{2n}}} \sqrt{1 - \frac{y^{2n}}{b^{2n}}} \left[ \begin{aligned} &D_{11} \left( \frac{\partial^2 w}{\partial x^2} \right)^2 + 2D_{12} \left( \frac{\partial^2 w}{\partial x^2} \right) \left( \frac{\partial^2 w}{\partial y^2} \right) + D_{22} \left( \frac{\partial^2 w}{\partial y^2} \right)^2 \\ &+ 4D_{16} \left( \frac{\partial^2 w}{\partial x^2} \right) \left( \frac{\partial^2 w}{\partial x \partial y} \right) + 4D_{26} \left( \frac{\partial^2 w}{\partial y^2} \right) \left( \frac{\partial^2 w}{\partial x \partial y} \right) + 4D_{66} \left( \frac{\partial^2 w}{\partial x \partial y} \right)^2 \\ &- N \left[ \left( \frac{\partial w}{\partial x} \right)^2 + \left( \frac{\partial w}{\partial y} \right)^2 \right] \end{aligned} \right] dx dy \quad (8)$$

The boundary conditions at the plate edges are given below:

$$w = 0 \quad \text{and} \quad M = 0 \quad (\text{for simply supported plates}) \quad (9)$$

$$w = 0 \quad \text{and} \quad \frac{\partial w}{\partial n_i} = 0 \quad (\text{for clamped plates}) \quad (10)$$

where M indicates the bending moment,  $\partial n_i$  is the outward normal of the periphery. The trial function is

$$\varphi_{ij} = \left( c_{00} + c_{02}y^2 + c_{20}x^2 + c_{22}x^2y^2 + c_{24}x^2y^4 + c_{04}y^4 \right) \left( c_{40}x^4 + c_{42}x^4y^2 + c_{06}y^6 + c_{60}x^6 \right) \quad (11)$$

$c_{ij}$  denotes the unknown coefficients and order of polynomial (r) is 6. The deflection function which satisfies the boundary conditions is given below

$$w(x, y) = \left( \frac{x^{2n}}{a^{2n}} + \frac{y^{2n}}{b^{2n}} - 1 \right)^p \varphi_{ij} \quad (12)$$

p denotes the boundary condition (p=1 for simply supported condition, p=2 for clamped condition).

In order to find the lowest critical buckling loads, Eq. (8) is minimized with respect to the coefficients  $c_{ij}$

$$\frac{\partial F}{\partial c_{ij}} = 0 \quad (13)$$

Then, the following equation is obtained for a non-trivial solution:

$$|K - \lambda_b M_b| = 0 \quad (14)$$

where  $\lambda_b$  is the buckling load parameter including material properties, characteristic dimensions and in-plane uniform load of the plate. K is the stiffness matrix related to the strain energy and  $M_b$  is the mass matrix related to potential energy. This is a generalized eigenvalue problem.

The solution of Eq. (14) leads to a characteristic equation involving a polynomial of tenth degree in  $\lambda_b$ , from which the lowest critical buckling loads ( $N_{cr}$ ) may be found.



## 2.2. The Galerkin Method

The Galerkin Method is known as one of the powerful weighted residual methods. The governing differential equation of symmetrically laminated composite plates under in-plane load is given below:

$$D_{11} \left( \frac{\partial^4 w}{\partial x^4} \right) + 4D_{16} \left( \frac{\partial^4 w}{\partial x^3 \partial y} \right) + 2(D_{12} + 2D_{66}) \left( \frac{\partial^4 w}{\partial x^2 \partial y^2} \right) + 4D_{26} \left( \frac{\partial^4 w}{\partial x \partial y^3} \right) + D_{22} \left( \frac{\partial^4 w}{\partial y^4} \right) + N \left[ \left( \frac{\partial^2 w}{\partial x^2} \right) + \left( \frac{\partial^2 w}{\partial y^2} \right) \right] = 0 \quad (15)$$

Where  $w$  indicates the deflection function, and  $D_{11}$ ,  $D_{12}$ ,  $D_{22}$ ,  $D_{16}$ ,  $D_{26}$ ,  $D_{66}$  denote the elements of the bending stiffness matrix  $D_{ij}$  which are already found in the Section 2.1.

Obviously, a residual ( $\epsilon_R$ ) is obtained if the deflection function (Equation 12) is inserted in the governing differential equation (Equation 15), because an approximate solution to the problem is searched. The Galerkin Method minimizes the integral of the product of this residual ( $\epsilon_R$ ) and the trial function ( $\varphi_{ij}$ ) over the super-elliptical region.

$$\int_{-a}^a \int_{-b}^b \sqrt[2n]{1 - \frac{x^{2n}}{a^{2n}}} \sqrt[2n]{1 - \frac{y^{2n}}{b^{2n}}} \epsilon_R \varphi_{ij} dx dy = 0 \quad (16)$$

The rest of the calculation will be similar to the above as expressed for Rayleigh-Ritz method. A set of homogeneous linear algebraic equations in the unknown displacement  $w$ , whose determinant must be identically zero, is obtained. The lowest value of  $N_{cr}$  that makes the determinant zero is the lowest critical compressive load.

## 3. NUMERICAL RESULTS

Critical buckling loads of isotropic and quasi-isotropic, cross-ply and angle-ply elliptical and super-elliptical plates under clamped and simply supported boundary conditions were calculated by the Rayleigh-Ritz method and the Galerkin Method based on the Classical Laminated Plate Theory (CLPT). Verification of the isotropic case, convergence study, and the effects of thickness, super-elliptical power ( $n$ ), aspect ratio and boundary conditions on the critical buckling load are investigated in this section.

### 3.1. Verification of the isotropic case

The critical buckling load ( $N_{cr}$ ) of elliptical ( $n=1$ ) thin isotropic plates under two different boundary conditions (simply supported or clamped) were compared with the results of Sato [31, 32] and Ghaheri et al. [17] given in Table 1. The results of the present study given in Table 1 seem to be in good agreement with the results of previous studies. Critical buckling loads decrease with the increase of the aspect ratio ( $a/b$ ) in both simply supported and clamped condition cases. The deflection function ( $r=6$ ) used in the verification calculations was given in Eq. (12).

Table 1 - Comparison of the critical buckling load ( $N_{cr}$ ) of elliptical ( $n=1$ ) isotropic plates under different edge conditions ( $\nu = 0.3, r=6$ ) obtained with Rayleigh-Ritz Method

a/b	Simply Supported			Clamped		
	Sato [31]	Ghaheri et al.[17]	Present study	Sato [32]	Ghaheri et al.[17]	Present study
1	4.198	4.198	4.198	14.682	14.682	14.682
2	3.051	3.051	3.051	10.434	10.434	10.434
3	2.911	2.911	2.911	9.966	9.966	9.969
4	2.820	2.820	2.820	9.803	9.803	9.825
5	2.757	2.757	2.757	9.721	9.736	9.796

3.2. Main parameters for composite case

In this study T300-934 coded carbon/epoxy selected as the plate material for numerical calculations. Mechanical properties of carbon/epoxy are given in Table 2 [33].

Table 2 - Mechanical properties of carbon/epoxy (T300-934) [33]

Longitudinal Young Modulus ( $E_{11}$ )	$148 \times 10^9$ (N/m <sup>2</sup> )
Transversal Young Modulus ( $E_{22}$ )	$9.65 \times 10^9$ (N/m <sup>2</sup> )
Longitudinal Shear Modulus ( $G_{12}$ )	$4.55 \times 10^9$ (N/m <sup>2</sup> )
Longitudinal Poisson ratio ( $\nu_{12}$ )	0.3
Lamina thickness (t)	$0.185 \times 10^{-3} - 0.213 \times 10^{-3}$ (m)

The short half side (a or b) is selected as 0.1 m. Six different aspect ratios (a/b or b/a=1, 1.2, 1.4, 1.6, 1.8, 2) are considered. Twenty-eight different types of symmetrically laminated quasi-isotropic, cross-ply and angle-ply super-elliptical plates are given in Table 3. Quasi-isotropic plates have four different sequences ( $-45^\circ, 0^\circ, 45^\circ$  and  $90^\circ$ ), cross-ply laminated plates consist of two different sequences ( $0^\circ$  and  $90^\circ$ ) and angle-ply laminates have two different sequences ( $-45^\circ$  and  $45^\circ$ ). Thickness of each lamina (t) is equal to 0.2 mm and total thickness of a plate is 3.2 mm.

Table 3 - Symmetrically laminated composite plate types

<b>LT1</b>	$[-45_2/0_2/45_2/90_2]_s$	<b>LT15</b>	$[45_2/0_2/-45_2/90_2]_s$
<b>LT2</b>	$[-45_2/0_2/90_2/45_2]_s$	<b>LT16</b>	$[45_2/0_2/90_2/-45_2]_s$
<b>LT3</b>	$[-45_2/45_2/0_2/90_2]_s$	<b>LT17</b>	$[45_2/90_2/-45_2/0_2]_s$
<b>LT4</b>	$[-45_2/45_2/90_2/0_2]_s$	<b>LT18</b>	$[45_2/90_2/0_2/-45_2]_s$

Table 3 - Symmetrically laminated composite plate types (continue)

<b>LT5</b>	$[-45_2/90_2/0_2/45_2]_s$	<b>LT19</b>	$[90_2/-45_2/0_2/45_2]_s$
<b>LT6</b>	$[-45_2/90_2/45_2/0_2]_s$	<b>LT20</b>	$[90_2/-45_2/45_2/0_2]_s$
<b>LT7</b>	$[0_2/-45_2/45_2/90_2]_s$	<b>LT21</b>	$[90_2/0_2/-45_2/45_2]_s$
<b>LT8</b>	$[0_2/-45_2/90_2/45_2]_s$	<b>LT22</b>	$[90_2/0_2/45_2/-45_2]_s$
<b>LT9</b>	$[0_2/45_2/-45_2/90_2]_s$	<b>LT23</b>	$[90_2/45_2/-45_2/0_2]_s$
<b>LT10</b>	$[0_2/45_2/90_2/-45_2]_s$	<b>LT24</b>	$[90_2/45_2/0_2/-45_2]_s$
<b>LT11</b>	$[0_2/90_2/-45_2/45_2]_s$	<b>LT25</b>	$[0_2/90_2/0_2/90_2]_s$
<b>LT12</b>	$[0_2/90_2/45_2/-45_2]_s$	<b>LT26</b>	$[90_2/0_2/90_2/0_2]_s$
<b>LT13</b>	$[45_2/-45_2/0_2/90_2]_s$	<b>LT27</b>	$[-45_2/45_2/-45_2/45_2]_s$
<b>LT14</b>	$[45_2/-45_2/90_2/0_2]_s$	<b>LT28</b>	$[45_2/-45_2/45_2/-45_2]_s$

### 3.3. Convergence study

Critical buckling loads of LT1 (  $[-45_2/0_2/45_2/90_2]_s$  ) plates with different support conditions (clamped or simply supported), for super-elliptical powers (n=1 and 10), for three different shape functions (Table 4) and for two solution methods (The Galerkin Method and The Rayleigh-Ritz Method) with increasing terms were calculated in order to reach convergence.

Table 4 - Selected three different deflection functions (p=1 for simply supported plate, p=2 for clamped plate)

	<b>Deflection Functions</b>
df1	$w = \left( \frac{x^{2n}}{a^{2n}} + \frac{y^{2n}}{b^{2n}} - 1 \right)^p \left( c_{00} + c_{20}x^2 + c_{02}y^2 + c_{22}x^2y^2 + c_{40}x^4 \right)$
df2	$w = \left( \frac{x^{2n}}{a^{2n}} + \frac{y^{2n}}{b^{2n}} - 1 \right)^p \left( c_{00} + c_{20} \frac{x^2}{a^2} + c_{02} \frac{y^2}{b^2} + c_{22} \frac{x^2 y^2}{a^2 b^2} + c_{40} \frac{x^4}{a^4} \right)$
df3	$w = \left( \frac{x^{2n}}{a^{2n}} + \frac{y^{2n}}{b^{2n}} - 1 \right)^p \left( c_0 + c_1 \left( \frac{x^{2n}}{a^{2n}} + \frac{y^{2n}}{b^{2n}} - 1 \right)^1 + c_2 \left( \frac{x^{2n}}{a^{2n}} + \frac{y^{2n}}{b^{2n}} - 1 \right)^2 + c_3 \left( \frac{x^{2n}}{a^{2n}} + \frac{y^{2n}}{b^{2n}} - 1 \right)^3 + c_4 \left( \frac{x^{2n}}{a^{2n}} + \frac{y^{2n}}{b^{2n}} - 1 \right)^4 + c_5 \left( \frac{x^{2n}}{a^{2n}} + \frac{y^{2n}}{b^{2n}} - 1 \right)^5 \right)$

**3.4. Effect of Super-Elliptical Power (n), Boundary Condition, Method of Solution and Deflection Function**

In this section the effect of super-elliptical power (n), boundary condition, method of solution and deflection function on the critical buckling load have been investigated and presented (Table 5-6) for LT1 ( $[-45_2/0_2/45_2/90_2]_s$ ) plate. Critical buckling loads obtained by Rayleigh-Ritz Method and Galerkin Method (for elliptical plate with clamped edge, that is,  $n=1$ ) are compared in Table 6. If the same shape functions are used, the same results were found with two different solution methods (Galerkin Method and Rayleigh-Ritz Method), as Reddy stated [12]. However, results were obtained much more rapidly with Rayleigh-Ritz method compared with the Galerkin Method. In addition, the results obtained by  $df1$  and  $df2$  were the same for both methods. Although the results calculated by using  $df3$  are close to  $df1$  and  $df2$  in the case of elliptical plate ( $n=1$ ), the solution required a longer processing time. The use of  $df3$  did not yield accurate results for both simply supported edge and clamped edge. For both elliptical ( $n=1$ ) and super-elliptical plates ( $n=10$ ),  $df1$  was found to be the most suitable option for the calculations. One of the reasons for not arriving at any results by the Galerkin Method for simply supported edge may be that there are fourth-degree derivatives in the governing differential equation used. Therefore, when the Galerkin Method is applied some derivative expressions disappear due to the shape function used during the calculation for the simple support boundary condition. On the other hand, because there are quadratic derivative expressions in the integral equation, such a problem does not occur in the solution with the Rayleigh-Ritz Method. After this investigation it was decided to use Rayleigh-Ritz Method with  $df1$  with up to 10 terms for the rest of the study.

Table 5 - Convergence study of critical buckling load  $N_{cr}$  (N/m) of super-elliptical LT1 ( $[-45_2/0_2/45_2/90_2]_s$ ) plate (clamped)

<b>n=1</b>	<b>Critical buckling load <math>N_{cr}</math> (N/m)</b>				
<b>Method of solution</b>	<b>Increasing terms</b>				
	<b>1</b>	<b>2</b>	<b>3</b>	<b>4</b>	<b>5</b>
Rayleigh-Ritz (df1)	272939	254156	248606	248518	248476
Rayleigh-Ritz (df2)	272939	254156	248606	248518	248476
Rayleigh-Ritz (df3)	272939	250793	250457	250455	250455
Galerkin (df1)	272939	254156	248606	248518	248476
Galerkin (df2)	272939	254156	248606	248518	248476
Galerkin (df3)	272939	250793	250457	250455	250455
<b>n=10</b>	<b>Critical buckling load <math>N_{cr}</math> (N/m)</b>				
<b>Method of solution</b>	<b>Increasing terms</b>				
	<b>1</b>	<b>2</b>	<b>3</b>	<b>4</b>	<b>5</b>
Rayleigh-Ritz (df1)	12505200	6319280	3593230	912713	656662
Rayleigh-Ritz (df2)	12505200	6319280	3593230	912713	656662
Rayleigh-Ritz (df3)	12505200	6616170	4836340	3963080	3437660

Table 6 - Convergence study of critical buckling load  $N_{cr}$  (N/m) of super-elliptical LTI ( $[-45_2/0_2/45_2/90_2]_s$ ) plate (simply supported)

n=1	Critical buckling load $N_{cr}$ (N/m)				
Method of solution	Increasing terms				
	1	2	3	4	5
Rayleigh-Ritz (df1)	89787	80186,4	72271,2	72154,8	72147,8
Rayleigh-Ritz (df2)	89787	80186,4	72271,2	72154,8	72147,8
Rayleigh-Ritz (df3)	89787	72375,4	72297,5	72297,4	72297,4
n=10	Critical buckling load $N_{cr}$ (N/m)				
Method of solution	Increasing terms				
	1	2	3	4	5
Rayleigh-Ritz (df1)	6004240	6003250	1592030	219160	185974
Rayleigh-Ritz (df2)	6004240	6003250	1592030	219160	185974
Rayleigh-Ritz (df3)	6004240	2089610	1416880	1135030	978255

It can be observed from Table 7 that the convergence achieved is sufficient, if a shape function with 10 terms ( $r=6$ ) is selected. Hence this shape function will be used for all calculations for the rest of the study.

Table 7 - Convergence study of critical buckling load  $N_{cr}$  (N/m) of LTI ( $[-45_2/0_2/45_2/90_2]_s$ ) with the Rayleigh-Ritz Method

Shape functions	Critical buckling load $N_{cr}$ (N/m)			
	Simply Supported		Clamped	
	n=1	n=10	n=1	n=10
$c_{00}$	89787.0	6004240	272939	12505200
$c_{00}+c_{20}x^2$	80186.4	6003250	254156	6319280
$c_{00}+c_{20}x^2+c_{02}y^2$	72271.2	1592030	248606	3593230
$c_{00}+c_{20}x^2+c_{02}y^2+c_{22}x^2y^2$	72154.8	219160	248518	912713
$c_{00}+c_{20}x^2+c_{02}y^2+c_{22}x^2y^2+c_{40}x^4$	72147.8	185974	248476	656662
$c_{00}+c_{20}x^2+c_{02}y^2+c_{22}x^2y^2+c_{40}x^4+c_{04}y^4$	72129.9	156480	248018	511536
$c_{00}+c_{20}x^2+c_{02}y^2+c_{22}x^2y^2+c_{24}x^2y^4+c_{40}x^4+c_{04}y^4$	72129.8	144653	248017	436023
$c_{00}+c_{20}x^2+c_{02}y^2+c_{22}x^2y^2+c_{24}x^2y^4+c_{40}x^4+c_{04}y^4+c_{42}x^4y^2$	72129.6	101350	248017	244432
$c_{00}+c_{20}x^2+c_{02}y^2+c_{22}x^2y^2+c_{24}x^2y^4+c_{40}x^4+c_{04}y^4+c_{42}x^4y^2+c_{60}x^6$	72129.6	100192	248017	239047
$c_{00}+c_{20}x^2+c_{02}y^2+c_{22}x^2y^2+c_{24}x^2y^4+c_{40}x^4+c_{04}y^4+c_{42}x^4y^2+c_{60}x^6+c_{06}y^6$	72129.6	99773.5	248012	235721

**3.5. Effect of super-elliptical power (n)**

The effect of some selected super-elliptical powers (n=1, 2, 4, 6, 8, 10) on the critical buckling loads of super-elliptical plate LT1 ( $[-45_2/0_2/45_2/90_2]_s$ ) was investigated and the results are presented in Table 8-9. From the results one can see that the critical buckling load ( $N_{cr}$ ) generally increases with the increase of the super-elliptical power (n), while  $N_{cr}$  decreases with the increase of the aspect ratios (a/b, b/a).

It is interesting to see from the results of simply supported boundary conditions (Table 8) that critical buckling loads for n=1 (elliptical plates) and n=2 are lower than rectangular plates. A similar situation is observed in clamped boundary conditions for n=2 and 4 cases (Table 9). As shown in Table 7, in the analyzes performed it was only possible to reach a maximum of 10 terms (r=6) and a super-elliptical power up to n=10 using Wolfram Mathematica software. Analyses for higher number of terms and super-elliptical powers can be achieved by using computers with high computational capacity.

Table 8 - Critical buckling load  $N_{cr}$  (N/m) of super-elliptical LT1 ( $[-45_2/0_2/45_2/90_2]_s$ ) plate (simply supported r=6)

a/b	Critical buckling load (N/m)						
	n=1	n=2	n=4	n=6	n=8	n=10	Rectangle [30]
1	72129.6	76729.2	87361.9	92150.8	95897.9	99773.5	87155
1.2	56678.2	60865.7	69666.9	73602.3	76632.1	79719.0	69227
1.4	48209.8	51387.6	58590	61823.4	64343.9	66955.8	57983
1.6	43197.7	45287.7	51168.7	53835.6	55979.2	58289.4	50452
1.8	40029.5	41137.5	45950.3	48161.7	50006.7	52089.7	45166
2.0	37906.3	38188.8	42143.9	43988.4	45589.4	47474.9	41321
<b>b/a</b>							
1	72129.6	76729.2	87361.9	92150.8	95897.9	99773.5	87155
1.2	66815.0	69286.9	77740.7	81619	84801.6	88295.5	77739
1.4	64334.6	64893.8	71564.1	74693.7	77397	80591.1	71597
1.6	63049.7	62100.2	67353.7	69884.2	72175.9	75087.	67340
1.8	62278.9	60219.	64356.1	66415.6	68346.2	71001.7	64265
2	61729.0	58892.3	62147.8	63841.6	65463.7	67858.6	61971

Table 9 - Critical buckling load  $N_{cr}$  (N/m) of super-elliptical LT1 ( $[-45_2/0_2/45_2/90_2]_s$ ) plate (clamped, r=6)

a/b	Critical buckling load (N/m)						
	n=1	n=2	n=4	n=6	n=8	n=10	Rectangle
1	248012	225054	225518	228595	231984	235721	227709

Table 9 Critical buckling load  $N_{cr}$  (N/m) of super-elliptical LTI ( $[-45_2/0_2/45_2/90_2]_s$ ) plate (clamped,  $r=6$ ) (continue)

a/b	Critical buckling load (N/m)						
	n=1	n=2	n=4	n=6	n=8	n=10	Rectangle
1.2	196040	176456	176691	179033	181661	184591	178374
1.4	167180	150143	150208	152135	154293	156713	151954
1.6	149911	134807	134727	136389	138235	140278.	136733
1.8	138913	125319	125108	126581	128189	129943.	127432
2.0	131522	119149	118819	120141	121554	123088	121464
<b>b/a</b>							
1.0	248012.	225054.	225518	228595	231984	235721	227709
1.2	227783	209483.	210036	212935	216001	219284	212665
1.4	217549.	202952	203603	206363	209136	211999	206921
1.6	211801	200298	201071	203670	206139	208623	205120
1.8	208244	199361	200271	202680	204861	207003	205019
2	205856	199189	200237	202439	204350	206151	205632

3.6. Effect of plate thickness

Table 10 - Critical buckling load  $N_{cr}$  (N/m) of different thinner or thicker super-elliptical plates (simply supported,  $r=6$ ,  $n=1$ )

a/b	Critical buckling load (N/m)					
	[-45 <sub>2</sub> /0 <sub>2</sub> /45 <sub>2</sub> /90 <sub>2</sub> ] <sub>s</sub> (t=3.2 mm)		[-45 <sub>3</sub> /0 <sub>3</sub> /45 <sub>3</sub> /90 <sub>3</sub> ] <sub>s</sub> (t=4.8mm)		[-45 <sub>4</sub> /0 <sub>4</sub> /45 <sub>4</sub> /90 <sub>4</sub> ] <sub>s</sub> (t=6.4 mm)	
	Rayleigh-Ritz	FEM	Rayleigh-Ritz	FEM	Rayleigh-Ritz	FEM
1	72129.6	71104	243394	237267	576957	553980
1.2	56678.2	55956	189291	187189	449779	439457
1.4	48209.8	47562	159836	159295	380402	373716
1.6	43197.7	42548	142542	142576	339570	334755
1.8	40029.5	39345	131703	131866	313916	309727
2	37906.3	37168	124503	124581	296830	292680
b/a	Critical buckling load (N/m)					
	[-45 <sub>2</sub> /0 <sub>2</sub> /45 <sub>2</sub> /90 <sub>2</sub> ] <sub>s</sub> (t=3.2 mm)		[-45 <sub>3</sub> /0 <sub>3</sub> /45 <sub>3</sub> /90 <sub>3</sub> ] <sub>s</sub> (t=4.8mm)		[-45 <sub>3</sub> /0 <sub>3</sub> /45 <sub>3</sub> /90 <sub>3</sub> ] <sub>s</sub> (t=4.8mm)	
	Rayleigh-Ritz	FEM	Rayleigh-Ritz	FEM	Rayleigh-Ritz	FEM
1	72129.6	71104	243394	237267	576957	553980
1.2	66815.0	65754	227851	219525	538753	512939

Table 10 - Critical buckling load  $N_{cr}$  (N/m) of different thinner or thicker super-elliptical plates (simply supported,  $r=6, n=1$ ) (continue)

b/a	Critical buckling load (N/m)					
	[-45 <sub>2</sub> /0 <sub>2</sub> /45 <sub>2</sub> /90 <sub>2</sub> ]s (t=3.2 mm)		[-45 <sub>3</sub> /0 <sub>3</sub> /45 <sub>3</sub> /90 <sub>3</sub> ]s (t=4.8mm)		[-45 <sub>3</sub> /0 <sub>3</sub> /45 <sub>3</sub> /90 <sub>3</sub> ]s (t=4.8mm)	
	Rayleigh-Ritz	FEM	Rayleigh-Ritz	FEM	Rayleigh-Ritz	FEM
1.4	64334.6	63194	221132	210982	521865	493092
1.6	63049.7	61796	217934	206320	513614	482264
1.8	62278.9	60889	216109	203320	508829	475294
2	61729.0	60272	214780	201239	505368	470491

Table 11 - Critical buckling load  $N_{cr}$  (N/m) of different thinner or thicker super-elliptical plates (clamped,  $r=6, n=1$ )

a/b	Critical buckling load (N/m)		
	[-45 <sub>2</sub> /0 <sub>2</sub> /45 <sub>2</sub> /90 <sub>2</sub> ]s	[-45 <sub>3</sub> /0 <sub>3</sub> /45 <sub>3</sub> /90 <sub>3</sub> ]s	[-45 <sub>4</sub> /0 <sub>4</sub> /45 <sub>4</sub> /90 <sub>4</sub> ]s
	t=3.2 mm	t=4.8 mm	t=6.4 mm
1	248012	834717	1979940
1.2	196040.	653874	1554180
1.4	167180	553977	1318610
1.6	149911	494608	1178330
1.8	138913	457075	1089450
2	131522	432041	1030030

b/a	Critical buckling load (N/m)		
	[-45 <sub>2</sub> /0 <sub>2</sub> /45 <sub>2</sub> /90 <sub>2</sub> ]s	[-45 <sub>3</sub> /0 <sub>3</sub> /45 <sub>3</sub> /90 <sub>3</sub> ]s	[-45 <sub>4</sub> /0 <sub>4</sub> /45 <sub>4</sub> /90 <sub>4</sub> ]s
	t=3.2 mm	t=4.8 mm	t=6.4 mm
1	248012.	834717	1979940
1.2	227783	773429	1830780
1.4	217549.	743275	1756840
1.6	211801	726584	1715790
1.8	208244	716238	1690380
2	205856	709216	1673220



Table 12 - Critical buckling load  $N_{cr}$  (N/m) of different thinner or thicker super-elliptical plates (simply supported,  $r=6, n=10$ )

a/b	Critical buckling load (N/m)		
	[-45 <sub>2</sub> /0 <sub>2</sub> /45 <sub>2</sub> /90 <sub>2</sub> ]s	[-45 <sub>3</sub> /0 <sub>3</sub> /45 <sub>3</sub> /90 <sub>3</sub> ]s	[-45 <sub>4</sub> /0 <sub>4</sub> /45 <sub>4</sub> /90 <sub>4</sub> ]s
	t=3.2 mm	t=4.8 mm	t=6.4 mm
1	99773.5	329924	786523
1.2	79719.	261649	625061
1.4	66955.8	218973	523162
1.6	58289.4	190137	454730
1.8	52089.7	169687	405734
2	47474.9	154633	369886
b/a	Critical buckling load (N/m)		
	[-45 <sub>2</sub> /0 <sub>2</sub> /45 <sub>2</sub> /90 <sub>2</sub> ]s	[-45 <sub>3</sub> /0 <sub>3</sub> /45 <sub>3</sub> /90 <sub>3</sub> ]s	[-45 <sub>4</sub> /0 <sub>4</sub> /45 <sub>4</sub> /90 <sub>4</sub> ]s
	t=3.2 mm	t=4.8 mm	t=6.4 mm
1	99773.5	329924	786523
1.2	88295.5	294463	700661
1.4	80591.1	271005	643257
1.6	75087.	254299	602562
1.8	71001.7	241897	572141
2	67858.6	232343	548957

In this section, critical buckling loads for super-elliptical plates for three selected different thicknesses (3.2, 4.8 and 6.4 mm), super-elliptical powers ( $n=1$  and  $10$ ), boundary conditions (clamped and simply supported) and aspect ratios ( $a/b$  and  $b/a$ ) were investigated. The results are given in Table 10-13. From these results, critical buckling loads increase with the increase of the plate thickness as expected. As may be seen from the Tables (10-13), critical buckling loads decreases with the increase of the aspect ratio. Critical buckling loads of clamped plates are higher than simply supported plates for all cases.

Table 13 - Critical buckling load  $N_{cr}$  (N/m) of different thinner or thicker super-elliptical plates (clamped,  $r=6, n=10$ )

a/b	Critical buckling load (N/m)		
	[-45 <sub>2</sub> /0 <sub>2</sub> /45 <sub>2</sub> /90 <sub>2</sub> ]s	[-45 <sub>3</sub> /0 <sub>3</sub> /45 <sub>3</sub> /90 <sub>3</sub> ]s	[-45 <sub>4</sub> /0 <sub>4</sub> /45 <sub>4</sub> /90 <sub>4</sub> ]s
	t=3.2 mm	t=4.8 mm	t=6.4 mm
1	235721	797535	1889260
1.2	184591	617921	1467230
1.4	156713	520596	1238340

Table 13 - Critical buckling load  $N_{cr}$  (N/m) of different thinner or thicker super-elliptical plates (clamped,  $r=6$ ,  $n=10$ ) (continue)

a/b	Critical buckling load (N/m)		
	[-45 <sub>2</sub> /0 <sub>2</sub> /45 <sub>2</sub> /90 <sub>2</sub> ]s	[-45 <sub>3</sub> /0 <sub>3</sub> /45 <sub>3</sub> /90 <sub>3</sub> ]s	[-45 <sub>4</sub> /0 <sub>4</sub> /45 <sub>4</sub> /90 <sub>4</sub> ]s
	t=3.2 mm	t=4.8 mm	t=6.4 mm
1.6	140278.	463805	1104200
1.8	129943.	428404	1020290
2	123088	404905	964996
b/a	Critical buckling load (N/m)		
	[-45 <sub>2</sub> /0 <sub>2</sub> /45 <sub>2</sub> /90 <sub>2</sub> ]s	[-45 <sub>3</sub> /0 <sub>3</sub> /45 <sub>3</sub> /90 <sub>3</sub> ]s	[-45 <sub>4</sub> /0 <sub>4</sub> /45 <sub>4</sub> /90 <sub>4</sub> ]s
	t=3.2 mm	t=4.8 mm	t=6.4 mm
1	235721	797535	1889260
1.2	219284	750242	1772210
1.4	211999	731457	1724620
1.6	208623	724438	1705180
1.8	207003	722194	1697880
2	206151	721874	1695730

### 3.7. Effect of lamination types, boundary conditions and aspect ratios

Twenty-eight different types of quasi-isotropic, cross-ply and angle-ply plates shown in Table 3 are used for the calculations of the critical buckling loads  $N_{cr}$  (N/m) of super-elliptical plates ( $r=6$  and  $n=10$ ) under simply supported or clamped conditions, and the results are presented in Figure 2-5.

It can be seen from the results that the critical buckling loads depend on the types of lamination. Critical buckling loads decrease with the increase of aspect ratios ( $a/b$  and  $b/a$ ) and change with the selection of the short half side of the plates ( $a$  or  $b$ ). It is also observed that the results change with the boundary restraints. Critical buckling loads for simply supported conditions are lower than those for clamped conditions. The lowest critical buckling load of the plates seems to decrease as the aspect ratio increases for both the simply supported case and the clamped case.

The principal objective of this parametric study is to seek the best possible lamination among 28 alternatives under uniform in-plane load, which is in fact the one with the highest value of lowest critical buckling load.

From the Figure 2-5, it is seen that the critical buckling values of 24 different quasi-isotropic plates (LT1-24) in pairs and 2 different types of angle-ply (LT27-28) plates have the same values.

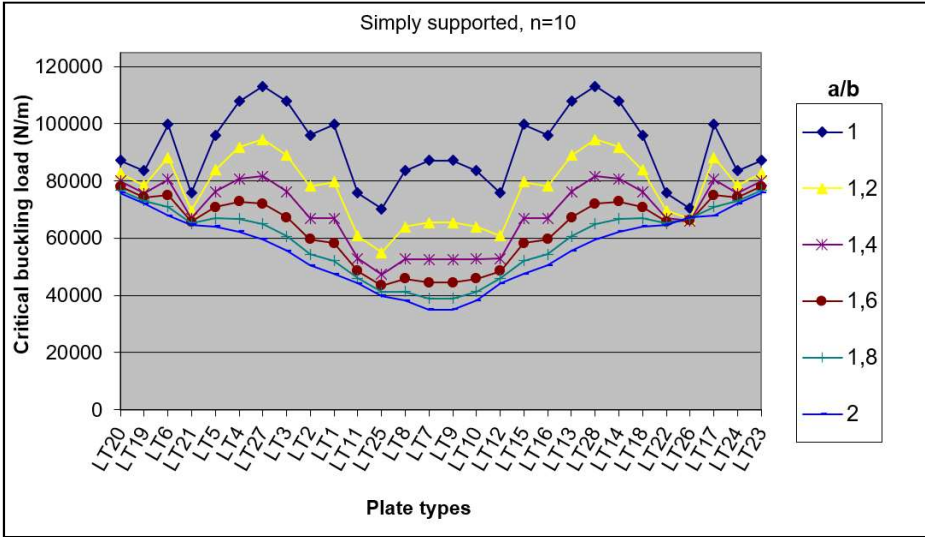


Figure 2 - Critical buckling load  $N_{cr}$  (N/m) of super-elliptical plates (simply supported  $r=6, n=10$ )

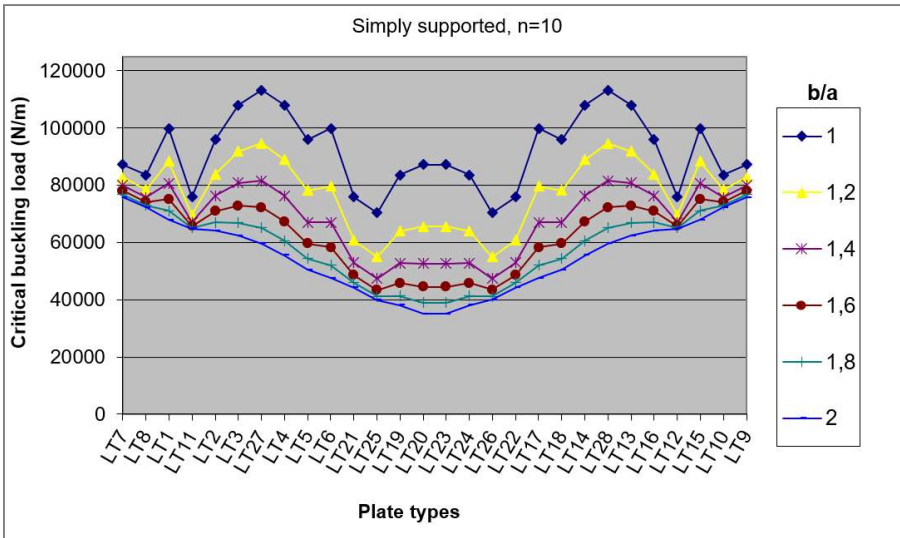


Figure 3 - Critical buckling load  $N_{cr}$  (N/m) of super-elliptical plates (simply supported  $r=6, n=10$ )

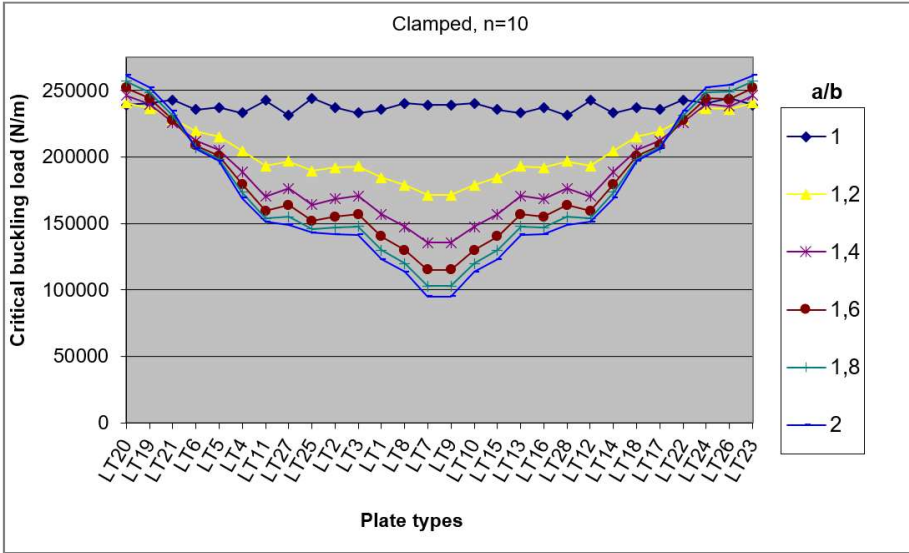


Figure 4 - Critical buckling load  $N_{cr}$  (N/m) of super-elliptical plates (clamped)  $r=6$ ,  $n=10$

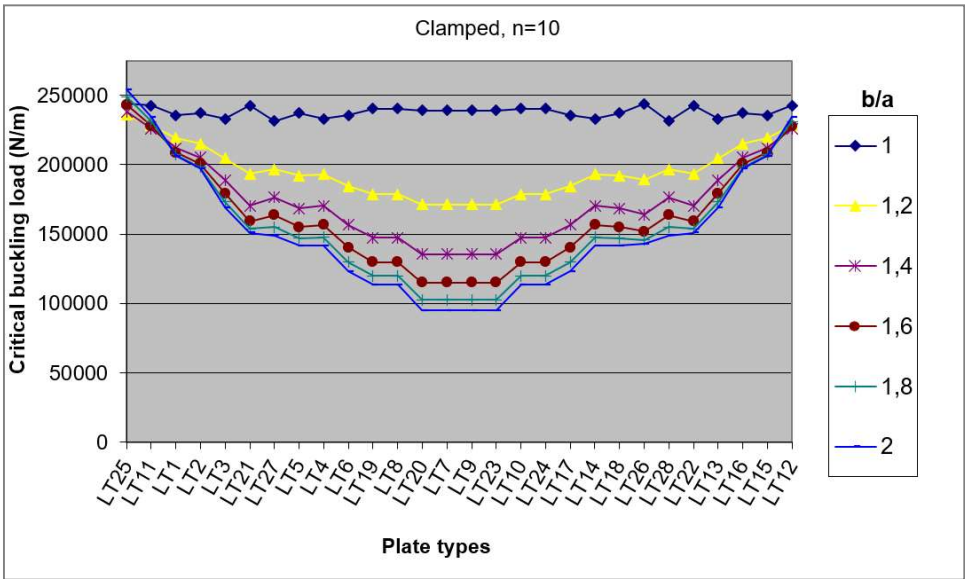


Figure 5 - Critical buckling load  $N_{cr}$  (N/m) of super-elliptical plates (clamped)  $r=6$ ,  $n=10$

#### 4. CONCLUSIONS

Buckling analyses of elliptical and super-elliptical quasi-isotropic, cross-ply and angle-ply plates have been carried out based on the Classical Lamination Plate Theory (CLPT) by using the Rayleigh-Ritz Method for different boundary restraints (clamped or simply supported). Computations were done by Wolfram Mathematica [34] and MATLAB [35] software platforms.

The critical buckling loads of plates with different super-elliptical powers ( $n$ ), thicknesses, aspect ratios and lamination types were investigated. The verification of the isotropic case for two different boundary conditions (clamped and simply supported) and for different aspect ratios (1 to 5) was compared with some available studies in the literature and reliable convergence was obtained.

Convergence studies of up to five terms were carried out with the Rayleigh-Ritz Method and the Galerkin Method, known as a powerful weighted residual method using three different shape functions for clamped and simply supported boundary conditions in Section 3.4. From these results, it was observed that buckling analysis for super-elliptical plates ( $n=1,10$ ), for simply supported or clamped boundary conditions, Rayleigh-Ritz Method with suitable shape function is the more proper method in terms of less computational time and accurate results.

It can be seen from the convergence analysis of the LT1 ( $[-45_2/0_2/45_2/90_2]_s$ ) plate that reasonable accuracy was obtained for a trial function with 10 terms with Rayleigh-Ritz Method. It was observed that critical buckling loads of plates are influenced by the change of the super-elliptical power, lamination types, boundary conditions, thickness and aspect ratios. It was also observed that critical buckling loads of simply supported super-elliptical plates are lower than those of clamped super-elliptical plates.

From the tabulated results and graphics critical buckling loads increase with an increase in the thickness. However, they generally decrease with increase of the aspect ratios. It can also be concluded that some lamination types have favorable circumstances with regard to the critical buckling load, as given in Section 3.2.

It was observed that from the results of highest value for the lowest critical buckling loads ( $N_{cr}$ ) of super-elliptical plates ( $n=10$ ), angle-ply plates are more advantageous than cross-ply and quasi-isotropic plates for lowest aspect ratio is ( $a/b=1, 1.2$  and  $1.4$ ). Besides, quasi-isotropic plates are more advantageous than others for highest aspect ratios ( $a/b=1.6, 1.8$  and  $2$ ) similar to the rectangular plate in previous work [30] for the simply supported boundary condition. However, quasi-isotropic plates are more advantageous than others for all aspect ratios for clamped boundary conditions. From the results of elliptical plates ( $n=1$ ) for simply supported and clamped boundary conditions, quasi-isotropic plates are more advantageous than angle-ply and cross-ply plates for all aspect ratios.

Critical buckling loads of symmetrically laminated elliptical plates (super-elliptical power  $n=1$ ) have been demonstrated in Appendix A (Figures A1.–A4.) for designers. Some mode shapes of laminated quasi-isotropic, cross-ply and angle-ply elliptic plate types ( $n=1$ ) in simple support boundary condition was obtained with FEM software ANSYS [36] and presented in Appendix B (Figures B1, B2 and B3.).

Consequently, in the preliminary design of composite structures, it is possible to obtain optimum data sets with parametric analyzes as illustrated in this study. The Rayleigh-Ritz

method gives faster and more convenient results than the Galerkin Method for buckling analysis of elliptical and super-elliptical plates when the appropriate shape function is selected.

### **Acknowledgements**

The authors dedicate this article to Prof. Dr. Uğur GÜVEN (Yildiz Technical University).

### **References**

- [1] Sheno, R.A. and Wellicome, J.F.), *Composite Materials in Maritime Structures, (Fundamental Aspects) Volume-I*. Cambridge University Press, NY., 1993a.
- [2] Sheno, R.A. and Wellicome, J.F, *Composite Materials in Maritime Structures, (Practical Considerations) Volume-II*. Cambridge University Press, NY., 1993b.
- [3] Mouritz, A.P., Gellert, E., Burchill, P. and Challis, K., Review of advanced composite structures for naval ships and submarines, *Compos. Struct.* 53(1):21–41, 2001.
- [4] Altekin, M., Free transverse vibration of shear deformable super-elliptical plates, *Wind and Struct.* 24(4),307-331, 2017.
- [5] Kumar, Y., The Rayleigh–Ritz method for linear dynamic, static and buckling behavior of beams, shells and plates: A literature review., *J. Vibr. and Cont.* 24(7): 1205-1227, 2018.
- [6] Timoshenko, S.P. and Gere, J.M., *Theory of Elastic Stability*, 2nd Edition. McGraw-Hill Book Company, USA, 1961.
- [7] Szilard, R., *Theories and Applications of Plate Analysis: Classical Numerical and Engineering Methods*, John Wiley & Sons, Inc., Hoboken, NJ, USA, 2004.
- [8] Dawe, D.J. and Craig, T.J., The vibration and stability of symmetrically-laminated composite rectangular plates subjected to in-plane stresses, *Compos. Struct.*5(4): 281-307, 1986.
- [9] Leissa, A.W., A review of laminated composite plate buckling, *App. Mech. Rev.* 40(5), 1987.
- [10] Aiello, M.A. and Ombres, L., Buckling and vibrations of unsymmetric laminates resting on elastic foundations under in-plane and shear forces, *Compos. Struct.* 44: 31-41, 1999.
- [11] Darvizeh, M., Darvizeh A., Ansari, R. and Sharma, C.B., Buckling analysis of generally laminated composite plates (generalized differential quadrature rules versus Rayleigh–Ritz method, *Compos. Struct.* 63:69–74, 2004.
- [12] Reddy, J.N., *Mechanics of laminated composite plates and shells: Theory and Analysis*, 2nd ed., Boca Raton, FL, CRC Press, 2004.

- [13] Shufrin, I., Rabinovitch, O. and Eisenberger, M., Buckling of symmetrically laminated rectangular plates with general boundary conditions – A semi analytical approach, *Compos. Struct.* 82: 521–531, 2008.
- [14] Seifi, R., Khoda-Yari, N. and Hosseini, H., Study of critical buckling loads and modes of cross-ply laminated annular plates, *Compos. Part B Eng.* 43(2): 422-430, 2012.
- [15] Altunsaray, E. and Bayer, İ., Buckling of symmetrically laminated quasi-isotropic thin rectangular plates, *Steel and Compos. Struct.* 17(3): 305-320, 2014.
- [16] Afsharmanesh, B., Ghaheri, A. and Taheri-Behrooz, F., Buckling and vibration of laminated composite circular plate on winkler-type foundation, *Steel and Compos. Struct.* 17(1): 1-19, 2014.
- [17] Ghaheri, A., Keshmiri, A. and Taheri-Behrooz, F., Buckling and vibration of symmetrically laminated composite elliptical plates on an elastic foundation subjected to uniform in-plane force, *J. Eng. Mech.* 140(7): 04014049-1-10, 2014.
- [18] Liew, K.M., Kitipornchai, S. and Lim, C.W., Free vibration analysis of thick superelliptical plates, *J. Eng. Mech.* 124 (2): 137-145, 1998.
- [19] Wang, C.M., Wang, L. and Liew, K.M., Vibration and buckling of super elliptical plates, *J. Sound Vib.* 171(3): 301-31, 1994.
- [20] Altekin, M., Free linear vibration and buckling of super-elliptical plates resting on symmetrically distributed point-supports on the diagonals, *Thin Wall. Struct.* 46:1066-1086, 2008.
- [21] Hasheminejad, S.M., Keshvari, M.M. and Ashory, M.R., Dynamic stability of super-elliptical plates resting on elastic foundations under periodic in-plane loads, *J. Eng. Mech.* 140(1):172-181, 2014.
- [22] Jazi, S.R. and Farhatnia, F., Buckling analysis of functionally graded super elliptical plate using pb-2 Ritz Method, *Adv. Mat. Res. Vols.383-390: 5387-5391*, 2012.
- [23] Sayyad, A.S. and Ghugal, Y.M., On the buckling of isotropic, transversely isotropic and laminated composite rectangular plates, *Int. J. Struct. Stab. Dyn.* 14(7): 1450020, 2014.
- [24] Ghaheri, A., Nosier, A. and Keshmiri, A., Parametric stability of symmetrically laminated composite super-elliptical plates, *J. Compos. Mat.* 50(28): 3935-3951, 2016.
- [25] Zhang, D.G., Nonlinear bending and thermal post-buckling analysis of FGM super elliptical thin plates, *Res.& Rev.: J. Mat. Sci.* 5(6): 64-73, 2017.
- [26] Altekin, M., Bending of super-elliptical Mindlin plates by finite element method, *Teknik Dergi*, 29, No:4, 8469-8496, 2018.
- [27] Mirzaei, M., Thermal buckling of temperature-dependent composite super elliptical plates reinforced with carbon nanotubes, *J. Therm. Str.* 41(7): 920-935, 2018.
- [28] Altunsaray, E. and Bayer, İ., Deflection and free vibration of symmetrically laminated quasi-isotropic thin rectangular plates for different boundary conditions, *Ocean Eng.* 57:197-222, 2013.

[29] Altunsaray, E., Free vibration of symmetrically laminated quasi-isotropic super-elliptical thin plates" *Steel and Compos. Struct.* 29(4): 493-508, 2018.

[30] Altunsaray, E. and Bayer, İ., Buckling Analysis of Symmetrically Laminated Rectangular Thin Plates under Biaxial Compression" *Teknik Dergi*, 29, No:4, 2021.

[31] Sato, K., Free flexural vibrations of a simply supported elliptical plate subjected to an in-plane force, *Theo. App. Mech. Jap.* 50: 165–181, 2001.

[32] Sato, K., Vibration and buckling of a clamped elliptical plate on elastic foundation and under uniform in-plane force, *Theo. App. Mech. Jap.* 51:49–62, 2002.

[33] Tsai, S.W., *Composites design.* (4th Edition), Think Composites, 1988.

[34] Wolfram Mathematica, Dokuz Eylul University.

[35] MATLAB, Dokuz Eylul University.

[36] ANSYS, Dokuz Eylul University.

**APPENDIX A**

In this section, the results of the critical buckling loads found for the simply support and clamped boundary conditions, edge ratios  $a/b$  and  $b/a$  by the Rayleigh-Ritz Method analysis of the elliptical plates ( $n=1$ ) are shown in (Figure A1-A4).

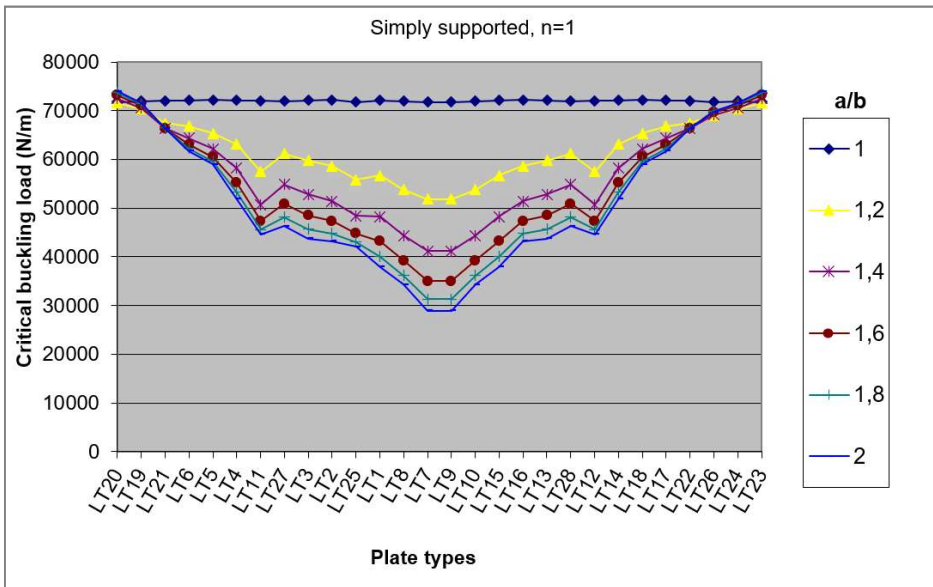


Figure A1 - Critical buckling load  $N_{cr}$  (N/m) of super-elliptical plates (simply supported)  $r=6, n=1$



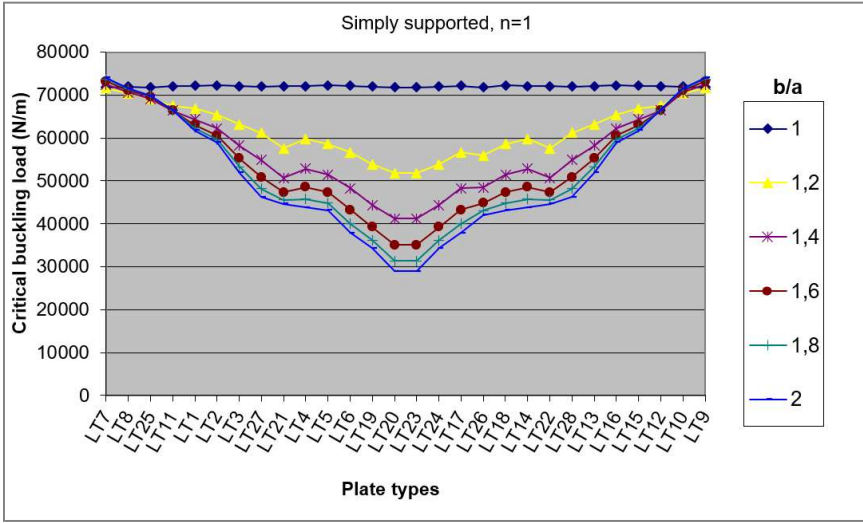


Figure A2 - Critical buckling load  $N_{cr}$  (N/m) of super-elliptical plates (simply supported)  $r=6, n=1$

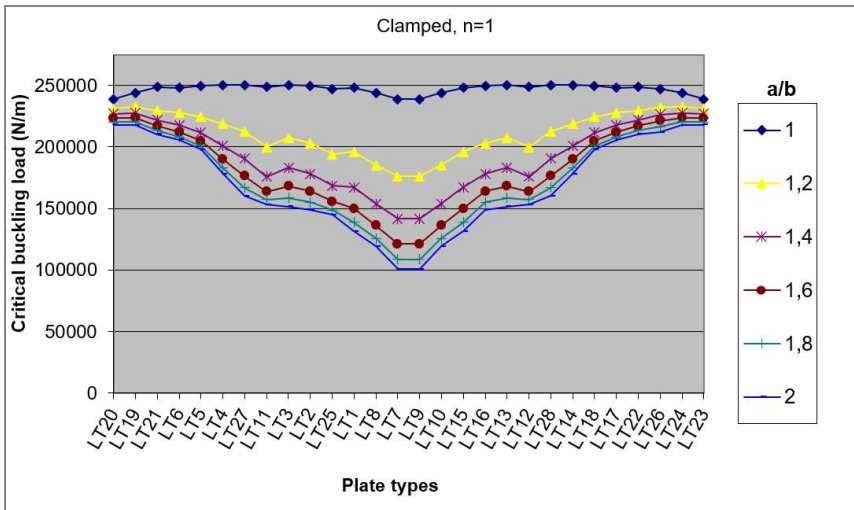


Figure A3 - Critical buckling load  $N_{cr}$  (N/m) of super-elliptical plates (clamped)  $r=6, n=1$

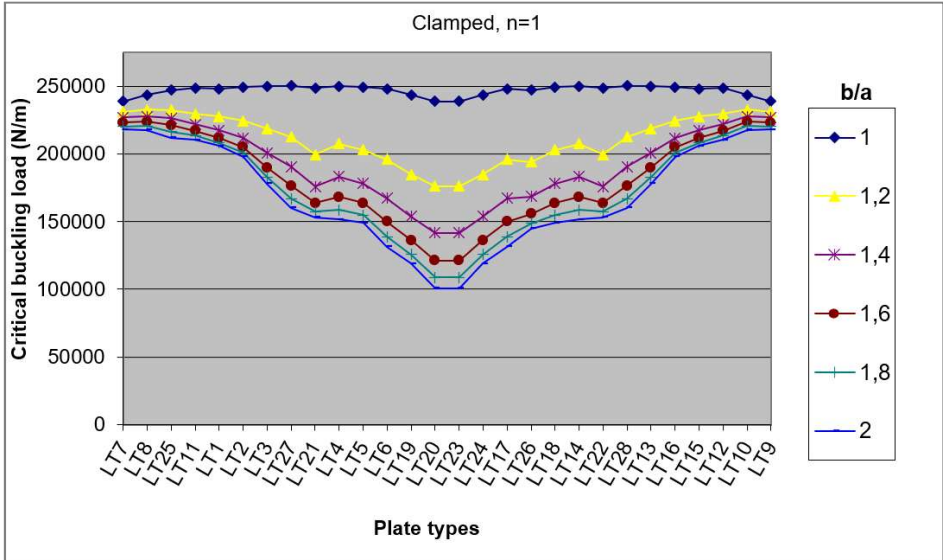


Figure A4 - Critical buckling load  $N_{cr}$  (N/m) of super-elliptical plates (clamped)  $r=6$ ,  $n=1$

**APPENDIX B**

In this section, first three mode shapes of some elliptic plate ( $n=1$ ) types (quasi-isotropic, cross-ply and angle-ply laminates) in simply supported boundary condition were calculated and plotted in the FEM analysis program ANSYS [36] (Figure B1, B2 and B3). No result could be obtained with the program for the clamped boundary conditions or super-elliptical plates ( $n=10$ ).

It may be seen from Figure B1 ( $a/b=1$ ), LT27 (angle-ply plate) has the highest critical buckling loads for mode-1 and mode-2, LT25 (cross-ply plate) has the highest critical buckling load for mode-3. From Figure B2 ( $a/b=2$ ), LT19 (quasi-isotropic plate) has the highest critical buckling loads for mode-1, LT27 (angle-ply plate) has the highest critical buckling loads for mode-2 and LT25 (cross-ply plate) has the highest critical buckling load for mode-3.

Similar to the results found in the previous studies of the authors [30] in which they analyzed rectangular plates, although the critical buckling loads of some plates in super-elliptical plates are the same in this study, these results change when the aspect ratio changes. For instance, LT8 and LT19 plates have equal critical buckling loads for the  $a/b=1$  case, but mode shapes are different (Figure B1). However, as seen in Figure B2 and B3, the critical buckling loads and mode shapes of the LT8 and LT19 plates are different in the  $a/b=2$  and  $b/a=2$  cases.

In general, there are two types of construction systems called transverse system or longitudinal system depending on the placement directions of supporting structural members in composite hull design. In this study, one of the reasons for calculating ratios of  $a/b$  and  $b/a$  separately is that the designers would be able to prefer either transverse or longitudinal construction system. For instance, as can be seen in Figure B2 and B3, plate numbered LT8

gives the same critical buckling values as plate numbered LT19 in case of edge ratio  $b/a=2$  when the edge ratio is  $a/b=2$ . It is recommended that a designer may prefer the plate type LT8 for production in the transverse system, and the plate type LT19 for production in the longitudinal construction system.

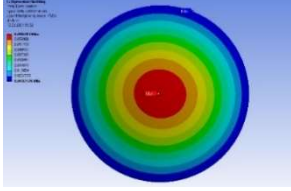
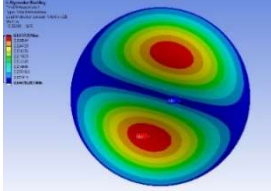
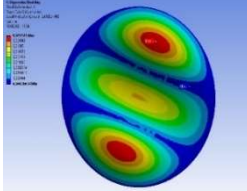
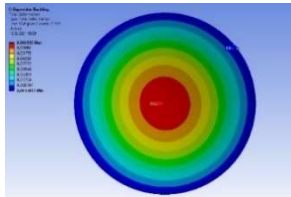
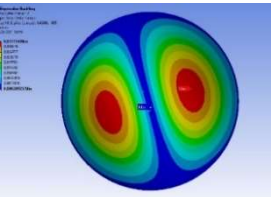
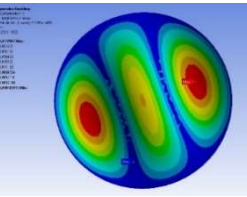
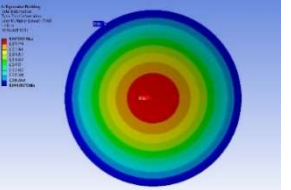
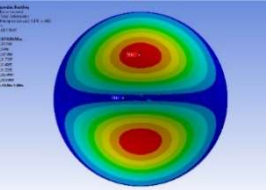
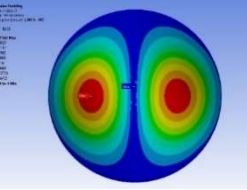
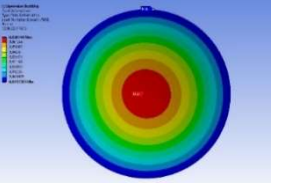
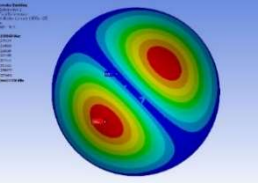
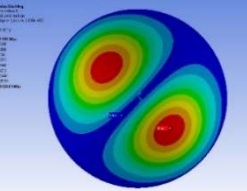
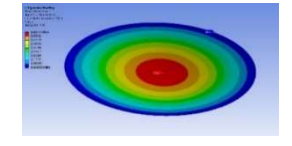
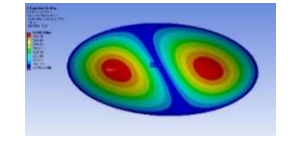
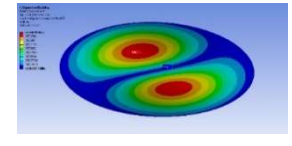
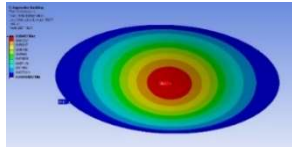
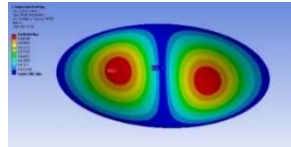
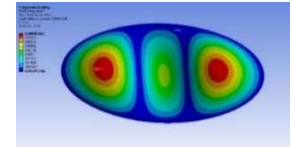
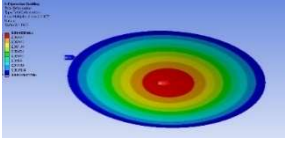
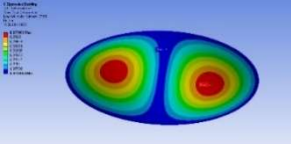
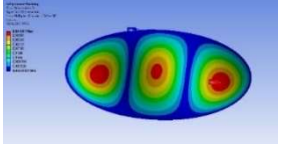
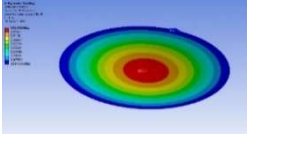
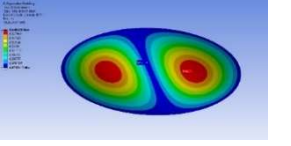
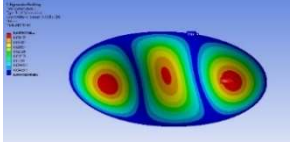
		
LT8 $[0_2/-45_2/90_2/45_2]_s$ mode1= 71223 N/m	LT8 $[0_2/-45_2/90_2/45_2]_s$ mode2= 142470 N/m	LT8 $[0_2/-45_2/90_2/45_2]_s$ mode3= 243650 N/m
		
LT19 $[90_2/-45_2/0_2/45_2]_s$ mode1= 71224 N/m	LT19 $90_2/-45_2/0_2/45_2]_s$ mode2= 142460 N/m	LT19 $[90_2/-45_2/0_2/45_2]_s$ mode3= 243650 N/m
		
LT25 $[0_2/90_2/0_2/90_2]_s$ mode1=71303 N/m	LT25 $[0_2/90_2/0_2/90_2]_s$ mode2=167510 N/m	LT25 $[0_2/90_2/0_2/90_2]_s$ mode3=266310 N/m
		
LT27 $[-45_2/45_2/-45_2/45_2]_s$ mode1=71282 N/m	LT27 $[-45_2/45_2/-45_2/45_2]_s$ mode2=167850 N/m	LT27 $[-45_2/45_2/-45_2/45_2]_s$ mode3=26580 N/m

Figure B1 - Some mode shapes of laminated plates (quasi-isotropic, cross-ply, angle-ply) ( $a/b=1, n=1$ )

*Buckling of Laminated Elliptical and Super-Elliptical Thin Plates*

		
LT8 $[0_2/-45_2/90_2/45_2]_s$ mode1= 34050 N/m	LT8 $[0_2/-45_2/90_2/45_2]_s$ mode2= 71657 N/m	LT8 $[0_2/-45_2/90_2/45_2]_s$ mode3= 124900 N/m
		
LT19 $[90_2/-45_2/0_2/45_2]_s$ mode1= 70237 N/m	LT19 $[90_2/-45_2/0_2/45_2]_s$ mode2= 89999 N/m	LT19 $[90_2/-45_2/0_2/45_2]_s$ mode3= 120140 N/m
		
LT25 $[0_2/90_2/0_2/90_2]_s$ mode1=41837 N/m	LT25 $[0_2/90_2/0_2/90_2]_s$ mode2=77156 N/m	LT25 $[0_2/90_2/0_2/90_2]_s$ mode3=150210 N/m
		
LT27 $[-45_2/45_2/-45_2/45_2]_s$ mode1=45783 N/m	LT27 $[-45_2/45_2/-45_2/45_2]_s$ mode2=91731 N/m	LT27 $[-45_2/45_2/-45_2/45_2]_s$ mode3=149030 N/m

*Figure B2 - Some mode shapes of laminated plates (quasi-isotropic, cross-ply, angle-ply) ( $a/b=2, n=1$ )*

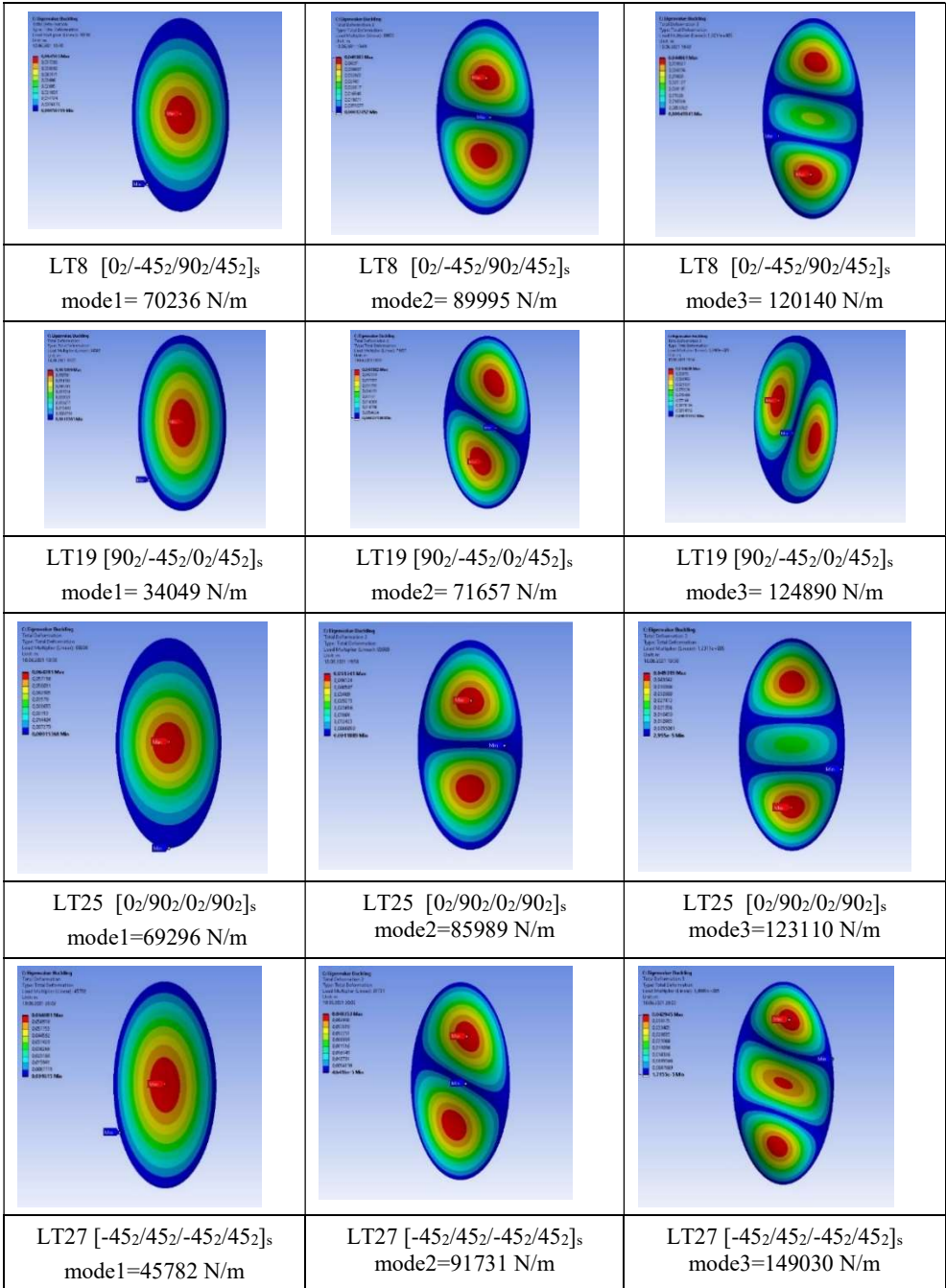


Figure B3 - Some mode shapes of laminated plates (quasi-isotropic, cross-ply, angle-ply) ( $b/a=2, n=1$ )



# **Modification in Response of a Bridge Seismically Isolated with Lead Rubber Bearings Exposed to Low Temperature**

**Esengul CAVDAR<sup>1</sup>**  
**Volkan KARUK<sup>2</sup>**  
**Gokhan OZDEMIR<sup>3</sup>**

## **ABSTRACT**

This study investigates the response modification in a bridge seismically isolated with lead rubber bearings (LRBs), due to change of ambient temperature from 20°C to -30°C. Accordingly, a large-size LRB was tested after being conditioned at corresponding temperatures and changes in its hysteretic properties were noted. Use of analytical tool in modeling nonlinear response of the tested LRB was justified by comparing the experimentally observed and analytically obtained force-displacement curves. Then, verified analytical representation of an LRB was employed in nonlinear response history analyses conducted to quantify the change in response of a representative LRB isolated bridge when subjected to bidirectional ground motion excitations at 20°C and -30°C. Analyses results are also employed to assess the use of property modification factor,  $\lambda$ , to change isolator properties in order to represent low temperature behavior. It is revealed that for the selected ground motion records, the average isolator force remains almost the same for both ambient temperatures. Moreover, using property modification factor will result in accurately estimated isolator displacements, but overestimated isolator forces, in an average sense.

**Keywords:** Seismic isolation, lead rubber bearing, low temperature, lead core heating, bridge.

---

## Note:

- This paper was received on February 16, 2021 and accepted for publication by the Editorial Board on August 13, 2021.
- Discussions on this paper will be accepted by November 30, 2022.
- <https://doi.org/10.18400/tekderg.880787>

1 Eskisehir Technical University, ESQUAKE Seismic Isolator Test Laboratory, Eskisehir, Turkey  
esengulcavdar@eskisehir.edu.tr - <https://orcid.org/0000-0003-1497-0908>

2 Eskisehir Technical University, ESQUAKE Seismic Isolator Test Laboratory, Eskisehir, Turkey  
volkankaruk@eskisehir.edu.tr - <https://orcid.org/0000-0002-6782-7972>

3 Eskisehir Technical University, ESQUAKE Seismic Isolator Test Laboratory, Eskisehir, Turkey  
gokhan\_ozdemir@eskisehir.edu.tr - <https://orcid.org/0000-0002-2962-2327>

## **1. INTRODUCTION**

Seismic isolation is an earthquake resistant design strategy which is adopted to protect structures against adverse effects of ground motions. It relies on lengthening of natural period of structures by introducing systems that possess low horizontal stiffness between the superstructure and substructure. Accordingly, in case of a seismic excitation, rather than the seismically isolated structure, seismic isolators will undergo large deformations and dissipate energy. Among various seismic isolation systems, lead rubber bearings (LRB) are among the most widely used seismic isolators. They are composed of alternate layers of rubber and steel plates with a lead core at the center that passes through the height of the bearing. Rubber layers are responsible for the lateral stiffness of the bearing whereas lead core provides the required lateral strength. Since they were invented by Robinson in the 1970s, LRBs have been used in several structures (bridges, hospitals, data centers etc.) around the world [1-3]. In parallel, several research programs have been conducted to determine performance of LRBs under the effect of different parameters [4-10]. One of these parameters is the change in ambient temperature.

Mechanical properties of LRBs, mainly post yield stiffness and characteristic strength, are related to properties of rubber and lead, respectively. Although there are numerous studies that focused on the change in rigidity of rubber at low temperatures [11-17], very few experimental data are available for modification of LRB properties at low temperatures [18-20]. The LRB tested by Hasegawa et al. [18] was 250 mm in diameter with a lead core diameter of 38 mm. Displacement controlled LRB tests were conducted at temperatures of 40, 20, 0 and -20°C for a shear strain of 100% at 0.3 Hz. It was reported that the exposure time of the bearing to these temperatures is 5 hours. Similarly, Constantinou et al. [7] conducted tests with an LRB having rubber and lead core diameters of 381 mm and 70 mm, respectively. Isolator tests were carried out at a shear strain of 58% and loading frequency was 0.35 Hz. Constantinou et al. [7] stated that LRB was conditioned at -26°C and 20°C for 48 hours prior to tests. Compared to LRBs used in experimental studies of Hasegawa et al. [18] and Constantinou et al. [7], LRB tested by Cho et al. [19] was a large size bearing with rubber and lead core diameters of 860 mm and 170 mm, respectively. The total rubber thickness was 288 mm and tested at a shear strain of 15%. Temperatures considered by Cho et al. [19] were -20, -10, 0 and 23°C. It is to be mentioned that 15% shear strain is very low to be representative of seismic behavior of an LRB designed to undergo large deformations. Accordingly, variation in mechanical properties of a large size LRB exposed to low temperature was revisited by Park et al. [20]. Rubber and lead core diameters of the LRB were 800 mm and 180 mm, respectively and tested at a shear strain of 100%. All of the studies cited above reported that both characteristic strength and post yield stiffness of the isolator increase due to reduction in ambient temperature. Moreover, characteristic strength was observed to be more sensitive to change in ambient temperature by having large amount of increments compared to post yield stiffness.

The studies discussed so far specifically were interested in cyclic tests of LRBs exposed to different temperatures and reported solely the variations in stiffness and strength of bearings on a comparable manner based on displacement controlled test results. In recent studies, seismic performance of bridges, isolated by LRBs, under the effects of both ground motion excitations and low temperature have also been investigated. For instance, Billah and Todorov [21] examined the seismic response of an LRB isolated bridge in case of subfreezing



temperature. The authors performed nonlinear response history analyses (NRHA) using a bridge model subjected to different ground motions representative of earthquakes in Eastern Canada. In their study, LRBs were modeled with two different non-deteriorating bilinear force-displacement curves to idealize hysteretic behavior of LRBs at “summer” (25°C) and “winter” (-30°C) with properties provided by manufacturer. Another study that has focused on seismic response of LRB isolated bridge under low temperatures was conducted by Deng et al. [22]. Similarly, in the analytical model, they used a non-deteriorating hysteretic representation for LRBs where stiffness and strength of LRB was modified in accordance with an empirical formulation. LRB properties used in the analyses were computed for temperatures changing from -30°C to 40°C. However, it must be mentioned that both Billah and Todorov [21] and Deng et al. [22] neglected the deterioration in strength of LRBs due to temperature rise in the lead core under cyclic motion. Thus, those results are based on bounding analyses where hysteretic properties such as strength and stiffness of LRB do not change during the applied motion. On the other hand, it is well documented that considering the actual response (deteriorating force-displacement curve) of LRBs under cyclic motion may result in substantially different response quantities compared to analyses performed with non-deteriorating idealizations of LRBs [23-28]. In this sense, study of Wang et al. [29] presents valuable data related to performance of LRBs under ground motion excitations at low temperatures. In their research, gradual reduction in strength of isolator has been taken into account by employing the proposal of Kalpakidis et al. [30-31] for modeling of LRBs. These authors considered two different LRBs in the analytical model that can be classified as small- and moderate-size. Modeling of both LRBs was based on property modification factors proposed by Constantinou et al. [7] and Li et al. [32] rather than experimental data. From this point of view, study of Wang et al. [29] is in lack of discussion related to suitability of using these factors, which are sensitive to geometry of LRB, manufacturer of the bearing, loading protocol (shear strain and frequency) and exposure time to low temperature.

Literature review related to experimental studies show that LRBs are classified as small- to moderate-size with diameters ranging between 250 mm and 860 mm. However, the use of large-size LRBs with diameters greater than 1000 mm gets widespread interest, and the validity of available test data for such large bearings needs to be questioned. Besides, analytical studies mostly address the use of empirical formulations for modification of LRB properties rather than employing the related test data of the analyzed isolators. Furthermore, analytical representation of LRBs was performed by non-deteriorating force-displacement curves by neglecting the actual strength deterioration. Thus, there is a need to perform complementary research, composed of both experimental and analytical phases, to investigate the response of LRB isolated bridges exposed to low temperatures. The objectives of this study are (i) to determine the variation in seismic performance of an LRB isolated bridge considering their modified mechanical properties when exposed to low temperatures and (ii) to evaluate the effectiveness of property modification factors (suggested for low temperatures) employed in bounding analysis of seismically isolated structures. For this purpose, first, a large-size LRB was tested after it was conditioned at both room (20°C) and low (-30°C) temperatures under dynamic conditions. Change in the mechanical properties of this LRB will be reported. Then, the experimental data is used to verify the success of analytical model employed to idealize hysteretic response of LRBs. Accordingly, deteriorating hysteretic behavior of the LRB obtained from both experiments and analytical models were compared. Once the use of analytical model to idealize nonlinear hysteretic

behavior of LRBs has been shown to be appropriate for both conditions, a representative bridge isolated with LRBs, will be analyzed under the effect of both near-field and large-magnitude small-distance ground motions. In the analyses, both horizontal components of selected ground motions were subjected to structural model simultaneously. Finally, analyses were repeated for the same bridge model where LRBs are modelled by non-deteriorating force-displacement relations constructed by using property modification factors suggested to modify isolator characteristics in order to represent low ambient temperature. Results are presented in a comparative manner to assess the validity of evaluated response modification factors. Maximum isolator displacements (MIDs) and maximum isolator forces (MIFs) were the response quantities used to quantify the variation in seismic performance of LRB isolated bridge exposed to low temperature.

## 2. LRB TESTS

The bearing tested in this study is a large-size LRB with rubber and lead core diameters of 1020 mm and 190 mm, respectively. Height of the bearing is 436 mm including the top and bottom plates together with the end shim at the top. It is composed of 28 layers of rubber each of which has 10 mm thickness with a total rubber height of 280 mm. Geometrical properties of the tested LRB are presented in Figure 1.

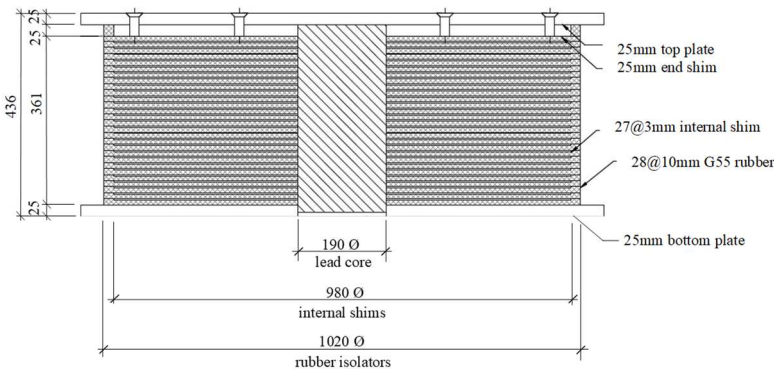


Figure 1- Section cut of test specimen (all units are in mm)

In order to determine the mechanical properties of the specimen, its hysteretic response in shear was recorded under a constant compressive load. Accordingly, the LRB was subjected to three cycles of sinusoidal motion with amplitude equal to 280 mm that corresponds to 100% shear strain. Frequency of the motion was 0.1 Hz where the maximum velocity is 176 mm/s. The axial force acting on the bearing was 4500 kN which results in 6 MPa normal stress. The LRB was first tested at a room temperature of 20°C after conditioning for 24 hours inside the laboratory and tested again at room temperature after conditioning at -30°C for 24 hours inside the air conditioned room (Figure 2.a). Selection of -30°C with an exposure time of 24 hrs is based on the study of Guay and Bouaanani [33] where the authors focused on the low temperature exposure for design of elastomeric bridge bearings in Canada. They investigated the number of consecutive days that the ambient temperature remains below a

specific value. The authors showed that the frequency of  $-30\text{ }^{\circ}\text{C}$  for 24 hrs is in the order of 1 %. Any exposure time longer than 24 hrs was found to have almost zero frequency. This is why 24 hrs of exposure to  $-30\text{ }^{\circ}\text{C}$  is considered in the present study. Tests were conducted at ESQUAKE Seismic Isolator Test Laboratory of Eskişehir Technical University where air conditioned room and test setup are facilitated next to each other. As a result, the time spent to initiate the isolator test after conditioning is less than 10 min. Application of 4500 kN vertical force took 45 s with a loading rate of 100 kN/s. Thus, the isolator test was completed within 12 min. (10 min. + 45 s + 30 s for 3 cycles of motion with 0.1 Hz) after conditioning. The test setup of ESQUAKE shown in Figure 2.b is capable of applying dynamic motions in both horizontal and vertical directions. Table 1 presents the loading capacities of ESQUAKE test setup. Horizontal force-displacement curves obtained from tests for  $20\text{ }^{\circ}\text{C}$  and  $-30\text{ }^{\circ}\text{C}$  are given in Figure 3.

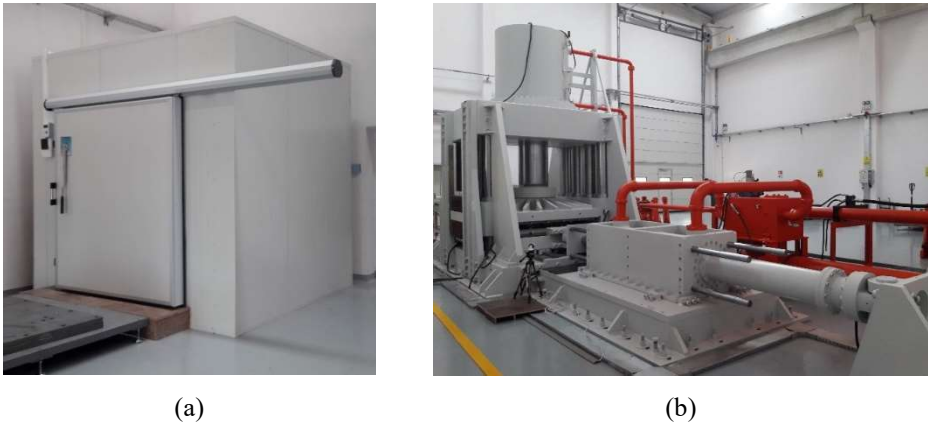


Figure 2 - (a) Air-conditioned room and (b) seismic isolator test setup of ESQUAKE

Table 1 - Properties of ESQUAKE test setup.

Max. Vertical Load:	20.000 kN
Max. Horizontal Load:	2.000 kN
Max. Horizontal Stroke:	$\pm 600$ mm
Max. Velocity:	1.000 mm/s

Mechanical properties of the tested LRB such as post-yield stiffness ( $K_d$ ) and characteristic strength ( $Q_d$ ) for temperatures of  $20\text{ }^{\circ}\text{C}$  and  $-30\text{ }^{\circ}\text{C}$  are presented in Table 2. Data given in Table 2 are computed by means of Eqns. (1)-(2) and Figure 4. In Eqns. (1) and (2),  $Q_1'$ ,  $Q_1''$ ,  $Q_2'$  and  $Q_2''$  are the isolator forces at 50% of the maximum positive and negative horizontal displacements  $d_{\max}$  and  $d_{\min}$  as per ISO 22762-1 [34].  $Q_1$  and  $Q_2$  are the isolator forces at  $d_{\max}$  and  $d_{\min}$ , respectively (see Figure 4).

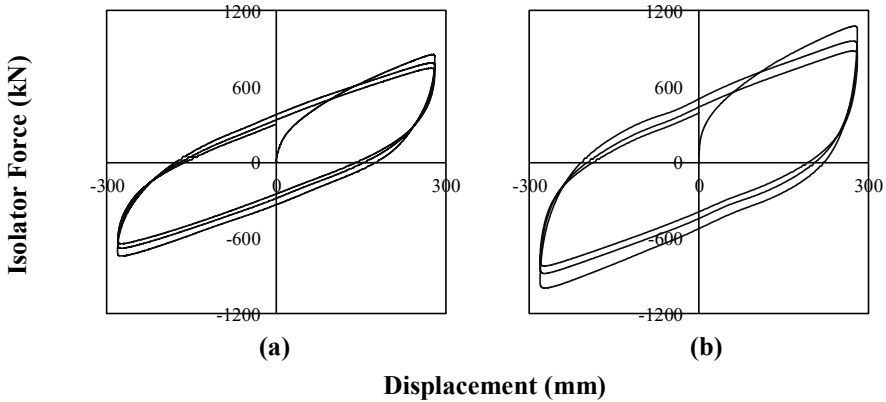


Figure 3 - Force-displacement curves of LRB tested at a) 20°C and b) -30°C.

Table 2 - Mechanical properties of LRB at 20°C and -30°C

Exposure Temperature	Cycle	$Q_d$ (kN)	$K_d$ (kN/m)
-30°C	1	489	2020
	2	414	1919
	3	372	1864
20°C	1	324	1833
	2	286	1796
	3	260	1766

$$Q_d = \left[ \frac{Q_1'' d_{max} / 2 - Q_1' d_{min} / 2}{(d_{max} - d_{min}) / 2} - \frac{Q_2' d_{max} / 2 - Q_2'' d_{min} / 2}{(d_{max} - d_{min}) / 2} \right] / 2 \quad (1)$$

$$K_d = \left[ \frac{Q_1' - Q_1''}{(d_{max} - d_{min}) / 2} + \frac{Q_2'' - Q_2'}{(d_{max} - d_{min}) / 2} \right] / 2 \quad (2)$$

Comparison of test results obtained for temperatures of 20°C and -30°C reveals the following conclusions. Characteristic strength (force intercept at zero displacement)  $Q_d$  of the tested LRB increases when the exposure temperature drops to -30°C. The amount of increase in  $Q_d$  is 50% for the first cycle whereas it is 45% and 43% for the second and third cycles, respectively. Similarly, post-yield stiffness  $K_d$  of the LRB increases as the temperature decreases. However, the amount of variations in  $K_d$ , which are 10%, 7% and 5% for first, second and third cycles, respectively, are relatively small compared to those computed for  $Q_d$ . Considering the test results, it is evident that amount of variation in mechanical properties of LRB is not constant at all loading cycles and the trend is to decrease with increasing

number of cycles. The reason for such reduction is the temperature rise in the lead core of LRB during cyclic motion as discussed in the next section.

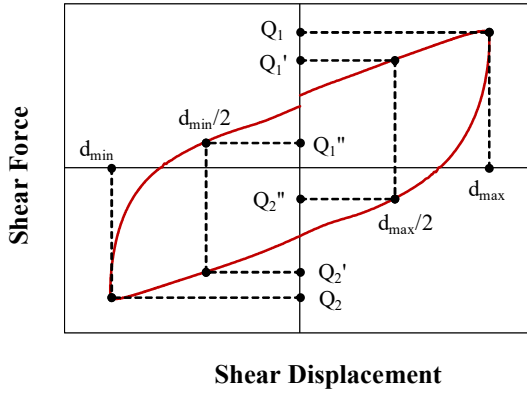


*Figure 4 - Force-displacement definitions for LRBs.*

### 3. DETERIORATING HYSTERETIC RESPONSE OF LRB

The hysteretic behavior of isolators is generally modeled by a generic non-deteriorating force-deformation relation. However, as shown in Figure 3, force-displacement curve of LRBs deteriorates under cyclic motion. Figure 3 clearly demonstrates the gradual reduction in strength of the tested bearing at each cycle. The primary reason of such a variation in strength of LRBs has been identified as the temperature rise in the lead core during cyclic motion by Kalpakidis and Constantinou [30]. Their mathematical model enables one to modify the initial strength of lead as a function of lead core temperature. Accordingly, the horizontal strength of the LRB decreases gradually when subjected to motion. The model considers the instantaneous temperature rise in the lead core and allows calculating the reduction in strength of isolator via reducing the initial yield stress of the lead ( $\sigma_{YL0}$ ), instantly. According to this model, the relation between the lead core temperature  $T_L$  and the strength of lead ( $\sigma_{YL0}$ ) is defined by Eqn. (3) where  $E_2$  is a constant that relates the temperature and yield stress and equals to  $0.0069/^\circ\text{C}$ . For detailed information about deteriorating hysteretic response of an LRB, reference is made to Kalpakidis and Constantinou [30].

$$\sigma_{YL}(T_L) = \sigma_{YL0} \exp(-E_2 T_L) \tag{3}$$

For the sake of completeness and refraining queries regarding the analytical representation of the tested LRB in this study, Figure 5 is presented. In Figure 5, force-displacement curves obtained from experiments are compared with the analytical ones computed by means of the mathematical model proposed by Kalpakidis and Constantinou [30] for both  $20^\circ\text{C}$  and  $-30^\circ\text{C}$ . OpenSees [35] is the structural analysis program by which the computations were performed. It is to be noted that the deteriorating cyclic behavior of LRB addressed in analytical modeling requires the definition of an initial yield stress for lead which is equal to the characteristic strength obtained from corresponding test result divided by the cross-sectional

area of the lead core. For detailed information about analytical modeling of LRB in OpenSees, please refer to Kumar et al. [27]. Figure 5 shows that hysteretic response of the tested LRB can be idealized realistically with great success in the analyses regardless of the ambient temperature.

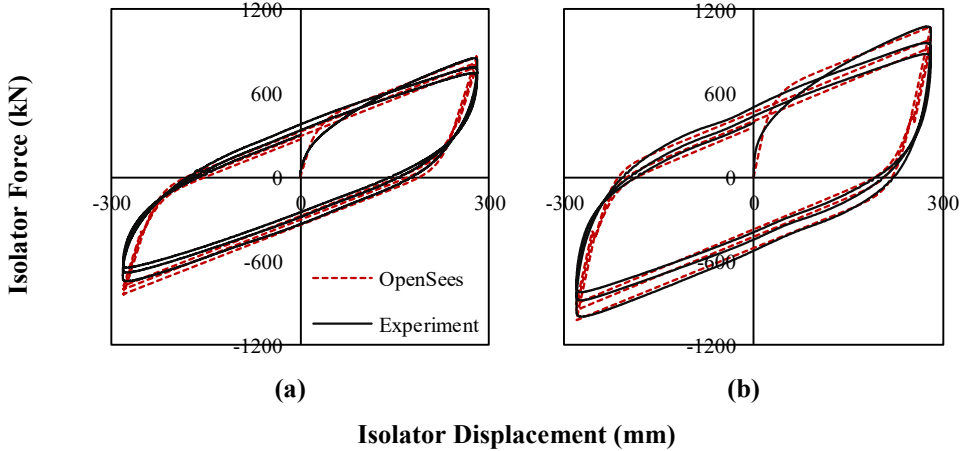


Figure 5 - Comparison of experimental and analytical hysteretic curves of LRB tested at a) 20°C and b) -30°C.

#### 4. SEISMICALLY ISOLATED BRIDGE MODEL

The analyzed bridge was originally not seismically isolated and designed for U.S. Department of Transportation Federal Highway Administration seismic design course [36]. Then, it was slightly modified (diaphragms in the box girder were added at both abutments and piers) by Constantinou et al. [7] in order to facilitate seismic isolation units between each pier/abutment and the box girder. It is a cast-in-place concrete box girder bridge with a 30-degree skew. The length of the bridge is 97.5m and has three spans with lengths of 30.5m, 36.5m and 30.5m. Intermediate bents consist of two 1.22m circular columns and a cap beam with dimensions of 1.22mx1.83m. The total weight of the bridge above the isolation level is 24956 kN (box girder and each diaphragm weigh 229 kN/m and 657 kN, respectively). The section at one of the intermediate bents is presented in Figure 6.a.

As shown in Figure 6.a, isolation system is composed of two LRBs at each abutment and pier with a total of eight isolators. They are modeled by deteriorating hysteretic behavior described in the previous section. Nonlinear bidirectional interaction of LRBs in case of simultaneous excitations of ground motions in both horizontal directions is defined in the following section. The bridge superstructure was assumed to have infinite in-plane rigidity [37-38]. Analytical representation of the bridge bent is given in Figure 6.b where  $M_{\text{superstructure}}$  is defined based on the tributary weight of the superstructure plus the additional weight of the diaphragm and equals to 8330 kN (isolation period based on the post-yield stiffness of the tested LRB at 20°C is 3 s). Total mass of the bent components,  $M_{\text{bent}}$ , is lumped equally at the column tops. In the analytical model, member rigid end zone segment is taken into account to represent the bent stiffness properly. The bridge superstructure and columns are

modeled as elastic based on the assumption that structure remains within the elastic range due to seismic isolation by means of *elasticbeamcolumn* element of OpenSees [35]. Accordingly, the elastic modulus of concrete is taken as 24 820 MPa. Bridge structure is assumed to be fixed at the foundation level.

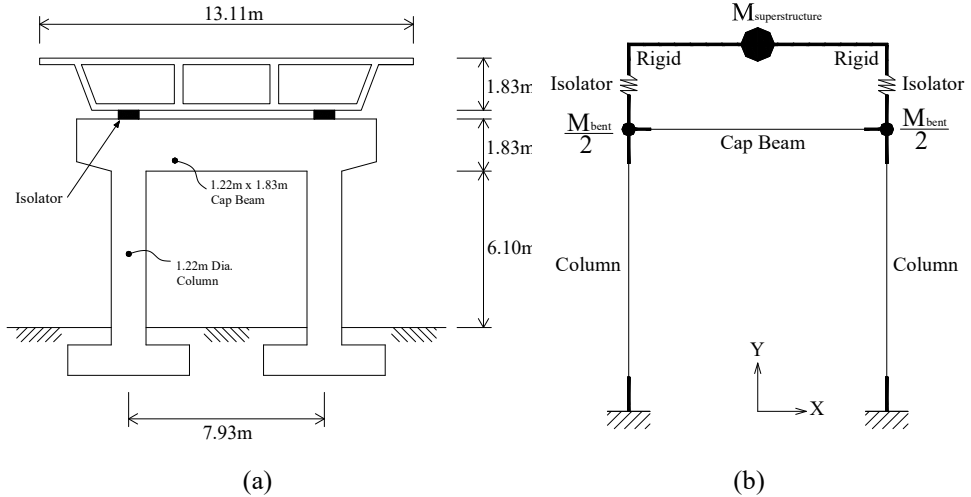


Figure 6 - (a) Bent geometry and (b) analytical model of the bent. Reprinted from [39]

### 5. BIDIRECTIONAL RESPONSE OF LRBS

The bidirectional bilinear hysteretic model used for modeling of LRBS was developed by Park et al. [40]. Validity of the model for idealizing the hysteretic response of isolators subjected to bidirectional ground motion excitations was tested and verified by Mokha et al. [41]. Analytical model proposed by Park et al. [40] enables assembling the isolator forces by taking into account the bidirectional interaction effects when isolators behave nonlinearly in both of the horizontal directions. Accordingly, isolator forces are calculated by Eqns. (4)-(6). By means of the off-diagonal terms of Eqn. (6), the interaction between the isolator forces in two orthogonal horizontal directions are taken into account.

$$\begin{Bmatrix} F_x \\ F_y \end{Bmatrix} = c_d \begin{Bmatrix} \dot{U}_x \\ \dot{U}_y \end{Bmatrix} + K \begin{Bmatrix} U_x \\ U_y \end{Bmatrix} + (\sigma_{yL} (T_L) A_L) \begin{Bmatrix} Z_x \\ Z_y \end{Bmatrix} \tag{4}$$

$$Y \begin{Bmatrix} \dot{Z}_x \\ \dot{Z}_y \end{Bmatrix} = (A[I] - B[\Omega]) \begin{Bmatrix} \dot{U}_x \\ \dot{U}_y \end{Bmatrix} \tag{5}$$

$$[\Omega] = \begin{Bmatrix} Z_x^2 [\text{sgn}(\dot{U}_x Z_x) + 1] & Z_x Z_y [\text{sgn}(\dot{U}_y Z_y) + 1] \\ Z_x Z_y [\text{sgn}(\dot{U}_x Z_x) + 1] & Z_y^2 [\text{sgn}(\dot{U}_y Z_y) + 1] \end{Bmatrix} \tag{6}$$

In the above equations,  $F_x$  and  $F_y$  are the isolator forces and  $U_x$  and  $U_y$  are the isolator displacements in  $x$  and  $y$  directions, respectively.  $Y$  and  $K$  are the yield displacement and post-yield stiffness of the bilinear force-deformation relation of isolators, respectively.  $c_d$  stands for the energy dissipation of the rubber and  $A_L$  is the cross-sectional area of the lead core.  $Z_x$  and  $Z_y$  are hysteretic dimensionless quantities that account for the interaction of hysteretic seismic isolator forces in orthogonal horizontal directions and vary between +1 and -1. In Eqn. (5),  $A$  and  $B$  values should satisfy the relation of  $A = 2B$  [41] in order to assure that the force and displacement vectors are in the same direction (specifically,  $A=1$  and  $B=0.5$ ). Additionally,  $[I]$  is the unit matrix,  $sgn$  stands for the signum function and overdot refers to differentiation with respect to time.

**6. GROUND MOTIONS**

Two sets of ground motions previously used by Warn and Whittaker [37], were considered in the analyses. Each ground motion set is composed of 10 pairs of records. They were clustered to represent characteristics of near-field (NF) and large-magnitude small-distance (LMSD) records. These motions were used so that analyses results represent a broad range of seismic demand in terms of maximum isolator displacement.

*Table 3 - Characteristics of selected near-field ground motions.*

#	Event	Station	M <sub>w</sub>	Comp. <sup>1</sup>	PGA (g)	PGV (cm/s)	PGD (cm)	Distance <sup>2</sup> (km)
1	Tabas, Iran	Tabas	7.4	FN	0.90	109.7	55.5	1.2
				FP	0.98	105.8	74.9	
2	Loma, Prieta	Lex Dam	7.0	FN	0.69	178.7	56.6	6.3
				FP	0.37	68.7	25.4	
3	Cape Mendocino	Petrolia	7.1	FN	0.64	62.9	14.1	8.5
				FP	0.65	46.5	10.3	
4	Erzincan, Turkey	Erzincan	6.7	FN	0.43	119.1	42.1	2.0
				FP	0.46	58.1	29.5	
5	Landers	Lucerne	7.3	FN	0.71	136.1	11.2	1.1
				FP	0.80	70.3	184.3	
6	Northridge	Rinaldi	6.7	FN	0.89	174.2	38.3	7.5
				FP	0.39	60.9	17.3	
7	Northridge	Olive View	6.7	FN	0.73	122.1	30.7	6.4
				FP	0.60	53.9	9.1	
8	Kobe	JMA	6.9	FN	1.09	160.2	40.1	3.4
				FP	0.57	72.4	15.9	
9	Chi-Chi, Taiwan	TCU065	7.	West	0.81	126.2	92.6	1.0
				North	0.60	78.8	60.8	
10	Chi-Chi, Taiwan	TCU075	7.6	West	0.33	88.3	86.5	1.5
				North	0.26	38.2	33.2	



The magnitudes of ground motions grouped as near-field are in between 6.7 and 7.6 with closest distances to the fault rupture less than 10 km. Large-magnitude small-distance ground motions have magnitudes greater than 6.5 while closest distances to fault rupture are in between 10 km and 30 km. Tables 3 and 4 give the characteristics of the considered ground motions where PGA, PGV and PGD stands for peak ground acceleration, peak ground velocity and peak ground displacement, respectively. Selected ground motions were downloaded from both the Pacific Earthquake Engineering Research (PEER) Center [42] database and library of QuakeManager [43] software. 5% damped response spectra of ground motions listed in Tables 3 and 4 are given in Figure 7 where the “strong” and “weak” components are designated based on PGVs of ground motions. The horizontal component with the larger PGV is denoted as strong component [39].

Table 4 - Characteristics of selected large-magnitude small-distance ground motions.

#	Event	Station	M <sub>w</sub>	Comp.	PGA (g)	PGV (cm/s)	PGD (cm)	Distance <sup>2</sup> (km)
1	Loma Prieta	Gilroy Array #1	6.9	0	0.41	31.6	6.4	11.2
				90	0.47	33.9	8.5	
2	Kocaeli, Turkey	Gebze	7.4	0	0.24	50.3	42.8	17.0
				270	0.14	29.7	27.6	
3	Loma Prieta	Saratoga Aloha Ave	6.9	0	0.51	41.2	16.3	13.0
				90	0.32	42.6	27.6	
4	Cape Mendocino	Rio Dell Over Pass FF	7.1	270	0.39	43.8	21.7	18.5
				360	0.55	41.9	19.5	
5	Landers	Joshua Tree	7.3	0	0.27	27.5	9.5	11.6
				90	0.28	43.1	14.3	
6	Loma Prieta	Gilroy Array #2	6.9	0	0.37	32.9	7.2	12.7
				90	0.32	39.1	12.1	
7	Landers	Yermo Fire Station	7.3	270	0.25	51.4	43.9	24.9
				360	0.15	29.7	24.6	
8	Kobe	Abeno	6.9	0	0.22	20.7	9.1	23.8
				90	0.24	24.2	10.0	
9	Duzce, Turkey	Bolu	7.1	0	0.73	56.4	23.1	17.6
				90	0.82	62.1	13.6	
10	Northridge	Canoga Park Topanga Can	6.7	106	0.36	32.1	9.1	15.8
				196	0.42	60.7	20.3	

<sup>1</sup> FN – Fault Normal, FP – Fault Parallel

<sup>2</sup> Closest distance to fault rupture

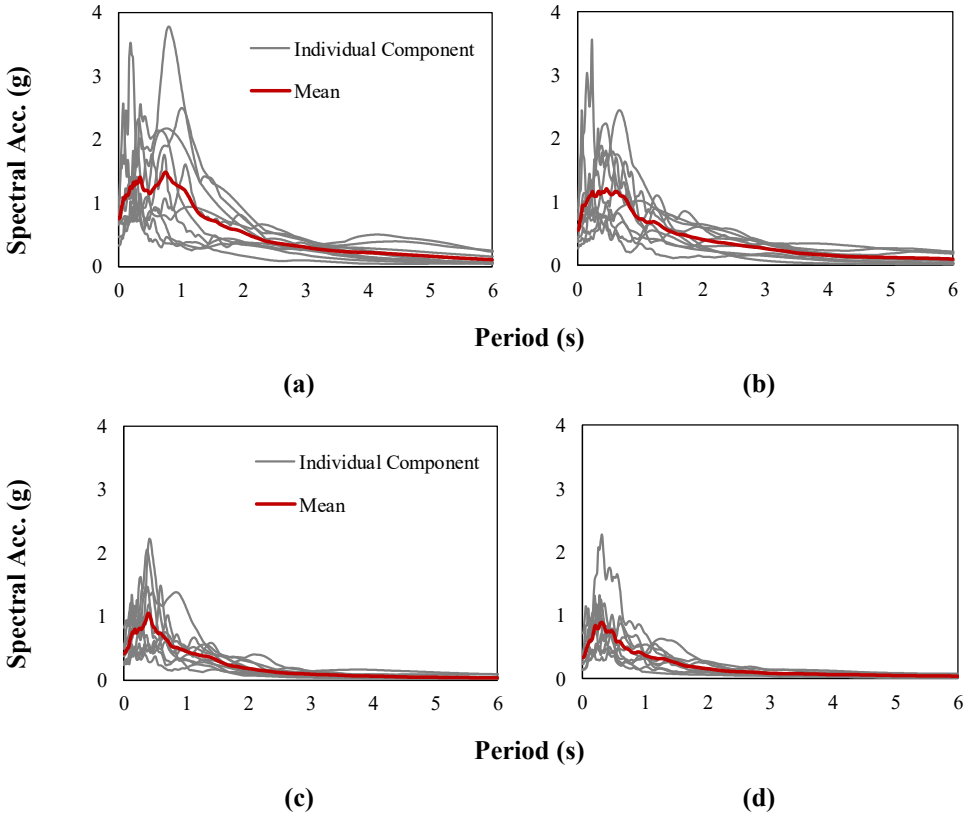


Figure 7 - 5% damped response spectra for (a) strong and (b) weak components of NF ground motions, (c) strong and (d) weak components of LMSD ground motions.

## 7. DYNAMIC ANALYSIS RESULTS

Nonlinear response history analyses were performed in OpenSees [35] with due consideration of deteriorating hysteretic representation of LRBs under bidirectional excitations of ground motions given Tables 3 and 4 in order to evaluate the variation in response quantities of the SIB due to change in environmental temperature. Accordingly, maximum isolator displacements (MIDs) and base shears in the pier are presented in a comparative manner for 20°C and -30°C. Moreover, the effect of seismicity level in combination with the change of environmental temperature is discussed based on analyses results obtained by using both NF and LMSD ground motion records.

### 7.1. Maximum Isolator Displacements

One of the important predictions for a seismically isolated bridge is the resultant displacement of the isolation system. It dominates the design of the isolator geometry together with the peak shear force transferred to the pier columns. This section presents the

observations related to variation of MID of the analyzed structural system due to change in ambient temperature. Figure 8 shows the comparison of MIDs obtained for 20°C and -30°C for both ground motion sets of NF and LMSD. Averages of MIDs recorded for all of the considered ground motion records are also given in Figure 8 where MIDs were calculated by taking the maxima of  $\sqrt{(D_x^2 + D_y^2)}$ . Here,  $D_x$  and  $D_y$  are the isolator displacements in horizontal x- and y-directions, respectively. Figure 8.a, where MIDs for NF ground motions are presented, reveals that MID reduces significantly when the ambient temperature drops from 20°C to -30°C. The amount of reductions in MID ranges from 8% to 53% with an average value of 19%. Similar comparison for LMSD ground motions is given in Figure 8.b. In this case, the amounts of change in MIDs for individual ground motion records range from 33% to -52% with an average of -16% when the temperature changes from 20°C to -30°C. At the end of analyses, the corresponding temperature rises in the lead core of the LRB are computed by means of the formulations proposed by Kalpakidis and Constantinou [30] for both ground motion sets and presented in Figure 9.

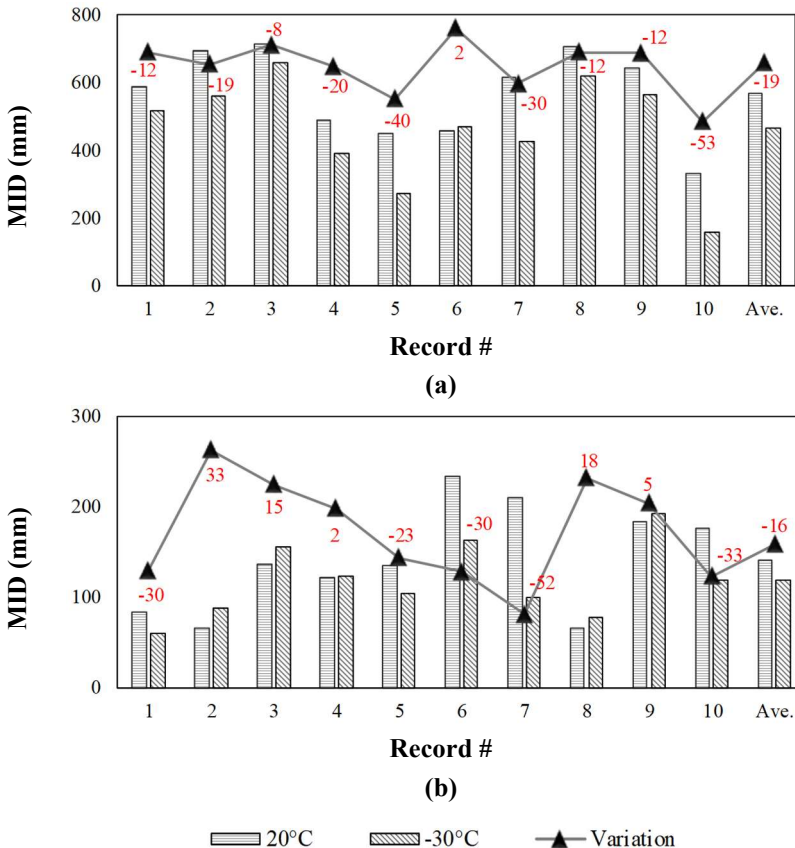


Figure 8 - Comparison of MIDs for (a) NF and (b) LMSD ground motions at 20°C and -30°C.

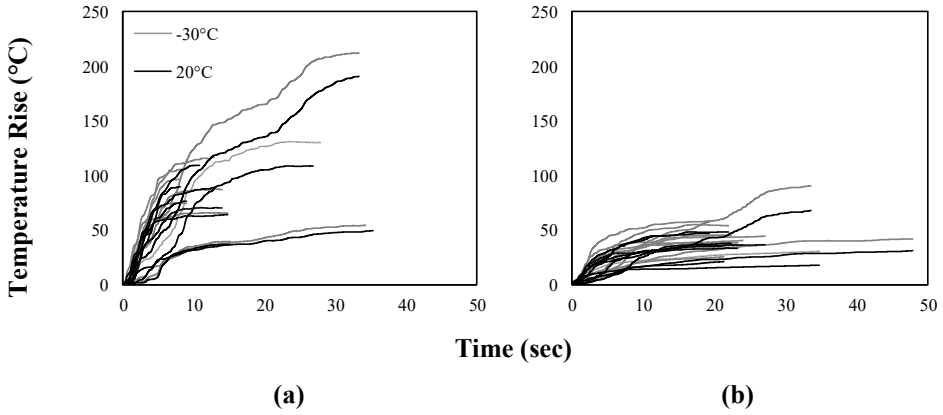


Figure 9 - Temperature rises in lead core for (a) NF and (b) LMSD ground motions at temperatures of 20°C and -30°C.

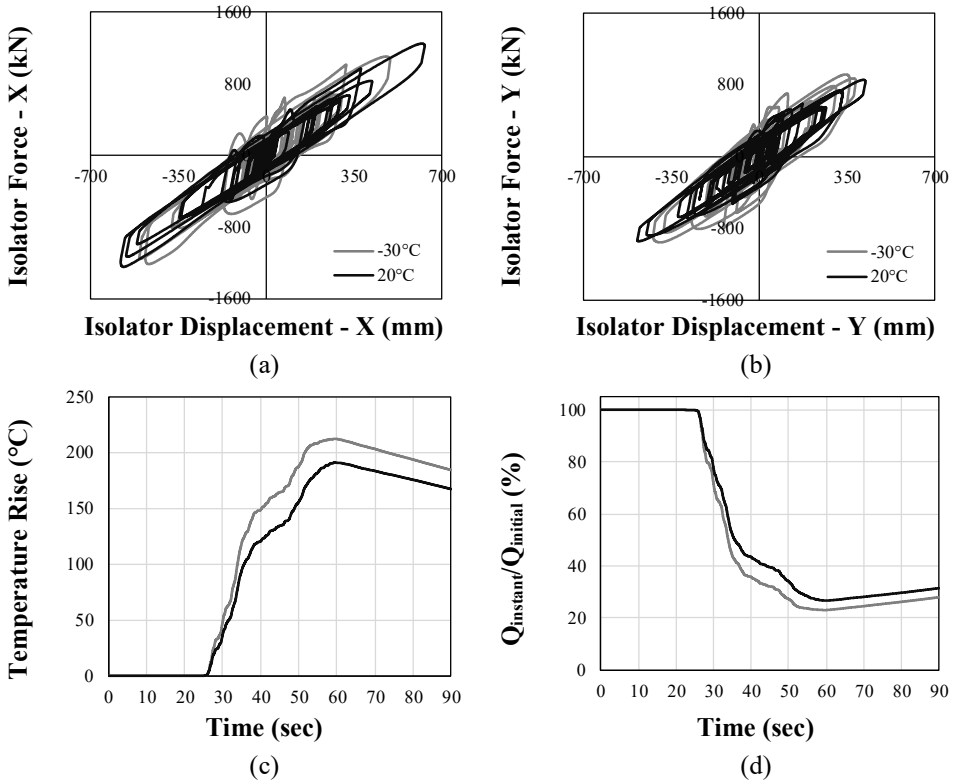


Figure 10 - (a) force-displacement curve in x-direction, (b) force-displacement curve in y-direction, (c) rise in lead core temperature, (d) change in strength of LRB for NF record #9 at 20°C and -30°C.

Since amplitudes of displacements that the LRB undergoes are larger for NF ground motions compared to LMSD ones, temperature rises in the lead core are greater for NF motions. In order to highlight the significance of strength deterioration in LRB during the analyses, Figure 10 shows force-displacement curves of the LRB for NF record #9 which has the peak value of temperature rise in Figure 9.a. Figure 10 also presents temperature rise in the lead core of the analyzed LRB and corresponding change in strength of the bearing. It is observed that the amount of temperature rise in the lead core is larger at low temperature. For record #9, maximum lead core temperatures were calculated as 213°C and 191°C for ambient temperatures of -30°C and 20°C, respectively (Figure 10.c). The corresponding losses in the initial strength of the LRB are 77% and 73%, in the same order (Figure 10.d). The reason for such high temperature rises in the lead core is the large amplitude displacement at several cycles.

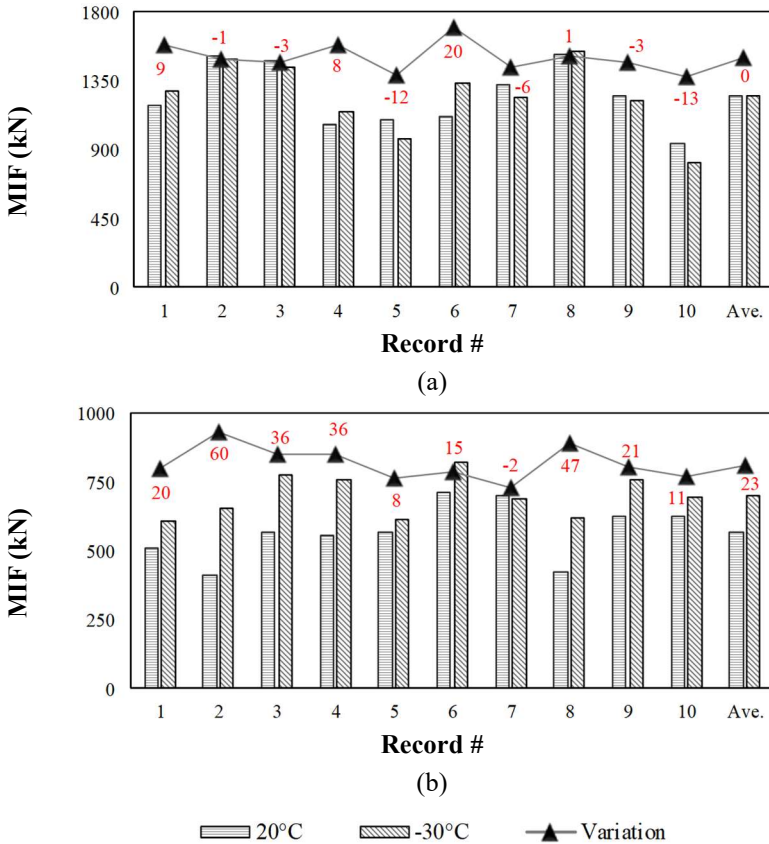


Figure 11 - Comparison of MIFs for (a) NF and (b) LMSD ground motions at 20°C and -30°C.

### 7.2. Base Shears in the Piers

It is of crucial importance in both performance-based design and performance assessment of a seismically isolated bridge to estimate the shear force transferred from isolation system to the piers. In this section, variation of base shear forces acting on each column of the bridge (see Figure 6) is presented in Figure 11 as a function of ambient temperature and seismicity level. For near field ground motions, Figure 11.a shows that the amounts of variation in isolator force are in between -13% to 20% when temperature decreases from 20°C to -30°C. However, it is interesting to observe that when the averages of base shears are of concern, they are identical for both 20°C to -30°C with a magnitude of 1248 kN. Although the initial strength and stiffness of isolator increases due to reduced ambient temperature, the average shear force does not change for both 20°C to -30°C. Even though initial strength and stiffness of the bearing increases at -30°C due to reduced isolator displacements (compared to 20°C case) the maximum shear force transferred by the isolator remain the same in an average sense (see Figure 10.a).

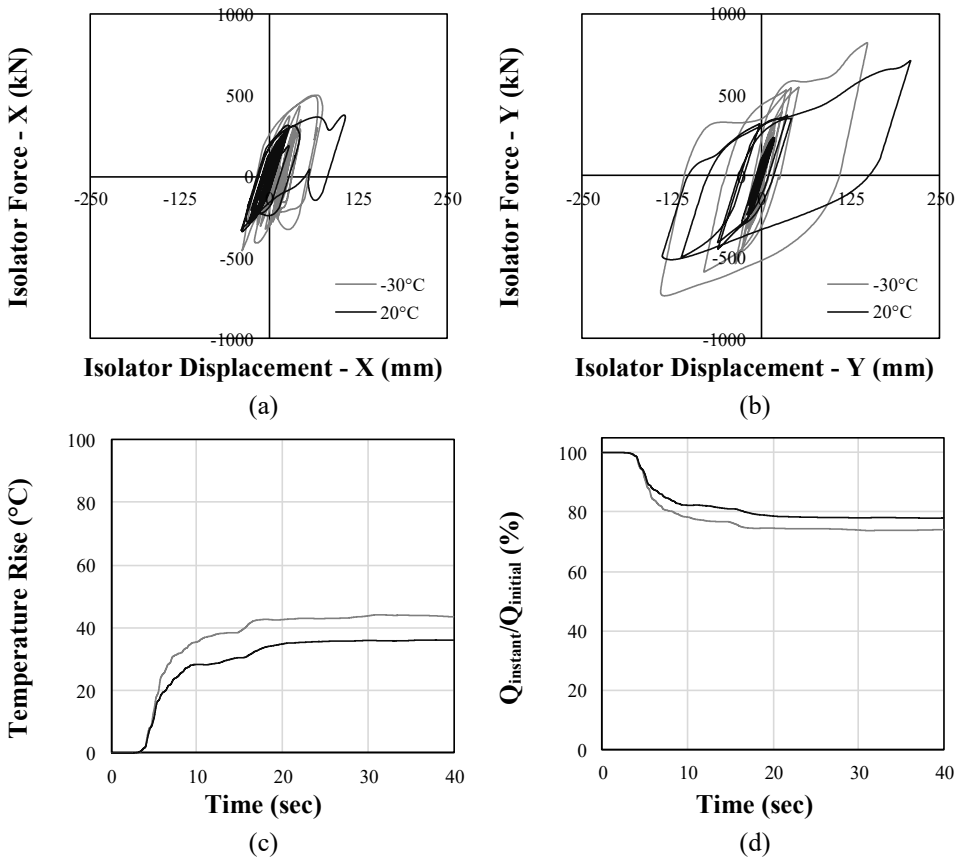


Figure 12 - (a) force-displacement curve in x-direction, (b) force-displacement curve in y-direction, (c) rise in lead core temperature, (d) change in strength of LRB for LMSD record #6 at 20°C and -30°C.

Figure 11.b is shown to investigate the variation of isolator force for large-magnitude small-distance ground motion set when the ambient temperature is reduced from 20°C to -30°C. Figure 11.b reveals that although the average value of amplification in isolator force is calculated as 23%, for the selected ground motions it may be up to 60%, individually. In order to understand better the change in hysteretic behavior of LRB, Figure 12 is presented for record #6 of LMSD ground motion set. As clearly shown in Figures 12.a and 12.b, the isolator undergoes a larger displacement for 20°C compared to the 30°C case. However, isolator displacement is not large enough to overcome the isolator force recorded for -30°C scenario where the initial strength and stiffness values are greater than those of 20°C case. Since the isolator displacements are small, computed temperature rises in the lead core are relatively low and equal to 36°C and 43°C (Figure 12.c) and corresponding amounts of loss in initial strengths are 22% and 26% (Figure 12.d) for ambient temperatures of 20°C and -30°C, respectively.

## **8. ASSESSMENT OF USING PROPERTY MODIFICATION FACTOR**

The current design approach for modeling the hysteretic behavior of seismic isolators is to perform bounding analyses. It assures that the nominal properties (defined as the average among the three cycles of force-displacement curve obtained at normal temperature) of the isolator is modified to consider the effects of aging, contamination, ambient temperature, history of loading and heating during cyclic motion. For this purpose, corresponding property modification factors,  $\lambda$ , are employed as defined by the design guidelines [44]. Modified properties of the isolator are used to construct non-deteriorating force-displacement curves that will represent both upper and lower bound characteristics of LRB in NRHA. Such modeling approach aims to estimate the boundaries where the probable isolator response will take place in between, rather than focusing on the real performance of the isolator. Once property modification factors are determined, it will be possible for the designer to consider the envelope response of seismically isolated structure where maximum and minimum isolator properties are established. Although it is suggested to determine the property modification factors based on test results which are specific to isolator under investigation, in the literature there are some default values used in bounding analysis. This section is devoted to assessing the validity of using the available default values of property modification factors, suggested to represent change in ambient temperature, to estimate critical response quantities of a seismically isolated structure, namely maximum isolator displacement and maximum isolator force. In this sense, property modification factors suggested by three different investigations to mimic the change in LRB properties at low temperatures are considered and listed in Table 5. It is to be noted that, these values are specific only to isolators tested by the researchers at an ambient temperature of -30°C. The manufacturer, size of bearing, shear modulus of rubber, exposure time to low temperature and loading frequency of the studies cited in Table 5 are all different from each other. As a result, there is a diversity in the suggested property modification factors for characteristic strength  $Q$  and post-yield stiffness  $K$  of the LRB. Property modification factors of Table 5 are used to modify the nominal values of  $Q$  and  $K$  computed by considering the test results presented in Table 2 for 20°C ambient temperature. Figure 13 presents the corresponding non-deteriorating force-displacement curves used in additional nonlinear response history analyses together with the hysteretic representation for nominal characteristics of the LRB tested in this study.

Table 5 - Property modification factors suggested for -30°C

	$\lambda_Q$	$\lambda_K$
Constantinou et al. (2007)	1.80	1.30
Li et al. (2009)	1.59	1.30
Imai et al. (2008)	1.57	1.41

The maximum isolator displacements and forces obtained from NRHA performed by using non-deteriorating hysteresis loops ( $MID_{non-deteriorating}$ ,  $MIF_{non-deteriorating}$ ) for modeling of LRBs with the ones where deteriorating force-deformation relation ( $MID_{deteriorating}$ ,  $MIF_{deteriorating}$ ) of LRBs was defined based on the experimental data (see Figure 5.b) are compared. Results are illustrated in Figure 14 where grey straight lines represent the case that the response quantities obtained by both non-deteriorating and deteriorating hysteretic representations of LRB are identical to each other. The motivation for evaluation of using property modification factors to estimate the nonlinear response of LRBs at low temperatures (-30°C in this specific case) is to see whether they can be addressed in preliminary design stage of isolated bridges to aid the designer.

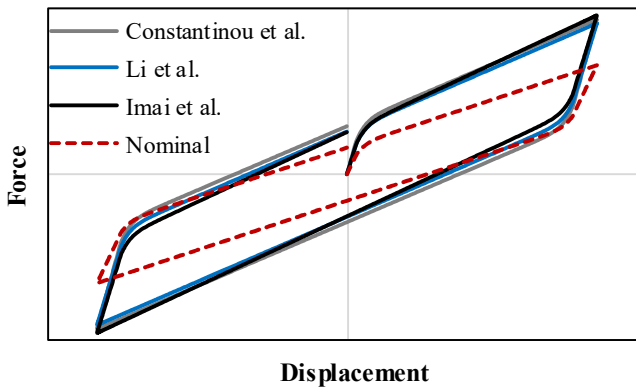


Figure 13 - Force-displacement curves constructed by property modification factors suggested for -30°C.

In Figure 14, in addition to individual results obtained from analyses performed by using each record of ground motion sets (black geometrical forms), their averages are also presented by geometric shapes in red color. In an average sense, Figures 14.a and 14.b demonstrate that using property modification factors of the cited studies is highly effective in estimation of MIDs in comparison to actual deteriorating behavior of LRB. Evaluated property modification factors result in almost the same MIDs for both ground motion sets. For near-field ground motion set, the average MIDs obtained from analysis using property modification factors of Constantinou et al. [7], Li et al. [32] and Imai et al. [45] are 424 mm, 454 mm and 452 mm, respectively while it is 464 mm when the actual deteriorating behavior is used to model isolator response. Average values of MIDs of large-magnitude small-distance ground motion set are 116 mm, 120 mm and 120 mm, in the same order whereas it



is 118 mm for deteriorating hysteretic representation of LRB. In Figure 14.a, it is revealed that for some ground motions, using property modification factors result in under-estimated isolator displacements. In order to assess the reason of such observation, Figure 15 is depicted where force-displacement curves of deteriorating and non-deteriorating (for property modification factors suggested by Constantinou et al. [7]) representations are presented. Figure 15 clearly shows that as the number of large amplitude cycles increases, the corresponding temperature rise in the lead core results in reduced isolator strength for the deteriorating hysteretic representation. Consequently, the isolator experiences amplified displacements. On the other hand, the non-deteriorating hysteretic representation is not sensitive to number of cycles and isolator strength does not change during the cyclic motion. Thus, it is strongly suggested to perform bounding analysis accompanied by the analyses where actual deteriorating force-displacement curve of LRB is taken into account.

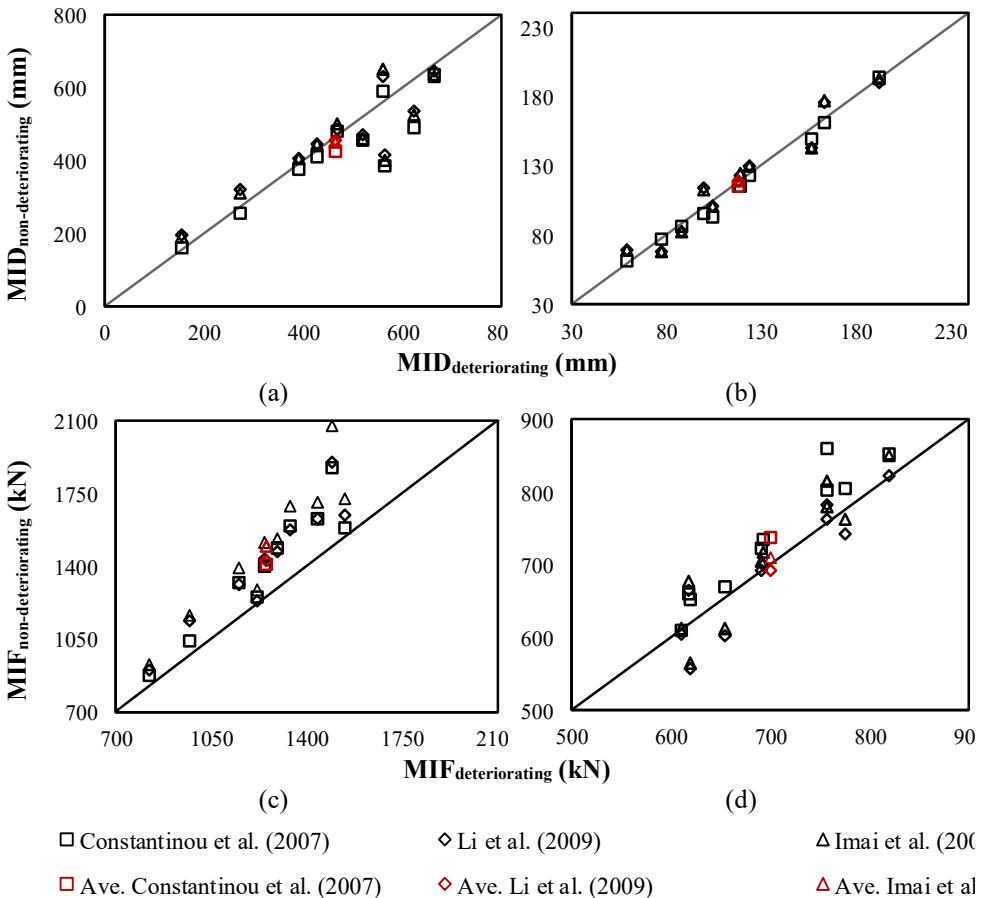


Figure 14 - Accuracy of using property modification factors in prediction of isolator response at -30°C for (a) MID in near-field ground motions, (b) MID in large-magnitude small-distance ground motions, (c) MIF in near-field ground motions, (d) MIF in large-magnitude small-distance ground motions.

Figures 14.c and 14.d show the accuracy of using property modification factors in terms of MIFs. For both ground motion sets, MIFs are over-estimated by non-deteriorating hysteretic representation of LRBs in an average sense. The average amounts of over-estimations range from 10% to 20% for near-field motions while it is less than 5% for large-magnitude small-distance motions. It states that, as the isolator displacement increases, the amount of over-estimation in MIF increases, as well. Thus, the dimensions of bridge piers may be over-sized at the design stage when non-deteriorating representations constructed by property modification factors are used to idealize LRB behavior at an ambient temperature of  $-30^{\circ}\text{C}$ .

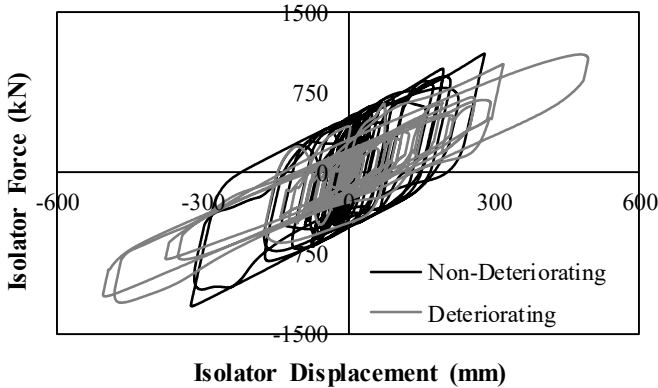


Figure 15 - Comparison of deteriorating and non-deteriorating hysteretic representations for LRB behavior.

## 9. CONCLUSIONS

This study quantifies the variation in both mechanical properties of an LRB and response of a representative LRB isolated bridge when subjected to bidirectional excitations of ground motions at ambient temperatures of  $20^{\circ}\text{C}$  and  $-30^{\circ}\text{C}$ . Hence, a set of complementary experimental and analytical investigations were performed. First, cyclic tests of the considered LRB were conducted and change in hysteretic behavior of the bearing was noted. Then, the recorded hysteretic behavior was compared with the analytically estimated one and the superior ability of the available mathematical model to mimic the force-displacement curve of LRBs under cyclic motion was presented at both ambient temperatures. Using the verified analytical tool for nonlinear behavior of LRB at  $20^{\circ}\text{C}$  and  $-30^{\circ}\text{C}$ , nonlinear response history analyses were conducted with two sets of motions representative of both near-field and large-magnitude small-distance records. Results are also used to assess the success of property modification factors in estimation of LRB response at low temperature. Experimental and analytical investigations have revealed the following conclusions:

- Characteristic strength and post-yield stiffness of bilinear force-displacement curve of the tested LRB increases when the temperature drops from  $20^{\circ}\text{C}$  to  $-30^{\circ}\text{C}$ . The amplifications in strength and stiffness are observed to be in the order of 50% and 10%, respectively. As the number of cycles increases, these values decrease gradually.

- For the selected ground motions and structural model, in an average sense, MIDs obtained from NRHA conducted with NF motions at  $-30^{\circ}\text{C}$  are about 20% less than the ones computed for  $20^{\circ}\text{C}$ . For LMSD motions, it is computed as 16%.
- When the averages of maximum isolator forces obtained from NRHA conducted at  $-30^{\circ}\text{C}$  and  $20^{\circ}\text{C}$  were compared, it was found that they are identical for NF motions. On the other hand, average base shear at  $-30^{\circ}\text{C}$  is about 30% larger than that of  $20^{\circ}\text{C}$  for LMSD motions.
- Using property modification factors cited in this study results in very accurate estimations for maximum isolator displacement regardless of the ground motion set. However, maximum isolator forces are over-estimated compared to actual deteriorating behavior of LRB. The amount of over-estimation in isolator force increases with increasing isolator displacement. Bounding analysis should be complemented with further analysis where deteriorating hysteretic behavior of LRBs is taken into account.

It is to be mentioned that although the cited studies suggest to use different property modification factors for characteristic strength and post-yield stiffness, they are found to be very effective in estimation of maximum isolator displacement which is the key parameter considered in the design of seismically isolated structures. This observation is important because even though these factors are sensitive to geometry of LRB, manufacturer of the bearing, loading protocol (shear strain and frequency), it is shown that they still provide a good prediction for a randomly selected isolator (different geometry, manufacturer and shear strains). In order to refrain from an over generalization, it should be kept in mind that presented results are specific to both selected ground motions and the tested LRB.

### **Acknowledgments**

This study was supported by research grant No.1505F460, Commission of Scientific Research Projects, Eskisehir Technical University.

### **References**

- [1] Skinner, R.I., Robinson, W.H., McVerry, G.H., *An Introduction to Seismic Isolation*. Chichester: John Wiley & Sons, 1993.
- [2] Naeim, F., Kelly J., *Design of Seismic Isolated Structures: From Theory to Practice*. New York: John Wiley & Sons, 1999.
- [3] Kunde, M.C., Jangid, R.S., *Seismic Behavior of Isolated Bridges: A-state-of-the-art review*. *Electronic Journal of Structural Engineering*, 3, 140–170, 2003.
- [4] Robinson, W.H., *Lead Rubber Hysteretic Bearings Suitable for Protecting Structures During Earthquake*. *Earthquake Engineering and Structural Dynamics*, 10(4), 593–604, 1982.
- [5] Nagarajaiah, S., Sun, X., *Response of Base Isolated USC Hospital Building in Northridge Earthquake*. *Journal of Structural Engineering (ASCE)*, 126(10), 1177–1186, 2000.

- [6] Roeder, C.W., Proposed Design Method for Thermal Bridge Movements. *Journal of Bridge Engineering*, 8(1), 12-19, 2003.
- [7] Constantinou, M.C., Whittaker, A.S., Kalpakidis, Y., Fenz, D.M., Warn, G.P., Performance of Seismic Isolation Hardware Under Service and Seismic Loading, Technical report, NY: MCEER=07-2012, Buffalo, 2007.
- [8] Benzoni, G., Casarotti, C., Effects of Vertical Load, Strain Rate and Cycling on The Response of Lead-Rubber Seismic Isolators. *Journal of Earthquake Engineering*, 13(3), 293-312, 2009.
- [9] Erdoğan, H., Çavdar, E., Özdemir, G., Türk Deprem Yönetmelikleri (DBYBHY ve TBDY) Spektrum Tanımlarının Deprem Yalıtım Sistemi Tasarımı Özelinde Karşılaştırılması. *Teknik Dergi*, 32(5), 2021.
- [10] Pinarbasi, S., Akyuz, U., Sismik İzolasyon ve Elastomerik Yastık Deneyleri. *İMO Teknik Dergi*, 237, 3581-3598, 2005.
- [11] Roeder, C.W., Stanto, J.F., Taylor A.W., Performance of Elastomeric Bearings (No. 298). Washington, DC: National Cooperative Highway Research Program, Transportation Research Board, 1987.
- [12] Ritchie, D.F., Neoprene Bridge Bearing Pads, Gaskets and Seals. *Rubber World*, Lippincott & Petto Inc. 200(2), 27-31, 1989.
- [13] Eyre, R., Stevenson, A., Performance of Elastomeric Bridge Bearings at Low Temperatures. *Proceedings 3rd World Congress on Joint Sealing and Bearing Systems for Concrete Structures*, 736-762. Toronto, Canada, 1991.
- [14] Yakut, A., Yura, J.A., Evaluation of Low-Temperature Test Methods for Elastomeric Bridge Bearings. *Journal of Bridge Engineering*, 7(1), 50-56, 2002(a).
- [15] Yakut, A., Yura, J.A., Parameters Influencing Performance of Elastomeric Bearings at Low Temperatures. *Journal of Structural Engineering*, 128(8), 986-994., 2002(b).
- [16] Fuller, K.N.G., Gough, J., Thomas, A.G., The Effect of Low-Temperature Crystallization on The Mechanical Behavior of Rubber. *Journal of Polymer Science: Part B: Polymer Physics*, 42(11), 2181-2190, 2004.
- [17] Cardone, D., Gesualdi, G., Nigro, D., Effects of Air Temperature on The Cyclic Behavior of Elastomeric Seismic Isolators. *Bulletin of Earthquake Engineering*, 9(4), 1227-55, 2011.
- [18] Hasegawa, O., Shimoda, I., Ikenaga, M., Characteristic of Lead Rubber Bearing by Temperature. *Summaries of Technical Papers of Annual Meeting Architectural Institute of Japan*, B-2, Structures II, Structural Dynamics Nuclear Power Plants, Architectural Institute of Japan, pp: 511-512, 1997.
- [19] Cho, C.B, Kwahk, I.J., Kim, Y. J., An Experimental Study for The Shear Property and The Temperature Dependency of Seismic Isolation Bearings. *Journal of the Earthquake Engineering Society of Korea*, 12(1), 67-77, 2008.
- [20] Park, J.Y., Jang, K.S., Lee, H.P., Lee, Y.H., Kim, H., Experimental Study on The Temperature Dependency of Full-Scale Low Hardness Lead Rubber Bearing. *Journal of Computational Structural Engineering*, 25(6), 533-540, 2012.

- [21] Billah, M., Todorov, B., Effects of Subfreezing Temperature on The Seismic Response of Lead Rubber Bearing Isolated Bridge. *Soil Dynamics and Earthquake Engineering*, 126, 1-13, 2019.
- [22] Deng, P., Gan, Z., Hayashikawa, T., Matsumoto, T., Seismic Response of Highway Viaducts Equipped with Lead-Rubber Bearings Under Low Temperature. *Engineering Structures*, 209:110008, 2019.
- [23] Kalpakidis, I.V., Constantinou, M.C., Whittaker, A.S., Modeling Strength Degradation in Lead-Rubber Bearings Under Earthquake Shaking. *Earthquake Engineering and Structural Dynamics*, 39(13), 1533–49, 2010.
- [24] Ozdemir, G., Avsar, O. Bayhan, B., Change in Response of Bridges Isolated with LRBs Due to Lead Core Heating. *Soil Dynamics and Earthquake Engineering*, 31(7), 921-929, 2011.
- [25] Ozdemir, G., Dicleli, M., Effect of Lead Core Heating on The Seismic Performance of Bridges Isolated with LRB In Near-Fault Zones. *Earthquake Engineering and Structural Dynamics*, 41(14), 1989-2007, 2012.
- [26] Ozdemir, G., Lead Core Heating in LRBs Subjected to Bidirectional Ground Motion Excitations in Various Soil Types. *Earthquake Engineering and Structural Dynamics*, 43(2), 267-285, 2014.
- [27] Kumar, M., Whittaker, A.S., Constantinou, M.C., An Advanced Numerical Model of Elastomeric Seismic Isolation Bearings. *Earthquake Engineering and Structural Dynamics*, 43(13), 1955–1974, 2014.
- [28] Ozdemir, G., Bayhan, B., Gulkan, P., Variations in The Hysteretic Behavior of LRBs as a Function of Applied Loading. *Structural Engineering and Mechanics*, 67(1), 69-78, 2018.
- [29] Wang, H., Zheng, W.Z., Li, J., Gao, Y.Q., Effects of Temperature and Lead Core Heating on Response of Seismically Isolated Bridges Under Near-Fault Excitations. *Advances in Structural Engineering*, 22(14), 2966-2981, 2019.
- [30] Kalpakidis, I.V., Constantinou, M.C., Effects of Heating on The Behavior of Lead-Rubber Bearings. I: Theory. *Journal of Structural Engineering*, 135(12), 1440–1449, 2009a.
- [31] Kalpakidis, I.V., Constantinou, M.C., Effects of Heating on The Behavior of Lead-Rubber Bearings. II: Verification of Theory. *Journal of Structural Engineering*, 135(12), 1450–1461, 2009b.
- [32] Li, J., Ye, K., Jiang, Y.C., Thermal Effect on The Mechanical Behavior of Lead-Rubber Bearing. *Journal of Huazhong University of Science and Technology Urban Science*, 138(7), 867-876, 2009.
- [33] Guay, L.P. and Bouaanani, N., Assessment of low temperature exposure for design and evaluation of elastomeric bridge bearings and seismic isolators in Canada. *Canadian Journal of Civil Engineering*, 43(9), 851-863, 2016.
- [34] ISO (International Organization for Standardization). ISO 22762-1:2005: Elastomeric seismic-protection isolators – Part 1: Test methods, 2005.

- [35] OpenSees, Open System for Earthquake Engineering Simulation; Version: 2.1.0, University of California, Pacific Earthquake Engineering Research Center, Berkeley, California, 2001.
- [36] Berger/Abam Engineers, Inc. Federal Highway Administration Seismic Design Course, Design Example No.4, 1996. <https://ntrl.ntis.gov/NTRL/dashboard/searchResults/titleDetail/PB97142111.xhtml>
- [37] Warn, G.P., Whittaker, A.S., Performance Estimates in Seismically Isolated Bridge Structures. *Engineering Structures*, 26(9), 1261–78, 2004.
- [38] Dicleli, M., Performance of Seismic-Isolated Bridges in Relation to Near-Fault Ground-Motion and Isolator Characteristics. *Earthquake Spectra*, 22(4), 887-907, 2006.
- [39] Avşar, O., Ozdemir, G., Response of Seismic-Isolated Bridges in Relation to Intensity Measures of Ordinary and Pulselike Ground Motions. *Journal of Bridge Engineering*, 18(3), 250-260, 2013.
- [40] Park, Y.J., Wen, Y.K., Ang, A.H., Random Vibration of Hysteretic Systems Under Bi-Directional Ground Motions. *Earthquake Engineering and Structural Dynamics*, 14(4), 543-557, 1986.
- [41] Mokha, A.S., Constantinou, M.C., Reinhorn, A.M., Verification of Friction Model of Teflon Bearings Under Triaxial Load. *Journal of Structural Engineering (ASCE)*, 119(1), 240-261, 1993.
- [42] Pacific Earthquake Engineering Research (PEER) Center. Strong motion data base, 2012. Available from <https://ngawest2.berkeley.edu/>
- [43] QuakeManager, A software framework for ground motion record management selection, analysis and modification; Version:1.80. <https://www.eqsol.com/QuakeManager.html>
- [44] Warn, G.P., Whittaker, A.S., Property Modification Factors for Seismically Isolated Bridges. *Journal of Bridge Engineering*, 11(3), 371-377, 2006.
- [45] Imai, T., Satoh, T., Nishimura, T., Tanaka, H., Mitamura, H., The Performance Evaluations of Rubber Bearings for Bridges in Cold Districts. *Proceeding of Hokkaido Chapter of JSCE*, p. A-18, 2008.

# Comparing Performances of Machine Learning Techniques to Forecast Dispute Resolutions

Murat AYHAN<sup>1</sup>

Irem DIKMEN<sup>2</sup>

M. Talat BIRGONUL<sup>3</sup>

## ABSTRACT

This paper compares classification performances of machine learning (ML) techniques for forecasting dispute resolutions in construction projects, thereby mitigating the impacts of potential disputes. Findings revealed that resolution cost and duration, contractor type, dispute source, and occurrence of changes were the most influential factors on dispute resolution method (DRM) preferences. The promising accuracy of the majority voting classifier (89.44%) indicates that the proposed model can provide decision-support in identification of potential resolutions. Decision-makers can avoid unsatisfactory processes using these forecasts. This paper demonstrated the effectiveness of ML techniques in classification of DRMs, and the proposed prediction model outperformed previous studies.

**Keywords:** Construction disputes, dispute resolution methods, multiclass classification, dispute management.

## 1. INTRODUCTION

Encountering conflicts is almost inevitable in construction projects particularly due to the complex, fragmented, and dynamic nature of the construction industry along with involvement of numerous parties usually in an adversarial relationship [1]. In case the parties in a conflict cannot reach a satisfactory outcome, the conflict may progress into a dispute [2]. Awwad et al. [3] stated that the construction industry is exceptionally susceptible to conflicts and disputes, and these may often escalate to lawsuits. At the same time, a growth in the number and severity of construction disputes were reported by several researchers [3, 4, 5]. Moreover, construction disputes can be detrimental as they have the potential to disrupt the

---

Note:

- This paper was received on April 29, 2021 and accepted for publication by the Editorial Board on September 20, 2021.
- Discussions on this paper will be accepted by November 30, 2022.

• <https://doi.org/10.18400/tekderg.930076>

1 Gazi University, Civil Engineering Department, Ankara, Turkey  
muratayhan@gazi.edu.tr - <https://orcid.org/0000-0002-2011-4190>

2 Middle East Technical University, Civil Engineering Department, Ankara, Turkey  
idikmen@metu.edu.tr - <https://orcid.org/0000-0002-6988-7557>

3 Middle East Technical University, Civil Engineering Department, Ankara, Turkey  
birgonul@metu.edu.tr - <https://orcid.org/0000-0002-1638-2926>

workflow and lead to delayed schedules, budget overruns, poor communication, and damaged business relationships [6]. Therefore, it would be beneficial to avoid disputes; however, if the occurrence of disputes cannot be precluded, management personnel need to resolve them through various resolution processes [7]. Selecting an appropriate dispute resolution method (DRM) to resolve a dispute is crucially important as it paves the way for successful project completion [8]. However, management personnel have difficulties in reaching satisfactory outcomes out of disputed cases.

A best method that handles all disputes is not available as projects vary in scale, complexity, nature, and so forth [9]. Numerous interrelated factors should be considered to successfully manage disputes, making it a challenging decision-making problem. Contrarily, the construction industry relies on the experience and the level of knowledge of the decision-maker in such decisions [10]. On the other hand, a study on Turkish construction industry unveiled that the dispute management decision-making is characterized as an unconscious process, and the industry requires novel tools to overcome this deficit. It is also highlighted that there is a need for a more systematic approach to DRM selection instead of the industry's reliance on the current subjective approach [11].

The techniques available in the Artificial Intelligence (AI) domain has the potential to mitigate the subjectivity, which dominates dispute management decision-making, by providing systematical decision-support [8]. Solving an engineering problem via AI techniques involves learning from data while simulating underlying functional relationships that are difficult to rationalize, even if the interdependencies between inputs and outputs are unknown. Among various AI applications, machine learning (ML) domain focuses on developing systems capable of learning from data about a specific task automatically. It is possible to perform data classification tasks via ML techniques as these techniques can develop algorithms that utilize prespecified features to predict target labels [12].

This paper argues that appropriate DRM can be forecasted systematically, given the circumstances of the case, so that early-warnings of potential resolutions can be achieved. For this reason, ML techniques were utilized to develop classification models that forecast the occurrence of disputes and their potential resolutions, thereby mitigating the negative impacts of potential disputes. In Ayhan et al. [13], the effectiveness of ML techniques in early prediction of dispute occurrence was demonstrated, and promising classification accuracy results were obtained. This paper builds upon the work by Ayhan et al. [13] and applies multiclass classification techniques to forecast potential resolutions prior to dispute occurrence. For this reason, initially, the variables affecting dispute resolutions were identified by an extensive literature review, and the findings were used to develop a novel conceptual model that depicts the common factors influencing dispute resolutions. Considering that understanding the influential factors underlying a dispute determines the performance of a construction project [14], this conceptual model is the basis for the proposed study. Then, using the established conceptual model, past project data were collected via questionnaires with the decision-making authorities of the projects. Then, Chi-square tests of association were performed on the collected dataset to identify the relationships between the influential factors and DRMs. Based on the results of the Chi-square tests, the attributes, which were identified as statistically significantly associated with DRM preferences, were kept and remaining attributes were eliminated. This resulted in establishment of a classification model for forecasting dispute resolutions. The obtained classification model



was experimented via alternative ML techniques and classifier performances were evaluated by 10-times repeated 10-fold cross-validation.

## **2. RESEARCH BACKGROUND**

The main concern of the studies from the dispute resolution literature is avoiding ineffectual DRMs, which generally involve processes leading to settlement in courts [15]. In construction industry, litigation is the conventional method of providing involuntary and binding dispute resolution despite being costly and lengthy. Moreover, in many industries (i.e., Turkish construction industry) litigation is commonly used rather than seeking other resolutions despite the widespread dissatisfaction related to the litigation [14]. Arbitration was initially an inexpensive and efficient alternative to litigation; however, following the growing dissatisfaction, its categorization as an alternative dispute resolution (ADR) technique has been criticized [16]. Consequently, construction professionals resorted to ADR techniques due to their cost and time advantages, less adversarial nature, and lower legal requirements; indeed, common ADR techniques such as dispute review boards (DRB), mediation, and negotiation have gained popularity in the construction industry [7]. The disputed cases in this research's dataset were resolved through six different techniques as (1) litigation (LIT); (2) arbitration (ARB); (3) DRB; (4) mediation (MED); (5) senior executive appraisal (SEA); and (6) negotiation (NEG). Litigation and arbitration are considered as conventional DRMs, and the remaining methods are considered as ADR techniques. Technical and legal details of these techniques will exceed the scope of this paper.

A review of the literature reveals that researchers focused mainly on the most adopted DRMs in a specific region, or the implementation and potential advantages/disadvantages of specific DRMs [3]. For example, King et al. [17] conducted a questionnaire among experts in Malaysian construction industry to identify the most beneficial and resorted DRMs in terms of cost, time, and satisfaction. Focusing on Sri Lankan construction industry, Illankoon et al. [18] identified 15 dispute causes and 13 factors affecting DRM selection from the literature along with the most effective ADR method from perspectives of various parties in a project. Specific to disputes in Nepalese road construction projects, Kisi et al. [6] conducted surveys with experts to identify the preference frequencies of DRMs, so that various parties can comprehend the best practices related to a claim category. Sinha and Jha [19] identified the causes of commonly occurring disputes that are followed by litigation and causing delays in Public-Private-Partnership (PPP) road projects in India along with the causes leading to utilization of certain DRMs. The aforementioned studies provide valuable statistical frameworks and reflect current tendencies related to the DRM selection in various regions, rather than providing systematical decision-support systems for management personnel. On the other hand, AI applications can enable systematical selection of dispute resolutions and provide the necessary decision-support to obtain satisfactory outcomes [20].

Among studies that utilized AI techniques, Cheung et al. [8] developed a Case-Based Reasoning (CBR) model that retrieves similar dispute cases. Chen [21] proposed a model for construction professionals facing potential litigation from change order related disputes using the K-Nearest Neighbor (KNN) algorithm, and the model allows its users to select the most similar cases. Liu et al. [22] proposed a CBR system to extract experiences from past projects by retrieving similar cases. However, acting solely on similar cases may not be adequate

because characteristics of disputes and possible resolutions differentiate, and finding a matching case is rather difficult.

It is observed that the literature is rich in studies on construction litigation, and there is a specific interest on predicting the outcomes of litigated cases. For example, Chau [23] aimed to generate insights on how a construction claim would be resolved if litigation were preferred by using a Particle Swarm Optimization (PSO) based Artificial Neural Network (ANN) model, which achieved 80.00% accuracy. Chen and Hsu [24] proposed a model that identifies the potential litigation probability of a case via ANN classifier with 84.61% accuracy. Using the same dataset of litigated cases filed in Illinois courts, several ML based models were developed to predict the outcomes of court rulings including ANN [25], Boosted Decision Trees (BDT) [26], and two hybrid systems [27, 28] that achieved 66.67%, 89.59%, 91.15%, and 96.02% accuracy, respectively. Specific to disputes caused by differences in site conditions, Mahfouz et al. [29] reviewed the links between 15 legal factors and litigation outcomes using several ML techniques, which led to the highest accuracy of 88.00% from the Naïve Bayes (NB) model. Although the advantages of predicting the outcomes prior to litigation are evident such that a party can keep away from courts upon identification of an unfavorable result, the mentioned studies do not offer any alternatives to litigation.

There are some other studies that are not limited with litigation and aim to provide decision-support during resolutions. Chong and Zin [2] utilized factor analysis approach to analyze DRM selection rationale of the decision-makers in the Malaysian construction industry. Chaphalkar et al. [30] claimed that if disputed parties can forecast the outcome with some certainty, they may prefer settling before conventional DRMs to avoid expenses and aggravation. For this reason, they developed a Multilayer Perceptron (MLP) model by using 204 variation claim cases resolved through arbitration processes in India, and classified these cases as accepted, rejected, or partly accepted based on 16 factors affecting decisions of the arbitrators. Although the model was significantly successful, it only targeted variation claims and arbitration cases.

Among other efforts, several ML models were developed by using a dataset of 152 PPP projects undertaken in Taiwan, and these cases were classified based on 15 features about the project and the dispute. Initially, Chou [31] performed DRM classification using single and ensemble ML models at two distinct phases as (1) project initiation; and (2) in the aftermath of dispute occurrence. The following study by Chou et al. [10] combined the capabilities of fuzzy logic, genetic algorithm, and Support Vector Machines (SVM) to forecast DRM selection. Once again by using several ML techniques, Chou et al. [32] discovered rule sets for classification of possible dispute resolutions. These studies can successfully forecast DRMs; however, the dataset was composed solely of instances with a certain project delivery system (i.e., PPP) from a certain construction industry (i.e., Taiwan).

Therefore, this study applied ML techniques to forecast the potential resolutions prior to dispute occurrence. The multiclass classification performances were compared with each other to select the best performing classifier for identification of potential resolutions, so that construction professionals can avoid unsatisfactory resolution processes, which will reduce the unnecessary costs, delays, and aggravation caused by using inconclusive processes. Moreover, management personnel can take the necessary precautions beforehand, thanks to the early-warnings of the proposed model.

### 3. RESEARCH METHODOLOGY

The methodology for this research is visualized in Figure 1, which involves three steps as (1) development of the conceptual model; (2) development of the classification model; and (3) finalization of the classification model.

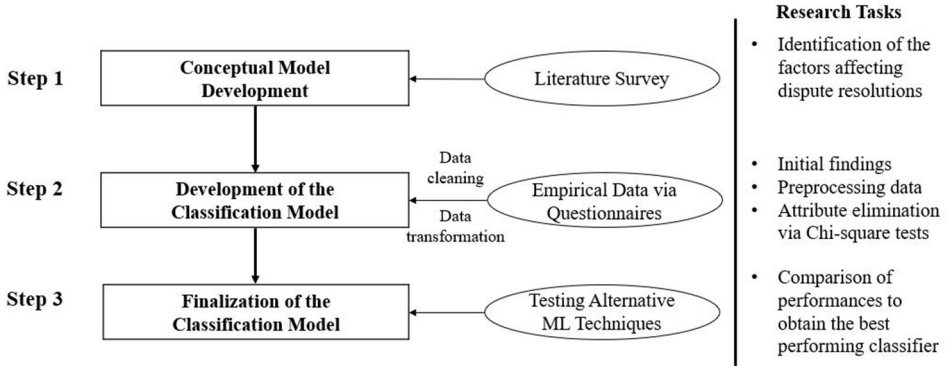


Figure 1 - Research methodology

#### 3.1. The Conceptual Model

Numerous factors affecting dispute resolutions were identified from the literature and the most frequently perceived ones were picked for use in the conceptual model. The findings revealed 42 frequently perceived attributes and these factors can be grouped in six categories as (1) project characteristics (i.e., contract value); (2) changes or unexpected events; (3) delays; (4) characteristics of the disputed case (i.e., disputed extension of time (EoT) amount); (5) DRM characteristics (i.e., resolution duration); and (6) knowledge level on the DRM. These categories were based on the findings of several research including (1) İltter [11] that identified 16 factors affecting the recommendations of the legal professionals in DRM selection; (2) Chou et al. [10] that identified project attributes impacting the utilized DRM; (3) Awwad et al. [3] that listed 12 factors affecting the choice of ADR; (4) Lee et al. [7] that related 29 factors with DRM selection.

The aforementioned six groups were utilized in categorization of the influential factors into a conceptual model. A thorough discussion on identification of the factors from the literature is available in Ayhan [33], which proposed conceptual models composed of variables affecting the dispute occurrence and their resolutions that led to development of two distinct classification models. These conceptual models are depicted in Figure 2. The first model classified dispute occurrence of construction projects as disputed and undisputed projects [13], which demonstrated the effectiveness of ML techniques in early prediction of dispute occurrence. The second model, which is the subject of this paper, applies multiclass classification techniques to forecast potential resolutions prior to dispute occurrence.

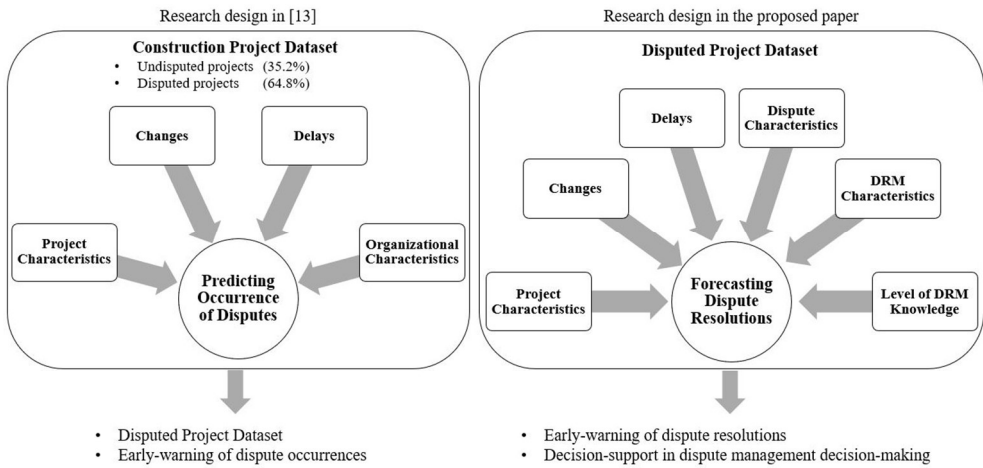


Figure 2 - The conceptual models

### 3.2. Development of the Classification Model

A questionnaire was prepared to collect past project data about the variables listed in the conceptual model. The questionnaire involved six distinct sections to collect (1) demographic information about the experts; (2) project specific information; (3) information to detect any variations or unexpected events during the course of the project; (4) dispute specific information; (5) information about the DRM characteristics; and (6) information about the level of knowledge of experts about certain DRMs. In section 5, participants were asked to rank the importance of DRM related features such as importance of preserving relationships, bindingness of the process, and so forth to understand what features the decision-makers consider during DRM selection. The questionnaire is available in the study by Ayhan [33].

Participants of the questionnaire raised their concerns in sharing disputed project data, and this was understandable considering the sensitive and confidential nature of dispute related data. Consequently, it was difficult to find participants willing to share such information. In order to overcome the difficulties in collecting dispute data, this study utilized a snowball sampling method.

The collected data was initially investigated, and noisy data was removed. Following the data cleansing, the next step was to understand the existence of associations among the variables because the effects of each attribute will be different. This research preferred to use Chi-square statistics, which a test of association among categorical variables [34]. Thus, at this point, the cleaned dataset was processed by converting numeric data to categories. The Chi-square analysis was performed by using the IBM SPSS Statistics, and this analysis enabled elimination of the attributes in the conceptual model that do not have a statistically significant association with dispute resolutions. As a result of attribute elimination, a simpler model for classification was obtained based on the collected dataset.

### 3.3. Finalizing the Classification Model

Alternative ML algorithms can be experimented on the developed classification model, and their performances can be compared to obtain the best classifier that will be proposed as the final classifier for forecasting dispute resolutions. The open-source WEKA 3.8.3. software was used for this purpose as it provides plenty of ready-to-use ML algorithms to its users. There is evidence in the literature that proves the software can generate stable results with equal or better performance compared with similar applications [35]. Moreover, rather than struggling with complicated computer codes, the optimization of algorithm hyperparameters can be conveniently performed via a simple graphical interface [36]. Therefore, WEKA can be confidently and easily used in data classification tasks in this research.

### 3.4. Machine Learning Techniques

The classification task in this research is a multiclass classification problem because the output is a multiple category variable. Due to differences in the characteristics of the data, an ML technique that can handle all data classification tasks do not exist [15]. To determine the best technique, the bias resulting from the ML algorithm should be coherent with the problem characteristics [36]. This can be achieved by experimenting promising single techniques on the dataset and comparing their performances with each other to select the best performer [27]. Therefore, this paper assessed the performances of several ML techniques.

The findings of a research identifying the top 10 data mining algorithms was the reference for the evaluated ML techniques in the proposed study [36]. Among the 10 algorithms, there were techniques for various purposes (i.e., data clustering); however, the task in this paper requires classification, and consequently, the classification algorithms were evaluated only. Apart from these algorithms, MLP was also tested because it is intensively preferred in construction domain. Within this context, the six ML techniques used in this paper are (1) NB; (2) KNN; (3) C4.5 Decision Tree (DT); (4) MLP; (5) Polynomial kernel SVM; and (6) Radial Basis Function (RBF) kernel SVM. The ML approach in this study is illustrated in Figure 3.

It should be noted that although there exists an enhanced release of C4.5 algorithm, called C5.0 algorithm, the researchers stucked with the C4.5 because it is freely available unlike the enhanced version. Moreover, it is revealed that C4.5 can still produce somehow equal or better performance compared with C5.0 [37, 38].

Binary classification capabilities of the ML algorithms may be extended for the multiclass problem in this research, except the SVM, which can only perform on binary tasks [39]. In the case of SVM algorithm, the problem should be decomposed into several binary classification tasks. WEKA supports four decomposition techniques as (1) one-vs-one (OvO); (2) one-vs-all (OvA); (3) random correction code (RCC); and (4) exhaustive correction code (ECC). In the OvA approach, for an output with  $k$  categories, there will be  $k$  binary classification tasks that aim to separate the instances belonging to a category from the combination of remaining categories, which will result in  $k$  classifiers [40]. Meanwhile, in the OvO technique, the instances belonging to a category are separated from only one other category. In other words, a classifier is trained to distinguish one class from another in a pairwise approach, which will result in  $k(k-1)/2$  classifiers [41]. In this training scheme, a voting strategy, which is based on each classifier's classification decision, makes the final

class assignment for a new instance [40]. Dietterich and Bakiri [42] proposed the error-correcting output codes (ECOC) method that decomposes a multiclass problem into a set of binary problems. In this decomposition, it is aimed to improve the classification performance by symbolizing each category of an output by bits of code words. WEKA has two extensions of the original ECOC, which are RCC and ECC. Although the ECC technique is more sophisticated than the RCC, an increment in the number of output categories causes an exponential growth in the number of classifiers to be generated in the ECC, which may result in infeasible solutions. In such cases, the RCC technique can be used where the only difference from the ECC is that there is randomization during the generation of the code word matrix at the beginning of operations [36]. In addition to solutions obtained from the ML techniques that can solve multiclass problems without using any further decomposition techniques, the multiclass problem in this research was solved by using the aforementioned decomposition techniques for all evaluated ML algorithms.

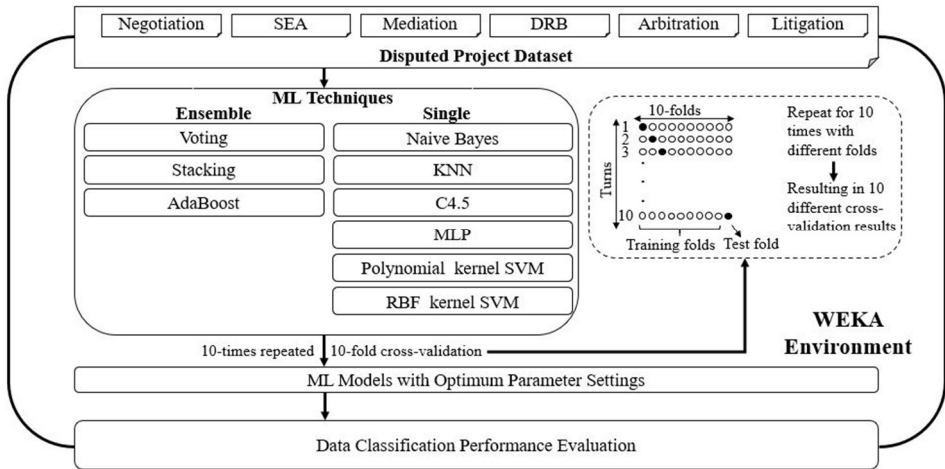


Figure 3 - The ML approach in this study

A convenient way to improve the performances of single ML techniques is to establish ensemble models that aim to compensate the errors in each single technique by synthesizing them [27]. In this paper, (1) voting; (2) stacked generalization; and (3) the AdaBoost algorithm were the techniques for ensemble model development. Voting is perceived as the easiest way of combining various classifiers [40], and due to this simplicity, it was utilized in this research. In voting, the class of an instance is the class that obtains the majority of the votes of the contained classifiers. However, when the minority decision is correct about the class of an instance, a misclassification problem may occur as the technique is not capable of determining which decision is the correct one. This shortcoming is addressed in stacking, where a meta-learner classifier is specifically trained to identify the reliable classifier (base-learner), and consequently, ensemble models obtained through stacking has the potential to perform better than voting [36]. The driving forces in developing ensemble models are (1) improving classification accuracy (as in stacking); (2) decreasing variance (as in bagging); and (3) decreasing bias (as in boosting). Unlike boosting where the next classifier is trained

on the misclassifications of the former classifier systematically, developing complementary classifiers is by chance in bagging [40]. Therefore, boosting was utilized in this research, and the AdaBoost algorithm was specifically preferred because it is commonly used, easy to implement, and adaptable to various ML techniques [36].

*Table 1 - Parameter configurations for the utilized ML techniques*

Algorithm	Parameter	Search Range
NB	No parameter optimization	-
KNN	k neighbors	1-50 (increment by 1)
	Distance measurement function	Chebyshev, Euclidean, Manhattan
	Distance weighting method	Equal, Inverse, Similarity
C4.5	Pruning	Yes, No
	Reduced error pruning	Yes, No
	Subtree raising	Yes, No
	Threshold factor for pruning	[0.01-0.50] (increment by 0.01)
	Lowest number of instances at leaves	[1-10] (increment by 1)
	Number of folds for pruning	[2-5] (increment by 1)
	Laplace counts at leaves	Yes, No
MLP	Number of hidden layers	0, 1, 2, (total number of inputs and outputs) / 2
	Epochs (cycles)	500, 1000
	Momentum	[0.1-0.9] (increment by 0.1)
	Learning rate	[0.1-0.9] (increment by 0.1)
Poly. SVM	Penalty parameter	$[2^{-2}-2^{15}]$ (increment exponentially by 1)
	Exponent	[1-10] (increment by 1)
RBF SVM	Penalty parameter	$[2^{-2}-2^{15}]$ (increment exponentially by 1)
	Gamma	$[2^{-15}-2^4]$ (increment exponentially by 1)
Voting	Combination rule	Majority Voting, Average of Probabilities

Table 1 - Parameter configurations for the utilized ML techniques (continue)

Algorithm	Parameter	Search Range
Stacking	Base-learner	Top 3 performing single classifiers in turns
	Meta-learner	Remaining 5 classifiers (excluding itself)
AdaBoost	Number of iterations	10
	Boosting mechanism	Resampling, Reweighting

Theoretical framework related to evaluated ML techniques exceeds the scope of this paper. However, it should be known that each ML technique has specific parameters that determines their success. Table 1 shows the parameters to be optimized for each algorithm, and the ranges to be searched. To determine the optimized value of a numeric parameter, there is a need to use a validation set or cross-validation method. WEKA has plenty of evaluators for this purpose such as cross-validated parameter selection and grid search.

#### 4. DATA COLLECTION AND DESCRIPTION

Initially, data about 151 construction projects were collected for this study. After removal of noisy and unrepresentative cases, there were 108 projects from 19 different countries. The data was collected by meetings with 78 experts individually, which represented 75 different companies. The participants were selected among professionals with decision-making authority. The average construction industry experience of the participants was 18 years, and 47.0% of them have worked for more than 15 years. Therefore, the opinions of experienced professionals were reflected in this study. Moreover, the dataset contained a broad array of projects to reflect the changes in the decision-making process to the research that result from varying characteristics of projects and disputes. In the dataset, it is observed that 38 projects were completed without any disputes (35.2%), while in 70 projects (64.8%), at least one disputed issue was experienced. These 70 disputed projects generated 82 distinct dispute cases, and the model was based on 54 dispute cases that the disputants reported satisfactory resolutions.

The attributes, their categories, and relative frequencies in the dataset are given in Table 2. This research used techniques such as Chi-square tests and NB algorithm that requires discrete data. Thus, all numeric attributes in the dataset were converted to categorical variables for computational purposes. This data transformation should be handled with care because the performance of the classification algorithm may be adversely affected if the distinctive features of the data are suppressed during discretization. With this consideration, WEKA provides an information gain-based supervised discretization method. In this method, discretization ranges can be defined based on the output so that the subjectivity during data conversion can be mitigated, and split points generating the maximum information gain can be determined so that the information loss can be diminished.



Table 2 - Attributes, categories, and relative frequencies

ID	Attribute	Categories and relative frequencies
PC1	Project location	Domestic (55.6%); International (44.4%)
PC2	Project value	< \$10 mil. (24.1%); \$10-\$100 mil. (35.2%); > \$100 mil. (40.7%)
PC3	Planned duration	< 1 year (14.8%); 1-2 years (31.5%); 2-3 years (25.9%); > 3 years (27.8%)
PC4	Type of construction	Housing (20.4%); Commercial (11.1%); Industrial (11.1%); Transportation (24.1%); Power plants/lines (3.7%); Medical (5.6%); Water supply/reservoir (7.4%); Sports, cultural and educational (9.3%); Public (5.6%); Soil works (1.9%)
PC5	Type of contractor	Single (79.6%); Joint venture (13.0%); Consortium (7.4%)
PC6	Type of employer	Public (46.3%); Private (40.7%); Public-Private-Partnership (13.0%)
PC7	Type of contract	Private (53.7%); Public procurement (14.8%); FIDIC red (20.4%); FIDIC silver/yellow (11.1%)
PC8	Payment method	Fixed (lump-sum) (46.3%); Unit price (53.7%)
PC9	Project delivery	Design-bid-build (63.0%); Design-build (18.5%); Engineering-procurement-construction (18.5%)
PC10	Design complexity	Very low (16.7%); Low (11.1%); Moderate (18.5%); High (35.2%); Very high (18.5%)
PC11	Construction complexity	Very low (9.3%); Low (13.0%); Moderate (14.8%); High (37.0%); Very high (25.9%)
C1	Changes	Yes (59.3%); No (40.7%)
D1	Delays (ratio)	0% (27.8%); 0%-20% (20.4%); 20%-40% (16.7%); > 40% (35.2%)
DC1	Disputant	Owner/employer (16.7%); Contractor (83.3%)
DC2	Phase	Construction (87.0%); Transfer/Repair/Maintenance (13.0%)
DC3	Dispute source	Cost of change orders (5.6%); Time & cost of change orders (31.5%); Measurement & valuation (11.1%); Delay in site handover (5.6%); Defects/errors/poor quality (11.1%); Imprudent contractor (11.1%); Late payments (5.6%); Errors/changes in quantities (7.4%); Site/soil investigation (9.3%); Interpretation of contract articles (1.9%)
DC4	Suspension of works	Yes (61.1%); No (38.9%)
DC5	Disputed amount	< 5 mil. \$ (44.4%); 5-25 mil. \$ (27.8%); 25-75 mil. \$ (14.8%); > 75 mil. \$ (13.0%)
DC6	Settled amount	\$0 (6.3%); < \$1 mil. (31.3%); \$1-\$5 mil. (31.3%); \$5-\$25 mil. (16.7%); > \$25 mil. (14.6%)
DC7	Success rate	0% (1.9%); 0%-25% (1.9%); 25%-50% (25.9%); 50%-75% (35.2%); > 75% (35.2%)
DC8	EoT claim occurrence	Yes (51.9%); No (48.1%)
DC9	Disputed EoT amount	0 days (51.9%); 0-6 months (18.5%); 6 months-1 year (11.1%); > 1 year (18.5%)
DC10	Settled EoT amount	0 days (53.7%); 0-6 months (16.7%); 6 months-1 year (14.8%); > 1 year (14.8%)
DC11	Success rate (EoT)	0% (53.7%); 0%-25% (0.0%); 25%-50% (0.0%); 50%-75% (7.4%); > 75% (38.9%)

Table 2 - Attributes, categories, and relative frequencies (continued)

ID	Attribute	Categories and relative frequencies
DRMC1	Resolution cost	\$0 (53.7%); < \$100k (9.3%); \$100k-\$350k (13.0%); \$350k-\$1 mil. (14.8%); > \$1 mil. (9.3%)
DRMC2	Resolution duration	< 2 weeks (20.4%); 2-4 weeks (18.5%); 1-3 months (29.6%); 3-6 months (3.7%); 0.5-2.5 years (14.8%); > 2.5 years (13.0%)
DRMC3	Preserving relationships	Rank-1 (33.3%); Rank-2 (5.6%); Rank-3 (5.6%); Rank-4 (7.4%); Rank-5 (16.7%); Rank-6 (9.3%); Rank-7 (5.6%); Rank-8 (0.0%); Rank-9 (5.6%); Rank-10 (11.1%)
DRMC4	Speed of process	Rank-1 (22.2%); Rank-2 (20.4%); Rank-3 (11.1%); Rank-4 (22.2%); Rank-5 (5.6%); Rank-6 (5.6%); Rank-7 (9.3%); Rank-8 (3.7%); Rank-9 (0.0%); Rank-10 (0.0%)
DRMC5	Cost of process	Rank-1 (9.3%); Rank-2 (14.8%); Rank-3 (16.7%); Rank-4 (16.7%); Rank-5 (5.6%); Rank-6 (5.6%); Rank-7 (16.7%); Rank-8 (11.1%); Rank-9 (3.7%); Rank-10 (0.0%)
DRMC6	Bindingness	Rank-1 (0.0%); Rank-2 (9.3%); Rank-3 (9.3%); Rank-4 (3.7%); Rank-5 (14.8%); Rank-6 (20.4%); Rank-7 (7.4%); Rank-8 (18.5%); Rank-9 (14.8%); Rank-10 (1.9%)
DRMC7	Confidentiality	Rank-1 (1.9%); Rank-2 (3.7%); Rank-3 (3.7%); Rank-4 (3.7%); Rank-5 (0.0%); Rank-6 (13.0%); Rank-7 (5.6%); Rank-8 (5.6%); Rank-9 (20.4%); Rank-10 (42.6%)
DRMC8	Fairness	Rank-1 (22.2%); Rank-2 (13.0%); Rank-3 (7.4%); Rank-4 (9.3%); Rank-5 (1.9%); Rank-6 (7.4%); Rank-7 (16.7%); Rank-8 (5.6%); Rank-9 (9.3%); Rank-10 (7.4%)
DRMC9	Flexibility in procedures	Rank-1 (1.9%); Rank-2 (1.9%); Rank-3 (16.7%); Rank-4 (13.0%); Rank-5 (11.1%); Rank-6 (5.6%); Rank-7 (14.8%); Rank-8 (18.5%); Rank-9 (7.4%); Rank-10 (9.3%)
DRMC10	Control over the process	Rank-1 (0.0%); Rank-2 (3.7%); Rank-3 (7.4%); Rank-4 (3.7%); Rank-5 (14.8%); Rank-6 (16.7%); Rank-7 (13.0%); Rank-8 (16.7%); Rank-9 (13.0%); Rank-10 (11.1%)
DRMC11	Reaching remedying solutions	Rank-1 (3.7%); Rank-2 (16.7%); Rank-3 (1.9%); Rank-4 (14.8%); Rank-5 (20.4%); Rank-6 (11.1%); Rank-7 (9.3%); Rank-8 (9.3%); Rank-9 (11.1%); Rank-10 (1.9%)
DRMC12	Willingness in reaching solutions	Rank-1 (5.6%); Rank-2 (11.1%); Rank-3 (20.4%); Rank-4 (5.6%); Rank-5 (9.3%); Rank-6 (5.6%); Rank-7 (1.9%); Rank-8 (11.1%); Rank-9 (14.8%); Rank-10 (14.8%)
K1	Litigation knowledge	Very low (7.4%); Low (11.1%); Moderate (16.7%); High (33.3%); Very high (31.5%)
K2	Arbitration knowledge	Very low (11.1%); Low (13.0%); Moderate (18.5%); High (38.9%); Very high (18.5%)
K3	DRB knowledge	Very low (25.9%); Low (5.6%); Moderate (20.4%); High (20.4%); Very high (27.8%)
K4	Mediation knowledge	Very low (5.6%); Low (5.6%); Moderate (18.5%); High (31.5%); Very high (38.9%)
K5	SEA knowledge	Very low (3.7%); Low (5.6%); Moderate (11.1%); High (20.4%); Very high (59.3%)
K6	Negotiation knowledge	Very low (0.0%); Low (1.9%); Moderate (5.6%); High (40.7%); Very high (51.9%)

## 5. RESULTS OF THE CHI-SQUARE TESTS

Table 3 - Results of Chi-square tests for attribute elimination

Identifier	Attribute	p-value	Selected for final model
PC1	Project location	0.236	NO
PC2	Project value	0.349	NO
PC3	Planned duration	0.221	NO
PC4	Type of construction	0.131	NO
PC5	Type of contractor	<b>0.003</b>	<b>YES</b>
PC6	Type of employer	0.581	NO
PC7	Type of contract	0.540	NO
PC8	Payment method	0.354	NO
PC9	Project delivery system	0.172	NO
PC10	Level of design complexity	0.601	NO
PC11	Level of construction complexity	0.342	NO
C1	Changes	<b>0.018</b>	<b>YES</b>
D1	Delays (ratio)	0.088	NO
DC1	Disputant	0.390	NO
DC2	Phase	0.406	NO
DC3	Dispute source	<b>0.014</b>	<b>YES</b>
DC4	Suspension of works	0.778	NO
DC5	Disputed amount	0.485	NO
DC6	Settled amount	0.668	NO
DC7	Success rate	0.910	NO
DC8	EoT claim occurrence	0.202	NO
DC9	Disputed EoT amount	0.976	NO
DC10	Settled EoT amount	0.709	NO
DC11	Success rate (EoT)	0.129	NO
DRMC1	Resolution cost	<b>0.000</b>	<b>YES</b>
DRMC2	Resolution duration	<b>0.000</b>	<b>YES</b>
DRMC3	Importance of preserving relationships	0.943	NO
DRMC4	Importance of speed of process	0.823	NO
DRMC5	Importance of cost of process	0.687	NO
DRMC6	Importance of bindingness	0.571	NO
DRMC7	Importance of confidentiality	0.521	NO

Table 3 - Results of Chi-square tests for attribute elimination (continue)

Identifier	Attribute	p-value	Selected for final model
DRMC8	Importance of fairness	0.069	NO
DRMC9	Importance of flexibility in procedures	0.308	NO
DRMC10	Importance of control over the process	0.468	NO
DRMC11	Importance of reaching remedying solutions	0.387	NO
DRMC12	Importance of willingness in reaching solutions	0.759	NO
K1	Knowledge level on litigation	<b>0.005</b>	<b>YES</b>
K2	Knowledge level on arbitration	<b>0.016</b>	<b>YES</b>
K3	Knowledge level on DRB	0.699	NO
K4	Knowledge level on mediation	0.480	NO
K5	Knowledge level on SEA	0.899	NO
K6	Knowledge level on negotiation	0.876	NO

Presence of insignificant attributes in the model causes an adverse impact on the performance of ML techniques and eliminating these attributes can improve the generalization performance [27]. Among attribute elimination techniques, Chi-square tests, which provide a practical method for revealing the relationships among categorical variables, was found to be suitable for this study’s dataset due to its capabilities in handling attributes with multiple categories and diverse data distributions, unlike other alternative techniques [43]. Although the existence of association between variables can be identified by using this method, the strength of the association cannot be determined. Fortunately, association’s strength can be detected among nominal variables by Cramer’s V measure and among ordinals by Somers’ d measure, where both measures can handle input and output variables with unequal numbers of categories [34].

Chi-square results were tabulated in Table 3 with their corresponding exact probability values (p-values). The p-value of a nominal variable was calculated by using the exact Pearson Chi-square statistics, while the p-value of an ordinal variable was calculated by using the Mantel-Haenszel linear association test. The p-values were evaluated using 95% confidence interval (CI) such that attributes were either eliminated from (p-value > 0.005) or selected for (p-value ≤ 0.005) the classification model. Chi-square results showed that statistical significance of the association with dispute resolutions can be proved in only seven attributes. Figure 4 shows the established classification model with seven attributes.

Table 4 is the contingency table showing Chi-square test results for the selected attributes in the classification model along with the strength of association values. For Cramer’s V values exceeding 0.25, there exists a very strong association between input and output variables [44]. Among nominal attributes, all three selected attributes (PC5, C1, and DC3) had a very

strong association with dispute resolutions. Without considering the signs in front of the value, Somers' d values exceeding 0.10 imply partially strong relationship, and values exceeding 0.40 imply a strong relationship [45]. Thus, DRMC1 and DRMC2 had strong association with dispute resolutions, while K1 and K2 had partially strong association.

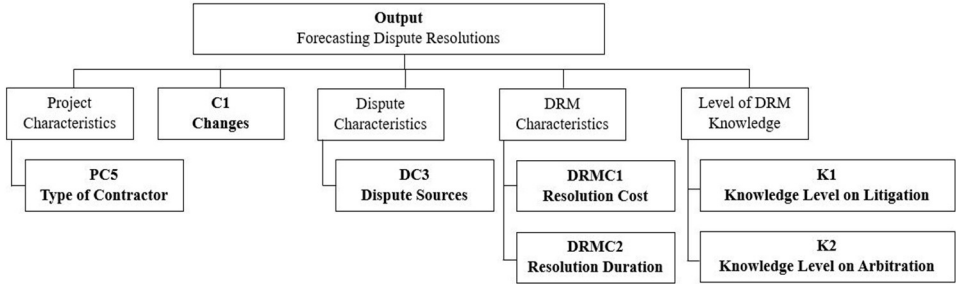


Figure 4 - The attributes in the classification model

Table 4 - Contingency table and strength of association values for the selected attributes

Attribute	Categories	Resolution method (Relative frequency (%))						Association Strength
		LIT	ARB	DRB	MED	SEA	NEG	
PC5 Type of contractor	Single	18.6	11.6	2.3	9.3	18.6	39.5	Cramer'sV 0.514
	JV	0.0	0.0	57.1	14.3	0.0	28.6	
	Consortium	25.0	25.0	0.0	0.0	50.0	0.0	
C1 Changes	Yes	6.3	18.8	9.4	12.5	25.0	28.1	Cramer'sV 0.491
	No	31.8	0.0	9.1	4.5	9.1	45.5	
DC3 Dispute source	Source 1	0.0	0.0	0.0	0.0	66.7	33.3	Cramer'sV 0.498
	Source 2	5.9	23.5	5.9	17.6	23.5	23.5	
	Source 3	50.0	0.0	16.7	0.0	33.3	0.0	
	Source 4	0.0	0.0	0.0	0.0	0.0	100.0	
	Source 5	33.3	0.0	0.0	16.7	0.0	50.0	
	Source 6	16.7	0.0	0.0	0.0	0.0	83.3	
	Source 7	33.3	0.0	0.0	0.0	33.3	33.3	
	Source 8	0.0	25.0	75.0	0.0	0.0	0.0	
	Source 9	20.0	20.0	0.0	20.0	0.0	40.0	
	Source 10	0.0	0.0	0.0	0.0	100.0	0.0	
DRMC1 Resolution cost	\$0	0.0	0.0	0.0	0.0	34.5	65.5	Somers' d -0.909
	\$0-\$100k	0.0	0.0	0.0	100.0	0.0	0.0	
	\$100k-\$350k	28.6	0.0	71.4	0.0	0.0	0.0	
	\$350k-\$1mil.	62.5	37.5	0.0	0.0	0.0	0.0	
	> \$1 mil.	40.0	60.0	0.0	0.0	0.0	0.0	

Table 4 - Contingency table and strength of association values for the selected attributes (continue)

Attribute	Categories	Resolution method (Relative frequency (%))						Association Strength
		LIT	ARB	DRB	MED	SEA	NEG	
DRMC2 Resolution duration	< 2 weeks	0.0	0.0	0.0	36.4	0.0	63.6	Somers' d -0.667
	2-4 weeks	0.0	0.0	0.0	10.0	10.0	80.0	
	1-3 months	0.0	0.0	31.3	0.0	43.8	25.0	
	3-6 months	0.0	0.0	0.0	0.0	100.0	0.0	
	0.5-2.5 years	25.0	75.0	0.0	0.0	0.0	0.0	
> 2.5 years	100.0	0.0	0.0	0.0	0.0	0.0		
K1 Litigation knowledge	Very low	0.0	0.0	0.0	0.0	50.0	50.0	Somers' d -0.309
	Low	0.0	0.0	16.7	0.0	16.7	66.7	
	Moderate	11.1	22.2	0.0	11.1	22.2	33.3	
	High	16.7	11.1	5.6	11.1	16.7	38.9	
	Very High	29.4	11.8	17.6	11.8	11.8	17.6	
K2 Arbitration knowledge	Very low	16.7	0.0	0.0	0.0	16.7	66.7	Somers' d -0.283
	Low	0.0	0.0	14.3	0.0	42.9	42.9	
	Moderate	40.0	0.0	0.0	10.0	10.0	40.0	
	High	4.8	19.0	4.8	19.0	19.0	33.3	
	Very High	30.0	20.0	30.0	0.0	10.0	10.0	

## 6. DATA CLASSIFICATION TESTS USING ML TECHNIQUES

In cases where the number of samples is limited, it is reasonable not to allocate instances to distinct sets for training, validation, and testing. Instead, all instances can be used for extracting knowledge to avoid loss of information in an already limited dataset. This can be achieved by cross-validation (CV), which aims to use all instances for training purposes, and then, the accuracy is obtained by resampling the dataset [46]. The *k*-fold CV is a commonly used version that is based on training and testing the model *k*-times randomly on different subsets of training data to generate an estimate of the performance of a classifier on new data [40]. The optimum value for *k* is put forth as 10 based on trials with diverse datasets and algorithms [20]. To avoid uneven representation among folds, stratification is used during resampling. Moreover, to decrease the high variance in CV results, the process was repeated 10 times and the final accuracy value is determined by averaging the results from each process [46]. Within this context, stratified 10-fold CV was utilized in this research by repeating the process 10 times.

Table 5 tabulates the outcomes from the 10-times repeated 10-fold CV analysis of the evaluated single ML techniques. All algorithms generated their best average classification results when ECC decomposition technique was used. The most successful classifiers are C4.5, NB, and MLP with 86.48%, 85.93%, and 83.33% average classification accuracy, respectively.

*Table 5 - 10-times repeated 10-fold CV performance of single classifiers*

Algorithm	Average Accuracy (%)	%95 CI Average Accuracy (%)
NB ECC	85.93	[84.50-87.35]
KNN ECC	74.63	[72.46-76.80]
C4.5 ECC	86.48	[85.08-87.88]
MLP ECC	83.33	[80.54-86.13]
Polynomial Kernel SVM ECC	82.04	[79.17-84.90]
RBF kernel SVM ECC	80.93	[79.84-82.02]

The top three algorithms are used as candidates during development of the ensemble classifiers. In voting, the ensemble classifier synthesized the classification decisions of these three algorithms. In stacking, two algorithms are merged as base-learner and meta-learner, where the learning process was performed on the complete dataset for base-learner, but the meta-learner can only access to the instances that are not misclassified by the base-learner. In this research, the aforementioned top three algorithms are used as base-learners in turns, and meta-learners were the remaining five techniques in turns, excluding the technique used as base-learner. Such an approach was preferred to avoid using classifiers of the same type during stacking [40]. This process brings out 15 stacked classifiers. The AdaBoost algorithm aims to transform weakly performing classifiers into successful ones and all six of the evaluated ML techniques are boosted via AdaBoost algorithm.

Although it is expected that ensemble models would improve the classification accuracy, they did not improve the performance at all times. Table 6 tabulates the outcomes from the 10-times repeated 10-fold CV analysis of the ensemble classifiers that performed better than their single counterparts. The stacked classifier combining C4.5 ECC and NB ECC classifiers achieved 86.67% average accuracy, while boosting of C4.5 ECC classifier by the AdaBoost algorithm generated 88.15% average accuracy. The most outstanding classification performance belonged to the classifier, which was generated by using the majority voting technique, and 89.44% average classification accuracy was achieved.

*Table 6 - 10-times repeated 10-fold CV performance of ensemble classifiers*

Algorithm	Average Accuracy (%)	%95 CI Average Accuracy (%)
Majority voting	89.44	[87.37-91.52]
Stacking: C4.5 ECC + NB ECC	86.67	[85.04-88.30]
AdaBoost: C4.5 ECC	88.15	[85.34-90.95]

## **7. DISCUSSION OF FINDINGS**

Among PC attributes, the only selected attribute was the type of contractor (PC5). In this dataset, it is observed that when the contractor is a consortium, in 50.0% of the cases, they resorted to conventional DRMs. Meanwhile, when the contractor is a joint-venture (JV), conventional DRMs were never used and instead, DRB was the most common technique for resolution, which was used in 57.1% of the cases. This is in line with the study by Lingard et al. [47], which stated that when the participating firms remain as independent entities that do not have joint liability (i.e., consortium), it is possible for one company to gain while the other suffers; therefore, it is more likely to use conventional DRMs that fit to this nature. On the other hand, JVs have joint liability so that both rewards and penalties are shared among the participating companies. Considering that settling through ADR processes can generate win-win results unlike the conventional DRMs that declare a winner and a loser [16], it is more likely for JVs to resolve their disputes through ADR methods. Among eliminated PC attributes, considering that DRM is specified prior to dispute occurrence via contract documents, it was interesting that the type of contract (PC7) was not significantly associated. This is because parties prefer using alternative DRMs that are not specified in the contract with the aim of using the method that best suits their needs (i.e., via addendum to contract).

The occurrence of changes (C1) during the execution of a construction project was found to be an influential factor on DRM selection. Indeed, there is supporting evidence in the literature stating that the occurrence of changes is a common problem in the construction industry that can trigger problems during the execution of a construction project such as cost and time related conflicts [48]. In this study's dataset, it is revealed that the disputes resulting from occurrence of changes are resolved through ADR techniques mostly (75%). Considering that most disputes resulting from changes end up in courts [48], the proposed classification model can offer alternative and efficient ways to decision-makers for resolution rather than resorting to court involved unsatisfactory processes immediately.

Among DC attributes, the only selected attribute was the dispute source (DC3). The association of dispute sources with DRM preferences was also considered as an influential factor in other similar models in the literature [10, 31].

Among DRMC attributes, resolution cost (DRMC1) and duration (DRMC2) were the most influential attributes in the classification model with the highest strength of association values. Other DRMC attributes that reflected 10 different features of DRMs were ranked based on their importance; however, none of them were in the final model. This shows that experts based their DRM preferences mainly on the cost and the time they are willing to allocate. This was an expected outcome. For example, in the study of Cheung and Suen [9] that developed a multi-attribute utility theory model for resolution strategy selection, the highest utility factors were obtained from resolution duration and cost among all DRM selection criteria. Similarly, Illankoon et al. [18] identified time to reach a settlement as the most influential factor during DRM selection.

Among K attributes, K1 and K2, which represent the knowledge level of the decision-maker on litigation and arbitration, were in the classification model. In other words, the experience of the experts with litigation and arbitration shapes their DRM preferences. It is observed that litigation preference is increasing with the increasing level of knowledge on litigation. This



is also valid for arbitration process. This reveals that experts that feel competent in litigation and/or arbitration prefer using these techniques over ADR methods.

The experiments revealed that C4.5, NB, and MLP are the three-best single ML classifiers (when ECC decomposition technique is used) for the dataset in question, which generated average accuracy values of 86.48%, 85.93%, and 83.33%, respectively. Consequently, it is evident that the C4.5 classifier outperformed the competing classifiers in this research. The superiority of DT was expected as it provides an effective structure in which alternative decisions can be evaluated when complex information with several variables should be considered [26].

Following the experiments with single ML techniques, ensemble classifiers were developed to enhance the classification performance. It is experimentally revealed that the majority voting technique, which synthesized the classification decisions of the three top performing single classifiers, produced the highest average classification accuracy value as 89.44%. Therefore, the final classification model for forecasting dispute resolutions is the majority voting classifier. Classification accuracies of the compared single and ensemble classifiers were visualized in Figure 5.

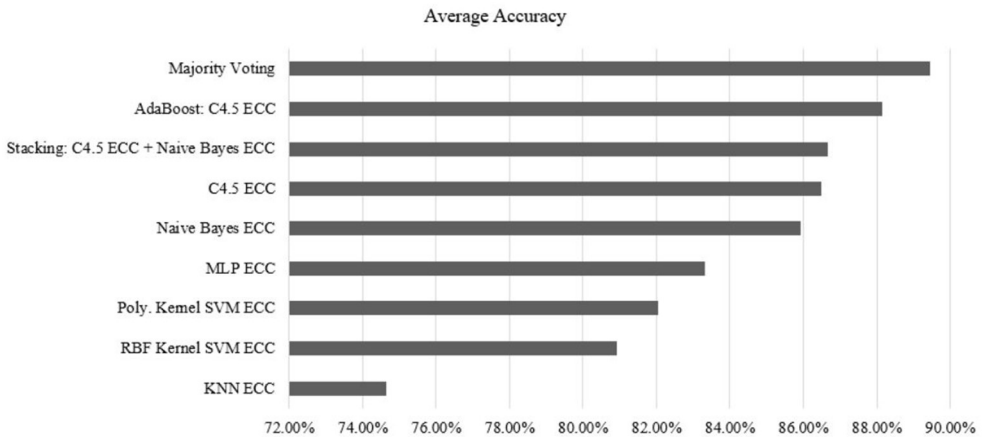


Figure 5 - Classification accuracies of the classifiers

Besides voting, 15 stacked classifiers were developed. Theoretically, when the classifiers that constitute the stacked classifier are diverse algorithms and their classification accuracies are high, the resultant ensemble model is expected to outperform the constituent classifiers [40]. However, this was not the case in many stacking trials. In this research, the most successful stacked classifier was developed by combining C4.5 ECC and NB ECC classifiers that achieved 86.15% average accuracy. A similar case was also observed for the classifiers boosted by the AdaBoost algorithm as some boosted classifiers showed weak performances. Theoretically, when the complexity of the single classifiers is high with respect to the amount of training instances, the outcome of the boosting is expected to be unsatisfactory [36]. The most successful AdaBoost model was obtained from boosting the C4.5 ECC classifier that resulted in an average accuracy value of 88.15%. In summary, the boosted classifier

improved the base-learner (C4.5) performance by 1.67%, while the stacked classifier improved the base-learner (C4.5) by 0.19% and the meta-learner (NB) by 0.74%.

Among limited empirical research on forecasting dispute resolutions, Chou [31] achieved 83.82% test set accuracy during project initiation phase, and 69.05% test set accuracy in the aftermath of dispute occurrence. On the other hand, the ensemble models in the same study enhanced the accuracy on the test set during project initiation phase by achieving 84.65% accuracy. In Chou et al. [10], based on 10-fold CV results on the test set, an average accuracy of 61.75% was obtained from single SVM classifiers for DRM classification. This performance was improved by combining SVM with genetic algorithm and fuzzy logic to achieve 77.04% average 10-fold CV accuracy for the test set. In Chou et al. [32], the best average 10-fold CV result was obtained as 81.12% through SVM. Benchmarking these, it is evident that the performance of the proposed classification model is higher, and the results are encouraging.

During identification of the factors affecting dispute resolutions, it is observed that numerous subjective factors are effectual. Thus, the main limitation of this research is its dependence to subjective judgments of participating experts. Scarcity of sample projects is one other constraint. Even though the collected sample of construction projects is representative, the sample size is nonetheless limited because of the difficulties in acquiring such sensitive information. The sample size can be enlarged to improve the generalization of the presented model. However, it should be noted that such data scarcity problems were also encountered in other research since historical data is scarce in nature for construction industry [49]. Finally, although various ML techniques were compared in this study, the extent of the experimented techniques were limited and considerable classification techniques, which might offer potential improvements in the accuracy, were not evaluated in this research, that can be done as further research.

## **8. CONCLUDING REMARKS**

In this research, dispute resolutions were forecasted by using alternative ML techniques, which included multiclass classification and ensemble models. A novel conceptual model was developed to identify the factors affecting dispute resolutions, and it is revealed that prediction models can be developed to provide decision-support that rely on the attributes in the conceptual model. The conceptual model can effectively guide decision-makers by highlighting factors to be considered during resolutions.

For construction professionals, the early-warnings of potential resolutions provided by the proposed model can enable avoiding the unnecessary costs, delays, and aggravation caused by using inconclusive resolution processes. The proposed model can help to reveal whether a selected DRM was appropriate or not, which may lead the decision-maker, upon identification of an inconclusive DRM, to settlement before deciding to implement certain resolution processes. For example, negotiation is generally the first choice in settling disputes, but if it is not the appropriate process for resolution, it would cause waste of time and money without reaching satisfactory outcomes. In such cases, the proposed model can be used to inform the users whether to give up negotiations, and resort to other DRMs.

In this research, the performances of various classifiers were compared with each other, and C4.5, NB, and MLP classifiers produced outstanding average classification accuracies of 86.48%, 85.93%, and 83.33% respectively, when the problem was decomposed into binary classification tasks using ECC decomposition technique. Moreover, three ensemble classifiers outperformed the single techniques. The first ensemble classifier was developed by stacking, which combined C4.5 ECC and NB ECC classifiers, and it achieved 86.67% average accuracy. The second one was developed by using AdaBoost algorithm on C4.5 ECC classifier, which achieved 88.15% average accuracy. The highest value was obtained as 89.44% from the majority voting model, which combined performances of C4.5, NB, and MLP classifiers. Therefore, the effectiveness of ML techniques in classification of DRMs has been demonstrated, and specifically, it is revealed that an appropriate combination of ML classifiers can further improve the classification performance. Moreover, the classification accuracy of the proposed prediction model outperformed previous studies.

Future work can focus on mitigation of data scarcity both by expanding the sample size, and by integrating the classification models with soft computing approaches. The improvement due to the proposed decision-support approach can be tested on other classification problems in construction management domain as a further study. Moreover, further improvement in classification accuracy can be pursued by using other classification techniques such as Random Forests and so forth.

### **References**

- [1] Alaloul, W. S., Hasaniyah, M. W., Tayeh, B. A., A Comprehensive Review of Disputes Prevention and Resolution in Construction Projects. 2nd Conference for Civil Engineering Research Networks, Bandung, Indonesia, 2019.
- [2] Chong, H. Y., Zin, R. M., Selection of Dispute Resolution Methods: Factor Analysis Approach. *Engineering Construction and Architectural Management*, 19(4), 428–443, 2012.
- [3] Awwad, R., Barakat, B., Menassa, C., Understanding Dispute Resolution in the Middle East Region from Perspectives of Different Stakeholders. *Journal of Management in Engineering*, 32(6), 2016.
- [4] Parikh, D., Joshi, G. J., Patel, D.A., Development of Prediction Models for Claim Cause Analyses in Highway Projects. *Journal of Legal Affairs and Dispute Resolution in Engineering and Construction*, 11(4), 2019.
- [5] Ustuner, Y. A., Tas, E., An Examination of the Mediation Processes of International ADR Institutions and Evaluation of the Turkish Construction Professionals' Perspectives on Mediation. *Eurasian Journal of Social Sciences*, 7(4), 11–27, 2019.
- [6] Kisi, K. P., Lee, N., Kayastha, R., Kovel, J., Alternative Dispute Resolution Practices in International Road Construction Contracts. *Journal of Legal Affairs and Dispute Resolution in Engineering and Construction*, 12(2), 2020.
- [7] Lee, C. K., Yiu, T. W., Cheung, S.O., Selection and Use of Alternative Dispute Resolution (ADR) in Construction Projects - Past and Future Research. *International Journal of Project Management*, 34(3), 494–507, 2016.

- [8] Cheung, S. O., Au-Yeung, R. F., Wong, V. W. K., A CBR Based Dispute Resolution Process Selection System. *International Journal of IT in Architecture Engineering and Construction*, 2(2), 129-145, 2004.
- [9] Cheung, S. O., Suen, H. C. H., A Multi-Attribute Utility Model for Dispute Resolution Strategy Selection. *Construction Management and Economics*, 20(7), 557–568, 2002.
- [10] Chou, J. S., Cheng, M. Y., Wu, Y. W., Improving Classification Accuracy of Project Dispute Resolution using Hybrid Artificial Intelligence and Support Vector Machine Models. *Expert Systems with Applications*, 40(6), 2263–2274, 2013.
- [11] İlt r, D., Opinions of Legal Professionals Regarding the Selection of Appropriate Resolution Method in Construction Disputes. *RICS COBRA Annual Construction Building and Real Estate Research Conference*, Paris, France, 2010.
- [12] Siam, A., Ezzeldin, M., El-Dakhakhni, W., Machine Learning Algorithms for Structural Performance Classifications and Predictions: Application to Reinforced Masonry Shear Walls. *Structures*, 22, 252–265, 2019.
- [13] Ayhan, M., Dikmen, I., Birgonul, M. T., Predicting the Occurrence of Construction Disputes using Machine Learning Techniques. *Journal of Construction Engineering and Management*, 147(4), 2021.
- [14]  evikbař, M., K ksal, A., An Investigation of Litigation Process in Construction Industry in Turkey, *Teknik Dergi*, 29(6), 8715–8729, 2018.
- [15] Pulket, T., Arditi, D., Construction Litigation Prediction System using Ant Colony Optimization. *Construction Management and Economics*, 27(3), 241–251, 2009.
- [16] Harmon, K. M. J., Resolution of Construction Disputes: A Review of Current Methodologies. *Leadership and Management in Engineering*, 3(4), 187–201, 2003.
- [17] King, L. S., Kamarazaly, M. A. H., Hashim, N., Yaakob, A. M., Man, N.H., Analysis on the Issues of Construction Disputes and the Ideal Dispute Resolution Method. *Malaysian Construction Research Journal*, 7(2), 153–165, 2019.
- [18] Illankoon, I. M. C. S., Tam, W. V. Y., Le, N. K., Ranadewa, K. A. T. O., Causes of Disputes, Factors Affecting Dispute Resolution and Effective Alternative Dispute Resolution for Sri Lankan Construction Industry. *International Journal of Construction Management*, 1–11, 2019.
- [19] Sinha, A. K., Jha, K. N., Dispute Resolution and Litigation in PPP Road Projects: Evidence from Select Cases. *Journal of Legal Affairs and Dispute Resolution in Engineering and Construction*, 12(1), 2020.
- [20] Chou, J. S., Cheng, M. Y., Wu, Y. W., Pham, A. D., Optimizing Parameters of Support Vector Machine using Fast Messy Genetic Algorithm for Dispute Classification. *Expert Systems with Applications*, 41(8), 3955–3964, 2014.
- [21] Chen, J. H., KNN Based Knowledge-Sharing Model for Severe Change Order Disputes in Construction. *Automation in Construction*, 17(6), 773–779, 2008.

- [22] Liu, J., Li, H., Skitmore, M., Zhang, Y., Experience Mining Based on Case-Based Reasoning for Dispute Settlement of International Construction Projects. *Automation in Construction*, 97, 181–191, 2019.
- [23] Chau, K. W., Application of PSO-Based Neural Network in Analysis of Outcomes of Construction Claims. *Automation in Construction*, 16(5), 642–646, 2007.
- [24] Chen, J. H., Hsu, S. C., Hybrid ANN-CBR Model for Disputed Change Orders in Construction Projects. *Automation in Construction*, 17(1), 56–64, 2007.
- [25] Arditi, D., Oksay, F. E., Tokdemir, O. B., Predicting the Outcome of Construction Litigation using Neural Networks. *Computer-Aided Civil and Infrastructure Engineering*, 13(2), 75–81, 1998.
- [26] Arditi, D., Pulket, T., Predicting the Outcome of Construction Litigation using Boosted Decision Trees. *Journal of Computing in Civil Engineering*, 19(4), 387–393, 2005.
- [27] Arditi, D., Pulket, T., Predicting the Outcome of Construction Litigation using an Integrated Artificial Intelligence Model. *Journal of Computing in Civil Engineering*, 24(1), 73–80, 2010.
- [28] Pulket, T., Arditi, D., Universal Prediction Model for Construction Litigation. *Journal of Computing in Civil Engineering*, 23(3), 178–187, 2009.
- [29] Mahfouz, T., Kandil, A., Davlyatov, S., Identification of Latent Legal Knowledge in Differing Site Condition (DSC) Litigations. *Automation in Construction*, 94, 104–111, 2018.
- [30] Chaphalkar, N. B., Iyer, K. C., Patil, S. K., Prediction of Outcome of Construction Dispute Claims using Multilayer Perceptron Neural Network Model. *International Journal of Project Management*, 33(8), 1827–1835, 2015.
- [31] Chou, J. S., Comparison of Multilabel Classification Models to Forecast Project Dispute Resolutions. *Expert Systems with Applications*, 39(11), 10202–10211, 2012.
- [32] Chou, J. S., Hsu, S. C., Lin, C. W., Chang, Y. C., Classifying Influential Information to Discover Rule Sets for Project Disputes and Possible Resolutions. *International Journal of Project Management*, 34(8), 1706–1716, 2016.
- [33] Ayhan, M., Development of Dispute Prediction and Resolution Method Selection Models for Construction Disputes. Ph.D. Thesis, Middle East Technical University, Ankara, 2019.
- [34] Weisburd, D., Britt, C., *Statistics in Criminal Justice*, 3rd ed, Boston. Springer, 2007.
- [35] Arasu, B. S., Seelan, B. J. B., Thamaraiselvan, N., A Machine Learning-Based Approach to Enhancing Social Media Marketing. *Computers & Electrical Engineering*, 86, 2020.
- [36] Witten, H. W., Frank, E., Hall, M. A., Pal, C. J., *Data Mining: Practical Machine Learning Tools and Techniques*, 4th ed, Burlington. Morgan Kaufmann, 2016.

- [37] Hssina, B., Merbouha, A., Ezzikouri, H., Erritali, M., A Comparative Study of Decision Tree ID3 and C4.5. *International Journal of Advanced Computer Sciences and Applications*, 4(2), 13–19, 2014.
- [38] Febriantono, M. A., Pramono, S. H., Rahmadwati, R., Naghdy, G.), Classification of Multiclass Imbalanced Data using Cost-Sensitive Decision Tree C5.0. *IAES International Journal of Artificial Intelligence*, 9(1), 65–72, 2020.
- [39] Cortes, C., Vapnik, V., Support-vector networks. *Machine Learning*, 20(3), 273–297, 1995.
- [40] Alpaydin, E., *Introduction to Machine Learning*, 2nd ed, Cambridge. MIT Press, 2010.
- [41] Hsu, C. W., Lin, C. J., A Comparison of Methods for Multiclass Support Vector Machines. *IEEE Transactions on Neural Networks*, 13(2), 415–425, 2002.
- [42] Dietterich, T. G., Bakiri, G., Solving Multiclass Learning Problems via Error-Correcting Output Codes. *Journal of Artificial Intelligence Research*, 2, 263–286, 1994.
- [43] McHugh, M. L., The Chi-Square Test of Independence. *Biochemia Medica*, 23(2), 143–149, 2013.
- [44] Akoglu, H., User’s Guide to Correlation Coefficients. *Turkish Journal of Emergency Medicine*, 18(3), 91–93, 2018.
- [45] Pollock III, P.H., *An SPSS Companion to Political Analysis*, 4th ed, Washington, DC. CQ Press, 2011.
- [46] Vanwinckelen, G., Blockeel, H., On Estimating Model Accuracy with Repeated Cross-Validation. *21st Belgian-Dutch Conference on Machine Learning*, Ghent, Belgium, 2012.
- [47] Lingard, H., Brown, K., Bradley, L., Bailey, C., Townsend, K., Improving Employees’ Work-Life Balance in the Construction Industry: Project Alliance Case Study. *Journal of Construction Engineering and Management*, 133(10), 807–815, 2007.
- [48] İltter, O., Çelik, T., Investigation of Organizational and Regional Perceptions on the Changes in Construction Projects. *Teknik Dergi*, 32(6), 2021.
- [49] Yu, W. D., Hybrid Soft Computing Approach for Mining of Complex Construction Databases. *Journal of Computing in Civil Engineering*, 21(5), 343–352, 2007.

# Transit Frequency Optimization in Bi-modal Networks Using Differential Evolution Algorithm

Mehmet Metin MUTLU<sup>1</sup>

İlyas Cihan AKSOY<sup>2</sup>

Yalçın ALVER<sup>3</sup>

## ABSTRACT

This study proposes a bi-level optimization model for the transit frequency setting problem in bi-modal networks. The objective of the upper-level problem is to obtain a solution set of bus line frequencies that provide the minimum total travel cost of the car and bus users. Differential Evolution (DE) algorithm is employed in the upper-level model to determine the optimal headways for a given route structure. The lower-level model is a congested multi-modal user equilibrium assignment model, which considers the interactions of car and bus flows, for determining joint mode/route preferences of the network users, which considers the interactions of car and bus flows. The developed model is tested on Mandl's benchmark network to evaluate its performance and applicability. The comparative experiments demonstrate that the proposed model leads to reductions in transportation costs. Also, the result of numerous optimization runs shows that DE performs well in finding similar frequency sets in independent optimizations.

**Keywords:** Transit frequency setting problem, bus frequency optimization, multi-modal assignment, differential evolution algorithm, bi-level optimization.

## 1. INTRODUCTION

Increasing population and urbanization, along with economic development, lead to higher mobility needs and transportation demand, especially in developing countries, such as Turkey. Commonly, the main policy of decision-makers is to mitigate transportation-related problems emerging due to increasing demand and meeting this demand by public transportation. However, unplanned public transit services may lead to insufficient supply

---

Note:

- This paper was received on May 11, 2021 and accepted for publication by the Editorial Board on January 11, 2022.
- Discussions on this paper will be accepted by November 30, 2022.
- <https://doi.org/10.18400/tekderg.935950>

1 Department of Civil Engineering, Aydın Adnan Menderes University, Aydın, Turkey  
metin.mutlu@adu.edu.tr - <https://orcid.org/0000-0003-0008-8279>

2 Department of Civil Engineering, Karamanoğlu Mehmetbey University, Karaman, Turkey  
icihanaksoy@kmu.edu.tr - <https://orcid.org/0000-0002-4256-8222>

3 Department of Civil Engineering, Ege University, İzmir, Turkey  
yalcin.alver@ege.edu.tr - <https://orcid.org/0000-0002-9833-4505>

causing high travel costs or oversupply causing high operational costs. Furthermore, it can increase private transportation travel times by discouraging the use of public transit. On the other hand, a well-planned transit system can enhance transportation system for both public and private transportation.

Public transit networks can be improved through measures such as redesigning bus line routes, optimizing operational decisions such as bus line frequency setting, and traffic control measures such as allocating road network lanes like exclusive bus lanes. Optimal transit operation planning is a four-stage process, namely, network route design, timetable development, vehicle scheduling, and crew scheduling [1]. All stages should be handled simultaneously to obtain the optimum design. However, it is not possible with modern computing technology due to complex nature of these kind of problems [2]. Accordingly, each stage is usually solved sequentially [3].

Urban Transportation Network Design Problems are usually formulated as bi-level problems to allow considering passengers' reactions in network design decisions. The bi-level transportation network optimization problem is generally an NP-hard problem [4] commonly characterized by inherent non-convexity [5]. Due to the complexity of the problem, meta-heuristics were proposed for network design problems in the literature for obtaining nearly global optimal solutions with high computation speeds at the expense of solution accuracy [6,7].

Total user travel cost and operator cost minimization are frequently used objective functions for transit network design problems. It is possible to satisfy these objectives in a transit network solely by optimizing bus frequencies, which is studied under Transit Network Frequency Setting Problems (TNFSP).

There are numerous studies conducted related to TNFSP using heuristic approaches for mono-modal networks. [8] is one of the early studies adopting the bi-level model approach, in which the frequency setting problem is handled using a projected sub-gradient algorithm in the upper level with the aim of minimizing the total travel time and waiting times. The proposed model is performed in the transit networks of Stockholm (Sweden), Winnipeg (Canada), and Portland (USA). The study of [9] determines the line frequencies using a basic heuristic minimization algorithm, and implementing the proposed model to a small-size network. [10] proposes a frequency setting model to maximize demand under frequency value and fleet size constraints utilizing a gradient projection method. [11] determines both optimal frequencies and optimal bus sizes to minimize the sum of the total user cost and operator cost. The frequencies are determined using the Hooke-Jeeves algorithm, while the congested transit assignment is performed using ESTRAUS simulation software. In [12], a frequency setting model that minimizes total travel time of all users and required fleet size for the operators by Tabu Search is tested on a real-size network for morning-peak and off-peak periods. [13] determines frequencies by two different frequency determination methods, named optimum frequency and demand-based frequency methods, on the routes obtained by Ant Colony Optimization. Lastly, [14] develops a frequency setting model based on a novel objective function with the aim of decreasing the spread of COVID-19 derived from crowding at transit stops. The model aims to minimize the total infection risk at the stops, under a limited fleet size, employing the Differential Evolution Algorithm (DE).



The studies presented above adopt the mono-modal assignment approach. This assumption is considered applicable for the networks where nonsignificant changes occur on the network since the minor improvements are unlikely to lead to user mode shifts between transit and private cars. However, if significant changes occur on the network, the network should be designed in consideration of elastic demand; thus, network design models should utilize multi-modal assignment. There are several transit frequency setting studies regarding the multi-modal assignment in the literature. [15] minimizes the weighted sum of users' costs, operator cost, and external cost using a heuristic algorithm, testing the model and the algorithm for a real-scale transit network. [16] determines the optimal frequency on a small-scale network with three transportation modes to minimize the total disutility using a stochastic user equilibrium assignment.

Reviewing the studies presenting the comparative performances of metaheuristics in different engineering fields; in [17], DE is compared to well-known metaheuristics, such as Genetic Algorithm (GA) and Simulated Annealing (SA), in the loop-layout design problem, and the findings show that DEA is superior to others; [18] addresses the performance comparison among the metaheuristics, Cuckoo-Search (CK), Particle Swarm Optimization (PSO), Differential Evolution (DE), and Artificial Bee Colony (ABC) by testing over 50 different benchmark functions. Statistical analysis demonstrates that the problem-solving success of DE and CK is relatively better than that of PSO and ABC; [19] presents a comparison of six meta-heuristic techniques to solve the multilevel thresholding problem: GA, PSO, DE, Ant Colony Optimization (ACO), SA, and Tabu Search (TS), and concluding that Differential Evolution is the most efficient in terms of the quality of the solution. Based on the results of these studies, in this study, DE is employed for performance evaluation in the problem of frequency optimization of transit lines in multi-modal networks.

In this study, a bi-level TNFSP model employing the Differential Evolution Algorithm (DE), an evolutionary metaheuristic algorithm, for optimizing frequencies in multi-modal networks is presented. The upper-level of the bi-level model is an optimization model that minimizes the total user cost by frequency setting, while the lower-level is a bi-modal assignment model that determines the transportation mode choice of the network users in addition to the route choices of private and public transportation modes. Therefore, the model proposed is suitable to be utilized as a decision support tool to optimize frequencies of public transportation lines considering the tradeoff between private car and public transportation use preferences, to minimize the costs of the users of both modes.

To our knowledge, there is no study employing DE for solving Transit Network Frequency Setting problems. The main contributions of this study are: proposing DE for a multi-modal TNFSP; examining the effect of different parameter values on the performance of DE in TNFSP; considering both private and public transportation modes in TNFSP for minimizing the total system cost by utilizing a multi-modal deterministic user equilibrium assignment in the lower-level model.

Section 2 of the study describes the upper-level and the lower-level models. Section 3 presents the numerical applications made on the benchmark network and discusses the results of the comparative experiments. Section 4 draws the conclusions of the study and highlights the possible directions for future research.

## 2. OPTIMIZATION MODEL

In transportation planning, the effect of network design decisions on the performance of the transportation system and network users must be taken into consideration. Therefore, the transportation network design problem is usually formulated as a bi-level problem. The upper-level of the bi-level structure represents the decision-maker, whereas the lower-level represents travelers. This structure allows the decision-maker to take the reactions of travelers as well as network performance into consideration.

In this study, TNFSP is handled as a bi-level problem. The upper-level is a frequency optimization problem to minimize the total travel cost, and the lower-level is a multi-modal assignment problem.

### 2.1. Upper-Level Model

The objective of the optimization model is to determine the bus line frequency set, minimizing the total car and bus travel cost in the transportation system, which can be formulated as in (Eq. 1):

$$\min \sum_{rs} (\sum_k q_k^{rs} \times t_k^{rs} + \sum_{\hat{k}} \hat{q}_{\hat{k}}^{rs} \times \hat{t}_{\hat{k}}^{rs}) \forall rs \in W, \forall k \in K_{rs}, \forall \hat{k} \in \hat{K}_{rs} \quad (1)$$

where  $W$  is the set of origin-destination (OD) pairs,  $K_{rs}$  is the set of car paths on road network connecting OD pair  $rs$ ,  $\hat{K}_{rs}$  is the set of transit paths on transit network connecting OD pair  $rs$ ,  $q_k^{rs}$  is the car flow on path  $k$ ,  $\hat{q}_{\hat{k}}^{rs}$  is the bus trip flow on path  $\hat{k}$ ,  $t_k^{rs}$  is the travel time on path  $k$ ,  $\hat{t}_{\hat{k}}^{rs}$  is the travel time on the path  $\hat{k}$ .

Car path travel time is the sum of congested travel time of member links. The bus travel time of passengers consists of in-vehicle travel time and congested waiting time. Bus in-vehicle travel time is congested link travel time affected by both car and bus vehicle flows. Operator cost is not considered in this study for determining the optimal frequencies. The design constraint of the upper-level model regarding the bus fleet size  $n_b$ , imposes  $0 < n_b \leq n_b^{max}$ , where  $n_b^{max}$  is the maximum allowed fleet size, and  $n_b$  is the minimum required number of buses to operate the transit network calculated by the frequency value and run time of each line.

Increased bus frequencies decrease waiting time, and consequently, total travel time decreases. Therefore, it is expected to result in shifts from private to public transportation. In this case, as the modal share of bus transportation increases, private car usage decreases, resulting in decreased car flows in the road network. As a result of lower car volumes, link travel times decrease. Subsequently, in a bi-modal transportation system, lower private car transportation costs induce shifts from public to private transportation. Decreasing bus frequencies, on the other hand, results in increased bus travel time and shifts from public to private transportation. In this case, increased link travel times due to high vehicle flow lead to an increase in travel times for both private and public transportation. An iterative process between the trip assignment model and optimization model is necessary to determine the optimal frequency set, minimizing the total travel cost. Due to the complex nature of the bi-level problems, it is not possible to determine the optimal solution using exact solution

methods, especially in large-scale networks. Therefore, meta-heuristics are applied to obtain near-optimal solutions, especially for real-scale problems [20].

We employed DE for optimizing transit line frequencies in multi-modal networks in this study. DE, developed by [21], is an evolutionary approach to solve continuous-space problems and is considered to be one of the most prominent metaheuristics. DE consists of three main operators like genetic algorithms: mutation, crossover, selection operators.

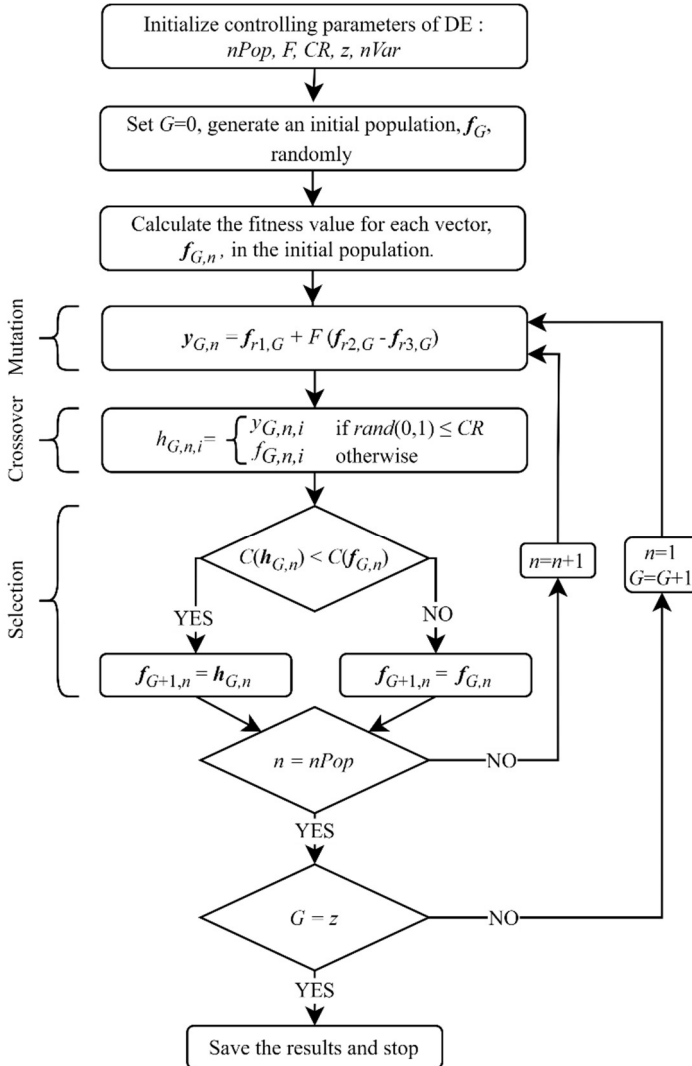


Figure 1 - The flowchart of traditional DE

In the mutation operator, a mutant vector is created by weighting three random vectors (i.e., parent chromosomes) selected from the current population using the mutation constant,  $F$ , which controls the amplification of the differential variation. It should be noted that the selected three vectors must be different from each other. Following the generation of the mutant vector, a trial vector is generated by combining the target vector and the mutant vector with the help of the crossover constant,  $CR$ , that controls which genes of mutant and target vectors contribute to the trial vector. Finally, in the selection operator, a new target vector for the next generation is selected between the current target vector and the trial vector based on their fitness values. If the trial vector yields a smaller fitness value than the target vector value, the trial vector is replaced in the next generation; otherwise, the target vector is retained. The traditional DE steps are presented as a flowchart in Figure (1).

The algorithm that we used to solve the multi-modal frequency setting problem using DE is outlined as follows:

**Step 0: Initialization.** For each agent of the population with size  $nPop$ , generate a set of elements (frequencies for each line,  $nVar$ )  $\mathbf{f}_n = \{f_{n,1}, f_{n,2}, \dots, f_{n,nVar}\}$ , with random positions (frequency values) in the search space ( $f_{min} < f < f_{max}$ ).

**Step 1: Calculation.** Calculate cost (total travel time on the transportation system) for each frequency set,  $\mathbf{f}_n$  by performing multi-modal trip assignment.

**Step 2:** For each agent of population,  $n \in \{1,2, \dots, nPop\}$ :

**Step 2.1: Mutation.** Randomly select three different frequency set indices  $a, b$  and  $c$  from the population and generate mutation vector:  $\mathbf{y}_n = \mathbf{f}_a + F(\mathbf{f}_b - \mathbf{f}_c)$  where  $\mathbf{y}_n = \{y_{n,1}, y_{n,2}, \dots, y_{n,nVar}\}$  and mutation constant,  $F \in [0,2]$ .

**Step 2.2: Crossover.** Generate a random index  $r \in \{1,2, \dots, nVar\}$  and for each element of an agent (frequency of line) generate a random number  $R_i \in [0,1]$ . For each element  $i \in \{1,2, \dots, nVar\}$ :  $h_{n,i} = \{y_{n,i} \text{ if } R_i \leq CR \text{ or } i = r; f_{n,i} \text{ otherwise}\}$ , where crossover constant,  $CR \in [0,1]$  is the crossover probability.

**Step 2.3: Selection.** Perform trip assignment with  $\mathbf{h}_n$ . Replace the corresponding element  $\mathbf{f}_n$ , with  $\mathbf{h}_n$  if the solution is improved:  $\mathbf{f}_n = \{\mathbf{h}_n \text{ if } C(\mathbf{h}_n) \leq C(\mathbf{f}_n); \mathbf{f}_n \text{ otherwise}\}$

**Step 3: Termination criterion.** Stop if the maximum iteration number  $z$  is reached and output the best solution; Otherwise, go to Step 2.

## 2.2. Lower-Level Model

Total travel cost calculation of the transportation system in the upper-level optimization model is possible through the output of the lower-level trip assignment model. The lower-level problem is a multi-modal network equilibrium assignment model with elastic demand in mode choice level, considering car and bus networks with flow interactions under the following assumptions: (1) All network users are assumed to choose the path minimizing their travel cost and transit network users are assumed to board the first arriving bus in the attractive lines set. (2) Transit stops are used as zones where demand originates and terminates. (3) Walking links are not included in the network; therefore, the assignment model does not allow passengers to walk between stops (4) All bus lines are assumed to have

the same in-vehicle travel times while passing through the same itineraries. (5) Road network trip costs are calculated using the BPR link cost function, which does not consider the costs occurring at intersections. Thus, the assignment model assumes that congestions occur only on links and there are no delays caused by spillback queues and traffic lights, etc. (6) For the sake of simplicity, the car occupancy rate is assumed 1 passenger/car. (7) It is assumed that all travelers have access to a car, and therefore all public transportation users are considered choice riders in this study.

The assignment model acquires a solution that both car and transit flows to satisfy the deterministic user equilibrium criterion. The modal distributions are calculated using a logit type mode choice function (Eq. 2). The mode choice function employs the minimum travel costs of modes between OD pairs as parameters, and road network link travel time is assumed to follow the Bureau of Public Roads (BPR) function (Eq. 3), including bus vehicle flows considering passenger car equivalency.

$$q_{rs} = \bar{q}_{rs} \frac{1}{1 + e^{\theta(u_{rs} - \hat{u}_{rs} - \Psi_{rs})}} \forall rs \in W \quad (2)$$

where  $q_{rs}$  is the car mode demand between OD pair  $rs$ ,  $\bar{q}_{rs}$  is total travel demand between  $rs$ ,  $u_{rs}$  is the cost of the shortest path between  $rs$  on the road network,  $\hat{u}_{rs}$  is the cost of the shortest path between  $rs$  on transit network,  $\Psi_{rs}$  is the car preference parameter.

$$t_a = t_a^0 \left[ 1 + \alpha \left( \frac{x_a + x_{a,bus} \times PCE_{bus}}{c_a} \right)^\beta \right] \forall a \in A \quad (3)$$

where  $t_a$  is congested link travel cost of link  $a$ ,  $t_a^0$  is the free-flow travel time of  $a$ ,  $x_a$  is car flow on  $a$ ,  $x_{a,bus}$  is bus vehicle flow on  $a$ ,  $PCE_{bus}$  is passenger car equivalency factor of bus,  $c_a$  is the practical capacity of  $a$ ,  $\alpha$  and  $\beta$  are calibration parameters.

Bus mode travel times are calculated utilizing a BPR-like function, given in Eq. 4, representing the effect of increased waiting time at stops due to congestion, as proposed by [22], in a transit network converted from line-segment representation to route-section representation as a proper method for handling common lines problem. It is possible to solve transit assignment problems similar to road network assignment problems utilizing route-section networks. The route section between a node pair consists of attractive lines that are a subset of bus lines that passengers can travel between the same node pair. In the route-section representation, nodes generally represent bus stops while links represent the route sections.

In this study, determining attractive lines to be included in each route section is based on the minimization of expected travel time as proposed in [23], and it is assumed that all lines passing through a road link have the same in-vehicle travel time. Consequently, all lines passing through the same road link sequence between a node pair are associated with a route section as attractive lines.

$$\hat{t}_s = \bar{t}_s + \left( \frac{\hat{\alpha}}{f_s} \right) + \hat{\beta} \times \left( \frac{x_s + \hat{x}_s}{\hat{c}_s} \right)^{\hat{\eta}} \forall s \in S \quad (4)$$

where  $\hat{t}_s$  is the total congested travel cost of route section  $s$ ,  $\bar{t}$  is the in-vehicle travel time of bus trips on  $s$  which depends on vehicle flows on corresponding road network link set  $A$ ,  $f$  is total frequencies of lines contained in  $s$ ,  $\hat{a}$  is the calibration parameter for non-congested wait time at the stop,  $\hat{x}_s$  is the number of passengers waiting for lines contained in  $s$ ,  $\tilde{x}_s$  is the total number of competitive passengers of  $s$ , who wait for other route sections that use lines contained in  $s$  in the same stop, and passengers boarding the lines contained in  $s$  at a node before the origin node of  $s$  and alighting after,  $\hat{C}_s$  is the practical capacity of  $s$ , which is the total capacity of the lines it contains,  $\hat{\beta}$  is the calibration parameter for congested wait time at the stop.

Flow interaction between road and transit network links due to shared lane usage together with flow interaction on transit network due to competitive flows in transit network results in an asymmetric cost function in the assignment model employed in this study. Therefore, the assignment problem can be solved using the diagonalization method, which is commonly used for trip assignment problems with asymmetric cost functions due to non-symmetric link flow interactions [24,25]. Diagonalization is an iterative method that involves diagonalization of link cost functions to fix cross-link effects by fixing all arguments of a link other than its own flow in each iteration to solve a sub-problem [26]. The sub-problem solved at each iteration of the diagonalization algorithm using Frank and Wolfe Algorithm [27] for the multi-modal assignment problem presented in this study is formulated as:

$$\min \tilde{z}^{(n)} = \sum_a \int_0^{x_a} t_a(\omega, x_{a,bus}^{(n)}) d\omega + \sum_s \int_0^{\hat{x}_s} \hat{t}_s(\omega, \tilde{x}_s^{(n)}, x_{s,car}^{(n)}) d\omega + \sum_{rs} \int_0^{\hat{q}_{rs}} \left( \frac{1}{\theta} \ln \frac{\omega}{\bar{q}_{rs} - \omega} + \Psi_{rs} \right) d\omega \quad (5a)$$

subject to

$$\sum_k X_k^{rs} = \bar{q}_{rs} - \hat{q}_{rs} \quad \forall rs; \quad (5b)$$

$$\sum_{\hat{k}} \hat{X}_{\hat{k}}^{rs} = \hat{q}_{rs} \quad \forall rs; \quad (5c)$$

$$X_k^{rs}, \hat{X}_{\hat{k}}^{rs} \geq 0 \quad \forall k, \hat{k}, rs \quad (5d)$$

Equation (5a) is the objective function of the assignment problem composed of three terms. The first term is the sum of the integrals of the road network link cost functions to satisfy the road network user equilibrium criterion where  $t_a$  is the road link cost function,  $(n)$  is the iteration number and  $x_{a,bus}^{(n)}$  is the bus vehicle flow on the link at the  $n^{\text{th}}$  iteration. The second term is the sum of the integrals of the route section network link cost functions to satisfy the transit network user equilibrium criterion where  $\hat{t}_s$  is the cost function of route section  $s$ ,  $\tilde{x}_s^{(n)}$  is the bus competitive flow vector of  $s$  at the  $n^{\text{th}}$  iteration, and  $x_{s,car}^{(n)}$  is the vector of car flows on the road network links that  $s$  incorporates, affecting the in-vehicle cost of  $s$  at the  $n^{\text{th}}$  iteration. The last term is the sum of integrals of the inverse of the logit demand function for each OD pair, ensuring the equilibrium criterion for the car and transit demand share as proposed by [26]. Equations (5b) and (5c) are flow conservation constraints for the road network and route section network, respectively, and equation (5d) is the nonnegativity of

flow constraint for both networks, where  $X_k^{rs}$  is the flow on path  $k$  between OD pair  $rs$  on the road network,  $\hat{X}_k^{rs}$  is the flow on path  $\hat{k}$  between  $rs$  on the route section network.

### 3. TEST NETWORK APPLICATION

The proposed model is tested on Mandl's Swiss network, which has been used by several authors in the literature [28-30]. The test network consists of 15 nodes and 42 unidirectional links. The line routes to be used are obtained from the study of [29]. Automatically generated route-section network with the given road network and bus lines consists of 282 unidirectional links. The original demand is increased by a factor of 2 considering the modal choice since the original network is used solely for the transit demand.

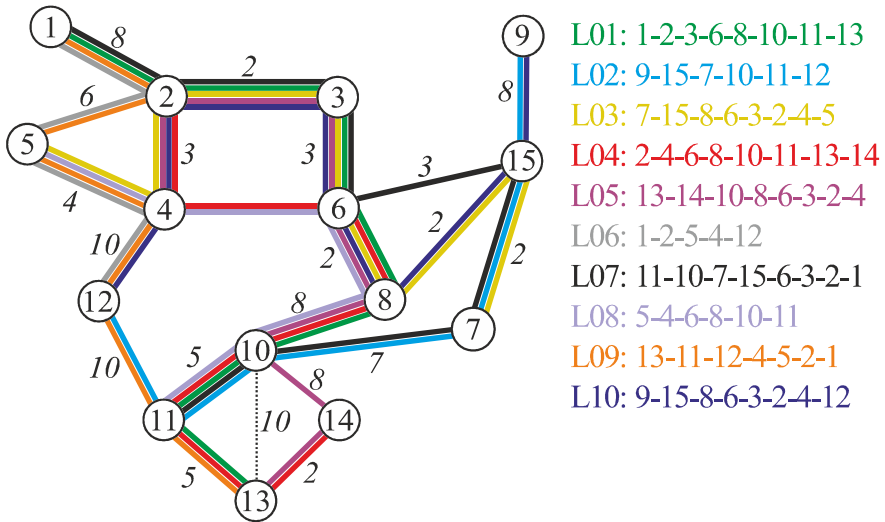


Figure 2 - Test network and bus lines

In Figure 2, the bus line routes of the test network are represented by different colors. The free-flow travel times of each link independent of directions, are indicated on the relevant link in minutes. The node sequence of each route in one direction is also presented on the right of the network. The OD matrix of the total trip demand in the analysis period used in numerical applications is given in Table 1.

In the transit network, assuming that the operator has a limited fleet size, a fleet size constraint is incorporated into the optimization model. Fleet size and bus capacities are assumed 300 buses and 100 passengers, respectively. For all links in the road network, practical capacities are 800 veh/h. Cost function parameters of the assignment model are defined as  $\theta = 0.3$ ,  $\Psi_{rs} = 0$ ,  $\alpha = 0.15$ ,  $\beta = 4$ ,  $PCE_{bus} = 3$ ,  $\hat{\alpha} = 0.5$ ,  $\hat{\beta} = 1$ ,  $\hat{n} = 1$ . Allowed minimum and maximum values of line frequency are defined as 1 and 60, respectively.

Table 1 - Node-to-node trip demand matrix used in test network application

OD	1	2	3	4	5	6	7	8	9	10	11	12	13	14	15
1	0	800	400	120	160	300	150	150	60	320	60	50	70	0	0
2	800	0	100	240	40	360	180	180	30	260	40	20	20	10	0
3	400	100	0	80	120	360	180	180	30	90	40	20	20	10	0
4	120	240	80	0	100	200	100	100	30	480	80	50	20	10	0
5	160	40	120	100	0	100	50	50	20	240	40	30	10	0	0
6	300	360	360	200	100	0	200	200	60	1760	120	30	30	20	0
7	150	180	180	100	50	200	0	100	30	880	70	20	20	10	0
8	150	180	180	100	50	200	100	0	30	880	70	20	20	10	0
9	60	30	30	30	20	60	30	30	0	280	40	10	0	0	0
10	320	260	90	480	240	1760	880	880	280	0	1200	500	1000	400	0
11	60	40	40	80	40	120	70	70	40	1200	0	150	190	30	0
12	50	20	20	50	30	30	20	20	10	500	150	0	140	0	0
13	70	20	20	20	10	30	20	20	0	1000	190	140	0	90	0
14	0	10	10	10	0	20	10	10	0	400	30	0	90	0	0
15	0	0	0	0	0	0	0	0	0	0	0	0	0	0	0

Algorithms used in this study were coded using MATLAB R2020a and carried out on a 64-bit computer with an AMD Ryzen 5 3600 3.60 GHz CPU and 16 GB RAM. The average duration of an optimization terminated at the 100<sup>th</sup> iteration is 280 minutes.

Metaheuristic algorithms are sensitive to the values of the parameters. In problems with numerous local optima such as TNFSP, reaching optimal or near-optimal solutions may be difficult and time-consuming for the algorithms because of improper parameter values. Thus, DE is executed with the different combinations of parameter values to better show the effect of different parameter values on the performance of DE.

Parameters  $F$  and  $CR$  values are chosen from the sets  $\{0.5, 1.0, 1.5, 2.0\}$  and  $\{0.2, 0.4, 0.6, 0.8\}$ , respectively, resulting in 16 combinations. Also, three replications for each combination are carried out to avoid statistical deviations, leading to 48 optimization runs in total. It is likely that the increase in nPop and  $z$  values obtain better solutions; therefore, the effects of these parameters are not investigated in this study. nPop and the maximum iteration number are defined as 50 and 100, respectively. Table 2 demonstrates the results of 16 different parameter combinations, showing the average total system cost of five optimizations for each parameter combination.

Table 2 clearly shows that the best combination of parameter values is obtained in the combination  $F = 0.5$  and  $CR = 0.6$ , with a cost of 901,757. To demonstrate the stability of the algorithm, 30 optimizations are performed using the calibrated parameter values. The obtained frequency sets and the corresponding costs of 30 optimization runs are given in Table 3.



Table 2 - The results of different combinations of parameter values (Average total system costs in min)

<i>F</i> \ <i>CR</i>	0.2	0.4	0.6	0.8
0.5	914,264	903,797	901,757	902,014
1.0	908,573	913,523	912,798	909,029
1.5	914,523	920,224	932,105	916,026
2.0	930,134	926,153	941,997	949,893

Standart Deviation = 14,885, Coefficient of Variation = 0.016 in 48 runs

Table 3 - The results of 30 solutions by the calibrated parameter values

Total System Cost (min)	Frequency values of the lines (runs/h) { <i>f</i> <sub>1</sub> , <i>f</i> <sub>2</sub> , <i>f</i> <sub>3</sub> , <i>f</i> <sub>4</sub> , <i>f</i> <sub>5</sub> , <i>f</i> <sub>6</sub> , <i>f</i> <sub>7</sub> , <i>f</i> <sub>8</sub> , <i>f</i> <sub>9</sub> , <i>f</i> <sub>10</sub> }	Frequency of Being Obtained as a Solution
899,220	{1.0,1.9,1.6,1.0,18.6,1.3,28.6,24.2,21.2,19.9}	1
900,079	{1.0,1.7,1.0,3.0,12.9,1.3,29.0,26.8,20.8,21.9}	4
900,686	{1.4,1.0,1.0,1.0,15.2,1.0,28.5,25.9,22.5,21.9}	1
900,691	{1.8,3.9,1.0,2.5,13.6,1.0,29.7,27.3,19.7,16.8}	2
902,120	{1.2,2.2,2.1,2.1,11.8,1.1,29.5,29.4,19.9,18.5}	2
902,309	{1.1,1.0,1.0,1.0,13.0,1.1,32.3,27.5,18.5,18.0}	2
902,509	{1.1,1.0,1.0,1.2,15.5,1.0,30.2,24.0,21.7,19.5}	1
902,795	{1.0,4.6,1.4,1.2,21.3,1.2,27.8,21.6,19.2,20.8}	4
902,845	{1.0,3.9,1.3,5.2,18.8,1.0,29.8,17.9,20.0,19.6}	1
902,866	{1.0,12.1,3.3,1.0,19.1,1.0,29.4,25.7,17.5,5.3}	2
902,991	{1.0,3.6,1.1,1.0,17.5,1.0,30.2,26.7,21.5,12.0}	1
903,329	{1.0,1.0,1.2,4.4,14.0,1.0,30.8,24.1,17.5,25.1}	1
905,035	{1.0,13.1,5.4,1.0,19.2,1.5,27.8,24.8,16.6,7.2}	2
905,343	{1.0,14.8,2.4,1.0,25.4,2.0,26.5,20.9,16.4,4.6}	1
906,114	{1.5,5.2,3.1,1.0,21.2,1.0,29.7,25.4,15.4,14.3}	2
906,743	{1.1,15.3,5.2,1.0,23.0,2.0,27.6,24.4,13.9,2.8}	1

Standard Deviation = 1,921, Coefficient of Variation = 0.0021 in 30 optimizations

The statistical outputs given in the last row of both tables affirm the necessity of the calibration process for the parameter values. The best solution obtained is given in the first row of Table 3, with a total system cost of 899,220. Network performance outputs, namely average travel times and modal share ratios, are calculated by running the combined mode choice assignment process using the frequency set obtained from the optimization. In the best

solution, the average travel times of car and bus trips are 17.38 min and 11.49 min per user, respectively, and the transit modal share is 40%. Figure 3 depicts the convergence process along 100 iterations for 30 runs by the calibrated parameter values. As can be seen, the algorithms complete the convergence process in approximately 40 iterations.

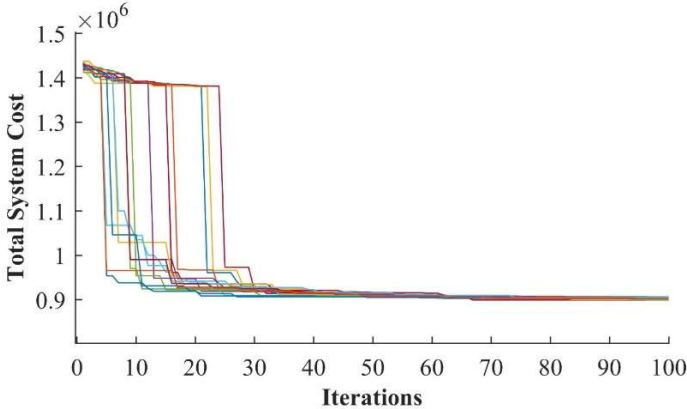


Figure 3 - Convergence of 30 solutions along with iterations

Firstly, the bus line frequencies are optimized using a model without a fleet size constraint. The results given in Table 4 show that minimum system cost is obtained with a fleet size of 339. Therefore, optimizing with a fleet size constraint greater than 339 buses is unnecessary since the same solution is expected to be obtained.

Table 4 - The results without fleet size constraint by the proposed model

Total System Cost (min)	Private Car Cost (min)	Public Transportation Cost (min)	Fleet Size	Frequency values of the lines (runs/h) $\{f_1, f_2, f_3, f_4, f_5, f_6, f_7, f_8, f_9, f_{10}\}$
874,568	504,033	370,534	339	{1.0,1.1,1.0,2.0,18.8,1.1,40.8,35.8,26.2,36.4}

In multi-modal networks with link flow interaction, the increase in the frequency of transit lines makes transit systems more attractive and leads to an increase in the use of transit systems. Thus, the congestion on the roads and the total system cost for all users are reduced. However, the further increase in frequency values of transit lines causes an increase in transit vehicle flow on the road links, triggering congestion for the vehicles of both modes. To prove this argument, following a simple assumption, the total system costs are calculated for the scenarios that all lines take the same frequency values between 1 and 60, as shown in Figure 4. The best frequency set is obtained using the frequency set of 18 runs/h for all lines with a minimum total system cost of 923,140, and 446 buses are needed to operate the network. Further improvement in total system cost is possible by optimizing the frequency values of lines individually.

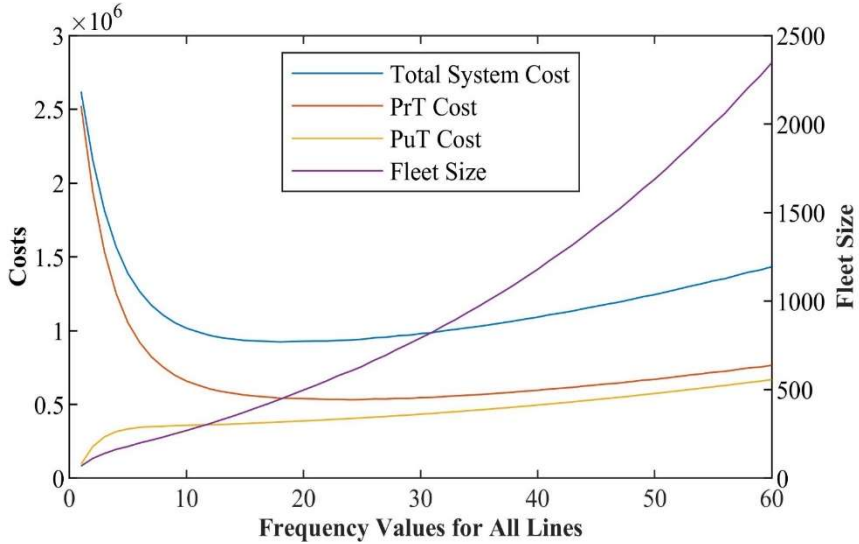


Figure 4 - Total system costs (min) for frequency sets in multi-modal networks

To assign the same frequency value to all lines, as shown in Figure 4, is a simple method; however, in order to demonstrate the stability and robustness of the proposed algorithm, we benefit from the solutions for comparison purposes. The frequency sets with 6, 12, and 15 runs/h for all lines require 199, 308, and 374 buses to operate the network, respectively. The optimization model is run with these fleet size constraints to compare the optimization model results with fixed-frequency calculation results in terms of private transportation and public transportation total user costs. The comparison results are given in Table 5. The reductions in total system costs for the optimizations with fleet size constraints of 199, 308, and 374 buses are 12%, 7%, and 6%, respectively.

Table 5 - The comparison between the results of the proposed model and the simple method

Fleet Size (bus)	Reduction (%)	Total System Cost (min)	Private Car Cost (min)	Public Trans. Cost (min)	Public Trans. Share (%)	Frequency values of the lines (runs/h) $\{f_1, f_2, f_3, f_4, f_5, f_6, f_7, f_8, f_9, f_{10}\}$
199	-12	1,115,326	765,749	349,576	32	{13.3,10.1,1.3,1.0,13.3,1.0,7.4,9.4,2.7,1.0}
		1,265,426	920,639	344,787	28	{6,6,6,6,6,6,6,6,6,6}
308	-7	901,333	544,349	356,983	39	{1.0,1.0,1.3,7.7,9.1,1.7,33.7,23.0,21.0,18.2}
		967,510	605,094	362,416	37	{12,12,12,12,12,12,12,12,12,12}
374	-6	877,787	511,514	366,273	42	{1.0,2.0,1.2,2.2,16.2,1.0,37.2,34.7,25.1,30.6}
		933,608	563,192	370,415	40	{15,15,15,15,15,15,15,15,15,15}

#### **4. CONCLUSION**

In this study, we propose a bi-level optimization model utilizing DE for TNFSP in bi-modal networks. The objective is to minimize the total travel cost in the transportation system for both car and bus modes. The proposed model is calibrated and tested on a benchmark network. The optimization results are compared with a simple fixed-frequency cost calculation approach. Numerous optimization runs resulted in similar and consistent solutions with significant decreases in cost, showing that DE is applicable in TNFSPs. Also, the significant reductions in the total system cost obtained using the proposed model are shown as proof of the necessity of optimization models for determining bus line frequencies.

Multi-modal assignment results indicate that bus link travel times are significantly affected by car flows. Consequently, bus travel time is always higher than car travel time since bus travel time also includes waiting time, even in uncongested situations, as expected. Therefore, the use of exclusive bus lanes can be considered to achieve a competitive public transit network leading to an increased modal share of bus mode.

Bi-level models with meta-heuristics in the upper level require numerous repetitions of the lower-level model. Therefore, a computationally less expensive static assignment model is utilized in this study to ensure reasonable optimization durations. However, using static models compared to dynamic assignment models or microscopic simulation models may lead to less realism regarding trip costs, path choices, etc. Another limitation of this study is that all public transportation users are considered choice riders and have access to a car.

In future studies, taking captive riders into consideration will lead to a more realistic trip assignment model. Additionally, to develop a more realistic and more sustainable transit network design model, the proposed model will be improved by including the exclusive bus lane location decisions in transit network design.

#### **Acknowledgments**

The authors would like to thank two anonymous reviewers for their constructive comments that contributed to improve this paper.

#### **References**

- [1] Ceder. A., *Public Transit Planning and Operation: Modeling, Practice and Behavior*, CRC Press, Boca Raton, USA, 2015.
- [2] Magnanti, T. L., Wong, R. T., *Network Design and Transportation Planning: Models and Algorithms*. *Transportation Science*, 18(1), 1–55, 1984.
- [3] Guihaire, V., Hao, J.-K. K., *Transit network design and scheduling: A global review*. *Transportation Research Part A: Policy and Practice*, 42(10), 1251–1273, 2008.
- [4] Zhao, F., *Large-Scale Transit Network Optimization by Minimizing User Cost and Transfers*. *Journal of Public Transportation*, 9(2), 107–129, 2006.
- [5] Yang, H., Bell, M. G. H., *Models and algorithms for road network design: a review and some new developments*. *Transport Reviews*, 18(3), 257–278, 1998.

- [6] Farahani, R. Z., Miandoabchi, E., Szeto, W. Y., Rashidi, H., A review of urban transportation network design problems. *European Journal of Operational Research*, 229(2), 281–302, 2013.
- [7] Ibarra-Rojas, O. J., Delgado, F., Giesen, R., Munoz, J. C., Planning, operation, and control of bus transport systems: A literature review. *Transportation Research Part B: Methodological*, 77, 38–75, 2015.
- [8] Constantin, I., Florian, M., Optimizing Frequencies in a Transit Network: A Nonlinear Bi-level Programming Approach. *International Transactions in Operational Research*, 2(2), 149–164, 1995.
- [9] Gao, Z., Sun, H., Shan, L. L., A continuous equilibrium network design model and algorithm for transit systems. *Transportation Research Part B: Methodological*, 38(3), 235–250, 2004.
- [10] Yoo, G. S., Kim, D. K., Chon, K. S., Frequency design in urban transit networks with variable demand: Model and algorithm. *KSCE Journal of Civil Engineering*, 14(3), 403–411, 2010.
- [11] dell'Olio, L., Ibeas, A., Ruisánchez, F., Optimizing bus-size and headway in transit networks. *Transportation*, 39(2), 449–464, 2012.
- [12] Giesen, R., Martinez, H., Mauttone, A., Urquhart, M. E., A method for solving the multi-objective transit frequency optimization problem. *Journal of Advanced Transportation*, 50 (8), 2323-2337, 2016.
- [13] Gholami, A., Tian, Z., The comparison of optimum frequency and demand based frequency for designing transit networks. *Case Studies on Transport Policy*, 7(4), 698–707, 2019.
- [14] Mutlu, M. M., Aksoy, İ. C., Alver, Y., COVID-19 transmission risk minimization at public transportation stops using Differential Evolution algorithm. *European Journal of Transport and Infrastructure Research*, 21(1), 53-69, 2021.
- [15] Gallo, M., D'Acierno, L., Montella, B., A multimodal approach to bus frequency design. 17<sup>th</sup> International Conference on Urban Transport and the Environment, Pisa, Italy, 2011.
- [16] Uchida, K., Sumalee, A., Watling, D., Connors, R., Study on Optimal Frequency Design Problem for Multimodal Network Using Probit-Based User Equilibrium Assignment. *Transportation Research Record: Journal of the Transportation Research Board*, 1923(1), 236-345, 2005.
- [17] Nearchou, A. C., Meta-heuristics from nature for the loop layout design problem. *International Journal of Production Economics*, 101(2), 312-328, 2006.
- [18] Civicioglu, P., Besdok, E., A conceptual comparison of the Cuckoo-search, particle swarm optimization, differential evolution and artificial bee colony algorithms. *Artificial Intelligence Review*, 39, 315-346, 2013.

- [19] Hammouche, K., Diaf, M., Siarry, P., A comparative study of various metaheuristic techniques applied to the multilevel thresholding problem. *Engineering Applications of Artificial Intelligence*, 23(5), 676-688, 2010.
- [20] Miandoabchi, E., Daneshzand, F., Szeto, W. Y., Farahani, R. Z., Multi-objective discrete urban road network design. *Computers & Operations Research*. 40(10), 2429–2449, 2013.
- [21] Storn, R., Price, K.,. Differential Evolution – A Simple and Efficient Heuristic for Global Optimization over Continuous Spaces. *Journal of Global Optimization*, 11, 341–359, 1997.
- [22] De Cea, J., Fernández, E., Transit Assignment for Congested Public Transport Systems: An Equilibrium Model. *Transportation Science*, 27(2), 133–147, 1993.
- [23] Chriqui, C., Robillard, P., Common Bu Lines. *Transportation Science*, 6(2), 115-121, 1975.
- [24] Florian, M., Spiess, H., The convergence of diagonalization algorithms for asymmetric network equilibrium problems. *Transportation Research Part B: Methodological*, 16(6), 477–483, 1982.
- [25] Miandoabchi, E., Farahani, R. Z., Szeto, W. Y., Bi-objective bimodal urban road network design using hybrid metaheuristics. *Central European Journal of Operations Research*, 20(4), 583–621, 2012.
- [26] Sheffi. Y., *Urban transportation networks*, Prentice-Hall, NJ, USA, 1985.
- [27] Frank, M., Wolfe, P., An algorithm for quadratic programming. *Naval Research Logistics*, 3(1-2), 95–110, 1956.
- [28] Mandl, C. E., Evaluation and optimization of urban public transportation networks. *European Journal of Operational Research*, 5(6), 396–404, 1980.
- [29] Arbex, R. O., da Cunha, C. B., Efficient transit network design and frequencies setting multi-objective optimization by alternating objective genetic algorithm. *Transportation Research Part B: Methodological*, 81(2), 355–376, 2015.
- [30] Jha, S. B., Jha, J. K., Tiwari, M. K., A multi-objective meta-heuristic approach for transit network design and frequency setting problem in a bus transit system. *Computers and Industrial Engineering*, 130, 166–186, 2019.

# **Numerical Study on the Deformation Behavior of Geosynthetic-Encased Stone Columns Supporting Embankments**

**Tuncay DOĞAN<sup>1</sup>**

**Mehmet Rifat KAHYAOĞLU<sup>2</sup>**

## **ABSTRACT**

The method of encasing the stone column with a proper type of geosynthetic material is a widely used technique to provide the required lateral confinement and to avoid the dispersion of granular column material into soft clay. Along with the improved ultimate load capacity and the reduced settlement and bulging, the geosynthetic encasement preserves the easy drainage ability of stone columns. This paper presents the finite element analysis results of a hypothetical embankment on a soft soil deposit which is improved by geotextile encased stone columns and geogrid reinforced sand mat on top. At first, numerical results of three dimensional (3D) finite element model (FEM) were validated via the experimental data of previous field studies. Afterward, parametric studies were carried out on the FEM considering the effect of the sand mat thickness, the stiffness of the geosynthetic reinforcement, and the geosynthetic encasing length and encasement stiffness on both the horizontal and vertical deformation of stone columns. Settlement differences between columns and soft soil in both the short term and long term were also determined. The optimum values of sand mat layer thickness, vertical encasement length, and geosynthetic stiffness are recommended to be used for preliminary designs.

**Keywords:** Stone column, geotextile encasement, geogrid reinforcement, sand mat, settlement, bulging.

## **1. INTRODUCTION**

The use of column-supported embankments (CSEs) provides rapid construction, quicker consolidation, total and differential settlement reduction, and adjacent facility protection [1-2]. However, it appears to be impossible to improve very soft clayey soils with CSEs, due to

---

Note:

- This paper was received on June 8, 2021 and accepted for publication by the Editorial Board on February 18, 2022.
- Discussions on this paper will be accepted by November 30, 2022.

• <https://doi.org/10.18400/tekderg.949826>

1 Department of Civil Engineering, Muğla Sıtkı Koçman University, Muğla, Turkey  
dogantuncay@msn.com - <https://orcid.org/0000-0002-6376-2163>

2 Department of Civil Engineering, Muğla Sıtkı Koçman University, Muğla, Turkey  
rkahyaoglu@mu.edu.tr - <https://orcid.org/0000-0002-9288-5277>

lack of lateral confinement and excessive lateral bulging of column material [3]. In such types of soils, insufficient confinement requirements can be persuaded by encasing the column with the proper type of geosynthetics [4-5].

The impact of geosynthetic stiffness increment on ultimate load capacity improvement, settlement, and bulging reduction of geosynthetic encased columns (GECs), and excess pore water pressure change in the soft ground was investigated through the field and scaled laboratory experiments [6-9]. Murugesan and Rajagopal (2007) asserted that the most effective parameter of the instrumented GECs was the tensile strength of encasement. They also indicated that since the greatest radial geosynthetic strain occurs at the upper part, columns should be encased in the length of the 4-fold diameter [6]. Liu et al. (2007) published the in-situ results of a case study of basal geogrid reinforced and pile-supported highway embankment [7]. The measured pressure on the piles was measured to be 14-fold bigger than that on the soil. The study reveals that soil arching transfers the loads from soil to the piles hereby excess pore pressure reduces significantly. Murugesan and Rajagopal (2010) examined the influence of material properties and the geometry of the model for both encased and non-encased stone columns in a large-scale laboratory test setup and suggested design codes for specific load and settlement conditions [8]. Yoo et al. (2015) conducted loading tests on an artificially sedimented clay ground reinforced by geotextile-encased sand piles (GESP) and conventional sand compaction piles (SCP). Results show that the failure mode of SCPs is bulging where it is buckling for GESPs thus, the geosynthetic stiffness has nearly no effect on the load-carrying capacity in the buckling failure [9].

Moreover, there are countless accomplished samples of numerical studies on encased granular columns in the literature [10-11]. Murugesan and Rajagopal (2006) implied that the geosynthetic encased stone columns (GESCs) were stiffer than ordinary stone columns [10]. Yoo (2015) presented charts for preliminary design on the estimation of the ultimate vertical deformation and the stress concentration ratio (SCR) [11]. Tabesh and Poulos (2007) declared that constructing floating columns is more feasible in cases where the column tip cannot reach the rigid ground [12]. The frictional force along the column length affects the GESCs behavior, therefore the settlement differences between the pile and the surrounding ground should be considered [13].

In recent years, the horizontal (basal) geogrid reinforcement has found an area of utilization combined with column supported embankments (CSEs) over soft clay soils in circumstances of high embankment loads to create a geosynthetic reinforced column supported embankment (GRCSE) [14-15]. Cheng et al. (2014) examined the ultimate load capacity of a geosynthetic reinforced column supported (GRCS) platform by analyzing the 15-month long in-situ data. They revealed the possible generation of soil arching for certain heights of fill, that way the GRCS system can improve the stability of the embankment and reduce bulging significantly. The results proved that the usage of the geogrid reinforcement over the composite ground improves the transfer of loads from the embankment into the stone columns [16]. Liu et al. (2017) conducted parametric analyses on several factors such as pile spacing, coefficient of shear strength, internal friction angle, and cohesion of fill material in order to compare how they affect the load transfer behavior. The study points out that the cohesion is more effective than the internal friction angle of embankment fill on the load transfer mechanism [17].

The published literature focusing on the long-term vertical and lateral deformation behavior of geosynthetic encased stone columns (GESC) is limited. Many recent studies have dealt with the load-carrying capacities and settlements of unreinforced embankments supported



with GESCs. Nevertheless, the effect of reinforcement at the base of the embankment has not been considered yet. Furthermore, the load transfer mechanism and the bulging (lateral deformation) behavior of the GESCs are not thoroughly determined.

This paper interprets the findings of finite element analysis (FEA) results of a hypothetical geotextile-encased stone column-supported embankment which is improved by a geogrid reinforced sand mat (GRSM) in soft soil. To enhance the performance of GESCs and to fill the gaps for the above-mentioned issues, the main objectives of the present study can be listed briefly as; (1) to investigate the performance of vertical encasement on stone columns and the geosynthetic reinforcement at sand mat layer, (2) to determine the optimum sand mat layer thickness and the optimum geogrid reinforcement stiffness, (3) to determine the optimum vertical geotextile encasement stiffness (tensile strength) and the adequate length of the column encasement, (4) to consider the effect of geotextile encasement on the settlement (vertical displacement) and lateral deformation (bulging) behavior of stone columns.

## 2. NUMERICAL ANALYSIS AND PARAMETRIC STUDY

A hypothetical composite soil system was idealized and simulated with 3D FE analyses using PLAXIS 3D (Plaxis v.b 2018) [18]. First, the model was verified with the soft ground at the study of Raju (1997) [19]. Then, parametric studies on the load-carrying capacity and the deformation behavior of vertically encased columns were carried out for various parameters including the sand mat layer thickness, the stiffness of reinforcement, and encasement. The 3D FEM, FE mesh and cross-section of the model are shown in Fig. 1(a), Fig. 1(b) and Fig. 1(c).

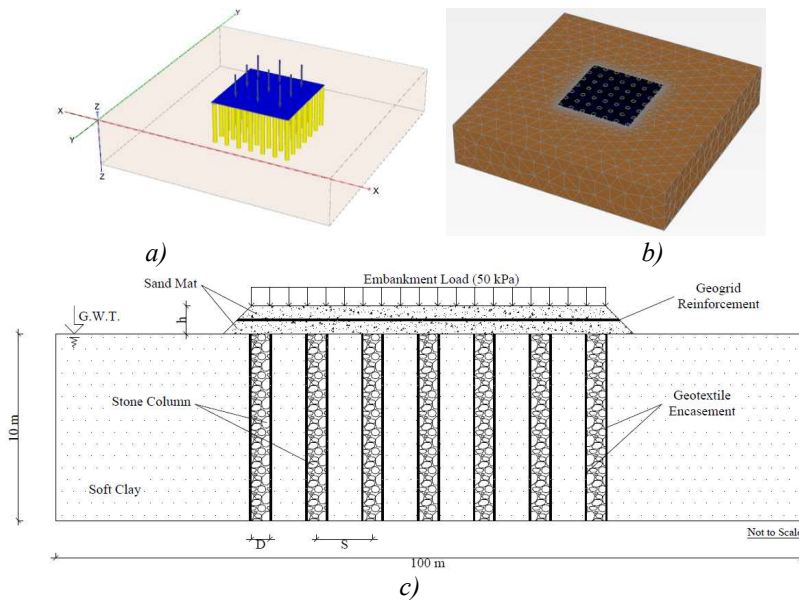


Fig. 1 - (a) 3D View of FEM, (b) FE Mesh of PLAXIS 3D Model, (c) Cross-Section of the Model

### 2.1. Material Properties

In this study, three types of soil materials have been used to simulate the soft ground, the sand mat, and the granular column. Known to be accurately corresponding to the behavior of the soft soil between columns, the Modified Cam-Clay (MCC) Model was used to simulate the ground in undrained condition, following the advice of Kaliakin et al. (2012) and Khabbazian et al. (2015) [20-21]. MCC model is defined by five parameters: the slope of the swelling line (K), the slope of the virgin consolidation line ( $\lambda$ ), the void ratio at unit pressure (e), the slope of the critical state line (M), and Poisson’s ratio ( $\nu$ ). Stone columns and the sand mat layer were modeled as granular soil and idealized by Mohr-Coulomb (MC) Model as a homogenous drained soil material [22]. Five material parameters are associated with this model, namely effective friction angle ( $\phi'$ ), effective cohesion (c'), dilation angle ( $\phi'$ ), elastic modulus (E), and Poisson’s ratio ( $\nu$ ). The Mohr-Coulomb and the Modified Cam Clay parameters used in the numerical analyses were similar to typical values with the previous studies e.g. [11, 20, 22]. Detailed information about soft soil, sand mat layer, and stone column are given below (Table 1).

Table 1 - Material properties used in the numerical analyses

Parameter	Column Material Stone / Soil [22]	Sand Mat Material Sacramento river sand [20]	Soft Clay Material Malaysian marine clay [23-25]
Model type	MC	MC	MCC
Effective unit weight, $\gamma'$ (kN/m <sup>3</sup> )	19	18	15
Effective friction angle, $\phi'$ (°)	43	32	-
Elastic modulus, E (kPa)	55000	15000	-
Poisson’s ratio, $\nu$	0.3	0.3	0.3
Effective cohesion, c' (kPa)	1	1	-
Permeability, k (m/s)	1x10 <sup>-2</sup>	1x10 <sup>-3</sup>	1x10 <sup>-6</sup>
Dilation angle, $\phi'$ (°)	10	3	-
Slope of the critical state line, M	-	-	1.0
Slope of the virgin cons. line, $\lambda$	-	-	0.4
Slope of swelling line, K	-	-	0.02
Void ratio at unit pressure, e	-	-	1.0

The geosynthetics used for both vertical encasement and basal reinforcement were modeled as linear elastic material with axial stiffness in elastic or elastoplastic forms, with an assumed Poisson’s ratio of 0.30 e.g. [7]. The secant stiffness of the geosynthetic (J) was defined as the ratio of the tensile force per unit width to the average strain in the geosynthetic. The initial

tensile modulus was computed at 3% axial strain to determine the geosynthetic elastic module. Geosynthetic encasement design values for stone column were documented as required tensile modulus (J) between 1000 and 4000 kN/m by Almeida et al. (2015) [26]. Therefore, values between J=500-3500 kN/m were used in the numerical analyses for encasement. Also, seven different reinforcements with stiffness of J=1000-7000 kN/m were used to investigate the influence of the basal reinforcement.

In order to model the interaction behavior between the geosynthetic and the granular column, and between the geosynthetic and the surrounding soft soil, interface elements that can be characterized by two sets of parameters were used. The coefficient of sliding friction ( $\mu$ ) between the geosynthetic and the granular column was selected to be 0.5 ( $\mu = 2/3 \tan\phi$ ) [27], where  $\phi$  is the friction angle of the column material. For interaction between the geosynthetic and the soft soil,  $\mu$  was assumed to be 0.3 ( $\mu = 0.7 \tan\phi$ ) [28], where  $\phi$  is the friction angle of the soft soil.

## **2.2. Geometry Model**

In the analyses, the FE model limits were designated 100 m x 100 m in the horizontal direction and 10 m in the vertical direction. The stone column length and depth of the soft clay layer were adopted as 10 meters to simulate the fixed column behavior. Ordinary (conventional) stone columns (OSC) and vertically encased stone columns (VESC) with varying diameters of 0.60, 1.00, and 1.40 m and varying center-to-center column spacing ratios (s/D) of 2, 3, and 4 were selected within the analyses.

## **2.3. Model Verification**

The case study by Raju (1997) in which a stone-column-supported embankment constructed in Kebun, Malaysia was adopted and simulated numerically with PLAXIS 3D [19]. The Kebun interchange is located near the city of Klang on the west coast of Malaysia. The upper soils in the coastal region are predominantly extremely soft marine clays having thicknesses of up to 35 m. and the very soft clay deposit is 11 m thick in the cone test carried out in Kebun. Tip resistances range between 0.1 MPa and 0.3 MPa in the soft clay deposit. Undrained shear strengths as low as 5 kPa and an increasing rate of about 1 kPa per meter in depth have been measured. 1m high embankment on untreated soil has failed. At the site, only the typical values for moisture content ( $w$ ), liquid limit ( $w_l$ ), plastic limit ( $w_p$ ), plasticity index (PI), clay, silt, and sand fractions, the sensitivity values ( $St$ ), and the coefficient of consolidation ( $c_v$ ) for the soft soils were encountered. Still, it is not possible to clearly determine the parameters of the Plaxis MCC model with these material properties accessed in the field. Yoo et al. (2007) [23] and Yoo and Kim (2009) [24] refer to the Malaysian clay in the study of Tan et al. (2008) [25], located in the region close to Raju (1997) study, in the validation of their finite element analysis. For this reason, soil properties determined in the Raju (1997) field study were converted into MCC material model parameters with the help of these studies [23-25] (Table 1).

At the measurement point in Kebun where the embankment height is 2.6 m, a settlement of about 40 cm has been measured (it should be kept in mind that the soil and stone column layout is different at the sites and the settlement magnitudes cannot be directly compared).

Here, only 25% of the settlement has taken place during embankment construction. The remaining settlement has taken place over a period of almost 8 months thereafter. In areas not treated with vibro replacement, settlements over 1.0 m were measured for comparable embankment heights and soil conditions. The load value corresponding to 2.6 m fill height was used as model loading in the validation study (50 kPa).

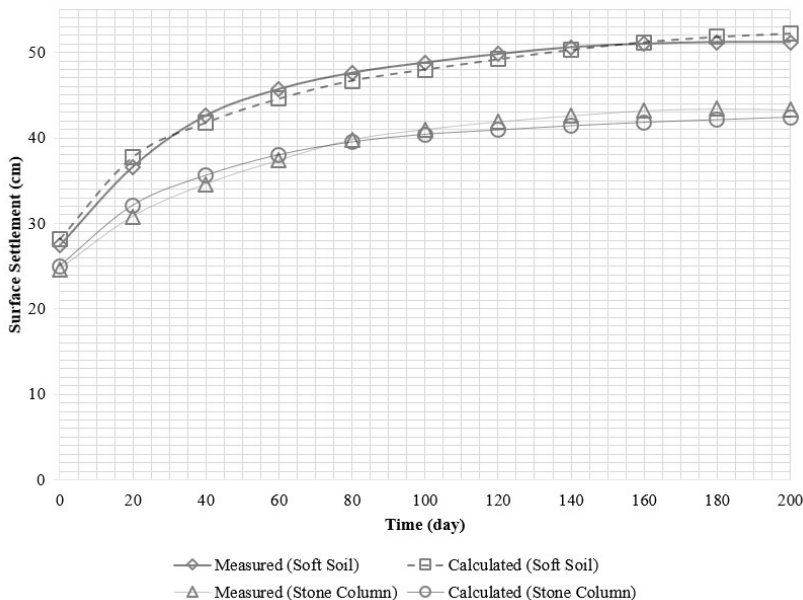


Fig. 2 - Comparison of Measured vs. Calculated Settlements of Soft Soil and Stone Column

The settlement results and the vertical stress transferred to both the column and the soft ground obtained from the numeric study were compared with those measured at the Kebun project (Fig. 2). Consistency between the measured settlement values from the Kebun, Malaysia project and calculated results from the above-mentioned analyses makes the numerical model convenient to apply to parametric studies.

### 2.4. Numerical Analyses

At first, to choose the most suitable column profile to be used in analyses, column diameter (D) was pre-selected as 0.60 meters and a relative settlement diagram was drawn for the increasing load for both drained and undrained conditions. Relative settlement can be described as the ratio of the settlements between the top of the stone column and the soft clay layer. In line with the experimental study of Debnath and Dey (2017) pressure causing a settlement of 20% of the diameter of the column was considered as the ultimate load-carrying capacity [29]. A uniform load was applied on sand mat until achieving this settlement value. Bearing capacity corresponding to the relative settlement of 20% D was determined as 165 kPa (Fig. 3).

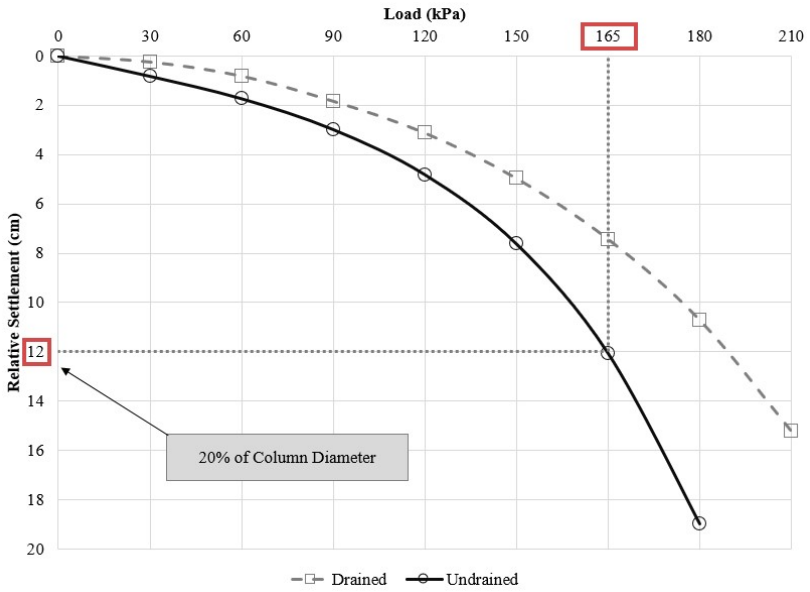
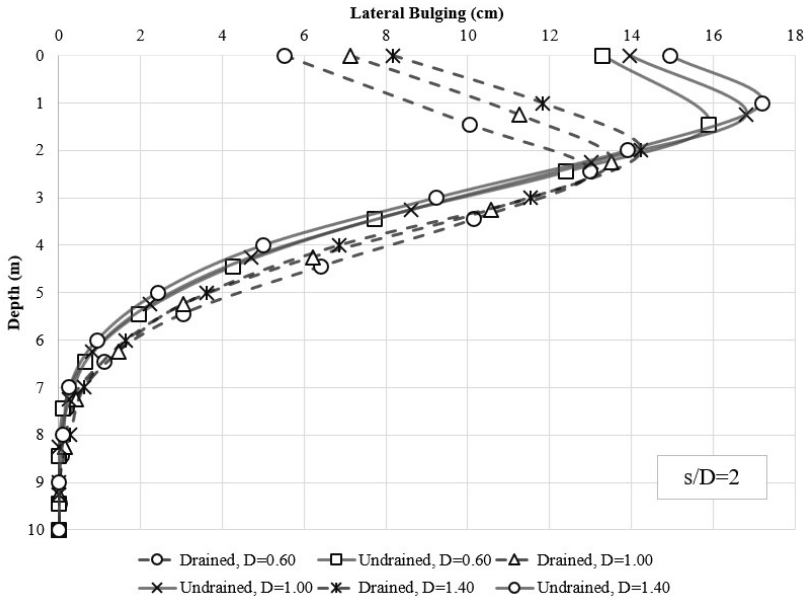


Fig. 3 - Load - Relative Settlement Relationship



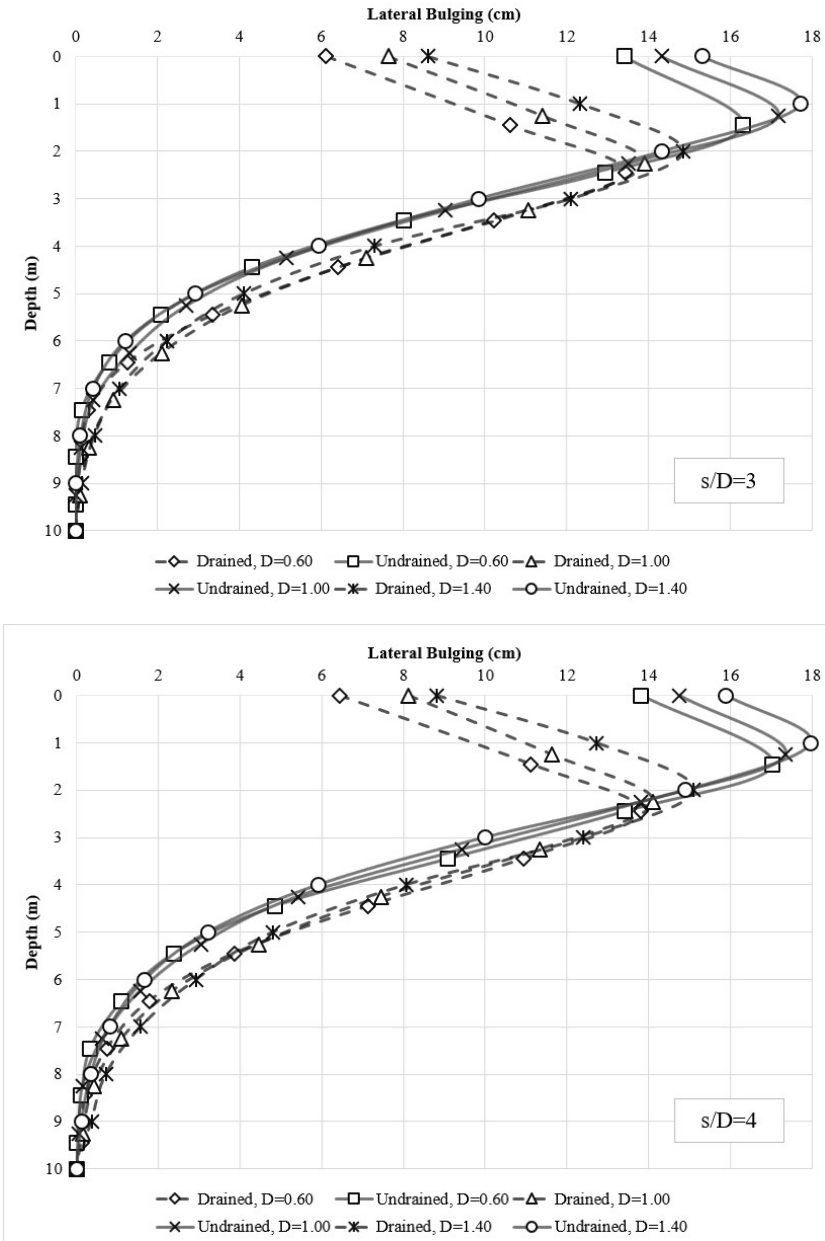


Fig. 4 - Bulging - Depth Relationship (a)  $s/D=2$ , (b)  $s/D=3$ , (c)  $s/D=4$

This capacity was decided to be used in the following analyses. Then, the stone column variations of 0.60 m, 1.00 m, and 1.40 m diameters (D) and spacing ratios ( $s/D$ ) of 2, 3, and

4 have been subjected to 165 kPa for both drained and undrained conditions, lateral deformation-depth diagrams were drawn and the maximum bulging values were noted on Fig. 4(a), Fig. 4(b) and Fig. 4(c).

Noted numerical data were reflected on the maximum lateral deformation-spacing ratio diagram (Fig. 5). In order to dilute the effect of column diameter and column spacing, the stone column profile with the least deviation was determined to be  $D=1.00$  m and  $s/D=3$  at undrained condition (UC) and it was decided to be used in the following analyses within the study. This way the stone columns were isolated from lateral/vertical deformation change depending on column diameter or column spacing and bearing capacity change caused by soil arching.

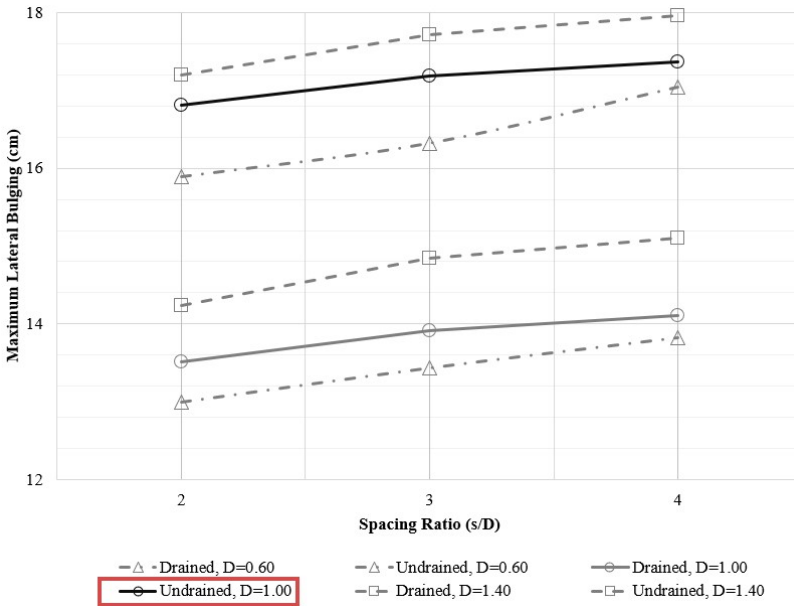


Fig. 5 - Maximum Lateral Deformation - Spacing Ratio (s/D) Relationship

Contrary to expectation, undrained settlement values are higher than drained settlement values as can be seen from Fig.5. A similar situation has been observed in previous studies and explained as follows. The consolidation of the soft soil surrounding the stone column can significantly affect both the response of the soil to loading and the load distribution between the column and the soil. The drainage of the column and the instantaneous dissipation of the excess pore-water pressure in the column causes an immediate load transfer to the column. During consolidation, there is a progressive load transfer from the soil to the column. And also, with a continuous consolidation of the soil, which is accelerated by the drainage effect of the columns, an improvement of the soil parameters of the in-situ soil becomes effective [30-31].

The varying material properties and reinforcement scenarios evaluated in the parametric study were summarized in Table 2.

Table 2 - Parameters evaluated in the parametric analyses

Parameter	
Soft soil layer height (H) (m)	10, 11, 12, 13, 14, 15, 16, 18, 20
Column diameter (m)	0.60, 1.00, 1.40
Spacing ratio (s/D)	2, 3, 4
Sand mat thickness (m)	0.00 D, 0.05 D, 0.10 D, 0.15 D, 0.20 D
Geogrid stiffness (J) (kN/m)	1000, 2000, 3000, 4000, 5000, 6000, 7000
Geotextile stiffness (E) (kN/m)	500, 1000, 1500, 2000, 2500, 3000, 3500

### 3. RESULTS AND DISCUSSIONS

#### 3.1. Effect of Sand Mat Thickness

An unreinforced sand mat layer (USM) that has a thickness varying between 0.0 D to 0.2 D with 0.05 D intervals was deployed on an OSC reinforced soft clay ground. While determining the sand mat thickness, the values given in the Dutch Design Guideline CUR226 [31] were considered. The sand mat layer was designated as two layers in order to lay the

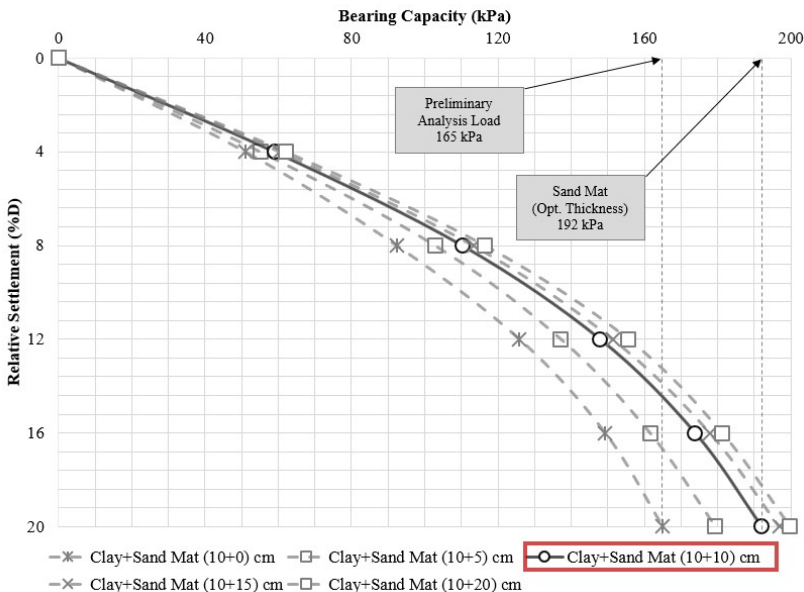


Fig. 6 - Bearing Capacity - Relative Settlement Diagram for Sand Mat Thickness



reinforcement material between these layers e.g., 0.10 D thick sand + geotextile reinforcement + 0.05 D thick sand for a 0.15 D meters thick sand mat. A series of numerical analyses were carried out and bearing capacity-relative settlement diagrams were drawn using the data obtained (Fig. 6).

Sand mat thickness appears to be improving the bearing capacity obviously until 0.2 D meters and beyond that, the effect is not obvious. A sand mat layer of 0.2 D thick was selected as the optimum sand mat and decided to be used at the continuing steps of the numerical study. An early study by Debnath and Dey (2017) indicates that a USM thickness of about 0.2 times the diameter of the footing (i.e., 0.2D) gives the maximum performance improvement in composite foundation systems [29]. The calculated sand mat thickness conforms to the referent study. The selected optimum sand mat was calculated to be causing an increase up to 1.16-fold on the bearing capacity of OSC installed in soft ground.

### 3.2. Effect of Geogrid Reinforcement Stiffness

The optimum sand mat of 0.2 D meters thick was reinforced with varying axial stiffness (J) of the geogrid reinforcement material; 1000, 2000, 3000, 4000, 5000, 6000, and 7000 kN/m representing a scale of low to very high strength geosynthetic material. Bearing capacity-relative settlement diagrams were drawn using the data obtained from the series of numerical analyses (Fig. 7).

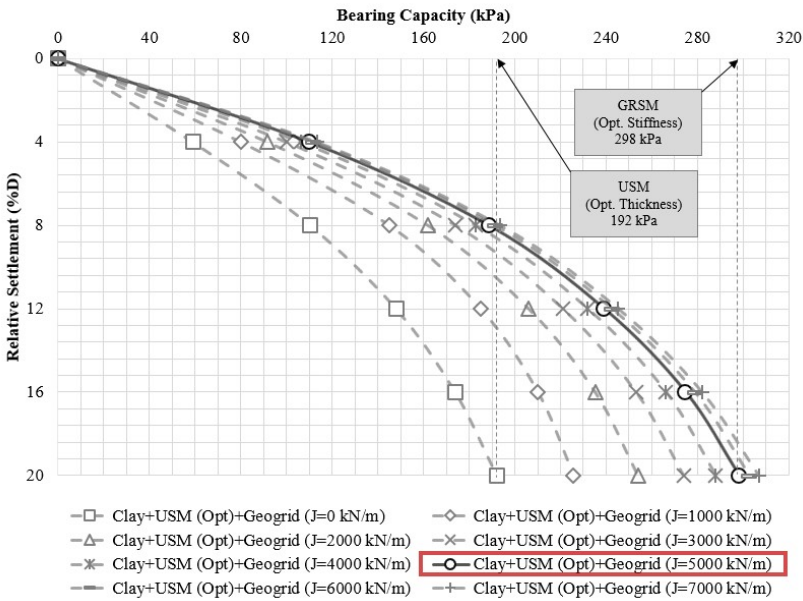


Fig. 7 - Bearing Capacity - Relative Settlement Diagram for Geogrid Stiffness

According to Fig. 7, bearing capacity increases with the increasing stiffness values of geogrid reinforcement until J=5000 kN/m. The improvement becomes insignificant after that level.

Similar results have also been reported in former studies [32-33]. Geogrid reinforcement with 5000 kN/m stiffness was selected as optimum and decided to be used in the ongoing numerical study. The selected optimum GRSM was calculated to be increasing the bearing capacity of the soft ground up to 1.55-fold and 1.81-fold compared to OSC+USM and OSC, respectively.

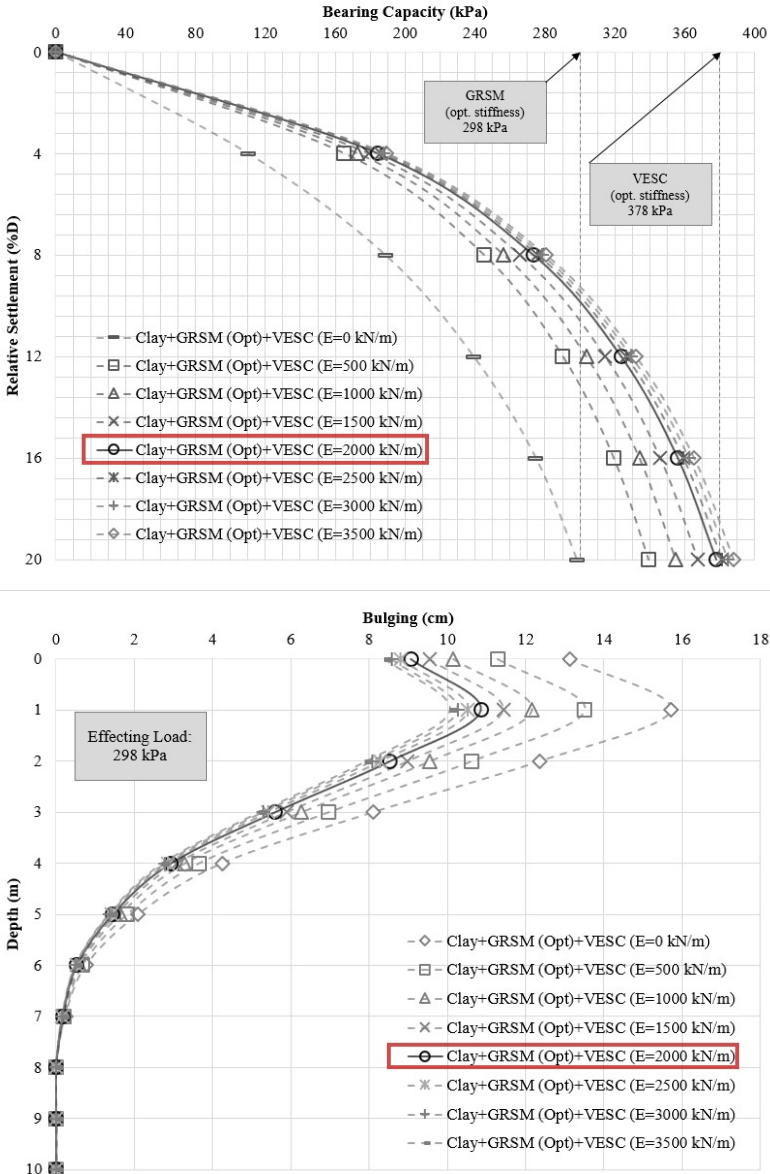


Fig. 8 - Diagrams for Geotextile Stiffness  
 (a) Bearing capacity-relative settlement, (b) Lateral deformation-depth

### 3.3. Effect of Geotextile Encasement Stiffness

The OSCs installed in the soft ground under optimum GRSM ( $m=0.2 D$  and  $J=5000 \text{ kN/m}$ ) were encased with varying axial stiffness of geotextile material; 500, 1000, 1500, 2000, 2500, 3000, and 3500  $\text{kN/m}$  representing a scale of low to very high strength geosynthetic material. The lateral deformation of the stone column was not measured in the Raju (1997) field study used for validation. In this numerical study, the lateral deformation of the stone column was calculated as the lateral deformation of the geosynthetic encasement. Bearing capacity-relative settlement diagram Fig. 8(a) and lateral deformation-depth diagram Fig. 8(b) were drawn, respectively by using the data obtained from the series of numerical analyses performed.

According to Fig. 8(a) and Fig. 8(b), additional confinement due to the increasing stiffness of the geosynthetic encasement material appears to be significantly contributing to both the ultimate load capacity and the bulging reduction. The contribution is obvious until the stiffness value of  $E=2000 \text{ kN/m}$  and beyond that enhancement is insignificant. For that matter, a stiffness value of 2000  $\text{kN/m}$  for vertical encasement was chosen as optimum and decided to be used at continuing steps of the numerical study. The selected optimum GRSM+VESC was calculated to be increasing the load-carrying capacity of the soft ground up to 1.27-fold, 1.97-fold, and 2.29-fold compared to GRSM+OSC, USM+OSC, and OSC and reducing the lateral deformation up to 31% compared to GRSM+OSC, respectively. Former studies conform the load-carrying capacity improvement and settlement reduction of SCs to the provision of the geosynthetic encasement [29, 34-37].

### 3.4. Effect of Geotextile Encasement Length

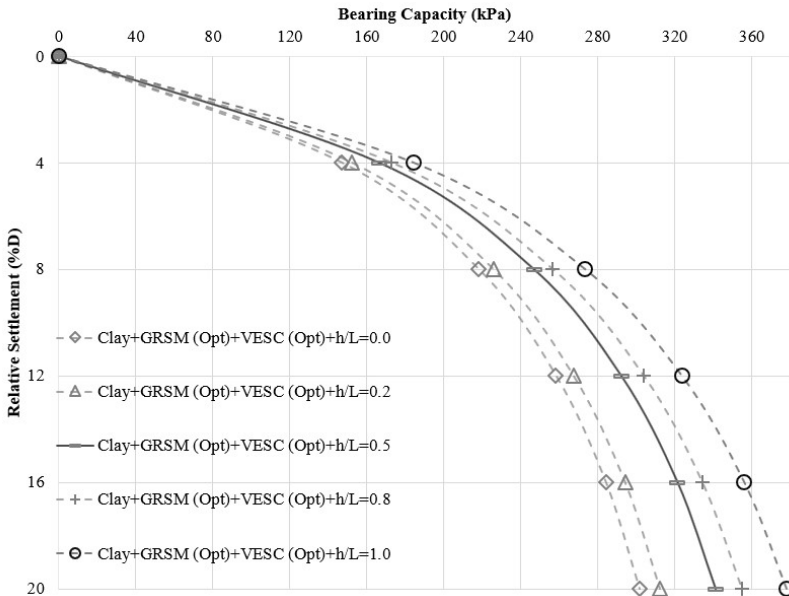


Fig. 9 - Bearing Capacity - Relative Settlement Diagram for Varying Encasement Lengths

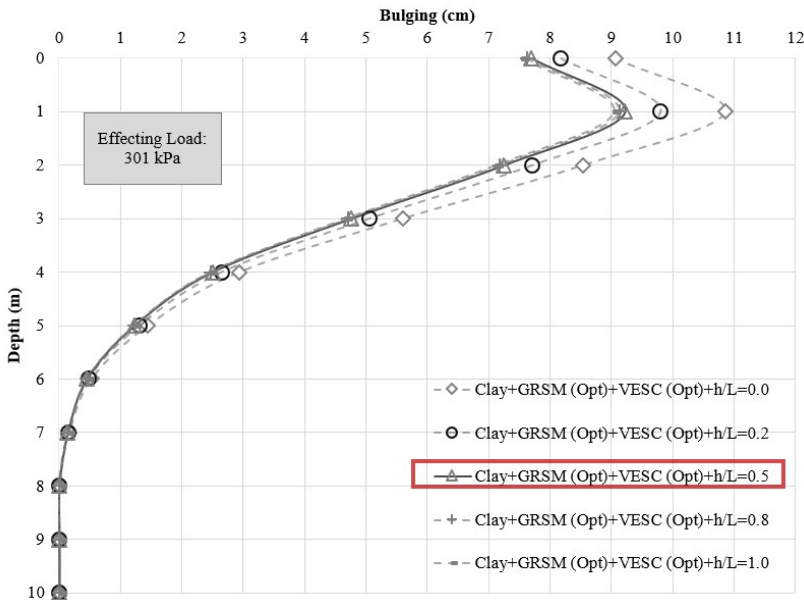


Fig. 10 - Lateral Deformation - Depth Diagram for Varying Encasement Lengths

The analyses on optimized GRSM reinforced ( $m=0.2$  D and  $J=5000$  kN/m) and VESC ( $E=2000$  kN/m) improved soil model were repeated for different encasement lengths of which the ratio of vertical encasement length to column length ( $h/L$ ) varied 0.0 to 1.0. Bearing capacity-relative settlement (Fig. 9) and lateral deformation-depth diagrams (Fig. 10) were drawn using the data obtained from analyses.

Fig. 9 and 10 show that a vertical encasement from the top to the middle of the column ( $h/L=0.5$ ) appears to be obviously contributing to both the bearing capacity and the bulging reduction of SC under GRSM. For lengths beyond the middle of the column, the encasement's contribution is insignificant. The bulging is still the main reason for failure of GESC independent to different encasement lengths. Similar results have been reported in former studies. Malarvizhi and Ilamparuthi (2007) indicate that the maximum bulging occurs at  $4D$  from the top of the column [34]. Ali et al. (2012) reveals that whether floating or end-bearing long unreinforced stone columns always fail by bulging whereas short floating columns always fail because of punching. Their study refers that encasement over full column length gives higher failure stress than encasement over the top half or quarter of the column length and also the higher failure stress still occurs at the upper half of the column [35].

Despite the fact of 50% encasement length reduction as a result of encasing the upper half of the stone column, the decrease of bearing ratio of composite ground is determined as 10%. This suggests that the stone column can be encased partially on the condition of reinforcing up to where lateral deformation is maximum. Tandel et al. (2012) imply a 14% decrease in maximum load capacity despite the 50% decrease at encasement length [36]. The calculated load-carrying performance of partially encased stone columns conforms to the referent study.

#### 4. CONCLUSIONS

The conclusions of the study are summarised respective to the analyses order:

(1) Composition of a sand mat at the base of the embankment reduces the settlement difference between the stone column and the soft ground. Sand mat thickness appears to be improving the bearing capacity obviously until  $0.2D$ . The effect becomes insignificant beyond that depth.

(2) Utilizing a layer of geogrid reinforcement in the sand mat increases the effect up to the axial stiffness of  $J=5000$  kN/m. The optimum GRSM ( $0.2D$  thick and reinforced by a  $J=5000$  kN/m geogrid layer) caused an increase up to 1.16-fold on the bearing capacity of OSC installed in soft ground.

(3) Geosynthetic encasement can significantly alter the stress/settlement response of the stone column. Besides, encasing the stone columns with a geotextile reduces the lateral displacements. Geotextile encasement up to the stiffness of  $E=2000$  kN/m appears to be the optimum, behind that contribution is insignificant. The optimum GRSM+VESC (vertically encased by a geotextile of  $E=2000$  kN/m stiffness) caused increasing the ultimate load capacity of the soft soil up to 1.27-fold, 1.97-fold, and 2.29-fold compared to GRSM+OSC, USM+OSC, and OSC and reducing the lateral deformation up to 31% compared to GRSM+OSC, respectively.

(4) For end-bearing (fixed) stone columns, an encasement length of  $0.5L$  appears to be contributing significantly to both the bearing capacity and the bulging reduction of SC under GRSM. For lengths beyond the middle of the column, the encasement's contribution is not obvious.

#### Nomenclature

$D$	Column Diameter
$L$	Column Length
$\varphi'$	Dilation Angle
$c'$	Effective Cohesion
$\phi'$	Effective Friction Angle
$\gamma'$	Effective Unit Weight
$E$	Elastic Modulus
$J$	Geogrid Stiffness
$E$	Geotextile Stiffness
$k$	Permeability
$\nu$	Poisson's Ratio
$K$	Slope of Swelling Line
$M$	Slope of the Critical State Line
$\lambda$	Slope of the Virgin Consolidation Line

<i>H</i>	Soft Clay Layer Height
<i>s</i>	Stone Column Spacing
<i>e</i>	Void Ratio at Unit Pressure

### References

- [1] Borges, J. and Marques, D., Geosynthetic-Reinforced and Jet-Grout Column Supported Embankments on Soft Soils: Numerical Analysis and Parametric Study. *Computers and Geotechnics*, 38(7):883-896, 2011. DOI: 10.1016/j.compgeo.2011.06.003
- [2] Hughes, J., Withers, N. and Greenwood, D.A., A Field Trial of the Reinforcing Effect of a Stone Column in Soil. *Géotechnique*, 25(1):31-44, 1975. DOI: 10.1680/geot.1975.25.1.31
- [3] Madhav, M.R. and Vanitha, L., Analysis and Design of Granular Pile Reinforced Ground. Proceedings of ATC-7 Workshop on Stone Column in Soft Deposits, Korea, Busan:1-17, 2006.
- [4] Van Impe, W. and Silence, P., Improving of the Bearing Capacity of Weak Hydraulic Fills by Means of Geotextiles. Proceedings of the 3rd International Conference on Geotextiles, Austria: Vienna:1411-1416, 1986.
- [5] Raithel, M., Kempfert, H.G. and Kirchner, A., Geotextile-Encased Columns (GEC) for Foundation of a Dike on very Soft Soils. Proceedings of the 7th ICG International Conference on Geosynthetics, France, Nice:1025-1028, 2002.
- [6] Murugesan, S. and Rajagopal, K., Model Tests on Geosynthetic Encased Stone Columns. *Geosynthetics International*, 14(6):346-354, 2007. DOI: 10.1680/gein.2007.14.6.346
- [7] Liu, H., Ng, C.W.W. and Fei, K., Performance of a Geogrid-Reinforced and Pile Supported Highway Embankment over Soft Clay: Case Study. *Journal of Geotechnical and Geo-Environmental Engineering*, 133(12):1483-1493, 2007. DOI: 10.1061/(ASCE)1090-0241(2007)133:12(1483)
- [8] Murugesan, S. and Rajagopal, K., Studies on the Behaviour of Single and Group Geosynthetic Encased Stone Columns. *The Journal of Geotechnical and Geo-Environmental Engineering*, 136(1):129-139, 2010. DOI: 10.1061/(ASCE)GT.1943-5606.0000187
- [9] Yoo, W., Kim, B. and Cho, W., Model Test Study on the Behaviour of Geotextile-Encased Sand Pile in Soft Clay Ground. *KSCE Journal of Civil Engineering*, 19(3):592-601, 2015. DOI: 10.1007/s12205-012-0473-4
- [10] Murugesan, S. and Rajagopal, K. Geosynthetic-Encased Stone Columns: Numerical Evaluation. *Geotextiles and Geomembranes*, 24(6):349-358, 2006. DOI: 10.1016/j.geotextmem.2006.05.001bulging
- [11] Yoo, C., Settlement Behaviour of Embankment on Geosynthetic-Encased Stone Column Installed Soft Ground - A Numerical Investigation. *Geotextiles and Geomembranes*, 43:484-492, 2015. DOI: 10.1016/j.geotextmem.2015.07.014

- [12] Tabesh, A. and Poulos, H., Design Charts for Seismic Analysis of Single Piles in Clay. *Geotechnical Engineering*, 160(2):85-96, 2007. DOI: 10.1680/geng.2007.160.2.85
- [13] Lu, Y., Abusharar, S., Zheng, J., Chen, B. and Yin, J., The Performance of an Embankment on Soft Ground Reinforced with Geosynthetics and Pile Walls. *Geosynthetics International*, 16:173-182, 2009. DOI: 10.1680/gein.2009.16.3.173
- [14] Briançon, L. and Simon, B., Performance of Pile Supported Embankment over Soft Soil: Full-Scale Experiment. *Journal of Geotechnical and Geo-Environmental Engineering*, 138(4):554-561, 2012. DOI: 10.1061/(ASCE)GT.1943-5606.0000561
- [15] Jelušič, P. and Žlender, B., Optimal Design of Reinforced Pad Foundation and Strip Foundation. *International Journal of Geomechanics*, 18(9), 2018. DOI: 10.1680/jgein.17.00039
- [16] Cheng, Q., Wu, J., Zhang, D. and Ma, F., Field Testing of Geosynthetic-Reinforced and Column-Supported Earth Platforms Constructed on Soft Soil. *Frontiers of Structural and Civil Engineering*, 8(2):124-139, 2014. DOI: 10.1007/s11709-014-0255-9
- [17] Liu, W., Qu, S., Zhang, H. and Nie, Z., An Integrated Method for Analysing Load Transfer in Geosynthetic-Reinforced and Pile-Supported Embankment. *KSCE Journal of Civil Engineering*, 21(3):687-702, 2017. DOI: 10.1007/s12205-016-0605-3
- [18] Brinkgreve, R.B.J., Engin, E. and Swolfs, W.M., *Plaxis 3D 2012 Manual*. Plaxis bv, the Netherlands, 2012.
- [19] Raju, V.R., *The Behavior of very Soft Cohesive Soils Improved by Vibroreplacement. Ground Improvement Geosystems – Densification and Reinforcement*. Thomas Telford, 253-259, 1997. DOI: 10.1680/gigdar.26056.0032
- [20] Kaliakin, V., Khabbazian, M. and Meehan, C., Modelling the Behaviour of Geosynthetic Encased Columns: Influence of Granular Soil Constitutive Model. *International Journal of Geomechanics*, 12(4):357–369, 2012. DOI: 10.1061/(ASCE)GM.1943-5622.0000084
- [21] Khabbazian, M., Kaliakin, V. and Meehan, C., Column Supported Embankments with Geosynthetic Encased Columns: Validity of the Unit Cell Concept. *Geotechnical and Geological Engineering*, 33:425-442, 2015. DOI: 10.1007/s10706-014-9826-8
- [22] Ambily, A. and Gandhi, S., Behaviour of Stone Columns Based on Experimental and FEM Analysis. *Journal of Geotechnical and Geo-Environmental Engineering*, 133(4):405-415, 2007. DOI: 10.1061/(ASCE)1090-0241(2007)133:4(405)
- [23] Yoo, C., Song, A.R., Kim, S.B., and Lee, D.Y., Finite Element Modelling of Geogrid-Encased Stone Column in Soft Ground. *Geotechnical Society*, 23 (10):133-150, 2007.
- [24] Yoo, C. and Kim, S.B., Numerical Modeling of Geosynthetic-Encased Stone Column-Reinforced Ground. *Geosynthetics International*, 16 (3):116-126, 2009. DOI: 10.1680/gein.2009.16.3.116
- [25] Tan, S.A., Tjahyono S. and Oo, K.K., Simplified Plane-Strain Modelling of Stone-Column Reinforced Ground. *Journal of Geotechnical and Geoenvironmental Engineering*, 134 (2):185-194, 2008. DOI: 10.1061/(ASCE)1090-0241(2008)134:2(185)

- [26] Almeida, M., Hosseinpour, I., Riccio, M. and Alexiew, D., Behaviour of Geotextile Encased Granular Columns Supporting Test Embankment on Soft Deposit. *Geotechnical and Geo-Environmental Engineering*, 141(3), 2015. DOI: 10.1061/(ASCE)GT.1943-5606.0001256.
- [27] Elias, V. Welsh, J. Warren, J., Lukas, R., Collin, G. Berg, R. R., *Ground Improvement Methods*, Vol. II. Federal Highway Administration, Washington, DC, USA, FHWA-NHI-06-020, 2006.
- [28] Abu-Farsakhl, M., Coronel, J., Tao, M., Effect of Soil Moisture Content and Dry Density on Cohesive Soil-Geosynthetic Interactions Using Large Direct Shear Tests, *Journal of Materials in Civil Engineering*, 19 (7):540-549, 2007. DOI:10.1061/(ASCE)0899-1561(2007)19:7(540).
- [29] Debnath, P. and Dey, A., Bearing Capacity of Geogrid Reinforced Sand over Encased Stone Columns in Soft Clay. *Geotextiles and Geomembranes*, 45:653-665, 2017. DOI: 10.1016/j.geotexmem.2017.08.006
- [30] Juran, I. and Guermazi, A., Settlement Response of Soft Soils Reinforced by Compacted Sand Columns. *Journal of Geotechnical Engineering*, 114 (8):930-943, 1988. DOI: 10.1061/(ASCE)0733-9410(1988)114:8(930)
- [31] Van Eekelen, S.J.M. and Brugman, M.H.A., *Design Guideline Basal Reinforced Piled Embankments*. CRC Press, SBR Kennisoverdracht B.V., 2016.
- [32] Zhang, N. et al., Evaluation of Effect of Basal Geotextile Reinforcement under Embankment Loading on Soft Marine Deposits. *Geotextiles and Geomembranes*, 43(6):506-514, 2015. DOI: 10.1016/j.geotexmem.2015.05.005
- [33] Kahyaoglu, M.R. and Vaníček, M.A., Numerical Study of Reinforced Embankments Supported by Encased Floating Columns. *Acta Geotechnica Slovenica*, 16(2):25-38, 2019. DOI: 10.18690/actageotechslv.16.2.25-38.2019
- [34] Malarvizhi, S. and Ilamparuthi, K., Comparative Study on the Behaviour of Encased Stone Column and Conventional Stone Column. *Soils and Foundations*, 47(5):873-885, 2007. DOI: 10.3208/sandf.47.873
- [35] Ali, K., Shahu, J. and Sharma, K., Model Tests on Geosynthetic-Reinforced Stone Columns: A Comparative Study. *Geosynthetics International*, 19(4):292-305, 2012. DOI:10.1680/gein.12.00016
- [36] Tandel, Y. and Solanki, C.H., Deformation Behaviour of Ground Improved by Reinforced Stone Columns. *Australian Geomechanics Journal*, 47:51-59, 2012.
- [37] Xu, Z., Sathiyamoorthy, R., Jian-Feng, C., Zhen, Z. and Liang-Yong, L., 3D Coupled Mechanical and Hydraulic Modelling of Geosynthetic Encased Stone Column-Supported Embankment Over Soft Clay. *Marine Georesources & Geotechnology*, 2020, DOI:10.1080/1064119X.2020. 1825571



# **Identification and Prioritization of Key Performance Indicators for the Construction Small and Medium Enterprises**

**Ozan OKUDAN<sup>1</sup>**  
**Cenk BUDAYAN<sup>2</sup>**  
**Yusuf ARAYICI<sup>3</sup>**

## **ABSTRACT**

**Purpose:** The central purpose of this study is to propose a set of key performance indicators (KPIs) to measure the performance of construction small and medium enterprises (SMEs) that have been ignored in the performance management literature so far. Secondly, this study aims to determine the most crucial KPIs by using the fuzzy VIKOR method to improve cost-effectiveness in the performance measurement of construction SMEs. At the first stage of this study, KPIs proposed by the existing studies were identified via a literature survey. Then, the KPIs extracted from the literature survey were verified, and eight new KPIs were proposed as a result of focus group discussions with 12 participants who are owners/managers of construction SMEs. Additionally, the Balanced Scorecard (BSC) was modified in line with the needs of construction SMEs, and each KPI was grouped into a BSC perspective. A questionnaire survey followed this grouping to gather data associated with the KPIs. Based on these data, KPIs were prioritized by using the fuzzy VIKOR. It is found out that external indicators such as “effectiveness of monitoring market conditions” are determined as the most important KPIs, in contrast to the findings in the studies about large-scale companies. Furthermore, “Attracting new customers”; “Reliability of financial performance” and, “Competency of managers” are identified as important indicators. Four KPIs proposed by experts during the focus group discussion are placed among the most important KPIs, which highlights the need for a specific performance measurement system (PMS) for construction SMEs.

**Keywords:** Performance measurement, KPIs, construction SMEs, fuzzy VIKOR, MCDM.

---

### Note:

- This paper was received on August 3, 2021 and accepted for publication by the Editorial Board on April 8, 2022.
- Discussions on this paper will be accepted by November 30, 2022.
- <https://doi.org/10.18400/tekderg.977849>

1 Department of Civil Engineering, Yildiz Technical University, Istanbul, Turkey  
okudan@yildiz.edu.tr - <https://orcid.org/0000-0001-7816-2761>

2 Department of Civil Engineering, Middle East Technical University, Northern Cyprus  
cbudayan@metu.edu.tr - <https://orcid.org/0000-0002-8433-2824>

3 Department of Architecture and Built Environment, Northumbria University, Newcastle, United Kingdom  
yusuf.arayici@northumbria.ac.uk - <https://orcid.org/0000-0001-5705-2272>

## **1. INTRODUCTION**

The construction SMEs are essential parts of the construction industry (CI). The Department for Business Innovations and Skills (2012) underlined that 85.1% of employment and 72.9% of total revenue in the UK construction industry is driven by construction SMEs. Construction SMEs contribute to construction projects in diverse ways. They can deliver small and medium-sized projects as main contractors and undertake specialist works as subcontractors in large projects due to the lack of skilled labour force in large construction companies. The industry relies on construction SMEs especially when it comes to off-site manufacturing such as design and procurement, on-site manufacturing, assembly, and supporting services in large construction projects (Rezgoui and Miles 2010). Therefore, construction SMEs' performances play a vital role in completing large construction projects successfully (Williams 2016).

Although the CI is considered one of the "locomotive industries", it is often criticized because of its low productivity and underperformance (Cui et al. 2018). Perhaps it is accurate to say that it performs the worst compared to other industries (Institution of Civil Engineering 2018). One of the most critical reasons for the low performance of the industry can be that most construction SMEs, as crucial players in the CI, show mediocre performance and fail to survive in the market. The report published by U.S. Small Business Administration (2012) stated that the survival rate of SMEs in the CI is less than 40% which is the lowest among the industries such as manufacturing, retail trade, food services & hotels. The report of the Institution of Civil Engineers (2018) also underlined the same issue. The report pinpointed that over 90% of construction SMEs experienced financial difficulties due to unfair and overdue payments in the UK. Considering that chronic performance issues of construction SMEs can have a drastic domino effect on the entire industry, more innovative and effective solutions must be developed for the construction SMEs to boost the overall performance of the industry.

Performance measurement could be an effective concept to boost the performance of construction SMEs. Performance measurement plays a crucial role in improving companies' performances since they provide the means to allocate and coordinate the resources (Melnyk et al. 2014). Besides, performance measurement ensures that all departments of an organization working to achieve the same corporate objectives. Therefore, the same performance measures and targets can be specified to measure and analyse the performance of all departments in the organization, which in turn, can lead to feedback loops across the organization (Kolehmainen 2010).

One of the outstanding concepts used for performance measurement is key performance indicators (KPIs), and this concept has been widely used in the CI. KPIs can be used to monitor the financial and non-financial success of a company (Tripathi et al. 2019), since "KPIs are measures that are indicative of the performance of associated process" (Beatham et al. 2004). Prioritization of KPIs is also crucial for effective performance measurement since monitoring all KPIs is not feasible and manageable (Luu et al. 2008b). KPIs in a PMS must be monitored by the management of SMEs to ensure that targets are met. In other words, each KPI must be measured repetitively, and the measurement data should be analysed, reported, and stored in the company periodically (Parmenter 2007). Therefore, the required time for performance measurement increases enormously as the number of KPIs increases. The information necessary to analyze these KPIs may be unavailable inside the organization,

and supplementary financial and human resources must be allocated to measure, analyze and store these KPIs (Kaplan and Norton 1996; Parmenter 2007). Thus, construction companies can save an enormous amount of time and money if they identify which KPIs are suitable for their needs (Ali et al. 2013). Since construction SMEs have limited resources and time compared to large companies, the complex and formalized performance measurement system may eventually become inefficient (Madsen 2015). Consequently, determination, prioritization, and monitoring of KPIs are vital for success in CI (Cox et al. 2003).

Performance measurement is widely known as a critical concept for construction companies. Therefore, multiple studies have been conducted to develop a PMS in the CI (Ali et al. 2013; Chan and Chan 2004; Cox et al. 2003; Luu et al. 2008a; Radujković et al. 2010; Skibniewski and Ghosh 2009; Tripathi and Jha 2018). However, Ciu et al. (2018) stated that this research area is not mature, and there is still some distance to be covered. Deficiencies of the existing body of knowledge from this perspective are continuously criticized by authors such as Liu et al. (2018a) and Okudan et al. (2020). Because most of the existing studies focus on the performance measurement of large construction companies and construction projects and ignore the construction SMEs. The PMSs developed for large construction companies and construction projects are not applicable for the construction SMEs due to their substantial differences which are elaborated within the scope of this study. Thus, the lack of the theoretical basis is a critical roadblock to the implementation of performance measurement practices in construction SMEs, causing the abovementioned issues within the entire industry. Since knowledge on performance measurement of construction SMEs is limited, construction practitioners keep implementing conventional management practices at the expense of their companies' future (Kagioglou et al. 2001; Skibniewski and Ghosh 2009). Therefore, there is still a gap in the performance measurement literature. Consequently, the cornerstone of this research is identifying a set of KPIs meeting the needs of construction SMEs. Additionally, existing studies mostly adopted simple descriptive methods which prioritize the KPIs based on a single criterion (Ali et al. 2013; Chan and Chan 2004; Cox et al. 2003; Luu et al. 2008a; Radujković et al. 2010; Skibniewski and Ghosh 2009; Tripathi and Jha 2018). Since such a prioritization should consider all strategic objectives of the construction SMEs, the multi-criteria decision-making (MCDM) approach becomes an essential need (Rogulj and Jajac 2018).

Consequently, the aims of this study are: (1) proposing a set of KPIs to measure the performance of construction SMEs which have been ignored in the performance management literature so far, (2) and determining the most important KPIs by using the fuzzy VIKOR method to improve cost-effectiveness in performance measurement. The practical implications of this study can be summarized as follows:

- Owners and/or managers of construction SMEs can measure their companies' performance and test outcomes of their managerial processes and decisions on performance by using the PMS developed in this study.
- The decision-makers within the construction SME can revise and refine managerial processes, as well as strategies, to ensure that the objectives of their construction SMEs are met. In this manner, the proposed system could function as a decision support framework by construction SMEs.

## 2. LITERATURE REVIEW

### 2.1. Performance Measurement in the Construction Industry

As stated above, there are many studies conducted to develop a PMS in the CI. The summary of these studies is shown in Table 1. Differences between this study and the existing studies in the construction management literature in terms of scope are provided to show the contribution of this study to the overall body of knowledge.

*Table 1 - Summary of performance management studies in the construction management literature*

Reference	Brief description of the study	Scope of the Study				
		A	B	C	D	E
Cox et al. (2003)	Developed a set of indicators that can be utilized to measure performance at the project level. 14 indicators were extracted from the literature, and analysis showed that 6 indicators were the most useful to measure the performance.		X			
Chan and Chan (2004)	Determined 14 KPIs that can be used for measuring the project performance. The application of the KPIs was demonstrated through case studies.		X			
Luu et al. (2008b)	Proposed 9 KPIs to benchmark construction projects. Later, the validity of KPIs was tested by considering three case studies.		X			
Luu et al. (2008a)	Identified strategic goals of large construction companies in Taiwan. They proposed 30 KPIs from a Balanced Scorecard perspective.			X		
Chan (2009)	Proposed 8 KPIs to measure the performance of the Malaysian construction industry	X				
Skibnewski and Gosh (2009)	Identified 9 KPIs and proposed a framework that uses Enterprise Resource Planning to collect data required to analyse KPIs.			X		
Radujkovic et al. (2010)	Proposed 36 KPIs that can be used to measure the performance of construction companies in Eastern Europe. The study adopted an in-depth literature review and descriptive methods as the research methodology.			X		
Ali et al. (2013)	Proposed KPIs for large construction companies and ranked KPIs by using the Relative Importance Index.			X		
Tripathi and Jha (2018)	Extracted 20 indicators from literature and ranked them using descriptive methods.		X			

Note: **A:** Measuring industries' overall performance; **B:** Measuring project performance; **C:** Measuring the performance of large companies; **D:** Measuring the performance of construction SMEs; **E:** Integrating MCDM to performance management field to link strategic objectives to performance measurement.

Considering the critical evaluation of the literature given in Table 1, there seems to be a clear gap in the literature review in areas related to performance measurement of construction SMEs and integrating MCDM to performance measurement to develop a PMS that is aligned with the construction SMEs' strategic objectives. Accordingly, the following section answers the question of why construction SMEs need their own PMS and KPIs.

## **2.2. The Reasons for Why Construction SMEs Need Their Own KPIs**

Kaplan and Norton (1996) emphasized the essentiality of companies' strategic objectives in performance measurement. The authors also asserted that effective PMS can only be designed when a company's strategic objectives are translated into a coherent set of performance measures (KPIs). Similarly, Garengo et al. (2005) and Nelly et al. (2002) pinpointed that a PMS must be designed and implemented in full accordance with a company's business strategy to link strategy into measurable objectives of functions, groups of people, and individuals. The design process of a PMS should include strategic planning and implementation. The performance measurement, therefore, highlights the gap between the company's current performance and its strategic objectives (Garengo et al. 2005; Garengo and Bititci 2007).

The main difference between construction SMEs, construction projects, and large companies regarding the performance measurement stems from the differences in strategic objectives, corporate governance, and business model (Garengo and Bititci 2007). Construction SMEs have their particular management style and needs compared to large construction companies and construction projects due to the uniqueness of the owner roles, ownership and management, culture and behaviour, processes and procedures, human resources and customers, markets management as well as the availability of resources (Madsen 2015; Sousa and Aspinwall 2010). Therefore, they need a PMS tailored to successfully fulfil their needs. For instance, while construction projects are temporary endeavours whose durations vary generally between 1 to 5 years, the lifespan of construction SMEs are longer than the construction projects. Thus, the managers of construction SMEs certainly have different perspectives than project managers. Due to the construction industry's unique dynamic and turbulent environment, construction SMEs cannot implement any PMS developed peculiarly for SMEs working in other industries. Consequently, an ideal PMS should be discussed and developed based on the perspectives and needs of construction SMEs.

The critical evaluation of the literature presented in Section 2.2 revealed that construction management literature lacks an appropriate PMS for construction SMEs. Instead, the existing studies chiefly focus either on construction projects or large companies. Thus, these measurement systems were developed based on the perspectives of the managers in large construction companies or projects. It is widely addressed in the literature that developing a PMS without considering the fundamental differences between construction SMEs, construction projects, and large companies results in poor adoption in practice (Hudson Smith and Smith 2007; Turner et al. 2005; Wiesner et al. 2007). Consequently, a PMS that works in large construction firms is, in many instances, less likely to work in construction SMEs and vice versa (Taylor and Taylor 2013). Therefore, the views of the managers/owners of construction SMEs should also be considered to develop an applicable PMS for them.

### 3. RESEARCH METHODOLOGY AND RESULTS

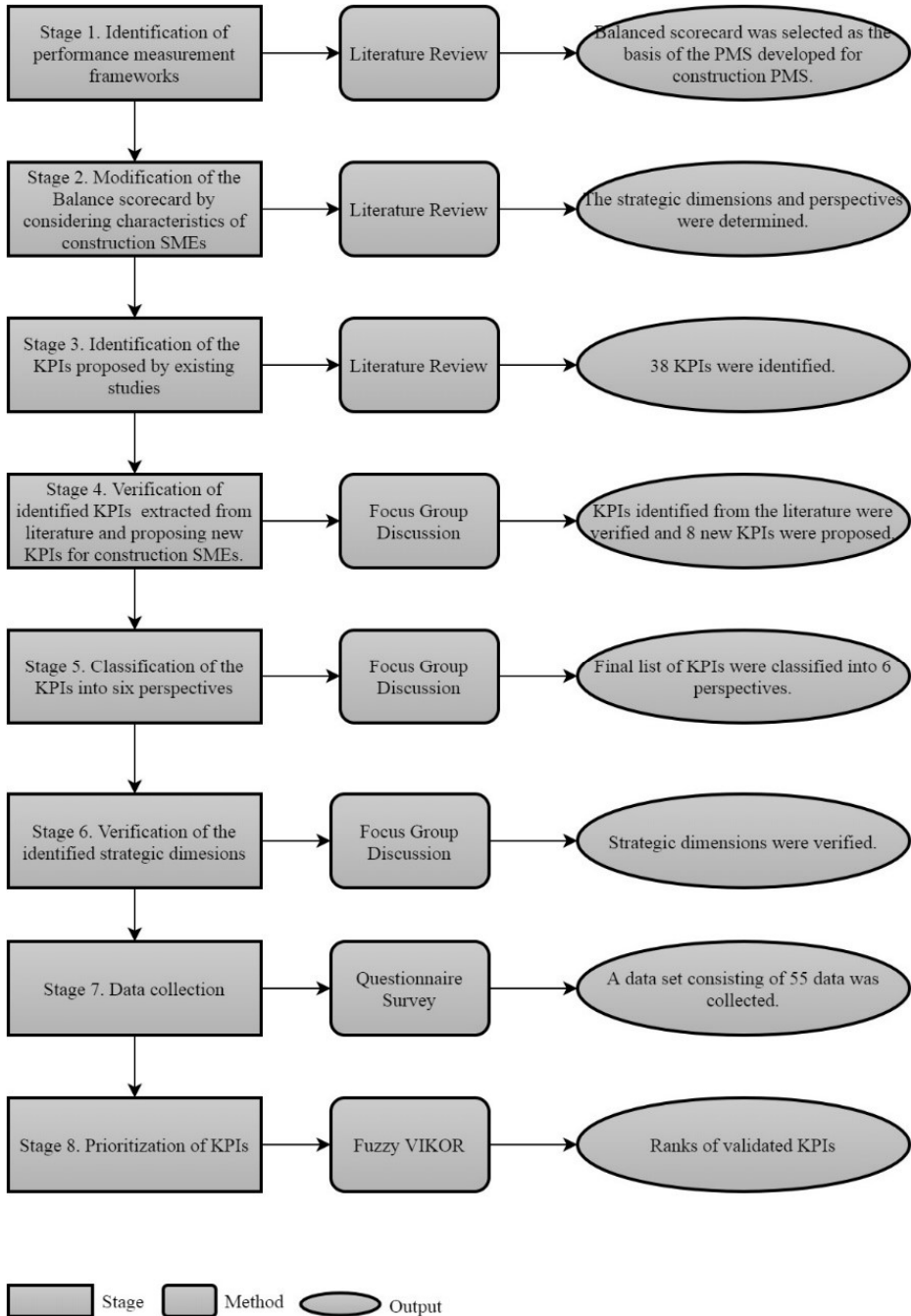


Figure 1 - Research Process Flowchart

The research methodology followed in this study is illustrated in Figure 1. At the first stage, a conceptual framework was developed by considering the existing performance measurement frameworks. Firstly, these frameworks were evaluated, and the balanced scorecard was selected. The balanced scorecard was revised and modified as in line with the needs of the construction SMEs. Then, a literature survey was conducted to determine KPIs for the construction SMEs. Besides, the strategic dimensions of SMEs were extracted from the survey. Therefore, the first stage of the study was completed.

Although the PMS was developed based on the existing literature, it was verified by conducting focus group sessions at the second stage. Then, a questionnaire was designed to rank the identified KPIs. The final step is the prioritization of KPIs of the construction SMEs by using fuzzy VIKOR analysis.

### **3.1. Stage 1. Identification of the Performance Management Frameworks**

In literature, many different frameworks have been developed to measure the performance of companies. However, in recent years, multidimensional frameworks are preferred to satisfy all strategic objectives of performance measurement. One of the most widely used multidimensional performance measurement frameworks is proposed by Kaplan and Norton (1996), namely the balanced scorecard (BSC) that satisfies a balance between the financial and non-financial indicators. Similarly, different multidimensional performance measurement frameworks, such as result and determinants framework (RDF) (Fitzgerald et al. 1991), performance prism (Neely et al. 2002), and dynamic multi-dimensional performance framework (DMPF) (Neetu and Mahim 2013) are developed. Among these multidimensional performance measurement frameworks, this study adopts the BSC since it is one of the most efficient business ideas (Bassioni et al. 2004). Besides, although there is no BSC-based PMS for construction SMEs yet, BSC has been used widely to develop PMSs for other construction companies. For instance, Yu et al. (2007a) developed a comparable PMS for large construction companies based on BSC. Similarly, Oyewobi et al. (2015) integrated the BSC into the business excellence model to develop a system that measures the strategic performance of construction organizations.

Kagioglou et al. (2001) defined BSC as a performance measurement framework that combines four main perspectives, namely finance, customer, internal business process, and learning and growth. BSC incorporates a wide range of indicators through various sub-measures under these four perspectives. Thus, companies can utilize performance drivers (leading indicators) and outcome measures (lagging indicators), while traditional PMSs only utilize outcome measures. A balance between the lagging and leading indicators should be established to develop an effective PMS (Wu 2012). Thus, by combining these lagging and leading measures, a common language is achieved, aligning top management and employees with the vision of the organization (Kaplan and Norton 1996).

The central purpose of BSC is to convey the mission and strategy of organizations into indicators that facilitate the analysis of results and decision-making processes. Therefore, the strategic objectives are identified according to the strategic priorities of organizations at the initial stage. These strategic objectives are then translated into performance measures.

### **3.2. Stage 2. Modification of the Balanced Scorecard**

The practicality of the BSC in construction SMEs has been thoroughly discussed in the literature, and BSC is determined as an efficient framework for measuring the performance of construction SMEs (Malagueño et al. 2018; Monte and Fontenete 2012). However, the BSC had initially been developed for large companies. Therefore, it should be modified by considering the characteristics of construction SMEs. Modified BSC should be faster and less complex so that construction SMEs can implement it with their limited resources and capabilities (Madsen and Stenheim 2014).

As stated above, traditional BSC considers the KPIs under four perspectives, though it is not mandatory. To reflect the organizational strategy, the traditional structure of BSC can be modified by adding divergent perspectives. Besides, Schneiderman (1999) and Neely and Bourne (2000) stated that four main perspectives are insufficient. Primarily due to the complex environment of the CI, new perspectives are proposed for construction companies. For instance, Ali et al. (2013) proposed the environment as a new perspective. Construction Excellence (2017) stated that one of the KPIs perspectives for construction companies should be the environment. The performance of construction SMEs is chiefly affected by factors derived from the outside of the organization (Banham 2010). Therefore, external factors are crucial as well. Consequently, in this study, two new perspectives are included to propose a comprehensive PMS.

BSC includes strategic objectives in the development of performance measurement. However, SMEs have to make frequent changes in strategic objectives since the business environments where they operate are not stable (Madsen 2015). Therefore, to increase the applicability rate of the BSC and to propose a generic PMS for the construction SMEs, the strategic dimensions that show the possible strategic orientations of the organizations are used. A literature review was performed to determine the generic strategic dimensions of construction SMEs for BSC. Fernandes et al. (2006) clustered the strategic objectives into three strategic dimensions while developing a strategy map for an SME based on BSC. Gomes et al. (2009) conducted a factor analysis and determined five strategic dimensions for SMEs. Monte and Fontenete (2012) proposed three dimensions for the small gas stations in Portugal. Likewise, Sofiyabadi et al. (2016) proposed eight research criteria for SMEs in the service business. Consequently, in this study, eight strategic dimensions were identified by combining the strategic dimensions proposed for SMEs in the literature. The strategic dimensions extracted from the literature are then validated through focus group discussion, as shown in Section 3.6.

### **3.3. Stage 3. KPIs Identification**

A comprehensive literature review was conducted via search engine Scopus to extract KPIs. At the end of this search, a total of 68 studies were retrieved. A first-level screening was performed by carefully reading the titles and abstracts. As a result, papers directly related to company performance were filtered, and the studies dealing with project performance were eliminated as projects and construction companies almost have entirely different management systems (Turner and Müller 2003). Based on this research, eleven existing studies related to performance measurement of construction companies proposing KPIs were identified. All the KPIs proposed in these studies were then extracted to prepare an initial



list. To prevent duplicates, these KPIs were re-evaluated to remove, merge, and/or rename some KPIs with similar meanings. Finally, thirty-eight KPIs were identified.

### **3.4. Stage 4. KPIs Verification**

The strategy and vision for the construction SMEs should also be verified since the BSC framework requires strategies as a guideline to develop KPIs. However, the extracted KPIs are proposed mainly for large construction companies. Therefore, they may not be in line with the strategy and vision of the construction SMEs. Besides, KPIs should be determined by considering the perspectives of BSC and classified into these perspectives. Therefore, to filter out irrelevant KPIs, a discussion session led by a moderator (one of the authors of this study) was conducted with a group of 12 experts. There is no determined rule about the size of the focus group. It is important to note that a large sample size such as 20 or even 50 could make the moderation of the session complex and hard to control. On the other hand, few participants may lead to low-reliability and inhibit the extraction of creative ideas from the sessions (Budayan et al. 2020). The experts were selected cautiously by considering their positions to increase the reliability of the group discussion sessions. Therefore, judgment sampling was applied to determine the participants. The following criteria were proposed to select the most appropriate participants. It should be noted that, during the expert selection, project types were not considered as a selection criterion. Unlike the project-specific studies which consider the effect of project types, the project type becomes a negligible criterion for the studies focusing on company performance (Ali et al., 2013; Radujković et al., 2010). Furthermore, when a performance measurement system is developed for a company that focuses on a single project type, it will have a limited practical implication since construction companies have to undertake various project types simultaneously.

1. The respondent should work in a construction SME that identifies itself as a specialist in residential building construction.
2. The respondent has a high-level management role.
3. The respondent's company has survived more than five years in the industry.
4. The respondent has worked for more than one year in a management role.

The profile of the participants and their companies is shown in Table 2. Although the participants were selected from construction SMEs, the total turnover and the total number of employees were also checked and verified. All companies have worked in the CI for at least five years. The experience levels and positions of the participants also show that these participants satisfy the predefined criteria. Consequently, the ideas captured from these participants can be considered reliable.

These KPIs were verified by following a similar methodology as described by Budayan et al. (2020). According to this methodology, firstly, the participants reviewed the suitability of KPIs considering the vision and strategy statement of construction SMEs. The participants assessed the suitability of each KPI based on a 1 to 5 Likert scale without discussion. The scale intervals are interpreted as follows: (1) not suitable; (2) partially suitable; (3) suitable; (4) very suitable; and (5) most suitable. Then, the responses of the participants were evaluated by conducting a descriptive analysis. Since the average of the appropriateness levels of all

KPIs was calculated higher than 3.5, none of the KPIs was eliminated at this stage. Then, these KPIs were discussed by the participants one by one to reach a final decision. At the end of this session, all KPIs were verified by the participants with a consensus. Besides, each of the experts was given an opportunity to propose a new KPI during this stage. Suggestions of each expert were discussed during the session with other participants. The discussion ended when a consensus about the appropriateness of KPIs was reached. At the end of this session, 8 new KPIs were proposed. Consequently, a final list of 46 KPIs was obtained and is shown in Table 3. It should be noted that the “\*” mark at the rightest column of Table 3 indicates that this KPI was proposed during the focus group discussion sessions.

Table 2 - Profile of participants participating in group discussion sessions.

Sample Specifications	Counts and Percentages	
<i>Role of Participants</i>	Owner 7 (58.33%)	Manager 5 (41.66%)
<i>Experience of the Company in CI (Year)</i>	5-10 5 (41.66%)	10-20 7 (58.33%)
<i>Experience of Participants in SMEs (Year)</i>	1-5 5 (41.66%)	5-15 7 (58.33%)
<i>Total Turnover of the Company (Million \$)</i>	0-3 6 (50%)	3-5 6 (50%)
<i>Number of Employees in the Company</i>	1-50 6 (50%)	50-250 6 (50%)
<i>Education Level</i>	BSc. 7 (58.33%)	MSc. 5 (41.66%)

### 3.5. Stage 5. Classification of the KPIs into six perspectives

The second session was conducted with the same participants to classify the KPIs according to the predefined six perspectives. The workflow conducted in this session is illustrated in Figure 2. Consequently, the participants classified the identified KPIs into six perspectives within a consensus, and the classification of KPIs to these six perspectives is illustrated in Table 3 as well.

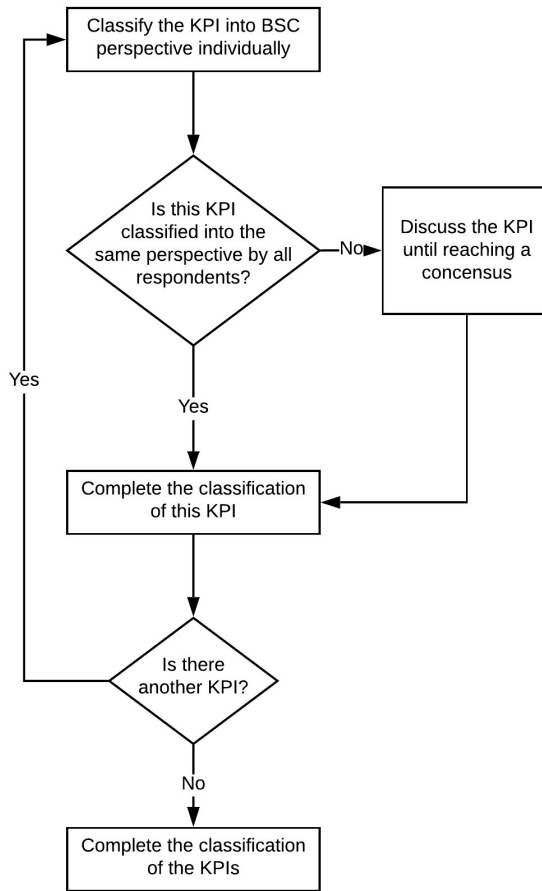


Figure 2 - Workflow of the third session

Table 3 - Perspectives and Sources of Key Performance Indicators

Key Performance Indicators	A	B	C	D	E	F	G	H	I	K	L	Count
<b>Financial</b>												
Profitability	—	X	X	—	X	X	X	X	X	X	X	9
Reliability of financial performance	—	—	—	—	—	—	—	—	—	X	—	1
Growth of organization	—	—	X	—	—	—	—	—	X	X	X	4
Financial stability	—	—	X	—	—	—	—	—	—	X	—	2
Proper cash flow	—	—	—	—	—	—	—	—	—	X	—	1
Percentage of loan interest from profit	—	—	—	—	—	—	—	—	—	X	—	1
Rate of return of an investment	—	—	—	—	—	—	—	—	—	—	—	*
The growth rate of annual revenue	—	—	—	—	—	—	—	—	—	—	—	*

Table 3 - Perspectives and Sources of Key Performance Indicators (continue)

Key Performance Indicators	A	B	C	D	E	F	G	H	I	K	L	Count
<b>Customer</b>												
The satisfaction of the internal customer	—	—	X	—	—	—	—	—	X	X	—	3
Attracting new customers	—	—	—	—	—	—	—	—	—	—	—	*
Good customer relationships	—	—	—	—	—	—	—	—	—	X	X	2
The satisfaction of external customers	—	X	X	—	X	X	X	—	X	X	X	8
Good service or/and product quality	—	—	—	X	X	—	—	—	X	X	—	4
Market share	—	—	X	—	—	X	—	X	—	X	X	5
Value of local currency	—	—	—	—	—	—	—	—	—	—	—	*
Competitive price	—	—	—	—	—	—	—	—	—	X	—	1
Effectiveness of managing contracts and legal disputes	—	—	—	—	—	—	—	—	X	—	—	1
<b>Internal Business Process</b>												
Productivity	X	X	—	—	—	X	X	X	X	X	X	8
Innovation	—	—	—	—	—	—	—	—	X	X	—	2
Healthy and safe working environment	X	X	—	X	X	—	X	X	—	X	X	8
Business productivity	—	—	X	—	—	—	—	—	X	X	—	3
Competency of managers	—	—	—	—	—	—	—	—	—	X	—	1
Effectiveness of planning	X	X	—	X	X	X	X	—	X	X	—	8
Labour force productivity	—	—	—	—	—	X	—	—	—	X	—	2
Effectiveness of resource management	—	—	—	—	—	—	—	—	—	X	—	1
Improving technological capacity	—	—	X	—	X	—	—	—	—	X	—	3
Rate of professional employee	—	—	—	—	X	—	—	—	—	—	—	1
Rework	X	—	—	—	—	—	—	—	X	X	X	4
Defects	—	X	—	—	—	—	—	—	X	X	—	3
Research and development level	—	—	X	—	—	X	—	—	—	X	—	3
Satisfaction of employees	—	—	—	—	—	—	—	—	X	—	X	2
Effectiveness of material planning	—	—	—	—	—	—	—	—	—	—	—	*
<b>Learning and Growth</b>												
Empowered workforce	—	—	—	—	—	—	—	—	—	X	—	1
Appropriateness of informatization	—	—	X	—	—	—	—	—	X	X	—	3
Continuous improvement	—	—	—	—	—	—	—	—	X	X	X	3
Training of personnel	—	—	X	—	X	X	—	—	—	X	—	4
The capability of the HR management team	—	—	—	—	—	—	—	—	—	X	—	1
Motivation	—	—	—	—	—	—	—	—	X	X	—	2

Table 3 - Perspectives and Sources of Key Performance Indicators (continue)

Key Performance Indicators	A	B	C	D	E	F	G	H	I	K	L	Count
<b>Environment</b>												
Impacts on society	—	—	—	—	—	—	—	—	—	X	X	2
Effectiveness of waste management	—	—	—	—	—	—	—	—	—	X	X	2
Optimizing energy use	—	—	—	—	—	—	—	—	—	X	X	2
Conformity to standards	—	—	—	—	—	—	—	—	—	—	—	*
<b>External</b>												
Effectiveness of Risk management	—	—	—	—	—	—	—	—	—	X	—	1
A good relationship with stakeholders	—	—	—	—	—	—	—	—	X	X	—	2
Effectiveness of monitoring and managing changes in policy or law	—	—	—	—	—	—	—	—	—	—	—	*
Effectiveness of monitoring market conditions	—	—	—	—	—	—	—	—	—	—	—	*

Note: A: (Cox et al. 2003); B:(Bassioni et al. 2004); C: (Yu et al. 2007b); D: (Luu et al. 2008b); E: (Luu et al. 2008a); F:(Chan 2009); G: (Skibniewski and Ghosh 2009); H: (Horta et al. 2010); I: (Radujković et al. 2010); K: (Ali et al. 2013); L: (Tripathi and Jha 2018).

### 3.6. Stage 6. Verification of the Identified Strategic Dimensions

The third session of group discussion was determined the strategic dimensions appropriate to the construction SMEs. To verify the identified strategic dimensions, each strategic dimension was discussed by the same participants one by one until they reached a consensus. At the end of this session, two strategic dimensions, namely effective risk management and atonement of HR strategy, were classified as unsuitable for construction SMEs and, consequently, eliminated. The final list of strategic dimensions is illustrated in Table 4.

Table 4 - The final list of strategic dimensions

Abbreviation	Criteria	Abbreviation	Criteria
C1	Ability to Run	C4	Key Results
C2	Business continuity	C5	Company Sales and Earnings
C3	Competitive Advantage	C6	Coordinated Strategy with the Enterprise Architecture

### 3.7. Stage 7. Data Collection

In this stage, a questionnaire was prepared by including the strategic dimensions and KPIs. The questionnaire consisted of three parts. In the first part, respondents provided information about themselves and their companies. In the second part, the respondents rated the KPIs with respect to each strategic dimension (given in Table 4) based on seven linguistic variables shown in Table 5. Fuzzy linguistic variables were used rather than numbers in this study

since the experts can reflect their opinions about the identified KPIs more precisely and ambiguity can be eliminated (Karwowski and Mital 1986). In this study, fuzzy membership function and fuzzy numbers suggested by Lin et al. (2006) were followed. In the third part of the questionnaire, the respondents also rated the importance of strategic dimensions for the construction SMEs using the same linguistic variables.

Table 5 - Linguistic variables and fuzzy numbers

Linguistic variables	Fuzzy numbers	Linguistic variables	Fuzzy numbers
Extremely low	(0,0.05,0.15)	Fairly high	(0.5,0.65,0.8)
Low	(0.1,0.2,0.3)	High	(0.7,0.8,0.9)
Fairly low	(0.2,0.35,0.5)	Extremely high	(0.85,0.95,1)
Medium	(0.3,0.5,0.7)		

This questionnaire study was conducted with 55 respondents who were selected by using judgment sampling, as shown in Section 3.4. The profile of the respondents and their companies are shown in Table 6.

Table 6 - Profile of respondents and their companies

Sample Specifications	Counts and Percentages			
	Owner		Manager	
<i>Role of respondents</i>	35 (63.63%)		20 (36.36%)	
<i>Experience of the company in CI (year)</i>	5-10 14(25.45%)	10-20 24(43.63%)	20-25 11(20%)	25-30 6(10.90%)
<i>Experience of respondents in SMEs (year)</i>	1-10 17(30.90%)	10-20 16(29.09%)	20-25 7(12.72%)	25-45 15 (27.27%)
<i>Total</i>				
<i>Turnover of the Company (Million \$)</i>	0-3 37(62.27%)		3-5 18(32.72%)	
<i>Number of employees in the company</i>	1-50 41(74.54%)		50-250 14(25.45%)	
<i>Education Level</i>	BSc. 35 (63.63%)		MSc. 11(20%)	Other 9(16.36%)

Based on this table, the experiences of respondents who are top-level managers satisfy the experience level criterion. Also, their companies survive longer than the criterion. Consequently, the positions of the respondents, their experience levels, and their companies' experiences satisfy all the predefined criteria. Finally, to avoid misunderstandings and increase the reliability of the study, all questionnaires were completed through face-to-face interviews.

### **3.8. Stage 8. Fuzzy VIKOR Analysis**

To determine the effectiveness of the KPIs in measuring the performance of the companies in achieving the determined strategic dimensions, a multiple-criteria decision making (MCDM) perspective was used. As an MCDM method, VIKOR analysis was selected, and all the processes were formulated accordingly. VIKOR is developed to determine a compromise solution for a discrete decision-making problem with conflicting criteria. The method is a convenient tool to use when decision-makers cannot select or do not know how to decide on the most suitable alternatives. VIKOR was selected because it has several advantages compared to other MCDM methods such as TOPSIS (Rostamzadeh et al. 2015). Unlike the TOPSIS that considers only group utility maximization and individual regret minimization, VIKOR also can fully reflect the experts' subjective preferences (Liu and Wu 2012; Opricovic and Tzeng 2004). The VIKOR method is used in various fields many times in the literature, such as performance management (Sofiyabadi et al. 2016) and risk management (Gul et al. 2019).

As stated above, the fuzzy theory was considered a viable alternative. The decision-makers make decisions under vague and uncertain conditions, leading to numerous uncertainties. Therefore, the scientific methods should be selected in the decision-making process carefully to reduce the risk of any uncertain decision environment (Sofiyabadi et al. 2016), and the fuzzy theory is an effective method for dealing with vague and risky problems. VIKOR method is also redesigned by using fuzzy theory and named as fuzzy VIKOR. Thus, the fuzzy VIKOR was used in this study.

#### **3.8.1. Appropriateness of the Collected Data for Fuzzy VIKOR Analysis**

Before performing the fuzzy VIKOR analysis, the appropriateness of the sample for this analysis was checked. Firstly, the sample size was considered. In the MCDM studies, the size of the sample is a quite subjective and contextual measure. Therefore, there is no strict rule for minimum sample size. However, MCDM methods such as VIKOR and TOPSIS do not require a large sample size for the analysis (Gupta 2018; Volmohammadi 2010). Consequently, the fundamental advantage of these methods is that they give reliable results with a small sample size (Bacalan et al. 2019). A large sample size may even cause unreliability due to *cold-called* respondents (Cheng and Li 2002), especially when the questionnaire takes a long time to complete the questionnaire used in this study. Besides, many authors pinpointed that MCDM techniques can offer reliable results with a small sample size of 10 or lower experts, stating that the findings of these techniques might be unrealistic with a large sample size since a large sample size can lead to a high degree of inconsistency (Pun and Hui 2001). Therefore, many researchers, such as Suganthi (2018) (3

experts), Liu et al. (2019) (6 experts), Liu et al. (2018b) (7 experts), Sofiyabadi et al. (2016) (8 experts), performed either VIKOR or fuzzy VIKOR methods with small sample size. Nonetheless, this study was conducted with 55 experts to maximize the reliability of the results. In this manner, the sample size used in this study is way above the sample size of similar studies as shown above.

Secondly, the reliability of this data set was reviewed. All questionnaires were collected via face-to-face interviews to increase the reliability of the data. For this reason, the data collection methodology used in this study is extremely reliable compared to studies collecting the data via e-mails (Lee and Yang 2018). Namely, this study maximized the quality of the data rather than the quantity.

**3.8.2. Application of Fuzzy VIKOR Analysis**

Although various software is available to perform fuzzy VIKOR analysis, an excel sheet was developed in-house by following the fuzzy VIKOR method proposed by Opricovic (2011) to have a broader knowledge about the method and its mechanism. The computational accuracy was tested by using the data presented in Sofiyabadi et al. (2016).

In this study, first, a decision matrix was prepared for each participant, and 55 decision matrices were obtained at the end. Later, these 55 matrices were merged to form an aggregated decision matrix before applying the fuzzy VIKOR analysis. By following the remaining steps of the fuzzy VIKOR, crisp Q values were obtained. Ranks of the KPIs were obtained by sorting Crisp Q values (given in Table 7) in descending order. A KPI with the smallest crisp Q value is the most important KPI, as understood from Table 7.

*Table 7 - Outputs of Fuzzy VIKOR*

KPIs	Crisp Q	KPIs	Crisp Q	KPIs	Crisp Q	KPIs	Crisp Q
A1	0,0610	A13	0,0332	A24	0,0381	A36	0,0873
A2	0,0304	A14	0,0450	A25	0,0497	A37	0,0726
A3	0,0575	A15	0,0671	A26	0,0709	A38	0,0527
A4	0,0636	A16	0,0779	A27	0,0665	A39	0,1267
A5	0,0343	A17	0,0645	A28	0,0689	A40	0,1274
A6	0,1209	A18	0,0879	A29	0,0700	A41	0,1287
A7	0,0795	A19	0,0566	A30	0,0673	A42	0,0345
A8	0,0730	A20	0,0893	A31	0,0647	A43	0,1288
A9	0,0586	A21	0,0704	A32	0,0724	A44	0,0918
A10	0,0182	A22	0,0316	A33	0,0616	A45	0,0396
A11	0,0398	A23	0,0517	A34	0,0618	A46	0,0163
A12	0,0424			A35	0,0606		



**4. RESULTS AND DISCUSSION OF FINDINGS**

**4.1. The Top KPIs**

The top ten KPIs shown in Table 8 are discussed in this section since the number of KPIs should be limited to eight to twelve while developing a PMS to improve its applicability (Kaplan and Norton 1996; Parmenter 2007).

According to Table 8, eight KPIs are non-financial indicators. Therefore, a PMS that involves only financial indicators such as conventional financial measurement systems is not accurate and applicable in practice. For this reason, a broader perspective is necessary to evaluate the performance of these companies. Additionally, “effectiveness of monitoring market conditions” and “effectiveness of monitoring and managing changes in policy or law” obtained very high scores as measures of external perspective. These results show that external factors play crucial roles in the performance of construction SMEs. The intensive dependence of construction SMEs on the external environment is also stated in the literature (Li et al. 2011).

Furthermore, four KPIs proposed by experts during the focus group discussion sessions obtained very high scores, highlighting the differences of construction SMEs. It is important to note that these KPIs had been neglected in the existing studies focusing on large construction companies and projects. Thus, the results verified that the perceptions of the managers in large construction companies are different from the construction SMEs. Due to this reason, construction SMEs need a PMS tailored according to their specific needs.

*Table 8 - Top ten KPIs*

KPIs	S	R	Q	Rank
Effectiveness of monitoring market conditions	1.127	0.245	0.0162	1
Attracting new customers	1.169	0.242	0.0182	2
Reliability of financial performance	1.233	0.259	0.0304	3
Competency of managers	1.314	0.248	0.0315	4
Good service and/or product quality	1.199	0.270	0.0332	5
Proper cash flow	1.235	0.267	0.0343	6
Conformity to standards	1.183	0.275	0.0344	7
Labour force productivity	1.282	0.267	0.0380	8
Effectiveness of monitoring and managing changes in policy or law	1.260	0.274	0.0396	9
Good customer relationship	1.271	0.273	0.0398	10

Another notable point is that three indicators placed in the top ten KPIs are customer-oriented, namely “attracting new customers”, “good service and product quality” and “good customer relationships”. Construction SMEs should develop good relationships with their customers since they generally utilize personal networks and rely on personal

recommendations to attract new customers. Most construction SMEs consider the most efficient marketing approach “word of mouth” (Buser and Carlsson 2014). Similarly, qualities of end products and satisfaction of external customers are also acknowledged as important KPIs for large construction companies (Ali et al. 2013; Radujković et al. 2010; Tripathi and Jha 2018)

“Effectiveness of monitoring market conditions” was presented as the most important KPI in this study. Construction SMEs should earn money as soon as possible after an investment; otherwise, they will be out of business. However, especially during an economic crisis, the money circulation in the market decreases, and these companies can confront difficulties in getting their payments. Hence, market imperfections, such as financial distress, affect construction SMEs severely (Belghitar and Khan 2013). Therefore, the owners or managers of construction SMEs should continuously monitor and control market conditions to forecast any fluctuations and should take precautions to keep their enterprises financially balanced. In this way, they can have a chance to establish more sustainable management.

Additionally, Ulubeyli et al. (2018) asserted that construction SMEs are more vulnerable to adverse market conditions than larger firms due to their relatively limited resources. However, in the study of Radujkovic et al. (2010), “effectiveness of monitoring market conditions” is not determined as one of the most significant KPIs since large construction companies can maintain a strong stance against the fluctuations in the market, unlike construction SMEs (Smallbone et al. 2012). This conclusion can also support the hypothesis of this study, stating that large construction companies and construction SMEs have different dynamics and strategic objectives, and therefore, a different PMS should be developed for construction SMEs.

“Competency of managers” was considered as the fourth most significant performance indicator by the respondents. Due to their economies of scale and limited resources, construction SMEs confront with more difficulties compared to large companies. However, they are more flexible and open to changes due to their simple internal management processes (Aragón-Sánchez and Sánchez-Marin 2005). In construction SMEs, most of the internal management processes are conducted by the CEO/entrepreneur or a small group of managers. Therefore, to gain an advantage of construction SMEs’ flexible nature, the managers should have competence, capabilities, and strong personality traits. Their capabilities and other features are crucial in the performance of construction SMEs (McAuley 2010). Consequently, the competency of managers must be measured both before and after the recruitment continuously.

“Proper cash flow” was ranked in the sixth order. Comparatively, construction SMEs rely on networking capital more than larger firms. Strictly speaking, the percentage of current assets and liabilities to total assets and total liabilities are higher in construction SMEs than larger companies (Padachi 2006). However, high investment in working capital can be one of the fundamental reasons for bankruptcy (Soenen 1993) due to the requirement of external finance which is more expensive for construction SMEs because of the asymmetric information (Belghitar and Khan 2013). However, the availability of cash flow can help companies to avoid the need for expensive external finance (Baños-Caballero et al. 2014). Companies having proper cash flow can exploit the advantages of high investment in working capital without dealing with expensive external finance. This advantage makes the availability of cash flow crucial for construction SMEs. Besides, since construction SMEs have relatively

higher transaction costs than larger companies due to the economies of scale, proper cash flow is profoundly demanded by construction SMEs (Tauringana and Adjapong Afrifa 2013). Indeed, Navon (1996) emphasized the importance of cash flow for the construction companies and indicated that most construction companies fail due to a lack of proper cash flow. For this reason, construction SMEs should continuously control this KPI.

The ninth most significant indicator is determined as “Effectiveness of monitoring and managing changes in policy or law”. Governments, together with their policies and laws, are the key factors affecting the development and success of SMEs in all industries (Smallbone and Welter 2001). Therefore, policies or regulations might act as enabling and/or constraining forces for SMEs. Bannock and Peacock (1989) explained the costs resulted from the changes in policy or law and defined the types of costs as direct costs and compliance costs. They argued that these costs are relatively higher for SMEs than larger companies due to small enterprises’ limited resources. Therefore, studies conducted for large construction companies generally neglected these KPIs in their PMSs. Consequently, owners or managers of construction SMEs must be aware of the significance of the changes in policies and laws and monitor this KPI.

#### **4.2. The Least Rated KPIs**

According to Table 7, all KPIs related to environmental issues except “conformity to standards” were considered as the least significant KPIs by the respondents. However, conformity to standards is determined as the seventh most important KPI. Two possible reasons can explain this conflict. The first reason might be that construction SMEs do not pay enough attention to examining their impact on the environment and stay passive in the face of sustainable development (Loucks et al. 2010). The second reason might be that respondents may not be thinking of environmental issues, which could help them improve their enterprise performance. The most possible perception is that they consider environmental issues as all about achieving laws and some standards.

Another interesting finding is that the KPIs related to human resource management are ranked in the list of least important KPIs. Although the positive relationship between the human resource management practices and organizational performance of SMEs is stated in the literature (Ogunyomi and Bruning 2016), most construction SMEs consider that the training of employees is expensive and the return of the investment from it is insignificant (Dainty et al. 2005) due to the high employee turnover and low retention rate in construction SMEs compared to large construction companies.

### **5. CONCLUSIONS AND RECOMMENDATIONS**

Although the importance of the performance of the construction SMEs for the CI and the whole economy is widely recognized, they do not perform the expected performance. Therefore, performance measurement is critical for these companies to improve their performance. This research attempted to determine the KPIs that can be used to measure the construction SMEs performances.

This research has shown that construction SMEs are vulnerable to external factors. Construction SMEs generally perform their operations with their limited resources. They do not have sufficient abilities and resources to adapt to the changes and resist crises in the market compared to the large construction companies. Therefore, these external factors affect construction SMEs in achieving their strategic objectives. In other words, there is a relationship between the performance of these companies and the external factors. Consequently, they should measure the effectiveness of their procedures to monitor market conditions and their performances.

This study also highlighted that the cash flow and the reliability of financial performance are more important than profitability. The construction SMEs prefer permanent earnings to high profitability since they conduct their operations based on working capital. This preference means that these companies do not hold a capital buffer for their immediate financial obligations required to survive in the market. Therefore, they should measure the reliability and stability of their cash flow and financial performance.

On the other hand, the least rated ten KPIs also provide crucial insights into the tendency of the respondents. Results show that all environmental indicators, except for conformity to standards, were ranked among the lowest-ranked indicators for measuring the performance of the construction SMEs. This finding reflects the general view of the CI. Construction companies consider making extra efforts for having good environmental performance as insignificant. The respondents regard that conformity to standards is adequate since they can avoid fines.

This study also hypothesizes that there are perspective differences between the managers and/or owners of construction SMEs, projects, and large construction companies. As stated before, the manager preferences on the implementation of the PMSs are as crucial as the structure of PMSs itself. The results of this study verified this hypothesis. For instance, although owners or managers of construction SMEs think that external factors have significant effects on their enterprises, the results of other performance measurement-related studies conducted for larger companies have opposite results. Consequently, the preferences and perspectives of the managers of construction SMEs should be revealed to develop a PMS specific to construction SMEs.

This study provides vital contributions to the literature. The applicability of BSC is in question due to the complexity of the BSC. However, this study develops a faster and more flexible PMS based on BSC by identifying the most significant KPIs and using the strategic dimensions. Therefore, owners and/or managers of construction SMEs who want to improve the performance of their enterprises can use the KPIs proposed in this study. Besides, they can develop a strategic map for their organizations by utilizing the findings of this study and revise their managerial processes to ensure that strategic objectives are met.

Although the validation is a substantial part of studies that used an MCDM approach, the validation of the findings of this study was not performed. However, to run this study, two different research methods, namely questionnaires and focus group discussions, were used with two separate groups. Similarities between the obtained results and the past studies are observed, which can be considered as a support for the findings of this study. In addition, one purpose of this study was to increase the practical application of BSC in SMEs. However, to improve the reliability of this study, a validation session should be conducted, which is also

planned as a case study in the future. On the other hand, the participants of the questionnaire survey and focus group discussions are all located in Turkey so that the results derived from their judgements are likely to be affected by their experience in the Turkish CI. Thus, although the list of KPIs can be considered generic, the ranking of the KPIs may change concerning a different group of participants experienced in other countries. For instance, as elaborated above, external KPIs related to macroeconomic conditions were given top priority by the participants. The fluctuating economic conditions of Turkey can be one of the reasons for this conclusion, however, in a more stable economy, the macroeconomic conditions can be considered uncritical. Contrarily, although environment related KPIs are considered among the least important KPIs, in a country where stricter environmental regulations are applied, these indicators can be ranked at the top level. Thus, the performance measurement framework proposed in this study should be perceived as a generic framework so that minimal modifications might be necessary based on the needs and conditions of a country.

In this study, the fuzzy VIKOR was selected due to its aforementioned benefits. However, in performance management literature, the effects of MCDM methods over the ranks of KPIs were not thoroughly investigated. However, there is a possibility that the ranks of the KPIs can vary among different MCDM methods. Consequently, the forthcoming studies should investigate this issue. Another essential step for improving the developed PMS is to determine how to measure KPIs within the system. For this purpose, future studies can promote a performance index based on the findings of this study. Furthermore, the differences between various industries can also be investigated to reveal how the characteristics of the industries affect the preferences of the managers on performance measurement in these industries.

## References

- [1] Ali, H. A. E. M., Al-Sulaihi, I. A., and Al-Gahtani, K. S. Indicators for measuring performance of building construction companies in Kingdom of Saudi Arabia. *J. King Saud Univ. - Eng. Sci.*, 25, 2, 125–134, 2013.
- [2] Aragón-Sánchez, A., and Sánchez-Marín, G. Strategic orientation, management characteristics, and performance: A study of Spanish SMEs. *J. small Bus. Manag.*, 43, 3, 287–308, 2005.
- [3] Bacalan, R., Cupin, M., Go, L. A., Manuel, M., Ocampo, L., and Govind, M. The Incubatees' Perspective on Identifying Priority Enabling Factors for Technology Business Incubators. *Eng. Manag. J.*, 31, 3, 177–192, 2019.
- [4] Banham, H. C. External environmental analysis for small and medium enterprises (SMEs). *J. Bus. Econ. Res.*, 8, 10, 19–26, 2010.
- [5] Bannock, G., and Peacock, A. *Government and Small Business*. Sage Publications Ltd., London 1989.
- [6] Baños-Caballero, S., García-Teruel, P. J., and Martínez-Solano, P. Working capital management, corporate performance, and financial constraints. *J. Bus. Res.*, 67, 3, 332–338, 2014.

- [7] Bassioni, H. A., Price, A. D. F., and Hassan, T. M. Performance measurement in construction. *J. Manag. Eng.*, 20, 2, 42–50, 2004.
- [8] Beatham, S., Anumba, C., Thorpe, T., and Hedges, I. KPIs: A critical appraisal of their use in construction. *Benchmarking An Int. J.*, 11, 1, 93–117, 2004.
- [9] Belghitar, Y., and Khan, J. Governance mechanisms, investment opportunity set and SMEs cash holdings. *Small Bus. Econ.*, 40, 1, 59–72, 2013.
- [10] Bourne, M., Franco-Santos, M., Micheli, P., and Pavlov, A. Performance measurement and management: A system of systems perspective. *Int. J. Prod. Res.*, Taylor & Francis, 56, 8, 2788–2799, 2018.
- [11] Budayan, C., Okudan, O., and Dikmen, I. Identification and prioritization of stage-level KPIs for BOT projects – evidence from Turkey. *Int. J. Manag. Proj. Bus.*, 13, 6, 1311–1337, 2020.
- [12] Buser, M., and Carlsson, V. Is anybody home? The role of company websites for small building contractors in Sweden. *Proceedings 30th Annu. ARCOM Conf.*, Association of Researchers in Construction Management, Portsmouth, 977–986, 2014.
- [13] Chan, A. P. C., and Chan, A. P. L. Key performance indicators for measuring construction success. *Benchmarking An Int. J.*, 11, 2, 203–221, 2004.
- [14] Chan, T. K. Measuring performance of the Malaysian construction industry. *Constr. Manag. Econ.*, 27, 12, 1231–1244, 2009.
- [15] Cheng, E. W. L., and Li, H. Construction partnering process and associated critical success factors: Quantitative investigation. *J. Manag. Eng.*, 18, 4, 194–202, 2002.
- [16] Construction Excellence. *UK Industry Performance Report 2017*.
- [17] Cox, R. F., Issa, R. R. A., and Ahrens, D. Management's perception of key performance indicators for construction. *J. Constr. Eng. Manag.*, 129, 2, 142–151, 2003.
- [18] Cui, C., Liu, Y., Hope, A., and Wang, J. Review of studies on the public–private partnerships (PPP) for infrastructure projects. *Int. J. Proj. Manag.*, Elsevier Ltd and Association for Project Management and the International Project Management Association, 36, 5, 773–794, 2018.
- [19] Dainty, A. R. J., Ison, S. G., and Briscoe, G. H. The construction labour market skills crisis: the perspective of small–medium-sized firms. *Constr. Manag. Econ.*, 23, 4, 387–398, 2005.
- [20] Department for Business Innovation & Skills. *Business Population Estimates 2012* 2012.
- [21] Fernandes, K. J., Raja, V., and Whalley, A. Lessons from implementing the balanced scorecard in a small and medium size manufacturing organization. *Technovation*, 26, 5, 623–634, 2006.
- [22] Fitzgerald, L., Johnston, R., Brignall, T. J., Silvestro, R., and Voss, C. *Performance measurement in service businesses*. Chartered Institute of Management Accountants London 1991.

- [23] Garengo, P., Biazzo, S., and Bititci, U. S. Performance measurement systems in SMEs: A review for a research agenda. *Int. J. Manag. Rev.*, 7, 1, 25–47, 2005.
- [24] Garengo, P., and Bititci, U. Towards a contingency approach to performance measurement: an empirical study in Scottish SMEs. *Int. J. Oper. Prod. Manag.*, 27, 8, 802–825, 2007.
- [25] Gomes, C. F., Yasin, M. M., and Lisboa, J. V. Benchmarking competitive methods and strategic choices of Portuguese SMEs. *Benchmarking An Int. J.*, Emerald Group Publishing Limited, 16, 6, 729–740, 2009.
- [26] Gul, M., Ak, M. F., and Guneri, A. F. Pythagorean fuzzy VIKOR-based approach for safety risk assessment in mine industry. *J. Safety Res.*, 69, , 135–153, 2019.
- [27] Gupta, H. Evaluating service quality of airline industry using hybrid best worst method and VIKOR. *J. Air Transp. Manag.*, Elsevier Ltd, 68, , 35–47, 2018.
- [28] Horta, I. M., Camanho, A. S., and Da Costa, J. M. Performance assessment of construction companies integrating key performance indicators and Data Envelopment Analysis. *J. Constr. Eng. Manag.*, 136, 5, 581–594, 2010.
- [29] Hudson Smith, M., and Smith, D. Implementing strategically aligned performance measurement in small firms. *Int. J. Prod. Econ.*, 106, 2, 393–408, 2007.
- [30] Institution of Civil Engineering. *Blockchain Technology in The Construction Industry: Digital Transformation for High Productivity* 2018.
- [31] Johnson, H. T. The search for gain in markets and firms: A review of the historical emergence of management accounting systems. *Accounting, Organ. Soc.*, 8, 2–3, 139–146, 1983.
- [32] Kagioglou, M., Cooper, R., and Aouad, G. Performance management in construction: a conceptual framework. *Constr. Manag. Econ.*, 19, 1, 85–95, 2001.
- [33] Kaplan, R. S., and Norton, D. *The Balanced Scorecard*. Harvard Business School Press, Boston 1996.
- [34] Karwowski, W., and Mital, A. Applications of approximate reasoning in risk analysis. *Appl. Fuzzy Set Theory Hum. Factors*, 227–243 1986.
- [35] Kennerley, M., and Neely, A. Measuring performance in a changing business environment. *Int. J. Oper. Prod. Manag.*, 23, 2, 213–229, 2003.
- [36] Kolehmainen, K. Dynamic Strategic Performance Measurement Systems: Balancing Empowerment and Alignment. *Long Range Plann.*, Pergamon, 43, 4, 527–554, 2010.
- [37] Lee, P. T. W., and Yang, Z. *Multi-Criteria Decision Making in Maritime Studies and Logistics*. Springer, Switzerland 2018.
- [38] Li, X., Segarra Roca, P., and Papaioikonomou, E. SMEs' responses to the financial and economic crisis and policy implications: an analysis of agricultural and furniture sectors in Catalonia, Spain. *Policy Stud.*, 32, 4, 397–412, 2011.

- [39] Lin, C. T., Chiu, H., and Chu, P. Y. Agility index in the supply chain. *Int. J. Prod. Econ.*, 100, 2, 285–299, 2006.
- [40] Lin, Q.-L., Liu, L., Liu, H., and Wang, D. J. Integrating hierarchical balanced scorecard with fuzzy linguistic for evaluating operating room performance in hospitals. *Expert Syst. Appl.*, 40, 6, 1917–1924, 2013.
- [41] Liu, A., Xiao, Y., Lu, H., Tsai, S. B., and Song, W. A fuzzy three-stage multi-attribute decision-making approach based on customer needs for sustainable supplier selection. *J. Clean. Prod.* 2019.
- [42] Liu, H. J., Love, P. E. D., Smith, J., Irani, Z., Hajli, N., and Sing, M. C. P. From design to operations: a process management life-cycle performance measurement system for Public-Private Partnerships. *Prod. Plan. Control*, 29, 1, 68–83, 2018a.
- [43] Liu, J., Love, P. E. D., Davis, P. R., Smith, J., and Regan, M. Conceptual framework for the performance measurement of Public-Private Partnerships. *J. Infrastruct. Syst.*, 21, 1, 04014023, 2015.
- [44] Liu, P., and Wu, X. A competency evaluation method of human resources managers based on multi-granularity linguistic variables and VIKOR method. *Technol. Econ. Dev. Econ.*, Taylor and Francis Ltd., 18, 4, 696–710, 2012.
- [45] Liu, Y., Wang, H., and Tzeng, G.-H. From Measure to Guidance: Galactic Model and Sustainable Development Planning toward the Best Smart City. *J. Urban Plan. Dev.*, 144, 4, 04018035, 2018b.
- [46] Loucks, E. S., Martens, M. L., and Cho, C. H. Engaging small and medium-sized businesses in sustainability. *Sustain. Accounting, Manag. Policy J.*, 1, 2, 178–200, 2010.
- [47] Love, P. E. D., and Holt, G. D. Construction business performance measurement: the SPM alternative. *Bus. Process Manag. J.*, 6, 5, 408–416, 2000.
- [48] Luu, T. Van, Kim, S. Y., Cao, H. L., and Park, Y. M. Performance measurement of construction firms in developing countries. *Constr. Manag. Econ.*, 26, 4, 373–386, 2008a.
- [49] Luu, V. T., Kim, S.-Y. Y., and Huynh, T.-A. A. Improving project management performance of large contractors using benchmarking approach. *Int. J. Proj. Manag.*, 26, 7, 758–769, 2008b.
- [50] Madsen, D. Ø. The balanced scorecard in the context of SMEs: A literature review. *Rev. Bus. Res.*, 15, 3, 75–86, 2015.
- [51] Madsen, D. Ø., and Stenheim, T. Perceived benefits of balanced scorecard implementation: some preliminary evidence. *Probl. Perspect. Manag.*, 12, 3, 81–90, 2014.
- [52] Malagueño, R., Lopez-Valeiras, E., and Gomez-Conde, J. Balanced scorecard in SMEs: effects on innovation and financial performance. *Small Bus. Econ.*, 51, 1, 221–244, 2018.



- [53] McAuley, A. Looking back, going forward: Reflecting on research into the SME internationalisation process. *J. Res. Mark. Entrep.*, 12, 1, 21–41, 2010.
- [54] Melnyk, S. A., Bititci, U., Platts, K., Tobias, J., and Andersen, B. Is performance measurement and management fit for the future? *Manag. Account. Res.*, 25, 2, 173–186, 2014.
- [55] Monte, A. P., and Fontenete, C. N. S. M. Balanced scorecard in SMEs—a proposal for small gas stations in Portugal. *World Acad. Sci. Eng. Technol.*, World Academy of Science, Engineering and Technology, 66, 6, 244–255, 2012.
- [56] Navon, R. Company-level cash-flow management. *J. Constr. Eng. Manag.*, 122, 1, 22–29, 1996.
- [57] Neely, A. The performance measurement revolution: why now and what next? *Int. J. Oper. Prod. Manag.*, MCB UP Ltd, 19, 2, 205–228, 1999.
- [58] Neely, A., and Bourne, M. Why measurement initiatives fail. *Meas. Bus. Excell.*, 4, 4, 3–6, 2000.
- [59] Neely, A. D., Adams, C., and Kennerley, M. *The performance prism: The scorecard for measuring and managing business success*. Prentice Hall Financial Times London 2002.
- [60] Neetu, Y., and Mahim, S. Performance measurement and management frameworks: Research trends of the last two decades. *Bus. Process Manag. J.*, Emerald Group Publishing Limited, 19, 6, 947–971, 2013.
- [61] Ogunyomi, P., and Bruning, N. S. Human resource management and organizational performance of small and medium enterprises (SMEs) in Nigeria. *Int. J. Hum. Resour. Manag.*, 27, 6, 612–634, 2016.
- [62] Okudan, O., Budayan, C., and Dikmen, I. Development of a conceptual life cycle performance measurement system for build–operate–transfer (BOT) projects. *Eng. Constr. Archit. Manag.*, ahead-of-p, ahead-of-print 2020.
- [63] Opricovic, S. Fuzzy VIKOR with an application to water resources planning. *Expert Syst. Appl.*, 38, 10, 12983–12990, 2011.
- [64] Opricovic, S., and Tzeng, G. H. Compromise solution by MCDM methods: A comparative analysis of VIKOR and TOPSIS. *Eur. J. Oper. Res.*, 156, 2, 445–455, 2004.
- [65] Oyewobi, L. O., Windapo, A. O., and Rotimi, J. O. B. Measuring strategic performance in construction companies: a proposed integrated model. *J. Facil. Manag.*, 13, 2, 109–132, 2015.
- [66] Padachi, K. Trends in working capital management and its impact on firms' performance: an analysis of Mauritian small manufacturing firms. *Int. Rev. Bus. Res. Pap.*, 2, 2, 45–58, 2006.
- [67] Parmenter, D. *Key Performance Indicators: Developing, Implementing, and Using Winning KPIs*. John Wiley & Sons, Inc., Hoboken, New Jersey 2007.

- [68] Pun, K. F., and Hui, I. K. An analytical hierarchy process assessment of the ISO 14001 environmental management system. *Integr. Manuf. Syst.*, MCB UP Ltd, 12, 5, 333–345, 2001.
- [69] Radujković, M., Vukomanović, M., and Dunović, I. B. Application of key performance indicators in South-Eastern European construction. *J. Civ. Eng. Manag.*, 16, 4, 521–530, 2010.
- [70] Rezgui, Y., and Miles, J. Exploring the potential of SME alliances in the construction sector. *J. Constr. Eng. Manag.*, 136, 5, 558–567, 2010.
- [71] Rogulj, K., and Jajac, N. Achieving a Construction Barrier-Free Environment: Decision Support to Policy Selection. *J. Manag. Eng.*, 34, 4, 04018020, 2018.
- [72] Rostamzadeh, R., Govindan, K., Esmacili, A., and Sabaghi, M. Application of fuzzy VIKOR for evaluation of green supply chain management practices. *Ecol. Indic.*, Elsevier B.V., 49, , 188–203, 2015.
- [73] Schneiderman, A. Why balanced scorecards fail. *J. Strateg. Perform. Meas.*, 2, 11, 6–11, 1999.
- [74] Skibniewski, M. J., and Ghosh, S. Determination of key performance indicators with enterprise resource planning systems in Engineering Construction Firms. *J. Constr. Eng. Manag.*, 135, 10, 965–978, 2009.
- [75] Smallbone, D., Deakins, D., Battisti, M., and Kitching, J. Small business responses to a major economic downturn: Empirical perspectives from New Zealand and the United Kingdom. *Int. Small Bus. J.*, 30, 7, 754–777, 2012.
- [76] Smallbone, D., and Welter, F. The Role of government in SME development in transition economies. *Int. Small Bus. J. Res. Entrep.*, 19, 4, 63–77, 2001.
- [77] Soenen, L. A. Cash conversion cycle and corporate profitability. *J. Cash Manag.*, 13, , 53–57, 1993.
- [78] Sofiyabadi, J., Kolahi, B., and Valmohammadi, C. Key performance indicators measurement in service business: a fuzzy VIKOR approach. *Total Qual. Manag. Bus. Excell.*, 27, 9–10, 1028–1042, 2016.
- [79] Sousa, S., and Aspinwall, E. Development of a performance measurement framework for SMEs. *Total Qual. Manag. Bus. Excell.*, 21, 5, 475–501, 2010.
- [80] Suganthi, L. Multi expert and multi criteria evaluation of sectoral investments for sustainable development: An integrated fuzzy AHP, VIKOR / DEA methodology. *Sustain. Cities Soc.*, Elsevier Ltd, 43, , 144–156, 2018.
- [81] Tauringana, V., and Adjapong Afrifa, G. The relative importance of working capital management and its components to SMEs' profitability. *J. Small Bus. Enterp. Dev.*, 20, 3, 453–469, 2013.

- [82] Taylor, A., and Taylor, M. International Journal of Production Research Factors influencing effective implementation of performance measurement systems in small and medium-sized enterprises and large firms: a perspective from Contingency Theory Factors influencing effective implementation of performance measurement systems in small and medium-sized enterprises and large firms: a perspective from Contingency Theory 2013.
- [83] Tripathi, K. K., Hasan, A., and Neeraj Jha, K. Evaluating performance of construction organizations using fuzzy preference relation technique. *Int. J. Constr. Manag.*, 1–14, 2019.
- [84] Tripathi, K. K., and Jha, K. N. An Empirical study on performance measurement factors for construction organizations. *KSCE J. Civ. Eng.*, 22, 4, 1052–1066, 2018.
- [85] Turner, J. R., and Müller, R. On the nature of the project as a temporary organization. *Int. J. Proj. Manag.*, 21, 1, 1–8, 2003.
- [86] Turner, T. J., Bititci, U. S., and Nudurupati, S. S. Implementation and impact of performance measures in two SMEs in Central Scotland. *Prod. Plan. Control*, 16, 2, 135–151, 2005.
- [87] Ulubeyli, S., Kazaz, A., and Sahin, S. Survival of construction SMEs in macroeconomic crises. *J. Eng. Des. Technol.*, 16, 4, 654–673, 2018.
- [88] US. Small Business Administration. *Do economic or industry factors affect business survival?* 2012.
- [89] Volmohammadi, C. Using the analytic network process (ANP) in business strategy selection: A case study. Australian. *Aust. J. Basic Appl. Sci.*, 4, 10, 5205–5213, 2010.
- [90] Wiesner, R., McDonald, J., and Banham, H. C. Australian small and medium sized enterprises (SMEs): A study of high performance management practices. *J. Manag. Organ.*, 13, 3, 1–29, 2007.
- [91] Williams, T. Identifying success factors in construction projects: A case study. *Proj. Manag. J.*, 47, 1, 97–112, 2016.
- [92] Wu, H.-Y. Y. Constructing a strategy map for banking institutions with key performance indicators of the balanced scorecard. *Eval. Program Plann.*, 35, 3, 303–320, 2012.
- [93] Yu, I., Kim, K., Jung, Y., and Chin, S. Comparable performance measurement system for construction companies. *J. Manag. Eng.*, 23, 3, 131–139, 2007a.
- [94] Yu, I., Kim, K., Jung, Y., Chin, S., Asce, A. M., Jung, Y., Chin, S., and Asce, M. Comparable performance measurement system for construction companies. *J. Manag. Eng.*, 23, 3, 131–139, 2007b.



# **Hydrological Considerations in Designing Roadways: Avoiding Hydroplaning**

Sevgi CAVDAR<sup>1</sup>

Ali UYUMAZ<sup>2</sup>

## **ABSTRACT**

High water levels on lanes poses high risk to the safety on highways. Since drainage structures are mostly focused on water spread issue at sideways, consequences of the build-up flow on the surface is overlooked . This study addresses whether optimizing cross slopes prevents hydroplaning. Water depths obtained using kinematic wave equation were tested against several studies for verification. Wide range of rainfall intensities and cross slopes were covered. Findings revealed that cross slope optimization for grades up to 10% prevents hydroplaning for intensities below 250mm/hr with widths up to 15m. The findings also shows cross slope optimization must be considered simultaneously with inlet design work.

**Keywords:** Cross slope optimization, hydroplaning, kinematic wave equation, roadway drainage, sheet flow on roadways.

## **1. INTRODUCTION**

High water depths on lanes risk safety that is essential for every highway. When the increased water depths create pressures equal to or more than the pressure due to weight of the vehicle, the vehicle hydroplanes—starts riding on the water with a lack of directional control and braking ability. There are two sources of water on traffic lanes that may create dangerous depths: (1) intrusion of flow adjacent to curb into the lanes, and (2) precipitation on the road surface. Latter is reduced through altered pavement cross slopes. Ross and Russam [11] and Gallaway et al. [6] investigated water depths experimentally with different roadway geometries. However, their solutions are limited to the tested conditions. Cristina and Sansalone [5] developed a rainfall-runoff kinematic wave model for highways, but the solution remains in differential form and of no practical use; they were only concerned with the concentration time of the flow. Studies on drainage facilities are concerned with the

---

Note:

- This paper was received on August 31, 2021 and accepted for publication by the Editorial Board on March 4, 2022.
- Discussions on this paper will be accepted by November 30, 2022.

• <https://doi.org/10.18400/tekderg.989134>

1 Department of Civil Engineering, Sivas Cumhuriyet University, Sivas, Turkey  
cavdars@cumhuriyet.edu.tr, cavdars@itu.edu.tr - <https://orcid.org/0000-0003-3958-4368>

2 Department of Civil Engineering, Istanbul Technical University, Istanbul, Turkey  
uyumaz@itu.edu.tr - <https://orcid.org/0000-0002-2530-6706>

sideway gutter flow and its spread, but the flow contributing to hydroplaning directly from the roadway surface is studied to a lesser extent and the geometric limits to antihydroplaning values are not well established.

This study employs a kinematic wave equation (KWE) and provides a water depth solution for roadways, which is then tested against several studies from the literature for verification. A wide range of rainfall intensity and cross slope values are covered to examine the significance of cross slope in combination with changing road width and grade. These flow depths could be compared with antihydroplaning flow depths obtained from the studies linking water depths to speed to get optimal cross slopes and peak flow in determining the size of the collection facilities.

## 2. BACKGROUND

Shortening the travel distance of a raindrop that lands on the road surface results in a water level decrease, which is possible by adjusting the cross slopes. The distance is determined by the angle alpha ( $\alpha$ ) (Figure 1A), which is the angle roadway centerline makes with the resultant of the cross and longitudinal slopes  $S_x$  and  $S_L$ , respectively (Figure 1B). If  $S_L = 0$ , then  $\alpha = \pi / 2$  and that reduces the travel path to roadway width, flow lines perpendicular to the curb—under the assumption that no ruts, local indentations, or bumps exist. However, in case of  $S_L \neq 0$ , the orthogonality assumption fails, increasing the length of flow. As the cross slope is a geometric factor that can best be controlled by the roadway designer, selecting an optimal value is essential for safer road design.

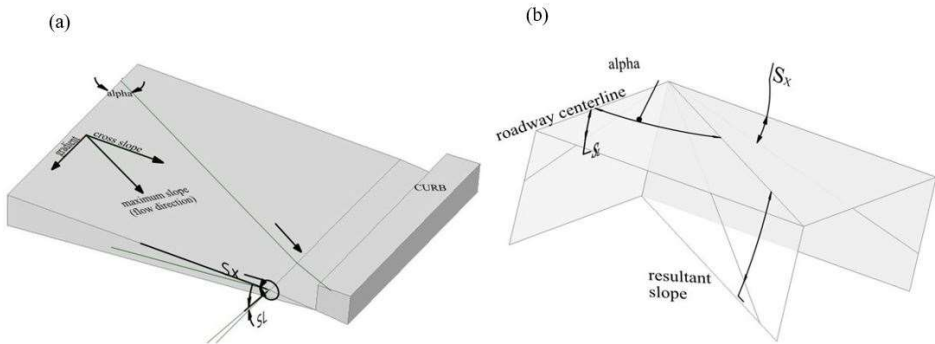


Figure 1 - Longitudinal and cross slopes forming the resultant, which helps obtain alpha and flow direction: (a) on a roadway section and (b) slopes at a magnified view.

### 2.1. Sheet Flow Solution to Traffic Lanes for Estimating Water Depths

Water on a roadway may move as sheet flow, shallow concentrated flow, open channel flow, or some combination of these. Time of concentration—the time required for rainfall landing on the farthest point of the roadway to reach the inlet-opening lip—can be calculated as the

sum of the travel times,  $T_i$ 's, within the various consecutive flow segments and some of these components are also essential for estimating the flow depth at the pavement-gutter intersection. Charbeneau et al. [3] conducted experiments measuring water depth-runoff on various roadway geometries under different rainfall intensities for sheet flow and concluded that hydraulic effects of rainfall were negligible. McCuen and Spiess [10] investigated the limiting criteria for sheet flow. They concluded that for the composite parameter  $nL / \sqrt{S}$  where  $n$  is the Manning roughness coefficient,  $L$  is the flow length, and  $S$  is the surface slope, values below 30 SI (International System of units) and 100 USC (United States Customary units) gives acceptable errors as a criterion and thus below that limit sheet flow assumption holds. If sheet flow exists, a kinematic wave equation may be employed to estimate the time of concentration, but if it does not, friction slope being different than the bed slope, kinematic wave assumption fails. For the most part, it is safe to assume that the criteria hold for the flow from the roadway centerline up to the pavement-gutter line, although it may not be the case for the gutter flow. In this study, the concern is the part up to the pavement-gutter intersection, so the sheet flow solution suffices with a single travel time,  $T_{ii}$ .

Table 1 - Manning's roughness coefficient ( $n$ ) for overland sheet flow (Eq. (9)), after HEC-22 [2].

Surface Description	Manning Number ( $n$ )
Smooth asphalt	0.011
Smooth concrete	0.012
Ordinary concrete lining	0.013

Using Manning's equation for sheet flow:

$$V = \frac{K_M}{n} z^{2/3} S^{1/2} \tag{1}$$

where  $K_M$  is the unit conversion factor 1 for SI and 1.486 for US units;  $n$  is Manning's roughness coefficient (Table 1);  $z$  is the flow depth, used in place of hydraulic radius for shallow flow and  $S$  is the energy grade line, which is equivalent to the pavement slope, defined as  $S = (S_x^2 + S_L^2)^{1/2}$ . If  $S_L = 0$ ,  $S$  equals the cross slope of the pavement,  $S_x$ .

Using the definition of unit discharge  $q$  one obtains

$$q = Vz = \frac{K_M}{n} z^{5/3} S^{1/2} \tag{2}$$

Thus, unit discharge for sheet flow can also be expressed as

$$q = kz^m \tag{3}$$

where  $k = K_M S^{1/2} / n$  and  $m = 5 / 3$ . Considering a Control Volume along the flow direction  $y$  with a representative cross section of  $z \Delta y$ , as depicted in Figure 2, as  $\Delta y$  and  $\Delta t \rightarrow 0$  inflow and outflow can be written as follows:

$$\begin{aligned} \text{inflow: } & (q_y + I \Delta y) \Delta t \\ \text{outflow: } & (q_y + \frac{\partial q}{\partial y} \Delta y) \Delta t \end{aligned} \tag{4}$$

where  $q_y$  is the unit discharge flow in the longitudinal direction,  $y$ , and  $I$  is the source term (rainfall intensity) in  $\text{mm hr}^{-1}$  (in.  $\text{hr}^{-1}$ ). Difference between the inflow and outflow in Eq. (4) equals the change in storage:

$$(q_y + I \Delta y) \Delta t - (q_y + \frac{\partial q}{\partial y} \Delta y) \Delta t = (z + \frac{\partial z}{\partial t} \Delta t) \Delta y - z \Delta y \tag{5}$$

Simplifying Eq. (5), one obtains the continuity equation for the sheet flow:

$$\frac{\partial q}{\partial y} + \frac{\partial z}{\partial t} = I \tag{6}$$

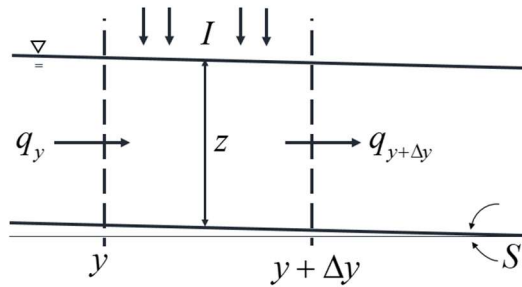


Figure 2 - Definition sketch for the continuity equation in the longitudinal section for sheet flow.

Using Eq. (6) in the form  $\left( \frac{dq}{dz} \right) \frac{\partial z}{\partial y} + \frac{\partial z}{\partial t} = I$ , and applying the method of characteristics,



one obtains:  $\frac{dy}{dq / dz} = \frac{dt}{1} = \frac{dz}{I}$ . Hence

$$\frac{dz}{dt} = I \rightarrow z = IT_{ii} \tag{7}$$

where  $T_{ii}$  is the travel time for the first segment of flow, i.e. travel time for the segment considered within the scope of this study. Since neither  $z$  nor  $T_{ii}$  is known, using Eq. (3) along with  $\frac{dy}{dt} = \frac{dq}{dz}$  (obtained from the method of characteristics) and inserting  $z$  in Eq. (7) one obtains

$$\frac{dq}{dz} = mkz^{m-1} \rightarrow \frac{dy}{dt} = 5 / 3k(IT_{ii})^{2/3} \tag{8}$$

After inserting  $k$  as defined in Eq. (3) and rearranging one obtains

$$T_{ii} = \frac{K_T}{I^{0.4}} \left( \frac{nL}{\sqrt{S}} \right)^{0.6} \tag{9}$$

where  $K_T$  is a coefficient equal to 6.92 or 0.933, in SI and USC, respectively. This is also the equation suggested by US Federal Highway Administration.

The angle resultant slope makes with the roadway centerline depicted in Figure 1,  $\alpha$ , is the crucial part in determining the length of flow  $L$  in Eq. (9), and defined:

$$\alpha = \sin^{-1} (S_x / S) \tag{10}$$

Since  $L = b / \sin \alpha$  with reference to Figure 1, using the aforementioned definition of  $S$ ,  $\alpha$  becomes,  $\alpha = \sin^{-1} \left( S_x / (S_x^2 + S_L^2)^{1/2} \right)$ . Thus,  $L / \sqrt{S}$  in Eq. (9) becomes:

$$\frac{L}{\sqrt{S}} = \frac{b / \sin \alpha}{\sqrt{S}} = \frac{b / (S_x / S)}{\sqrt{S}} = b \frac{(S_x^2 + S_L^2)^{0.25}}{S_x} \tag{11}$$

Eq. (11) inserted in Eq. (9) gives:

$$T_{ii} = \frac{K_T}{I^{0.4}} \left( n \frac{b / \sin \alpha}{\sqrt{S}} \right)^{0.6} = \frac{K_T}{I^{0.4}} \left( nb \frac{(S_x^2 + S_L^2)^{0.25}}{S_x} \right)^{0.6} = \frac{K_T}{I^{0.4}} (nb)^{0.6} \left( \frac{S_x^2 + S_L^2}{S_x^4} \right)^{0.15} \quad (12)$$

Using Eqs. (7) and (12) one obtains:

$$z = K_T (Inb)^{0.6} \left( \frac{S_x^2 + S_L^2}{S_x^4} \right)^{0.15} \quad (13)$$

Eq. (9) ignores the transverse path a droplet takes from the gutter-pavement line to the curb line as  $L$  is the flow length on the pavement excluding the gutter flow. This second leg of flow goes unmentioned because, despite curb-opening line mandates that all water travel across the gutter, it is unimportant in terms of the time spent and may be ignored. Additionally, not only does the accumulating water slowly form channel flow (therefore cannot be treated as sheet flow), but also (because of incoming flow in the gutter) not all over-lane flow is simultaneously conveyed to the curb line.

The flow on the pavement through lanes is considered dominated by sheet flow within the limits defined by McCuen and Spiess [10], and the relationship is obtained between the travel time and roadway geometry. The flow length,  $L$ , one of the major determinants of travel time, ranges from the roadway width for  $S_L = 0$  to the roadway length bounded by a sump, for  $S_x = 0$ . Using travel time, the depth of flow on the road is obtained from  $z = T_{ii} I$  for a design rainfall; any spills over into the road lanes from the continuous gutter section should be checked. Knowing the depth of water helps setting the optimal cross slopes for a given rainfall intensity to avoid unwanted incidents due to hazardous hydroplaning.

## 2.2. Verification of the Model

The magnitude of water depth, which is highly dependent on the cross slope of the pavement, is crucial in producing hydroplaning, and the correctness of water depths obtained using the kinematic wave equation depends on how well the travel time is estimated. This study checks whether the solution for travel time compares well with the experimental data made available by the previous work.

Various studies are conducted to determine the depth of rainwater experimentally. One of the earliest studies related to roadways was performed in the UK by Ross and Russam [11] on an 11 m x 5.5 m platform. After running experiments on two surfaces under various cross slopes with resultant slope ranging from 0.5% up to about 8% (flow path up to 11 m) and rainfall intensities from 10 mm hr<sup>-1</sup> to 200 mm hr<sup>-1</sup>, they recommended the use of Eq. (14).

$$z_{R\&R} = 0.474(LxI)^{1/2} S^{-1/5} \quad (14)$$

where  $z_{R\&R}$  is water depth in mm as reported by the Ross and Russam [11];  $L$  is drainage length in m;  $I$  is rainfall intensity in  $\text{mm hr}^{-1}$  and  $S$  is the slope of the flow path. For the comparison, travel times for Ross and Russam[11] were obtained using Eq. (7) after finding water depth from Eq. (14).

Wong [13] compared several time of concentration formulas with experimental data. They reported that formulation by Chen and Wong [4] estimates the best. However, the formulation by United States Corps of Engineers' [12] (USACE), Eq. (15), based on  $R^2$  (the quotient of the sum of squared errors and the total sum of squares) estimates the time of concentration better than the Chen and Wong [4] formulation. USACE recommendation for travel time is

$$t_{USACE} = (10.57 + 0.12 / S_L) (b / 30.48)^{(0.55 - 0.001 / S_L)} I^{-0.43} \tag{15}$$

where  $S_L$  is the longitudinal slope of the road and  $b$  is the width, while  $I$  is the rainfall intensity in  $\text{mm h}^{-1}$ .

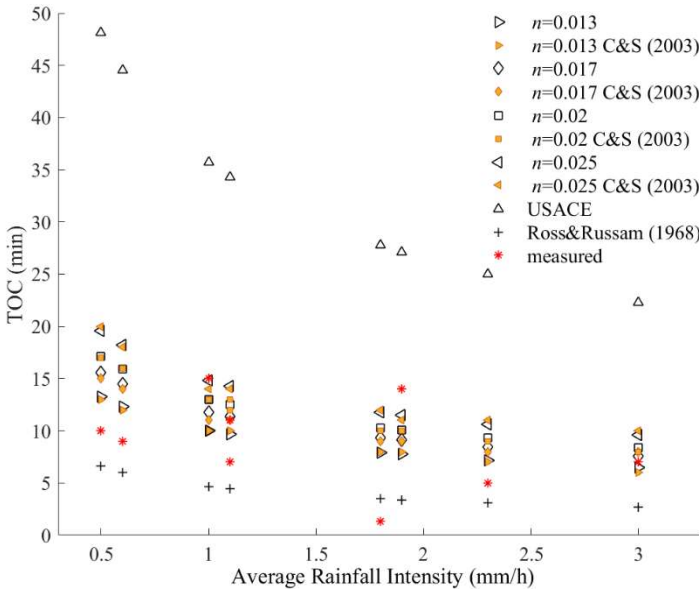


Figure 3 - Comparing our kinematic wave model with that of Cristina and Sansalone [5] (referred to as C&S (2003) in the figure) model and of the experimental results for 2% cross slope, 0.4% longitudinal slope for a road width of 20 m which remains within the criteria limits posted by McCuen and Spiess [10].

Cristina and Sansalone [5] mentioned the rarity of adopting kinematic wave equation for modelling impervious surfaces subject to traffic loadings. They developed a kinematic wave model and obtained flow depth using the finite difference method. They also compared their results with an experimental model where water moves perpendicular to traffic flow with a

2% cross slope. The experimental data from Cristina and Sansalone [5] are compared with their results as well as with USACE and Ross and Russam [11]’s empirical equation as provided in Eq. (14). Comparison between the Cristina and Sansalone findings and the findings of the present work are in good agreement as depicted in Figure 3. Yet the formulation presented in this work is easier to be used. In comparison with USACE, the kinematic wave solution outperforms; however, it should be kept in mind that the experiments are limited. Although Wong [13] showed that the USACE solution is the best in predicting the time of concentrations, both the present work’s and Ross and Russam [11] formulations are better than USACE results which highly overestimates. It is worth noting that selection of correct  $n$  value is very crucial for the implementation of kinematic wave approach. The tendency for the overestimation of the time of concentration with kinematic wave approach may be attributed to the abstractions in the runoff process.

### 2.3. Water Depth Variations under Different Design Rainfalls and Roadway Geometries

Water depths are determined from Eq. (13), and the results are plotted in Figure 4 and Figure 5. The roadway was considered to have a width of 15 m with multiple lanes and a Manning coefficient of  $n = 0.016$ , slightly higher than provided in Table 1.

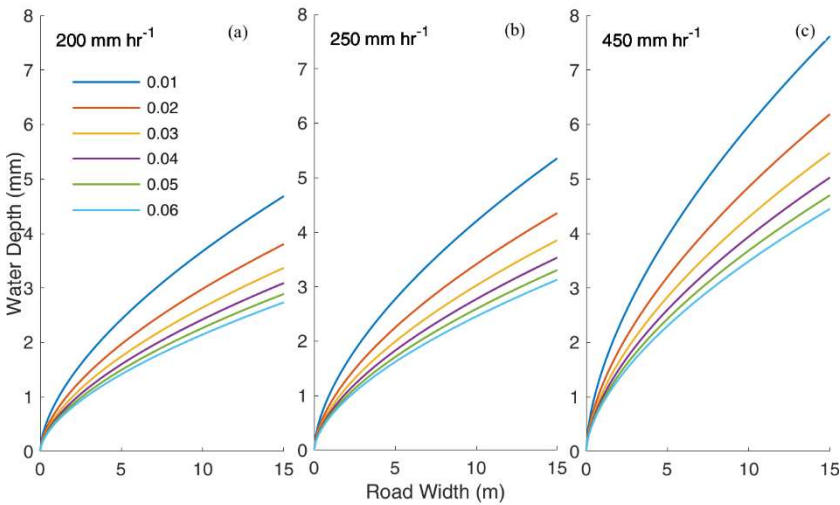


Figure 4 - For  $S_L = 0$ , the effect of changing cross slope on the flow depth as a function of width is provided for rainfall intensities (a) 200, (b) 250, and (c) 450 mm hr<sup>-1</sup>.

Figure 4 shows water depths topping over 4 mm even with the shortest paths (i.e.  $S_L = 0$ ) under design rainfall intensities of 200, 250, and 450 mm hr<sup>-1</sup> with the cross slope ranging from 1 to 6%. Depths reach up to 6 mm with rainfall intensity of 450 mm hr<sup>-1</sup> while 250 mm hr<sup>-1</sup> barely reaches 4 mm depth after the 10<sup>th</sup> meter hits in from the crown. 10-year frequency

constitutes the norm for roadway drainage practices, and it is understood that  $450 \text{ mm hr}^{-1}$  rainfall intensity is rare for a 10-year design frequency, but it provides a window into how the changes occur. At 15 m, for a cross slope of 1%, the water depth reaches up to 4.7 mm, while for 6% cross slope, the depth remains at 2.7 mm for a rainfall intensity of  $200 \text{ mm hr}^{-1}$ ; for  $250 \text{ mm hr}^{-1}$ , 5.36 mm and 3.13 mm, respectively (Table 2; Figure 4). It is obvious from Table 2 that at 15 m, while water depth is 5.36 mm for 1% cross slope and 4.35 mm for 2% with a difference of 1.01 mm, the difference is 0.17 mm when the cross slopes are 5 and 6% with water depths 3.3 and 3.13 mm, respectively (Figure 4). On the other hand, while water accumulation is 1.87 mm for 1% cross slope at the width of 3.25 m, it increases only to 2.84 mm at 6.5 m with the difference of 0.97 mm. For  $b = 6.5 \text{ m}$  under  $250 \text{ mm hr}^{-1}$  rainfall intensity, the water depth is 2.84 mm for 1% cross slope, 2.04 for 3%, and 1.66 mm for 6% cross slope while for  $b = 15 \text{ m}$  the depths are 5.36, 4.35, and 3.85 for cross slopes of 1, 2 and 3%, respectively.

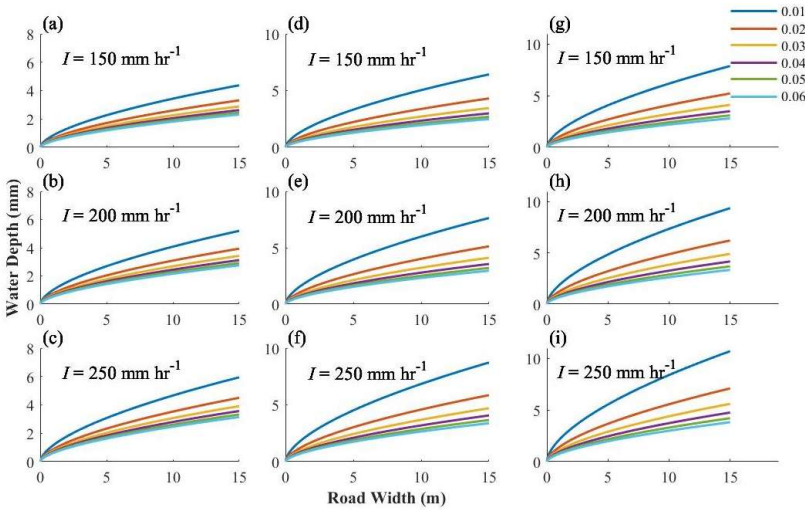


Figure 5 - Flow depths through roadway width for  $S_L = 0.01$  in (a), (b), and (c);

$S_L = 0.05$  in (d), (e), and (f); and  $S_L = 0.1$  in (g), (h), and (i) with cross slopes ranging from 1% to 6% under rainfalls of 150, 200 and  $250 \text{ mm hr}^{-1}$ .

Figure 5 shows the water depths for roadway grades of 1, 5, and 10% for rainfall intensities equal to 150, 200, and  $250 \text{ mm hr}^{-1}$ . Each subplot shows the corresponding water depths for cross slopes ranging from 1 to 6% within the roadway profile, as in Figure 4. Water-depth versus road-width shows that for  $b = 6.5 \text{ m}$  with  $S_x = 2\%$  and  $150 \text{ mm hr}^{-1}$ , rainfall the water depths are 1.94, 2.00, 2.61, and 3.16 mm for 0, 1, 5, and 10% longitudinal slopes, respectively. For  $200 \text{ mm hr}^{-1}$  at  $b = 15 \text{ m}$  water depths reach to 4.68, 5.2, 7.64, and 9.6 mm for the same longitudinal slopes of 0, 1, 5, and 10%, respectively.

Table 2 - Water depth (mm) values with  $I = 250 \text{ mm hr}^{-1}$  intensity under flat grades for various roadway widths.

$S_x$ $b(\text{m})$	0.01	0.02	0.03	0.04	0.05	0.06
3.25	1.87	1.52	1.35	1.23	1.15	1.09
6.5	2.84	2.30	2.04	1.87	1.75	1.66
15	5.36	4.35	3.85	3.53	3.30	3.13

The sheet flow assumption holds for all these cases, and therefore, the solution provided is valid.

### 3. DISCUSSIONS

Engineering most of the time is about setting the criteria and planning around the rare instances that can be highly hazardous, be it earthquakes, volcanic eruptions, winds, or floods. Effectively planning urban traffic involves many factors for the decision-makers [8], one of which is avoiding hydroplaning during rainstorms. Studies linking water depth and speed document that higher water depths increase hydroplaning risks at lower speeds. Hydroplaning may occur at speeds of  $89 \text{ km h}^{-1}$  with a water depth of 2 mm. However, depending on various factors influencing the conditions, hydroplaning can take place at lower speeds and depths (HEC-22 [2]). Gurganusa et al. [7], in their study to find flow depth using Light Detection and Ranging for existing roads speculated that “hydroplaning speed was at least 16 kph below the posted speed limit.” Gallaway et al. [6] recommend limiting water depths at or below 4 mm to prevent hydroplaning. Risk of partial hydroplaning continues at lower depths. It is assumed in this paper that flow depths below 2 mm do not constitute a danger for dynamic hydroplaning around the speeds of  $90 \text{ km hr}^{-1}$  (55 mph), and 4 mm is the limit depth above which must be avoided. The analyses exhibit the water depth results using kinematic wave equation with various longitudinal and cross slope values as the design rainfall intensity changes. Factors influencing hydroplaning are many. Design rainfall intensity is one that affects water depths immensely and is *fixed* for a given region; *Figure 4* shows how an increase in rainfall intensity leads to an increase in water depths. As a significant factor, the intensity may be obtained via solutions specific to the region under investigation to cope with changing climate [1]. Increases in the longitudinal slope and roadway width are two other factors that lead to higher accumulation of water, and in certain cases, the designer may not have much control over them. *Figure 6* shows the hydroplaning starting grades up to 10% for a given rainfall intensity; those analyses are conducted for a transverse slope of 1% and show that the area that falls below the lane-line is safe and requires no cross-slope optimization (i.e., 1% is enough), but the area above requires further investigation of proper cross slope to avoid hydroplaning. For example, for a 3-lane roadway with a cross slope of 1%, intensities up to  $75 \text{ mm hr}^{-1}$  require no further analysis to prevent hydroplaning (*Figure 6*; *Table 3*).

The present work revealed that the likelihood of a single-lane road hydroplaning is rare. However, once the roadway width or grade increases, cross slope optimization becomes inevitable because of increased water accumulation.

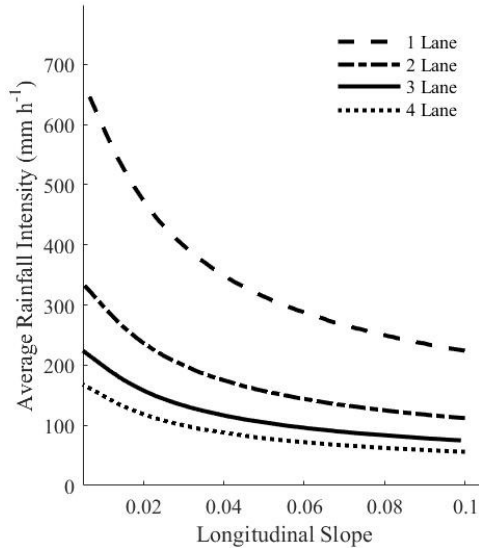


Figure 6 - Influence of increasing lane number on reaching a hydroplaning depth of 4 mm for a cross slope of 1%. Lane width is assumed 3.25 m.

Table 3 - With a minimum cross slope of 1% and a maximum grade of 10%, hydroplaning free rainfall intensities.

# of Lanes	1	2	3	4
Rainfall intensity	224 mm hr <sup>-1</sup>	112 mm hr <sup>-1</sup>	75 mm hr <sup>-1</sup>	56 mm hr <sup>-1</sup>

Cross slope is one of the primary factors that help lower water depths. Considering 3.25 m a lane width, a two-lane roadway under 250 mm hr<sup>-1</sup> design intensity leads to partial hydroplaning risks with water depths tipping 2 mm below 3% cross slopes, while higher values easily eliminate the risks. At the width of 15 m, full hydroplaning risks are faced if the cross slope is below 3% (Table 2). Figure 7 shows many configurations with the full hydroplaning limit of 4 mm, marked with dashed lines; plots start at 2 mm, the start of partial hydroplaning depth. Adjusting cross slopes prevents hazardous water depths for roadway grades up to 10% under the design rainfall intensity of 250 mm hr<sup>-1</sup> while for flat grades, cross slopes above 2% are optimal for roadway widths up to 15 m (Figure 7). It should be noted that increasing cross slope by the same percent produces different outcomes depending on the transverseness of the reference slope by increasing it from 1% to 2% with a difference of 1% is more pronounced than the difference between 5% and 6% with 1.01 mm and 0.17 mm depths, respectively, at 15 m with zero grade (Table 2; Figure 4; Figure 7). In other words, increasing the cross slopes after a certain value does not maximize the water depth drops and might be impractical in terms of comfort, but a minor increase at flatter percent leaves higher impacts in avoiding hydroplaning.

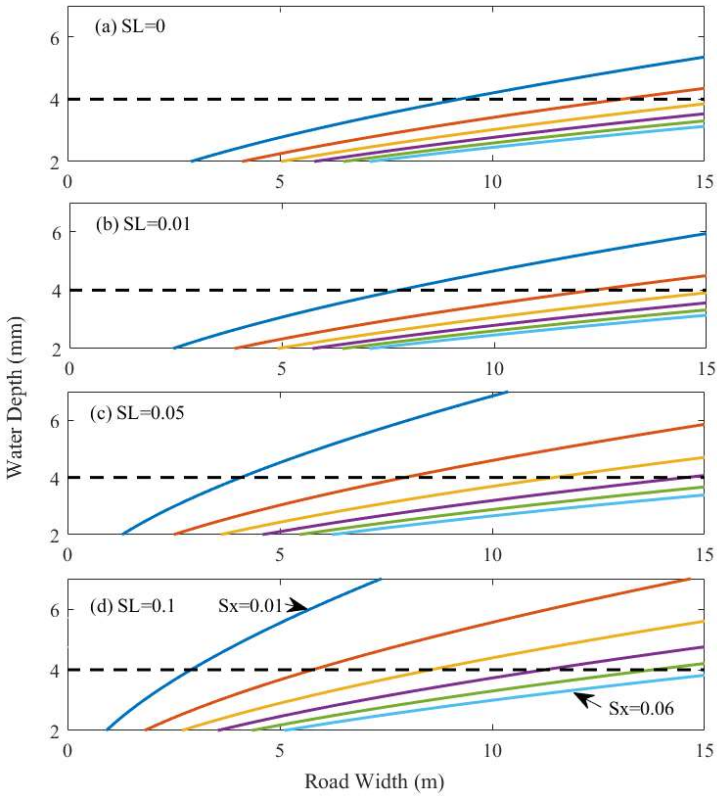


Figure 7 - Water depths profiles for 250 mm hr<sup>-1</sup> rainfall intensity, a 4 mm depth marking is used for ease in interpretation. Each color represents a different cross slope (0.01 to 0.06), with equal increments.

Flow depth may also be affected by factors besides the flow length, such as texture and tread depths. For bald tires, for example, hydroplaning may occur at depths as low as 0.3 mm (0.01 in.) while the treaded tires reportedly do not hydroplane even on low texture roads with flow depths below 2 mm (0.08 in.) as the grooves allow water to channel away [6] (1.6 mm (2/32 in.) is the standard tread depth and usually risks start when water depths are higher than groove depths). Guo et al. [8] considered the tread depth to be much deeper, but for this study, standard depth was considered in deciding hydroplaning standards.

#### 4. CONCLUSIONS

The most critical aspect of any roadway design is its capacity to self-drain for avoiding hydroplaning water depths. Factors affecting flow depth on a roadway include design rainfall intensity, roadway width, longitudinal slope, and cross slope. On roads where most or all water originates from precipitation, cross slope gains importance for drainage. The steepness of the cross slope is limited for safety considerations (the vehicle tends to veer towards the



low edge of the pavement), and the present work revealed that for up to 6% cross slopes show that increase in cross slope results in diminishing reduction effects on water depths. Overall, the present work has shown that the cross slope optimization was a safe way to avoid hydroplaning depths for grades up to 10% and widths up to 15m for intensities below 250 mm hr<sup>-1</sup>. Roadway width, as much as mandated by the need, may be judged based on the constrain, provided that a certain width is inconvenient in terms of drainage. In brief, while some factors that affect roadway water depth may not be controlled, the designer may restrain the cross slope; increasing cross slopes have diminishing reduction effects on water depths. Furthermore, the safest slope values are coupled with design intensities without hydroplaning threat beyond which cross slope adjustment is required to prevent hydroplaning because of shortened flow paths, and hence, water depths. With a zero-cross slope should not be used since then roads act as channels, not diverting the flow to the sides, and constantly cause an increase in the flow depth until sag is reached.

### Symbols

- $\alpha$  : the angle between resultant slope and the roadway centreline,  $\sin^{-1}(S_x / S)$
- $b$  : the width of the road, m (ft.)
- $I$  : rainfall intensity, in mm hr<sup>-1</sup> (in. hr<sup>-1</sup>)
- $k$  :  $K_M S^{1/2} / n$
- $K_M$  : unit conversion factor (1 for SI and 1.486 for US units)
- $K_T$  : a coefficient equal to 6.92 (0.933) in SI (US)
- $L$  : flow length m (ft.)
- $m$  : 5 / 3
- $n$  : Manning's roughness coefficient
- $S$  : energy grade line m m<sup>-1</sup> (ft. ft.<sup>-1</sup>), equal to  $(S_x^2 + S_L^2)^{1/2}$  (Figure 1B)
- $S_L$  : road grade m m<sup>-1</sup> (ft. ft.<sup>-1</sup>)
- $S_x$  : cross slope m m<sup>-1</sup> (ft. ft.<sup>-1</sup>)
- $q$  : unit discharge m<sup>2</sup> s<sup>-1</sup> (ft.<sup>2</sup> s<sup>-1</sup>)
- $T_{ii}$  : sheet flow travel time min
- $t_{USACE}$  : travel time for USACE equation min
- $z$  : flow depth m (ft.)
- $z_{R\&R}$  : water depth in mm as reported by the Ross and Russam [11] solution

## **Acknowledgments**

We acknowledge the contributions of two anonymous reviewers for their comments that were useful for improving the quality of this manuscript.

## **References**

- [1] Anilan, T., Yüksek, Ö, Fatih, S., & Orgun, E. (2022) Rainfall intensity-duration-frequency analysis in turkey, with the emphasis of eastern black sea basin. *Teknik Dergi*, 33(4)
- [2] Brown, S., Schall, J., Morris, J., Doherty, C., Stein, S., & Warner, J. (2009). Hydraulic engineering circular no. 22, 3rd edition: Urban drainage design manual. *National Highway Institute, Federal Highway Administration, Washington, DC*.
- [3] Charbeneau, R. J., Jeong, J., & Barrett, M. E. (2009). Physical modeling of sheet flow on rough impervious surfaces. *Journal of Hydraulic Engineering*, 135(6), 487-494.
- [4] Chen, C., & Wong, T. S. (1993). Critical rainfall duration for maximum discharge from overland plane. *Journal of Hydraulic Engineering*, 119(9), 1040-1045.
- [5] Cristina, C. M., & Sansalone, J. J. (2003). Kinematic wave model of urban pavement rainfall-runoff subject to traffic loadings. *Journal of Environmental Engineering*, 129(7), 629-636.
- [6] Gallaway, B., Ivey, D., Hayes, G., Ledbetter, W., Olson, R., Woods, D., & Schiller Jr, R. (1979). *Pavement and geometric design criteria for minimizing hydroplaning*. (Final Report No. FHWA-RD-79-31).
- [7] Gurganusa, C. F., Chang, S., & Gharaibeh, N. G. (2021). Evaluation of hydroplaning potential using mobile lidar measurements for network-level pavement management applications. *Road Materials and Pavement Design*, 1-10.
- [8] Gülhan, G., Özuysal, M., & Ceylan, H. (2020). Evaluation of intersection properties using MARS method for improving urban traffic performance: Case study of Tekirdağ, Turkey. *Teknik Dergi*, 32(6)
- [9] Guo, X., Zhang, C., Cui, B., Wang, D., & Tsai, J. (2013). Analysis of impact of transverse slope on hydroplaning risk level. *Procedia-Social and Behavioral Sciences*, 96, 2310-2319.
- [10] McCuen, R. H., & Spiess, J. M. (1995). Assessment of kinematic wave time of concentration. *Journal of Hydraulic Engineering*, 121(3), 256-266.
- [11] Ross, N., & Russam, K. (1968). *The depth of rain water on road surfaces*. (No. RRL LR 236). Crowthorne, Berkshire: Road Research Laboratory.
- [12] US Army Corps of Engineers. (1954). Data report, airfield drainage investigation.
- [13] Wong, T. S. (2005). Assessment of time of concentration formulas for overland flow. *Journal of Irrigation and Drainage Engineering*, 131(4), 383-387.

# **A Numerical Investigation on the Limitations of Design Equations for Steel Plate Shear Walls**

**Muhammed GÜRBÜZ<sup>1</sup>**  
**İlker KAZAZ<sup>2</sup>**

## **ABSTRACT**

In previous studies various design issues on steel plate shear wall (SPSW) systems under lateral loading were investigated using analytical and experimental methods. However, these studies examined the interactive effect of only a few of design parameters, such as panel aspect ratio, column flexibility parameter, axial load ratio on the boundary frame columns, web plate thickness, stiffness of horizontal and vertical boundary elements and top anchor beam, etc., on the drift capacity and shear force distribution among frame and panel components of SPSWs at a time. This study investigates the effect of all of these parameters in the same framework. A parametric study is conducted on finite element models of 292 3-story SPSWs with rigid beam-to-column connections and designed for specified parameters. By evaluating failure forms from finite element analyses, the limiting (undesired) cases resulting from different combinations of specified geometric properties are identified. A column flexibility factor of 2.2 is proposed instead of the current limit value of 2.5 for satisfactory column performance, improved drift capacity and balanced strength distribution among frame and panel of SPSW. The value of 0.75 for the ratio of plate shear force to total shear force has emerged as a critical threshold value for the strength distribution among plate and frame components in order to fulfill capacity design principles. This study provides a comprehensive view of the behavior of SPWS for determining the most suitable combination of various parameters in the design of SPSW structures.

**Keywords:** Steel plate shear wall, finite element analysis, failure, column flexibility, axial load, inclination angle.

## **1. INTRODUCTION**

Steel plate shear walls (SPSW) are structural components with high energy dissipation capacity, initial stiffness and ductility under lateral loads. Reduced seismic load due to

---

Note:

- This paper was received on October 6, 2021 and accepted for publication by the Editorial Board on April 8, 2022.
  - Discussions on this paper will be accepted by November 30, 2022.
- <https://doi.org/10.18400/tekderg.1005342>

1 Erzurum Technical University, Civil Engineering Department, Erzurum, Turkey  
muhammed.gurbuz@erzurum.edu.tr - <https://orcid.org/0000-0001-6628-3363>

2 Erzurum Technical University, Civil Engineering Department, Erzurum, Turkey  
ilkerkazazi@erzurum.edu.tr - <https://orcid.org/0000-0002-3885-1885>

reduced dead weight and thickness of the walls are some of the advantages of the steel plate shear walls. These characteristics make them attractive for resisting seismic loading and dissipating seismic energy. A typical unstiffened steel plate shear wall consists of vertical and horizontal boundary elements (VBE and HBE) and an infill steel plate. There are different types of steel infill plates such as corrugated, perforated or stiffened. In some studies, sandwich composite panels used as infill plates to investigate the energy dissipation capacity change compared to unstiffened steel infill panels [1]. The desired behavior of properly designed unstiffened SPSWs under lateral loading can be represented by four phases. Figure 1 illustrates the anticipated behavior phases of a typical steel plate shear wall. Under a low level of loading, the entire structure should be elastic. After this phase, prior to global yielding, the central region of each panel is expected to yield, but the boundary elements remain to be elastic. At the global yielding except for the corner regions most parts of each panel yield and plastic hinges form at the beam ends. Finally, the entire panel yields and the plastic hinges form at the ends of all the beams and the first story column bases. The uniform yielding mechanism is fully developed in this stage. Except for the plastic hinges at the ends of boundary elements, in span regions must remain elastic; even the steel panel and the plastic hinges exhibit significant nonlinearity [2]. To assure this mechanism, codes and guidelines incorporate design equations and recommendations on the SPSW component's strength and stiffness.

The design equations and processes developed for SPSWs are based on well-established mechanical models. The shear strength of steel plate shear walls has been investigated by previous experimental research and accurately established by analytical research. Thorburn et al. [3] proposed an analytical model of yielding infill steel plate known as strip model, where the inclined tension field was represented by a series of pin-ended strips as shown in Figure 1. Timler and Kulak [4] verified the strip model presented by Thorburn et al. [3] by an experimental study on SPSWs. Tension field inclination angle ( $\alpha$ ) is developed using the principle of least work in these studies and is given as;

$$\tan^4 \alpha = \frac{1 + \frac{t_w L_b}{2A_c}}{1 + t_w h_s \left[ \frac{1}{A_b} + \frac{h_s^3}{360I_c L_b} \right]} \quad (1)$$

where  $t_w$  is the thickness of the infill plate,  $h_s$  is the story height,  $L_b$  is the bay width,  $I_c$  is the moment of inertia of the vertical boundary element,  $A_c$  is the cross-sectional area of the vertical boundary element,  $A_b$  is the cross-sectional area of the horizontal boundary element and  $\alpha$  is the inclination angle of the strips.

The strip model enables the calculation of the shear capacity of SPSW. SPSW design requirements are given in AISC-341 [5], and practical low and high seismicity design processes are illustrated in AISC Design Guide 20 [6]. The story design shear strength given in AISC-341 originates from the strip model representing the collapse mechanism of a SPSW with simple connections, and it is derived as;

$$V_r = \frac{1}{2} F_y t_w L \sin 2\alpha \tag{2}$$

where  $F_y$  is the nominal yield stress of steel infill,  $L$  is the clear distance between VBE flanges (panel length) and other terms are as defined previously. For a frame with rigid beam-to-column connections, the overall shear capacity of a single-story frame  $V_r$  is defined as the sum of the shear capacities from moment frame and shear panel as presented in Eq.(3) [7].

$$V_r = \frac{1}{2} F_y t_w L \sin 2\alpha + \frac{4M_p}{h} \tag{3}$$

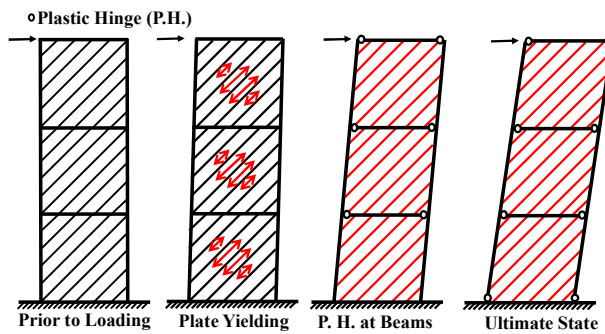


Figure 1- The anticipated sequence of failure mechanism of a multi-story steel plate shear wall with moment-resisting connections

In this equation,  $M_p$  is the smaller of plastic moment capacity of the beams or columns and  $h$  is the panel height. The shear force demand  $V_d$  under seismic loads are calculated using the soil class, maximum considered earthquake spectral response parameters, dead and live loads, etc. Taking  $V_r \geq V_d$  in Eq. (2), the angle of tension field should be estimated, since the plate thickness and size of HBE and VBE required to be input in Eq. (1) are not initially known. As an initial value of inclination angle ( $\alpha=45^\circ$ ) is assumed. Then, solving Eq. (2) for  $t_w$ , the thickness of the steel panel at a given story is determined. For these given equations to be valid, the size of boundary elements should be sufficiently stiff and strong for tension field development. Stiffness of bounding columns significantly affects the overall performance of steel plate shear wall (SPSW) systems under lateral loading conditions. Wagner's [8] analytical studies on diagonal tension fields provided the theoretical background on the flexibility coefficient of vertical boundary elements ( $\omega$ ). Wagner [3] derived the flange flexibility parameter by considering the elastic deformations of a cantilever plate girder under transverse loading. Kuhn et al. [9] simplified the flange flexibility parameter that is introduced by Wagner [8]. The simplified flexibility is used to specify the stiffness limits for the boundary frames. The given flexibility parameter is;

$$\omega_i \approx 0.7h_{st} \left( \frac{t_w}{(I_u + I_o)L} \right)^{0.25} \tag{4}$$

where  $h_{st}$  stands for the spacing between the neighboring stiffeners,  $I_u$  is the moment of inertia of bottom flange (corresponding to the tension column of SPSW),  $I_o$  is the moment of inertia of top flange (corresponds to the compression column of the SPSW). Montgomery and Medhekar [10] proposed that the column flexibility parameter  $\omega_i$  should not exceed 2.5 to form a relatively uniform tension field on steel plate shear walls. Considering both columns have the same moment of inertia and solving for  $I_c$ , Eq. (4) becomes:

$$I_c \geq \frac{0.00307t_w h_s}{L_b} \tag{5}$$

Similarly, the horizontal boundary element element has a moment of inertia about the strong axis,  $I_b$ , not less than;

$$I_b \geq \frac{0.0031L_b^4}{h_s} (t_{w,i+1} - t_{w,i}) \tag{6}$$

where  $t_{w,i}$  is the infill panel thickness of the  $i$ 'th story. As the steel panels have similar thicknesses at successive stories, Eq. (6) is ineffective to determine the beam size. In this study, a practical limit is adopted for  $I_c/I_b$  to determine  $I_b$  relative to column size. After designing the columns and beams, a refined estimation of tension field inclination angle is calculated using Eq. (1). Some iterations will help the design to be closer to have an optimal strength. Following the preliminary design, other calculations such as the boundary element compactness, shear strength, beam-to-column connection requirements, etc., should be checked.

Steel plate shear wall design equations briefly summarized above, are accommodated in various provisions and standards [5,11]. CAN\CSA 2009 [11] recommends that the infill plate of the SPSW should be designed to resist the entire load and neglects the contribution of the surrounding boundary frame as given in Eq. (2). AISC 2005 seismic provision [12] have the same approach on load resistance distribution over the infill plate and moment frame. The current building code, AISC 2016 [5], supersedes the previous approach and requires that the strength of the frame shall not be less than 25% of the total shear force, which finds a basis in the capacity design philosophy. The codes are ambiguous on whether the boundary frame contribution in the design of SPSW should be considered or not as given in Eq. (3). Purba and Bruneau [13] estimated the percentage of shear forces and suggested that the infill plates should be designed to resist the total story shear. Berman [14] analyzed the seismic behavior of a series of code-designed steel plate shear walls using nonlinear response history analysis with ground motions representing different hazard levels. The percentage of story shear resisted by the web plate relative to the boundary frame is between 60% and 80%, and it is relatively independent of panel aspect ratio, wall height or hazard level but is affected by the changes in plate thickness. Verma and Sahoo [15] studied the

contribution of boundary elements in resisting the lateral force considering their interaction with the web plates of SPSW systems. Results of nonlinear time-history analyses show that the percentage of lateral load resisted by infill plate depends on the aspect ratio of the infill and the number of stories. An expression was proposed to predict the lateral force contribution of the infill plate and the boundary frame of SPSWs based on stiffness. A series of code-designed steel plate shear walls (SPSWs) with different aspect ratios and number of stories were numerically analyzed to investigate the wall and frame contributions of SPSWs [16]. The design procedure that neglects the boundary frame-moment resisting action may result in quite different stiffness and ductility capacity on SPSWs with different aspect ratios under almost the same design lateral loads. The twenty-five percent frame resistance limit specified by the provision is somewhat arbitrary [17].

Another unclear issue in the preliminary design is the sizing of the horizontal boundary elements at the upper and lowermost levels. A lack of proper capacity design on the boundary elements may lead to the plastic hinges forming within the beam span or column height. These undesirable plastic mechanisms may induce significant inelastic deformations of the boundary elements and reduce the SPSW strength as it prevents the yielding of the corner region of the steel panels. Qin et al. [18] investigated the flexural behavior of anchor horizontal boundary element (top beam) in steel plate shear wall and found that the plastic flexural capacity of anchor HBE decreases from unity to the minimum as a result of an increase in shear force, axial force and vertical stresses. Dastfan and Driver [19] studied flexibility parameter limits for the top and bottom anchor beams and developed a new flexibility parameter ( $\omega_l$ ) for top and bottom anchor beams where the original assumptions do not apply. For the top beam, a limit of 2.5 is selected, and for the bottom panel an upper limit of 2 is proposed. A lower limit of  $\omega_l \geq 0.84\omega_i$  is also introduced.

Yu et al. [20] tested a 1/3-scale, one-bay and two-story SPSW specimen under quasi-static cyclic loading and an axial load ratio of 0.3 ( $0.3F_yA_g$ ) to investigate the behavior of steel plate shear walls with axially loaded vertical boundary elements. They conducted a parametric study of SPSW specimens with various width-to-height ratios of infill steel plates and axial load ratios of VBEs by the finite element analysis. They stated that without considering the effect of axial load, the VBE flexibility coefficient limit of 2.5 is applicable for the SPSWs with width-to-height ratio of 1.0 for the infill steel plate. However, with an increase of the infill steel plate's aspect ratio, the development of the tension field tends to be inadequate, while the shear capacity and stress uniformity of the infill steel plate decrease. As a result, the flexibility coefficient limit of 2.1 is recommended for the design of VBEs in SPSW structures. On the other hand, Curcovic et al. [21] stated that the current requirement for minimum column moment of inertia is conservative. Qu et al. [22] investigated the effect of column stiffness (flexibility) on drift concentration in steel plate shear walls. They stated that column stiffness should be a design parameter to ensure a reasonably uniform drift distribution and a more uniform infill plate yielding along the height of SPSW buildings. Qu and Bruneau [23] showed that the existing limit on  $\omega_i$  is not correlated with satisfactory in-plane and out-of-plane VBE performance. Based on experimental data and analytical investigations, they examined whether the significant inward VBE inelastic deformation and out-of-plane buckling observed in some instances were due to excessive VBE flexibilities or due to other causes such as shear yielding at the ends of the VBEs. Sahoo et al. [24] investigated the effect of the type of connections between the web plates and the boundary elements and the boundary members' flexibility along with pinned beam-to-column

connections under lateral loading conditions using an experimental study on two-story SPSW specimens. Based on the analytical and experimental results, various design issues of SPSW systems are discussed.

The panel aspect ratio is one of the critical parameters that affect the shear distribution between the infill plates and VBEs. In AISC 05 [12], the ratio of panel width ( $L$ ) to height ( $h$ ) is limited to  $0.8 \leq L/h \leq 2.5$ . Aspect ratio and bay width of the steel plate shear walls were studied extensively by researchers. Gholipour and Alinia [25] studied the behavior of 4, 7, 10, 13, 16, and 19 story code-designed steel plate shear wall structures regarding panel aspect ratios of 0.83, 1.67, and 2.5, and it was concluded that selection of a suitable bay-width produces a considerable reduction on the size of VBE sections, especially in high-rise SPSWs. Li and Tsai [2] tested narrow SPSWs and stated that the SPSW exhibited ductile hysteretic behavior comparable to larger aspect ratios. Formisano et al. [26] conducted finite element analyses of slender steel shear panels regarding different values of the thickness by varying the aspect ratio of the plate for assessing the design formulas and the influence of the geometry on the structural behavior of shear plates.

This study is a comprehensive comparative study covering all aspects of SPSW preliminary design parameters and expounds on the correlation of the parameters with structural behavior. For that purpose, a numerical parametric study is devised to investigate the effect of a wide range of parameters such as plate thickness, aspect ratio, axial load and relative stiffness of boundary elements on the behavior of SPSW models using finite element analysis. In the numerical models, the top anchor beam is designed using different flexibility coefficients, and resultant behavior modes are reported. Both code-limited columns (flexibility parameter less than 2.5) and columns that violate requirements (column flexibility parameter above the limit 2.5) are considered. A wide range of aspect ratios are investigated, and the effect of aspect ratio on shear force distribution between plate and frame is quantified in terms of most influential parameters. The findings of this study give an insight on the effect of the relative shear strength of the infill plate with respect to total wall strength on the overall system behavior. Although the damage limits and failure development stages are studied well for the conventional shear walls [27], there is also need for detailed studies for SPSWs. This study investigates the failure sequences of SPSWs under monotonic loading in detail.

At the first stage, the finite element modeling procedure is verified using the experimentally measured response of shear wall specimens. In the parametric study, a total of 292 shear wall models combining various parameters are analyzed. The primary parameters affecting shear wall response are determined and adequacy of design equations are evaluated in emphasis to non-conforming cases.

## **2. FINITE ELEMENT MODEL VERIFICATION**

Six different steel plate shear wall specimens from four different studies are selected for finite element model validation as displayed in Fig 2. Specific details of the specimens may be found elsewhere, so only necessary information is provided. A summary of the specimen properties that is used for validation is provided at Table 1.



Table 1- Properties of the specimens used for validation

Researcher	Specimen	No. of Stories	$t_w$ (mm)	$F_{yp}$ (MPa)	$F_{yf}$ (MPa)	Column Section	Beam Section
Lubell et al. (2000)	SPSW2	1	1.5	320	380	S75x8	S75x8
Wang et al. (2015)	TM2	3	4 <sup>a</sup>	288-418 <sup>b</sup>	323-365 <sup>b</sup>	250x200x8x12 <sup>a</sup>	200x200x8x12 <sup>a</sup>
Park et al. (2007)	WC4T	3	4	351-441 <sup>b</sup>	351-441 <sup>b</sup>	250x250x9x12	200x200x16x16
Park et al. (2007)	SC2T	3	2	351	351-441 <sup>b</sup>	250x250x20x20	200x200x16x16
Park et al. (2007)	SC4T	3	4	351-441 <sup>b</sup>	351-441 <sup>b</sup>	250x250x20x20	200x200x16x16
Choi and Park (2008)	FSPW2	3	4	299	353-385 <sup>b</sup>	150x150x22x22	150x100x12x20

$t_w$ : infill plate thickness;  $F_{yp}$ : Plate material yield strength;  $F_{yf}$ : Frame material yield strength.

<sup>a</sup> Control story (2<sup>nd</sup> story)

<sup>b</sup> Tensile coupon test result range of the material (different thicknesses)

The first specimen SPSW2 is a 1/4 scale model of a steel-framed office building core tested by Lubell [28] as displayed in Fig 2(a). The steel plate web thickness of SPSW2 is 1.5 mm. The distance between two vertical boundary elements centerlines is 900 mm. The steel plate has a width-to-height aspect ratio of 1. The second model specimen TM2 is a three-story unstiffened steel plate shear wall with a 1/3 scale [29]. Different plate thicknesses are used in different stories; 6 mm for the bottom story plate and 4 mm for the top two-story plates. The frame TM2 is designed as a moment frame with welded connections.

The third model (WC4T) shown in Fig 2(c) is a 1/3 model of three-story steel plate shear wall [30]. The infill plate thickness of the WC4T specimen is 4 mm. Plate and boundary member materials are SM490 (Korean Standard) with a yield strength of 330 MPa. Two other specimens from the same study namely SC2T and SC4T are also modelled and used for validation study. WC4T specimen has a column section of H-250×250×9×12 (H- overall depth × flange width × web thickness × flange thickness). SC4T and SC6T specimens have relatively strong columns (H-250×250×20×20). Infill plate thickness ( $t_w$ ) of SC4T and SC6T specimens are 4 mm and 6 mm respectively.

The last specimen used for validation is frame designated as FSPW2 from the study by Choi and Park [31]. The columns of the three-story model have a section of H-150×150×22×22. The beams at second and third stories are H-150×100×12×20 and the top beam is H-250×150×12×20. The infill plate thickness of the specimen is 4 mm made of SS400 (Korean Standard) steel grade.

Detailed three-dimensional models of the specimens are created in ANSYS APDL [32] software. SHELL 181 from the ANSYS element library is used to create steel web plate and boundary elements of the models. The element has four nodes with six degrees of freedom at each node: translations in the x, y, and z directions and rotations about the x, y, and z axes. SHELL 181 element is also suitable for large strain nonlinear applications. Material properties are specified to be compatible with the materials used in the experiments and defined separately for each component of the model. Rate-independent material model is selected because all the experimental models were tested under static loading conditions. The steel material stress-strain curves are established as bilinear elastoplastic with von Mises yield criterion. Kinematic hardening rule is adopted for the models.

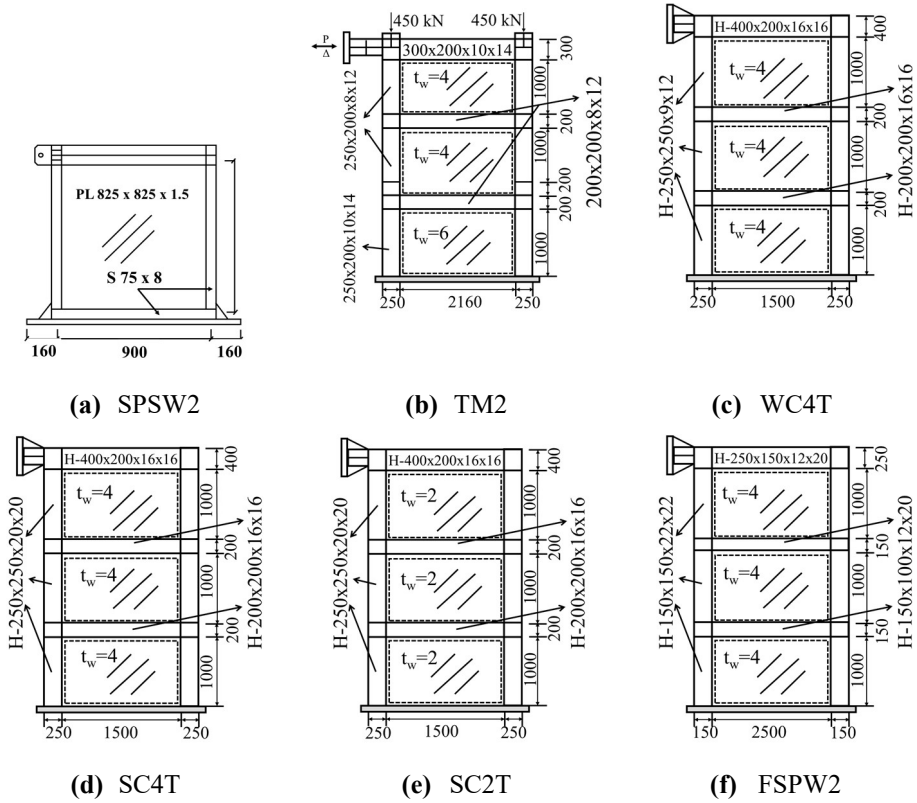


Figure 2- Drawings of experimental models (a) SPSW2 [28] (b) TM2 [29] (c) WC4T [30] (d) SC4T [30] (e) SC2T [30] and (f) FSPW2 [31]

Steel plates have imperfections due to fabrication errors such as initial distortion due to welding or bolting processes, misalignment of boundary elements and infill plates, etc. Therefore, a small disturbance load initiating the out of plane displacement of infill plate is found to be adequate to produce the inherent wavy tension field pattern. A small force of 50–100 N is applied to avoid the possible counterbalancing force effect on the plate due to large values. It is verified that the location of the disturbance load on the infill plate has no effect on the analysis results and buckling shape. So, the disturbance load is applied at the middle of the plate simultaneously with vertical loads before the lateral loading in all analyses. Axial loads are applied at the column tops. When defining the boundary conditions, the models are fixed at the base. Nodes in regions corresponding to lateral support locations are restrained as specified in related studies.

All specimens were subjected to cyclic quasi-static loading in the experimental programs. In all the tests, steel plate shear walls exhibit good ductility [28–31] capacity and desirable energy dissipation. Figure 3 plots the monotonic and cyclic analyses results in comparison to experimentally measured responses. The agreement between global experimental results and numerical prediction can be considered to be satisfactory for all models. For three specimens

as the story displacements are available from experimental work, the inter-story drift ratios are compared in Figure 4. From the findings of this exercise, it is concluded that the numerical modeling tool and approach can be safely used in the parametric study.

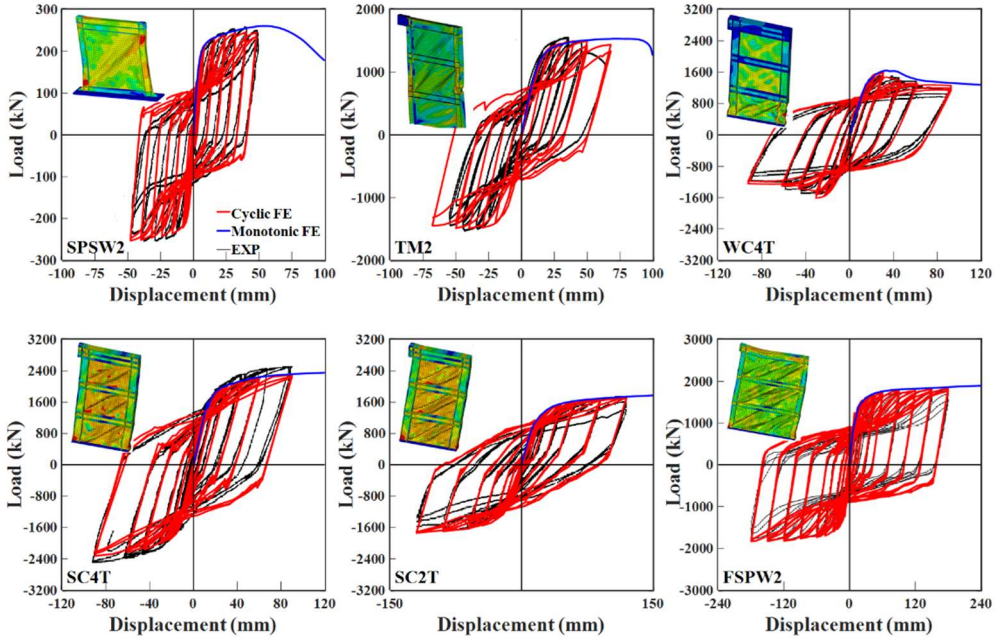


Figure 3 - Comparison of experimental and numerical load – top displacement curves

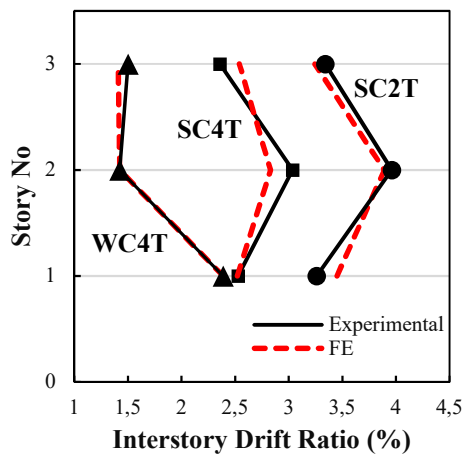


Figure 4 - Variations of maximum inter-story drift ratios

### 3. PARAMETRIC NUMERICAL STUDY ON SPSW SYSTEMS

#### 3.1. Model Parameters

Plate thickness, panel aspect ratio, stiffness of boundary elements and axial load ratio on VBE are considered as the parameters to investigate the SPSW behavior. Both material and geometric nonlinearities are included in the models. A typical three-story SPSW model illustrating and summarizing the parameters of the study is presented in Figure 5(b). In order to increase the resistance of the top beam against the bending action of internal steel plate forces an additional beam is attached to the top beam, and the beams are assumed to be constrained (share the same nodes) along the adjoining beam flanges as shown in Figure 5(a). The horizontal load is applied at the top left nodes of the models as shown in Figure 5(b). Although the frame-wall interaction effects that may be influential on the behavior of SPSWs may be disregarded in this way, the relatively constant shear force at the base of building systems legitimize these models as much as experimental models. Beam to column intersections at all story levels are considered as the lateral support locations. Out-of-plane displacements of the nodes in intersection regions are restrained at all story levels. As explained in section 2, in all models a constant 50 N out-of-plane load is applied at the middle of the infill plate to account for the imperfections.

Capacity design procedures might result in highly conservative sections in some cases [14]. In order not to limit the parameters and define a wide range of models, the capacity design process has not been followed. Thus, a better observation of the parameter effects on SPSW behavior have been made. The steel panel height  $h_s$  is constant in all models as 3000 mm, and the selected panel lengths  $L$  are 2000, 3000, 4000, 5000, and 6000 mm. In this way, plate aspect ratios, which is defined as the ratio of panel length to height  $L/h$ , ranging from 0.67 to 2 are considered. Models with a low panel aspect ratio of 0.67 are analyzed as it was reported previously that narrow steel plate shear walls performed satisfactorily and exhibited ductile hysteretic behavior, which can be compared to those with larger aspect ratios [2]. Plate thicknesses  $t_w$  are selected as 3, 4, 5, and 6 mm. Past research has focused on walls with a  $L/t_w$  ratio ranging from 300 to 800, although no limits are specified for that ratio as per AISC provisions [5]. The selected plate thickness and plate lengths cover a wide range of panel slenderness ( $300 < L/t_w < 3000$ ).

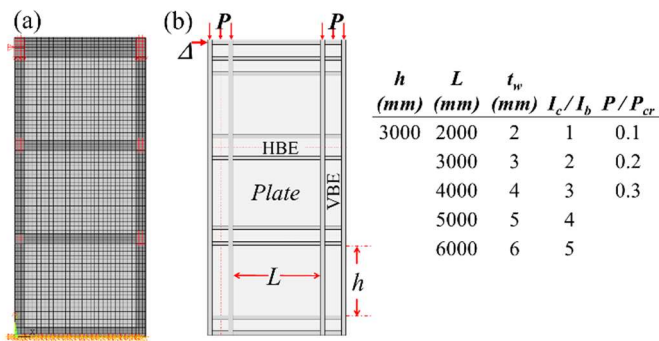


Figure 5 - (a) A representative finite element model of SPSWs used in this study, (b) typical steel plate shear wall configuration

European rolled wide-flange sections are used to design HBEs (HE sections) and VBEs (HD sections). Structural steel grades of S235 ( $F_y=235$  MPa,  $F_u=360$  MPa) and S355 ( $F_y=355$  MPa,  $F_u=510$  MPa) are used for steel infill panel and the boundary elements, respectively. Vertical boundary elements are chosen according to the stiffness requirements as per the AISC seismic provisions. After determining  $h$ ,  $L$ , and  $t_w$ , the required minimum value of column moment of inertia  $I_{c,min}$  is calculated using Eq. (5). Then, different models are generated with  $I_c$  equal to 1, 2, 4, 6, 8, 10 times the required minimum value  $I_{c,min}$ . The sections (HD and HE) are selected according to their moment of inertia. In all cases, the section with the closest moment of inertia to the calculated  $I_c$  is selected without further consideration.

Additionally, models that do not meet the column flexibility requirements (Eqs. 4 and 5) are created to investigate the effects of non-conforming column flexibility on the overall behavior of the structure. The column flexibility factors ( $\alpha$ ) of models varied from 1.18 to 2.7. The models that have a column flexibility parameter greater than 2.7 are not considered as their poor performance has been recognized in previous studies [29]. According to the seismic design principle of SPSW, the boundary elements shall remain elastic under the forces of a fully yielded web plate. Only plastic hinges at the ends of the horizontal boundary elements are permitted at this stage. The moment of inertia of the HBE depends on the difference of web plate thicknesses at neighboring stories. Since the plate thicknesses at all stories are constant, the demand on the beam is insignificant, which makes Eq. (6) useless. So, the moment of inertia of the horizontal boundary elements is selected depending on the  $I_c/I_b$  ratio ( $I_c$ =moment of inertia of VBE,  $I_b$ =moment of inertia of HBE). The adopted column-to-beam moment of inertia ratios are in a range of  $1 \leq I_c/I_b \leq 5$ . After specifying the sections for columns and beams, the tension field inclination angle is calculated using Eq. (1). For investigating the effect of axial load on the shear capacity, VBEs are subjected to axial load levels of 0.1, 0.2, and 0.3 times the critical axial load  $P_{cr}$ , where  $P_{cr}$  is equal to the yield strength of the VBE material ( $F_y$ ) times the cross-sectional area of the VBE ( $A_g$ ). The combination of these parameters gives a total of 292 different three-story SPSW models. After the design process, the beam flange width to beam height ratio ( $b_f/h_b$ ) and the beam flange width-to-thickness ratio ( $b_f/2t_f$ ) also emerge as parameters which are considered in the parametric evaluation. The  $b_f/2t_f$  ratio is used to determine whether the selected section is compact, non-compact, or slender with respect to limits specified in the standards. The lower the value of this parameter, the more compact the section is. With these two parameters, accurate observations could be made in cases where the  $I_c/I_b$  ratio was not sufficient to explain the beam behavior.

### 3.2. Structural Behavior under Monotonic Loading

As there is a large number of FE models for the analyses and considering the excessive solution time and the convergence difficulties in nonlinear cyclic loading analyses, all models are analyzed under monotonically increasing lateral load. Comparison of calculated load-deformation curves of experimental specimens under monotonic and cyclic loading indicates a larger drift capacity for the former than the latter for all experimental models as displayed in Figure 3. Traditionally, deformation limits of a subassembly should be derived using the experimentally obtained inelastic force–deformation cyclic response characteristics. Tests using monotonic loading are permitted to supplement the cyclic tests. However, the ultimate deformation need not be limited by that from the cyclic tests, where in-cycle rapid strength

loss did not occur during any cyclic test. In such cases, it is permitted to construct backbones from a combination of monotonic and cyclic data. The ultimate deformation of a cyclic test generally corresponds to the monotonic test capping displacement (at which the tangent stiffness becomes negative). The maximum displacement attained in the monotonic test is approximately 1.5 times that for the cyclic test. It is also known that the structural components (beam to column connections, infill plate, beams, and columns) may be exposed to more severe strength degradation under cyclic loading. So, it is occasionally argued that the cyclic loading protocol induced damage might be more severe than an actual seismic ground motion should do. Thus, there are cases where monotonic loading may produce more representative behavior of a subassembly. Monotonic loading adequately calculates the initial stiffness, maximum shear force and deformation characteristics within the eligible design drift ratio limits for all cases, which for this study is of interest.

Structural members and components are designed to exhibit a predetermined behavior under prescribed lateral load effect. So, the results of finite element analyses are evaluated on the basis of SPSW behavior. Buckling of infill steel plate is the first and inherent instability mode for all SPSW models. It should be useful to define the desired nonlinear behavior of an SPSW at this stage as a reference behavior type. The failure sequence of properly designed SPWS in reference to Figure 1 can be listed as;

- Buckling of steel infill plate and development of complete tension field action (yielding of the entire plate) at around 0.01 rad story drift ratio,
- Onset of yielding at the beam ends,
- Onset of yielding at column base,
- Plastic hinging at each end of the beam,
- Plastic hinging at the column base.

Obviously under such a variety of parametric combinations it should not be expected that all models will fail in this hierarchal order even if the design is performed under given limitations. It is observed that combination of parameters over a certain critical range leads to some unpredictable and undesirable failure patterns. By identifying these failure modes, the design parameters that cause such system behavior can be easily detected. For that purpose, the observed failure modes of SPSWs in the finite element analyses are identified as follows:

- Plastic hinge formation at horizontal boundary element,
- Plastic hinge formation at vertical boundary element,
- An apparent inward deformation on the vertical boundary element and in-plane shear yielding failure at the top end of VBE,
- Top anchor beam ends have in-plane plastic deformation under the axially acting column shear forces and steel panel-induced load,
- An in-span out-of-plane buckling at the top anchor beam,
- Yielding of beam-to-column junctions,
- Bending of VBE,
- VBE yielding along the height,
- In-span out-of-plane buckling along the height of the column.

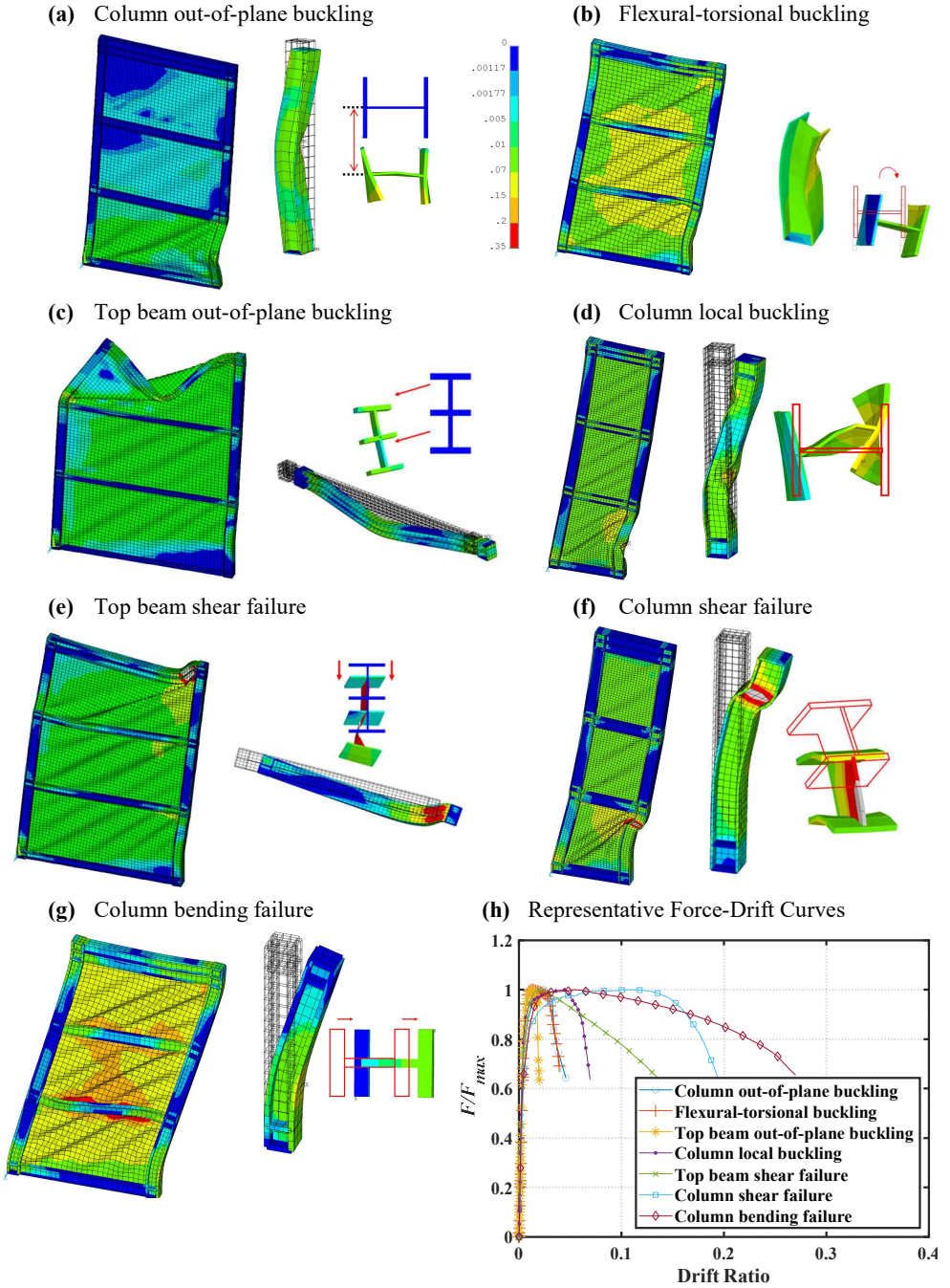


Figure 6 - Von-Mises strain plot of observed failure modes on models and specific column and beam members and representative lateral force-drift ratio curves of each mode

In the light of these failure definitions, seven main failure groups under monotonic loading are identified according to the dominant failure patterns as summarized in Figure 6. The von Mises strain plots for all failure modes are illustrated using the same contour levels given in Figure 6(a). It should be noted that some models may be classified under two or more groups as they exhibit more than one apparent failure modes. After grouping of models with similar failure patterns, the effects of design parameters on the SPSW behavior is investigated. The failure modes given in Figure 6(a-g) are studied in detail and the design parameters in relation to the specific failure pattern are determined by evaluating their effect on the load-deformation characteristics, i.e. shear force and lateral drift capacity. A representative lateral force-top drift ratio curve is selected from each group and they are plotted in Figure 6(h) for comparative and illustrative purposes.

The relationship between design parameters and the ratio of the shear force resisted by infill plate to total SPSW shear force ( $V_p/V_t$ ) is investigated. The plate shear force is calculated using the forces from the nodes at the middle level of the first-story plate. The representative  $V_p/V_t$  value is adopted as the yield point on the load-deformation curve. The concept of equivalent plastic energy is used to determine the yield point.

Although some parameters reveal apparent trends with respect to drift capacity of models, such as increasing the axial load ratio  $P/P_{cr}$  on the boundary columns has a decreasing effect on the ultimate drift ratio, the plot of individual parameters displays a weak correlation with the ultimate drift ratio for the entire data set. So, the relation of design parameters with ultimate drift ratio is separately evaluated for each failure group as plotted in Figures 7 to 13. The ultimate drift ratio is defined as the point where the base story shear force drops 85% of the maximum value on the load-displacement curve. However, such high axial load cases where the force-displacement curve gradually decreases after peak force, the ultimate drift limit is accepted as the drift level which corresponds to 50% of the peak shear force. In the following individual failure modes illustrated in Figure 6 are examined in more detail.

### **3.2.1. Column out-of-Plane Buckling**

As a general examination procedure, the correlation of SPSW design parameters with respect to ultimate drift ratio (first row) and ratio of plate shear force to total shear force  $V_p/V_t$  (second row) are plotted in Figure 7. This investigation procedure is also followed for all the remaining failure groups.

Main parameters affecting the column out-of-plane buckling are the column flexibility parameter  $\omega_t$  and the axial load ratio  $P/P_{cr}$ . Although buckling occurs with respect to the weak axis of VBE on this failure type, it is related to the  $\omega_t$ , since the weak axis and strong axis moment of inertias are inter-related. The lowest  $\omega_t$  value of models with an out-of-plane displacement of columns is 2.2 as shown in Figure 7(a) and (g). The average axial load level of models in this group is 0.21 and this is one of the highest values among the groups. In this set of models, the average ratio of beam flange width to beam height  $b_f/h_b$  is 0.97 with a low standard deviation of 0.07. The width-to-thickness ratio of the beam flanges ( $b_f/2t_f$ ) has a wide range and is not an indicative parameter for this group of models. The average drift ratio of the group is 0.039, which is the lowest average drift ratio among groups. Increasing the axial load and the plate aspect ratio reduces the drift ratio as shown in Figures 7(e)&(f). Both



parameters increase the axial demands on the columns and lead to early column failure as a result of column out-of-plane deformation as shown in Figure 6(a). Another parameter that contributes to the formation of this failure mode is the  $I_c/I_b$  ratio as displayed in Figure 7(h). For this failure mode most models have  $I_c/I_b = 1.0$  and the average  $I_c/I_b$  ratio is 1.58, which is the second lowest among groups. The use of relatively strong beams as indicated by  $I_c/I_b$  and  $b_f/h_b$  ratios increase the occurrence of column failure mechanism before the beams. The steel infill plate does not entirely yield in this type of failure mode. The observed failure sequence is as follows:

- Partial tension yielding at the steel infill plate,
- Yielding of beam-to-column junctions,
- Yielding starts at the compression column,
- In-span out-of-plane buckling occurs at the column.

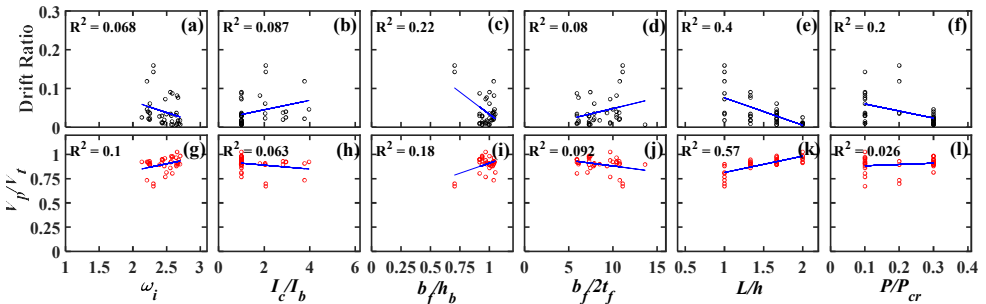


Figure 7 - Correlation of design parameters with drift and  $V_p/V_i$  ratios

In the design of steel plate shear walls, the boundary elements are expected to remain elastic until the entire plate yields. As the column failure starts prior to the entire plate yielding in this group, the frame contribution to the system shear capacity is minimal. The  $V_p/V_i$  ratio increases as the aspect ratio of the plate increases as displayed in Figure 7(k). Except for 4 of the 38 models in this group, all others have a  $V_p/V_i$  ratio greater than 0.8. These four models are characterized by the lowest column flexibility factor and aspect ratio of this failure group ( $L/h = 1.0$ ). So, these four models have the largest deformation capacity of this set due to the stronger column and lower aspect ratio when compared to other models. It can be concluded that this type of failure is most likely to occur in SPSW designs with relatively weak columns ( $\omega_i \geq 2.2$ ) and stiff and wide-flanged beams with  $I_c/I_b \leq 1.58$  and  $b_f/h_b \approx 0.97$ , respectively. High axial load level significantly catalysis the failure, yet the failure mode may also commence under low axial load combined with critical values of these parameters.

### 3.2.2. Flexural Torsional Buckling of the Column

Flexural torsional buckling of a column usually takes place when sudden twists and bends occur in the member. In this failure group, the column is loaded eccentrically by the plate forces because of the deformed wavy shape of the steel infill. As illustrated in Figure 6(b),

eccentric stresses induced by the plate cause the column to twist and axial load facilities flexural buckling (average  $P/P_{cr} = 0.18$ ). This group models have the second lowest average drift ratio level with an average value of 0.07. All models in this group have a plate aspect ratio of 1 and above as shown in Figure 8(k). The column flexibility factor is greater than 2.2 as in the first failure group as displayed in Figure 8(g). The average  $b_f/h_b$  ratio is 0.99 with a standard deviation of 0.04 as shown in Figure 8(i). The increasing axial load ratio and  $L/h$  ratio of the plate also correlates well with decreasing drift capacity in this group as displayed in Figures 8(e) and (f). In addition to increasing the compressive load on columns, high axial load also increases the P-delta effect and reduces the structural system's displacement capacity. The failure order of this failure type is:

- Tension yielding starts at steel infill panel while boundary elements remain elastic,
- Yielding develops at horizontal boundary element ends,
- Yielding initiates at vertical boundary element,
- Vertical boundary element cross-section rotates (twists) around the longitudinal axis of the member,
- An apparent inward deformation occurs at the vertical boundary element and VBE fails in the form of in-plane flexural buckling.

The  $V_p/V_t$  ratio is 0.73 and higher in all models. As the percentage of shear force resisted by the plate becomes dominant over the system strength, the drift ratio capacity of SPSW decreases. The plate shear force ratio has a strong relationship with the plate aspect ratio as shown in Figure 8(k). Although there is a correlation between drift and axial load level,  $V_p/V_t$  ratio remains insensitive to axial load level as displayed in Figures 8(f) and (l). The average column-to-beam stiffness ratio  $I_c/I_b$  and plate aspect ratio  $L/h$  of the first and second groups are 1.58 and 2.0 for the former and 1.5 and 1.22 for the latter, respectively. This indicates to relatively stiffer columns and narrower panel width for the second group than the first. Other parameters are similar in each group. It can be stated that narrow steel plate shear walls with  $\omega_t$  above 2.2 and  $I_c/I_b < 2.0$  may not prevent the columns from being damaged before beams.

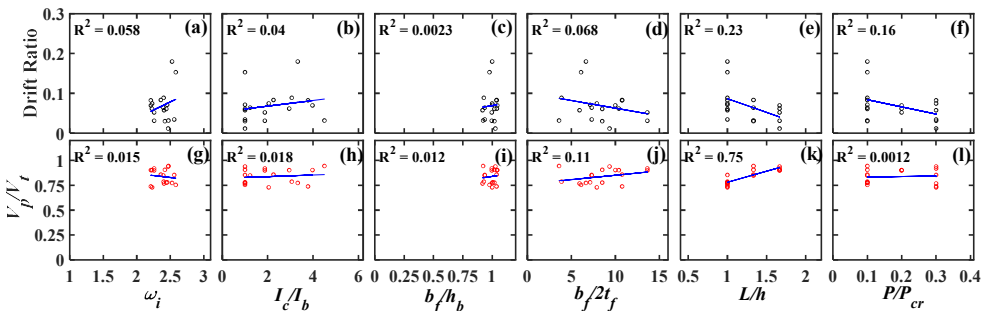


Figure 8 - Correlation of design parameters with drift and  $V_p/V_t$  ratios

### 3.2.3. Top Beam Out of Plane Buckling

Unlike the first two groups, the column flexibility factor covers a wide range of values for models of this group as shown in Figures 9(a) and (g). There is a significant decrease in the average axial load ( $P/P_{cr} = 0.14$ ) when compared to first two groups. Figures 9(e) and (k) display that the models with the highest aspect ratios are clustered in this group. In all models, the proportion of plate width to height is 1.67 or 2.00. The average  $I_c/I_b$  ratio is 3.22, which is among the highest of all failure groups. The models in this failure group have more flexible horizontal boundary elements than vertical elements with a larger span. Using weak beams at inter-story is not influential to sudden failure. However, even double beams are used at the top of the frame, the stiffness is insufficient to resist out-of-plane buckling loads as illustrated in Figure 6(c). In this failure group, sudden strength loss without any softening behavior is observed on the load-displacement curve. This failure group has the highest average beam slenderness ratio. The slenderness ratio is calculated by dividing the story length ( $L_s$ ) by the radius of gyration ( $r$ ) of the cross. Since buckling might occur about either of the axis, the radius of gyration about the weak axis is often becomes more important. As the beam length increases and the beam moment of inertia about weak axis decreases, the beams are more prone to buckling. Also, the low axial load prevents the columns from being damaged before the beams, which improves the systems lateral displacement capacity. The average ratio of the beam flange width to beam depth ( $b_f/h_b$ ) is 0.77, which is lower than the first two failure groups and indicates to less stiff beam in the out-of-plane direction. For top beams, sections with a high  $b_f/h_b$  ratio and low  $I_c/I_b$  ratio reduce the occurrence probability of this type failure. The observed failure mechanism of this group is as follows:

- Partial/full yielding of the steel infill,
- Yielding of beam-to-column junctions,
- Yielding at column base and beam ends,
- Out of plane buckling of the top beam.

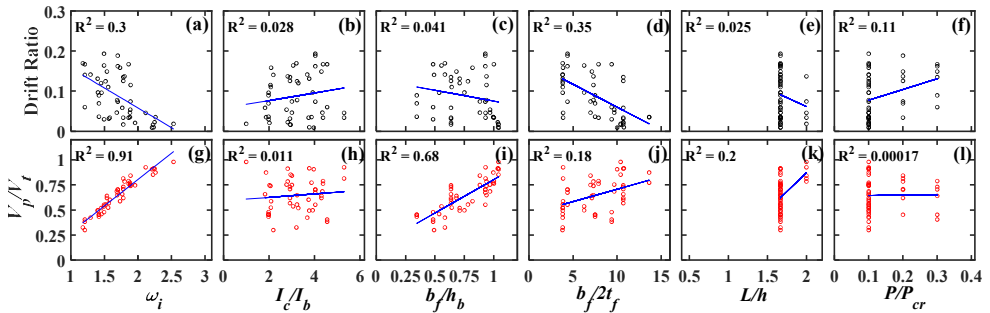


Figure 9 - Correlation of design parameters with drift and  $V_p/V_t$  ratios

The average drift ratio of this group is 0.09. There is an inverse correlation between column flexibility factor and drift ratio as displayed in Figure 9(a). The models in this failure group have stiffer columns than the models in the first two groups in terms of the moment of inertia. The average of column flexibility factors is 1.7. For  $V_p/V_t$  ratio, there is a noteworthy

correlation with the column flexibility factor (R-squared is 0.91) as plotted in Figure 9(g). The value of  $\omega_t$  varies between 1.21 and 2.53. The results show that this failure mode may also develop in models with relatively weak columns represented with column flexibility factor greater than 2.2. But, note that these models are in the largest beam width to flange thickness ratio ( $b_f/2t_f > 10$ ) group. Even if the model has relatively weak columns ( $\omega_t > 2.20$ ), the top beam out-of-plane failure may occur with a combination of high  $L/h$  and high beam  $b_f/2t_f$  ratios.

### **3.2.4. Column Local Buckling**

Among the failure groups this particular failure mode is placed in the medium range in terms of average drift ratio. The average column flexibility factor  $\omega_t$  is 2.14 with a lowest value of 1.7. Some models in this group can be classified under two or more groups as their deformed shape exhibit the failure properties of different modes at the same time. However, their common feature is that the failure initiates when local column flange buckling occurs and columns deform inwards as shown in Figure 6(d). In this group, the models with the highest aspect ratio ( $L/h=2.0$ ) have the lowest drift ratio as displayed in Figure 10(e). Even so, if a model with a low aspect ratio ( $L/h=0.67$ ) has a very high column flexibility factor, it may also fail at low drifts. In models with high aspect ratio, columns tend to deform nonlinearly before the entire infill panel yields. Models have a moderate axial load ratio (average is 0.18) in this group. In the models with the highest drift ratio, the local flange buckling usually occurs near the column base and leads to the formation of a plastic hinge. When the plastic hinges form in the column base and at the beam ends, this allows the structure to achieve high drift levels. When the plasticity develops within the column span, the drift ratio capacity decreases. In both scenarios, first the flange buckling initiates, and then instability develops. Two dominant failure sequences are:

- Yielding of the steel infill,
  - Yielding of the beam-to-column junction,
  - Yielding of beam ends,
  - Yielding starts at column base,
  - Plastic hinging at beam ends,
  - Column local flange buckling near the base,
  - Plastic hinging at the column base,
- and,
- Partial yielding of the steel infill,
  - Yielding of beam ends,
  - Yielding starts at column base,
  - Local flange buckling occurs in-span of the column,
  - In-plane deformation of the column,
  - Inward buckling – instability of the column.

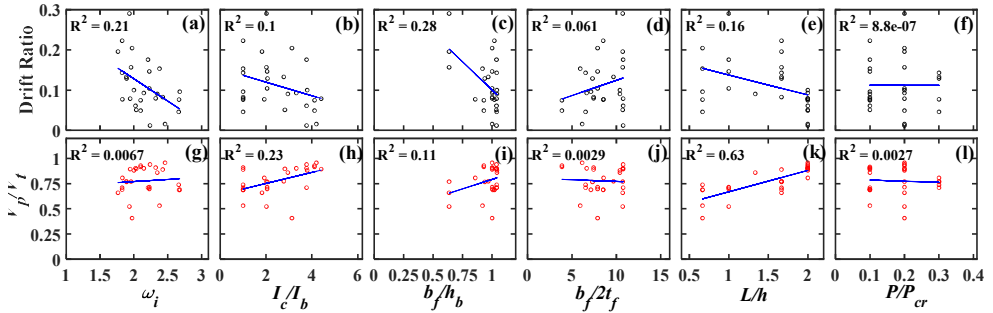


Figure 10 - Correlation of design parameters with drift and  $V_p/V_t$  ratios

Similar to other groups, the  $V_p/V_t$  ratio correlates with the plate aspect ratio as shown in Figure 10(k). Contribution of steel infill to the total base shear increases with the  $L/h$  ratio. This is because the columns fail before reaching their capacity. As seen in Figures 10(c) and (i), the  $b_f/h_b$  ratio of the models in this group is generally high. In models with high  $b_f/h_b$  ratio, while the beams have not been damaged yet, damage begins on the columns. In general, models with  $V_p/V_t$  ratio below 0.7 are models with a low plate aspect ratio and low column flexibility factor. Different combinations of these parameters can lead to different kinds of behavior.

### 3.2.5. Top Beam in-Plane Shear Failure

In this failure type, the top anchor beam end has inward deformation under steel panel-induced traction forces as displayed in Figure 6(e). The average  $\omega_e$  of the top beam shear failure group is 1.63, which is the lowest among all the failure groups. Strong columns enable models to reach high drift ratios. The average drift ratio of this group is 0.18, which is the second highest among groups. The average  $I_c/I_b$  ratio is the highest of all at 3.58. Some design parameters distinctly separate this group and the top beam out-of-plane deformation group discussed above. The plate aspect ratio  $L/h$  in the previous group is 1.7, which is the highest group average value, but in this group, this ratio is 1.2 and is one of the lowest. When the SPSW span length decreases, the upper beam is prone to shear failure with less possibility of out-of-plane deformation.

As given in Figure 11(a), column flexibility factor values of all models are less than 2.0 and the average  $b_f/h_b$  ratio is 0.68, which is the lowest of all groups. Only six models have an  $I_c/I_b$  ratio of less than 2.14. Although the value of beam stiffness is relatively large in these models, beam shear failure is triggered by low  $b_f/h_b$  ratio, which contributes to formation of local web or flange buckling at the upper beam's end under the unbalanced infill steel plate traction force. Models with a low  $b_f/h_b$  ratio do not always have low drift capacity. The low  $b_f/h_b$  ratio allows the models to have failure to form in beams rather than the columns, thus high drift ratios are achieved. The two main factors that permit this failure are low  $\omega_f$  for columns and high  $I_c/I_b$  and low  $b_f/h_b$  ratios for beams. The failure sequence is as follows:

- Yielding of the steel infill,
- Yielding of beam ends,

- Yielding starts at column base,
- Plastic hinging at beam ends,
- Plastic hinging at the column base or in-plane column global buckling,
- Excessive inward deformation of the top beam end.

Most of the models have  $V_p/V_t$  ratios less than 0.7 as plotted in Figure 11(a). There is a good correlation between the column  $\omega_i$  value and the  $V_p/V_t$  ratio as shown in Figure 11(g). A high  $\omega_i$  value increases the  $V_p/V_t$  ratio in this group as in the other groups. Only five models, which are characterized with high  $\omega_i$ , have  $V_p/V_t$  ratio above 0.7. It is also found that these five models have a  $b_f/h_b$  ratio of approximately 1 (see Figure 11(i)), which is quite above the average value and has high plate  $L/h$  ratio. Overall this group displays the strongest correlation between  $b_f/2t_f$  and  $V_p/V_t$  ratios. Both parameters increase the  $V_p/V_t$  ratio as illustrated in Figures 11(j-k). In this group, which generally includes models with strong columns, an increase in the ratio of beam width to beam thickness  $b_f/2t_f$  causes the upper beam to deform earlier. The drift ratios of these models are in the low to medium range.

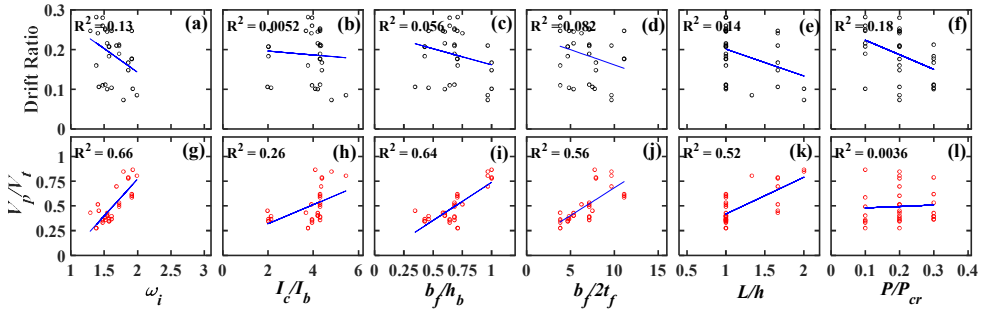


Figure 11 - Correlation of design parameters with drift and  $V_p/V_t$  ratios

### 3.2.6. Column Shear Failure

The models in this group have a shear failure at the compression column top end as illustrated in Figure 6(f). An apparent inward deformation occurs on the vertical boundary element and VBE fails in the form of in-plane shear yielding failure at the top. Only four models have column flexibility factor greater than 2.0 as seen in Figure 12(g). These four models have the lowest plate aspect ratio ( $L/h=0.67$ ) and the minimum  $I_e/I_b$  value (1.0). High shear forces induced by stiff and short beams and inward forces from the steel infill plate lead to the formation of the column failure. This result indicates that when models with stiff columns ( $\omega_i \leq 2.0$ ) are used together with beams of equal stiffness ( $I_e/I_b \approx 1.0$ ), the beams are not damaged and failure occurs at the column top. As the minimum  $I_e/I_b$  ratio is 1.0, using sections with lower width to thickness ratio (low  $b_f/2t_f$ ) makes the beams even more compact. For models with low  $\omega_i$  as in this group, column shear yielding failure only occur using beam sections with the lowest  $I_e/I_b$  ratio and the lowest width to thickness ratio ( $b_f/2t_f$ ) in the entire data set. This failure group has the lowest average  $I_e/I_b$  ratio (1.3) and the lowest average  $b_f/2t_f$  ratio (3.87) among groups. In this group, which has the strongest beams of all groups in terms of stiffness and  $b_f/2t_f$  ratio, the high shear force resulting from the opposing beam

and infill panel forces at the column top end ultimately leads to column shear failure. Although failure mechanism occurs on the columns, the average drift ratio of this group is 0.18, which is one of the highest. The failure sequence is as follows:

- Yielding of the steel infill,
- Yielding of beam ends,
- Yielding starts at column base and initiates through the height,
- Plastic inward deformation occurs at the column top level.

The  $V_p/V_t$  ratio of only two models in this group is above 0.75 as displayed in Figure 12. As seen in Figure 12(g), the  $V_p/V_t$  ratios plotted against the column flexibility factor  $\omega_t$  indicates a moderate correlation with large dispersion. When the plate aspect ratio  $L/h$  is considered trend is similar to previous failure groups. As the aspect ratio of the plate increases, the  $V_p/V_t$  ratio also increases. The  $V_p/V_t$  ratio also increases with increasing beam  $b_f/2t_f$  ratio. Models with the highest  $b_f/2t_f$  ratio get the lowest values of  $\omega_t$  in this failure group. The use of weaker columns and a higher  $b_f/2t_f$  ratio on beams generally reduces the frame contribution to the shear strength of SPSW system.

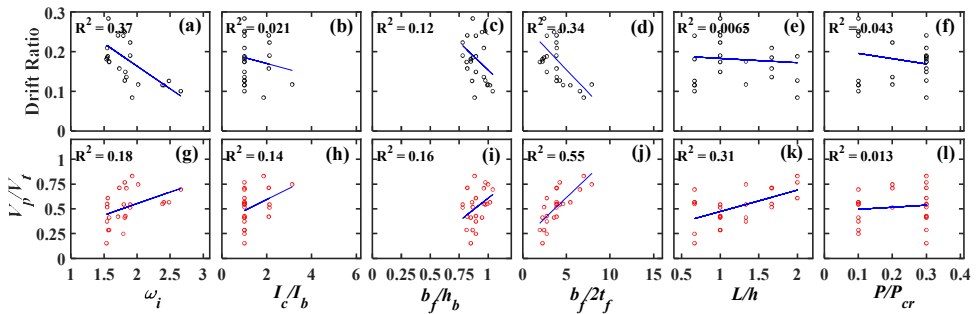


Figure 12 - Correlation of design parameters with drift and  $V_p/V_t$  ratios

### 3.2.7. Column Bending Failure

In this group, failure arises from the in-plane bending effect induced by infill plate forces along the column span. Local buckling does not form on the flanges and the web of the column, only flexural bending is observed along the length of the column as shown in Figure 6(g). The force-displacement curve of the SPSWs generally decrease gradually under bending and  $P-\Delta$  effects, and no sudden strength drop is observed as illustrated in Figure 6(h). After the plastic hinge development at the beam ends, the columns deform under bending force and axial load. This group has the highest average drift ratio ( $\approx 0.21$ ) as illustrated in Figure 13. The average axial load ratio is 0.22, which is one of the highest among groups. With a low column flexibility parameter, the SPSW system can have improved drift capacity even though the columns are exposed to high levels of axial load as in this failure type. The average value of the column flexibility factor is 1.67 as shown in Figures 13(a) and (g). Only 4% of the models in this group have  $\omega_t$  values greater than 2.2. These models have low plate aspect ratio and low axial load. The trend between axial load

and drift ratio shows that the drift capacity decreases with increasing axial load as plotted in Figure 13(f).  $I_c/I_b$  ratio ( $\approx 2.57$ ) of this group is higher than the column shear failure group and lower than the top beam shear failure group. Other parameters display similar tendencies with respect to drift and plate shear force ratio as with top beam shear failure and column shear failure groups. Based on these observations, it is concluded that the  $I_c/I_b$  ratio is an important parameter affecting the failure pattern of SPSWs. The failure sequence of this failure type is as follows:

- Yielding of the steel infill,
- Yielding of beam ends,
- Yielding starts at column base and initiates through the height,
- Plastic hinging at beam ends,
- Column bending.

Approximately 94% of the models have a  $V_p/V_t$  ratio below 0.75 as displayed in Figure 13(g). The average  $V_p/V_t$  ratio is 0.49, which is one of the lowest among the other groups. The  $V_p/V_t$  ratio has good correlation with  $b_f/2t_f$  and increases with higher beam  $b_f/2t_f$  ratio as shown in Figure 13(j). The  $V_p/V_t$  ratio also shows an increasing trend with increasing  $\omega_i$  and  $L/h$  ratios of the plate, similar to other groups, as shown in Figure 13(g) and (k), respectively.

In general, this failure type has average parameter values comparable to the top beam shear failure group. Although the average values for  $\omega_i$  and  $L/h$  are higher than the top beam shear failure group, the main reason for better drift performance is that the selected beams in this group are stiffer (average  $I_c/I_b=2.57$ ) and have a lower  $b_f/2t_f$  ratio, i.e. are strong beams.

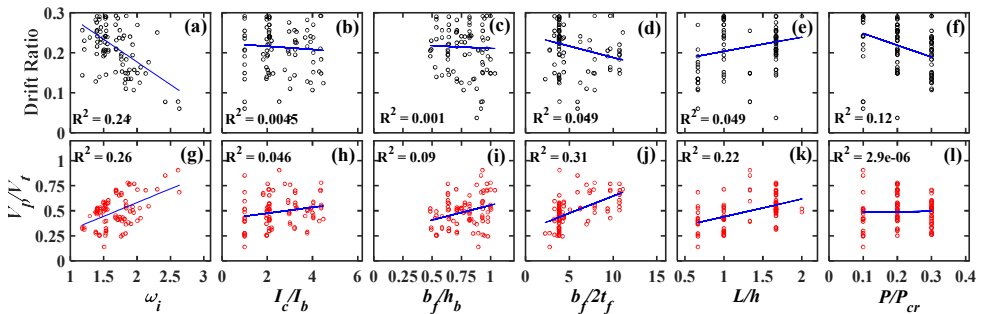


*Figure 13 - Correlation of design parameters with drift and  $V_p/V_t$  ratios*

### 3.3. Summary of Results

SPSW design parameters leading to different behavior types as identified above are summarized in Table 2 to gain better insight on the parametric relations that affect the failure pattern on SPSWs. In this way, effects of design parameters such as the axial load level and the stiffness of the horizontal boundary elements (in case of same thickness in adjacent stories), which are not addressed in the preliminary design code equations, can be evaluated comprehensively. Table 2 presents the average values of dependent and independent



variables calculated for seven groups. In Table 2, failure patterns are ordered with respect to decreasing column flexibility parameter  $\omega_t$ . Due to strong correlation between  $\omega_t$  and  $V_p/V_t$  ratio, group average  $V_p/V_t$  values also became listed in ascending order. By this way, first three modes with the highest  $\omega_t$  become failure modes effected by column local flange instabilities. These modes are also characterized by medium panel aspect ratios ( $\sim 1.5$ ). These column instabilities are accompanied by low drift ratio and high  $V_p/V_t$  ratio. Low  $I_c/I_b$  ratios, high  $b_f/h_b$  and  $b_f/2t_f$  ratios, i.e. relatively strong beams with respect to columns, are also peculiarities of these failure modes.

The last three failure modes in Table 2 are related to column and top beam in-plane deformations with high drift capacity and low  $V_p/V_t$  ratio. The main reasons of these behavior types are low column flexibility parameter  $\omega_t$  (stronger frames) and low  $L/h$  ratio (narrow SPSWs). Also, columns being stronger than beams characterized with high  $I_c/I_b$  ratio contributes to emergence of these failure modes. The fourth and fifth failure modes in Table 2 should be evaluated separately in our opinion. The top beam tends to experience outwards buckling when columns with moderate flexibility are utilized in high aspect ratio SPSWs. When the aspect ratio  $L/h$  of panel decrease, the instability of the top beam turns inwards.  $I_c/I_b$  ratio, another main ingredient of such behavior, is at the highest value for top beam shear buckling. Low  $b_f/h_b$  and  $b_f/2t_f$  ratios increase the effect of mentioned parameters on top beam failures as seen in Table 2.

Table 2 - Average values of effective design parameters according to failure types.

No	Failure Type	Drift ratio	$V_p/V_t$	$\omega_t$	$L/h$	$P/P_{cr}$	$I_c/I_b$	$b_f/h_b$	$b_f/2t_f$
1	Column out-of-plane buckling	0.04	0.89	2.46	1.50	0.21	1.58	0.97	8.49
2	Column flexural-torsional buckling	0.07	0.82	2.38	1.22	0.18	2.00	0.99	8.35
3	Column flange buckling	0.11	0.78	2.14	1.51	0.18	2.45	0.96	8.37
4	Top beam out-of-plane buckling	0.09	0.65	1.70	1.70	0.14	3.22	0.77	7.56
5	Top beam shear failure	0.18	0.49	1.63	1.20	0.20	3.80	0.68	6.62
6	Column shear failure	0.18	0.52	1.85	1.20	0.21	1.30	0.90	3.87
7	Column bending failure	0.21	0.49	1.67	1.30	0.22	2.57	0.78	5.47

When all groups are considered individually, a value of 2.2 emerges as a limiting value for the column flexibility factor for improved drift capacity and shear force distribution among the plate and frame parts of SPSW. In terms of drift ratio capacity, the  $\omega_t$  value of failure modes with the lowest drift capacity is above this limit. Models with a column flexibility factor greater than 2.2 may achieve high drift level, if certain criteria are met by other parameters. The number of these models has a very small percentage in the total data. The column flexibility factor above 2.2 leads to excessive column flexibility especially when high  $L/h$  and  $P/P_{cr}$  ratios are used. When the SPSW is designed for  $\omega_t$  values greater than 2.2, the wall is more likely to have a sudden strength drop on the load-deformation curve with the aggravating contribution of effects of other parameters to instability. The failure modes, such as partial yielding of the infill and sudden outward deformation failures of beams and columns, are more likely to occur in these models that do not meet the proper design considerations.

The use of high infill plate ratio  $L/h$  with high column flexibility factor results in failure modes with a relatively low drift capacity as discussed above. The failure modes with the highest drift capacity in Table 2 have the lowest  $L/h$  ratio. However, this should not indicate that wide SPSWs (with high  $L/h$  ratios) cannot be employed safely. When carefully combined with other parameters, it is observed that walls with high aspect ratios achieve high drift values. For example, in a model with the column flexibility factor  $\omega_t$  of 1.4 and the highest plate aspect ratio  $L/h=2.0$ , the column fails in global buckling by reaching a high level of drift. Another model with  $\omega_t = 1.96$  and  $L/h = 1.67$  can still achieve the highest drift ratio capacities.

According to the design equation given in Eq. (5), for the same  $t_w$  and  $h_s$ , as  $L$  increases, the required minimum column moment of inertia decreases. This is per the limit value of 2.5 is adopted for  $\omega_t$  for both narrow and broad SPSWs in the provisions. Thus, for models with high  $L/h$  ratio design code yields columns with lower minimum  $I_c$  value. However, according to results of this study,  $L/h$  ratio is inversely correlated to good behavior when used together with flexible columns. So, it should be safer to adopt the limiting  $\omega_t$  value of 2.2 for steel plate shear walls with large bay width ( $L/h \geq 1.67$ ). As the stress uniformity diminishes due to inadequate tension field development in high aspect ratio models, so columns should be stiffer to allow steel infill to develop a full tension field mechanism.

When the array with 292 models is evaluated considering the  $I_c/I_b$  ratio, for two failure groups with the highest average  $I_c/I_b$  ratio, the results indicate that both groups have failure at the top beam. Looking at the two groups with the lowest  $I_c/I_b$  ratio, the results show that the failures occur in the columns. According to the adequately designed SPSW's failure sequence, it is desirable that the hinging occurs first in the beams and then in the columns. In this case, this parameter can be chosen depending on the column flexibility factor. For instance, allowing a low  $I_c/I_b$  ratio ( $\leq 2.0$ ) for models with a column flexibility parameter higher than 2.2 may result in sudden failure in the columns while the beams are not yet damaged (column out-of-plane buckling and flexural-torsional buckling). An upper bound limit for  $I_c/I_b$  ratio is not suggested in this study. The model behavior with high  $I_c/I_b$  values can be improved by increasing the top beam stiffness. When the  $I_c/I_b$  ratio is above 3.0, the top anchor beam stiffness must be high enough to resist column and infill plate-induced forces. For the top beam, the code-based beam stiffness assumptions ( $\omega_t \leq 2.50$ ) do not apply in most cases. As a general rule, for models with  $\omega_t$  value above 2.2, the minimum value of  $I_c/I_b$  should be 2.0.

In the design phase, axial load ratio is among the challenging parameters. Drift ratio capacity decreases as the axial load ratio increases as expected. For models with high axial load, it is necessary to use columns with low column flexibility to achieve higher drift levels. For example, the average axial load value of beam buckling and column shear buckling groups are 2.21, but the average drift ratio capacities of these groups are 0.04 and 0.18, respectively. Here, the column flexibility factor shows the most dominant effect. However, it is clear that other parameters also influence the occurrence of this difference.

For the  $V_p/V_t$  ratio, 0.75 turns out to be a decisive limit between failure modes. When this ratio is above 0.75, boundary elements tend to fail before the infill panel fully yields. Partially yielded plates do not comply with the SPSW design philosophy and cause undesirable system behavior by producing non-uniform stress fields. The contribution of boundary frame to the total shear force generally shows strong correlation with the column flexibility factor and the

steel infill aspect ratio. The increase in both parameters causes an increase in the share of steel infill plate in the load distribution. Although the most effective parameters in the ratio  $V_p/V_t$  are  $\omega_i$  and  $L/h$ , other parameters also have reasonable effect on this ratio. The following equation is derived by regression analysis using all 292 analyses data for the prediction of  $V_p/V_t$  with design parameters. The R-squared value of the regression fit is 0.96.

$$\frac{V_p}{V_t} = 0.43\omega_i + 0.025\frac{I_c}{I_b} + 0.077\frac{b_f}{h_b} + 0.0056\frac{b_f}{2t_f} + 0.29\frac{L}{h} + 0.11\frac{P}{P_{cr}} - 0.773 \quad (7)$$

#### 4. EVALUATION OF THE EFFECT OF PARAMETERS ON DESIGN EQUATIONS

For further examining the effects of the parameters on the global system behavior, an investigation on the  $V_p/V_t$  ratio is conducted. The  $V_p/V_t$  ratios from analyses are plotted with respect to column flexibility factor in Figure 14. The 292 models are divided into three groups considering the infill plate aspect ratios. Accordingly, the plate  $L/h$  ratio of the models in the first group is 0.67, the average  $L/h$  ratios of models in the second group are 1.11 and 1.33, and the  $L/h$  ratios of the last group are 1.67 and 2.00.

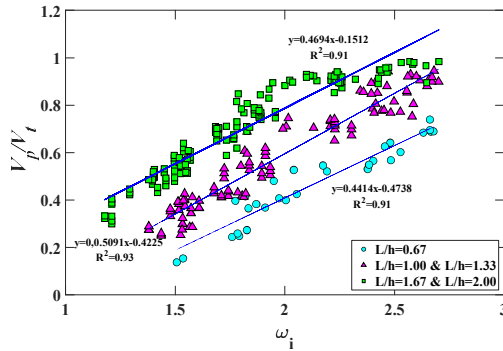


Figure 14- Relation of column flexibility factor  $\omega_i$  and  $V_p/V_t$ .

The plot reveals that the  $V_p/V_t$  ratio at yield is directly proportional to the column flexibility parameter, and as the  $L/h$  ratio increases, the percentage of shear carried by plate  $V_p$  increases. The  $\omega_i$  and  $L/h$  parameters are very effective in quantifying the shear percentage carried by plate and frame components of SPSW. All three datasets consist of models with different axial loads and different plate thickness. A general simplified form of Eq. (7) to predict the  $V_p/V_t$  ratio is calculated as;

$$\frac{V_p}{V_t} = 0.44 \times \omega_i + 0.31 \times \frac{L}{h} - 0.64 \quad (8)$$

The tension field inclination angles at all three stories are examined, but only the first story inclination angles are displayed here. The tension field inclination angle is determined based

on principal stress and principal strain directions. Figure 15(a) demonstrates the middle plate region on which tension field inclination angles are calculated. The width of the left and right column fields is  $L/4$ , and the middle plate field is  $L/2$ , where  $L$  is the infill plate length. Considering the inclined infill plate tension field mechanism, the principal strain and the principle stress angles with vertical direction are approximated to be tension field inclination angles. Both (principle stress and principle strain) angles are compared, and angles of the principal strains are found to be more stable and reliable. First story middle region tension field inclination angles that are obtained according to the principle strain angles are presented in Figure 15(b). According to the results, the permitted value of 40 degrees given by Seismic Provisions for Structural Steel Buildings [5] is found to be conservative, but an angle of 45 degrees is more realistic than 40 degrees. All models develop a tension field inclination angle between  $42^\circ$  and  $47^\circ$ . It is observed that the difference between the angle obtained from code-equation and FE analysis can rise to  $14^\circ$ . An inclination angle correction factor  $\beta$  for the code formula in Eq. (1) is proposed using the parameters;  $L$ ,  $h$ ,  $I_c$ ,  $I_b$ , and  $\omega$ . The right-hand-side of the tension field inclination angle equation is rearranged as;

$$\tan^4 \alpha = \beta \cdot \frac{1 + \frac{t_w L}{2A_c}}{1 + t_w h \left[ \frac{1}{A_b} + \frac{h^3}{360I_c L} \right]} \tag{9}$$

The correction factor,  $\beta$ , is derived by regression analysis as;

$$\beta = 2.5575 - 0.573 \frac{L}{h} - 0.526\omega + 0.0504 \frac{I_c}{I_b} \tag{10}$$

Comparison of inclination angles predicted by both uncorrected and the correction factor applied code formula in Eq. (9) with the values calculated from finite element analyses are plotted in Figure 15(c). As seen, the proposed inclination angle correction factor  $\beta$  significantly improves the prediction capacity of Eq. (9).

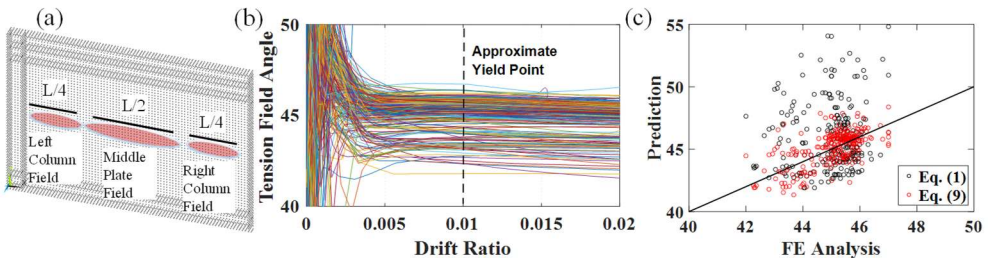


*Figure 15 - (a) Regions on steel plate considered for the calculation of tension field angle, (b) Variation of tension field angle with top drift ratio, and (c) Comparison of predictions of tension field angle equations with and without correction factor and analyses results*

As mentioned earlier, although provisions [5] incorporate equations such as Eq.(6) for the selection of horizontal boundary elements based on moments of inertia about an axis taken perpendicular to the plane of the web, a constant web plate thicknesses for all stories prevents us from using it. To better explore the effect of the horizontal boundary element stiffness on the behavior of SPSWs,  $I_b$  is introduced in proportion to  $I_c$ . All the analysis models are classified according to the  $I_c/I_b$  ratios. The  $I_c/I_b$  ranges of the groups are equal to 1, 1.8 to 2.2, 2.5 to 3.5 and greater than 3.5. For each group, the total shear force capacities from Eq. (3) and the analyses are compared in Figure 16(a). As seen in Figure 15, except for the  $I_c/I_b=1$ , the shear capacities calculated by Eq. (3) and finite element analyses agree well. When the moment frame shear force examined separately from the total shear, it is found that for  $I_c/I_b=1$ ,  $4M_p/h$  term calculating the frame contribution to total shear in Eq. (3) overestimates the shear strength of the frame approximately 2.2 times larger than FE analyses as displayed in Figure 16(b).

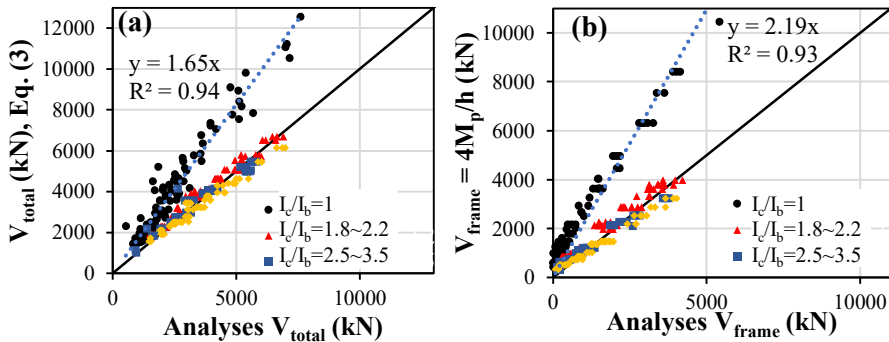


Figure 16 - Comparison of (a) the total SPSW shear force from FE analyses and prediction by Eq. (3), (b) the frame shear force from analyses and prediction by  $4M_p/h$

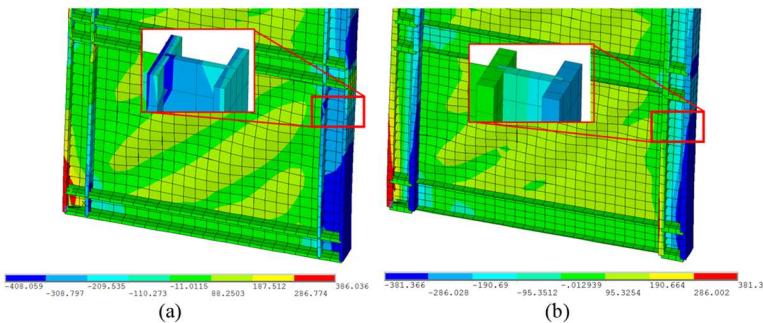


Figure 17 - Vertical stress distributions of a representative model with the ratio of (a)  $I_c/I_b$  equal to 1 and (b)  $I_c/I_b$  greater than 1

As given in Eq. (3), the contribution of frame to the total shear strength of SPSW is estimated as  $4M_p/h$  on the premise that the plastic hinge mechanism develops either at beam or column

ends. However, for the cases, which the equation overestimates the frame shear force, the column at the compression side of the SPSW is primarily under the effect of axial force and only a minor bending moment as indicated by the distribution of the vertical stress along the column section given in Figure 17(a). The increasing axial force and the plate-induced span loading causes in-span buckling of column and a hinge develops at around half height of the column. Due to this mechanism, the equilibrium of forces produces a small shear force on compression side columns. Therefore, the contribution of the VBEs to the total shear force decreases to a value, which is almost  $2M_p/h$ , primarily from the tension side column. Thus, if the ratio  $I_o/I_b$  is  $\approx 1$ , the expression  $4M_p/h$  given in Eq. (3) should be used as  $2M_p/h$ . Figure 17(b) presents the stress distribution on a model with  $I_o/I_b > 1$ . Tension and compression stresses at opposite flanges combine to form the bending moment acting on the section.

## 5. CONCLUSIONS

In this study, a total of 292 three-story steel plate shear wall systems are analyzed by using finite element method. The inelastic behavior of steel plate shear wall systems under monotonic loading are investigated. Limitations of preliminary design equations are determined on the basis of failure pattern, drift capacity and shear force distribution among panel and frame components of SPSWs on the FE models. The following main conclusions are derived from the parametric investigation.

- Seven different failure patterns are classified by evaluating the finite element analyses results and the relation of design parameters with these failure modes are evaluated. The failures related to column local instabilities (such as flange buckling or web twisting) is characterized with low drift ratio capacity and inefficient shear force distribution among frame and plate components of SPSW ( $V_p/V_i > 0.75$ ). In general, this behavior is observed when  $\omega_f > 2.2$ , and as the aspect ratio of wall becomes larger drift capacity reduces significantly. For such flexible systems ( $\omega_f > 2.2$  and  $L/h > 1.5$ ),  $I_o/I_b$  ratio should be greater than 2 for improving the performance of the SPSWs.
- A column flexibility factor of 2.2 is proposed as a limit value for satisfactory column performance, improved drift capacity and balanced strength distribution among frame and panel of SPSW. Below this value,  $L/h$  and  $I_o/I_b$  ratios play a key role on the failure mode of the SPSW. For  $\omega_f < 2$  and  $L/h$  and  $I_o/I_b$  ratios are higher than 1.5 and 3, respectively, models tend to experience a sudden failure due to top beam buckling without any softening behavior on the load-deformation curve. When  $L/h$  is smaller than 1.5 (narrow SPSW), but  $I_o/I_b$  ratio is still higher than 3, the top beam fails in shear mode. The best performance is obtained when  $\omega_f < 2.2$ ,  $L/h < 1.5$  and  $I_o/I_b < 2.5$ .
- When more compact beams (represented by small  $b_f/2t_f$  ratio) are used with strong columns (low  $\omega_f$ ) drift capacity increases. First three failure modes with the highest drift capacity, have the lowest average beam  $b_f/2t_f$  ratios.
- The axial load ratio is an important determining parameter in the formation of patterns. A structure without vertical load is far from reality and also leads to inadequate code-limit definitions as shown in this study. This parameter affects both the drift capacity of the structure and the stability of the column.

- The value of 0.75 for  $V_p/V_t$  ratio has emerged as a critical threshold value for the strength distribution among plate and frame. According to the results of this study, design of boundary frame according to twenty-five percent boundary frame resistance is found to be reasonable to obtain improved SPSW performance.
- Tension field inclination angle at yield varies between 42 degrees and 47 degrees for all 292 models. The 45 degree value is found to be an effective value to use for design purposes. A correction factor that increases the accuracy of predictions is introduced into traditional inclination angle formula.
- Infill plate-shear wall interaction is strongly dependent on the aspect ratio of the infill plate and column flexibility factor of the system. No strong correlations are found with regard to infill plate thickness and axial load. When the aspect ratio ( $L/h$ ) is smaller, infill plate shear force ratio to total shear force is lower. Greater column flexibility factor increases the percentage of shear force resisted by infill plate. An equation is proposed to estimate the ratio of the plate strength over total strength.
- When the column moment of inertia and beam moment of inertia ratio ( $I_c/I_b$ ) becomes close to 1, SPSW shear strength formula given by Eq. (3) overestimates the total shear strength of the system. This overestimation mainly originates from the plastic hinge mechanism, which is assumed to develop at beam or column ends. However, when beams and columns have equal stiffness columns are prone to develop in span hinges.

### **Symbols**

$A_b$	Beam cross sectional area
$A_c$	Column cross sectional area
$b_f$	Beam flange width
$h_b$	Beam depth
$h$	Infill plate height
$I_b$	Beam moment of inertia about the strong axis
$I_c$	Column moment of inertia about the strong axis
$I_{c,min}$	Minimum allowed moment of inertia of the column
$L$	Infill plate length
$M_{pb}$	Plastic moment capacity of the beam
$M_{pc}$	Plastic moment capacity of the column
$P_{cr}$	Nominal strength of the column
$t_f$	Beam flange thickness
$t_w$	Infill plate thickness
$V_d$	Shear force demand

$V_p$	Shear strength of the plate
$V_s$	Design shear strength
$V_t$	Total shear strengths of frame and infill plate
$\alpha$	Inclination angle
$\sigma_u$	Ultimate strength of the material
$\sigma_y$	Yield strength of the material
$\nu$	Poisson ratio
$\omega_i$	Column flexibility parameter
$\omega_L$	Flexibility parameter of top and bottom beams

### References

- [1] Dusak S, Yalçın C, Yelgin AN. Experimental investigation of using sandwich panels as infill plate in a steel plate shear wall. *Teknik Dergi/Technical Journal of Turkish Chamber of Civil Engineers* 2020;31:10413–39. <https://doi.org/10.18400/TEKDERG.559036>.
- [2] Li CH, Tsai KC. Experimental responses of four 2-story narrow steel plate shear walls. *Proceedings of 2008 Structural Congress*, vol. 314, Vancouver, Canada, 2008. [https://doi.org/10.1061/41016\(314\)101](https://doi.org/10.1061/41016(314)101).
- [3] Thorburn LJ, Montgomery CJ, Kulak GL. *Analysis of steel plate shear walls*. Edmonton, Canada, 1983.
- [4] Timler PA, Kulak GL. *Experimental Study of Steel Plate Shear Walls*, 1983. <https://doi.org/10.7939/R3C24QV49>.
- [5] AISC. *Seismic Provisions for Structural Steel Buildings*. ANSI/AISC 341 2016;16.
- [6] Sabelli R, Bruneau M. *Steel Plate Shear Walls (Steel Design Guide 20)*. American Institute of Steel Construction Inc, 2006.
- [7] Berman J, Bruneau M. Plastic analysis and design of steel plate shear walls. *Journal of Structural Engineering* 129:1448–56, 2003.
- [8] Wagner H. Flat sheet metal girder with very thin metal web: Part 1: General theories and assumptions. *National Advisory Committee for Aeronautics*, 1931.
- [9] Kuhn P, Peterson JP, Levin LR. *A summary of diagonal tension Part I: methods of analysis*, 1952.
- [10] Montgomery CJ, Medhekar M, Lubell AS, Prion HGL, Ventura CE, Rezai M. Unstiffened steel plate shear wall performance under cyclic loading. *Journal of Structural Engineering* 127:973–5, 2001. [https://doi.org/10.1061/\(ASCE\)0733-9445\(2001\)127:8\(973\)](https://doi.org/10.1061/(ASCE)0733-9445(2001)127:8(973)).



- [11] CAN CSA. CSA-S16-09 limit states design of steel structures. Rexdale, Canadian Standard Association, 2009.
- [12] AISC. Seismic Provisions for Structural Steel Buildings. Chicago, Illinois, 2005.
- [13] Purba R, Bruneau M. Seismic performance of steel plate shear walls considering two different design philosophies of infill plates. II: Assessment of collapse potential (2014 b). *Journal of Structural Engineering (United States)* 141:1–12, 2015. [https://doi.org/10.1061/\(ASCE\)ST.1943-541X.0001097](https://doi.org/10.1061/(ASCE)ST.1943-541X.0001097).
- [14] Berman JW. Seismic behavior of code designed steel plate shear walls. *Engineering Structures* 33:230–44, 2011. <https://doi.org/10.1016/j.engstruct.2010.10.015>.
- [15] Verma A, Sahoo DR. Estimation of lateral force contribution of boundary elements in steel plate shear wall systems. *Earthquake Engineering and Structural Dynamics* 46:1081–98, 2017. <https://doi.org/10.1002/eqe.2845>.
- [16] Hosseinzadeh SAA, Tehranizadeh M. Behavioral characteristics of code designed steel plate shear wall systems. *Journal of Constructional Steel Research* 99:72–84, 2014. <https://doi.org/10.1016/j.jcsr.2014.04.004>.
- [17] Uang CM, Bruneau M. State-of-the-Art Review on Seismic Design of Steel Structures. *Journal of Structural Engineering* 144, 2018. [https://doi.org/10.1061/\(ASCE\)ST.1943-541X.0001973](https://doi.org/10.1061/(ASCE)ST.1943-541X.0001973).
- [18] Qin Y, Lu JY, Huang LCX, Cao S. Flexural behavior of anchor horizontal boundary element in steel plate shear wall. *International Journal of Steel Structures* 17:1073–86, 2017. <https://doi.org/10.1007/s13296-017-9017-6>.
- [19] Dastfan M, Driver RG. Flexural stiffness limits for frame members of steel plate shear wall systems. *Proceeding, Annual Stability Conference*, p. 321–34, 2008.
- [20] Yu JG, Feng XT, Li B, Hao JP, Elamin A, Ge ML. Performance of steel plate shear walls with axially loaded vertical boundary elements. *Thin-Walled Structures* 125:152–63, 2018. <https://doi.org/10.1016/j.tws.2018.01.021>.
- [21] Curkovic I, Skejic D, Dzeba I. Impact of column flexural stiffness on behaviour of steel plate shear walls. *Ce/Papers* 1:3023–32, 2017. <https://doi.org/10.1002/cepa.354>.
- [22] Qu B, Guo X, Pollino M, Chi H. Effect of column stiffness on drift concentration in steel plate shear walls. *Journal of Constructional Steel Research* 83:105–16, 2013. <https://doi.org/10.1016/j.jcsr.2013.01.004>.
- [23] Qu B, Bruneau M. Behavior of vertical boundary elements in steel plate shear walls. *Engineering Journal* 47:109–22, 2010.
- [24] Sahoo DR, Sidhu BS, Kumar A. Behavior of unstiffened steel plate shear wall with simple beam-to-column connections and flexible boundary elements. *International Journal of Steel Structures* 15:75–87, 2015. <https://doi.org/10.1007/s13296-015-3005-5>.
- [25] Gholipour M, Alinia MM. Behavior of multi-story code-designed steel plate shear wall structures regarding bay width. *Journal of Constructional Steel Research* 122:40–56, 2016. <https://doi.org/10.1016/j.jcsr.2016.01.020>.

- [26] Matteis GDE, Formisano A, Mazzolani FM. Numerical analysis of slender steel shear panels for assessing design formulas. *International Journal of Structural Stability and Dynamics* 2007;7:273–94.
- [27] Kazaz İ, Gülkan P. Süneklik düzeyi yüksek betonarme perdelerdeki hasar sınırları. *Teknik Dergi/Technical Journal of Turkish Chamber of Civil Engineers* 23:6113–40, 2012. <https://doi.org/10.18400/td.74396>.
- [28] Lubell AS. Performance of unstiffened steel plate shear walls under cyclic quasi-static loading. University of British Columbia, 1997.
- [29] Wang M, Shi Y, Xu J, Yang W, Li Y. Experimental and numerical study of unstiffened steel plate shear wall structures. *Journal of Constructional Steel Research* 112:373–86, 2015. <https://doi.org/10.1016/j.jcsr.2015.05.002>.
- [30] Park H-G, Kwack J-H, Jeon S-W, Kim W-K, Choi I-R. Framed steel plate wall behavior under cyclic lateral loading. *Journal of Structural Engineering* 133:378–88, 2007. [https://doi.org/10.1061/\(asce\)0733-9445\(2007\)133:3\(378\)](https://doi.org/10.1061/(asce)0733-9445(2007)133:3(378)).
- [31] Choi IR, Park HG. Ductility and energy dissipation capacity of shear-dominated steel plate walls. *Journal of Structural Engineering* 134:1495–507, 2008. [https://doi.org/10.1061/\(ASCE\)0733-9445\(2008\)134:9\(1495\)](https://doi.org/10.1061/(ASCE)0733-9445(2008)134:9(1495)).
- [32] ANSYS. ANSYS Mechanical APDL. © ANSYS, Inc 2011:www.ansys.com. <https://doi.org/www.ansys.com>.

# **Evaluation of Occupational Safety in the Operation and Maintenance Activities of Dams**

**Özge AKBOĞA KALE<sup>1</sup>**  
**Ömer Levend AŞIKOĞLU<sup>2</sup>**  
**Selim BARADAN<sup>3</sup>**

## **ABSTRACT**

The accidents occurred during the operation/maintenance activities of US dams between 1984-2018 were analyzed from the OSHA database and 88 cases were selected. The objective of our study is to identify and investigate potential hazards and risk sources responsible for and affecting OHS performance in the operation/maintenance activities. Furthermore, the factors responsible for injuries and fatalities happened during these activities are determined. It is found out that 5.2% of precaution negligence was related to the facility and wrong design and poor maintenance were the main negligence factors. The important point to be noted is that these negligence factors result in fatal accidents, albeit few. The results also show that machine safeguarding was not available or provided in most of the cases and 12.7% of those who had occupational accidents did not use appropriate PPE or did not use PPE at all.

**Keywords:** Construction Safety, Accident Cause, Operation and Maintenance, Dams

## **1. INTRODUCTION**

The construction industry is one of the most hazardous industries in the world because of its diverse and complex nature [1-7]. Moreover, the construction industry ranks higher in fatal occupational injuries than any other sector due to the nature of work [8-12]. So, it mandates that the activities of construction industry have to be studied and further analyzed for reducing accident rates. However, to achieve more efficient results in terms of occupational safety, it is necessary to examine the construction sector which is an integral component of diverse sectors for growth and development. In this study the construction sector is studied by categorizing it based on the end-use of the project such as residential, industrial,

---

Note:

- This paper was received on December 14, 2021 and accepted for publication by the Editorial Board on July 22, 2022.
- Discussions on this paper will be accepted by November 30, 2022.
- <https://doi.org/10.18400/tekderg.1036732>

1 İzmir Demokrasi University, Department of Civil Engineering, Izmir, Turkey  
ozge.akbogakale@idu.edu.tr - <https://orcid.org/0000-0002-3848-0578>

2 Ege University, Department of Civil Engineering, Izmir, Turkey  
omer.asikoglu@ege.edu.tr - <https://orcid.org/0000-0002-2981-5903>

3 Ege University, Department of Civil Engineering, Izmir, Turkey  
selim.baradan@ege.edu.tr - <https://orcid.org/0000-0002-9172-8552>

infrastructure, and road or dam construction. Since the construction processes of diverse sectors are different from each other, these construction branches should be examined separately.

Dams, which are one of the most fundamental infrastructures required by any country, have provided many benefits for human survival and have been utilized thousands of years by mankind [13]. Additionally, dams provide a wide range of economic, environmental, and social benefits, including recreation, flood control, water supply, hydroelectric power, waste management, river navigation, and wildlife habitat [14]. So, dam constructions are done in all ages of mankind, and it is a necessity for humans to survive. According to estimates, over \$2 trillion was spent on constructing dams around the world in the 20th century [13]. In addition, most of the dam construction potential has been realized, especially in developed countries (Table 1). Apart from the potential hazards and risks that may arise during dam construction, there are specific risks in terms of occupational safety when the operation and maintenance activities are performed in existing dams, reservoirs, and auxiliary facilities.

There are literatures on “dam safety” that address the problems when demolishing of a dam and/or seek solutions to prevent it [15-19]. However, unfortunately there is almost no literature that deals with the occupational health and safety (OHS) problems in dam constructions. This issue is reflected in the ICOLD bulletin 73 (1989) as “in the majority of dam sites, the risk of fatal accident risk for workers during the construction is higher than the risk of dam break failure” [20].

Based on the various studies [21-24], it is concluded that rate of severe accidents and fatal accidents that occur in dam construction very high and alarming when compared to other construction sites. Hussien et al. (2020) revealed that the annual occupational injury prevalence of the dam construction site was 57.8% [25]. Further, Yılmaz and Başağa (2018) also stated that dam constructions are the second most hazardous construction site where accidents occur at a rate of 19.6% [23]. It is noted that existing research on the subject only focuses more on surveys or observation studies [25-31]. Although it is useful to conduct surveys and use descriptive statistics, using information, such as how the accident occurred and who was involved is not always sufficient to identify the most important contributing factors.

Therefore, analyzing past accident reports to support findings from surveys could be invaluable in accident causation studies. The databases created on the subject were not enough and the work accidents that occurred in the dam sites were not analyzed statistically before. Besides, accidents occur not only during the construction phase but also during operation and maintenance activities of dams. Developed countries have completed constructions of large dams long back, but the operation and maintenance of these dams is continuing and will continue for decades. Nowadays accidents occur during the operation and maintenance activities rather than in construction activities in developed countries. While there are very few studies in the field of OHS in dam construction, there is no study focusing on OHS during the operation and maintenance activities.

The aim of this study is (1) to identify the risk sources that have potential hazards and influence OHS performance, (2) to find the factors responsible for the injuries and fatalities occurred during operation and maintenance activities of dams, reservoirs, and dam auxiliary facilities, and (3) to investigate the frequency distributions of these factors. Subsequently,

these findings will provide guidelines and further necessary safety measures to be adapted to preventing future accidents. Further, it is expected that the findings of the study will guide the employees responsible for operation and maintenance works, guide the occupational safety departments of the dam sites, inform the occupational safety experts about the industry and inspire the researchers.

*Table 1 - Number of dams in the topmost 25 countries*

	<b>Country</b>	<b>ICOLD World Register of Dams 2020</b>	<b>Percentage of total dams (%)</b>
1	China	23841	41.7
2	United States of America	9263	16.2
3	India	4408	7.7
4	Japan	3130	5.5
5	Brazil	1365	2.4
6	Korea (Rep. of)	1338	2.3
7	Canada	1150	2.0
8	South Africa	1116	2.0
9	Spain	1064	1.9
10	Turkey	973	1.7
11	France	706	1.2
12	Iran	594	1.0
13	United Kingdom	580	1.0
14	Australia	567	1.0
15	Mexico	543	0.9
16	Italy	541	0.9
17	Germany	371	0.6
18	Norway	347	0.6
19	Albania	308	0.5
20	Zimbabwe	256	0.4
21	Romania	241	0.4
22	Portugal	234	0.4
23	Austria	232	0.4
24	Thailand	220	0.4
25	Sweden	190	0.3
	Others	3621	6.3
	<b>Total</b>	<b>57199</b>	<b>100.0</b>

## **2. THE OPERATION AND MAINTENANCE ACTIVITIES OF DAMS WITH COMMON POTENTIAL HAZARDS**

The operation and maintenance (if necessary, repair) activities of dams is significantly important for efficient operation of a dam and utilities to function effectively throughout their economic life. To evaluate the operation and maintenance of dams, reservoirs, and auxiliary facilities in terms of occupational safety, the various parts of a dam should be considered. While the controls and inspections of these parts are carried out within the scope of the operation and maintenance activities, the topics that need to be evaluated are summarized and presented in the flowchart (Figure 1).

The operation, surveillance, maintenance, and if necessary repair processes can be carried out by automation and require the presence of personnel at the dam site. Moreover, the risk potential for work accidents is higher in maintenance and repair activities since the activities require people to be available and work on sites.

Workers may be exposed to dangers such as collapses, cave-ins, toxic or suffocating gas emissions, gas explosions, dust explosions, component falls, electrocution, and floods. Apart from that, many heavy equipment works simultaneously in dam construction areas may pose problems. The utilization of heavy equipment such as excavator, loader, dump trucks, scrapers and so on comprised of great portion of construction operations in dam projects. Moreover, numerous workers are also present in these areas. Working on or around heavy equipment is high-risk work. If an incident occurs, the result is often a life-altering injury such as a broken bone, head injury, or, in many cases, loss of life. Incidents involving heavy equipment deeply affect not only the person who is injured but also the person operating the equipment or any co-workers nearby [32]. The work environment, which is complicated by the nature of the work, causes various accidents. Heavy equipment striking or slamming pedestrians are the prominent types of accidents. Further, noisy working environment prevents the vehicle sensors from being heard by the workers which result in accidents [24].

## **3. METHODS**

### **3.1. Data Acquisition**

The study specifically focuses on the operation and maintenance of dams, reservoirs, and auxiliary facilities. Because of this reason, data mining should be done to the database consisting of retrospective and comprehensive accident reports. The OSHA report database contains all research details and is very suitable for academic studies. Moreover, there are more than 90,000 dams in the United States according to the American Society of Civil Engineers (Figure 2) spread across the country [33]. OSHA accident reports were selected, because of all these reasons, to examine the accidents that occurred during the operation and maintenance activities of the dams, which are still functioning effectively in the United States.

#### Sluiceway

- In the tunnel-conduit structures examination,
  - Leakage, moisture or deterioration in the concrete and tunnel structures.
  - A problem in tunnel ventilation system, lighting equipment and discharge structures.
- In the penstock examination,
  - The pipe is observed for corrosion and / or leakage.
  - Material thickness measurements and paint thickness measurements are evaluated by comparing the values in the project / instructions.
- In the control of the valves,
  - Regulation (or intake) valve and discharge valve,
  - The operation of the control mechanism and The leakage of the valves.

#### Spillway

- The gate lifting device,
- Rust on the lifting device and gates and a need for paint.
- Change in downstream conditions.
- The deterioration of the approach channel concrete,
  - discharge channel concrete,
  - threshold structure concrete,
  - energy breaker concrete and stone supports
- Stability check for the slopes.

#### Dam Body

- A warning sign at the dam entrance and a warning sign in the crest
- Lighting on the crest,
- Any deformation or slump on the crest and any slope instability,
- Excessive leakage in the foundation of the dam,
- Trees, shrubs, grass in upstream and downstream and rip-rap deterioration,
- Any destructive condition in injection and drainage galleries, and
- Any crack in the dam concrete-face,

#### Reservoir Area

- Warning sign,
- Planting or settlement,
- The presence of a guard,
- The availability and functionality of a camera system,
- Gauge and its functionality,
- Limnigraph and its functionality

#### Power Plant

- Inspection of intake area, impounding structures, pipeline, sluice(s).
- Turbine functional checks and inspection.
- Drive belt and drive coupling inspection.
- Gearbox oil condition and bearing inspection.
- Generator inspection.
- Hydraulic system inspection and controller functions check.

Figure 1 - The operation and maintenance activities.

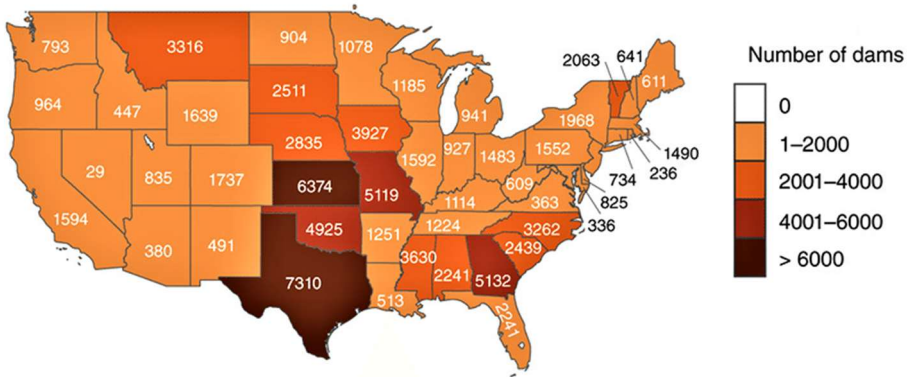


Figure 2 - Distribution of dams in the contiguous US [34].

Further, it should be noted that the Standard Industrial Classification System (SIC), a system for classifying industries by a four-digit code, was used as a limitation of data mining [35]. SIC codes related to construction within the scope of the study were used. Accidents occurring during operation and maintenance works of dams, reservoirs and auxiliary facilities were selected. Extensive elimination of accident cases was performed to achieve accurate and reliable data that is free from bias. Finally, 88 cases were remained that resulted in injuries and fatalities and they were used to create the database of accidents in operation and maintenance works of dams, reservoirs, and auxiliary facilities from 1984 to 2017.

### 3.2. Causes of Accidents in Operation and Maintenance of Dams, Reservoirs, and Auxiliary Facilities

It is observed that operation and maintenance activities often carried out by employees in areas which are not familiar to them. Even if they do not know the conditions very well or are familiar with environmental conditions, they work in areas where they do not pay much attention to the environmental conditions as their intention is to finish the job as soon as possible. Therefore, statistics and experience show that a large majority of accidents occur during the execution of corrective maintenance activities [36].

All tools, equipment, machinery, and installations need maintenance and repair periodically. Once the dam construction has been completed, regular inspections and maintenance are required to keep it in proper and efficient operating condition. Operation and maintenance activities contain some potential hazards, which necessitate the importance of proper safety and accident prevention throughout this process. According to Karimi et al. (2019) poor maintenance management (25%) tops the ranking of underlying causes of accidents [28]. Fatihkuşan (2011) indicated that 10%–15% of fatal accidents occur in maintenance and repair activities based on EUROSTAT statistics [37]. In European countries, between 10% and 20% of all work accidents and between 10% and 15% of all fatal work accidents can be attributed to maintenance operations [38].



The database used in this study classifies the injuries into fatal and nonfatal. When the accidents occurring in dam maintenance and repair works are investigated, it is found that 68.2% of these accidents result in loss of life (Table 2). Accident characteristics variables (nature of injury, type of injury) reveal plenty of information regarding the incident and injury; in other words, they describe the accident. Therefore, examination of these variables may give important information in learning the root causes of the accident. When the “type of injury” variable was examined, it is found that “drowning” and “falling from height” were the prime causes of accidents with data showing 34.1% and 14.8% frequencies, respectively. According to Hussen et al. (2020) falling from height is the most common type of injury in dam construction [25]. It is also observed from the studies that asphyxia (29.5%) and fractures (13.6%) were the most encountered injuries.

Table 2 - Distribution of accidents characteristics

Variables	Categories	Frequency	Percent	Cumulative Percent	
Degree of injury	Fatality	60	68.2	68.2	
	Hospitalized injury	28	31.8	100.0	
Nature of Injury	Asphyxia	26	29.5	29.5	
	Fractures	12	13.6	43.1	
	Bruises/Contusions/Abrasions	4	4.5	47.6	
	Electrical shock	4	4.5	52.1	
	Cuts/Lacerations	3	3.4	55.5	
	Burn/Scald (heat)	3	3.4	58.9	
	Sprain/Strain	2	2.3	61.3	
	Dislocation	2	2.3	63.5	
	Concussion	1	1.1	64.6	
	Amputation	1	1.1	65.8	
	Other	30	34.1	100.0	
	Type of Injury	Drown	30	34.1	34.1
		Fall from height	13	14.8	48.9
Struck by falling object /projectile		11	12.5	61.4	
High pressure		8	9.1	70.5	
Caught between		7	8.0	78.5	
Electric shock, other and unknown cause		5	5.7	84.2	
Asphyxiation/Inhalation of toxic vapor		3	3.4	87.6	
Traffic accident		3	3.4	91.0	
Wall collapse		2	2.3	93.3	
Slip		1	1.1	94.3	
Other	5	5.7	100.0		

It is found that most victims were operators (13.6%) or special trade construction (8.0%) based on the results. But the occupation of 39.8% of the victims was not reported in the data. Further, it can be observed in Table 3 that people working in the dam site for operation and maintenance show a wide variety of professional fields. It is very important to note that more than half of the workers involved in work-related accidents were non-union workers (54.5%) (Table 3). This shows us an indication that workers who were not members of union were more likely to have accidents or injuries due to lack of safety training [39].

*Table 3 - Distribution of worker characteristics*

Variables	Categories	Frequency	Percent	Cumulative Percent
Occupation	Occupation not reported	35	39.8	39.8
	Operators	12	13.6	53.4
	Construction trades	7	8.0	61.4
	Electrical power installers and repairers	7	8.0	69.3
	Construction laborer	6	6.8	76.1
	Labors except construction	6	6.8	83.0
	Structural metal workers	2	2.3	85.2
	Plumbers, pipefitters, and steamfitters	2	2.3	87.5
	Farm worker	2	2.3	89.8
	Timber cutting and logging occupations	2	2.3	92.0
	Welders and cutters	1	1.1	93.2
	Carpenter	1	1.1	94.3
	Supervisors, brick masons, stonemasons, tile setters	1	1.1	95.5
	Painters, construction, and maintenance	1	1.1	96.6
	Firefighting occupations	1	1.1	97.7
	Forestry workers except logging	1	1.1	98.9
	Guards and police excluding public service	1	1.1	100.0
Union	Union	40	45.5	45.5
Status	Non-union	48	54.5	100.0
Ownership	Private	68	77.3	77.3
	Local Government	20	22.7	100.0

Initial violations and penalties of the selected cases are also presented to emphasize post-accidental responsibilities of the companies. Totally 165 violations were seen in four main categories, namely, serious, wilful, repeat, and other. Serious category could be assigned

when companies had the potential to foresee a risk but did not protect or poorly protected the workers. When examined the data set, it is observed that serious violation has the highest frequency. The companies getting penalties in the serious category will be summoned most frequently by the OSHA and carry the highest fees [40]. Further, wilful violations include an intentional violation of OSHA rules by the employer or blatantly/deliberately disregard of the safety rules will result in highest penalties. Violations in the repeat category associated to a condition in which an OSHA regulation was infringed, and a company has been issued a citation within the last 3 years (unless that citation is currently under appeal). Fortunately, repeat violations are in the minority in the created data set which might be a sign of improved safety rules of the companies (Figure 3).

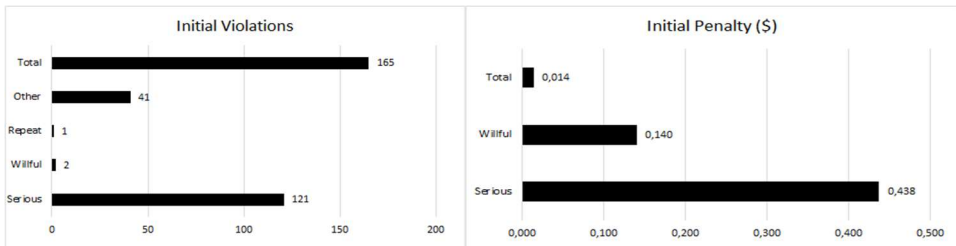


Figure 3 - Initial violation and penalty (\$M\$) summaries of selected cases.

#### 4. RESULTS AND DISCUSSION

As mentioned above, 88 work-related injury cases that occurred in operation and maintenance of dams, reservoirs and auxiliary facilities were selected and focused by our studies. Further, the database used in this study has classified the injuries into nonfatal and fatal. The causes of accidents were investigated by categorizing them into four major groups (Table 4).

In the first group, the evaluation was done based on the facility. Based on the results, it is found out that 5.2% of precaution negligence was related to the facility and wrong design and poor maintenance were the main negligence factors. To give an example of this negligence; “Employee #1 and coworkers were building a work platform made of dirt and held in place by a retaining wall next to the Buffalo Bill Dam. Employee #1 was operating a D Caterpillar when the wall and fill failed, causing him and the Caterpillar to fall into the reservoir. Employee #1 drowned.” Güranlı also mentioned that, almost 60% of fatal accidents are related to design decisions made before the work starts [41]. As a matter of fact, it has been stated that the designers' consideration of occupational safety during the planning and design phases of projects will greatly contribute to ensuring construction safety. It is ensured that the field decisions that contractors and builders must take during the implementation phase and that may lead to accidents are prevented on the project [42]. Each building construction project is different and unique, in addition to standard training, informing about the project by the designers ensures that the risks are reduced [43]. The important point to be noted is that these negligence factors result in fatal accidents, albeit few in number (Table 5).

Table 4 - Distribution of accident causes

Cause of accident	Precaution negligence	Number of accidents	Total number of accidents	%
Facility	Wrong design	5	13	5.2
	Poor maintenance	8		
Machine Safeguarding	Not available	17	19	7.6
	Not appropriate	1		
Personal Protective Equipment	Defective	1	32	12.7
	Not available	18		
	Not appropriate	6		
Training, Supervision, Surveillance	Not used	8	187	74.5
	Inadequate protection measure	44		
	Violate the rules	42		
	Poor inspection	41		
	Improper working method	40		
	Inadequate training	20		

Table 5 - Relationship of precaution negligence of facility and degree of injury

		Facility		
			Wrong design	Poor maintenance
Degree of Injury (DOI)	Fatal	Count	4	7
		% within DOI	80.0%	87.5%
	Nonfatal	Count	1	1
		% within DOI	20.0%	12.5%
Total	Count	5	8	

Machine guarding is a barrier basically guarding or protecting moving parts of the machines that are the most dangerous as well as prevent the workers from getting physical contact with the machines. Table 4 demonstrates the usage of machine safeguards. Investigations revealed that machine safeguarding was not available in most of the cases. In addition, it is found that accidents have occurred in cases where the machine safeguarding was not appropriate, as well as defective, which resulted in loss of life (Table 6). OSHA also, specifically states that machinery workers sustain 18,000 injuries and 800 deaths every year. While injuries can occur from machines in different ways, one of the most common ways is lack of guarding [44].

Table 6 - Relationship of machine safeguarding and degree of injury

		Machine safeguarding			
		Not available	Not appropriate	Defective	
Degree of Injury (DOI)	Fatal	Count	9	1	1
		% within DOI	52.9	100.0	100.0
	Nonfatal	Count	8	-	-
		% within DOI	47.1	-	-
Total	Count	17	1	1	

Tragically, in this study, it is determined that 12.7% of those who had occupational accidents did not use appropriate personal protective equipment (PPE) or did not use PPE at all. The noteworthy finding is that all victims using inappropriate PPE have died (Table 7). According to the last Bureau of Labor Statistics report on Personal Protective Equipment revealed that when a worker was injured, they were not using PPE in most cases [45]. Among the workers who sustained head injuries, 84% of them were not wearing hard hats, and 99% of workers who suffered facial injuries were not using face protection devices [45]. In United Kingdom, the data show that around 9,000 accidents related to PPE are reported to the health and safety executive every year. This data is similar to construction industry, which has the largest number of fatal accidents and one of the highest fatal injury rates and it proves how important it is to use correct PPE [46].

Table 7 - Relationship of PPE and degree of injury

		Personal Protective Equipment			
		Not available	Not appropriate	Defective	
Degree of Injury (DOI)	Fatal	Count	7	6	3
		% within DOI	38.9	100.0	37.5
	Nonfatal	Count	11	-	5
		% within DOI	61.1	-	62.5
Total	Count	18	6	8	

The results of the investigations show that workers who worked with inadequate protection measures had the most number of injuries. Moreover, it has been determined that violation of the rules, poor inspection and improper working methods lead to accidents. If safety and health training is provided, then it may act as a tool in reducing injury severity [47]. However,

it was found that training was inadequate in the accidents examined (Table 8). To prevent future accidents the following steps must be undertaken to reduce the accidents: the registration system should be installed, the maintenance should be done by the experts, the personnel and the protectors should be inspected effectively, and the advice of the machine builders should be paid attention. Furthermore, maintenance, repair, and control instructions should be prepared for each machine and facility and should be adhered strictly.

*Table 8 - Relationship of Training, Supervision, Surveillance, and degree of injury.*

		Training, supervision, surveillance					Inadequate training
		Inadequate protection measure	Violate the rules	Poor inspection	Improper working method		
Degree of Injury (DOI)	Fatal	Count	29	31	28	25	15
		% within DOI	65.9	73.8	68.3	6.5	75.0
	Nonfatal	Count	15	11	13	15	5
		% within DOI	34.1	26.2	31.7	37.5	25.0
Total	Count	44	42	41	40	20	

## 5. CONCLUSIONS

In this study, the accidents occurred during the operation/maintenance activities of US dams between 1984-2018 were analyzed from the OSHA database and 88 cases were selected and classified.

This study investigated the risks that may arise in operation and maintenance works and the causes of accidents in dams, reservoirs and auxiliary facilities and further examined the precautions to be taken against these risks. Eighty-eight accidents were selected from the larger database of OSHA since they fulfilled the requirements to perform the statistical analyses.

The precautions to be taken to prevent future accidents according to the distribution of accident causes are summarized below.

- Operation and maintenance works should not be rushed and should be done in a planned manner.
- Permits should be obtained from the competent authorities, and the permitting authorities should make the necessary checks. A proper inspection and auto control mechanism should be established and maintained.
- Operation and maintenance should be done by experts or expert teams. Adequate training should be provided to the maintenance team on the principles of machine protection, electrical and mechanical safety, operating permits for maintenance work.

- Any machine part, function, or process that might cause injury must be safeguarded. If the operation of a machine or accidental contact with it could injure the operator or others in the vicinity, the hazards must be either controlled or eliminated.
- Various situations or malfunctions during normal operation at machine benches and facilities should be recorded, and these records should be used during major revision and maintenance works.

Limitations of this study include the occurrence on OSHA accident reports, unavailability of data before 1984, unfilled information categories especially in older accident reports, and inadequacy of employment data solely of dam companies.

Further research efforts could consider performing comparative studies between dam construction/maintenance work and other construction/maintenance sectors. The study presented here focused mostly on identifying risks and hazards that dam workers are exposed to on job sites. It was observed that accidents such as drowning, which are unlikely to happen on other construction sites, could be encountered more frequently on dam construction / maintenance activities. If there is adequate additional data, the findings of this study could be helpful in a future study that analyzes and discuss whether dam maintenance/construction is any different from other construction work.

Operation and maintenance workers also experience various risks that may cause occupational diseases such as noise (hearing loss), dust (respiratory system diseases), and ergonomics (musculoskeletal system disorders). However, note that our study does not cover occupational diseases. In future studies, the subject can also be investigated from this aspect.

### References

- [1] Khosravi, Y., Asilian-Mahabadi, H., Hajizadeh, E., Hassanzadeh-Rangi, N., Bastani, H., Behzadan, A.H. Factors influencing unsafe behaviors and accidents on construction sites: A review. *International Journal of Occupational Safety and Ergonomics*, 20(1), 111-125, 2014.
- [2] Im, H.J., Kwon, Y.J., Kim, S.G., Kim, Y.K., Ju, Y.S., Lee, H.P. The characteristics of fatal occupational injuries in Korea's construction industry, 1997–2004. *Safety Science*. 47(8), 1159-1162, 2009.
- [3] Cameron, I., Hare, B., Davies, R. Fatal and major construction accidents: a comparison between Scotland and the rest of Great Britain. *Safety Science*, 46(4), 692-708, 2008.
- [4] Arquillos, A.L., Romero, J.C.R., Gibb, A. Analysis of construction accidents in Spain, 2003-2008. *Journal of Safety Research*, 43(5-6), 381-388, 2012.
- [5] Chong, H.Y., Low, T.S. Accidents in Malaysian construction industry: statistical data and court cases. *International Journal of Occupational Safety and Ergonomics*, 20(3), 503-513, 2002.
- [6] Jannadi, O.A., Bu-Khamsin, M.S. Safety factors considered by industrial contractors in Saudi Arabia. *Building and Environment*, 37(5), 539-547, 2002.

- [7] Tözer, K.D., Çelik, T., Gürcanlı, G.E. Classification of Construction Accidents in Northern Cyprus. *Teknik Dergi*, 29 (2), 8295-8316, 2018.
- [8] Hallowell, M.R. Safety-knowledge management in American construction organizations. *Journal of Management in Engineering*, 28(2), 203-211, 2012.
- [9] Ore, T., Stout, N. Traumatic occupational fatalities in the US and Australian construction industries. *American Journal of Industrial Medicine*, 30(2), 202-206, 1996.
- [10] Kazar, G., Çomu, S. Developing a Virtual Safety Training Tool for Scaffolding and Formwork Activities. *Teknik Dergi*, 33(2), 11729-11748, 2022.
- [11] Akboğa Kale, Ö., Baradan, S. Identifying Factors that Contribute to Severity of Construction Injuries using Logistic Regression Model. *Teknik Dergi*, 31 (2), 9919-9940, 2020.
- [12] Larsson, T.J., Field, B. The distribution of occupational injuries risks in the Victorian construction industry. *Safety Science* 40(5), 439-456, 2002.
- [13] MIT. Dams and reservoirs. <http://12.000.scripts.mit.edu/mission2017/dams-and-reservoirs/> Accessed July 22, 2020.
- [14] FEMA. Benefits of dams. <https://www.fema.gov/benefits-dams> Accessed July 22, 2020.
- [15] Froehlich, D.C. Predicting peak discharge from gradually breached embankment dam. *Journal of Hydrologic Engineering*, 21(11), 2016.
- [16] Pisaniello, J. D., Dam, T.T., Tingey-Holyaok, J.L. International small dam safety assurance policy benchmarks to avoid dam failure flood disasters in developing countries. *Journal of Hydrology*, 531(3), 1141-1153, 2015.
- [17] Dam, T.T., Burritt, R.L., Pisaniello, J. D. Adequacy of policy and practices for small agricultural dam safety accountability and assurance in Vietnam. *Agricultural Water Management*, 112, 63-74, 2012.
- [18] Zhang, L.M., Xu, Y., Jia, K.S. Analysis of earth dam failures: A database approach. *Georisk*, 3(3), 184–189, 2009.
- [19] Alcrudo, F., Mulet, J. Description of the Tous Dam break case study (Spain). *Journal of Hydraulic Research*, 45(1), 45-58, 2007.
- [20] Hydrocoop. 2013. Dam Construction Sites Accident Prevention. ICOLD Bulletin 80, <http://www.hydrocoop.org/dam-construction-sites-accident-prevention/> Accessed August 9, 2020.
- [21] Rico, M., Benito, G., Salgueiro, A.R., Diez-Herrero, A., Pereira, H.G. Reported tailings dam failures. A review of the European incidents in the worldwide context. *Journal of Hazardous Materials*, 152(2), 846-852, 2008.
- [22] Yunfeng, Y.E., Zhang, S., Jiaming, R.A., Haiqing, W.A., Yang, L.I., Shengyong, W.A., Xiaomei, D.O. Analysis of national major work safety accidents in China, 2003-2012. *Iranian Journal of Public Health*, 45(1), 6-13, 2016.



- [23] Yılmaz, G.K., Başağa, H.B. Assessment of occupational accidents in construction sector: A case study in Turkey. *Journal of Construction Engineering, Management & Innovation*, 1(2), 95-107, 2018.
- [24] Aşıkoglu, O.L., Akboğa Kale., O. Occupational health and safety in dam construction sites. *International Journal of Modern Engineering Research*, 7(8), 57-60, 2017.
- [25] Hussen, J., Dagne, H., Yenealem, D.G. Factors associated with occupational injury among hydropower dam construction workers, South East Ethiopia, 2018. *BioMed Research International*, Article ID 6152612, 2020.
- [26] Wardahni, N.I., Latief, Y., Machfudiyanto, R.A. Development of safety plan to improve OHS (occupational health and safety) performance for construction of dam (supporting infrastructure) based on WBS (work breakdown structure). *IOP Conference Series: Earth and Environmental Science*, 426(1), 012017, 2020.
- [27] Acakpovi, A., Dzamikumah, L. An investigation of health and safety measures in a hydroelectric power plant. *Safety and Health at Work*, 7(4), 331-339, 2016.
- [28] Karimi, S., Jafari, H., Anbardan, S.A., Esfahani, Z.K. Analysis of the amputation-leading accidents during a mechanical excavator repair using the tripod beta and SCAT combined method in a dam construction project. *Journal of Occupational Hygiene Engineering*, 6(3), 9-19, 2019.
- [29] Maleki, A., Darvishi E., Moradi, A. Safety culture assessment and its relationship with the accidents in a dam construction project. *Journal of Health and Safety at Work*, 4(4), 59-68, 2015.
- [30] Colvin, M., Dalvie, A., Myers, J.E., Macun, I.A., Sharp B. Health and safety in the Lesotho Highlands Dam and tunnel construction program. *International Journal of Occupational and Environmental Health*, 4(4), 231-235, 1998.
- [31] Yuksel, I., Kurt, M., Dizdar, E.N. The analysis of labour accident in the construction of Atatürk dam and hydroelectric power station. *Teknoloji*, (3)4, 105-111, 2002.
- [32] Ihsa.ca. Infrastructure Health & Safety Association. Struck-By Incidents and Heavy Equipment. 2018.
- [33] ASCE - American Society of Civil Engineers. 2019. Policy Statement 280 - Dam Safety, Repair, Retrofit, And Rehabilitation. <https://www.asce.org/issues-and-advocacy/public-policy/policy-statement-280---dam-safety,-repair,-retrofit,-and-rehabilitation/> Accessed: August 12, 2020.
- [34] Ryan, B.J., Duda, J.J., Craig, L.S., Greene, S.L., Torgersen, C.E., Collins, M.J., Vittum, K. Status and trends of dam removal research in the United States. *Wiley Interdisciplinary Reviews: Water*, 4(2), 1-13, 2016.
- [35] OSHA (Occupational Safety and Health Administration) 2017. Standard Industrial Classification (SIC) System Search. [https://www.osha.gov/tutorials/sic\\_help.html](https://www.osha.gov/tutorials/sic_help.html) Accessed July 22, 2020.

- [36] Antonov, A.E., Buica, G., Beiu, C. Management and Control of Occupational Risk Related To Maintenance Activities Of Work Equipment In Companies By Using Software Tools. *Environmental Engineering and Management Journal*, 13(6), 1361-164, 2014.
- [37] Fatihkuşan, M. 2011. Bakım Onarım Hizmetlerinin Türk Mevzuatındaki Yeri. (In Turkish). [https://www.mess.org.tr/media/filer\\_public/e3/70/e3701b6b-a606-4f77-b123-d30f91d8e735/fatih\\_usan\\_uyumluluk\\_modu.pdf](https://www.mess.org.tr/media/filer_public/e3/70/e3701b6b-a606-4f77-b123-d30f91d8e735/fatih_usan_uyumluluk_modu.pdf) Accessed August 17, 2020.
- [38] EU-OSHA. 2010. Factsheet 90-Maintenance and OSH – A Statistical Picture. [http://osha.europa.eu/en/publications/factsheets/en\\_90.pdf/view](http://osha.europa.eu/en/publications/factsheets/en_90.pdf/view) Accessed August 12, 2021.
- [39] Lew, J., Abraham, D., Wirahadikusumah, R., Irizarry, J., Arboleda, C. 2002. Excavation and trenching safety: existing standards and challenges. <https://engineering.purdue.edu/CSA/publications/trenching02> Accessed August 12, 2020.
- [40] Eskişar, T., Akboğa Kale, Ö. Evaluation of pile driving accidents in geotechnical engineering. *International Journal of Occupational Safety and Ergonomics*. <https://doi.org/10.1080/10803548.2019.1685195>. 2020.
- [41] Gürcanlı, G.E. Yeni ve Zorunlu Bir Kavram Olarak “İş Güvenliği İçin Tasarım”. 3. İşçi Sağlığı ve İş Güvenliği Sempozyumu, 21-23 October 2011, Çanakkale.
- [42] Kurt, M., İ. İnşaat Sektöründe Proje Aşamasında Koruyucu ve Önleyici İş Sağlığı ve Güvenliği Uygulamalarının Değerlendirilmesi. *Uzmanlık Araştırması. Çalışma ve Sosyal Güvenlik Bakanlığı İş Sağlığı ve Güvenliği Genel Müdürlüğü, Ankara, 2012.*
- [43] Gambatese, J. Addressing Construction Worker Safety in the Design Phase Designing for Construction Worker Safety. *Automation in Construction*, 643-649, 1999.
- [44] Safety Company. 2017, What is Machine Safeguarding and Why it is important?. <https://www.safetycompany.com/safetyblog/what-is-machine-guarding-and-why-is-it-important/> Accessed: August 9, 2020.
- [45] Kluksdahl, A. Personal Protective Equipment: Be Safe not Sorry, <https://n-o-v-a.com/blog/personal-protective-equipment-safe-not-sorry/> Accessed August 10, 2020.
- [46] HSE - Health and Safety Executive. 2006. Evidence base for identifying potential failures in the specification, use and maintenance of PPE at work, Research Report 419. <https://injury-lawyersuk.com/blog/personal-protective-equipment-facts-and-statistics/> Accessed August 9, 2020.
- [47] Bilir, S., Gürcanlı, G.E. A method for determination of accident probability in construction industry. *Teknik Dergi*, 29(4), 8537-8561, 2018.

***TECHNICAL NOTE***



# Effect of Blasting During Tunnel Excavation on an Existing Adjacent Tunnel

Van Kien DANG<sup>1</sup>  
Trong Hung VO<sup>2</sup>

## ABSTRACT

In recent decades, the effects of blast loads on existing structures have gained considerable attention due to the increase in threat from various activities. Site-specific empirical relationships for calculation of blast-induced vibration parameters like Peak Particle Velocity (PPV), Peak Particle Acceleration (PPA), and Peak Particle Displacement (PPD) are commonly used for the estimation of the impact of blasting vibration on an existing adjacent tunnel. However, these relationships are not able to consider the variation in rock parameters and uncertainty of in situ conditions such as modern rock mass classifications (i.e., RMR, Q-system, RQD). In this paper, a published blast data of various researchers in different rock sites at Croix-Rousse tunnel in France have been collected and used to propose a generalized regression model for PPV by considering the effects of rock parameters like Rock Mass Rating (RMR) system, damping ratio “ $\xi$ ”, Dynamic Young’s modulus “ $E_d$ ”. By using the numerical analysis method, the proposed regression model of PPV (Empirical Formula) function of a variable and multivariate can be directly used in the prediction of blast-induced vibrations in rocks.

**Keywords:** PPV, blasting vibration, multivariate equations, RMR, twin tunnels.

## 1. INTRODUCTION

An important consideration for tunnel excavation in urban areas using the drilling and blasting method is to avoid damage to existing buildings and structures as this method generates ground vibrations. Nowadays, many parameters are used to estimate blast-induced vibration as particle velocity and particle acceleration, particle displacement... However, particle velocity is the most suitable parameter for assessing vibration-associated risks. The particle velocity is also used for most standards in the world because it can be measured by Geophone sensors. The amplitude of blast-induced vibrations and the PPV are influenced by the type of

---

Note:

- This paper was received on September 30, 2021 and accepted for publication by the Editorial Board on January 7, 2022.
  - Discussions on this paper will be accepted by November 30, 2022.
- <https://doi.org/10.18400/tekderg.1002681>

1 Faculty of Civil Engineering, Hanoi University of Mining and Geology, Hanoi, Vietnam  
dangvankien@humg.edu.vn - <https://orcid.org/0000-0001-8821-9178>

2 Faculty of Civil Engineering, Hanoi University of Mining and Geology, Hanoi, Vietnam  
votronghung@humg.edu.vn - <https://orcid.org/0000-0001-5923-5806>

explosives used and the charge weight per delay and the distance between the blast face and the monitoring point, as well as geological and geotechnical conditions of the rock units in the excavation area. Different methods have been suggested to evaluate the ground vibrations level during blasting such as: the in-situ measurement based on sensors, the empirical approach model, the numerical simulation model ... The parameter values of rock mass is available in tunneling projects. It is very effective to find out the rule between PPV and parameter values of rock mass quality such as RMR, Q, RQD. By this relation, it allows quick and efficient determination of PPV values according to rock mass parameters. However, up to now, there has not been a scientific work to effectively propose the relationship between PPV and rock mass parameters.

In tunneling, the use of concrete is often restricted near the area where blasting takes place, due to the risk of vibration damage. An important example is the driving of two parallel tunnels that requires coordination between the two excavations so that blasting in one tunnel does not, through vibrations, damage temporary support systems in the other tunnel prior to installation of robust, permanent support, see Figure 1.

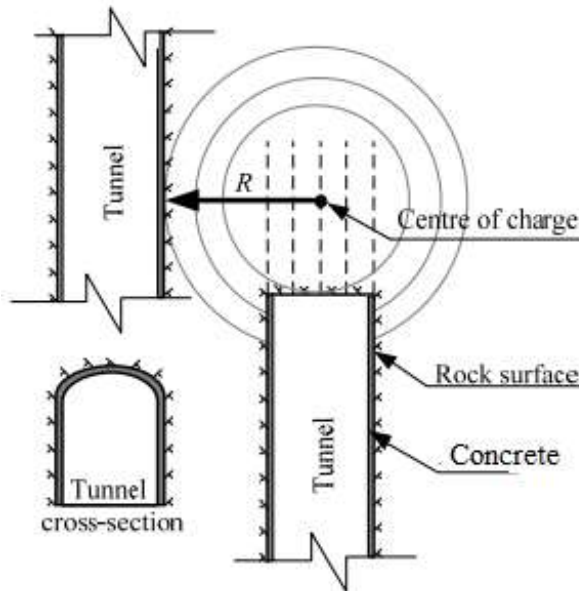


Figure 1 - Construction of two parallel tunnels [2]

Based on the measurement data and numerical model available at the Croix-Rousse tunnel project, Lyon, France, the paper was carried out to build the relationship between PPV and parameters based on numerical methods. It allows quick determination of the PPV value under the same conditions as the Croix-Rousse tunnel. This study was carried out to determine the relationship between PPV and parameters based on numerical methods.

The Croix-Rousse tunnel is located in Lyon, France, between the Rhône and the Saone rivers. The length of the tunnel is 1757 m with a cross-section area of 84.10m<sup>2</sup>. A new tunnel was

excavated in parallel to the existing one. The distance wall to wall between these two tunnels is around 29.27m (Figure 2). The cover depth of the tunnels varies between 70 and 100m [1].

In addition, some authors also studied the impact of blasting on existing tunnel structure such as following cases: The effect of an internal explosion in a tunnel on a neighboring buried tunnel and free surface [1]; the impact of the explosion which is placed on the ground to the tunnels; the impact of a bomb explosion at the surface on fortifications [7], [11]. The paper was used the measuring results at Croix-Rousse tunnel project, Lyon, France to study to establish empirical (regression function) between PPV and parameters according to many criteria simultaneous influences (multiple variables). Characteristics of the Croix-Rousse tunnel project were introduced in articles [4] ÷ [6].

The blasting vibrations induced in the existing tunnel during the excavation of the new Croix-Rousse tunnel were monitored using sensors of the Geophone type. The sensors (A, P, and T as seen in Fig.3) were embedded in the concrete lining along the tunnel axis. Results of the PPV values are monitored in three directions, including transverse direction, vertical direction, and the longitudinal direction of the tunnel. The maximum value of the three orthogonal components (x, y, z) is presented in Table 1 [13].

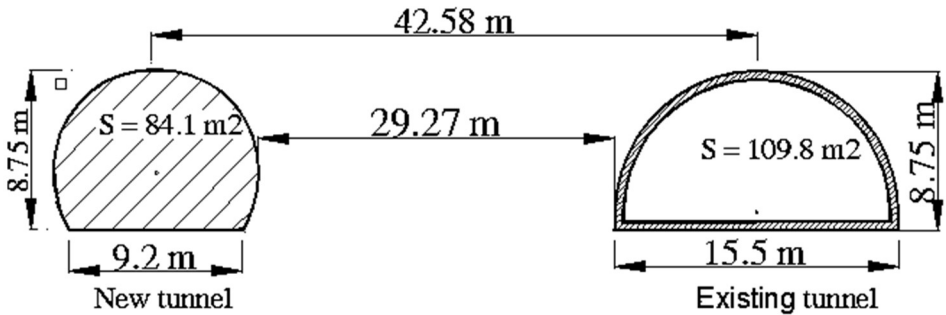


Figure 2 - Construction of two parallel tunnels in Croix-Rousse tunnel, Lyon, France

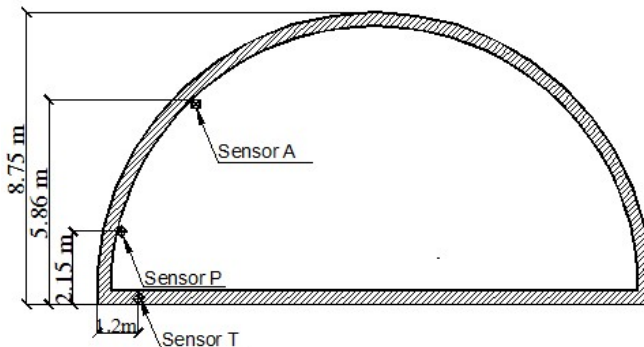


Figure 3 - Location of sensors in the existing tunnel at Croix-Rousse tunnel

Impact of blasting at tunnel face on an existing adjacent tunnel at Croix-Rousse tunnel was performed using the Finite Element Method with the Abaqus/Explicit 6.11-2 software by 2D and 3D model by author. The result of research by numerical models shows the relation between PPV (mm/s) on damping ratio “ $\xi$ ”, dynamic Young’s modulus “ $E_d$ ”, and time “ $t$ ” (s) such as Table 3 ÷ Table 6 [12].

Table 1 - Monitoring data of blasting velocity

Order number of blasting	Explosion weight: $Q_{max}$ (kg)	PPV <sub>max</sub> (mm/s)
230	544.0	3.58
231	574.5	8.99
232	647.0	12.12
233	662.0	15.36
234	1153.0	14.59
235	870.0	10.08
236	871.0	7.21
239	849.0	5.69

## 2. SOME MEASURING RESULTS AT CROIX-ROUSSE, LYON, FRANCE

Based on the measuring data at Croix-Rousse tunnel by sensors in the existing tunnel, multivariate equations estimated to present a relation between PPV (mm/s) and damping ratio “ $\xi$ ”, time “ $t$ ” (s) at Table 2. The multivariate equations are estimated to present the relation between the PPV (mm/s) on “ $E_d$ ” and “ $t$ ” (s) in Table 3.

Table 2 - PPV value (mm/s) depends on damping ratio “ $\xi$ ” and time “ $t$ ” (s)

t(s)	PPV (mm/s) and damping “ $\xi$ ”								
	Field data	$\xi=3\%$	$\Delta, \%$	$\xi=4\%$	$\Delta, \%$	$\xi=5\%$	$\Delta, \%$	$\xi=6\%$	$\Delta, \%$
0.0064	9.23	16.54	44.22	13.50	31.67	11.42	19.19	9.89	6.71
0.033	7.17	15.75	54.44	12.65	43.26	10.61	32.39	9.08	20.99
0.061	9.52	15.27	37.65	11.99	20.61	9.81	2.980	8.32	14.42
0.163	10.10	14.66	31.11	11.30	10.62	9.16	10.20	7.71	30.98
0.264	8.05	17.08	52.82	14.96	46.17	12.58	35.97	10.92	26.21
0.366	12.16	18.75	35.15	14.70	17.29	12.40	1.980	10.58	14.91
0.568	9.81	15.78	37.81	14.59	32.75	13.17	25.50	11.34	13.45
0.771	10.24	17.35	40.97	13.546	24.36	10.298	0.500	8.348	22.74

Note:  $\Delta\%$  - The difference between field data and numerical result



Table 3 - PPV value depends on “ $E_d$ ” and “ $t$ ” (s)

t(s)	Giá trị PPV (mm/s) with $E_d$ (GPa)								
	Field data	$E_d=40$ GPa	$\Delta, \%$	$E_d=50$ GPa	$\Delta, \%$	$E_d=60$ GPa	$\Delta, \%$	$E_d=70$ GPa	$\Delta, \%$
0.0064	9.23	5.84	36.72	11.72	21.24	11.42	19.18	9.63	4.15
0.033	7.17	7.22	0.69	12.386	42.11	10.61	32.42	8.5	15.65
0.061	9.52	9.7	1.86	12.48	23.72	9.81	2.96	7.43	28.13
0.163	10.10	13.8	26.81	12.56	19.59	9.16	10.26	6.5	35.64
0.264	8.05	1.23	84.72	9.7	17.01	12.58	36.01	11.29	28.69
0.366	12.16	4.16	65.79	13.1	7.18	12.4	1.94	10.3	15.29
0.568	9.81	-0.047	100.48	8.36	14.78	13.17	25.51	11.85	17.21
0.771	10.24	14.73	30.48	14.41	28.94	10.29	0.49	7.73	24.51

Note:  $\Delta\%$  - The difference between field data and numerical result

Based on field data in Table 4, the depends on PPV on Damping “ $\xi$ ” and “ $t$ ” (s) and the depends on PPV “ $E_d$ ” (GPa) and “ $t$ ” (s) are given such as on at Table 4 and Table 5.

Table 4 - PPV value depends on Damping “ $\xi$ ” and “ $t$ ” (s)

N <sub>o</sub>	PPV (mm/s)	t(s)	$\xi$ (%)
1	16.54	0.0064	3.0
2	15.75	0.033	3.0
3	15.27	0.061	3.0
4	14.66	0.163	3.0
5	17.08	0.264	3.0
6	18.75	0.366	3.0
7	15.78	0.568	3.0
8	17.35	0.771	3.0
9	13.50	0.0064	4.0
10	12.65	0.033	4.0
11	11.99	0.061	4.0
12	11.30	0.163	4.0
13	14.96	0.264	4.0
14	14.70	0.366	4.0
15	14.59	0.568	4.0
16	13.546	0.771	4.0
17	11.42	0.0064	5.0
18	10.61	0.033	5.0

Table 4 - PPV value depends on Damping " $\xi$ " and " $t$ " (s) (continue)

<b>Nº</b>	<b>PPV (mm/s)</b>	<b>t(s)</b>	<b><math>\xi</math> (%)</b>
19	9.81	0.061	5.0
20	9.16	0.163	5.0
21	12.58	0.264	5.0
22	12.4	0.366	5.0
23	13.17	0.568	5.0
24	10.29	0.771	5.0
25	9.63	0.0064	6.0
26	8.50	0.033	6.0
27	7.43	0.061	6.0
28	6.50	0.163	6.0
29	11.29	0.264	6.0
30	10.30	0.366	6.0
31	11.85	0.568	6.0
32	7.73	0.771	6.0

Table 5 - PPV value depends on " $E_d$ " (GPa) and " $t$ " (s)

<b>Nº</b>	<b>PPV (mm/s)</b>	<b>t(s)</b>	<b><math>E_d</math> (GPa)</b>
1	5.84	0.0064	40.0
2	7.22	0.033	40.0
3	9.70	0.061	40.0
4	13.8	0.163	40.0
5	1.23	0.264	40.0
6	4.16	0.366	40.0
7	14.73	0.771	40.0
8	11.72	0.0064	50.0
9	12.386	0.033	50.0
10	12.48	0.061	50.0
11	12.56	0.163	50.0
12	9.70	0.264	50.0
13	13.1	0.366	50.0
14	8.36	0.568	50.0
15	14.41	0.771	50.0
16	11.42	0.0064	60.0
17	10.61	0.033	60.0
18	9.81	0.061	60.0

Table 5 - PPV value depends on “E<sub>d</sub>” (GPa) and “t” (s) (continue)

N <sup>o</sup>	PPV (mm/s)	t(s)	E <sub>d</sub> (GPa)
19	9.16	0.163	60.0
20	12.58	0.264	60.0
21	12.4	0.366	60.0
22	13.17	0.568	60.0
23	10.29	0.771	60.0
24	9.63	0.0064	70.0
25	8.50	0.033	70.0
26	7.43	0.061	70.0
27	6.50	0.163	70.0
28	11.29	0.264	70.0
29	10.3	0.366	70.0
30	11.85	0.568	70.0
31	7.73	0.771	70.0

### 3. STUDY TO DETERMINE REGRESSION MODEL BY A FUNCTION OF A VARIABLE PPV = F (RMR)

The study tunnel area with PM200÷PM600 of Croi-Rousse tunnel and RMR value presents Figure 4 and Table 6. Inconsistent measurement results from sensors will be removed before finding the relationship between the parameters “K”, “α” (in Chapot's formula), and the "RMR" value of the rock mass. Using a formula of Chapot (1980) (1) in the French standards are often used to investigate o the relation between the (PPV) and S<sub>D</sub>,  $S_D = (\frac{D}{\sqrt{Q_c}})^{-\alpha}$ :

$$PPV = K. (\frac{D}{\sqrt{Q_c}})^{-\alpha} \quad (Chapot\ 1980) \quad (1)$$

PPV- Pick Particle Velocity (mm/s); D - is the distance from the blasting source to the point of monitoring (m); Q<sub>c</sub> - is the maximum charge weight per delay (kg); K and α are constants that depend on the ground condition as well as the conditions of blasting;

Analysis of recording vibrations in the Croix-Rousse tunnel by using the recording result at sensor A or sensor P (Figure 3). We can find the relation Relation between the maximum value of (PPV) and scaled charge explosive S<sub>D</sub> in sensor P. The layout of the two tunnels is presented in Figure.5. H represents the distance from the section in the existing tunnel to the tunnel face of the new tunnel. The numerical results indicate that the biggest particle velocity induced in the tunnel lining of the existing tunnel is obtained when the section is closer to the blasting location (the case of H = 0 in Figure.5). By analyzing the measurement data obtained from the sensor P, paper is obtained a relationship between “Ln(K)” and “α” in the Chapot formula with “RMR” value is described on Figure 6.

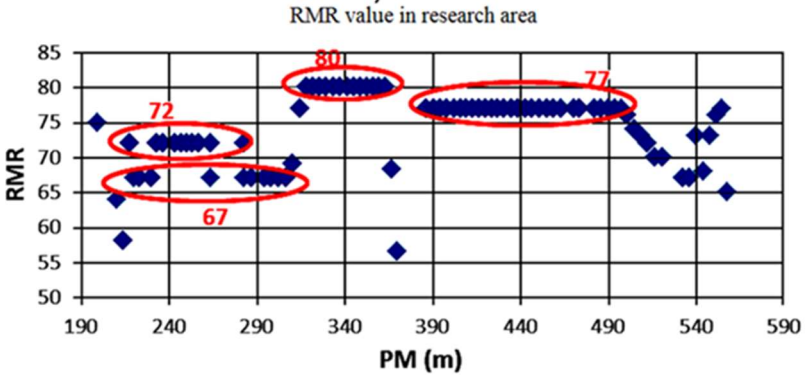


Figure 4 - RMR value in the research area

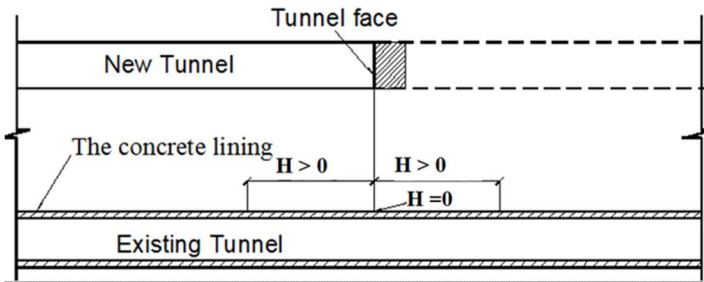


Figure 5 - Layout of two tunnels

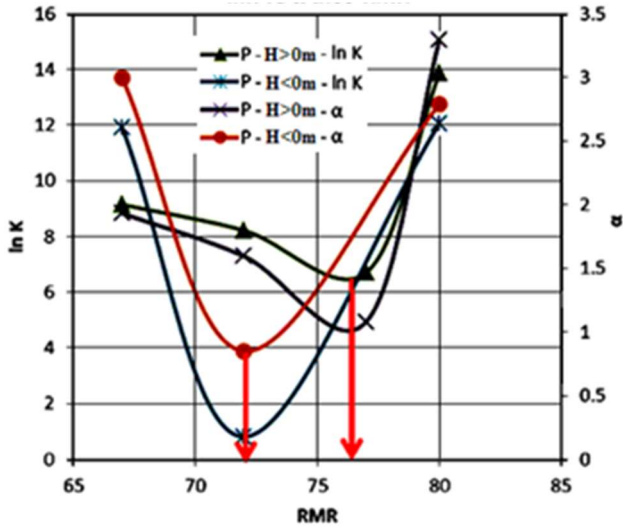


Figure 6 - Relationship between “Ln (K)” and “ $\alpha$ ” in the Chapot formula with “RMR” value at sensor P

By using the measuring value of sensor P at Croix- Rousse tunnel, the relation between PPV and RMR is established for granite rock with the function of a variable obtained formula (2). A flowchart in this study of the determined regression model functions using different types of regression is presented in Figure 7.

Table 6 - Location of the research areas in the tunnel

Research Areas	From KP	To KP	Length of research area, m	Rock type
1	200	600	400	Granit
2	640	750	110	Gonai
3	750	1430	680	Granit

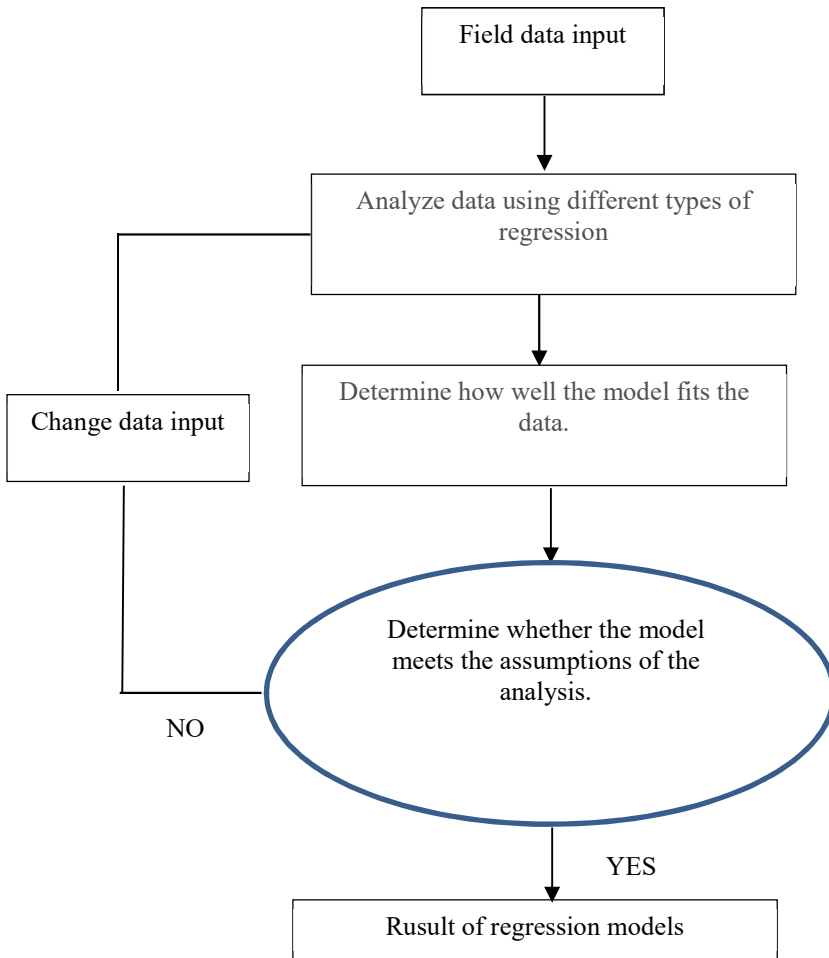


Figure 7 - Flowchart of the determine regression model functions

By using the measuring value of sensor P, the relation between PPV and RMR is established for granite rock with the function of a variable obtained formula (2):

$$PPV = (7.10^8 \cdot e^{-0.171 \cdot RMR}) \cdot (D/\sqrt{Q})^{-\left(\frac{2.4991 \cdot RMR^3 - 53.79 RMR^2 + 38736 \cdot RMR - 921961}{+38736 \cdot RMR - 921961}\right)} \quad (2)$$

Although it is the function of a variable, but it is very useful to give so fast PPV value based on the actual value RMR of surrounding rock mass conditions. It also is a good trend to continue studies on this problem in the future.

#### 4. STUDY TO DETERMINE REGRESSION MODEL BY FUNCTION OF TWO VARIABLES $PPV=F(t, \xi)$

After using the output data of Table 3, PPV value depends on "t" (s) and "ξ" obtained program found multi-variable experimental functions in Pascal programming language. The result has given 9 regression models (Empirical Formula) of two variables  $PPV=F(t, \xi)$  such as:

➤ Regression model (Empirical Formula) first:

$$PPV = 22.79 + 1.86 - 2.39 \times \xi; \quad R=0.89; \quad (2)$$

➤ Regression model (Empirical Formula) second:

$$PPV = 44.22 \times (T)^{(0.019)} \times (\xi)^{(-0.85)}; \quad R=0.86; \quad (3)$$

➤ Regression model (Empirical Formula) third:

$$PPV = 28.34 + 0.25 \times \ln(T) - 10.39 \times \ln(\xi); \quad R=0.89; \quad (4)$$

➤ Regression model (Empirical Formula) fourth:

$$PPV = e^{(28.43+0.15 \times T - 0.19 \times \xi)}; \quad R=0.87; \quad (5)$$

➤ Regression model (Empirical Formula) fifth:

$$PPV = 2.42 - 0.00037 \times (1/T) + 42.58 \times (1/\xi); \quad R=0.87; \quad (6)$$

➤ Regression model (Empirical Formula) sixth:

$$PPV = 30.83 \times (T)^{(0.019)} \times e^{(-0.19 \times \xi)}; \quad R=0.86; \quad (7)$$

➤ Regression model (Empirical Formula) seventh:

$$PPV = 40.79 \times (e)^{[(0.15) \times T]} \times (\xi)^{(-0.85)}; \quad R=0.86; \quad (8)$$

➤ Regression model (Empirical Formula) eighth:

$$PPV = 40.79 \times (e)^{[(0.15) \times T]} \times (\xi)^{(-0.85)}; \quad R=0.86; \quad (9)$$

➤ Regression model (Empirical Formula) ninth:

$$PPV = (30.82) \times (T)^{(0.019)} \times e^{[(-0.19) \times \xi]}; \quad R=0.86 \quad (10)$$

Where: F - type of regression model (empirical formula); PPV - Peak Particle Velocity; T - time; ξ- damping value; R - multiples correlation coefficient.

After comparing the multiples' correlation coefficient of regression model (empirical formula) (2),(10), the biggest of multiples correlation coefficient obtained with regression model second,  $R= 0,89$ . This regression model can be the original model to determine “The largest amount of explosives for one explosion” on the actual condition.

## 5. STUDY TO DETERMINE REGRESSION MODEL FUNCTION OF TWO VARIABLES $PPV=F(t, E_d)$

After using output data of Table 4, PPV value depends on “ $E_d$ ” and “ $t$ ”(s) obtained program found multi-variable experimental functions in Pascal programming language. The result has given 9 regression models (Empirical Formula) of two variables  $PPV=F(t, E_d)$  such as.

➤ Regression model (Empirical Formula) first:

$$PPV = (6.45 + 1.06xT + 0.055XE); \quad R=0,196; \quad (11)$$

➤ Regression model (Empirical Formula) second:

$$PPV = 1,041 \times (T)^{(0,008698489)} \times (E)^{(0,554901612)}; \quad R=0,24; \quad (12)$$

➤ Regression model (Empirical Formula) third:

$$PPV = 64,39 + 0,25 \times Ln(T) - 12,88 \times Ln(E); \quad R=0,89; \quad (13)$$

➤ Regression model (Empirical Formula) fourth:

$$PPV = e^{(6,008417125 + ,210416129 \times T + 0,085759656 \times E)}; \quad R=0,238; \quad (14)$$

➤ Regression model (Empirical Formula) fifth:

$$PPV = -0,124 - 0,00036 \times (1/T) + 667,19 \times (1/E); \quad R=0,88; \quad (15)$$

➤ Regression model (Empirical Formula) sixth:

$$PPV = 6,42 \times (T)^{(0,0093)} \times (e)^{[(0,087) \times E]}; \quad R=0,21; \quad (16)$$

➤ Regression model (Empirical Formula) seventh:

$$PPV = 1,0113 \times (e)^{[(0,2055) \times T]} \times (E)^{(0,543)}; \quad R=0,270; \quad (17)$$

➤ Regression model (Empirical Formula) eighth:

$$PPV = 6,0084 \times (e)^{[(0,2104) \times T]} \times (e)^{[(0,085) \times E]}; \quad R=0,23 \quad (18)$$

➤ Regression model (Empirical Formula) ninth:

$$PPV = (6,427) \times (T)^{(0,0093)} \times e^{[(0,087) \times E]}; \quad R=211; \quad (19)$$

Where: F - the type of regression model (empirical formula); PPV- Peak Particle Velocity; T - time (s);  $E_d$ - Dynamic Young’s modulus of rock mass; R - multiples correlation coefficient.

After comparing the multiples' correlation coefficient of regression model (empirical formula) (11)÷(19), the biggest of multiples correlation coefficients obtained with regression model in equation (13),  $R = 0,89$ . This regression model can be the original model to determine “The largest amount of explosives for one explosion” on the actual condition.

Received results also show that in the practice when building new tunnels near the existing tunnel to reduce effects of vibration of blasting can be predicted PPV value based on the Dynamic Young’s modulus ( $E_d$ ) of rock mass and time ( $t$ ). Comparing the value of the calculated PPV value with the corresponding allowed value of the standards can indicate rocks mass and tunnel lining works have stabilized under the effect of blasting load.

**6. STUDY TO DETERMINE REGRESSION MODEL WITH FUNCTIONS OF THREE VARIABLES**

According to the above results, after using field data at Croix-Rousse, Lyon, France on Table 2 ÷ Table 5, the effect of PPV on three parameters: “ $\xi$ ” and “ $t$ ” and “ $E_d$ ” is present in Table 5.

Table 5 - PPV value depends on three parameters “ $\xi$ ” and “ $t$ ” and “ $E_d$ ”

No	PPV	T	E	$\xi$	H
1	11.72	0.0064	50.0	5.0	0
2	11.3	0.163	70.0	4.0	0
3	10.61	0.033	60.0	5.0	0
4	8.32	0.061	50.0	6.0	0
5	7.73	0.771	70.0	6.0	0
6	7.43	0.061	70.0	6.0	0

After using the output data of Table 5, a program found multi-variable experimental functions in the Pascal programming language. The result has given 9 regression models (Empirical Formula) of the following three variables function:

$$PPV = F(t, E_d, \xi)$$

➤ Regression model (Empirical Formula) first:

$$PPV = 26.49 + 0.48 \times T - 0.086x E - 2.197x \xi; \quad R=0.97; \quad (20)$$

➤ Regression model (Empirical Formula) second:

$$PPV = 5,47 \times (T)^{(-0,024317111)} \times (E)^{(-0,37108331)} \times (\xi)^{(-1,072039643)}; \quad R=0.96; \quad (21)$$

➤ Regression model (Empirical Formula) third:

$$PPV = 38,05 - 0,269 \times Ln(T) - 3,076 \times Ln(E) - 9,98 \times Ln(\xi); \quad R=0.97; \quad (22)$$

➤ Regression model (Empirical Formula) fourth:

$$PPV = e^{(4,061958308 + ,056244176 \times T - 0,009530558 \times E - 0,234058115 \times \xi)}; \quad R=0.97; \quad (23)$$

➤ Regression model (Empirical Formula) fifth:

$$PPV = -2,33 + 0,012 \times (1/T) + 140,88 \times (1/E) + 47,31 \times (1/\xi); \quad R=0.97; \quad (24)$$



➤ Regression model (Empirical Formula) sixth:

$$PPV = 4,35 \times (T)^{(-0,023100363)} \times (e)^{[(-0,006446419) \times E]} \times (x)^{(-1,073281227)}; \quad R=0.96; \quad (25)$$

➤ Regression model (Empirical Formula) seventh:

$$PPV = 4,89 \times (T)^{(-0,018614246)} \times (E)^{(-0,376230868)} \times (e)^{[(-0,217764272) \times \xi]}; \quad R=0.97; \quad (26)$$

➤ Regression model (Empirical Formula) eighth:

$$PPV = 6,57 \times (e)^{[(0,042906918) \times T]} \times (E)^{(-0,589078741)} \times (\xi)^{(-1,159819879)}; \quad R=0.96; \quad (27)$$

➤ Regression model (Empirical Formula) ninth:

$$PPV = 4,77 \times (e)^{[(0,048844617) \times T]} \times (e)^{[(-0,010078617) \times E]} \times (\xi)^{(-1,160663177)}; \quad R=0.96; \quad (28)$$

➤ Regression model (Empirical Formula) tenth:

$$PPV = 5,77 \times (e)^{[(0,051432765) \times T]} \times (E)^{(-0,55901163)} \times (e)^{[(-0,234192886) \times \xi]}; \quad R=0.97 \quad (29)$$

➤ Regression model (Empirical Formula) eleventh:

$$PPV = (3,75) \times (T)^{(-0,017619142)} \times e^{[(-0,006486009) \times E]} \times e^{[(-0,217789924) \times \xi]}; \quad R=0.97 \quad (30)$$

Where: F – the type of regression model (empirical formula); PPV- Peak Particle Velocity; T-time (s);  $E_d$ - Dynamic Young’s modulus of rock mass;  $\xi$  – damping value in the numerical model; R - multiples correlation coefficient.

After comparing the multiples' correlation coefficient of the regression model (empirical equation (20) to equation (30)), the biggest of multiples correlation coefficients obtained with regression model in equation (30),  $R=0,97$ . This regression model can be an original model to determine “The largest amount of explosives for one explosion” on the actual condition. The above results show that using the result of numerical models with the field data investigations on the effect of the blasting in a new tunnel on the surrounding rock mass and on the existing tunnel can be carried out by regression model. The research results show that not only predicting the tunnel lining damage zone under the impact of blast loads but also determination peak maximum of explosion at the same time at the tunnel face by equation (1).

## 7. CONCLUSION

By obtained result in this study, several conclusions can be drawn as follows:

➤ PPV value is dependent on many different parameters such as physical-mechanics properties of the rock around the blasting area ( $E_d$  -Dynamic Young’s modulus;  $\xi$ -damping value, t- time at the investigated point from the time of blasting, H -the distance from an investigated point to explosion point and some parameters).

➤ The first time, the relation between PPV and RMR is established for granite rock with the function of a variable in the Croix-Rousse tunnel by equation (2). Although this equation is the function of a variable, it is useful to give so fast PPV value based on the actual value RMR of projects the same conditions as the Croix-Rousse tunnel. It is a result to applied in equivalent conditions and also a new direction to study in the future.

➤ Paper was also carried out to investigate the PPV value on above some parameters and to establish regression models thought the relation between PPV and effect parameters by a function of two variables such as equation (2) to equation (19). The PPV value also is a function of three variables of dependent parameters such as equation (20) to equation (30). However, PPV is a function of multivariate so reflection on the effect of all the actual conditions on PPV value is not fully. So, it is necessary to consider the importance of the variables for a project.

### **Symbols**

PPV - Peak Particle Velocity (mm/s);

PPA -Peak Particle Acceleration ( $\text{mm/s}^2$ );

PPD -Peak Particle Displacement (mm);

RMR- Rock Mass Rating;

Q-System is a classification system for rock masses with respect to stability of underground openings;

RQD- Rock Quality Designation;

$\xi$ - Damping ratio;

$\Delta\%$  - The difference between field data and numerical result;

$E_d$  - Dynamic Young's modulus (MPa);

t- time (s);

D - is the distance from the blasting source to the point of monitoring (m);

$Q_c$  - is the maximum charge weight per delay;

K and  $\alpha$  are constants that depend on the ground condition as well as the conditions of blasting;

$S_D$  - Scaled charge explosive;

KP- distance from the tunnel portal to point of monitoring (m);

R- Multiples' correlation coefficient of regression model;

F- function of variables;

### **References**

- [1] Clayton, E., Soler, B., Voiron, J.,. Renovation of Croix. Rouse tunnel - Specific points of the technical design. AFTES, page 135. Congrès International, Lyon1, 2011.

- [2] Vladimir Feldgun et al., . The Effect of an Internal Explosion in a Tunnel on a Neighboring Buried Structure and Free Surface- The 15th International Symposium on Interaction of the Effects of Munitions with Structures (ISIEMS 15), At Potsdam, Germany, 2016.
- [3] Vo Trong Hung, Dang Van Kien. A new research direction on the impact of the tunnel construction explosion shock on the adjacent tunneling structure. *Journal of Mining Industry*, Issue No.4, pages 78-84, Hanoi, Vietnam, 2017.
- [4] J.H. Yanga et al, 2D numerical analysis of rock damage induced by dynamic in-situ stress redistribution and blast loading in underground blasting excavation. *Tunneling and Underground Space Technology* 70, 221–232, 2017.
- [5] Zihan Liu et al., Influence of tunnel blasting construction on adjacent highway tunnel: A case study in Wuhan, China. *International Journal of Protective Structures*. Volume: 11 issue: 3, page(s): 283-303. Crossref DOI link: <https://doi.org/10.1177/2041419619888936>. September 1, 2020.
- [6] J.H. Yang et al., 2D numerical analysis of rock damage induced by dynamic in-situ stress redistribution and blast loading in underground blasting excavation. *Tunneling and Underground Space Technology* Volume 70, Pages 221-232, November 2017.
- [7] Ao Li et al., Safety Distance of Shotcrete Subjected to Blasting Vibration in Large-Span High-Speed Railway Tunnels., Article ID 2429713, 14 pages. <https://doi.org/10.1155/2019/2429713>, *Shock and Vibration* Volume 2019.
- [8] Dang Van Kien, Vo Trong Hung, Do Ngoc Anh. Studying the effects of blasting shock on the lining structure of adjacent tunnels during tunnel excavation by using the blasting method. *Journal of Vietnam Construction*. Issue No.7, pages 203-207, Hanoi, Vietnam, 2017.
- [9] Dang, K.Van. Assessment of the effect of blasting vibration on tunnel lining of Hai Van Pass Tunnel during expanding excavation the auxiliary tunnel by drilling and blasting method (in Vietnamese). *Journal of Mining and Earth Sciences*. 61, 6 (Dec, 2020), 131-138. DOI:<https://doi.org/10.46326/JMES.HTCS2020.18>. 2020.
- [10] Cilsal Murat. The Effect of Geotechnical Factors on Blasting Induced Ground Vibration Particle Velocity. *Tunneling and Underground Space Technology* 21(3):235-235. May 2006.
- [11] QCVN 02-2008-BCT. National technical regulation on safety in the process of producing, testing, performing check and acceptance, storage, transportation, use, disposal of industrial explosive materials, and storage of explosive precursors, Viet Nam, 2008.
- [12] Dang V.K., Dias D., Do N.A., Vo T.H. (2018), Impact of Blasting at Tunnel Face on an Existing Adjacent Tunnel. *International Journal of GEOMATE*, July 2018 Vol.15, Issue 47, pp.22-31, 2018.
- [13] Lin Da-neng, (2011), The mitigation negative effect of tunnel-blasting-induced vibrations on existing tunnel and buildings, *Journal of coal science & engineering*. Pp.28-33, Vol.17 No.1 Mar. 2011.

- [14] Van Kien Dang, Trong Hung Vo, Ngoc Anh Do, The estimation of the vibration effects caused by tunnel blasts: a case study in the croix-Rousse tunnel, Proceedings of the international conferences on earth sciences and sustainable geo-resources development (ESASGD), ISBN: 978-604-76-1171-3, pp: 339-346, Ha Noi, Viet Nam, 2016.
- [15] Tran Tuan Minh, Nguyen Quang Huy. Effect of blasting on the stability of lining during excavation of new tunnel near the existing tunnel. Civil Engineering Journal. Vol. 30 No. 1 (2021). <https://doi.org/10.14311/CEJ.2021.01.0004>, 2021.

## TEKNİK DERGİ MANUSCRIPT DRAFTING RULES

1. The whole manuscript (text, charts, equations, drawings etc.) should be arranged in Word and submitted in ready to print format. The article should be typed on A4 (210 x 297 mm) size paper using 10 pt (main title 15 pt) Times New Roman font, single spacing. Margins should be 40 mm on the left and right sides and 52.5 mm at the top and bottom of the page.
2. Including drawings and tables, articles should not exceed 25 pages, technical notes 10 pages.
3. Your contributed manuscript must be sent over the DergiPark system. (<http://dergipark.gov.tr/tekderg>)
4. The text must be written in a clear and understandable language, conform to the grammar rules. Third singular person and passive tense must be used, and no inverted sentences should be contained.
5. Title must be short (10 words maximum) and clear, and reflect the content of the paper.
6. Sections should be arranged as: (i) abstract and keywords, (ii) title, abstract and keywords in the other language, (iii) main text, (iv) symbols, (v) acknowledgements (if required) and (vi) references.
7. Both abstracts should briefly describe the object, scope, method and conclusions of the work and should not exceed 100 words. If necessary, abstracts may be re-written without consulting the author. At least three keywords must be given. Titles, abstracts and keywords must be fitted in the first page leaving ten line space at the bottom of the first page and the main text must start in the second page.
8. Section and sub-section titles must be numbered complying with the standard TS1212.
9. Symbols must conform to the international rules; each symbol must be defined where it appears first, additionally, a list of symbols must be given in alphabetic order (first Latin, then Greek alphabets) at the end of the text (before References).
10. Equations must be numbered and these numbers must be shown in brackets at the end of the line.
11. Tables, drawings and photographs must be placed inside the text, each one should have a number and title and titles should be written above the tables and below the drawings and photographs.
12. Only SI units must be used in the manuscripts.
13. Quotes must be given in inverted commas and the source must be indicated with a reference number.
14. Acknowledgement must be short and mention the people/ institutions contributed or assisted the study.
15. References must be numbered (in brackets) in the text referring to the reference list arranged in the order of appearance in the text. References must include the following information:  
If the reference is an article: Author's surname, his/her initials, other authors, full title of the article, name of the journal, volume, issue, starting and ending pages, year of publication.  
Example : Naghdi, P. M., Kalnins, A., On Vibrations of Elastic Spherical Shells. J. Appl. Mech., 29, 65-72, 1962.  
If the reference is a book: Author's surname, his/her initials, other authors, title of the book, volume number, editor if available, place of publication, year of publication.  
Example : Kraus. H., Thin Elastic Shells, New York. Wiley, 1967.  
If the reference is a conference paper: Author's surname, his/her initials, other authors, title of the paper, title of the conference, location and year.  
If the source is a thesis: Author's surname, his/her initials, thesis title, level, university, year.  
If the source is a report: Author's surname, his/her initials, other authors, title of the report, type, number, institution it is submitted to, publication place, year.
16. Discussions to an article published in Teknik Dergi should not exceed two pages, must briefly express the addressed points, must criticize the content, not the author and must be written in a polite language. Authors' closing remarks must also follow the above rules.
17. A separate note should accompany the manuscript. The note should include, (i) authors' names, business and home addresses and phone numbers, (ii) brief resumes of the authors and (iii) a statement "I declare in honesty that this article is the product of a genuinely original study and that a similar version of the article has not been previously published anywhere else" signed by all authors.
18. Copyright has to be transferred to UCTEA Turkish Chamber of Civil Engineers. The standard copyright form signed by the authorised author should therefore be submitted together with the manuscript.

# CONTENTS

Utilising Building Information Models in Facility Maintenance and Operations.....	12351
<b>Esa HALMETOJA, Natalija LEPKOVA</b>	
Experimental Investigation on Hydraulic Efficiency of Vertical Drop Equipped with Vertical Screens.....	12379
<b>Rasoul DANESHFARAZ, Sina SADEGHFAM, Vadoud HASANNIYA, John ABRAHAM4, Reza NOROUZI</b>	
Seismic Performance of a Hybrid Coupled Wall System Using different Coupling Beam Arrangements ..	12401
<b>Molham SALAMEH, Mohsenali SHAYANFAR, Mohammad Ali BARKHORDARI</b>	
Investigating the Service Quality of Kocaeli Tram Service Using Artificial Neural Networks.....	12429
<b>Selim DÜNDAR</b>	
Improvement of Shear Strength of Zeolite-Bentonite Liner Material under High Temperatures with Tincal and Pumice .....	12457
<b>Sukran Gizem ALPAYDIN, Esra GUNERI, Yeliz YUKSELEN-AKSOY</b>	
Challenges and Benefits of the Use of AASHTOWare for 3 Climatic Regions in Turkey.....	12473
<b>Beyhan IPEKYUZ, Hediye TUYDES YAMAN, Hande Isik OZTURK</b>	
Investigating the Influence of Dam-Breach Parameters on Dam-Break Connected Flood Hydrograph.....	12501
<b>Mohamed NAJAR, Ali GÜL</b>	
Buckling of Laminated Elliptical and Super-Elliptical Thin Plates.....	12525
<b>Erkin ALTUNSARAY, İsmail BAYER</b>	
Modification in Response of a Bridge Seismically Isolated with Lead Rubber Bearings Exposed to Low Temperature.....	12553
<b>Esengul CAVDAR, Volkan KARUK, Gokhan OZDEMIR</b>	
Comparing Performances of Machine Learning Techniques to Forecast Dispute Resolutions .....	12577
<b>Murat AYHAN, Irem DIKMEN, M. Talat BIRGONUL</b>	
Transit Frequency Optimization in Bi-modal Networks Using Differential Evolution Algorithm.....	12601
<b>Mehmet Metin MUTLU, İlyas Cihan AKSOY, Yalçın ALVER</b>	
Numerical Study on the Deformation Behavior of Geosynthetic-Encased Stone Columns Supporting Embankments.....	12617
<b>Tuncay DOĞAN, Mehmet Rifat KAHYAOĞLU</b>	
Identification and Prioritization of Key Performance Indicators for the Construction Small and Medium Enterprises .....	12635
<b>Ozan OKUDAN, Cenk BUDAYAN, Yusuf ARAYICI</b>	
Hydrological Considerations in Designing Roadways: Avoiding Hydroplaning.....	12663
<b>Sevgi CAVDAR, Ali UYUMAZ</b>	
A Numerical Investigation on the Limitations of Design Equations for Steel Plate Shear Walls.....	12677
<b>Muhammed GÜRBÜZ, İlker KAZAZ</b>	
Evaluation of Occupational Safety in the Operation and Maintenance Activities of Dams .....	12709
<b>Özge AKBOĞA KALE, Ömer Levend AŞIKOĞLU, Selim BARADAN</b>	
<b>TECHNICAL NOTE</b>	
Effect of Blasting During Tunnel Excavation on an Existing Adjacent Tunnel .....	12725
<b>Van Kien DANG, Trong Hung VO</b>	